Springer Handbook of Auditory Research

Geoffrey A. Manley
Anthony W. Gummer
Arthur N. Popper
Richard R. Fay *Editors*

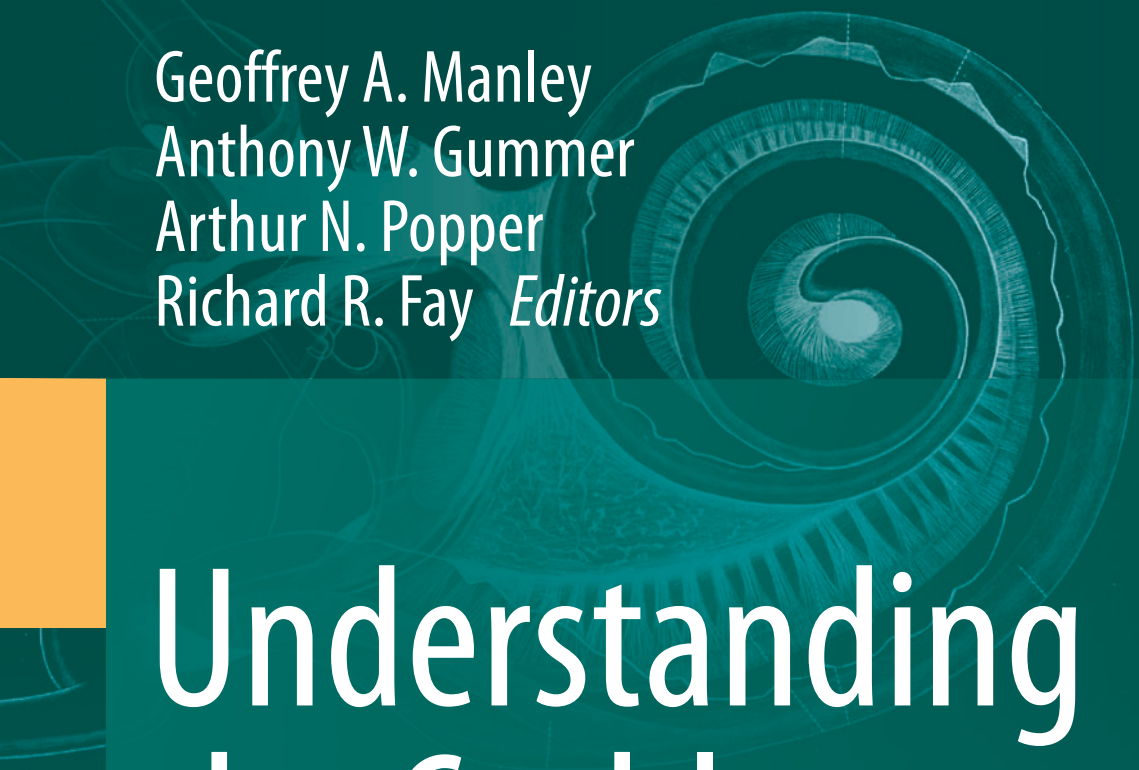

Understanding the Cochlea

ASA Press

Springer

Springer Handbook of Auditory Research

Volume 62

More information about this series at http://www.springer.com/series/2506

The ASA Press

The ASA Press imprint represents a collaboration between the Acoustical Society of America and Springer dedicated to encouraging the publication of important new books in acoustics. Published titles are intended to reflect the full range of research in acoustics. ASA Press books can include all types of books published by Springer and may appear in any appropriate Springer book series.

ASA Press

Geoffrey A. Manley · Anthony W. Gummer
Arthur N. Popper · Richard R. Fay
Editors

Understanding the Cochlea

With 71 Illustrations

ASA Press

Springer

Editors
Geoffrey A. Manley
Cochlear and Auditory Brainstem Physiology, Department of Neuroscience, School of Medicine and Health Sciences and Cluster of Excellence Hearing4all
Research Centre Neurosensory Science, Carl von Ossietzky University Oldenburg
Oldenburg
Germany

Anthony W. Gummer
Section of Physiological Acoustics and Communication, Faculty of Medicine
University of Tübingen
Tübingen
Germany

Arthur N. Popper
Department of Biology
University of Maryland
College Park, MD
USA

Richard R. Fay
Loyola University Chicago
Chicago, IL
USA

ISSN 0947-2657 ISSN 2197-1897 (electronic)
Springer Handbook of Auditory Research
ISBN 978-3-319-52071-1 ISBN 978-3-319-52073-5 (eBook)
DOI 10.1007/978-3-319-52073-5

Library of Congress Control Number: 2017945680

Printed on acid-free paper

This Springer imprint is published by Springer Nature
The registered company is Springer International Publishing AG
The registered company address is: Gewerbestrasse 11, 6330 Cham, Switzerland

Acoustical Society of America

The purpose of the **Acoustical Society of America** (www.acousticalsociety.org) is to generate, disseminate, and promote the knowledge of acoustics. The Acoustical Society of America (ASA) is recognized as the world's premier international scientific society in acoustics, and counts among its more than 7,000 members, professionals in the fields of bioacoustics, engineering, architecture, speech, music, oceanography, signal processing, sound and vibration, and noise control.

Since its first meeting in 1929, the ASA has enjoyed a healthy growth in membership and in stature. The present membership of approximately 7,000 includes leaders in acoustics in the USA and around the world. The ASA has attracted members from various fields related to sound including engineering, physics, oceanography, life sciences, noise and noise control, and architectural acoustics; psychological and physiological acoustics; applied acoustics; music and musical instruments; speech communication; ultrasonics, radiation, and scattering; mechanical vibrations and shock; underwater sound; aeroacoustics; macrosonics; acoustical signal processing; bioacoustics; and many more topics.

To assure adequate attention to these separate fields and to new ones that may develop, the Society establishes technical committees and technical groups charged with keeping abreast of developments and needs of the membership in their specialized fields. This diversity and the opportunity it provides for interchange of knowledge and points of view has become one of the strengths of the Society.

The ASA's publishing program has historically included the *The Journal of the Acoustical Society of America, JASA-Express Letters, Proceedings of Meetings on Acoustics*, the magazine *Acoustics Today*, and various books authored by its members across the many topical areas of acoustics. In addition, ASA members are involved in the development of acoustical standards concerned with terminology, measurement procedures, and criteria for determining the effects of noise and vibration.

The editors dedicate this book to our friend, colleague, and mentor Professor Emeritus Brian Manning Johnstone for his numerous and major contributions to understanding the cochlea, the topic of this book. His seminal publications encompass most chapter topics, including cochlear mechanical preprocessing, afferent and efferent neural activity, ionic and fluid homeostasis, otoacoustic emissions, and comparative auditory research as well as applied and clinical aspects of cochlear research. Brian always attracted dedicated basic scientists, clinicians, and audiologists with whom he generated new ideas and a myriad of research findings. Everyone was inspired by his amazing breadth of knowledge, his pioneering research, and his passion for science. This book honors an eminent scientist and a dear friend.

Series Preface

The following preface is the one that we published in volume 1 of the Springer Handbook of Auditory Research back in 1992. As anyone reading the original preface, or the many users of the series, will note, we have far exceeded our original expectation of eight volumes. Indeed, with books published to date and those in the pipeline, we are now set for over 60 volumes in SHAR, and we are still open to new and exciting ideas for additional books.

We are very proud that there seems to be consensus, at least among our friends and colleagues, that SHAR has become an important and influential part of the auditory literature. While we have worked hard to develop and maintain the quality and value of SHAR, the real value of the books is very much because of the numerous authors who have given their time to write outstanding chapters and to our many co-editors who have provided the intellectual leadership to the individual volumes. We have worked with a remarkable and wonderful group of people, many of whom have become great personal friends of both of us. We also continue to work with a spectacular group of editors at Springer. Indeed, several of our past editors have moved on in the publishing world to become senior executives. To our delight, this includes the current president of Springer US, Dr. William Curtis.

But the truth is that the series would and could not be possible without the support of our families, and we want to take this opportunity to dedicate all of the SHAR books, past and future, to them. Our wives, Catherine Fay and Helen Popper, and our children, Michelle Popper Levit, Melissa Popper Levinsohn, Christian Fay, and Amanda Fay Sierra, have been immensely patient as we developed and worked on this series. We thank them and state, without doubt, that this series could not have happened without them. We also dedicate the future of SHAR to our next generation of (potential) auditory researchers—our grandchildren—Ethan and Sophie Levinsohn, Emma Levit, and Nathaniel, Evan, and Stella Fay.

Preface 1992

The Springer Handbook of Auditory Research presents a series of comprehensive and synthetic reviews of the fundamental topics in modern auditory research. The volumes are aimed at all individuals with interests in hearing research including advanced graduate students, post-doctoral researchers, and clinical investigators. The volumes are intended to introduce new investigators to important aspects of hearing science and to help established investigators to better understand the fundamental theories and data in fields of hearing that they may not normally follow closely.

Each volume presents a particular topic comprehensively, and each serves as a synthetic overview and guide to the literature. As such, the chapters present neither exhaustive data reviews nor original research that has not yet appeared in peer-reviewed journals. The volumes focus on topics that have developed a solid data and conceptual foundation rather than on those for which a literature is only beginning to develop. New research areas will be covered on a timely basis in the series as they begin to mature.

Each volume in the series consists of a few substantial chapters on a particular topic. In some cases, the topics will be ones of traditional interest for which there is a substantial body of data and theory, such as auditory neuroanatomy (Vol. 1) and neurophysiology (Vol. 2). Other volumes in the series deal with topics that have begun to mature more recently, such as development, plasticity, and computational models of neural processing. In many cases, the series editors are joined by a co-editor having special expertise in the topic of the volume.

Arthur N. Popper, College Park, MD, USA
Richard R. Fay, Chicago, IL, USA

SHAR logo by Mark B. Weinberg, Potomac, Maryland, used with permission.

Volume Preface

This volume in the Springer Handbook of Auditory Research (SHAR) highlights exciting and significant developments in research into the mammalian cochlea since publication of the first *The Cochlea* volume in 1996 (volume 8, Dallos, Popper, and Fay). Rather than attempting a comprehensive review of the cochlea in this new volume because this would overlap with the first volume, we have selected key areas in which there have been major advances in the last three decades. These developments give an entirely new perspective on cochlear function, and the book concentrates on these themes. We hope that the insights gained from these studies will spark the interest of the next generation of researchers and bring current researchers and clinicians up-to-date on the latest findings to assist them in their work. This volume is conceived of as an urgently needed update in a central theme of auditory research and clinical practice.

Chapter 1 by Geoffrey A. Manley and Anthony W. Gummer provides a road map for the volume by introducing, summarizing, and integrating salient concepts from the different chapters.

In Chap. 2, Geoffrey A. Manley asks the question as to the real nature of the mammalian coiled cochlea. Manley describes its origin during the evolution of therian mammals and elucidates the changes in structure and especially physiology that belong to its unique combination of features.

Chapter 3 by Andrew K. Groves and Donna M. Fekete brings together new research on the development of the cochlea, with special focus on the sensory hair cells, a central theme of this volume.

The bundles of stereocilia on the apical surface of the hair cells are the subject of Chap. 4, where David P. Corey, Dáibhid Ó Maoiléidigh, and Jonathan F. Ashmore focus on identification of the molecular machinery of mechanoelectrical transduction and new biophysical principles of hair bundle mechanics.

One of the major discoveries in the hair cells was the motor protein, prestin, in the basolateral membrane of the outer hair cells by Peter Dallos and colleagues in the early 2000s. Two chapters discuss this molecule and its implications for hair cell function. In Chap. 5, Joseph Santos-Sacchi, Dhasakumar Navaratnam, Rob Raphael, and Dominik Oliver describe the biophysical and molecular properties

of prestin and discuss how this protein might be coupled to the plasma membrane and cytoskeleton to generate somatic electromechanical force. Then, in Chap. 6, Anthony W. Gummer, Wei Dong, Roozbeh Ghaffari, and Dennis M. Freeman address how somatic forces are coupled into the cochlear partition with sufficient magnitude and with appropriate phase to achieve the astounding cochlear properties of gain, frequency selectivity, and temporal precision.

Concepts of mechanical preprocessing for optimal stimulation of the hair bundles of inner and outer hair cells having been discussed in the previous three chapters, Chap. 7 by Michael E. Schnee and Anthony Ricci discusses how the inner hair cell faithfully encodes deflection of its hair bundle and describes specializations at the afferent synapse that enables high-fidelity neural coding.

Chapter 8 by Mark Sayles and Michael G. Heinz describes the properties of and concepts associated with the discharge patterns of afferent auditory nerve fibers for both single-tone stimulation and complex stimulation. Emphasis is placed on the relationship between neurophysiology and perception for both normal and hearing-impaired conditions.

All of the processes described in the preceding chapters require ionic currents, batteries, and solute balance. Chapter 9 by Philine Wangemann and Daniel C. Marcus focuses on the transport mechanisms required to maintain the ionic compositions and electrochemical gradients and also describes the consequences of their dysfunction.

A by-product of the active processes responsible for the exquisite filtering properties of the cochlea is otoacoustic emissions. In Chap. 10, Christopher Bergevin, Sarah Verhulst, and Pim van Dijk present a huge array of experimental and theoretical studies describing the origin and characteristics of emissions and examine what these data indicate about cochlear function under normal and pathological conditions.

In the past 21 years, a wealth of concepts associated with sound processing in the cochlea has derived from experiments with in vitro preparations. Now, Chap. 11 by Karl Grosh considers two methods of locally stimulating the cochlea in vivo—one electrical and the other optical—to elucidate physical properties and operating principles.

Although the cochlea has only been the subject of one specific SHAR volume, the aforementioned volume 8, there have been other volumes dealing with the inner ear, including its development (volume 26, 2005, *Development of the Inner Ear*, ed. by Kelly, Wu, Popper, and Fay) and hair cell function (volume 27, 2006, *Vertebrate Hair Cells*, ed. by Eatock, Fay, and Popper). Active processes in the auditory periphery was the subject of volume 30 (2008, *Active Processes and Otoacoustic Emissions*, ed. by Manley, Fay, and Popper), and innervation of the cochlea was the subject of volume 52 (2015, *The Primary Auditory Neurons of the Mammalian Cochlea*, ed. by Dabdoub, Fritzsch, Popper, and Fay). Clinical aspects of the cochlea have been considered in two volumes focusing on cochlear implants, volume 20 (2004, *Cochlear Implants: Auditory Prostheses and Electric Hearing*, ed. by Zeng, Popper, and Fay) and volume 39 (2011, *Auditory Prostheses: New Horizons*, ed. by Zeng, Popper, and Fay) as well as in two volumes on pathology

and diagnosis, volume 7 (1996, *Clinical Aspects of Hearing*, ed. by van de Water, Popper, and Fay) and volume 31 (2007, *Auditory Trauma, Protection, and Repair*, ed. by Schacht, Popper, and Fay).

In addition to these volumes, the inner ear has been discussed in chapters in many other SHAR volumes, with the focus ranging from the ears of nonmammalian species and evolution to its molecular biology and genetics.

Geoffrey A. Manley, Oldenburg, Germany
Anthony W. Gummer, Tübingen, Germany
Arthur N. Popper, College Park, MD, USA
Richard R. Fay, Chicago, IL, USA

Contents

Contributors

Jonathan F. Ashmore Department of Neuroscience, Physiology, and Pharmacology and UCL Ear Institute, University College London (UCL), London, UK

Christopher Bergevin Department of Physics and Astronomy and Centre for Vision Research, York University, Toronto, ON, Canada

David P. Corey Howard Hughes Medical Institute and Department of Neurobiology, Harvard Medical School, Boston, MA, USA

Wei Dong VA Loma Linda Healthcare System, Loma Linda, CA, USA; Department of Otolaryngology and Head and Neck Surgery, Loma Linda University Health, Loma Linda, CA, USA

Donna M. Fekete Center for Integrative Neuroscience, Department of Biological Sciences, and Purdue University Center for Cancer Research, Purdue University, West Lafayette, IN, USA

Dennis M. Freeman Research Laboratory of Electronics, Massachusetts Institute of Technology, Cambridge, MA, USA

Roozbeh Ghaffari Research Laboratory of Electronics, Massachusetts Institute of Technology, Cambridge, MA, USA

Karl Grosh Department of Mechanical Engineering, The University of Michigan, Ann Arbor, MI, USA; Department of Biomedical Engineering, The University of Michigan, Ann Arbor, MI, USA

Andrew K. Groves Departments of Neuroscience and Molecular and Human Genetics and Program in Developmental Biology, Baylor College of Medicine, Houston, TX, USA

Anthony W. Gummer Section of Physiological Acoustics and Communication, Faculty of Medicine, University of Tübingen, Tübingen, Germany

Michael G. Heinz Department of Speech, Language, and Hearing Sciences and Weldon School of Biomedical Engineering, Purdue University, West Lafayette, IN, USA

Geoffrey A. Manley Cochlear and Auditory Brainstem Physiology, Department of Neuroscience, School of Medicine and Health Sciences and Cluster of Excellence Hearing4all, Research Centre Neurosensory Science, Carl Von Ossietzky University Oldenburg, Oldenburg, Germany

Daniel C. Marcus Cellular Biophysics Laboratory, Kansas State University, Manhattan, KS, USA

Dhasakumar Navaratnam Departments of Neurology and Neuroscience, Yale University School of Medicine, New Haven, CT, USA

Dáibhid Ó Maoiléidigh Howard Hughes Medical Institute and Laboratory of Sensory Neuroscience, The Rockefeller University, New York, NY, USA

Dominik Oliver Department of Neurophysiology, Philipps-Universität Marburg, Marburg, Germany

Rob Raphael Department of Biomedical Engineering, Rice University, Houston, TX, USA

Anthony Ricci Department of Otolaryngology, Department of Molecular and Cellular Physiology, Stanford University, Stanford, CA, USA

Joseph Santos-Sacchi Departments of Surgery (Otolaryngology), Neuroscience, and Cellular and Molecular Physiology, Yale University School of Medicine, New Haven, CT, USA

Mark Sayles Laboratory of Auditory Neurophysiology, Department of Neurosciences, University of Leuven, Leuven, Belgium; Department of Speech, Language, and Hearing Sciences and Weldon School of Biomedical Engineering, Purdue University, West Lafayette, IN, USA

Michael E. Schnee Department of Otolaryngology, Stanford University, Stanford, CA, USA

Pim van Dijk Department of Otorhinolaryngology, Head and Neck Surgery, University Medical Center Groningen, University of Groningen, Groningen, The Netherlands

Sarah Verhulst Hearing Technology at WAVES, Department of Information Technology, Ghent University, Zwijnaarde, Belgium

Philine Wangemann Cell Physiology Laboratory, Kansas State University, Manhattan, KS, USA

Chapter 1
Major Advances in Cochlear Research

Geoffrey A. Manley and Anthony W. Gummer

Abstract The exquisite spectral and temporal properties of the cochlea are achieved by functional integration of specialized subsystems. Being highly integrated, these components had remained technically inaccessible in vivo for fundamental research and clinical diagnosis without damaging the whole system. In the last three decades, however, great steps forward in our understanding of cochlear function have been made possible by technical developments in biophysics, molecular biology, genetics, and imaging. The following chapters provide comprehensive descriptions of the fundamental principles and experimental results associated with various subsystems and their integration. This chapter highlights the major concepts and findings described in each chapter and links them across chapters, demonstrating the major advances in cochlear research.

Keywords Amplification · Auditory coding · Auditory synapse · Development · Hair cell · Ionic homeostasis · Mammalian cochlea · Noise damage · Optical stimulation · Otoacoustic emissions · Transduction

1.1 Introduction

It has been 21 years since the *Springer Handbook of Auditory Research* (SHAR) published a book dedicated to the whole cochlea (Dallos et al. 1996). This time period, an eternity in scientific terms, saw the development of a plethora of new

G.A. Manley (✉)
Cochlear and Auditory Brainstem Physiology, Department of Neuroscience,
School of Medicine and Health Sciences and Cluster of Excellence Hearing4all,
Research Centre Neurosensory Science, Carl Von Ossietzky University Oldenburg,
26129 Oldenburg, Germany
e-mail: geoffrey.manley@uni-oldenburg.de

A.W. Gummer
Section of Physiological Acoustics and Communication, Faculty of Medicine,
University of Tübingen, Elfriede-Aulhorn-Strasse 5, 72076 Tübingen, Germany
e-mail: anthony.gummer@uni-tuebingen.de

G.A. Manley et al. (eds.), *Understanding the Cochlea*, Springer Handbook
of Auditory Research 62, DOI 10.1007/978-3-319-52073-5_1

research techniques that have dramatically increased the ability of researchers to study different aspects of the structure and function of the cochlea. It brought many new mammalian fossils to light and special CT scanners that permit looking into details of fossils still embedded in rock (Clack et al. 2016). There has been an explosion of new study methods in molecular biology that have catapulted molecular techniques into dominance, allowing not only detailed genetic studies of evolutionary history but also a host of biochemical and physiological phenomena that control cochlear development and allow the regulated expression of genes that govern functions such as mechanoelectrical transduction, the cochlear ionic environment, electromechanical transduction, and synaptic transmission. New technical developments using highly sensitive optical, sound-recording, and mechanical techniques have permitted previously impossible studies of the nano- and macromechanics of the movements of the basilar membrane, organ of Corti, and tectorial membrane and of otoacoustic emissions. Together, the results from these research areas represent a very significant leap forward in understanding the cochlea and provide the title for this book.

This chapter summarizes and links the salient aspects of each chapter.

1.2 The Cochlea: What It Is, Where It Came From, and What Is Special About It

Chapter 2 by Geoffrey A. Manley asks the question as to the real nature of the mammalian coiled cochlea: How, when, and why did this unique structure originate? Manley describes its origin during the evolution of therian mammals and elucidates the changes in structure and especially the physiology that distinguish its unique combination of features from those of other vertebrate groups. One crucial event was the invasion of bone into the soft tissues of the cochlea, after which bone surrounded the scalae, the ganglion, and the nerve fascicles and also provided a stiffer support for the basilar membrane. Coiling itself came later and resulted in the loss of the lagenar macula, a vestibular organ originally at the tip of the cochlea. This loss likely led to a dramatic fall in the concentration of Ca^{2+} in the cochlear endolymph because there were no longer otoconia that needed high Ca^{2+} levels. This change in Ca^{2+} concentration initiated a profound series of changes in the structure of the tectorial membrane, in the endocochlear potential, in the physiology of the transduction channels, and in the structure and activity of prestin molecules. Together, these changes compensated for any deleterious effects in the fall of Ca^{2+} levels and, together with the stiffness provided by the bony supports, set the stage for the evolution of the ability to hear much higher frequencies than the ancestors. After full coiling, the length limits on hearing organs were greatly increased, leading in many lineages not only to longer cochleae but also to much larger space constants that permit much more precise analysis of narrow frequency ranges.

1.3 New Directions in Cochlear Development

Chapter 3 by Andrew K. Groves and Donna M. Fekete brings together new research on the development of the cochlea, especially that of the sensory hair cells. New techniques in molecular biology now make developmental biology pivotal in understanding not only normal cochlear structure and function but also the huge number of genetic mutational diseases among the human population. Since the SHAR volume on development 19 years ago (Rubel et al. 1998), the number of advances has been very significant. Groves and Fekete describe new discoveries related to the embryonic origin of the cochlea, the genetic control of the induction of the cellular domain that gives rise to the hearing organ, the genetic coordination of spatiotemporal gradients in cell cycle exit and differentiation, the fine-grained patterning of cell types in the organ of Corti, and the establishment of cochlear afferent and efferent innervation. New research has elucidated the remarkable complexity of the localized and time-limited gene expression patterns that control the origin of the otic capsule from head ectoderm and the series of steps that differentiate the dorsal section into a vestibular apparatus and a ventral section into the cochlear duct. During the past 10 years, there has also been considerable progress in understanding what regulates the induction and differentiation of the prosensory and the neighboring nonsensory domains. Here, special attention has been paid to clarifying the time-limited gene expression patterns that determine, for example, the specification and patterning of hair and supporting cells, including their distribution relative to the pillar cells (i.e., inner and outer hair cells) and the size and orientation of the sensory bundles on the hair cells. These events occur in a wave of cell cycle exit and cell differentiation in a basal-to-apical direction whose coordination is still unresolved. Parallel to these events, the differentiation of the afferent and efferent innervations of the vestibular and cochlear components of the inner ear takes place, involving the differential growth of the axon populations toward the different hair cell types, an exploratory phase during which axon cell connections are established, and a later phase where these are either broken or stabilized.

1.4 Mechanical Transduction Processes in the Hair Cell

Chapter 4 by David P. Corey, Dáibhid Ó Maoiléidigh, and Jonathan F. Ashmore provides an introduction to the interface between acoustic stimuli that arrive in the cochlea and the responses of the hair cells to these stimuli. Mechanoelectrical transduction is the process in sensory cells whereby mechanical energy is used to change molecular structures such that an electrical response, the receptor current, arises. As Corey, Ó Maoiléidigh, and Ashmore show, in hair cells this process is very fast indeed because the stimulus energy is coupled directly and mechanically to the hair cell bundle substructure. Corey, Ó Maoiléidigh, and Ashmore elucidate those structures of the bundle that are crucial for transduction and describe what is

now known about the organization of this molecular complex. The interaction of different protein components of the transduction apparatus with the ionic environment and the results of changes in channel conductance are fascinatingly complex and provide vital insight into how hair cells can be as sensitive as they are.

One of the most important molecular advances in knowledge of this transduction machinery in the past two decades is the discovery by Kachar et al. (2000) of the composition of the tip link. It is composed of two cadherin (CDH) dimers: a parallel dimer of PCDH15 forms the lower end of the tip link that is joined to a parallel dimer of CDH23 to form the upper end of the link. That is, nature has again hijacked ubiquitous proteins, in this case, extracellular adhesion proteins, and constructed an extracellular filament, the tip link. Based on the atomic structure and molecular dynamic simulations of this tetramer, it is now believed that the tip link is too stiff to be the gating spring. Instead, as explained by Corey, Ó Maoiléidigh, and Ashmore (Chap. 4), it is being proposed that the gating spring is an "elastic tether protein" connecting the transduction channel to the actin core of the stereocilium. Recently, fast Ca^{2+} imaging has provided evidence for the transduction channel being located near the lower extremity of the tip link. However, the "Holy Grail" of transduction research, the identity of the channel protein, remains elusive. Nevertheless, promising channel candidates are emerging, in particular the transmembrane channel-like (TMC) proteins TMC1 and TMC2, which appear to satisfy most of the criteria for the transduction channel. Other proteins belonging to the transduction machinery together with their interactions are being identified. However, without knowing the channel protein, understanding of the molecular basis of mechanoelectrical transduction is still in its infancy.

Earlier studies on the biophysics of hair bundle mechanics were primarily based on experiments from the vestibular and auditory systems of nonmammals. Many important principles derive from these seminal studies; they serve as a basis for understanding mechanoelectrical transducer function in the mammalian cochlea. Recent technical advances, such as faster stimulus and recording systems, together with experimental preparations of the isolated organ of Corti rather than the isolated hair cell are now enabling a detailed study of this transducer in the mammalian cochlea. There appear to be some important differences between the functional properties of the mammalian and nonmammalian systems. Two examples are highlighted by Corey, Ó Maoiléidigh, and Ashmore (Chap. 4). First, in nonmammalian land vertebrates (e.g., frogs and turtles), two adaptation processes can be distinguished experimentally, one with a time constant on the order of tens of milliseconds and the other on the order of a millisecond. There is evidence that the faster adaptation is mediated by Ca^{2+} binding to the channel to alter its development of mechanical force, whereas the slower adaptation is mediated by Ca^{2+}-dependent modulation of tension on the channel. In the mammalian cochlea, however, separation into two distinct adaptation processes is more difficult and time constants are, as might be expected, at least an order of magnitude faster. Second, although in the nonmammal there is ample direct experimental evidence that the hair bundle can oscillate spontaneously, there is no such evidence for the mammal. It is not known whether the differences are real or artifactual because, with the hair cell responses

being so extremely fast and complex, measurements are still made at the extreme of the capabilities of modern technology. These are important differences because, as explained by Corey, Ó Maoiléidigh, and Ashmore, adaptation can produce a region of negative slope in the displacement-force function of the hair bundle. A negative slope is necessary for the generation of spontaneous hair bundle oscillations, which, in turn, might provide evidence for cochlear amplification being primarily based on the mechanoelectrical transducers in the outer hair cell stereocilia rather than on the electromechanical transducers in the soma. Importantly, spontaneous oscillations of hair cells are known and manifest themselves outside the cochlea as spontaneous otoacoustic emissions (e.g., Bergevin, Verhulst, and van Dijk, Chap. 10). Thus, these aspects are not only important for this chapter but also for the chapters discussing the role of prestin in cochlear amplification (Santos-Sacchi, Navaratnam, Raphael, and Oliver, Chap. 5) and the mechanisms of power transfer (Gummer, Dong, Ghaffari, and Freeman, Chap. 6) as well as the properties of otoacoustic emissions, both spontaneous and sound evoked (Chap. 10).

Corey, Ó Maoiléidigh, and Ashmore (Chap. 4) use biophysical models of hair bundle mechanics to discuss the likely origins of possible differences in mammalian and nonmammalian transduction systems. For example, they emphasize that (1) a single adaptation process can produce a step response with two time constants; (2) state diagrams based on different adaptation processes can have the same structure; (3) frequency selectivity, dynamic range, and distortion products depend on the proximity of the operating point to a Hopf bifurcation; and (4) although the mammalian hair bundle might be too stiff to possess negative stiffness and oscillate spontaneously, when mass loaded, for example, by the tectorial membrane, it can oscillate spontaneously, at least theoretically. Whether the hair bundle of outer hair cells produces active force for cochlear amplification or is "simply" a passive element inputting to an active electromechanical transducer in the soma has yet to be determined experimentally.

The elucidation of the precise nature of the complex processes underlying sensory transduction and active processes in the cochlea remains one of the greatest technical and theoretical challenges.

1.5 Prestin: Molecular Mechanisms Underlying Outer Hair Cell Electromotility

The soma of the outer hair cell is an electromechanical transducer, generating mechanical force in response to a change in the transmembrane potential. Our present understanding of the molecular basis of electromechanical transduction is, when compared with that of mechanoelectrical transduction, no longer in its infancy. The reason is that unlike the transducer channel in the stereocilia, the protein serving as the molecular motor in the soma of the outer hair cell has been identified. This monumental task was accomplished by Zheng et al. (2000); appropriately, they named the protein prestin. Chapter 5 by Joseph Santos-Sacchi, Dhasakumar Navaratnam, Rob Raphael, and Dominik Oliver describes the

biophysical and molecular properties of prestin and inquires how this protein might be coupled to the plasma membrane and cytoskeleton to generate somatic electromechanical force up to at least 100 kHz.

Prestin is member A5 of an anion transporter family (SLC26). This is an example of protein hijacking, whereby protein modification has, in this case, enabled a solute carrier to become a motor. Expressed in heterologously transfected cells, prestin exhibits all known biophysical properties of outer hair cells. Knock-in prestin experiments (Dallos et al. 2008) have produced convincing evidence that prestin and, therefore, somatic electromechanical force are the bases for the amplification of faint sounds in the cochlea. Nevertheless, it is still not fully understood how sufficient force is generated because the electrical drive for the transducer is voltage, not current; the problem is that the voltage is attenuated and phase shifted by the electrical impedance of the basolateral membrane. This topic is also addressed by Corey, Ó Maoiléidigh, and Ashmore (Chap. 4) where the possibility of active force from the mechanoelectrical transducer is considered and by Gummer, Dong, Ghaffari, and Freeman (Chap. 6) where compensatory roles by structures such as the tectorial membrane are discussed.

Structural information on prestin, derived recently from crystallographic data of SLC26 relatives and molecular modeling, is beginning to shed light on molecular mechanisms of prestin function, such as the nature of the voltage sensor and the conformational states leading to electromotility. As emphasized by Santos-Sacchi, Navaratnam, Raphael, and Oliver (Chap. 5), there is "remarkable" agreement between structural and biophysical data.

There is also a large research effort attempting to identify prestin-associated proteins and understand their functional roles. For example, there exist links, called pillars, between the plasma membrane and the cytoskeleton, which are thought to be important for coupling and synchronizing molecular movements of prestin to the cytoskeleton to generate force along the longitudinal axis of the cell. Despite many attempts in many laboratories over the past two decades, the molecular composition of the pillars remains unknown. Santos-Sacchi, Navaratnam, Raphael, and Oliver (Chap. 5) discuss candidate proteins, such as microtubule-associated proteins (MAPs) and calcium/calmodulin-dependent serine protein kinase (CASK), which were recently shown to interact with prestin and actin. Related to this topic, experiments using knock-in mice expressing prestin fused to yellow fluorescent protein suggest that there is minimal lateral diffusion of prestin within the plasma membrane; the confinement mechanisms are unknown.

In general, molecular identification and functional characterization of prestin-associated proteins will eventually improve our understanding of the action of prestin under normal and pathological conditions. Moreover, such studies will also help understand the evolution of the incorporation of this molecule into the function of the organ of Corti that eventually enabled very high frequency hearing.

1.6 Electromechanical Feedback Mechanisms and Power Transfer in the Mammalian Cochlea

It is now well established that mechanical force produced by the outer hair cell is responsible for the extraordinary sensitivity, frequency selectivity, temporal fidelity, and dynamic range of the mammalian cochlea. To date, as discussed by Santos-Sacchi, Navaratnam, Raphael, and Oliver (Chap. 5), experimental evidence points overwhelmingly to prestin and, therefore, to somatic electromechanical force as being the source of this force. Nevertheless, given the mechanical and electrical impedances of cellular and acellular cochlear components, it is still not known how this force is coupled into the cochlear partition with sufficient magnitude and appropriate phase to achieve these astounding properties. Chapter 6 by Anthony W. Gummer, Wei Dong, Roozbeh Ghaffari, and Dennis M. Freeman addresses this topic, first by presenting results from velocity-pressure-voltage experiments that provide persuasive evidence for power amplification and for somatic electromechanical force being the source of this amplification. Second, based on the mechanical and electrokinetic properties of the tectorial membrane as well as vibration measurements at the tectorial membrane and reticular lamina, the essential role of the tectorial membrane for coupling this electromechanical force to the stereocilia is described.

Direct experimental evidence of power amplification requires the measurement of both velocity and fluid pressure because instantaneous power is the product of these two parameters. By comparing the phases of basilar membrane displacement and fluid pressure, Dong and Olson (2013) recently provided the first and, to date, the only direct evidence of power amplification at low sound pressure levels (<50-dB SPLs) around the best frequency (BF) of the recording place (−0.7 octave to 0.1 octave re BF). Moreover, by comparing the phase of the extracellular potential at the pressure-measurement place to the phase of basilar membrane displacement, these researchers provided evidence for somatic electromechanical force being the source of the power amplification. Chapter 6 exploits these experiments to illustrate many of the concepts associated with traveling-wave motion and active amplification in the cochlea.

How mechanical force from the outer hair cell is coupled into the organ of Corti to ensure amplification is an area of vigorous research. Being located in the vicinity of the stereocilia, the tectorial membrane has long been suspected to be an essential mechanical component of cochlear amplification, even before electromotility was discovered or the term cochlear amplifier was coined. Beginning around the turn of the millenium (Legan et al. 2000), mutations in various tectorial membrane genes have provided compelling experimental evidence that the tectorial membrane is indeed an essential component of the cochlear amplifier. Based on experiments with the tectorial membrane in isolation, in vitro, and in vivo, Gummer, Dong, Ghaffari, and Freeman (Chap. 6) explore mechanisms by which the tectorial membrane might contribute to amplification. Here, just three important results are highlighted. First, the tectorial membrane supports longitudinal traveling-wave motion at acoustic

frequencies (Ghaffari et al. 2007). That is, the stereocilia of neighboring outer hair cells are dynamically coupled, offering the possibility that the bandwidth is sufficiently wide to achieve temporal fidelity despite high gain. Second, up to at least 3 kHz in each cochlear turn, somatic electromechanical force causes counterphasic motion between the lower surface of the tectorial membrane and the reticular lamina at the inner hair cell (Nowotny and Gummer 2006). Counterphasic motion causes pulsatile fluid motion in the subtectorial space, offering the possibility of direct stimulation of the stereocilia of the inner hair cells. Third, recent vibration experiments employing optical coherence tomography in vivo and genetically manipulated cochlear components (Ren et al. 2016) are dissecting the phase relationships between the basilar membrane, tectorial membrane and reticular lamina to understand, for example, how somatic electromechanical force is coupled into the organ of Corti.

Paramount to these research efforts are experiments on isolated tectorial membrane reporting that it appears to be an anisotropic viscoelastic material, which also has electrokinetic properties (Ghaffari et al. 2013). These are extremely important findings because (1) viscoelasticity has hardly been featured in the mainly inertial models of tectorial membrane action and (2) it has generally been assumed that the tectorial membrane acts as a purely mechanical structure stimulating the stereocilia and fluid in the subtectorial space.

In the future, new stimulus and measurement paradigms, enabling more physiologically controlled experiments in vivo than has been hitherto possible in vitro, will elucidate fundamental processes associated with cochlear amplification. Chapter 11 by Grosh expands on this theme, considering some new experimental paradigms and their possible impact on understanding cochlear mechanical function.

1.7 Hair Cells and Their Synapses

Although the outer hair cell is the basis of mechanical amplification (e.g., Gummer, Dong, Ghaffari, and Freeman, Chap. 6), the inner hair cell and its afferent synapses form the neural encoder, transducing deflection of its stereocilia into a receptor potential to drive its afferent synapses and generate postsynaptic action potentials. The amplifier establishes the necessary nonlinear, frequency-dependent amplitude and phase properties of the mechanical input to the stereocilia to enable high-fidelity signal processing of sound. The inner hair cell must faithfully encode this mechanical signal with components at its disposal that have limited dynamic range, are inherently slow, and fatigue. Chapter 7 by Michael E. Schnee and Anthony Ricci describes specializations at the afferent synapse that enable high-fidelity neural coding.

A large part of the chapter deals with the so-called synaptic ribbon, a presynaptic density located at each afferent terminal. The synaptic ribbon is also a feature of other neural cells responding to graded stimuli with sustained transmitter release. Schnee and Ricci (Chap. 7) discuss the possibility that the synaptic ribbon binds

transmitter vesicles, providing a pool of vesicles that can be rapidly or readily released without depletion. Voltage-dependent Ca^{2+} channels (exclusively $Ca_V1.3$) are densely packed beneath the ribbon. These channels are rapidly gated and have mostly noninactivating properties that are required for the fast and sustained release of vesicles. How Ca^{2+} actually controls vesicular fusion remains unknown.

Mechanisms for the rapid clearance of Ca^{2+} are also still being explored. In contrast to other systems, the ribbon synapse contains otoferlin, a protein postulated to be the Ca^{2+} sensor. Schnee and Ricci (Chap. 7) also discuss further possibilities for the action of otoferlin, such as vesicle trafficking and endocytosis. Vesicular release mechanisms are also discussed, and the possibility that release might be multivesicular and that this might be the source of the rapid, large-amplitude excitatory postsynaptic currents (EPSCs), which, in turn, might provide a rapid and precise signal ensuring that an action potential is generated for each EPSC (i.e., without summation of EPSCs).

At the moment, the list of unanswered questions at the synapse is endless, but experiments combining electrophysiology with new molecular and genetic techniques promise exciting answers.

1.8 Afferent Coding and Efferent Control in the Normal and Impaired Cochlea

The preceding chapters have presented the biophysical and molecular principles associated with high-fidelity, mechanical-preprocessing, and neural encoding of sound, beginning at the stereocilia (Corey, Ó Maoiléidigh, and Ashmore, Chap. 4) and terminating in the afferent synapses (Schnee and Ricci, Chap. 7). Those chapters mainly deal with (single-tone) response properties at a single place along the cochlea. Now, Chap. 8 by Mark Sayles and Michael G. Heinz describe properties of and concepts associated with the discharge patterns of afferent auditory nerve fibers for both single-tone and complex stimulation. Emphasis is placed on the relationship between neurophysiology and perception. Being the main source of preventable hearing impairment, noise overexposure is the focus for studying pathological neural responses in Chap. 8.

For single-tone stimulation at the BF of a fiber, the dependence of mean firing rate on the SPL can largely be explained by a synergy between the nonlinear amplitude response of the basilar membrane (or, equivalently, of the inner hair cell stereocilia; e.g., Gummer, Dong, Ghaffari, and Freeman, Chap. 6) and fibers of different thresholds innervating a single inner hair cell (e.g., Chap. 7). Thus, as pointed out by Sayles and Heinz (Chap. 8), middle-to-high threshold, low spontaneous rate fibers have larger dynamic ranges than low-threshold, high spontaneous rate fibers because they are responsive in the compressive region of the basilar membrane nonlinearity as opposed to the low-intensity linear region. Indeed, phenomenological auditory models with a single parameter associated with electromechanical feedback from the outer hair cells and a single parameter for the

sensitivity of the inner hair cell stereocilia or synapse can account for neural effects of noise overexposure, such as threshold elevation, loss of frequency selectivity, and reduced dynamic range, for single-tone stimulation recorded from a single fiber. However, the wide perceptual dynamic range ($\sim$120 dB) compared with the limited dynamic range of a single fiber (less than $\sim$50 dB) remains unsolved. Mechanisms discussed by Sayles and Heinz are, for example, (1) pooled responses incorporating the spread of excitation to BFs away from the tone frequency, (2) pooling over restricted populations of BF, (3) dynamic-range adaptation, (4) efferent feedback, and (5) level-dependent temporal synchrony.

To discuss temporal coding, the acoustic signal is decomposed into the product of a rapid "temporal fine structure" component and a slower "envelope" component. For the two components, Sayles and Heinz (Chap. 8) discuss mechanisms defining, for example, (1) cutoff frequency, (2) synchronization, (3) temporal adaptation, and (4) temporal suppression. Properties are discussed for single-tone and complex stimuli under quiet hearing conditions and in the presence of background noise for both normal hearing thresholds and for hearing impairment.

Sayles and Heinz (Chap. 8) highlight some of the roles of the efferent system: the medial system synapsing with the outer hair cell soma and the lateral system with the inner hair cell afferent dendrites. For example, there is evidence that, by reducing cochlear-amplifier gain, the medial efferents can improve the detection of transient signals in background noise by decreasing neural adaptation to the noise and also assist in protection against damage from sound overexposure. There is evidence that the lateral efferents can also play a protective role against acoustic trauma as well as maintain interaural balance in excitability, possibly to ensure high sensitivity to interaural level differences.

Sayles and Heinz (Chap. 8) also emphasize one of the most important recent research topics in cochlear afferent function or better dysfunction, called "hidden hearing loss." This hearing impairment only becomes evident at suprathreshold sound intensities; the auditory thresholds are normal. Synaptopathy is believed to underlie this type of impairment, which, in turn, is hypothesized to involve glutamate excitotoxic damage to and eventual loss of auditory nerve fibers, predominantly the low spontaneous rate fibers. It is suspected that these fibers are particularly vulnerable because their spiral ganglion cells have a low number of mitochondria compared with those of high spontaneous rate fibers. Mitochondria are important for Ca^{2+} homoeostasis (e.g., Wangemann and Marcus, Chap. 9); Ca^{2+} overload is a major trigger for neural excitotoxicity.

At least three areas of intensified research into afferent coding are expected for the future: (1) effects of cochlear damage on the coding of speech, (2) effects of cochlear damage on neural coding in the brainstem and higher centers, and (3) development of diagnostic tools for the differential diagnosis of pathologies of the outer and inner cells as well as the afferent and efferent systems.

1.9 Ion and Fluid Homeostasis in the Cochlea

Many of the most common types of hereditary-based sensorineural hearing loss derive from malfunction of cells associated with the ionic homeostasis of endolymph. This luminal fluid, bathing the tectorial membrane (e.g., Gummer, Dong, Ghaffari, and Freeman, Chap. 6) and the apical surface of the hair cells where mechanoelectrical transduction (e.g., Corey, Ó Maoiléidigh, and Ashmore, Chap. 4) occurs, is unusual for an extracellular fluid because it has a high concentration of K^+, low concentration of Na^+, and exceedingly low concentration of Ca^{2+}. Moreover, the endolymph is at a positive potential relative to the perilymph, the fluid bathing the basal surface of the hair cells where neural (e.g., Schnee and Ricci, Chap. 7 and Sayles and Heinz, Chap. 8) and electromechanical (e.g., Santos-Sacchi, Navaratnam, Raphael, and Oliver, Chap. 5 and Gummer, Dong, Ghaffari, and Freeman, Chap. 6) transduction occurs. This potential, called the endocochlear potential, acts as one of the two batteries for hair cell transduction and is essential for cochlear amplification. Chapter 9 by Philine Wangemann and Daniel C. Marcus focuses on the transport mechanisms required to maintain these ionic compositions and electrochemical gradients. The chapter begins by explaining concepts associated with transepithelial transport in general as well as with the requirements of ion and solute homeostasis in the cochlea.

In the past two decades, there has been a meteoric advance in unraveling some of the myriad of processes associated with ion and solute homeostasis in the inner ear. It is well known that the stria vascularis plays a central role in homeostasis and is responsible for the high concentration of endolymphatic K^+ and generation of the endocochlear potential. Now, channels responsible for these two processes have been located and molecularly identified, with the endocochlear potential mainly originating from the basal cell-intermediate cell layer and the active K^+ secretion by the marginal cell layer. Reissner's membrane contributes to maintaining a low endolymphatic concentration of Na^+ by absorption through epithelial Na^+ channels and appears to provide acid-base control of endolymph via $Ca^{2+}/2H^+$ exchange. Ca^{2+} is secreted into the endolymph by the transport protein, plasma membrane Ca^{2+}-ATPase, located in the stereocilia and in Reissner's membrane. Processes associated with the recycling of K^+ from the sensory cells are presented, for example, through gap junction-coupled epithelial cells into spiral ligament fibrocytes and then into the stria vascularis. There is still much to be discovered about K^+ recycling.

Acid-base balance and water flow across cell membranes mediated by aquaporins are extremely important topics of this chapter. For example, H^+ has been shown to be secreted from the stria vascularis and HCO_3^- is secreted via the Cl^-/HCO_3^- exchanger pendrin, expressed in strial spindle cells, spiral prominence, and sulcus epithelial cells. Mutations in the *SLC26A4* gene encoding for pendrin are the most common cause of syndromic deafness. This is just one of the genetic factors underlying hearing loss that is presented by Wangemann and Marcus (Chap. 9). In animal models, a result of the pendrin mutation is a reduction in pH and elevation in

Ca^{2+} concentration in the endolymph. Various isoforms of aquaporin have been located in the inner ear, and in some cases, diffusion and signaling properties have been studied. However, the involvement of aquaporins in cochlear homeostasis remains unchartered territory. Another exceedingly important and broad topic covered by Wangemann and Marcus is the hormonal regulation of ion and solute homeostasis under normal and pathological (e.g., sound overexposure, drug exposure, and Ménière's disease) conditions.

In general, new genetic technology is expected to produce breakthroughs in our understanding of these homeostatic systems.

1.10 Remote Sensing the Cochlea: Otoacoustics

One result of the active processes discussed in Chaps. 4–6 is the existence of otoacoustic emissions (OAEs), discovered by Kemp (1978). That is, some of the energy generated by active processes in the inner ear is often measureable outside the eardrum as very faint sounds. Those sounds, known as spontaneous emissions or, if induced by stimuli, evoked emissions, have been an enormous boon to auditory research. On the one hand, the study of spontaneous emissions provides a means of remote sensing of cochlear operation in the absence of interfering stimuli. Especially where spontaneous emissions are normally absent (as in virtually all laboratory mammals except primates), emissions evoked by various kinds of sound are a useful tool. In Chap. 10, Christopher Bergevin, Sarah Verhulst, and Pim van Dijk examine the various kinds of emissions and review a huge array of experimental studies describing their origin and characteristics and examining what these data indicate regarding cochlear function.

OAEs are obviously closely tied to active processes in the cochlea (e.g., Corey, Ó Maoiléidigh, and Ashmore, Chap. 4) and show, despite very large differences in the size and structural configurations of the hearing organs of various organisms, remarkable similarities in their characteristics across species. The ability to examine emission properties without using invasive techniques or, at most, using low-level sounds is an enormous advantage because it eliminates many uncertainties that plague experiments carried out using invasive methods. In addition, the ability to compare emission characteristics across a wide variety of hearing organ structures makes it possible to elucidate what is common to all ears and ask the question as to why that is so, especially given the existence in mammals of at least two mechanisms underlying active processes. The failure of most mammalian ears to produce spontaneous emissions is also an important fact that implies that only minor differences in structure can hinder the loss of active-process energy to the outside world. But what are those minor differences?

Combining stimuli to produce, for example, distortion-product emissions, provides a pool of data that is important for cochlear modeling. Inducing emissions using sound stimuli is also an increasingly useful clinical tool that permits rapid evaluation of the condition of cochleae, whether they produce spontaneous

emissions or not, that in the meantime has become standard procedure in the screening of infants for hearing problems. These and other issues are described by Bergevin, Verhulst, and van Dijk (Chap. 10) as the basis of an important new area of auditory research and of clinical procedures.

1.11 Localized Internal Stimulation of the Living Cochlea Using Electrical and Optical Methods

In the past several decades, a wealth of concepts associated with sound processing in the cochlea have derived from experiments with in vitro preparations of isolated cells, the organ of Corti with or without the attached tectorial membrane, and cochlear explants. Many concepts derived from such experiments are presented in earlier chapters, in particular Chaps. 4–6 and 9. Today, with recent advances in optical imagining and, even, stimulation, it is becoming experimentally feasible to interrogate cochlear components and subsystems in vivo, confident that the physiological condition of the cochlea remains relatively unperturbed by the preparation procedure. Chapter 11 by Karl Grosh presents two methods of locally stimulating the cochlea, one electrical and the other optical, and illustrates how these techniques are elucidating principles of signal processing in the cochlea.

Although intracochlear electrical stimulation is not a new technique for probing cochlear function (e.g., Gummer, Dong, Ghaffari, and Freeman, Chap. 6), when combined with newly developed optical measurement technology, such as low-coherence heterodyne interferometry, it produces exciting new results. For example, with such a device, it is now possible to make in vivo vibration measurements not only from the basilar membrane but also from the reticular lamina to understand how electromechanical force from the outer hair cell is coupled into the organ of Corti. Using a blocker of prestin activity (salicylate) or a mutated tectorial membrane ($Tecta^{C1509G/C1509G}$), for example, has provided further compelling evidence that the feedback force derives from the soma. Related questions are, for example, (1) Is the electrical time constant of the outer hair cell indeed lower in vivo than in vitro, as suggested by an organ of Corti preparation compared with isolated-cell preparations or (2) does tectorial membrane motion possess a significant inertial component, as suggested by electrical stimulation in a cochlear explant but not supported by impedance measurements of isolated tectorial membrane? Although it is still not possible to differentiate between the vibration responses of the lower side of the tectorial membrane and the reticular lamina, as it is in a cochlear explant (e.g., Chap. 6), the necessary technological developments are expected in the near future. Even using standard laser Doppler vibrometry, Grosh discusses how localized electrical stimulation well above the BF for a given place on the basilar membrane could provide information about the local material and fluid properties of the cochlear partition and their contribution to the electromechanical response.

The second presented technique uses laser light to mechanically stimulate structures within the cochlea. This technique has recently been introduced into cochlear

mechanical research. Relying on the photoacoustic effect, the light energy is absorbed by the structure, heating it and inducing an acoustic emission as a result of rapid expansion, cooling, and, finally, compression. As with electrical stimulation, this type of optical stimulation can produce basilar membrane vibration responses that are similar to acoustic responses and, consistent with earlier findings based on single-unit (Cody and Johnstone 1981) and basilar membrane (Nilsen and Russell 2000) experiments, can demonstrate that enhanced frequency selectivity is produced by outer hair cells feeding force into the cochlear partition directly basal to the BF place. This research tool is still in its infancy. Conceivable advantages of this type of optical stimulation are, for example, the ability to achieve at least an order of magnitude spatially more focused stimulation than with (bipolar) electrical stimulation and also the ability to stimulate at a point within the depth of the cochlear partition.

The in vivo experiments using these relatively new paradigms and optical technologies are producing results that are remarkably consistent with knowledge gained from in vitro experiments and will vastly extend it when further developed and combined with genetic techniques, electrophysiological techniques, and pressure measurements.

1.12 Summary and Outlook

Today, cochlear research is being carried out using an unprecedented array of new and precise techniques and from all angles, from the initial evolution and ontogeny of this complex sense organ through electrophysiological and micromechanical studies of the function of the hearing organ through to remote sensing approaches that provide a noninvasive method of examining details of cochlear function from outside the ear. Enormous advances have been made in understanding how the cochlea came to be formed and differentiated as it is in therian mammals and how in development the precise structural configurations arise through the remarkably coordinated expression of many different genes in different tissues. Modern techniques in electrophysiological recording and in the mechanical stimulation of single hair cells and the living organ of Corti now permit a much more detailed and well understood description of hair cell transduction and the feedback system involving prestin that contributes uniquely to the response sensitivity and patterns of the hair cells. This new level of understanding provides a solid base for clinical research into innovative ways of stimulating and functionally assessing cochleae that, for one reason or another, are no longer healthy. Basic research is providing the crucial information needed to improve the lives of the hard of hearing and the deaf.

Compliance with Ethics Requirements Geoffrey A. Manley declares that he has no conflict of interest. Anthony W. Gummer declares that he has no conflict of interest.

References

Clack, J. A., Fay, R. R., & Popper, A. N. (Eds.). (2016). *Evolution of the Vertebrate Ear—Evidence from the Fossil Record*. New York: Springer International Publishing Switzerland.

Cody, A. R., & Johnstone, B. M. (1981). Acoustic trauma: Single neuron basis for the "half-octave shift." *The Journal of the Acoustical Society of America,* 70(3), 707–711.

Dallos, P., Popper, A. N., & Fay, R. R. (Eds.). (1996). *The Cochlea*. New York: Springer-Verlag.

Dallos, P., Wu, X., Cheatham, M. A., Gao, J., Zheng, J., Anderson, C. T., Jia, S., Wang, X., Cheng, W. H., Sengupta, S., He, D. Z., & Zuo, J. (2008). Prestin-based outer hair cell motility is necessary for mammalian cochlear amplification. *Neuron,* 58(3), 333–339.

Dong, W., & Olson, E. S. (2013). Detection of cochlear amplification and its activation. *Biophysical Journal,* 105(4), 1067–1078.

Ghaffari, R., Aranyosi, A. J., & Freeman, D. M. (2007). Longitudinally propagating traveling waves of the mammalian tectorial membrane. *Proceedings of the National Academy of Sciences of the United States of America,* 104(42), 16510–16515.

Ghaffari, R., Page, S. L., Farrahi, S., Sellon, J. B., & Freeman D. M. (2013). Electrokinetic properties of the mammalian tectorial membrane. *Proceedings of the National Academy of Sciences of the United States of America,* 110(11), 4279–4284.

Kachar, B., Parakkal, M., Kurc, M., Zhao, Y., & Gillespie, P. G. (2000). High-resolution structure of hair cell tip links. *Proceedings of the National Academy of Sciences of the United States of America*, 97, 13336–13341.

Kemp, D. (1978). Stimulated acoustic emissions from within the human auditory system. *The Journal of the Acoustical Society of America,* 64(5), 1386–1391.

Legan, P. K., Lukashkina, V. A., Goodyear, R. J., Kössl, M., Russell, I. J., & Richardson, G. P. (2000). A targeted deletion in α-tectorin reveals that the tectorial membrane is required for the gain and timing of cochlear feedback. *Neuron,* 28, 273–285.

Nilsen, K. E., & Russell, I. J. (2000). The spatial and temporal representation of a tone on the guinea pig basilar membrane. *Proceedings of the National Academy of Sciences of the United States of America,* 97(22), 11751–11758.

Nowotny, M., & Gummer, A. W. (2006). Nanomechanics of the subtectorial space caused by electromechanics of cochlear outer hair cells. *Proceedings of the National Academy of Sciences of the United States of America*, 103(7), 2120–2125.

Ren, T., He, W., & Barr-Gillespie, P. G. (2016). Reverse transduction measured in the living cochlea by low-coherence heterodyne interferometry. *Nature Communications,* 7, 10282. doi:10.1038/ncomms10282.

Rubel, E. W, Popper, A. N., & Fay, R. R. (Eds.). (1998). *Development of the Auditory System*. New York: Springer-Verlag.

Zheng, J., Shen, W., He, D. Z., Long, K. B., Madison, L. D., & Dallos, P. (2000). Prestin is the motor protein of cochlear outer hair cells. *Nature,* 405(6783), 149–155.

Chapter 2
The Cochlea: What It Is, Where It Came From, and What Is Special About It

Geoffrey A. Manley

Abstract The snail shell-shaped hearing organ of therian mammals is a unique development among vertebrate animals, and even egg-laying mammals (monotremes) do not have this specialization. Although there have been several ideas concerning ways in which the peculiar shape of the modern cochlea might positively affect certain aspects of its function, as yet no convincing hypothesis has been forwarded to explain its origin except that it packs a long structure into a small space. Its origin was accompanied by the loss of the vestibular lagenar macula and a large drop in the Ca^{2+} content of the endolymph, an event the consequences of which still need to be thoroughly examined. The specific shape and size of the cochlea in each species is governed by many factors, not only the adult animal's size but also its lifestyle, including sound localization, communication, and echolocation signaling. Before the spiral cochlea evolved, bone had invaded the soft tissues of the organ of Corti and the new laminae presumably enabled a better mechanical match to the mammalian middle ear, eventually providing the substrate for very high frequency hearing. The protein prestin evolved in parallel, developing high-frequency amplifying capabilities that were independently developed even further in bats and toothed whales.

Keywords Cochlea · Cochlear coiling · Cochlear evolution · Mammalian cochlea

G.A. Manley (✉)
Cochlear and Auditory Brainstem Physiology, Department of Neuroscience, School of Medicine and Health Sciences, and Cluster of Excellence Hearing4all, Research Centre Neurosensory Science, Carl Von Ossietzky University Oldenburg, 26129 Oldenburg, Germany
e-mail: geoffrey.manley@uni-oldenburg.de

G.A. Manley et al. (eds.), *Understanding the Cochlea*, Springer Handbook of Auditory Research 62, DOI 10.1007/978-3-319-52073-5_2

2.1 Introduction

What is the cochlea? In early literature about the mammalian inner ear, the hearing part, which looked remarkably like the shell of a land snail (*Helix pomatia*), was first called the cochlea by Fallopio in 1561 (Gitter 1990). The name "cochlea" is derived from the Latin for *snail shell*, which in turn is from the Greek κοχλίας (snail or screw). In the later literature, the endolymph-containing central channel (scala media), one of the three ducts within the cochlea, became known as the cochlear duct. Over time, and because this duct is a common feature of all inner ears of all amniote vertebrates ("reptiles," birds, and mammals), the term cochlear duct and cochlea were often applied to all amniote hearing structures irrespective of whether they are coiled or not. Although this makes etymological nonsense, it is perhaps acceptable in view of the evolutionarily close and direct relationships between these structures. In this short chapter, however, to emphasize its unique nature, the term cochlea will only be used for the hearing component of the inner ear of therian mammals.

The group known as therian mammals specifically excludes the few extant mammalian species known as monotremes, or egg-laying mammals such as the platypus (*Ornithorhynchus anatinus*), the echidnas or spiny anteaters of Australia (*Tachyglossus aculeatus*), and the three long-beaked echidna species of New Guinea (*Zaglossus* spp.), whose hearing epithelia are not coiled (Ladhams and Pickles 1996). The therian group also excludes other extinct lineages, such as the Multituberculata, a large group that existed ~200 million years ago (Ma) but, like the Monotremata, never evolved a coiled cochlea, even though the echidna organ of Corti is as long as that of the mouse (Luo and Ketten 1991; Fig. 2.1). In fact, the monotreme cochlea is a curved structure, but the curvature bends in the opposite direction to that of the therian cochlea (Ladhams and Pickles 1996). Therian mammals all have a coiled cochlea, produce live offspring without an external egg stage (i.e., they are viviparous), and include both the marsupials or pouched mammals (Metatheria) and the placental mammals (Eutheria). The term placental is misleading, however, because not only marsupials but also many unrelated viviparous species, those that directly produce live offspring (e.g., some skinks, some sharks), also use some kind of placenta to nourish their young before birth. In placental mammals, however, the placenta is generally very much larger because the young are retained in the mother's body for a longer time period than in marsupials, which are born in a very immature state and develop further in the mother's pouch.

The coiled mammalian cochlea can most generally be represented by a *conical, helical, often logarithmic* spiral. The individual coils are thus not in the same plane and become smaller toward the apex. In addition, the distance between the turns generally becomes larger toward the base (i.e., the volume of the cochlear turns increases), although the differences between turns can vary widely between species (e.g., Ekdale 2013).

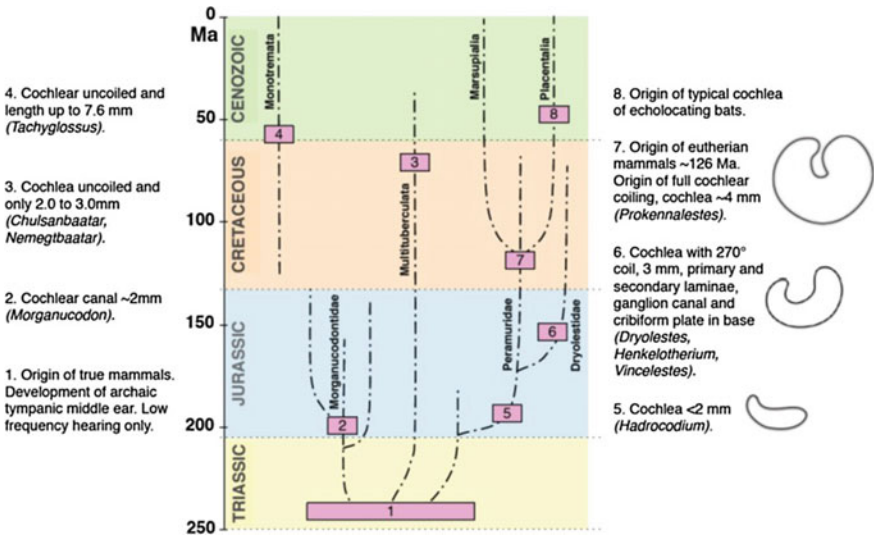

Fig. 2.1 Schematic diagram of the evolution of mammalian cochleae since the beginning of the Mesozoic era. *Left side*: Egg-laying mammals (Monotremata) and their lesser known fossil relatives such as the Multituberculates. None of these mammalian lineages evolved a coiled cochlea and the longest basilar membranes were ~8 mm in length. The middle ear was less evolved and stiff, the lagena was still present, and there was no bony integration into the soft tissues of the cochlear duct. *Right side*: Evolutionary lineages of the pouched mammals (Metatheria) and the placentals (Eutheria). Over a period of 100 million years ago (Ma), the cochlea elongated until ~120 Ma ago almost a full coil had been achieved at a length of ~4 mm. In these therian mammals the middle ear is highly evolved and very light, the cochlear ganglion is surrounded by bone, and the basilar membrane is partially supported by bone. The lagenar macula is no longer present and the prestin proteins of the outer hair cells are highly evolved (see Santos-Sacchi, Navaratnam, Raphael, and Oliver, Chap. 5). After Manley (2012), with permission

2.2 Where Did the Cochlea Come From?

Contrary to intuition, the widest part of the hearing epithelium (the low-frequency area) is at the narrow tip of the cochlea and the narrowest part (the high-frequency area) is in the much wider cochlear base. The reason for this lies in the history of amniote hearing organs, which began with only a low-frequency processing epithelium located near the connection to the saccule (Manley 2000). An increase in the length of the sensory epithelium that was accompanied by an increase in the upper frequency limit of hearing resulted in the ancestral, low-frequency area being pushed further away from the connection to the saccule.

Mammals as a group can be traced back to synapsid reptiles that were distinguished from all other lineages by a specific set of apertures in the skull and that diverged from stem reptiles ~300 Ma and thus earlier than the divergences to other

amniote groups. This fact makes it clear that the hearing organ configurations of mammals and other therian lineages evolved quite independently of each other. The features that are unique to modern therian mammals did not arise simultaneously but arose over many millions of years during which mammalian ancestors showed a mosaic of characteristics. The mixed, so-called heterodont dentition of typical mammals, for example, was a feature already clearly seen in their cynodont (mammal-like reptile) ancestors (Carroll 1987). Mammals, as it were, arose gradually over a long time. Taxonomically, however, there is no such thing as a half mammal, and taxonomists need some clear criteria to distinguish clades from each other. In the case of mammals, the distinguishing feature(s) had to be bony (i.e., not the possession of hair or milk glands) because the distinction had also to be made for fossil material. The feature that most distinguished mammals from their ancestors was the adoption of a secondary jaw articulation. The subsequent presence of redundant bones from the ancestral articulation precipitated the events leading to the evolution of mammalian, three-ossicle middle ears. Even if the tiny middle ear bones are missing in fossil material (a very common occurrence), the jaw articulation type remains uniquely recognizable. If we define the transition to true mammals as being marked by the origin of the three-ossicle tympanic middle ear (in the early Triassic period $\sim$220 Ma ago), then we can say definitely that at that time, no mammals possessed a cochlea. Instead, the auditory sensory epithelium was probably quite short (<1 mm), with only a few hundred hair cells. As described later in this section, the "true" cochlea with the specific shape of the therian cochlea only arose 100 Ma later, around 120 Ma ago (reviewed in Manley 2012).

It is likely that the first true mammals were not monophyletic, which is to say that mammals did not arise in a single evolutionary transition as one group. It is likely that the condition of "a three-ossicle middle ear" (thus defining them as mammals) arose independently twice, perhaps even more often (reviewed in Manley 2010). Remarkably, at the time of the critical transition 220 Ma ago, not only mammalian ancestors but also the ancestors of all amniote lineages (e.g., birds and lizards) were evolving tympanic middle ears of various kinds (Clack 2002). It is not yet known why this was the case, but it was almost certainly linked to changes in diet. The two middle ear types (one and three ossicle) did not, however, arise in the equivalent locations in the head. Whereas the mammalian middle ear arose fairly ventrally, near the new jaw joint, the single-ossicle middle ears that arose several times in bird and lizard ancestors arose somewhat dorsally at the location of the ancestral spiracle. The latter thus inherited an open connection to the mouth cavity. This connection in mammals (the Eustachian tube) is an independent evolutionary event as witnessed by the different relationships between the structures in development (Takechi and Kuratani 2010).

As in all amniote lineages, the advent of the tympanic middle ear greatly affected further evolution of the inner ear. The resulting and substantial increase in hearing sensitivity and thus the frequency bandwidth on the low- and high-frequency flanks drove, in most lineages, a slow but progressive increase in the length of the hearing

epithelium (Manley 2012). Thus until the origin of therian mammals 100 Ma later, the hearing organ in most groups was elongating into a generally curved epithelium covered in thousands of sensory hair cells. In all vertebrate groups, the response frequencies of the hair cells are systematically arranged in a so-called tonotopic ("tone-place") organization. An increase in hearing organ dimensions can be used to either increase the space devoted to a given frequency range (and thus raise, for example, the potential frequency resolution, which is the ability to clearly distinguish between neighboring frequencies, or increase parallel processing in more nerve fibers) or add new frequency ranges or both can happen. In the various lineages of therian mammals, the increase in length had different consequences (see, e.g., Heffner et al. 2001).

In mammals, the inner ear is effectively contained within a single bone of the skull, the petrosal, and this may have been the precondition that led to coiling. Coiling avoided the developmental issues involved in growing complex bony and soft tissue channels across borders between individual bones. Coiling made it possible for a longer epithelium to be accommodated without great changes in the shape and length of the periotic portion of the petrosal. Despite the potential advantages associated with increasing the size of the epithelium, the process was a very slow one; mammalian epithelia did not exceed a few millimeters in length for the first 100 Ma after the origin of the tympanic middle ear! This extremely slow increase is interesting because, in some respects, the characteristics of coiled cochleae arose before the actual coiling; the typical characteristics of the organ of Corti are much older than coiling (Manley 2012). The invasion of bone into the soft tissues of the cochlear duct, which is unique to the therian cochlea, formed a stiff support for the hearing organ. It also resulted in a bony enclosure of the cochlear ganglion and the need for openings in the bone to permit bundles of nerve fibers to reach the hearing epithelium (the habenula perforata). This important event occurred before full coiling was achieved. The bony laminae partially supporting the basilar membrane are discussed further in Sect. 2.3.2.

About 125 Ma ago, probably shortly before marsupials and placentals diverged, the coiling epithelium had reached about 4 mm in length in therian ancestors and the tip was close to the base, i.e., a 360° coil had nearly been achieved (e.g., in the fossil species *Prokennalestes*; Wible et al. 2001; Fig. 2.1). Longer lengths were thereafter only possible once the second coil began to grow above the basal area of the first coil. Once this perhaps difficult developmental step had been achieved, cochlear length increased much more quickly and greatly in some lineages.

2.3 What Is Special About the Cochlea?

There are at least three important aspects of structure and function that make the therian cochlea unique.

2.3.1 The Loss of the Lagena

It is likely that coiling that exceeded 360° was only achieved through a great modification of the cochlear apex that led to the tip becoming quite narrow and the vestibular sensory epithelium known as the lagena macula being lost during this process. Like all nonmammals, nontherian mammals (the monotremes, which have no coiled cochlea) still possess this organ. Apart from the loss of vestibular sensory input from the lagena in therian mammals, it is not clear whether this change had any additional structural consequences. However, there must have been biochemical consequences. For example, the otoconia of the vestibular maculae require a Ca^{2+} equilibrium between the endolymph and the lagenar otoconia themselves to maintain their integrity. This equilibrium requires a Ca^{2+} concentration in the cochlear–lagenar endolymph much higher than the known 20–40 μM Ca^{2+} measured in therians. In amphibians, the concentration is at least 200 μM (Martin et al. 2003), whereas in one lizard species it was measured at 1 mM (Manley et al. 2004). The loss of the lagena macula thus presumably also resulted in or made possible the loss of the necessity to maintain high Ca^{2+} levels in the endolymph. Because Ca^{2+} is a highly important ion that affects many aspects of cell function, especially in sensory cells and neurons, it might be expected that this event had substantial consequences, possibly both positive and negative. To date, however, we do not know how this change influenced the further evolution of therian hair cells, for example, by influencing selective pressures on mechanotransduction channels. Recent studies of Ca^{2+}-dependent hair cell adaptation in rats and mice are somewhat contradictory and do not yet permit conclusions to be reached (Peng et al. 2013; Corns et al. 2014).

In birds, it has been demonstrated that Ca^{2+} plays a very important role in the electrical tuning of hair cells (reviewed in Köppl et al. 2000; Manley and van Dijk 2008). Ca^{2+}-activated K^+ channels are an essential part of the mechanism enabling electrical tuning (Rosenblatt et al. 1997) and these channels possess accessory subunits that are systematically distributed along the tonotopic axis (Ramanathan et al. 1999). Electrophysiological studies have confirmed the ionic basis of tuning in both tall and short hair cells along the basilar papilla of chickens (Tan et al. 2013).

2.3.2 The Advent of Bony Laminae

Preceding the origin of the fully coiled cochlea was a change that probably had a much greater impact on further cochlear evolution than the coiling itself. The bone of the bony canal of the cochlea invaded and became integrated into ledges supporting the basilar membrane on both the neural and abneural sides (Ruf et al. 2009; Luo et al. 2010), forming the primary and secondary bony laminae. In all other amniotes, including the monotreme mammals, the soft tissues are entirely separated from the bone so that the hearing organ exists as a soft tube surrounded by, but not

firmly connected to, the bony canal. Initially, the invasion of bone had no great effect on the extension of the epithelium, and it is a big question as to the function it fulfilled. Although some paleontologists (based on the distribution of secondary bony laminae in modern species; e.g., Ruf et al. 2009; Luo et al. 2010) assume that a secondary bony lamina immediately conferred high-frequency hearing on these cochleae, this is unlikely in these ancestral forms because other changes to processing were necessary for high-frequency hearing. Instead, the invasion of bone may have been a response to the fact that the mammalian middle ear has a high stiffness. Thus, the match between the hearing epithelium and the middle ear would have been improved by stiffening the epithelial surrounds without necessarily a significant and immediate impact on the frequency responses. That the stiffness would be compatible with higher frequency responses and indeed act as a preadaptation to them is, however, obvious. The stiffness of the middle ear is made clear, for example, in the much lower sensitivity of the mammalian middle ear to pressure changes across the tympanic membrane than seen in nonmammalian middle ears (van Dijk and Manley 2013). This increased stiffness of the hearing epithelium was likely a selective advantage in early mammals that were generally very small, in which the concurrent and subsequent increases in epithelial length and changes in the molecular configuration of the prestin proteins of the outer hair cells likely resulted in an improvement toward higher frequency hearing. Because sound localization is much easier for small animals at high frequencies (Heffner et al. 2001), the selective pressures supporting higher frequency hearing likely improved the species' survival and therefore reproductive future.

In more modern species, however, such bony laminae are not a consistent feature of all therian cochleae, being much more prominent in basal areas of very high frequency cochleae such as those of some bats and of toothed whales (Vater et al. 2004). Coleman and Boyer (2012) compared primate cochleae and remarked on the absence of secondary bony laminae in the squirrel monkey *Saimiri sciureus*, although this species is known to hear well into the ultrasonic range (Beecher 1974; Fig. 2.2). Even in bats, perhaps the quintessential land-bound users of ultrasonic frequencies, bony laminae are only really prominent in those using constant frequencies in their calls. Pye (1966) wrote, "However, in *Rhinolophus ferrumequinum* [sic horseshoe bats] it persists only into the third half-turn and in *Hipposideros* [sic roundleaf bats] it is restricted to the base of the cochlea. It is absent from all the other species of bats examined." This inconsistent prominence of bony laminae in many modern mammals may suggest that cochlear laminae in early mammalian cochleae really were a phenomenon initially associated with establishing impedance matching in early peripheral systems. Nonetheless, it is a reasonable conclusion that the future processing of higher frequencies was favored by these preadaptations of the middle ear and the bony laminae in early therian mammals.

Just when really high-frequency hearing, defined as being above the human hearing range of 16 kHz at maximum, arose is uncertain. Simply because most early mammals were quite small and would have benefitted from hearing higher frequencies provides no clues. After all, most other, even modern, amniotes are also

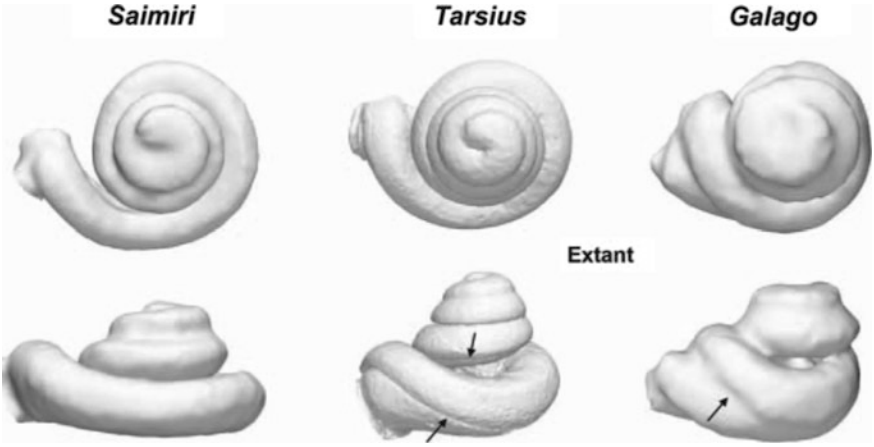

Fig. 2.2 Cochlear endocast models from computer-aided tomography for three living primates, *Saimiri* (squirrel monkey), *Tarsius* (tarsier), and *Galago* (galago). *Arrows* point to traces of the secondary bony laminae that are not visible in the squirrel monkey. As a scale, the length of the cochlea in the squirrel monkey is 26 mm. From Coleman and Boyer (2012), with permission from Wiley Periodicals, Inc.

small to very small and they do not process high frequencies. The transition to longer cochleae stiffened by laminae no doubt provided suitable conditions for the gradual and continued evolution of high-frequency hearing, a process that likely took tens of millions of years and was, as noted in Sect. 2.2, dependent on the further evolution of prestin molecular structure in outer hair cells (see Manley 2012; Sect. 2.3.3). The earliest bats (>55 Ma) had cochleae of "normal" dimensions (e.g., Habersetzer and Storch 1992) and only later fossil bats of age ~50 Ma began to show inflated cochleae typical of those of modern bats that hear very high ultrasonic frequencies. Toothed whales, that also evolved hearing at high ultrasonic frequencies, evolved much later, nearer 35 Ma ago.

2.3.3 Modifications of the Prestin Molecule

The prestin molecule has been extensively studied since its first description (Dallos and Fakler 2002). Its properties provided an explanation for the electromotility of therian outer hair cells, a property that was described almost 20 years earlier (Brownell 1983). The electromotility manifests itself as very fast changes in the configuration of prestin, which is located in densely packed complexes in the lateral cell membranes of outer hair cells (and not in this density in inner hair cells; Zheng et al. 2000). There is extensive evidence that prestin provides the power that is available as an active process in the outer hair cells and that the resulting active changes in the length of these cells are, collectively, able to drive the entire organ of

Corti at the preferred local frequency (Hallworth and Jensen-Smith 2008). This drive greatly amplifies the mechanical response to low-level sound stimuli. In addition to another, more ancestral active process in the hair cell bundles (Martin 2008), this mechanism enables mammalian cochleae to be very sensitive to sound, even at high frequencies (Hudspeth 2008).

Unsurprisingly, there has been strong selective pressure on the properties of prestin molecules, and the differences in the amino acid sequences of prestin molecules of different vertebrate groups are accompanied by differences in their physiological performance (Tan et al. 2012). Remarkably, in bats and toothed whales, which perceive frequencies sometimes exceeding 100 kHz, the same molecular changes in prestin have occurred independently (Li et al. 2012; Liu et al. 2012) during different evolutionary eras and are thus very likely to be precisely those specializations that improve responses to such frequencies.

2.4 Did Coiling Have Any Effect on Function?

Arguably, the points discussed in Sect. 2.3.3 had a far greater influence on therian hearing than did coiling per se. In the past, the greater length of the therian basilar papilla was assumed to permit responses to high frequencies. This, however, is at best a rough correlation that tells little about causality and most attempts to find patterns in cochlear dimensions and cochlear responses have not permitted profound conclusions to be made (West 1985; Nadol 1988; Echteler et al. 1994) except to the extent that the longer cochleae are associated with improved low-frequency hearing (Wannaprasert and Jeffery 2015). High frequencies are perceived quite well by rodents that often, like the mouse, have an organ of Corti that is shorter than the hearing organ of some birds. Yet the mouse (*Mus musculus*; ~7-mm organ) hears up to perhaps 80 kHz (Heffner et al. 2001), whereas the barn owl (*Tyto alba*; ~11-mm organ) hears only to 12 kHz (Köppl 1997). The hearing organ of an elephant is many times longer than that of the mouse, yet its upper frequency limit (~10.5 kHz; Heffner and Heffner 1980) is below that of humans and even barn owls. In many mammals that hear very high frequencies, such as small rodents and bats, on the other hand, the lower frequency limit is really high compared with that of most mammals. Thus the constraints of space have acted differently in different lineages: Adding higher frequencies without a concomitant increase in the length of the cochlea requires either smaller space constants (standard stretches of epithelium for each octave) and thus the loss of afferent innervation that provides neural parallel processing capacity, or the loss of some lower octaves. In many longer hearing organs, such as in humans, the space devoted to a single octave is large (e.g., >2.5 mm). In the mouse, it is <1 mm (Ekdale 2013).

There is thus no simple correlation between cochlear length and frequency limits (West 1985; Wannaprasert and Jeffery 2015). This information can be summarized by saying that the dimensions of the cochlea in therian mammals are group and species specific and that the lower and upper frequency limits and the space per

octave are interrelated and quite difficult to predict simply by looking at a cochlea. The space constant need not even be uniform within one cochlea. In some so-called constant-frequency bats, for example, that have an auditory "fovea," the space constant for a very tiny segment of the frequency range exceeds the total cochlear length by far (i.e., >50 mm per octave in rhinolophid bats). The fossil history of therian cochleae does not suggest that coiling per se was responsible for improved high-frequency hearing. However, longer epithelia that became possible through coiling were clearly correlated with the origin of high-frequency hearing. Within the primates, Braga et al. (2015) described a disproportionate growth of the cochlear length in the human lineage that "….show cochlear relative lengths and oval window areas larger than expected for their body mass, two features corresponding to increased low-frequency sensitivity more recent than 2 million years ago." This may be an indication that the intensified and differentiated use of sound communication in human ancestors correlated with this cochlear evolution.

Although it is clear that cochlear coiling is a highly efficient method of encapsulating an otherwise awkwardly long organ (in humans, its tip would otherwise penetrate $\sim$3 cm into the brain on each side and in some other mammals, straight cochleae, if possible, would overlap in the middle of the brain), until recently no further hypotheses were forwarded in which coiling was associated with "improvement." Indeed, a model by Steele and Zais (1985) had suggested that coiling did not influence mechanical processing in the cochlea. Recently, however, a hypothesis has been described that suggests that coiling is associated with improved low-frequency hearing (Cai et al. 2005; Manoussaki et al. 2008). In that model, calculations predicted how sound waves travel in a coiled cochlear tube and suggested that especially in the apical, low-frequency region, sound energy manifest in the slow traveling wave along the epithelium becomes concentrated along the outer wall of the cochlea. The authors demonstrate that the shape of the cochlea in species perceiving really low frequencies (such as baleen whales) differs characteristically from that of high-frequency cochleae. If these considerations turn out to be true, this would be a kind of preadaptation of coiling, since historically, coiling began at cochlear lengths of 4 mm and was most likely simply the result of spatial constraints. Thus while such an improvement in low-frequency hearing is unlikely to have favored the origin of cochlear coiling, it can be regarded as a fortuitous consequence or even a side effect of that coiling, just like high-frequency hearing itself. Thus in contrast to a commentary in *Nature* on this hypothesis (Ball 2006), the supposed improvement of low-frequency hearing made possible by coiling certainly does not explain *why* the cochlea is coiled but does suggest what one much later result of that coiling might be.

Huang et al. (2012) suggested on theoretical grounds that a coiled cochlea would perform better than a straight cochlea for sound localization in the vertical axis but only for bone-conducted sound. How such a mechanism might perform and what its relevance might be for real-life conditions has not yet been examined.

2.5 The Cochlea (Also) Determines the Hearing Range

For many years, it was assumed that because all airborne sound components enter the inner ear through the middle ear, the middle ear itself must be the prime determinant of which frequencies pass through and of the efficiency with which they do so (reviewed in Ruggero and Temchin 2002). In other words, the frequency limits of hearing are at least mainly due to the characteristics of the middle ear. However, measurements of middle ear responses in the guinea pig (Manley and Johnstone 1974) showed that over most of its frequency range, the velocity of the middle ear system followed the velocity of air particles (equal sound pressure means equal air particle velocity across frequency) but with a small frictional loss. Above 30–35 kHz, however, the system changed its behavior dramatically, with a sharp break to a steep slope in which the velocity fell rapidly to unmeasurably low levels. The most obvious explanation for this change was that as frequencies rose above 35 kHz, the highest frequency along the map of the organ of Corti had been exceeded (Robertson and Manley 1974). The organ of Corti had no further sensory areas that responded to these higher frequencies and thus ceased to respond to sound (i.e., the basilar membrane moved less and less). This resulted in a sudden increase in the input impedance of the inner ear that was directly reflected in a fall in the ability of the middle ear to "drive" the system, like putting the brakes on a car if it exceeds a certain speed. Similar data were measured from the middle ear of a species of bat (*Eptesicus pumilus*; Manley 1972) that had a much higher behavioral frequency limit. The pattern shown by the middle ear velocity as a function of frequency was very similar to that of the guinea pig, except that the "system collapse" occurred at frequencies above 70 kHz, not unexpected in an echolocating species. Thus it is apparent that it is not the fluid impedance that shapes the transfer function of the middle ear but the hearing organ itself.

Slightly different experiments with lizard middle ears also suggested that the middle ear response was not autonomous but depended on inner ear impedance. Destroying the inner ear epithelium (including making a hole in the "round window") changed the middle ear response at the highest frequencies (here above 4 kHz, about the normal limit of hearing in those species).

These concepts were later more formalized by Ruggero and Temchin (2002, p. 13206) who discuss data from six species. They concluded: "… show that the middle ear by itself is not responsible for limiting high-frequency hearing …. we propose that the tonotopic organization of the cochlea plays a crucial role in setting the frequency limits of cochlear sensitivity and hence in determining the bandwidth of hearing."

2.6 Variation in Cochlear Form and Dimensions

The therian mammalian cochlea varies in length from ~7 mm (mouse) to >70 mm (blue whale; Vater et al. 2004). The length of human cochleae varies (see Würfel et al. 2014 for a review) between the sexes (being 3.4% longer in males, Miller 2007; or 2% longer in males, Würfel et al. 2014) but not systematically between the left and right sides of the head (Würfel et al. 2014). Between all individual human ears, different authors give different values for the length variations (up to 18%, Erixon et al. 2009; or up to 36%, Würfel et al. 2014). The number of hair cells (14,600–20,400) and of nerve fibers of the auditory nerve (22,800–40,000; reviewed in Miller 1985) also show variations between the ears of humans. If the frequency range processed by all human cochleae remains the same, the space constants must likewise vary in proportion. With regard to the variations in cochlear length and form, there are instructive recent reviews, especially of cetacean (Ketten 2000) and primate (Coleman and Colbert 2010; Wannaprasert and Jeffery 2015) inner ears.

On average, the length of the basilar papilla does not strongly correlate with frequency range or frequency selectivity except in the few cases where long stretches of epithelium are devoted to extremely small ranges of frequency (as, for example, in the cochleae of *Rhinolophus* bats, where a so-called "fovea" exists, in analogy to optic foveae, in this case in the narrow frequency range of the Doppler-shifted call echoes). Larger cochleae with longer basilar membranes are associated with lower frequency hearing (Coleman and Colbert 2010; Wannaprasert and Jeffery 2015), but there is no such correlation for high-frequency hearing, presumably because high-frequency octaves occupy, in terms of space per hertz, much less space. If cochleae are short or long, they can cover the same frequency range by using different standard stretches of epithelium for each octave. However, this does, of course, mean that if the space constant is small, fewer hair cells and auditory nerve fibers are available for each octave. As noted above, in humans the space constant is about 2.5 mm per octave, whereas in mice it is nearer 1 mm per octave. In addition, having an acoustic fovea may be associated with dramatic increases in frequency selectivity (Kössl and Vater 1995; Vater et al. 2004) but does not guarantee this. In a bird, the barn owl, a nocturnal hunter, fully half the length of the hearing organ is devoted to one octave, but the frequency selectivity there is not exceptional (Köppl et al. 1993). Thus such a fovea is likely to be used, for example, to provide a great increase in the parallel input of many more nerve fibers. Those fibers may then make it possible to process other information such as the timing of signals better. Barn owls have a highly exceptional phase locking in their auditory nerve fibers (Köppl 1997) correlated with the processing of one clue for sound localization. However, sharp-tuning and high-timing resolution are mutually exclusive (at least if using the same data channels). Thus in any given species over evolutionary time, the hearing range, frequency resolution, and time processing will all have exerted selection pressures to produce a species cochlea that has a unique configuration.

2.7 Cochleae and Other Hearing Organs

Despite all the specializations discussed in Sect. 2.6 and in contrast to statements found in many publications, when compared with the hearing organs of other amniotes and in the frequency ranges where they overlap and can be compared, the ordinary therian mammalian cochlea is commonly not more sensitive and not more frequency selective than the auditory epithelia of birds or even some lizards (Manley and Köppl 1998; Manley 2000). Especially at really low frequencies (infrasound), the sensitivity of some birds is unsurpassed (e.g., Hill et al. 2014). Increases in sensitivity are, however, sometimes seen at the behavioral level in mammals and birds. It is apparent that the pinnae and inflated bullae of mammals and the facial masks of some birds (as in owls) can add 20 dB to the behavioral sensitivity. Thus it must concluded that in the past, the meaning of the cochlear structure in therian mammals, especially of the organ of Corti that favors such sensitivity and selectivity, has been overinterpreted as some kind of pinnacle of evolution. During the long evolutionary time periods, other amniotes have evolved other equally effective middle and inner ear structures and processes that also led to superbly sensitive and selective hearing organs.

2.8 Summary

The snail shell-shaped hearing organ of therian mammals is a unique development among vertebrate animals, and even egg-laying mammals (monotremes) do not have this specialization. Although there have been several ideas concerning ways in which the peculiar shape of the modern cochlea might positively affect certain aspects of its function, as yet no convincing hypothesis has been forwarded to explain its origin, except that it packs a long structure into a small space. Its origin was accompanied by the loss of the vestibular lagenar macula accompanied by a large drop in the Ca^{2+} content of the endolymph, an event the consequences of which still need to be thoroughly examined. The specific shape and size of the cochlea in each species is governed by many factors, such as the adult animal's size, but also its lifestyle, including sound localization, communication, and echolocation signaling. Before the spiral cochlea evolved, bone had invaded the soft tissues of the organ of Corti and the new laminae presumably enabled a better mechanical match to the mammalian middle ear, eventually providing the substrate for very high frequency hearing. The protein prestin evolved in parallel, developing high-frequency amplifying capabilities that were independently developed even further in bats and toothed whales.

Compliance with Ethics Requirements Geoffrey A. Manley declares that he has no conflict of interest.

References

Ball, P. (2006). Ear's spiral responds to bass. *Nature*. doi:10.1038/news060313-2.

Beecher, M. (1974). Pure tone thresholds of the squirrel monkey (*Saimiri sciureus*). *The Journal of the Acoustical Society of America*, 55, 196–198.

Braga, J., Loubes, J.-M., Descouens, D., Dumoncel, J., Thackeray, J. F., Kahn, J.-L., de Beer, F., Riberon, A., Hoffman, K., Balaresque, P., & Gilissen, E. (2015). Disproportionate cochlear length in genus *Homo* shows a high phylogenetic signal during apes' hearing evolution. *PLoS ONE,* 10(6), e0127780. doi:10.1371/journal.pone.0127780.

Brownell, W. E. (1983). Observations on a motile response in isolated outer hair cells. In D. B. Webster & L. M. Aitkin (Eds.), *Neural Mechanisms of Hearing* (pp. 5–10). Clayton, VIC, Australia: Monash University Publishing.

Cai, H., Manoussaki, D., & Chadwick, R. S. (2005). Effects of coiling on the micromechanics of the mammalian cochlea. *Journal of the Royal Society Interface*, 2, 341–348.

Carroll, R. L. (1987). *Vertebrate Paleontology and Evolution*. New York: Freeman.

Clack, J. A. (2002). Patterns and processes in the early evolution of the tetrapod ear. *Journal of Neurobiology*, 53, 251–264.

Coleman, M. N., & Colbert, M. W. (2010). Correlations between auditory structures and hearing sensitivity in non-human primates. *Journal of Morphology*, 271, 511–532.

Coleman, M. N., & Boyer, D. M. (2012). Inner ear evolution in primates through the Cenozoic: Implications for the evolution of hearing. *The Anatomical Record*, 295, 615–631.

Corns, L. F., Johnson, S. L., Kros, C. J., & Marcottia, W. (2014). Calcium entry into stereocilia drives adaptation of the mechanoelectrical transducer current of mammalian cochlear hair cells. *Proceedings of the National Academy of Sciences of the United States of America*, 111, 14918–14923.

Dallos, P., & Fakler, B. (2002). Prestin, a new type of motor protein. *Nature Reviews in Molecular Cell Biology*, 3, 104–111.

Echteler, S. M., Fay, R. R., & Popper, A. N. (1994). Structure of the mammalian cochlea. In R. R. Fay & A. N. Popper (Eds.), *Comparative Hearing: Mammals* (pp. 134–172). New York: Springer-Verlag.

Ekdale, E. G. (2013). Comparative anatomy of the bony labyrinth (inner ear) of placental mammals. *PLoS ONE,* 8(6), e66624. doi:10.1371/journal.pone.0066624.

Erixon, E., Högstorp, H., Wadin, K., & Rask-Andersen, H. (2009). Variational anatomy of the human cochlea: Implications for cochlear implantation. *Otology & Neurotology*, 30, 14–22.

Gitter, A. H. (1990). Eine kurze Geschichte der Hörforschung II. Renaissance. *Laryngo-Rhino-Otology*, 69, 495–500.

Habersetzer, J., & Storch, G. (1992). Cochlea size in extant chiroptera and middle eocene microchiropterans from Messel. *Naturwissenschaften*, 79, 462–466.

Hallworth, R., & Jensen-Smith, H. C. (2008). The morphological specializations and electromotility of the mammalian outer hair cell. In G. A. Manley, R. R. Fay, & A. N. Popper (Eds.), *Active Processes and Otoacoustic Emissions in Hearing* (pp. 145–190). New York: Springer-Verlag.

Heffner R., & Heffner H. (1980). Hearing in the elephant (*Elephas maximus*). *Science*, 218, 518–520.

Heffner R. S., Koay G., & Heffner, H. E. (2001). Audiograms of five species of rodents: Implications for the evolution of hearing and the perception of pitch. *Hearing Research*, 157, 138–152.

Hill, E. M., Koay, G., Heffner, R. S., & Heffner, H. E. (2014). Audiogram of the chicken (*Gallus gallus domesticus*) from 2 Hz to 9 kHz. *Journal of Comparative Physiology A*, 200, 863–870.

Huang, X., Xu, C., & Bai, L. (2012). Is the cochlea coiled to provide sound localization? *Europhysics Letters*, 98, 58002.

Hudspeth, A. J. (2008). Making an effort to listen: Mechanical amplification in the ear. *Neuron*, 59, 530–545.

Ketten, D. R. (2000). Cetacean ears. In W. W. L. Au, R. R. Fay, & A. N. Popper (Eds.), *Hearing by Whales and Dolphins* (pp. 43–108). New York: Springer-Verlag.

Köppl, C. (1997), Phase locking to high frequencies in the auditory nerve and cochlear nucleus magnocellularis of the barn owl, *Tyto alba*. *The Journal of Neuroscience*, 17, 3312–3321.

Köppl, C., Gleich, O., & Manley, G. A. (1993). An auditory fovea in the barn owl cochlea. *Journal of Comparative Physiology A*, 171, 695–704.

Köppl, C., Manley, G. A., & Konishi, M. (2000). Auditory processing in birds. *Current Opinion in Neurobiology*, 10, 474–481.

Kössl, M., & Vater, M. (1995). Cochlear structure and function in bats. In A. N. Popper & R. R. Fay (Eds.), *Hearing by Bats* (pp. 191–235). New York: Springer-Verlag.

Ladhams, A., & Pickles, J. O. (1996). Morphology of the monotreme organ of Corti and macula lagena. *The Journal of Comparative Neurology*, 336, 335–347.

Li, Y., Liu, Z., Shi, P., & Zhang, J. (2012). The hearing gene *Prestin* unites echolocating bats and whales. *Current Biology*, 20, R55–R56.

Liu, Y., Cotton, J. A., Shen, B., Han, X., Rossiter, S. J., & Zhang, S. (2012). Convergent sequence evolution between echolocating bats and dolphins. *Current Biology*, 20, R53–R54.

Luo, Z.-X., & Ketten, D. R. (1991). CT scanning and computerized reconstructions of the inner ear of multituberculate mammals. *Journal of Vertebrate Paleontology*, 11, 220–228.

Luo, Z.-X., Ruf, I., Schulz, J. A., & Martin, T. (2010). Fossil evidence on evolution of inner ear cochlea in Jurassic mammals. *Proceedings of the Royal Society B: Biological Sciences*, 278, 28–34.

Manley, G. A. (1972). Frequency response of the middle ear of geckos. *Journal of Comparative Physiology*, 81, 251–258.

Manley, G. A. (2000). Cochlear mechanisms from a phylogenetic viewpoint. *Proceedings of the National Academy of Sciences of the United States of America*, 97, 11736–11743.

Manley, G. A. (2010). An evolutionary perspective on middle ears. *Hearing Research*, 263, 3–8.

Manley, G. A. (2012). Evolutionary paths to mammalian cochleae. *Journal of the Association for Research in Otolaryngology*, 13, 733–743.

Manley, G. A., & Johnstone, B. M. (1974). Middle-ear function in the guinea pig. *The Journal of the Acoustical Society of America,* 56, 571–576.

Manley, G. A., & Köppl, C. (1998). Phylogenetic development of the cochlea and its innervation. *Current Opinion in Neurobiology*, 8, 468–474.

Manley, G. A., & van Dijk, P. (2008). Otoacoustic emissions in amphibians, lepidosaurs, and archosaurs. In: G. A. Manley, R. R. Fay, & A. N. Popper (Eds.), *Active Processes and Otoacoustic Emissions in Hearing* (pp. 211–260). New York: Springer-Verlag.

Manley, G. A., Sienknecht, U., & Köppl, C. (2004). Calcium modulates the frequency and amplitude of spontaneous otoacoustic emissions in the bobtail skink. *Journal of Neurophysiology*, 92, 2685–2693.

Manoussaki, D., Chadwick, R. S., Ketten, D. R., Arruda, J., Dimitriadis, E. K., & O'Malley, J. T. (2008). The influence of cochlear shape on low-frequency hearing. *Proceedings of the National Academy of Sciences of the United States of America*, 105, 6162–6166.

Martin, P. (2008). Active hair-bundle motility of the hair cells of vestibular and auditory organs. In G. A. Manley, R. R. Fay, & A. N. Popper (Eds.), *Active Processes and Otoacoustic Emissions in Hearing* (pp. 93–144). New York: Springer-Verlag.

Martin, P., Bozovic, D., Choe, Y., & Hudspeth, A. J. (2003). Spontaneous oscillation by hair bundles of the bullfrog's sacculus. *The Journal of Neuroscience*, 23, 4533–4548.

Miller, J. D. (2007). Sex differences in the length of the organ of Corti in humans. *The Journal of the Acoustical Society of America*, 121, EL151–EL155.

Miller, M. R. (1985). Quantitative studies of auditory hair cells and nerves in lizards. *The Journal of Comparative Neurology*, 232, 1–24.

Nadol, J. B. (1988). Comparative anatomy of the cochlea and the auditory nerve in 14 mammals. *Hearing Research*, 34, 253–266.

Peng, A. W., Effertz, T., & Ricci, A. J. (2013). Adaptation of mammalian auditory hair cell mechanotransduction is independent of calcium entry. *Neuron*, 80, 960–972.

Pye, A. (1966). The structure of the cochlea in chiroptera. I. Microchiroptera: Emballonuroidea and Rhinolophoidea. *Journal of Morphology*, 118, 495–510.

Ramanathan, K., Michael, T. H., Jiang, G.-J., Heil, H., & Fuchs P. A. (1999). A molecular mechanism for electrical tuning of cochlear hair cells. *Science*, 283, 215–217.

Robertson, D., & Manley, G. A. (1974). Manipulation of frequency analysis in the cochlear ganglion of the guinea pig. *Journal of Comparative Physiology*, 91, 363–375.

Rosenblatt, K. P., Sun, Z.-P., Heller, S., & Hudspeth, A. J. (1997). Distribution of Ca^{2+}-activated K^+ channel isoforms along the tonotopic gradient of the chicken's cochlea. *Neuron*, 19, 1061–1075.

Ruf, I., Luo, Z.-X., Wible, J. R., & Martin, T. (2009). Petrosal anatomy and inner ear structures of the late Jurassic *Henkelotherium* (Mammalia, Cladotheria, Dryolestoidea): Insight into the early evolution of the ear region in cladotherian mammals. *Journal of Anatomy*, 214, 679–693.

Ruggero, M. A., & Temchin, A. N. (2002). The roles of the external, middle, and inner ears in determining the bandwidth of hearing. *Proceedings of the National Academy of Sciences of the United States of America*, 99, 13206–13210.

Steele, C. R., & Zais, J. G. (1985). Effect of coiling in a cochlear model. *The Journal of the Acoustical Society of America*, 77, 1849–1852.

Takechi, M., & Kuratani, S. (2010). History of studies on mammalian middle ear evolution: A comparative morphological and developmental biology perspective. *Journal of Experimental Zoology (Molecular and Developmental Evolution)*, 314B, 417–433.

Tan, X., Pecka, J. L., Tang, J., Lovas, S., Beisel, K. W., & He, D. Z. Z. (2012). A motif of eleven amino acids is a structural adaptation that facilitates motor capability of eutherian prestin. *Journal of Cell Science*, 125, 1039–1047.

Tan, X., Beurg, M., Hackney, C., Mahendrasingam, S., & Fettiplace, R. (2013). Electrical tuning and transduction in short hair cells of the chicken auditory papilla. *Journal of Neurophysiology*, 109, 2007–2020.

van Dijk, P., & Manley, G. A. (2013). The effects of air pressure on spontaneous otoacoustic emissions of lizards. *Journal of the Association for Research in Otolaryngology*, 14, 309–319.

Vater, M., Meng, J., & Fox, R. C. (2004). Hearing organ evolution and specialization: Early and later mammals. In G. A. Manley, A. N. Popper, & R. R. Fay (Eds.), *Evolution of the Vertebrate Auditory System* (pp. 256–288). New York, Springer-Verlag.

Wannaprasert, T., & Jeffery, N. (2015). Variations of mammalian cochlear shape in relation to hearing frequency and skull size. *Tropical Natural History*, 15, 41–54.

West, C. D. (1985). The relationships of the spiral turns of the cochlea and the length of the basilar membrane to the range of audible frequencies in ground dwelling mammals. *The Journal of the Acoustical Society of America*, 77, 1091–1101.

Wible, J. R., Rougier, G. W., Novacek, M. J., & McKenna, M. C. (2001). Earliest eutherian ear region: A petrosal referred to *Prokennalestes* from the early Cretaceous of Mongolia. *American Museum Novitates*, 3322, 1–44.

Würfel, W., Lanfermann, H., Lenarz, T., & Majdani, O. (2014). Cochlear length determination using cone beam computed tomography in a clinical setting. *Hearing Research*, 316, 65–72.

Zheng, J., Shen, W., He, D. Z., Long, K. B., Madison, L. D., & Dallos, P. (2000). Prestin is the motor protein of cochlear outer hair cells. *Nature*, 405, 149–155.

Chapter 3
New Directions in Cochlear Development

Andrew K. Groves and Donna M. Fekete

Abstract The mammalian cochlea is a highly specialized structure in the inner ear whose sensory organ, the organ of Corti, allows for exquisitely precise discrimination of sound frequencies over a huge range of sound amplitudes. The cochlea grows out as a ventral elaboration of the otocyst and is patterned by a variety of extracellular signals that originate both within the cochlear duct itself and from tissues adjacent to the cochlea. In this chapter, we describe the embryonic origins of the cochlear duct and spiral ganglion, the signals that induce the organ of Corti, the precise arrangement of the auditory hair cells and supporting cells, and recent work on how the hair cells become innervated by afferent and efferent neurons before the onset of hearing.

Keywords Bone morphogenetic protein · Cell cycle · Fibroblast growth factor · Hair cell · Inner ear · Morphogen · Otic placode · Patterning · Planar cell polarity · Retinoic acid · Sonic hedgehog · Sensory · Supporting cell · Tonotopy · Wnt

3.1 Introduction

The mammalian cochlea is specialized to detect sound of varying intensities, deconstructing it into its component frequencies and sending this information to the brain through the afferent axons of the spiral ganglion neurons. The brain also feeds

A.K. Groves (✉)
Departments of Neuroscience and Molecular and Human Genetics
and Program in Developmental Biology, BCM295, Baylor College of Medicine,
1 Baylor Plaza, Houston, TX 77030, USA
e-mail: akgroves@bcm.edu

D.M. Fekete
Center for Integrative Neuroscience, Department of Biological Sciences,
and Purdue University Center for Cancer Research, Purdue University,
915 W. State Street, West Lafayette, IN 47907, USA
e-mail: dfekete@purdue.edu

G.A. Manley et al. (eds.), *Understanding the Cochlea*, Springer Handbook of Auditory Research 62, DOI 10.1007/978-3-319-52073-5_3

back to the cochlea via two distinct efferent pathways. Due, in part, to the power of mouse genetics, remarkable progress has been made in the past 10–15 years to reveal molecular-genetic mechanisms of inner ear development in general and cochlear development in particular (see Kelley et al. 2005 for many aspects of inner ear development). This review describes a subset of these new discoveries related to the embryonic origin of the cochlea, the induction of its prosensory domain, the coordination of spatiotemporal gradients in cell cycle exit and differentiation, the fine-grained patterning of cell types in the organ of Corti, and the establishment of cochlear innervation. Some of the unresolved questions remaining in these areas are highlighted to encourage future studies.

3.2 Embryonic Origin of the Mammalian Cochlea

3.2.1 Defining the Cardinal Axes of the Inner Ear

The otic placode forms adjacent to the posterior hindbrain as the body plan of the embryo is being laid down after gastrulation and subsequently invaginates to form the otocyst. It is now well established that inducing signals that specify the anteroposterior (A-P) and dorsoventral (D-V) pattern of the embryonic nervous system as a whole are co-opted by the otocyst to define the cardinal axes of the future inner ear. Early in the development of the nervous system, the hindbrain undergoes a precise division into developmental compartments or rhombomeres (Trainor and Krumlauf 2000). Because the otocyst develops adjacent to rhombomeres 5 and 6 of the hindbrain, many developmental biologists hypothesized that these were the source of signals that defined the A-P axis of the ear. However, surgical manipulation of the posterior hindbrain in chicken embryos did not significantly affect otocyst patterning (Bok et al. 2005). Rather, the embryonic ectoderm surrounding the otocyst appeared to specify the A-P axis of the ear, and this activity could be mimicked by retinoic acid (RA; Bok et al. 2011). RA-synthesizing enzymes such as Raldh2 are expressed in the mesoderm posterior to the developing otocyst, whereas RA-degrading enzymes such as Cyp26C1 are expressed in the ectoderm anterior to the otocyst (Bok et al. 2011), thus providing a source and sink of RA to establish a gradient of RA responses across the otocyst. Treatment of either chick or mouse embryos with RA resulted in an expansion of posterior markers of the otocyst, such as *Tbx1*, whereas supplying an ectopic anterior source of RA resulted in an otocyst consisting of two mirror image posterior halves (Bok et al. 2011; Fig. 3.1).

Although the hindbrain does not appear to directly regulate the A-P axis of the otocyst, 180° rotation of the hindbrain on its D-V axis causes severe otocyst patterning defects (Bok et al. 2005). Sonic hedgehog (Shh) is a likely candidate for a signal that specifies ventral fate given its expression in the floor plate of the hindbrain and notochord and its demonstrated role in specification of ventral identity in the neural tube (Cohen et al. 2013). The role of Shh in specifying the

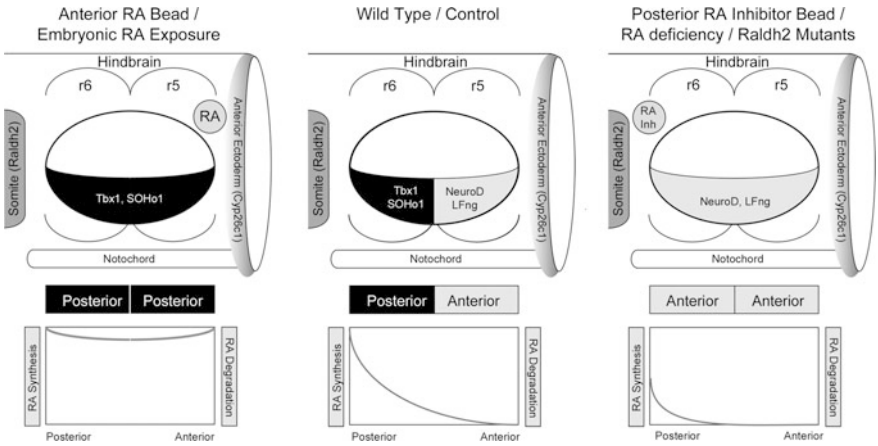

Fig. 3.1 Anteroposterior patterning of the otocyst. The mammalian otocyst is patterned in its anteroposterior axis by a gradient of retinoic acid (RA). The gradient is generated by a region of mesenchyme posterior to the otocyst (r6) that expresses the RA-synthesizing enzyme Raldh2 and a region of ectoderm anterior to the otocyst (r5) that expresses the RA-degrading enzyme Cyp26c1. As a result, the RA concentration is high in the posterior region of the otocyst and lower in the anterior region. This leads to the establishment of distinct gene expression domains (*Tbx1* and *SOHo-1* in the posterior half and *NeuroD* and *LFng* in the anterior half). Perturbations of the RA gradient by gain- or loss-of-function approaches lead to a disruption of the anteroposterior character of the otocyst

D-V pattern in the otocyst is supported by gain- and loss-of-function studies in mouse and chicken embryos (Riccomagno et al. 2002; reviewed in Wu and Kelley 2012).

Does Shh act directly on the otocyst or indirectly through its patterning of neural tissues? Studies on the transcriptional effectors of Shh signaling suggest that both mechanisms function to impart D-V identity to the ear. The Gli family of zinc finger transcription factors that mediate Shh signaling are expressed in the otocyst, with the transcriptional activators Gli1 and Gli2 being restricted to its most ventral regions (Bok et al. 2007). Gli3 can act as both a transcriptional activator and a repressor; in the absence of Shh signaling, it is partially degraded to release an N-terminal domain (Gli3 repressor [Gli3R]) that represses Shh targets, whereas in the presence of Shh, Gli3 remains intact (Gli3 activator [Gli3A]) and activates Shh targets (Wang et al. 2000). Thus, graded increases in Shh signaling gradually reduce Gli3R and progressively increase Gli3A, with the amount of Shh signal received by a given cell being the net output of Gli3R and Gli3A activities. In the ear, the apical region of the cochlear duct fails to form in *Gli2*$^{-/-}$*; Gli3*$^{-/-}$ mutants or the *Gli3D699* mutant, which only generates the Gli3R form (Bok et al. 2007). This suggests that the apical (ventral) regions of the cochlear duct, which are closest to Shh sources (floor plate and notochord), require Gli3A function.

Shh levels also affect the development of more dorsal components of the ear. Analysis of the same *Gli* mutants suggests that basal regions of the cochlear duct

and the saccule may be induced by progressively lower exposure to Shh, leading to a balance of Gli3A and Gli3R activities. Indeed, the basal regions of the cochlear duct and saccule are missing in *Shh* mutants (which cannot activate *Gli* genes and therefore have more Gli3R activity) but persist in $Shh^{-/-}$; $Gli3^{-/-}$ mice (which lack both Gli3A *and* Gli3R functions; Bok et al. 2007). More dorsally, $Gli3^{-/-}$ mice (in which Gli3A function is compensated by Gli2 and Gli1 but which lack any Gli3R activity) have malformed semicircular canals, which suggested that Gli3R activity is necessary to allow these structures to form properly (Bok et al. 2007). However, a more recent study that conditionally inactivated the Shh receptor Smoothened (Smo) in the otocyst found that the cochlea and saccule were completely absent but that dorsal components of the inner ear (the semicircular canals, endolymphatic duct, cristae, and utricle) appeared to develop quite normally (Brown and Epstein 2011). Reconciling these conflicting studies suggests that Shh acts on the ventral otocyst directly but that the dorsal otocyst is indirectly dependent on Shh through its patterning effects on tissues adjacent to the otocyst, such as the neural tube (Groves and Fekete 2012; Wu and Kelley 2012; Fig. 3.2).

Members of the Wnt family are good candidates to regulate dorsal fates in the otocyst. Within the neural tube, the action of Shh ventrally is opposed by Wnt signals in the dorsal neural tube and ectoderm. In the case of the otocyst, Wnts may play a similar role to specify dorsal identity, although initially they probably act in a paracrine fashion that is then enhanced or replaced by autocrine signaling. *Wnt6* is expressed at the neural plate border immediately adjacent to the otic placode (Jayasena et al. 2008). Both *Wnt1* and *Wnt3a* are later expressed in the dorsal neural tube (Riccomagno et al. 2005) adjacent to the otocyst. *Wnt2b* is expressed in the dorsomedial otocyst (Riccomagno et al. 2005), with another 14 Wnt ligands expressed in the otocyst by embryonic day 11.5 (E11.5; Summerhurst et al. 2008). As the placode invaginates and closes to form the otocyst, Wnt-reporter mice exhibit a D-V gradient of reporter activity, indicated by Lef/TCF-mediated transcriptional activation of transgenes (Riccomagno et al. 2005; Ohyama et al. 2006). Moreover, *Wnt1; Wnt3a* double mutants completely lack dorsal inner ear structures, with the remaining cochlea persisting as a rudimentary cyst (Riccomagno et al. 2005). Conversely, activation of Wnt signaling in cultured otocysts causes many dorsal markers to expand into ventral regions, and these same markers are reduced by ablation of the dorsal neural tube in chicken embryos (Riccomagno et al. 2005).

3.2.2 *Transforming the Ventral Otocyst into the Cochlear Duct*

The cochlear duct forms as an elaboration of the ventral otocyst by E11 in the mouse, with a clear protrusion that marks the beginning of the cochlear duct (Wu and Kelley 2012; Brown et al. 2015). The cochlear duct then elongates and coils until it reaches its full one and three-quarter turns in mice, although there is considerable variation in cochlear length and width between mammals (Ekdale 2015).

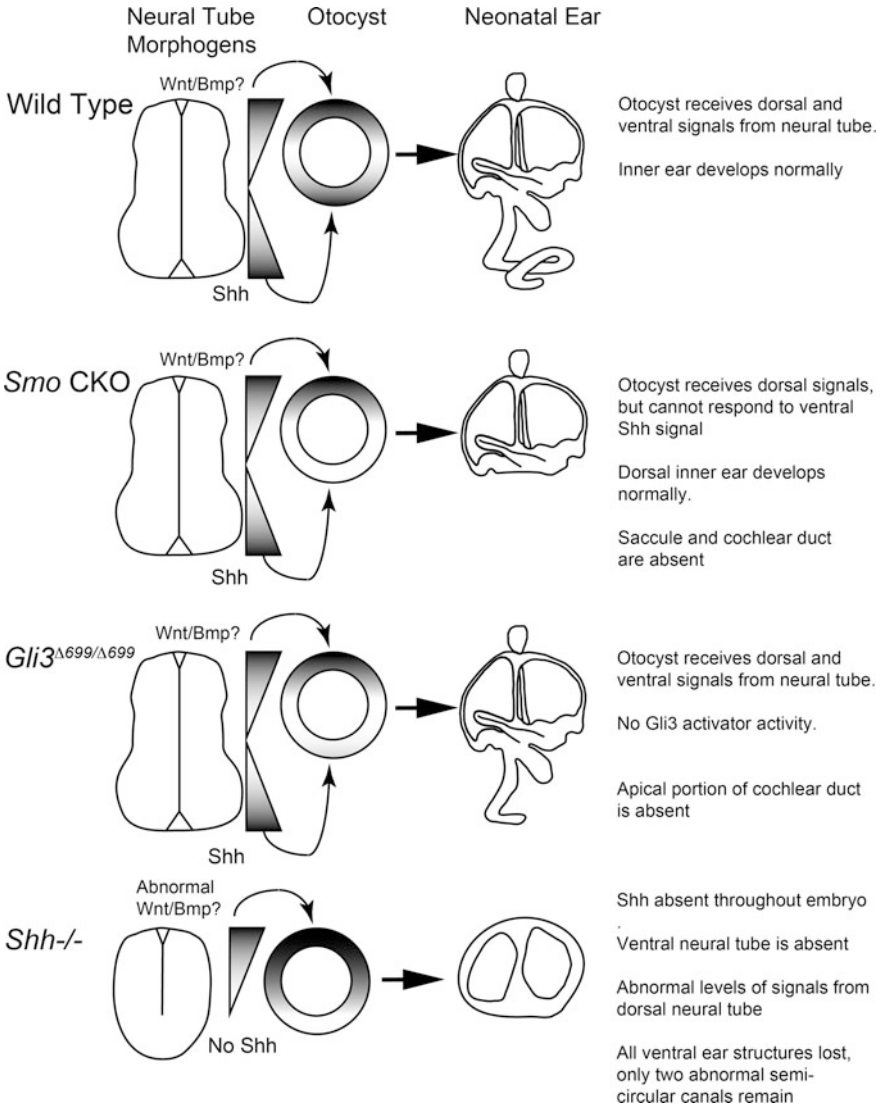

Fig. 3.2 Dorsoventral patterning of the otocyst. Dual morphogen gradients of Sonic hedgehog (Shh) released from the floor plate and Wnts and possibly bone morphogenetic proteins (BMPs) released from the roof plate pattern the dorsoventral axis of the otocyst. If the Shh receptor Smoothened (Smo) is deleted in the otocyst, the dorsal half of the otocyst develops normally in response to Wnt and BMP signals, but the saccule and cochlear duct are absent. In mice carrying a point mutation of *Gli3,* which removes its activator activity, only the most apical part of the cochlear duct is absent. However, in the absence of all Shh activity, the neural tube develops abnormally, and this removes ventral structures and causes dorsal structures to develop abnormally

Fate mapping using a *Neurog1-CreER* transgenic mouse to track *Neurog1*-expressing progenitors that arise in the anteroventral otocyst at E9 shows a significant contribution to the utricle, saccule, and VIIIth ganglion (Koundakjian et al. 2007; Raft et al. 2007). However, only a few descendants of these *Neurog1*-expressing cells are found in the cochlear duct and almost none in the organ of Corti itself (Koundakjian et al. 2007; Raft et al. 2007). Fate mapping using either a CreER line driven by Wnt-responsive Lef/TCF binding sites (*TOP-CreER*) or a *Gbx2-CreER* line shows that some Wnt-responsive progenitors located in the medial wall of the otocyst between E9.5 and E11.5 will contribute to the sensory epithelium of the cochlear duct by spreading ventrally (Riccomagno et al. 2005; Brown et al. 2015).

The elongating cochlear duct can be thought of as a tube divided into at least five sectors in cross section (Fig. 3.3). Rotating clockwise from the anterior region, these sectors are the roof of the cochlear duct (becomes Reissner's membrane), the lateral wall (becomes the stria vascularis), the lateral nonsensory floor (becomes the outer sulcus), the prosensory floor (becomes the organ of Corti), and the medial nonsensory floor/wall (becomes the greater epithelial ridge/inner sulcus; Kelley 2007; Wu and Kelley 2012). Several key genes that pattern these cochlear domains are shown in Fig. 3.3 and include *Otx2* (roof; Vendrell et al. 2015), *Pax2* (strial wall; Burton et al. 2004), *bone morphogenetic protein 4* (*Bmp4*; lateral floor; Ohyama et al. 2010), *Sox2* and *Jag1* (prosensory domain; Ohyama et al. 2010), and *Lfng* and *fibroblast growth fiber 10* (*Fgf10*; medial floor/wall; Morsli et al. 1998; Urness et al. 2015). As the cochlear duct grows in length, these domains elongate in the manner of striped toothpaste being squeezed out of a tube, thus preserving their respective territories along the length of the cochlear duct (Fig. 3.3).

3.2.3 Outstanding Issues Concerning the Embryonic Origin of the Cochlea

The cochlear duct likely developed in coordination with the basilar papilla as they arose and enlarged within the sarcopterygian or amphibian lagenar recesses (Fritzsch et al. 2013). As amniotes diverged from the anamniote relatives, the enlarging basilar papilla gradually displaced the lagenar macula to the distal end of what became the cochlear duct (Smotherman and Narins 2004; Fritzsch et al. 2013). The lagena has been lost from the cochlea of all modern mammals with the exception of the egg-laying monotremes (Manley 2012). How were gene regulatory networks co-opted to permit the appearance of the basilar papilla as a distinct sensory organ and the enlargement of the lagenar recess to form a cochlear duct? Evidence from mouse mutants has generated a rapidly growing list of genes that can regulate the growth of the cochlear duct and organ of Corti, including transcription factors or cofactors, signaling ligands and receptors, and regulators of the cytoskeleton. However, it is not known whether any of these genes or the regulatory networks in which they reside were deployed during the derivation of the cochlear

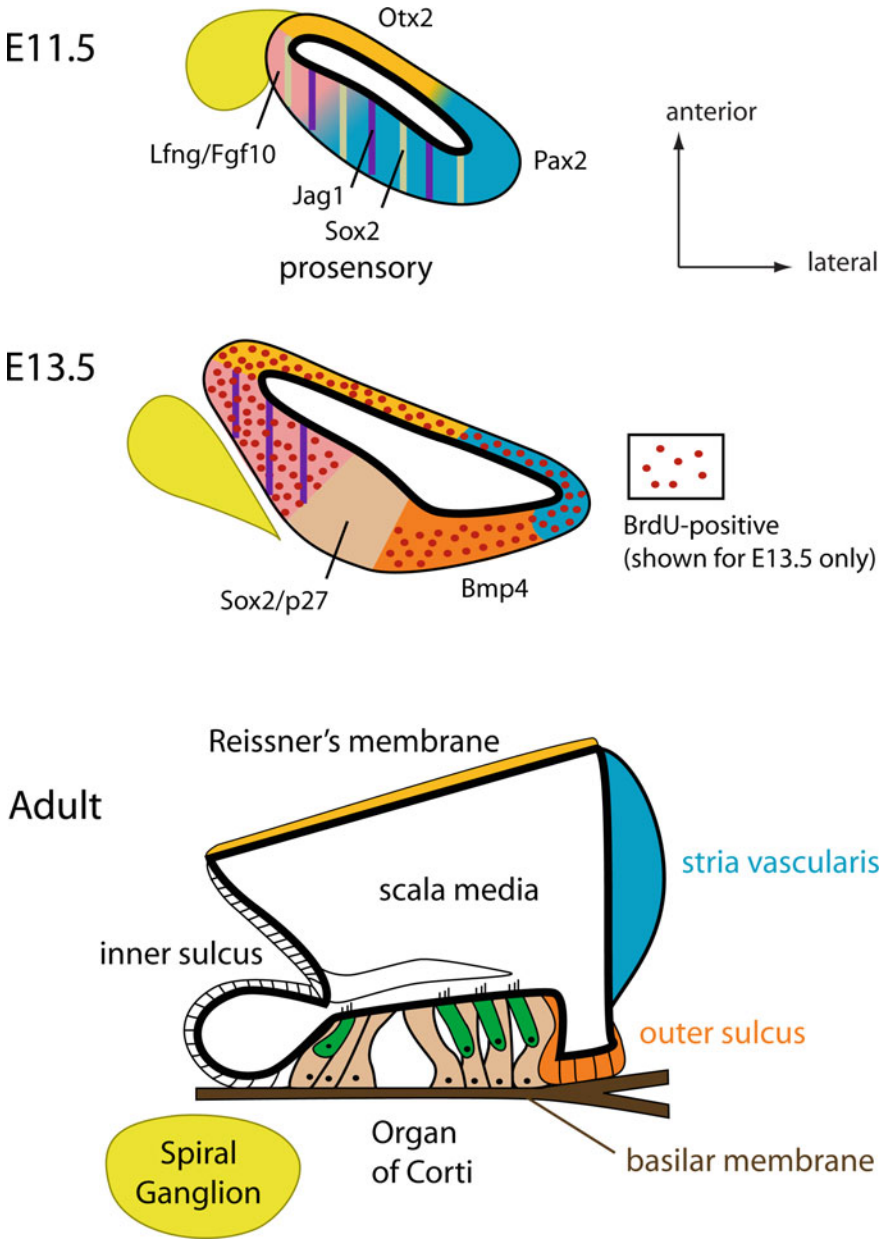

Fig. 3.3 Schematic of regional subdivision of the developing cochlear duct. This schematic highlights a small subset of the genes that gradually emerge as early markers of different cochlear tissues

duct from the lagenar recess or whether the appearance and expansion of the sensory and nonsensory components were coordinated together (perhaps by a cochlear "master gene") or separately as independent events.

What are the signals that establish the different territories of the cochlea in the ventral otocyst? As discussed in Sect. 3.2.1, conditional deletion of the Shh receptor *Smo* in the otocyst prevents the formation of the cochlear duct without significantly affecting other regions of the inner ear (Brown and Epstein 2011), suggesting that Shh signaling may lie upstream from regional determinants of cochlear identity. Interestingly, the anterior and ventral regions of the otocyst that express *Neurog1* and *LFng* are not strongly affected in *Smo* conditional mutants (Brown and Epstein 2011), although they normally contain some progenitors that can give rise to nonsensory regions of the cochlea in addition to the utricle, the saccule, and their associated maculae (Koundakjian et al. 2007; Raft et al. 2007). It will be of interest to determine whether these cochlear progenitors are diverted to other fates if they are unable to receive Shh signals or whether they simply die.

The signals responsible for the posteroventral stripe of *Bmp4* expression in the otocyst that will become the future outer sulcus of the cochlea are presently unknown, although a recent identified, long noncoding RNA, *Rubie*, that is located upstream from the *Bmp4* locus has been shown to be expressed in an identical pattern as *Bmp4* itself (Roberts et al. 2012) and may play a role in the fine tuning of *Bmp4* expression. The observation that the organ of Corti derives from Wnt-responsive progenitors (Riccomagno et al. 2005; Brown et al. 2015) suggests that Wnt signaling may play a direct or indirect role in the expression or maintenance of early markers of the prosensory domain/future cochlear duct such as *Sox2* and *Jag1* (Munnamalai and Fekete 2013). It is also possible that these signals may act to repress ventrolateral genes such as *Otx2* that will be expressed in the roof of the cochlear duct. A recent study of *Otx2* conditional mutant mice suggests that Otx2 may repress *Sox2* expression in the nascent cochlear duct, suggesting potential cross-repressive interactions in the division of the medial and lateral territories of the ventral otocyst (Vendrell et al. 2015).

3.3 Formation of the Cochlear Prosensory Domain

3.3.1 Role of Notch Signaling and Sox2 *in the Formation of Prosensory Patches*

Over the past decade, considerable progress has been made in understanding what regulates the specification and size of the prosensory domains. Each inner ear prosensory domain (organ of Corti, three cristae ampullae, and two maculae) expresses both *Sox2* and *Jag1* (Kiernan 2013). In the vestibular organs of chicken and mice, Jag1-Notch signaling helps specify the size and position of the prosensory patches through a mechanism of Notch-mediated lateral induction (Kiernan 2013; Neves et al. 2013). In this model, activation of Notch receptors by Jag1

ligands leads to the upregulation of *Sox2* in the signal-receiving cell. Evidence for this comes from both loss-of-function studies in which the mutation of either *Jag1* or *Sox2* leads to missing or greatly reduced prosensory patches throughout the ear (Kiernan et al. 2005a; Brooker et al. 2006) or gain-of-function studies in which ectopic expression of *Sox2, Jag1*, or the canonical Notch-signaling pathway can induce ectopic prosensory patches in regions of the ear that would normally form nonsensory tissue (reviewed in Neves et al. 2013).

Does this Notch-driven pathway also act within the prosensory domain of the cochlea? To be sure, ectopic activation of either *Sox2* or the canonical Notch-signaling pathway in nonsensory regions of the cochlea can induce the formation of ectopic sensory regions containing hair cells and supporting cells (Kiernan 2013; Pan et al. 2013), and severe *Sox2* hypomorphic mutations also prevent formation of the cochlear prosensory domain and the organ of Corti (Kiernan et al. 2005b). However, although conditional deletion of *Jag1* causes significant loss of cochlear sensory tissue (Kiernan et al. 2006), some prosensory markers still persist in these mutants (Basch et al. 2011). Also, in mice with conditional deletion of *Rbpjk*, the transcriptional mediator of canonical Notch signaling, hair cells continue to form, although these rapidly die (Basch et al. 2011; Yamamoto et al. 2011). Although some of these discrepancies may be due to technical differences in markers used or stages analyzed, it is also important to note that unlike in other prosensory patches, Jag1 is downregulated from the prosensory domain of the cochlea shortly after outgrowth commences and becomes restricted to the nonsensory epithelium of Kölliker's organ on the neural side of the cochlear duct (Fig. 3.3). This restriction of Jag1 is regulated in part by Bmp4, which is expressed on the opposite, abneural side of the duct (Ohyama et al. 2010). This establishes an asymmetry in Jag1 expression and in the activation of Notch signaling at the border between the Jag1 domain and the adjacent Sox2 domain, where the first inner hair cells will form (Murata et al. 2006). It is possible that this asymmetrical pattern of Notch activation leads to the asymmetrical pattern of the organ of Corti, where its polarized array of inner and outer hair cells contrasts with the more symmetrical arrangement of hair cells seen in the cristae and maculae of the vestibular organs.

3.3.2 *Role of Other Signaling Pathways in the Induction of the Cochlear Prosensory Domain: Fibroblast Growth Factors, Bone Morphogenetic Proteins, and Wnts*

The current conflicting results of the effect of Notch pathway mutants on the induction of the cochlear prosensory domain raise the possibility that other pathways may also act to induce this region of the cochlea in a manner distinct from other sensory organs of the ear. Fgf signaling is one such candidate pathway

because *Fgfr1* conditional mutants have very few hair cells in the cochlea but apparently normal numbers of hair cells in the vestibular organs (Pirvola et al. 2002). *Fgfr1* conditional mutants also show a decrease in proliferation in some regions of the young cochlea, particularly the greater epithelial ridge (Pirvola et al. 2002), but this study did not directly examine the presence of markers of the prosensory domain. Thus it is not clear whether the defects in these mutants are due to a failure of prosensory induction per se, reduced proliferation of prosensory progenitors, abnormal differentiation of the prosensory region, or a combination of all three effects. Candidate Fgfs, such as Fgf8, −10, or −20, either are not expressed early enough in the cochlea to influence prosensory induction (*Fgf8*; Jacques et al. 2007) or do not compromise the induction of the prosensory domain when mutated (*Fgf10* and *Fgf20*; Huh et al. 2012; Urness et al. 2015).

Bmp4 is expressed on the abneural side of the cochlear duct in the future outer sulcus and establishes a gradient of Bmp signaling across the abneural-neural axis of the duct (Ohyama et al. 2010). Disruption of Bmp signaling of the *Bmpr1a* and *Bmpr1b* receptors in compound conditional mutants causes a complete failure of prosensory domain formation. Instead, the cochlear duct continues to express Jag1 across the entire neural-abneural axis and develops with the molecular identity of Kölliker's organ (Ohyama et al. 2010). The prosensory domain would normally form in the region of the cochlear duct that receives medium doses of Bmp signaling. Thus, it is possible that moderate activation of the Bmp pathway acts to *directly* induce the prosensory domain or, alternatively, simply acts *indirectly* to downregulate Jag1, thereby allowing other inducing signals to function.

Recent evidence also raises the possibility that canonical Wnt signaling may play a role in the induction of the prosensory domain. Wnt-responsive *TCF/Lef* fluorescent reporter mice show a strong activation of the canonical Wnt-signaling pathway across the entire radial (neural-abneural) axis of the cochlear duct at E12.5 (Jacques et al. 2014), and pharmacological or genetic activation of the canonical Wnt pathway in the cochlea leads to an expansion of prosensory markers into nonsensory regions of the cochlea (Jacques et al. 2012; Shi et al. 2014). In contrast, pharmacological or genetic inhibition of the canonical Wnt pathway at E12.5 in these studies did not significantly affect the development of the prosensory domain. However, because the prosensory domain is already present at this time, further experiments will be necessary to determine if canonical Wnt signaling is necessary for induction of the cochlear prosensory domain as opposed to being necessary for maintaining prosensory identity.

3.3.3 *Outstanding Issues Concerning the Induction and Radial Patterning of the Prosensory Domain*

As discussed in Sect. 3.3.1, the role of Notch signaling in the induction of the prosensory domain of the cochlea has yet to be settled because different studies have used different approaches to disrupt Notch signaling, and to date, none have

resulted in a total and exclusive loss of Notch function. For example, in *Rbpjk*-mutant mice, all canonical Notch signaling is disrupted; however, because this protein acts as a transcriptional repressor in the absence of Notch signaling (Tanigaki and Honjo 2010), some *Rbpjk*-mutant phenotypes may be due to a combination of derepression of genes that are normally repressed by Notch signaling as well as a loss of Notch signaling itself. Although *Jag1* is the only Notch ligand to be strongly expressed in prosensory areas in the ear, different sensory organs are differentially affected in *Jag1* conditional mutant mice, for example, the utricular macula is almost completely absent, whereas the saccular macula remains largely intact (Kiernan et al. 2006). This variable phenotype could be caused by persistence of the Jag1 protein after conditional mutation of the *Jag1* gene or by compensation by another Notch ligand, possibly one of the several "noncanonical" Notch-interacting membrane proteins such as DNER or Dlk-1 (D'Souza et al. 2010). Ultimately, this issue will only be addressed by a complete conditional inactivation of all Notch receptors in the inner ear from as early a stage as possible.

An unresolved question about cochlear development is whether diffusible morphogens underlie radial axis patterning. A defining characteristic of a morphogen is that it is expressed in a gradient, and cells respond differently to different threshold concentrations of the morphogen. Morphogen gradients are often established across an equipotential field of progenitors by the presence of an asymmetric source at one end, which can be enhanced by a sink at the other end. In the developing cochlea, molecules associated with BMP, Wnt, and Fgf signaling are asymmetrically expressed within or adjacent to the presumptive organ of Corti as it segregates into morphologically distinct parts: medial (border cells, inner hair cells, and inner phalangeal cells), middle (pillar cells), and lateral (outer hair cells and Deiters and other supporting cell types). At E11.5–E12.5, *Fgf10* is expressed in the medial nonsensory flank of the organ, *Wnt5a* is expressed in a gradient that is highest on the medial half of the duct, and *Bmp4* is expressed in the lateral nonsensory flank. These three morphogen family members might serve instructive roles in subdividing the radial axis, although further experiments are required to definitely show that any of these has classical morphogen-like activity on cochlear progenitors (discussed further in Groves and Fekete 2012).

3.4 Coordinating Developmental Gradients of Differentiation and Cell Cycle Exit in the Cochlea

3.4.1 The Unusual Pattern of Cell Cycle Exit and Differentiation in the Cochlea

Once the cochlear prosensory domain has been induced, its progenitors begin to exit the cell cycle and differentiate into the distinct hair cell and supporting cell types of the organ of Corti. In contrast to the mammalian vestibular sensory organs,

where cell cycle exit and differentiation appear to initiate in the center of each organ and spread outward radially over an extended period of time (Kirkegaard and Nyengaard 2005; Burns et al. 2012), the prosensory region of the cochlea shows a radically different pattern of cell cycle withdrawal and differentiation (reviewed in Basch et al. 2016). Cell cycle exit commences in the most apical (tip) region of the cochlear prosensory domain on E12.5 in mice and spreads toward the base of the duct over the next few days, although the most basal cells do not complete their final cell division until E15.0 (Lee et al. 2006). Shortly after the onset of cell cycle exit in the apex, cells in the midbasal region begin differentiating into hair cells by expressing the Atoh1 transcription factor (Cai et al. 2013). Atoh1 expression then spreads to the base in one direction and in the other direction toward the apex over the next 3–4 days. Thus, the *first* cells to exit the cell cycle at the apex of the cochlea on E12.5 are the *last* ones to differentiate into hair cells. At present, very little is known about how cell cycle exit is initiated in the apex nor how this wave of withdrawal from the cell cycle propagates along the cochlea.

In the last 15 years, a number of cell cycle regulators have been implicated in the cell cycle exit of the cochlear prosensory domain. The G_1 cyclin CyclinD1 is expressed in proliferating progenitors at this stage and is maintained by canonical Wnt signaling (Jacques et al. 2012). Concomitant with cell cycle exit on E12–E13.5, the cyclin-dependent kinase inhibitor $p27^{kip1}$ (*Cdkn1b*) is expressed in the cochlea in an apical-basal gradient (Chen and Segil 1999; Lee et al. 2006). The prolonged period of cell proliferation in the apical regions of the $p27^{kip1}$-mutant cochlea causes an overproduction of both hair cells and supporting cells (Chen and Segil 1999; Lowenheim et al. 1999). In postmitotic supporting cells, $p27^{kip1}$ becomes enriched, whereas other cyclin-dependent kinase inhibitors such as $p19^{ink4d}$ (*Cdkn2d*) and $p21^{cip1}$ (*Cdkn1a*) become upregulated in hair cells and supporting cells. Mutation of these genes causes abnormal cell cycle reentry and death in the organ of Corti (reviewed in Schimmang and Pirvola 2013). Other cell cycle regulators such as the pocket protein family (*Rb1, Rbl1/p107,* and *Rbl2/p130*) also maintain the postmitotic state of hair cells and supporting cells, although different members appear to play different roles in the developing and mature cochlea (Rocha-Sanchez and Beisel 2007; Rocha-Sanchez et al. 2011).

In searching for genes that control or coordinate the onset of cell cycle withdrawal and differentiation in the mouse cochlea, investigators studied the mammalian homologs of so-called heterochronic genes that regulate developmental timing in the nematode worm *C. elegans* (Golden et al. 2015). Two of these genes, *Lin28* and *let-7*, oppose each other in controlling the timing of cell lineage decisions. *Lin28* encodes an RNA-binding protein that promotes stemness and prevents differentiation by stabilizing the transcripts of growth-promoting genes. *Lin28* also blocks the biogenesis of mature *let-7* microRNA. Conversely, *let-7* microRNAs repress the translation of *Lin28* as well as other genes that enhance proliferation. These counteracting effects on developmental timing are partly conserved in the mouse cochlea. *Lin28b* transcript levels fall as the prosensory cells pull out of

division between E13 and E16, while the levels of several *let-7* family members rise from E13 to E18 as cells differentiate. Overexpression of human *LIN28B* before E13 delays hair cell differentiation by causing a 16-hour delay in cell cycle exit. This is accompanied by an 80% decrease in *let-7* and significant increases in several *let-7* target transcripts, including *N-myc* and *cyclin D1* that promote cell proliferation in the cochlea. As might be expected, forcing the premature expression of a modified form of *let-7g* that is resistant to negative regulation by *Lin28b* causes precocious cell cycle exit and shortens the cochlea by 40% because of an insufficient number of prosensory cells. However, despite pulling out of division early, hair cells do not immediately differentiate (Golden et al. 2015). That is, the *Lin28b/let-7* network is partly uncoupled in the cochlea compared with the worm. This underscores the cochlea's unusual systematic lengthening of the interval between cell cycle exit and the onset of cell differentiation in progressing from base to apex. These data suggest that the timing of hair cell differentiation is held in check through a *let-7*-independent mechanism, possibly through the activity of Shh, as described in Sect. 3.4.2.

3.4.2 How Are Cell Cycle Exit and Differentiation Uncoupled in the Cochlea?

The temporal and spatial uncoupling of cell cycle exit and differentiation in the mammalian cochlea is very unusual because progenitor cells in other systems typically exit the cell cycle and differentiate almost simultaneously, with differentiation signals often triggering cell cycle exit. Mammalian vestibular sensory organs and all nonmammalian sensory organs tend to have a radially symmetrical pattern of hair cells and supporting cells, with a single hair cell surrounded by between 4 and 8 supporting cells (Goodyear and Richardson 1997). This radial pattern appears to be generated by establishing a central region of differentiation and cell cycle exit that expands outward circumferentially. This pattern of cell behavior has been observed in both the mammalian utricle and bird basilar papilla (Katayama and Corwin 1989; Burns et al. 2012). However, one may speculate that the precise and invariant pattern of one inner hair cell, three outer hair cells, and their associated supporting cell types that is repeated serially in the organ of Corti along its length may require the entire progenitor domain to become postmitotic before differentiation commences. In support of this, mouse mutants that delay cell cycle exit in the cochlea have disrupted proportions of hair cells and supporting cells, especially in the apical regions where cell cycle exit normally begins (Chen and Segil 1999).

What delays the onset of hair cell differentiation in the cochlea relative to cell cycle exit? Studies of a number of mouse mutants suggest a role for neurons of the spiral ganglion in holding the differentiation of hair cell progenitors in abeyance.

Prosensory progenitors in *Neurog1*-mutant mice exit from the cell cycle about 24–36 hour earlier than normal, and hair cell differentiation starts in the apical, not the basal, region of these mutants (Matei et al. 2005). A similarly abnormal pattern of hair cell differentiation is seen in *Neurod1*-mutant mice (Jahan et al. 2010). Because *Neurod1* and *Neurog1* are not expressed in the cochlea at detectable levels during differentiation of the prosensory domain, it is unlikely that these transcription factors are regulating hair cell differentiation directly but indirectly by controlling spiral ganglion neurogenesis. Both genes are expressed in neuronal progenitors that delaminate from the anteroventral otocyst earlier in development (Raft et al. 2004) and *Neurod1* or *Neurog1* mutations severely compromise neurogenesis, leading to an absence or severe hypoplasia of the spiral ganglion (Ma et al. 2000; Kruger et al. 2006). These data suggest that signals from the developing spiral ganglion may regulate the timing of differentiation of cochlear hair cells.

Clues as to the identity of the signal released by the spiral ganglion came from studies of mutants in the Shh-signaling pathway. Hypomorphic mutants of the Shh mediator *Gli3* ($Gli3^{\Delta 699}$), a mouse model of Pallister-Hall syndrome, contain ectopic hair cells (Driver et al. 2008), and treatment of developing cochlear explants with Shh or the Shh inhibitor cyclopamine causes a decrease or increase in the number of hair cells, respectively (Driver et al. 2008). *Shh* is expressed in the spiral ganglion (Liu et al. 2010; Bok et al. 2013) and is downregulated from basal regions of the spiral ganglion at a similar time to the onset of *Atoh1* expression in the corresponding basal regions of the cochlea, providing a circumstantial link between the disappearance of the Shh signal and the initiation of hair cell differentiation. This circumstantial link was independently confirmed by conditional inactivation of *Shh* in the spiral ganglion (Bok et al. 2013) and inactivation of the Shh receptor *Smo* in the cochlear duct (Tateya et al. 2013). Both conditional mutants have a truncated cochlea in which prosensory cells exit the cell cycle and differentiate prematurely. Strikingly, the expression of *Atoh1* and later hair cell markers in these mutants follows an apical-to-basal gradient instead of the normal basal-to-apical gradient seen in the presence of Shh (Bok et al. 2013; Tateya et al. 2013).

3.4.3 Outstanding Issues Concerning Cell Cycle Exit and Differentiation in the Prosensory Domain

The separate waves of cell cycle exit and differentiation of the prosensory domain along the apical-basal axis of the cochlea are without precedent in the mammalian nervous system. It is still unclear how these patterns are initiated and propagated along the cochlear duct. In the case of cell cycle exit, transgenic reporter lines have clearly demonstrated that the apical-basal gradient of $p27^{kip1}$ is regulated at both the transcriptional and posttranscriptional levels (Lee et al. 2006). Although cell cycle exit in the mouse cochlea is partially dependent on Shh signaling (Bok et al. 2013),

loss of Shh specifically from the spiral ganglion has a far less severe effect on cell cycle exit than on the onset and position of hair cell differentiation (Bok et al. 2013). However, because the progenitors for the future apex of the cochlea are likely to be located in the ventral and medial region of the otocyst, it is possible that Shh from the notochord and floor plate of the hindbrain may partially compensate for the loss of Shh in spiral ganglion conditional knockouts of *Shh*. Another possibility is that the regulation of cell cycle exit by Lin28B occurs independently of Shh.

The basal-apical wave of hair cell differentiation does not appear to require an intact cochlear duct or direct contact with the spiral ganglion or underlying mesenchyme because dissected pieces of the mouse cochlear duct are capable of initiating hair cell differentiation in an approximately normal temporal sequence even when cultured separately (Montcouquiol and Kelley 2003). Although loss of Shh from the spiral ganglion clearly leads to precocious hair cell differentiation in vivo, it is unclear whether there is an additional positively acting hair cell differentiation signal that is normally held in check by Shh. *Atoh1* has been shown to be regulated by a variety of other signals, such as Bmps, Fgfs, and Wnts (reviewed in Mulvaney and Dabdoub 2012; Cai and Groves 2014). If these factors are acting in the cochlea in vivo, it will be of interest to understand how they initiate hair cell differentiation precisely at the boundary of the prosensory domain and Kölliker's organ (Cai et al. 2013).

An understanding of the mechanisms leading to the acquisition of positional information along the basal-apical axis is another unresolved area of mammalian cochlear development. Once development is completed, there will be numerous biophysical, morphological, and biochemical gradients along the longitudinal axis of the cochlea that correlate systematically with frequency response. As recently as 2011, a review of the development of cochlear tonotopy indicated a remarkable dearth of molecular candidates that might impart basal-apical positional information (Mann and Kelley 2011). Three years later, significant progress was made using the chicken basilar papilla as a model system, where tonotopy is also associated with basal (proximal) to distal (apical) position. Transcriptome comparisons of large longitudinal sectors of the basilar papilla led to the discovery of molecular gradients unrelated to those involved in cell cycle withdrawal (Mann et al. 2014; Thiede et al. 2014). Transcripts for *Bmp7* and a Bmp inhibitor, *chordin-like 1*, are expressed in counter-gradients on E6.5 (Mann et al. 2014). Manipulation of Bmp signaling (up or down) alters hair cell differentiation in a manner that is consistent with a reprogramming of proximal-distal identity. A parallel study revealed a longitudinal gradient in the transcripts for a RA synthetic enzyme, Raldh3, which is highest proximally on E6.5 but reverses direction from E10 onward (Thiede et al. 2014). Based on experimental manipulations where high RA signaling is a powerful inducer of distal hair cell morphologies, the latter gradient appears to be functionally relevant (Thiede et al. 2014). It remains to be determined what sets up the initial Bmp7 gradient in the bird cochlea, nor is it known whether Bmp- and RA-signaling pathways can influence the tonotopic organization of the mammalian cochlea.

3.5 Fine-Grained Patterning and Cell-Type Specification in the Organ of Corti

As discussed in Sect. 3.3.2, the coordinated activation of a number of signaling pathways in a graded manner across the neural-abneural axis of the prosensory domain leads to the formation of three distinct regions in the organ of Corti defined by inner hair cells, pillar cells, and outer hair cells (Raphael and Altschuler 2003; see also Groves and Fekete 2012). Although other vertebrate species display morphological and functional variation of hair cells in the neural-abneural and basal-apical axes of their hearing organs (basilar papillae; Manley 2000), the separation of inner and outer hair cell regions by pillar cells is an exclusively mammalian innovation that can be observed in even the most basal mammals, the egg-laying monotremes (Ladhams and Pickles 1996). Whatever evolutionary events led to the specialization of the organ of Corti from a basilar papilla, it required the layering of distinct signals and gene regulatory networks to specify distinct cell types on top of the pathways that specified generic hair cell versus supporting cell fate decisions.

3.5.1 Notch Signaling as a Mechanism to Distinguish Hair Cells from Supporting Cells

The Notch-signaling pathway is an evolutionarily ancient mechanism of cell contact-mediated fate specification that can specify a fine-grained pattern of so-called primary cell fates versus secondary cell fates and can also specify and sharpen boundaries (Artavanis-Tsakonas and Muskavitch 2010). The alternating mosaic of hair cells and supporting cells seen in all vertebrate hearing and balance organs was first suggested as an excellent candidate for regulation by Notch signaling by Julian Lewis over 25 years ago (Lewis 1991). Since then, it has been firmly established that differentiating hair cells express Notch ligands (typically Dll1, Dll3, and Jag2) that signal to Notch receptors expressed by supporting cells (Kiernan 2013). The activation of Notch signaling leads to the repression of hair cell-specific transcription factors such as Atoh1, which in turn prevents the expression of hair cell-specific Notch ligands (Fig. 3.4). The resultant lateral inhibition (as distinct from lateral induction of prosensory specification mentioned earlier) has negative feedback that leads to the generation of a stable array of hair cells delivering Notch signals to neighboring supporting cells. Accordingly, genetic or pharmacological disruption of Notch signaling in a variety of vertebrate species leads to the development of extra hair cells at the expense of supporting cells (Kiernan 2013).

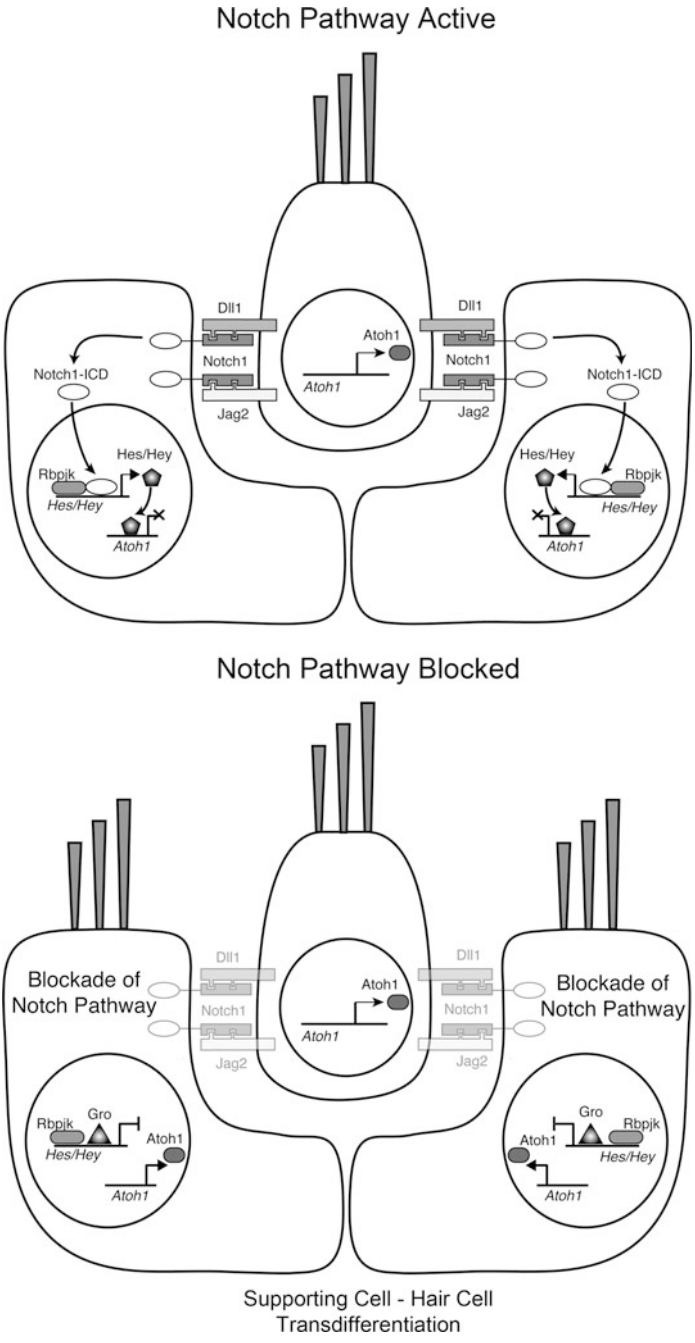
Notch Pathway Active
Dll1
Notch1
Jag2
Atoh1
Atoh1
Dll1
Notch1
Jag2
Notch1-ICD
Hes/Hey
Rbpjk
Hes/Hey
Atoh1
Notch1-ICD
Hes/Hey
Rbpjk
Hes/Hey
Atoh1
Notch Pathway Blocked
Blockade of Notch Pathway
Dll1
Notch1
Jag2
Atoh1
Atoh1
Dll1
Notch1
Jag2
Blockade of Notch Pathway
Rbpjk
Gro
Hes/Hey
Atoh1
Atoh1
Gro
Rbpjk
Atoh1
Hes/Hey
Atoh1
Supporting Cell - Hair Cell Transdifferentiation

◂**Fig. 3.4** A simple model of Notch signaling between hair cells and supporting cells. Hair cells express the Atoh1 transcription factor, which induces the expression of Notch ligands. These signal to supporting cells via Notch receptors, leading to the formation of an activation complex between the Notch intracellular domain (Notch1-ICD) and the coactivator RBPJκ. This activates expression of Notch downstream target genes (such as the Hes and Hey transcription factors). These suppress Atoh1 expression and hair cell fate in the supporting cells. If Notch signaling is blocked genetically or pharmacologically, the transcriptional activation complex cannot form and a RBPJκ-Groucho repression complex blocks Notch downstream genes. Atoh1 is thus induced in the supporting cells, driving them to a hair cell fate

Despite the widespread acceptance of the regulation of hair cell and supporting cell fate by Notch signaling, many studies in the past 10 years suggest that this simple model cannot explain all aspects of hair cell and supporting cell patterning in the organ of Corti. First, simple models of lateral inhibition typically generate a radial pattern of a hair cell surrounded by a series of supporting cells of the sort observed, at least to the first approximation, in bird hearing organs and mammalian vestibular organs (Goodyear et al. 1995) rather than the alternating rows of hair cells and supporting cells seen in the organ of Corti (Kelley 2006). Second, although conditional mutants of the *Notch1* receptor or compound mutants of *Jag2* and *Dll1* ($Jag2^{-/-}$; $Dll1^{hyp/-}$) cause many supernumerary hair cells at the expense of supporting cells, some supporting cells appear to be unaffected in these mutants (Kiernan et al. 2005a). Many inner pillar cells persist in these mutants (see Sect. 3.5.2 below), and $Jag2^{-/-}$; $Dll1^{hyp/-}$ mutants also appear to retain multiple border and inner phalangeal cells beneath supernumerary inner hair cells (Kiernan et al. 2005a). In other words, the increase in hair cells is not always matched by an expected decline in supporting cells as evidence of a cell fate switch. Moreover, the presence of occasional persistent bromodeoxyuridine (BrdU)-labeled cells suggests that the Notch pathway may also regulate cell cycle exit of at least some organ of Corti progenitors (Kiernan et al. 2005a). It is possible that residual supporting cell differentiation in these mutants reflects a failure to completely abolish all Notch signaling in the cochlea, and a resolution of this issue must await analysis of mice in which all Notch receptors expressed in the ear are completely mutated.

3.5.2 Specification of Subtypes of Hair Cells and Supporting Cells in the Organ of Corti

Although Notch signaling is used repeatedly in development to generate fine-grained patterns of alternating cell types, a given strength of Notch activation typically does not discriminate between different variants of a particular class of cells by itself. Thus, in the cochlea, disruption of Notch signaling generates supernumerary hair cells at the expense of some supporting cells, but the identity of these supernumerary hair cells, inner versus outer, is consistent with the location of their normal counterparts in the organ of Corti (e.g., Kiernan et al. 2005b).

Although some genes are expressed specifically in either inner or outer hair cells from an early stage, for example, *Fgf8* in inner hair cells (Jacques et al. 2007) and the transcription factor *Insm1* in outer hair cells (Lorenzen et al. 2015), many genes that distinguish inner from outer hair cells are expressed later as the organ of Corti matures (Liu et al. 2014), and the signals and transcriptional effectors that induce them are largely unknown at present.

The situation is somewhat different for supporting cells, where a number of genes that become restricted to particular classes of supporting cells, such as *Prox1* (Bermingham-McDonogh et al. 2006), $p75^{LNGFR}$ (Mueller et al. 2002), *Spry2* (Shim et al. 2005), *Hey1,* and *Hey2* (Benito-Gonzalez and Doetzlhofer 2014), are initially expressed in the prosensory domain before or concomitant with hair cell differentiation. In addition, other members of the *Hes* and *Hey* gene families that are commonly thought of as being Notch responsive show dynamic changes as the cells differentiate, with different combinations of *Hes* and *Hey* genes being expressed in different types of supporting cells (Doetzlhofer et al. 2009). *Hes* and *Hey* genes can be differentially regulated by Notch signaling in a number of ways, for example, the number and arrangement of high- and low-affinity binding sites for cleaved Notch intracellular domains varies between different *Hes* and *Hey* gene promoters (Ong et al. 2006). However, because neither the expression of Notch ligands by inner and outer hair cells nor the expression of Notch receptors by different supporting cells appear to differ significantly, it is likely that other signaling mechanisms collaborate with the Notch pathway to specify distinct supporting cell types.

The best-characterized example of how Notch signaling interacts with other signaling pathways in the cochlea is the specification of pillar and Deiters cell fates by Fgf signaling (Fig. 3.5). Pillar cells are the only supporting cell type that does not transdifferentiate into hair cells in the absence of Notch signaling (Kiernan et al. 2005b; Doetzlhofer et al. 2009). Pillar cells and Deiters cells express the Fgfr3 receptor and develop in close proximity to inner hair cells, which express Fgf8 very shortly after they differentiate. Pharmacological blockade of Fgf signaling, conditional deletion of *Fgf8*, or deletion of *Fgfr3* disrupt the differentiation of pillar cells (Jacques et al. 2007; Puligilla et al. 2007), and overexpression of Fgfs in the cochlea can activate pillar cell markers at the expense of markers of outer hair cells and Deiters cells (Jacques et al. 2007; Doetzlhofer et al. 2009). While pillar cells are differentiating, *Hey2* becomes downregulated from the prosensory domain and is restricted to pillar cells (Doetzlhofer et al. 2009). Although *Hey2* is typically thought of as a target of Notch signaling, *Hey2* is also regulated by Fgf signaling, for example, treatment of cochlear cultures with Fgfs upregulates Hey2 protein in many supporting cells (Doetzlhofer et al. 2009). Moreover, Hey2 expression and pillar cell fate are unaffected by inhibition of either Notch or Fgf receptors, but simultaneous inhibition of FGF and Notch signaling downregulates Hey2 and converts pillar cells into hair cells (Fig. 3.5). Finally, genetic deletion of *Hey2* allows pillar cells to convert into hair cells when Notch signaling is blocked (Doetzlhofer et al. 2009).

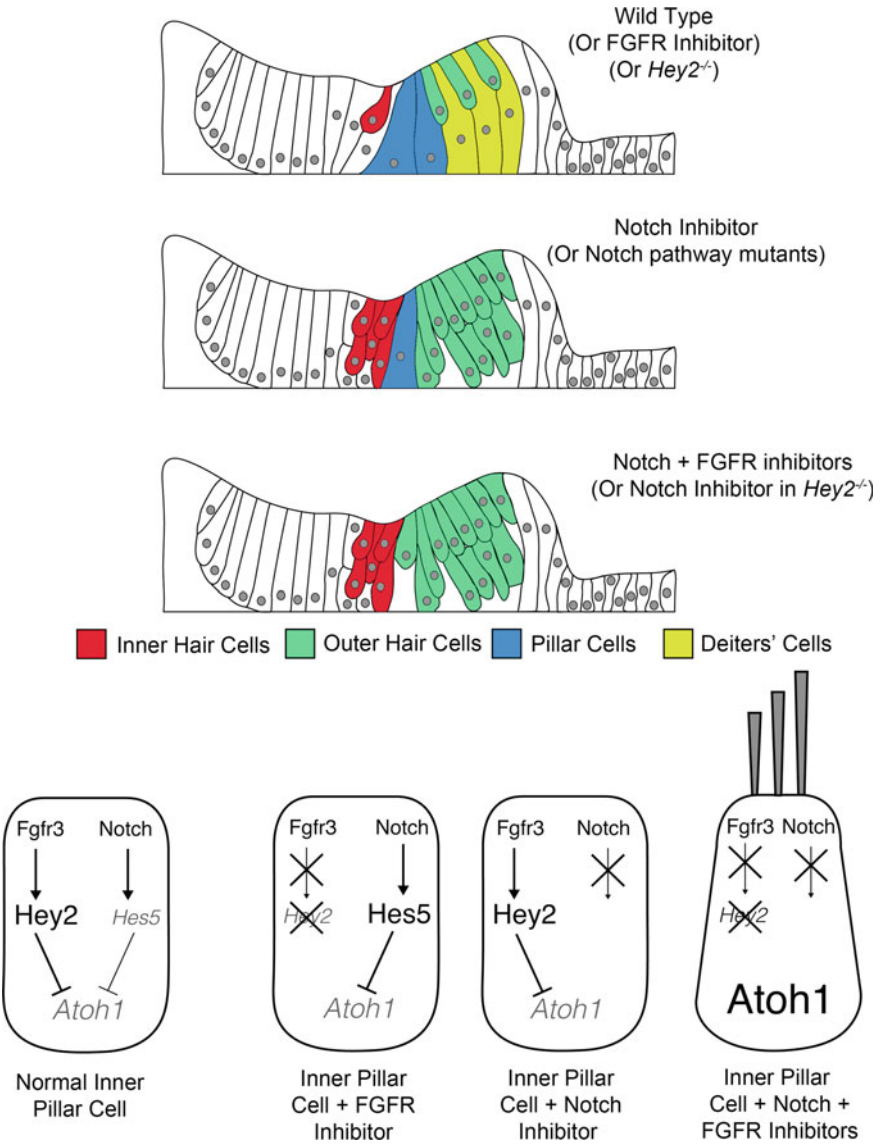

Fig. 3.5 The roles of fibroblast growth factor (FGF) and Notch signaling in pillar and Deiters cell identity. In wild-type embryos, pillar cells separate the inner and outer hair cell regions. If the Notch pathway is blocked, most supporting cells transdifferentiate into hair cells, but outer pillar cells remain because FGF signaling from the inner hair cells maintains Hey2 expression in these cells. If FGF signaling is blocked or in *Hey2*-mutant embryos, the Notch pathway upregulates Hes5, preserving pillar fate. If both pathways are blocked, Atoh1 expression is activated and the outer pillar cells convert into hair cells

A precise level of Fgf signaling appears to distinguish between pillar and Deiters cells and to maintain their distinct identities in mature animals (Fig. 3.6). The Fgf antagonist *Sprouty2* is expressed in pillar and Deiters cells, suggesting that a gradient of Fgf8 emanating from inner hair cells specifies pillar cells at high levels of Fgf signaling and Deiters cells at lower levels. Indeed, *Sprouty2*-mutant mice show a postnatal transformation of Deiters cells into pillar cells and the *Sprouty2*-mutant phenotype can be rescued by lowering Fgf signaling through the loss of one allele of *Fgf8* (Shim et al. 2005). Moreover, mouse models of the *Fgfr3* mutation found in Muenke syndrome also show a postnatal transformation of Deiters cells into pillar cells (Mansour et al. 2013). Here, however, the mutation in *Fgfr3* allows the receptor to become responsive to another Fgf expressed in the cochlea, Fgf10, thus increasing Fgf signaling in an analogous manner to the loss of *Spry2*. These remarkable results indicate that the fates of pillar and Deiters cells remain plastic even after the onset of hearing.

3.5.3 Outstanding Issues Concerning the Specification of Hair Cell and Supporting Cell Subtypes

Our understanding of the signals and gene regulatory networks that distinguish different types of hair cells and supporting cells from each other during development is currently limited by the dearth of unique markers. The difficulty of obtaining pure populations of different cell types and the relatively small number of cells present in the organ of Corti militate against obtaining a good survey of the genes expressed by each cell type. However, with recent technical advances in RNA sequencing from very small numbers of cells (or even single cells; Burns et al. 2015; Waldhaus et al. 2015), a much clearer picture of the gene expression patterns that distinguish cells in the organ of Corti should soon emerge.

Although there clearly are features that are common to all inner ear hair cells, the factors that regulate the development of auditory versus vestibular hair cells or of inner hair cells versus outer hair cells in the cochlea are unknown. *Atoh1* is a generic hair cell transcription factor, but it is not known whether it only regulates genes common to all hair cells or, alternatively, has access to different regions of chromatin in hair cell subtypes that are made differentially available by region-specific signaling pathways. In the case of the cochlea, it is possible that the signaling pathways that help divide the embryonic organ of Corti along its neural-abneural axis may provide a cellular context in which different transcription factors can cooperate with Atoh1 to specify different types of hair cells. In the case of supporting cells, a generic transcription factor that is expressed in all supporting cell types has yet to be identified. Hey2 is currently the only transcription factor that singles out one supporting cell type (pillar cells) from other supporting cells, although other supporting cells can be defined by specific combinations of other *Hes* and *Hey* genes.

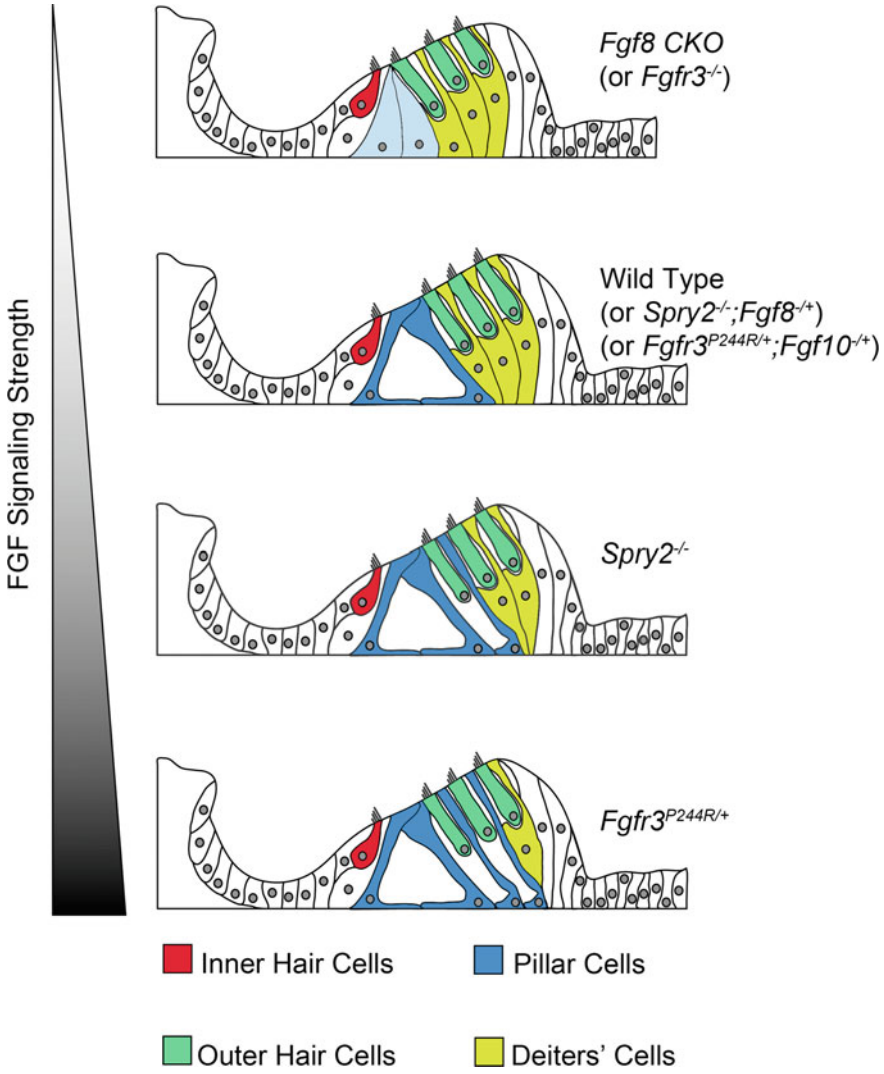

Fig. 3.6 An FGF gradient maintains pillar and Deiters cell fates in postnatal animals. FGF8 from inner hair cells creates a neural-abneural gradient of FGF signaling that allows differentiation of pillar cells and Deiters cells. If FGF8 signaling is reduced or blocked (by mutation of *FGF8* or the *FGFR3* receptor; *top panel*), pillar cells cannot differentiate properly. If the FGF inhibitor *Spry2* is mutated, increased FGF signaling causes some Deiters cells to convert into pillar cells (*third panel from top*). In the Muenke syndrome $FGFR3^{P244R}$ mutant (*bottom panel*), the receptor becomes responsive to FGF10 as well as to FGF3, and the further increase in FGF signaling causes more rows of Deiters cells to convert to a pillar cell fate. Further evidence of the dose-dependent effect of FGF signaling is shown by the fact that double mutants of genes that have opposing effects, such as *Fgf8; Spry2* mutants or $FGFR3^{P244R}$; *Fgf10* mutants, are phenotypically normal (*second panel from top*)

3.6 Innervation of the Organ of Corti

3.6.1 Neurogenesis of the Spiral Ganglion

The spiral ganglion neurons of the cochlea originate from a neurosensory domain in the ventromedial otocyst (Fig. 3.7). This region expresses several transcription factors (*Eya1, Six1, Sox2*) considered essential for initiating neurogenesis (reviewed by Appler and Goodrich 2011; Goodrich 2016). An adjacent posteroventral region expresses *Tbx1*, a transcription factor that blocks neurogenesis (Raft et al. 2004). The earliest evidence of neural fate specification in the otocyst is the salt-and-pepper appearance of Neurogenin1 (*Neurog1/Ngn1*)-expressing progenitors within the otic

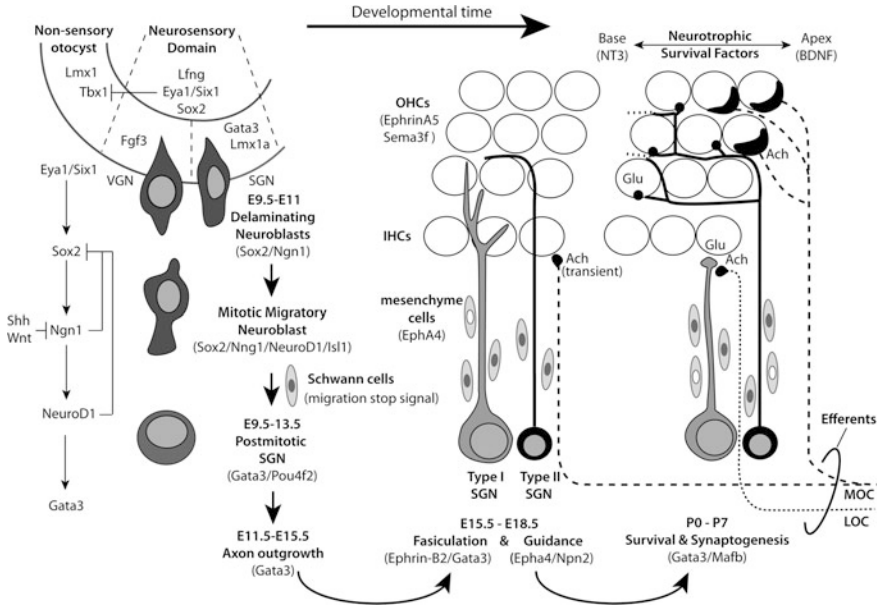

Fig. 3.7 Neurogenesis and the development of cochlear innervation. *Left to right*: neuroblasts are first recognized within the otocyst due to expression of *Neurog1 (Ngn1).* This initiates a cascade of neurogenic transcription factors. Progression of cells along a neural differentiation pathway requires both negative feedback loops to repress progenitor genes and loss of responsiveness to secreted factors like Shh and Wnt. Precursors of spiral ganglion neurons (SGNs) maintain expression of a different constellation of genes than those of vestibular ganglion neurons (VGNs), most notably *Gata3.* The final placement of the neuronal cell bodies is influenced by stop signals in the surrounding environment. Radial bundling of afferent neurites is influenced by Eph-to-Ephrin reverse signaling. Type I and type II afferents take distinct pathways across the tunnel of Corti (not shown) as they mingle with inner hair cells (IHCs) and outer hair cells (OHCs). An exploratory phase of axon outgrowth within the cochlea is influenced by Ephrin-to-Eph forward repulsive signaling and Semaphorin-to-Neuropilin repulsive signaling. SGN survival is mediated by the neurotrophins BDNF and NT3. Finally, refinement of connections takes place in the postnatal period for the type I afferents and both medial olivocochlear (MOC) and lateral olivocochlear (LOC) efferents. Ach, acetylcholine; Glu, glutamate

epithelium, some of which also express *Neurod1* and *Isl1* (Raft et al. 2007; Deng et al. 2014). Notch signaling is involved in the specification of neuronal precursors (Abello and Alsina 2007; Abello et al. 2007) and a role for Fgf signaling is also implicated in the chicken (Alsina et al. 2004). Neuroblasts delaminate from the epithelium and gather together as a common statoacoustic ganglion adjacent to the otocyst and the hindbrain. Negative feedback circuits then repress *Neurog1* (Raft and Groves 2015) and *Sox2* (Evsen et al. 2013) in the neuroblasts. *Neurog1* is required for neural specification (Ma et al. 1998, 2000), whereas *Neurod1* is necessary for delamination and survival of postmigratory neuroblasts (Liu et al. 2000; Kim et al. 2001). As the delaminated cells exit the cell cycle, *Neurod1* and *Isl1* are reduced, whereas *Pou4f1* and then *Pou4f2* are increased (Deng et al. 2014). The transition states of premigratory and migratory neuroblasts were identified through single-cell gene expression analysis (Durruthy-Durruthy et al. 2014), which revealed that genes related to Shh and Wnt responsiveness are downregulated as neuronal differentiation progresses. This change appears to be permissive for further neuronal development (Brown and Epstein 2011).

After the statoacoustic ganglion is formed, it then splits to create the vestibular ganglion and the spiral ganglion (Sandell et al. 2014). These two fates may be imposed earlier, while the neuroblasts are still residents of the otocyst, based on their sites of origin and gene expression profiles. The more anterolateral pool expresses *Fgf3*, emigrates earlier, is born first, and becomes vestibular. The more posteromedial pool expresses *Lmx1* and *Gata3*, emigrates later, pulls out of division last, and becomes auditory (Koo et al. 2009). Lineage and fate-mapping experiments in the chicken embryo are consistent with a mostly separate origin of vestibular and auditory neurons (Satoh and Fekete 2005; Bell et al. 2008). In mice, *Gata3* is expressed by neurons in both ganglia by the time they have separated at E12.5. However, within 1 day, it is rapidly downregulated in most vestibular ganglion neurons (Lawoko-Kerali et al. 2004; Lu et al. 2011). A severely reduced statoacoustic ganglion in *Gata3* mutants has been interpreted to mean that spiral ganglion neurons are selectively lost (Karis et al. 2001). Indeed, by delaying the knockout of *Gata3*, a persistent dependence of spiral ganglion neurons on this transcription factor was confirmed; *Gata3* is required for their differentiation, timing of axon outgrowth, and survival (Duncan et al. 2011; Luo et al. 2013). In the absence of *Gata3,* peripheral neurites sprout prematurely, meander excessively, and fail to form radial bundles while en route to the organ of Corti, perhaps because they arrive in advance of or are unable to respond to appropriate guidance cues (see Sect. 3.6.2; Appler et al. 2013). The number of ribbon synapses per inner hair cell is reduced by 50–70% (Yu et al. 2013). Gene expression profiling of *Gata3*-knockout spiral ganglia at E13.5 reveals a requirement for *Gata3* in upregulating the transcription factor *Mafb*. *Mafb* expression by spiral ganglion neurons is itself essential for the elaboration of the postsynaptic density associated with afferent innervation of hair cells at ribbon synapses (Yu et al. 2013). Thus, a cell autonomous defect in the postsynaptic partner, due primarily to the absence of *Mafb*, may explain why there are so few ribbons per inner hair cell after a delayed loss of *Gata3* in the neurons. This is

supported by a gene rescue experiment; restoration of *Mafb* (with an appropriate transgenic allele) in *Gata3*-knockout neurons restored about half of the missing ribbon synapses (Yu et al. 2013). Gene expression profiling also indicates that *Gata3* is required to reinforce the distinction of auditory versus vestibular ganglion neurons, at least for a small fraction of the genes that are differentially expressed across these two populations (Lu et al. 2011; Appler et al. 2013).

As it separates from the vestibular ganglion at E10.5, the spiral ganglion is encased in a sleeve of neural crest cells that also then pile up near the leading edge of the peripheral neurites at E12.5 (Sandell et al. 2014). Some of these cells associate with the spiral ganglion neurons as Schwann and satellite cells. The Schwann cells apparently provide a central stop signal because in their absence, the spiral ganglion neurons drift away from the sensory epithelium into the modiolus (Morris et al. 2006; Mao et al. 2014). An additional peripheral stop signal, mediated by Slit/Robo signaling, confines the neuronal soma to Rosenthal's canal and prevents them from scattering toward the sensory periphery after E14 (Wang et al. 2013). As development progresses, the spiral ganglion acquires its characteristic shape by elongating alongside the coiling cochlea.

3.6.2 Development of Afferent Innervation

An understanding of the cellular mechanisms underlying the development of cochlear afferent innervation has been explored for many years, both in vivo and in vitro. Evidence from a variety of studies suggests that the presence of hair cells, even ectopic ones, is sufficient to attract afferents, but hair cells are not strictly necessary for the spiral ganglion to send out processes that reach the sensory periphery (reviewed by Fritzsch et al. 2005b; Fekete and Campero 2007). The laboratory of Bernd Fritzsch championed the use of lipophilic fluorescent dyes in fixed specimens for track tracing of both afferent and efferent neurons into the embryonic mouse cochlea (Yang et al. 2011). Phenotyping a variety of mouse mutants with this technique has yielded a collection of genes that either indirectly (transcription factors) or directly (ligands and receptors) affect cochlear innervation patterns. Among the latter are the Ntrk2 and Ntrk3 receptors that bind to two key neurotrophins, brain-derived neurotrophic factor and neurotrophin-3. Although best known for their role in survival (Fritzsch et al. 2016), altering the time and place of their expression through genetic swaps has shown that these neurotrophins can also attract afferents (Tessarollo et al. 2004; Fritzsch et al. 2005a).

Recent work that has revealed additional molecular mechanisms guiding spiral ganglion neurites toward their final targets is summarized in Fig. 3.7 and has been expertly reviewed (Coate and Kelley 2013; Delacroix and Malgrange 2015). Timed induction of Cre recombination in a drug-inducible *Neurog1-CreER*^{T2} driver line permits a fraction of the neurons to be labeled in their entirety, yielding Golgi-like staining patterns. With this method, some spiral ganglion neurons are seen to possess bipolar morphologies by E12.5, with projections directed both centrally and

peripherally (Koundakjian et al. 2007). Peripheral neurites traverse through the mesenchyme toward the sensory epithelium and by E16.5, they are arranged in tight parallel bundles of 50–100 axons. This fasciculation requires *EphA4* expression in the mesenchyme, which is under the transcriptional control of *Pou3f4* (Coate et al. 2012). In the latter study, axonal fasciculation defects were observed in cochleae lacking *Pou3f4*, *EphA4*, or *Ephrin-B2* (the latter specifically absent from neurons). The same group used in vitro coculture assays to interfere with neuron-mesenchymal cell interactions by altering the levels of EphA4 or Ephrin-B2. In summary, the tight fasciculation into radial bundles probably serves to minimize repulsive interactions with surrounding mesenchymal cells, such as those mediated through Eph-to-Ephrin "reverse" signaling. Similarly disorganized radial bundles form in mice when neural crest-derived Schwann cells are missing due to targeted deletion of *Erbb2* or *Sox10* (Morris et al. 2006; Mao et al. 2014). In those mutants, it is unclear whether defasciculation is a direct consequence of the missing Schwann cells or whether it is because of the unusual distance between spiral ganglion cell bodies and their peripheral targets. The fasciculation defect found with *Gata3* conditional deletion (Appler et al. 2013) is likely to be due to intrinsic changes in the neurons.

In the next phase of outgrowth, peripheral processes reach the cochlear epithelium and send branches among the hair cells and supporting cells. Crossing the inducible *Neurog1-Cre* driver with mouse lines carrying floxed STOP fluorescent reporters brings a temporal dimension to the analysis because it allows for time-lapse imaging of neurites as they navigate within the sensory epithelium. This has provided a new appreciation of how active, complex, and transient individual axonal branches are as they explore, retract, and then stabilize their connections (Coate et al. 2015; Druckenbrod and Goodrich 2015). Initially in rodents, both type I and type II afferents project beyond the inner hair cell row, cross the tunnel, and travel among immature outer hair cells. By postnatal week (P) 0, type II afferents are spiraling longitudinally between the outer hair cell rows, having first crossed closer to the floor of the tunnel of Corti compared with the presumed type I afferents (Druckenbrod and Goodrich 2015). In mature ears, type II processes invariably turn toward the base (except in the apical turn), travel a long distance, and then build large terminals onto multiple outer hair cells (Nayagam et al. 2011). In contrast, each mature type I radial process will terminate with a simple ending that synapses exclusively with a single inner hair cell (Nayagam et al. 2011). But before this happens, type I neurons enjoy an exploratory phase with clawlike branches that contact a range of cell types on either side of the tunnel of Corti, including outer hair cells (Druckenbrod and Goodrich 2015).

During the first postnatal week in mice, outer hair cells express numerous puncta of presynaptic ribbon components, composed of Ribeye protein that is immunolabeled with Ctbp2 antibodies (Huang et al. 2012). These puncta have been interpreted as evidence of transient synapses between type I neurons and outer hair cells because they mostly disappear by P6, and this coincides with the full retraction of type I projections from the outer hair cell domain (Huang et al. 2012).

The remaining puncta on P6 may represent stabilized synapses with type II terminals. However, the presence of transient functional synapses between type I neurons and outer hair cells is still unresolved. First, only 14% and 9% of radial (possible type I) terminals are located among the outer hair cells on P0 and P3, respectively, and these almost never project past the first row of outer hair cells (Druckenbrod and Goodrich 2015), whereas the Ribeye puncta are present in all three rows (Huang et al. 2012). Second, on E18.5, the presumed type I processes are highly motile and individual branches frequently and rapidly undergo retractive movements when exploring the outer hair cell domain (Druckenbrod and Goodrich 2015). These retractions are likely to be a response to repulsive cues. Indeed, the perinatal outer hair cell region expresses two known axon repellents: secreted Semaphorin-3F and membrane-bound Ephrin-A5 (Defourny et al. 2013; Coate et al. 2015). It is assumed that the Ephrin-A5 ligand on the outer hair cells interacts with the EphA4 receptor expressed by a subset of type I neurites through "forward" signaling (as compared with the earlier role of EphA4-to-EphrinB2 reverse signaling from mesenchymal cells to these same neurites). The presence of these repellents offers a mechanism for why type I afferents fail to find permanent purchase among outer hair cells. This interpretation is bolstered by the phenotypes seen in mutants lacking these repellents or their receptors; an excess of afferent fibers mingles among outer hair cells after the critical period when type I processes should have become restricted to inner hair cells (Defourny et al. 2013; Coate et al. 2015). The Ephrin and Semaphorin repellents may be partially redundant, with Ephrin being more robust, because *Neuropilin2* mutants have only a mild excess of presumed type I projections into the outer hair cell region on E16.5 and this phenotype does not persist postnatally (Coate et al. 2015).

Why are the type II neurons not also subject to repulsion by Semaphorin-3F and Ephrin-A5? In part, this is probably because they do not express the EphA4 receptor thought to bind Ephrin-A5 (Defourny et al. 2013). However, type II neurites do express Neuropilin2, the presumed Semaphorin-3F receptor (Coate et al. 2015). It is possible that type II fibers outcompete type I fibers for outer hair cell targets because they find the environment less repulsive.

Additional repulsive, permissive, or attractive cues may guide the type II cochlear afferents. The search for transcriptional regulators of type II guidance cues could begin with Prox1, which is present at the right time and place to regulate the expression of axon guidance molecules both in the outer hair cell domain and in the type II neurons that project there. By birth, type II spiral fibers lacking *Prox1* fail to form tight bundles between Deiters cells, their projections are disorganized, and many axons turn toward the apex instead of toward the base (Fritzsch et al. 2010). This misguidance must be cell autonomous to the type II neurons because it is evident even when the outer hair cell domain (but not the spiral ganglion neurons) has normal *Prox1* gene expression. An analysis of the genes misregulated in the organ of Corti versus the spiral ganglion of *Prox1* mutants may identify the relevant guidance factors and receptors, respectively.

3.6.3 Development of Efferent Innervation

In mammals, efferent axons that project into the cochlea originate from two separate pools of neurons in the brainstem called the medial olivocochlear and the lateral olivocochlear neurons (Brown 2011). In the mature cochlea, these pools maintain separate projections on each side of the tunnel of Corti: medial olivocochlear neurons target outer hair cells and lateral olivocochlear neurons target the terminals of type I afferents beneath inner hair cells. However, during development, a more promiscuous phase of synaptic connections is seen for the medial olivocochlear efferents, as discussed in the following paragraph (Fig. 3.7).

Relatively little is known about the molecules guiding cochlear efferent axons from the periolivary complex in the brainstem through the VIIIth cranial nerve and into the organ of Corti. Efferent neurons express *Gata3* and in its absence on E12.5 in the mouse, they show midline-crossing defects and their axons are misrouted into the facial nerve (Karis et al. 2001). It is generally assumed that efferent axons track along the VIIIth nerve to reach the cochlea (Ma et al. 2000; Huang et al. 2001), with the pioneers arriving at the spiral ganglion by E12.5 (Fritzsch and Nichols 1993). After passing through the ganglion, at least some efferent fibers depart from afferents to create the intraganglionic spiral bundle at the periphery of the ganglion. The formation of this spiral bundle requires the presence and normal localization of the spiral ganglion cell bodies (Kim et al. 2001; Morris et al. 2006). Efferent fibers then travel along the afferent radial bundles to reach the organ of Corti by E16.5 (Simmons et al. 2011).

The first two weeks after birth are a period of synaptic plasticity in the cochlea; some synapses are retracting as others are consolidating (Pujol et al. 1998; Katz and Elgoyhen 2014). Most notable are transient axosomatic contacts between medial olivocochlear efferent fibers and inner hair cells observed from birth to postnatal day 14 (Simmons 2002). The final targets for medial olivocochlear fibers are not inner but outer hair cells, which they contact via large axosomatic terminals. As the medial olivocochlear efferents depart from the inner hair cells, they are replaced by afferents. Finally, late-arriving lateral olivocochlear efferents make small axodendritic synapses onto type I afferents beneath inner hair cells. Interestingly, functional synapses between inner hair cells and medial olivocochlear axons can reappear in aging cochleae concomitant with the loss of outer hair cells and of the afferent innervation of inner hair cells (Lauer et al. 2012; Zachary and Fuchs 2015).

3.6.4 Unresolved Questions in Afferent and Efferent Innervation of the Cochlea

Time-lapse imaging of cochlear afferents in the early postnatal period may help to resolve the question of whether type I neurites stop exploring long enough to form synapses with outer hair cells. If so, physiological recordings are necessary to

determine if any of these transient synapses are functional. There are still many unknown aspects of type II pathfinding within the cochlea, including what molecular mechanisms instruct them to make a characteristic sharp turn as they reach the outer hair cells or why they spiral basally for 100–200 μm before establishing synapses with a cluster of outer hair cells. The development of the cochlear efferents is also in need of further study. Selective and temporal deletion of *Gata3* in the efferent neurons, followed by transcriptomic analysis of the mutant cells, may be a fruitful strategy to catalog and then test potential guidance factors that direct these neurons through their complex trajectories to reach first their transient targets and then their final targets.

3.7 Concluding Thoughts

This chapter has summarized recent research on cochlear development. Although this review may appear to focus excessively on the organ of Corti, this is a fair reflection of the focus of research on the functional sensory tissue, with far fewer development studies devoted to nonsensory regions. This final section considers a few other aspects of cochlear development that have received less attention and suggests that some of these areas are ripe for investigation in the future.

3.7.1 How Does the Cochlea Grow and Coil?

The first area in which research on nonsensory areas of the cochlea has lagged behind studies of the development of the organ of Corti is, ironically, the development of the coiled shape that gives the cochlea its name (see Manley, Chap. 2). Others have described how the planar cell polarity pathway regulates cell rearrangements of convergent extension and radial intercalation that thin the prosensory domain into an array of hair cells and supporting cells (Ezan and Montcouquiol 2013). Although this extension clearly contributes to the thinning and lengthening of the prosensory domain and organ of Corti (Chacon-Heszele and Chen 2009), it is unlikely to be the only mechanism involved in cochlear outgrowth and coiling. Indeed, the wide range of cochlear lengths and morphologies seen across mammals and differences in cochlear dimensions, volumes, and thickness of the basilar membrane (Ekdale 2015) suggest that cochlear cell shape, cell division, and cell polarity are likely to be regulated at many levels and by many gene regulatory networks. At present, the field lacks even basic quantitative measurements of how the cochlea grows out from the otocyst and undergoes coiling. The ability to localize fluorescent proteins to cell nuclei and membranes in a cell- and tissue-specific manner, however, together with recent advances in high-resolution imaging of large volumes of cleared tissue samples (Kopecky et al. 2012) suggest that it will be possible to develop a complete picture of cochlear growth and coiling,

at least in mice. The large number of mouse mutants in which the shape and length of the cochlear duct are altered offers a rich resource that can be combined with imaging technology to understand the cellular and genetic regulation of cochlear morphology.

The epithelium of the mature cochlear duct is suspended between two chambers, the scala vestibuli and scala tympani. These contain the perilymph fluid responsible for conduction of sound waves along the cochlear duct. These two chambers are carved out of the mesenchyme surrounding the cochlear duct through the local death or dispersion of mesenchymal cells. Interestingly, this process proceeds from base to apex with approximately the same timing as the differentiation of the organ of Corti (Kopecky et al. 2012). It is tempting to speculate that signals regulating the basal-apical gradient of differentiation in the cochlea, such as Shh, may also regulate the behavior of the surrounding mesenchyme, although there are a variety of other signals exchanged between the otic epithelium and mesenchyme that may also affect mesenchymal cell behavior and transcription.

3.7.2 *Reissner's Membrane and the Stria Vascularis: The Importance of Nonsensory Cochlear Development*

The perilymph of the scala vestibuli is separated from the endolymph of the scala media of the cochlea by Reissner's membrane. This delicate membrane is composed of two cell populations: one derived from a single layer of cochlear epithelium and the other from two layers of periotic mesenchymal cells (Slepecky 1996). As expected from a membrane that separates two extracellular fluid compartments of very different ionic compositions, the cells of the mature Reissner's membrane express a variety of different ion channels and exchangers (Lang et al. 2007). The epithelial cells of Reissner's membrane are derived from *Otx1*- and *Otx2*-expressing cells in the ventrolateral region of the otocyst that will contribute to the roof of the cochlear duct (Wu and Kelley 2012; Vendrell et al. 2015). Conditional mutants of *Otx2* completely lack Reissner's membrane, with an ectopic prosensory region and organ of Corti developing in its place (Vendrell et al. 2015). The association between the epithelial and mesenchymal layers of Reissner's membrane is promoted by Fgf9 expressed in nonsensory otic epithelium. This source of Fgf signaling is necessary for the correct formation of Reissner's membrane because *Fgf9*-mutant mice have disorganized mesenchymal cells loosely attached to the epithelial layer (Pirvola et al. 2004). Reissner's membrane is also missing in *Fgf10*-mutant mice (Urness et al. 2015). However, there are very few other studies that have investigated the process that leads to the thinning of the epithelium of Reissner's membrane and the development of the association between its epithelial and mesenchymal cell layers.

The development and morphology of Reissner's membrane can also be affected indirectly by defects in the development and composition of endolymph fluid (e.g., Somma et al. 2012), which is regulated by another component of the cochlear duct, the stria vascularis (see Wangemann and Marcus, Chap. 9). Like Reissner's membrane, different components of the stria vascularis are derived from several embryonic sources. The marginal cells that line the wall of the cochlear duct and contact the endolymph are derived from the cochlear epithelium (Ohyama and Groves 2004). The pigmented intermediate cell layer is derived from migrating cranial neural crest cells that differentiate into melanocyte-like cells (Steel and Barkway 1989). Fibrocytes of the mesenchymal spiral ligament form a basal layer that interdigitates with marginal and intermediate cells (Spicer and Schulte 1991). These three cell populations are invaded by a dense network of capillaries that give the stria vascularis its name. Although genes have been identified that influence the development of particular components of the stria, little is known about the developmental events that orchestrate the integration of these different cell types. For example, several transcription factors such as *Tbx18, Sox9*, and *Pou3f4* are expressed in the periotic mesenchyme and later in the basal cells of the stria, and mutation of these genes all cause strial defects. As expected, genes involved in the differentiation of neural crest melanocytes (such as *Pax3, Sox10*, and *c-kit*, whose mutation causes Waardenburg syndrome) can also affect the formation and function of the stria vascularis (e.g., Kim et al. 2014). The orphan nuclear receptor *estrogen-related receptor β/Nr3b2* is expressed in the developing marginal cells of the stria, and conditional mutants of this gene cause severe cochlear defects, including collapse of Reissner's membrane and the loss of multiple ion channels and transporters from the marginal cells (Chen and Nathans 2007). These mutants also have secondary defects in the adjacent capillaries and marginal cells. Given the importance of the stria vascularis in the formation and maintenance of the endolymph and the role of strial degeneration in age-related hearing loss, understanding how the different cells of the stria develop and integrate with each other requires continued scrutiny.

Highlighting the developmental plasticity of the cochlear epithelium is evidence that the anlagen of the stria vascularis and Reissner's membrane have at least a transient ability to form ectopic prosensory tissue and an ectopic organ of Corti containing hair cells and supporting cells. This is suggested by results from gain-of-function experiments where *Sox2* or the active intracellular domain of the Notch1 receptor are overexpressed in the otocyst (Pan et al. 2010, 2013). Moreover, *Otx2* conditional mutants also have ectopic prosensory/hair cell-containing regions in place of Reissner's membrane (Vendrell et al. 2015). It will be of interest to carefully map the duration for which the progenitors for these two structures remain competent to differentiate into sensory tissue and to determine whether the mechanism of this competence involves the upregulation of *Sox2* to act as a multipotency or proneural factor (Raft and Groves 2015).

3.7.3 *Postmitotic Maturation of the Organ of Corti*

As can be seen from the preceding sections, current research on cochlear development tends to focus on the events that regulate the pattern and orientation of hair cells and supporting cells in the organ of Corti. However, once the numbers and disposition of cells in the organ of Corti have been fixed and before the onset of hearing, both hair cells and supporting cells undergo a period of morphological and functional maturation, which in mice encompasses a two-week period after birth. In the case of the inner and outer hair cells, much of this maturation centers on the development and growth of their stereociliary bundles and the expression of protein complexes and ion channels that will support mechanotransduction and synaptic transmission (Schwander et al. 2010). The morphological maturation of supporting cells has received much less attention, which is somewhat surprising given the extraordinary changes in cell morphology exhibited by these cells. Pillar cells and Deiters cells elongate dense actin-rich processes and produce large phalangeal processes at their apical extremity. These interconnect with the apical surfaces of hair cells to form the reticular lamina of the organ of Corti. With the exception of some of the adhesion molecules that organize the apical surfaces of hair cells and supporting cells (Togashi et al. 2011), very little is known about the molecular composition of these specialized support structures. As discussed in Sect. 3.6, the observation of plasticity between pillar cell and Deiters cell phenotypes in the postnatal mouse (Shim et al. 2005; Mansour et al. 2013) suggests that the mature phenotype of these cells may be maintained in the adult through ongoing signaling. Understanding the signals and transcriptional effectors that drive and maintain the differentiated state of hair cells and supporting cells is highly relevant to the questions relating to the inherent regenerative capacity of the organ of Corti. However, the small amount of tissue that can be isolated from the organ of Corti has made biochemical analysis of mature hair and supporting cell specializations difficult, although recent success in using mass spectrometry to identify components of stereociliary bundles (Shin et al. 2013) suggests that it may also be possible to apply these techniques to the reticular lamina if a suitable method of isolating it can be found.

Acknowledgements We dedicate this chapter to the memory of Julian Lewis (1946–2014), a visionary scientist whose hypothesis about the role of Notch signaling in patterning the cochlea was just one of his many contributions to the field of developmental biology.

Compliance with Ethics Requirements Andrew K. Groves declares that he has no conflict of interest. Donna M. Fekete declares that she has no conflict of interest.

References

Abello, G., & Alsina, B. (2007). Establishment of a proneural field in the inner ear. *International Journal of Developmental Biology,* 51(6–7), 483–493.

Abello, G., Khatri, S., Giraldez, F., & Alsina, B. (2007). Early regionalization of the otic placode and its regulation by the Notch signaling pathway. *Mechanisms of Development,* 124(7–8), 631–645.

Alsina, B., Abello, G., Ulloa, E., Henrique, D., Pujades, C., & Giraldez, F. (2004). FGF signaling is required for determination of otic neuroblasts in the chick embryo. *Developmental Biology,* 267(1), 119–134.

Appler, J. M., & Goodrich, L. V. (2011). Connecting the ear to the brain: Molecular mechanisms of auditory circuit assembly. *Progress in Neurobiology,* 93(4), 488–508.

Appler, J. M., Lu, C. C., Druckenbrod, N. R., Yu, W. M., Koundakjian, E. J., & Goodrich, L. V. (2013). Gata3 is a critical regulator of cochlear wiring. *The Journal of Neuroscience,* 33(8), 3679–3691.

Artavanis-Tsakonas, S., & Muskavitch, M. A. (2010). Notch: the past, the present, and the future. *Current Topics in Developmental Biology,* 92, 1–29.

Basch, M. L., Ohyama, T., Segil, N., & Groves, A. K. (2011). Canonical Notch signaling is not necessary for prosensory induction in the mouse cochlea: Insights from a conditional mutant of RBPjκ. *The Journal of Neuroscience,* 31(22), 8046–8058.

Basch, M. L., Brown, R. M., II, Jen, H. I., & Groves, A. K. (2016). Where hearing starts: The development of the mammalian cochlea. *Journal of Anatomy,* 228(2), 233–254.

Bell, D., Streit, A., Gorospe, I., Varela-Nieto, I., Alsina, B., & Giraldez, F. (2008). Spatial and temporal segregation of auditory and vestibular neurons in the otic placode. *Developmental Biology,* 322(1), 109–120.

Benito-Gonzalez, A., & Doetzlhofer, A. (2014). Hey1 and Hey2 control the spatial and temporal pattern of mammalian auditory hair cell differentiation downstream of Hedgehog signaling. *The Journal of Neuroscience,* 34(38), 12865–12876.

Bermingham-McDonogh, O., Oesterle, E. C., Stone, J. S., Hume, C. R., Huynh, H. M., & Hayashi, T. (2006). Expression of Prox1 during mouse cochlear development. *The Journal of Comparative Neurology,* 496(2), 172–186.

Bok, J., Bronner-Fraser, M., & Wu, D. K. (2005). Role of the hindbrain in dorsoventral but not anteroposterior axial specification of the inner ear. *Development,* 132(9), 2115–2124.

Bok, J., Dolson, D. K., Hill, P., Ruther, U., Epstein, D. J., & Wu, D. K. (2007). Opposing gradients of Gli repressor and activators mediate Shh signaling along the dorsoventral axis of the inner ear. *Development,* 134(9), 1713–1722.

Bok, J., Raft, S., Kong, K. A., Koo, S. K., Drager, U. C., & Wu, D. K. (2011). Transient retinoic acid signaling confers anterior-posterior polarity to the inner ear. *Proceedings of the National Academy of Sciences of the United States of America,* 108(1), 161–166.

Bok, J., Zenczak, C., Hwang, C. H., & Wu, D. K. (2013). Auditory ganglion source of Sonic hedgehog regulates timing of cell cycle exit and differentiation of mammalian cochlear hair cells. *Proceedings of the National Academy of Sciences of the United States of America,* 110 (34), 13869–13874.

Brooker, R., Hozumi, K., & Lewis, J. (2006). Notch ligands with contrasting functions: Jagged1 and Delta1 in the mouse inner ear. *Development,* 133(7), 1277–1286.

Brown, A. S., & Epstein, D. J. (2011). Otic ablation of smoothened reveals direct and indirect requirements for Hedgehog signaling in inner ear development. *Development,* 138(18), 3967–3976.

Brown, A. S., Rakowiecki, S. M., Li, J. Y., & Epstein, D. J. (2015). The cochlear sensory epithelium derives from Wnt responsive cells in the dorsomedial otic cup. *Developmental Biology,* 399(1), 177–187.

Brown, M. C. (2011). Anatomy of olivocochlear neurons. In D. K. Ryugo, R. R. Fay, & A. N. Popper (Eds.), *Auditory and Vestibular Efferents* (pp. 17–37). New York: Springer-Verlag.

Burns, J. C., On, D., Baker, W., Collado, M. S., & Corwin, J. T. (2012). Over half the hair cells in the mouse utricle first appear after birth, with significant numbers originating from early postnatal mitotic production in peripheral and striolar growth zones. *Journal of the Association for Research in Otolaryngology*, 13(5), 609–627.

Burns, J. C., Kelly, M. C., Hoa, M., Morell, R. J., & Kelley, M. W. (2015). Single-cell RNA-Seq resolves cellular complexity in sensory organs from the neonatal inner ear. *Nature Communications,* 6, 8557.

Burton, Q., Cole, L. K., Mulheisen, M., Chang, W., & Wu, D. K. (2004). The role of Pax2 in mouse inner ear development. *Developmental Biology,* 272(1), 161–175.

Cai, T., & Groves, A. K. (2014). The role of atonal factors in mechanosensory cell specification and function. *Molecular Neurobiology*, 52(3), 1315–1329.

Cai, T., Seymour, M. L., Zhang, H., Pereira, F. A., & Groves, A. K. (2013). Conditional deletion of Atoh1 reveals distinct critical periods for survival and function of hair cells in the organ of Corti. *The Journal of Neuroscience,* 33(24), 10110–10122.

Chacon-Heszele, M. F., & Chen, P. (2009). Mouse models for dissecting vertebrate planar cell polarity signaling in the inner ear. *Brain Research,* 1277, 130–140.

Chen, J., & Nathans, J. (2007). Estrogen-related receptor β/NR3B2 controls epithelial cell fate and endolymph production by the stria vascularis. *Developmental Cell,* 13(3), 325–337.

Chen, P., & Segil, N. (1999). p27(Kip1) links cell proliferation to morphogenesis in the developing organ of Corti. *Development,* 126(8), 1581–1590.

Coate, T. M., & Kelley, M. W. (2013). Making connections in the inner ear: Recent insights into the development of spiral ganglion neurons and their connectivity with sensory hair cells. *Seminars in Cell and Developmental Biology,* 24(5), 460–469.

Coate, T. M., Raft, S., Zhao, X., Ryan, A. K., Crenshaw, E. B., III, & Kelley, M. W. (2012). Otic mesenchyme cells regulate spiral ganglion axon fasciculation through a Pou3f4/EphA4 signaling pathway. *Neuron,* 73(1), 49–63.

Coate, T. M., Spita, N. A., Zhang, K. D., Isgrig, K. T., & Kelley, M. W. (2015). Neuropilin-2/Semaphorin-3F-mediated repulsion promotes inner hair cell innervation by spiral ganglion neurons. *eLife,* 4, e07830.

Cohen, M., Briscoe, J., & Blassberg, R. (2013). Morphogen interpretation: The transcriptional logic of neural tube patterning. *Current Opinion in Genetics and Development,* 23(4), 423–428.

Defourny, J., Poirrier, A. L., Lallemend, F., Mateo Sanchez, S., Neef, J., Vanderhaeghen, P., Soriano, E., Peuckert, C., Kullander, K., Fritzsch, B., Nguyen, L., Moonen, G., Moser, T., & Malgrange, B. (2013). Ephrin-A5/EphA4 signalling controls specific afferent targeting to cochlear hair cells. *Nature Communications,* 4, 1438.

Delacroix, L., & Malgrange, B. (2015). Cochlear afferent innervation development. *Hearing Research,* 330(Pt B), 157–169.

Deng, M., Yang, H., Xie, X., Liang, G., & Gan, L. (2014). Comparative expression analysis of POU4F1, POU4F2 and ISL1 in developing mouse cochleovestibular ganglion neurons. *Gene Expression Patterns,* 15(1), 31–37.

Doetzlhofer, A., Basch, M. L., Ohyama, T., Gessler, M., Groves, A. K., & Segil, N. (2009). Hey2 regulation by FGF provides a Notch-independent mechanism for maintaining pillar cell fate in the organ of Corti. *Developmental Cell,* 16(1), 58–69.

Driver, E. C., Pryor, S. P., Hill, P., Turner, J., Ruther, U., Biesecker, L. G., Griffith, A. J., & Kelley, M. W. (2008). Hedgehog signaling regulates sensory cell formation and auditory function in mice and humans. *The Journal of Neuroscience,* 28(29), 7350–7358.

Druckenbrod, N. R., & Goodrich, L. V. (2015). Sequential retraction segregates SGN processes during target selection in the cochlea. *The Journal of Neuroscience,* 35(49), 16221–16235.

D'Souza, B., Meloty-Kapella, L., & Weinmaster, G. (2010). Canonical and non-canonical Notch ligands. *Current Topics in Developmental Biology,* 92, 73–129.

Duncan, J. S., Lim, K. C., Engel, J. D., & Fritzsch, B. (2011). Limited inner ear morphogenesis and neurosensory development are possible in the absence of GATA3. *International Journal of Developmental Biology,* 55(3), 297–303.

Durruthy-Durruthy, R., Gottlieb, A., Hartman, B. H., Waldhaus, J., Laske, R. D., Altman, R., & Heller, S. (2014). Reconstruction of the mouse otocyst and early neuroblast lineage at single-cell resolution. *Cell,* 157(4), 964–978.

Ekdale, E. G. (2015). Form and function of the mammalian inner ear. *Journal of Anatomy*, 228(2), 324–337.

Evsen, L., Sugahara, S., Uchikawa, M., Kondoh, H., & Wu, D. K. (2013). Progression of neurogenesis in the inner ear requires inhibition of Sox2 transcription by neurogenin1 and neurod1. *The Journal of Neuroscience,* 33(9), 3879–3890.

Ezan, J., & Montcouquiol, M. (2013). Revisiting planar cell polarity in the inner ear. *Seminars in Cell and Developmental Biology,* 24(5), 499–506.

Fekete, D. M., & Campero, A. M. (2007). Axon guidance in the inner ear. *International Journal of Developmental Biology,* 51(6–7), 549–556.

Fritzsch, B., & Nichols, D. H. (1993). DiI reveals a prenatal arrival of efferents at the differentiating otocyst of mice. *Hearing Research,* 65(1–2), 51–60.

Fritzsch, B., Pauley, S., Matei, V., Katz, D. M., Xiang, M., & Tessarollo, L. (2005a). Mutant mice reveal the molecular and cellular basis for specific sensory connections to inner ear epithelia and primary nuclei of the brain. *Hearing Research,* 206(1–2), 52–63.

Fritzsch, B., Matei, V. A., Nichols, D. H., Bermingham, N., Jones, K., Beisel, K. W., & Wang, V. Y. (2005b). Atoh1 null mice show directed afferent fiber growth to undifferentiated ear sensory epithelia followed by incomplete fiber retention. *Developmental Dynamics,* 233(2), 570–583.

Fritzsch, B., Dillard, M., Lavado, A., Harvey, N. L., & Jahan, I. (2010). Canal cristae growth and fiber extension to the outer hair cells of the mouse ear require Prox1 activity. *PLoS ONE,* 5(2), e9377.

Fritzsch, B., Pan, N., Jahan, I., Duncan, J. S., Kopecky, B. J., Elliott, K. L., Kersigo, J., & Yang, T. (2013). Evolution and development of the tetrapod auditory system: An organ of Corti-centric perspective. *Evolution and Development,* 15(1), 63–79.

Fritzsch, B., Kersigo, J., Yang, T., Jahan, I., & Pan, N. (2016). Neurotrophic factor function during ear development: Expression changes define critical phases for neuronal viability. In A. Dabdoub, B. Fritzsch, A. N. Popper, & R. R. Fay (Eds.), *The Primary Auditory Neurons of the Mammalian Cochlea* (pp. 49–84). New York: Springer.

Golden, E. J., Benito-Gonzalez, A., & Doetzlhofer, A. (2015). The RNA-binding protein LIN28B regulates developmental timing in the mammalian cochlea. *Proceedings of the National Academy of Sciences of the United States of America,* 112(29), E3864–E3873.

Goodrich, L. V. (2016). Early development of the spiral ganglion. In A. Dabdoub, B. Fritzsch, A. N. Popper, & R. R. Fay (Eds.), *The Primary Auditory Neurons of the Mammalian Cochlea* (pp. 11–48). New York: Springer.

Goodyear, R., & Richardson, G. (1997). Pattern formation in the basilar papilla: Evidence for cell rearrangement. *The Journal of Neuroscience,* 17(16), 6289–6301.

Goodyear, R., Holley, M., & Richardson, G. (1995). Hair and supporting-cell differentiation during the development of the avian inner ear. *The Journal of Comparative Neurology,* 351(1), 81–93.

Groves, A. K., & Fekete, D. M. (2012). Shaping sound in space: The regulation of inner ear patterning. *Development,* 139(2), 245–257.

Huang, E. J., Liu, W., Fritzsch, B., Bianchi, L. M., Reichardt, L. F., & Xiang, M. (2001). Brn3a is a transcriptional regulator of soma size, target field innervation and axon pathfinding of inner ear sensory neurons. *Development,* 128(13), 2421–2432.

Huang, L.-C., Barclay, M., Lee, K., Peter, S., Housley, G. D., Thorne, P. R., & Montgomery, J. M. (2012). Synaptic profiles during neurite extension, refinement and retraction in the developing cochlea. *Neural Development,* 7, 38.

Huh, S. H., Jones, J., Warchol, M. E., & Ornitz, D. M. (2012). Differentiation of the lateral compartment of the cochlea requires a temporally restricted FGF20 signal. *PLoS Biology,* 10 (1), e1001231.

Jacques, B. E., Montcouquiol, M. E., Layman, E. M., Lewandoski, M., & Kelley, M. W. (2007). Fgf8 induces pillar cell fate and regulates cellular patterning in the mammalian cochlea. *Development,* 134(16), 3021–3029.

Jacques, B. E., Puligilla, C., Weichert, R. M., Ferrer-Vaquer, A., Hadjantonakis, A. K., Kelley, M. W., & Dabdoub, A. (2012). A dual function for canonical Wnt/β-catenin signaling in the developing mammalian cochlea. *Development,* 139(23), 4395–4404.

Jacques, B. E., Montgomery, W. H., 4th, Uribe, P. M., Yatteau, A., Asuncion, J. D., Resendiz, G., Matsui, J. I., & Dabdoub, A. (2014). The role of Wnt/β-catenin signaling in proliferation and regeneration of the developing basilar papilla and lateral line. *Developmental Neurobiology,* 74 (4), 438–456.

Jahan, I., Pan, N., Kersigo, J., & Fritzsch, B. (2010). Neurod1 suppresses hair cell differentiation in ear ganglia and regulates hair cell subtype development in the cochlea. *PLoS ONE,* 5(7), e11661.

Jayasena, C. S., Ohyama, T., Segil, N., & Groves, A. K. (2008). Notch signaling augments the canonical Wnt pathway to specify the size of the otic placode. *Development,* 135(13), 2251–2261.

Karis, A., Pata, I., van Doorninck, J. H., Grosveld, F., de Zeeuw, C. I., de Caprona, D., & Fritzsch, B. (2001). Transcription factor GATA-3 alters pathway selection of olivocochlear neurons and affects morphogenesis of the ear. *The Journal of Comparative Neurology,* 429(4), 615–630.

Katayama, A., & Corwin, J. T. (1989). Cell production in the chicken cochlea. *The Journal of Comparative Neurology,* 281(1), 129–135.

Katz, E., & Elgoyhen, A. B. (2014). Short-term plasticity and modulation of synaptic transmission at mammalian inhibitory cholinergic olivocochlear synapses. *Frontiers in Systems Neuroscience,* 8, 224.

Kelley, M. W. (2006). Regulation of cell fate in the sensory epithelia of the inner ear. *Nature Reviews: Neuroscience,* 7(11), 837–849.

Kelley, M. W. (2007). Cellular commitment and differentiation in the organ of Corti. *International Journal of Developmental Biology,* 51(6–7), 571–583.

Kelley, M. W., Wu, D. K., Popper, A. N., & Fay, R. R. (Eds.). (2005). *Development of the Inner Ear.* New York: Springer-Verlag.

Kiernan, A. E. (2013). Notch signaling during cell fate determination in the inner ear. *Seminars in Cell and Developmental Biology,* 24(5), 470–479.

Kiernan, A. E., Pelling, A. L., Leung, K. K., Tang, A. S., Bell, D. M., Tease, C., Lovell-Badge, R., Steel, K. P., & Cheah, K. S. (2005a). Sox2 is required for sensory organ development in the mammalian inner ear. *Nature,* 434(7036), 1031–1035.

Kiernan, A. E., Cordes, R., Kopan, R., Gossler, A., & Gridley, T. (2005b). The Notch ligands DLL1 and JAG2 act synergistically to regulate hair cell development in the mammalian inner ear. *Development,* 132(19), 4353–4362.

Kiernan, A. E., Xu, J., & Gridley, T. (2006). The Notch ligand JAG1 is required for sensory progenitor development in the mammalian inner ear. *PLoS Genetics, 2*(1), e4.

Kim, H., Ankamreddy, H., Lee, D. J., Kong, K. A., Ko, H. W., Kim, M. H., & Bok, J. (2014). Pax3 function is required specifically for inner ear structures with melanogenic fates. *Biochemical and Biophysical Research Communications,* 445(3), 608–614.

Kim, W. Y., Fritzsch, B., Serls, A., Bakel, L. A., Huang, E. J., Reichardt, L. F., Barth, D. S., & Lee, J. E. (2001). NeuroD-null mice are deaf due to a severe loss of the inner ear sensory neurons during development. *Development,* 128(3), 417–426.

Kirkegaard, M., & Nyengaard, J. R. (2005). Stereological study of postnatal development in the mouse utricular macula. *The Journal of Comparative Neurology,* 492(2), 132–144.

Koo, S. K., Hill, J. K., Hwang, C. H., Lin, Z. S., Millen, K. J., & Wu, D. K. (2009). Lmx1a maintains proper neurogenic, sensory, and non-sensory domains in the mammalian inner ear. *Developmental Biology,* 333(1), 14–25.

Kopecky, B., Johnson, S., Schmitz, H., Santi, P., & Fritzsch, B. (2012). Scanning thin-sheet laser imaging microscopy elucidates details on mouse ear development. *Developmental Dynamics,* 241(3), 465–480.

Koundakjian, E. J., Appler, J. L., & Goodrich, L. V. (2007). Auditory neurons make stereotyped wiring decisions before maturation of their targets. *The Journal of Neuroscience,* 27(51), 14078–14088.

Kruger, M., Schmid, T., Kruger, S., Bober, E., & Braun, T. (2006). Functional redundancy of NSCL-1 and NeuroD during development of the petrosal and vestibulocochlear ganglia. *European Journal of Neuroscience,* 24(6), 1581–1590.

Ladhams, A., & Pickles, J. O. (1996). Morphology of the monotreme organ of Corti and macula lagena. *The Journal of Comparative Neurology,* 366(2), 335–347.

Lang, F., Vallon, V., Knipper, M., & Wangemann, P. (2007). Functional significance of channels and transporters expressed in the inner ear and kidney. *American Journal of Physiology - Cell Physiology,* 293(4), C1187–C1208.

Lauer, A. M., Fuchs, P. A., Ryugo, D. K., & Francis, H. W. (2012). Efferent synapses return to inner hair cells in the aging cochlea. *Neurobiology of Aging,* 33(12), 2892–2902.

Lawoko-Kerali, G., Rivolta, M. N., Lawlor, P., Cacciabue-Rivolta, D. I., Langton-Hewer, C., van Doorninck, J. H., & Holley, M. C. (2004). GATA3 and NeuroD distinguish auditory and vestibular neurons during development of the mammalian inner ear. *Mechanisms of Development,* 121(3), 287–299.

Lee, Y. S., Liu, F., & Segil, N. (2006). A morphogenetic wave of p 27Kip1 transcription directs cell cycle exit during organ of Corti development. *Development,* 133(15), 2817–2826.

Lewis, J. (1991). Rules for the production of sensory cells. *Ciba Foundation Symposium,* 160, 25–39; discussion 40–53.

Liu, H., Pecka, J. L., Zhang, Q., Soukup, G. A., Beisel, K. W., & He, D. Z. (2014). Characterization of transcriptomes of cochlear inner and outer hair cells. *The Journal of Neuroscience,* 34(33), 11085–11095.

Liu, M., Pereira, F. A., Price, S. D., Chu, M. J., Shope, C., Himes, D., Eatock, R. A., Brownell, W. E., Lysakowski, A., & Tsai, M. J. (2000). Essential role of *BETA2/NeuroD1* in development of the vestibular and auditory systems. *Genes and Development,* 14(22), 2839–2854.

Liu, Z., Owen, T., Zhang, L., & Zuo, J. (2010). Dynamic expression pattern of Sonic hedgehog in developing cochlear spiral ganglion neurons. *Developmental Dynamics,* 239(6), 1674–1683.

Lorenzen, S. M., Duggan, A., Osipovich, A. B., Magnuson, M. A., & Garcia Añoveros, J. (2015). Insm1 promotes neurogenic proliferation in delaminated otic progenitors. *Mechanisms of Development,* 138(Pt 3), 233–245.

Lowenheim, H., Furness, D. N., Kil, J., Zinn, C., Gultig, K., Fero, M. L., Frost, D., Gummer, A. W., Roberts, J. M., Rubel, E. W, Hackney, C. M., & Zenner, H. P. (1999). Gene disruption of p 27(Kip1) allows cell proliferation in the postnatal and adult organ of Corti. *Proceedings of the National Academy of Sciences of the United States of America,* 96(7), 4084–4088.

Lu, C. C., Appler, J. M., Houseman, E. A., & Goodrich, L. V. (2011). Developmental profiling of spiral ganglion neurons reveals insights into auditory circuit assembly. *The Journal of Neuroscience,* 31(30), 10903–10918.

Luo, X.-J., Deng, M., Xie, X., Huang, L., Wang, H., Jiang, L., Liang, G., Hu, F., Tieu, R., Chen, R., & Gan, L. (2013). GATA3 controls the specification of prosensory domain and neuronal survival in the mouse cochlea. *Human Molecular Genetics,* 22(18), 3609–3623.

Ma, Q., Chen, Z., del Barco Barrantes, I., de la Pompa, J. L., & Anderson, D. J. (1998). Neurogenin1 is essential for the determination of neuronal precursors for proximal cranial sensory ganglia. *Neuron,* 20(3), 469–482.

Ma, Q., Anderson, D. J., & Fritzsch, B. (2000). Neurogenin 1 null mutant ears develop fewer, morphologically normal hair cells in smaller sensory epithelia devoid of innervation. *Journal of the Association for Research in Otolaryngology,* 1(2), 129–143.

Manley, G. A. (2000). Cochlear mechanisms from a phylogenetic viewpoint. *Proceedings of the National Academy of Sciences of the United States of America,* 97(22), 11736–11743.

Manley, G. A. (2012). Evolutionary paths to mammalian cochleae. *Journal of the Association for Research in Otolaryngology,* 13(6), 733–743.

Mann, Z. F., & Kelley, M. W. (2011). Development of tonotopy in the auditory periphery. *Hearing Research,* 276(1–2), 2–15.

Mann, Z. F., Thiede, B. R., Chang, W., Shin, J. B., May-Simera, H. L., Lovett, M., Corwin, J. T., & Kelley, M. W. (2014). A gradient of Bmp7 specifies the tonotopic axis in the developing inner ear. *Nature Communications,* 5, 3839.

Mansour, S. L., Li, C., & Urness, L. D. (2013). Genetic rescue of Muenke syndrome model hearing loss reveals prolonged FGF-dependent plasticity in cochlear supporting cell fates. *Genes and Development,* 27(21), 2320–2331.

Mao, Y., Reiprich, S., Wegner, M., & Fritzsch, B. (2014). Targeted deletion of Sox10 by Wnt1-cre defects neuronal migration and projection in the mouse inner ear. *PLoS ONE,* 9(4), e94580.

Matei, V., Pauley, S., Kaing, S., Rowitch, D., Beisel, K. W., Morris, K., Feng, F., Jones, K., Lee, J., & Fritzsch, B. (2005). Smaller inner ear sensory epithelia in Neurog1 null mice are related to earlier hair cell cycle exit. *Developmental Dynamics,* 234(3), 633–650.

Montcouquiol, M., & Kelley, M. W. (2003). Planar and vertical signals control cellular differentiation and patterning in the mammalian cochlea. *The Journal of Neuroscience,* 23(28), 9469–9478.

Morris, J. K., Maklad, A., Hansen, L. A., Feng, F., Sorensen, C., Lee, K. F., Macklin, W. B., & Fritzsch, B. (2006). A disorganized innervation of the inner ear persists in the absence of ErbB2. *Brain Research,* 1091(1), 186–199.

Morsli H., Choo, D., Ryan, A., Johnson, R., & Wu, D. K. (1998). Development of the mouse inner ear and origin of its sensory organs. *The Journal of Neuroscience*, 18(9), 3327–3335.

Mueller, K. L., Jacques, B. E., & Kelley, M. W. (2002). Fibroblast growth factor signaling regulates pillar cell development in the organ of Corti. *The Journal of Neuroscience,* 22(21), 9368–9377.

Mulvaney, J., & Dabdoub, A. (2012). Atoh1, an essential transcription factor in neurogenesis and intestinal and inner ear development: Function, regulation, and context dependency. *Journal of the Association for Research in Otolaryngology,* 13(3), 281–293.

Munnamalai, V., & Fekete, D. M. (2013). Wnt signaling during cochlear development. *Seminars in Cell and Developmental Biology,* 24(5), 480–489.

Murata, J., Tokunaga, A., Okano, H., & Kubo, T. (2006). Mapping of notch activation during cochlear development in mice: Implications for determination of prosensory domain and cell fate diversification. *The Journal of Comparative Neurology,* 497(3), 502–518.

Nayagam, B. A., Muniak, M. A., & Ryugo, D. K. (2011). The spiral ganglion: Connecting the peripheral and central auditory systems. *Hearing Research,* 278(1–2), 2–20.

Neves, J., Abello, G., Petrovic, J., & Giraldez, F. (2013). Patterning and cell fate in the inner ear: A case for Notch in the chicken embryo. *Development Growth and Differentiation,* 55(1), 96–112.

Ohyama, T., & Groves, A. K. (2004). Generation of Pax2-Cre mice by modification of a Pax2 bacterial artificial chromosome. *Genesis,* 38(4), 195–199.

Ohyama, T., Mohamed, O. A., Taketo, M. M., Dufort, D., & Groves, A. K. (2006). Wnt signals mediate a fate decision between otic placode and epidermis. *Development,* 133(5), 865–875.

Ohyama, T., Basch, M. L., Mishina, Y., Lyons, K. M., Segil, N., & Groves, A. K. (2010). BMP signaling is necessary for patterning the sensory and nonsensory regions of the developing mammalian cochlea. *The Journal of Neuroscience,* 30(45), 15044–15051.

Ong, C. T., Cheng, H. T., Chang, L. W., Ohtsuka, T., Kageyama, R., Stormo, G. D., & Kopan, R. (2006). Target selectivity of vertebrate notch proteins. Collaboration between discrete domains and CSL-binding site architecture determines activation probability. *Journal of Biological Chemistry,* 281(8), 5106–5119.

Pan, W., Jin, Y., Stanger, B., & Kiernan, A. E. (2010). Notch signaling is required for the generation of hair cells and supporting cells in the mammalian inner ear. *Proceedings of the National Academy of Sciences of the United States of America,* 107(36), 15798–15803.

Pan, W., Jin, Y., Chen, J., Rottier, R. J., Steel, K. P., & Kiernan, A. E. (2013). Ectopic expression of activated notch or SOX2 reveals similar and unique roles in the development of the sensory cell progenitors in the mammalian inner ear. *The Journal of Neuroscience,* 33(41), 16146–16157.

Pirvola, U., Ylikoski, J., Trokovic, R., Hebert, J. M., McConnell, S. K., & Partanen, J. (2002). FGFR1 is required for the development of the auditory sensory epithelium. *Neuron,* 35(4), 671–680.

Pirvola, U., Zhang, X., Mantela, J., Ornitz, D. M., & Ylikoski, J. (2004). Fgf9 signaling regulates inner ear morphogenesis through epithelial-mesenchymal interactions. *Developmental Biology,* 273(2), 350–360.

Pujol, R., Lavigne-Rebillard, M., & Lenoir, M. (1998). Development of sensory and neural structures in the mammalian cochlea. In E. W Rubel, A. N. Popper, & R. R. Fay (Eds.), *Development of the Auditory System* (pp. 146–192). New York: Springer-Verlag.

Puligilla, C., Feng, F., Ishikawa, K., Bertuzzi, S., Dabdoub, A., Griffith, A. J., Fritzsch, B., & Kelley, M. W. (2007). Disruption of fibroblast growth factor receptor 3 signaling results in defects in cellular differentiation, neuronal patterning, and hearing impairment. *Developmental Dynamics,* 236(7), 1905–1917.

Raft, S., & Groves, A. K. (2015). Segregating neural and mechanosensory fates in the developing ear: Patterning, signaling, and transcriptional control. *Cell and Tissue Research,* 359(1), 315–332.

Raft, S., Nowotschin, S., Liao, J., & Morrow, B. E. (2004). Suppression of neural fate and control of inner ear morphogenesis by Tbx1. *Development,* 131(8), 1801–1812.

Raft, S., Koundakjian, E. J., Quinones, H., Jayasena, C. S., Goodrich, L. V., Johnson, J. E., Segil, N., & Groves, A. K. (2007). Cross-regulation of Ngn1 and Math1 coordinates the production of neurons and sensory hair cells during inner ear development. *Development,* 134(24), 4405–4415.

Raphael, Y., & Altschuler, R. A. (2003). Structure and innervation of the cochlea. *Brain Research Bulletin,* 60(5–6), 397–422.

Riccomagno, M. M., Martinu, L., Mulheisen, M., Wu, D. K., & Epstein, D. J. (2002). Specification of the mammalian cochlea is dependent on Sonic hedgehog. *Genes and Development,* 16(18), 2365–2378.

Riccomagno, M. M., Takada, S., & Epstein, D. J. (2005). Wnt-dependent regulation of inner ear morphogenesis is balanced by the opposing and supporting roles of Shh. *Genes and Development,* 19(13), 1612–1623.

Roberts, K. A., Abraira, V. E., Tucker, A. F., Goodrich, L. V., & Andrews, N. C. (2012). Mutation of Rubie, a novel long non-coding RNA located upstream of Bmp4, causes vestibular malformation in mice. *PLoS ONE,* 7(1), e29495.

Rocha-Sanchez, S. M., & Beisel, K. W. (2007). Pocket proteins and cell cycle regulation in inner ear development. *International Journal of Developmental Biology,* 51(6–7), 585–595.

Rocha-Sanchez, S. M., Scheetz, L. R., Contreras, M., Weston, M. D., Korte, M., McGee, J., & Walsh, E. J. (2011). Mature mice lacking Rbl2/p 130 gene have supernumerary inner ear hair cells and supporting cells. *The Journal of Neuroscience,* 31(24), 8883–8893.

Sandell, L. L., Butler Tjaden, N. E., Barlow, A. J., & Trainor, P. A. (2014). Cochleovestibular nerve development is integrated with migratory neural crest cells. *Developmental Biology,* 385 (2), 200–210.

Satoh, T., & Fekete, D. M. (2005). Clonal analysis of the relationships between mechanosensory cells and the neurons that innervate them in the chicken ear. *Development,* 132(7), 1687–1697.

Schimmang, T., & Pirvola, U. (2013). Coupling the cell cycle to development and regeneration of the inner ear. *Seminars in Cell and Developmental Biology,* 24(5), 507–513.

Schwander, M., Kachar, B., & Muller, U. (2010). Review series: The cell biology of hearing. *Journal of Cell Biology,* 190(1), 9–20.

Shi, F., Hu, L., Jacques, B. E., Mulvaney, J. F., Dabdoub, A., & Edge, A. S. (2014). β-Catenin is required for hair cell differentiation in the cochlea. *The Journal of Neuroscience,* 34(19), 6470–6479.

Shim, K., Minowada, G., Coling, D. E., & Martin, G. R. (2005). Sprouty2, a mouse deafness gene, regulates cell fate decisions in the auditory sensory epithelium by antagonizing FGF signaling. *Developmental Cell,* 8(4), 553–564.

Shin, J. B., Krey, J. F., Hassan, A., Metlagel, Z., Tauscher, A. N., Pagana, J. M., Sherman, N. E., Jeffery, E. D., Spinelli, K. J., Zhao, H., Wilmarth, P. A., Choi, D., David, L. L., Auer, M., & Barr-Gillespie, P. G. (2013). Molecular architecture of the chick vestibular hair bundle. *Nature Neuroscience,* 16(3), 365–374.

Simmons, D. D. (2002). Development of the inner ear efferent system across vertebrate species. *Journal of Neurobiology,* 53(2), 228–250.

Simmons, D. D., Duncan, J., Crapon de Caprona, D., & Fritzsch, B. (2011). Development of the inner ear efferent systems. In D. K. Ryugo, R. R. Fay, & A. N. Popper (Eds.), *Auditory and Vestibular Efferents* (pp. 187–216). New York: Springer-Verlag.

Slepecky, N. B. (1996). Structure of the mammalian cochlea. In P. Dallos, A. N. Popper, & R. R. Fay (Eds.), *The Cochlea* (pp. 44–129). New York: Springer-Verlag.

Smotherman, M., & Narins, P. (2004). Evolution of the amphibian ear. In G. A. Manley, A. N. Popper, & R. R. Fay (Eds.), *Evolution of the Vertebrate Auditory System* (pp. 164–199). New York: Springer-Verlag.

Somma, G., Alger, H. M., McGuire, R. M., Kretlow, J. D., Ruiz, F. R., Yatsenko, S. A., Stankiewicz, P., Harrison,, W., Funk, E., Bergamaschi, A., Oghalai, J. S., Mikos, A. G., Overbeek, P. A.,& Pereira, F. A. (2012). Head bobber: An insertional mutation causes inner ear defects, hyperactive circling, and deafness. *Journal of the Association for Research in Otolaryngology,* 13(3), 335–349.

Spicer, S. S., & Schulte, B. A. (1991). Differentiation of inner ear fibrocytes according to their ion transport related activity. *Hearing Research,* 56(1–2), 53–64.

Steel, K. P., & Barkway, C. (1989). Another role for melanocytes: Their importance for normal stria vascularis development in the mammalian inner ear. *Development,* 107(3), 453–463.

Summerhurst, K., Stark, M., Sharpe, J., Davidson, D., & Murphy, P. (2008). 3D representation of Wnt and Frizzled gene expression patterns in the mouse embryo at embryonic day 11.5 (Ts19). *Gene Expression Patterns,* 8(5), 331–348.

Tanigaki, K., & Honjo, T. (2010). Two opposing roles of RBP-J in Notch signaling. *Current Topics in Developmental Biology,* 92, 231–252.

Tateya, T., Imayoshi, I., Tateya, I., Hamaguchi, K., Torii, H., Ito, J., & Kageyama, R. (2013). Hedgehog signaling regulates prosensory cell properties during the basal-to-apical wave of hair cell differentiation in the mammalian cochlea. *Development,* 140(18), 3848–3857.

Tessarollo, L., Coppola, V., & Fritzsch, B. (2004). NT-3 replacement with brain-derived neurotrophic factor redirects vestibular nerve fibers to the cochlea. *The Journal of Neuroscience,* 24(10), 2575–2584.

Thiede, B. R., Mann, Z. F., Chang, W., Ku, Y. C., Son, Y. K., Lovett, M., Kelley, M. W., & Corwin, J. T. (2014). Retinoic acid signalling regulates the development of tonotopically patterned hair cells in the chicken cochlea. *Nature Communications,* 5, 3840.

Togashi, H., Kominami, K., Waseda, M., Komura, H., Miyoshi, J., Takeichi, M., & Takai, Y. (2011). Nectins establish a checkerboard-like cellular pattern in the auditory epithelium. *Science,* 333(6046), 1144–1147.

Trainor, P. A., & Krumlauf, R. (2000). Patterning the cranial neural crest: Hindbrain segmentation and Hox gene plasticity. *Nature Reviews: Neuroscience,* 1(2), 116–124.

Urness, L. D., Wang, X., Shibata, S., Ohyama, T., & Mansour, S. L. (2015). Fgf10 is required for specification of non-sensory regions of the cochlear epithelium. *Developmental Biology,* 400 (1), 59–71.

Vendrell, V., Lopez-Hernandez, I., Alonso, M. B., Feijoo-Redondo, A., Abello, G., Gálvez, H., Giráldez, F., Lamonerie, T., & Schimmang, T. (2015). Otx2 is a target of N-myc and acts as a suppressor of sensory development in the mammalian cochlea. *Development*, 142(16), 2792–2800.

Waldhaus, J., Durruthy-Durruthy, R., & Heller, S. (2015). Quantitative high-resolution cellular map of the organ of Corti. *Cell Reports,* 11(9), 1385–1399.

Wang, B., Fallon, J. F., & Beachy, P. A. (2000). Hedgehog-regulated processing of Gli3 produces an anterior/posterior repressor gradient in the developing vertebrate limb. *Cell,* 100(4), 423–434.

Wang, S. Z., Ibrahim, L. A., Kim, Y. J., Gibson, D. A., Leung, H. C., Yuan, W., Zhang, K. K., Tao, H. W., Ma, L., & Zhang, L. I. (2013). Slit/Robo signaling mediates spatial positioning of spiral ganglion neurons during development of cochlear innervation. *The Journal of Neuroscience,* 33(30), 12242–12254.

Wu, D. K., & Kelley, M. W. (2012). Molecular mechanisms of inner ear development. *Cold Spring Harbor Perspectives in Biology,* 4(8), a008409.

Yamamoto, N., Chang, W., & Kelley, M. W. (2011). Rbpj regulates development of prosensory cells in the mammalian inner ear. *Developmental Biology,* 353(2), 367–379.

Yang, T., Kersigo, J., Jahan, I., Pan, N., & Fritzsch, B. (2011). The molecular basis of making spiral ganglion neurons and connecting them to hair cells of the organ of Corti. *Hearing Research,* 278(1–2), 21–33.

Yu, W.-M., Appler, J. M., Kim, Y.-H., Nishitani, A. M., Holt, J. R., & Goodrich, L. V. (2013). A Gata3-Mafb transcriptional network directs post-synaptic differentiation in synapses specialized for hearing. *eLife,* 2, e01341.

Zachary, S. P., & Fuchs, P. A. (2015). Re-emergent inhibition of cochlear inner hair cells in a mouse model of hearing loss. *The Journal of Neuroscience,* 35(26), 9701–9706.

Chapter 4
Mechanical Transduction Processes in the Hair Cell

David P. Corey, Dáibhid Ó Maoiléidigh, and Jonathan F. Ashmore

Abstract The conversion of the mechanical stimulus of sound into an electrical signal by hair cells of the cochlea is the central event in hearing. Their bundles of actin-rich stereocilia bear the proteins essential for hearing at their tips. Filamentous tip links, composed of the cadherins PCDH15 and CDH23, stretch between the tips of adjacent stereocilia. Deflection of the bundle increases tension in tip links, which pull open mechanically gated ion channels that include TransMembrane Channel-like 1 (TMC1) and TMC2. Channel opening allows entry of the receptor current that can depolarize hair cells with a submillisecond time constant, generating a neural signal. Adaptation, mediated by at least two different mechanisms, relaxes the receptor current in milliseconds even with maintained bundle deflection. Different adaptation mechanisms cause the bundle to exert force, powering mechanical feedback to amplify the mechanical stimulus and tune the response to a certain frequency. Mammalian cochlear hair cells also show a voltage-dependent motility mediated by SLC26A5 (prestin) in the lateral wall, which contributes to amplification and tuning. Although much is understood about hair cell function, remaining questions include the molecular structure of the transduction complex, the nature of fast adaptation, and how motility of different components is integrated to produce amplification and tuning.

D.P. Corey (✉)
Howard Hughes Medical Institute and Department of Neurobiology,
Harvard Medical School, Boston, MA 02115, USA
e-mail: dcorey@hms.harvard.edu

D. Ó Maoiléidigh
Howard Hughes Medical Institute and Laboratory of Sensory Neuroscience,
The Rockefeller University, New York, NY 10065, USA
e-mail: domaoileid@mail.rockefeller.edu

J.F. Ashmore
Department of Neuroscience, Physiology, and Pharmacology and UCL Ear Institute,
University College London (UCL), London WC1E 6BT, UK
e-mail: j.ashmore@ucl.ac.uk

G.A. Manley et al. (eds.), *Understanding the Cochlea*, Springer Handbook
of Auditory Research 62, DOI 10.1007/978-3-319-52073-5_4

Keywords Active bundle motility · Adaptation · Cochlea · Cochlear amplification · Electromotility · Hair cell · Hair bundle · Hopf bifurcation · Mechanoelectrical transduction · Stereocilia · Outer hair cell · Saccule · Tip link · TransMembrane Channel-like 1

4.1 Hair Bundle Transduction and Adaptation

The conversion of the mechanical stimulus of sound into an electrical signal by hair cells of the cochlea is the central event in hearing. It follows the complex amplification and delivery of sound vibration to the organ of Corti and precedes the even more complex interpretation of neuronal signals by auditory circuits of the central nervous system. But without the core process of mechanoelectrical transduction (MET), hearing does not happen. Here, concepts associated with this process are summarized. For more complete descriptions, the reader is referred to excellent recent reviews (Fettiplace and Kim 2014; Zhao and Müller 2015).

4.1.1 Structure, Mechanics, and Cohesion of the Hair Bundle

The ciliary bundle emanating from the apical surface of a hair cell has long been recognized as the cell's defining feature, and it gives the hair cell its name. Hair bundles in different species and organs have 30–300 stereocilia, and they range in height from $\sim$1 μm in high-frequency cochlear hair cells to almost 30 μm in vestibular hair cells of nonmammalian vertebrates. Each bundle has one true cilium, termed a kinocilium, that contains a 9 + 2 arrangement of microtubules similar to those in beating cilia. Only rarely have hair bundle kinocilia been observed to beat, however, and this form of motility is not thought to play a role in hair cell function. The kinocilium disappears during development in mammalian cochlear hair cells but not in other parts of the ear in any vertebrate.

Most of a bundle's cilia are similar to microvilli, with a dense core of several hundred actin filaments; they are called stereocilia or (less commonly) stereovilli. Stereocilia in all organs and species are arranged in rows of increasing height, creating a staircase-like structure that defines the bundle's polarity. The growth and maintenance of the stereocilium lengths is an important problem but beyond the scope of this chapter. Deflection of a bundle toward the tallest stereocilia (the positive direction) is excitatory (Flock and Wersäll 1962). Although all hair cells display the staggered heights of stereocilia, their arrangement into a bundle varies, with most hair cells in nonmammalian vertebrates showing a compact bundle but mammalian cochlear hair cells displaying a straight or V-shaped palisade (Fig. 4.1).

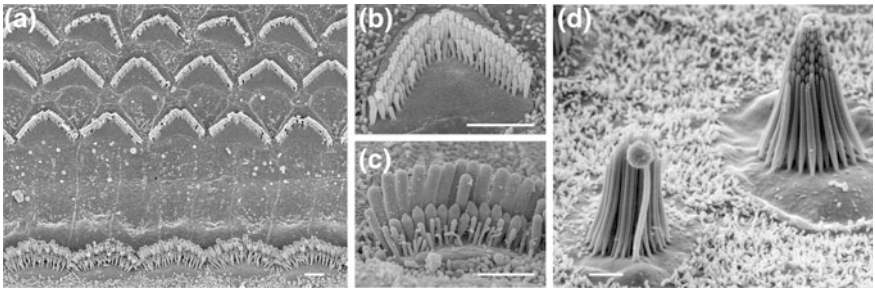

Fig. 4.1 Cochlear and vestibular hair cell bundles. **a** Organ of Corti from a 16-week mouse showing one row of IHCs and three rows of OHCs. **b** Single bundle on an OHC from an adult mouse. **c** Single bundle on an IHC from an adult mouse. **d** Bundles of hair cells on a bullfrog sacculus. *Scale bars* 2 μm. **a** From Xudong Wu, Harvard Medical School; **b**, **c** from Andrew Forge and Ruth Taylor, UCL Ear Institute, London; **d** from John Assad and David Corey, Harvard Medical School

Actin filaments are cross-linked by several proteins, including FSCN2 (fascin 2) and PLS1 (plastin 1/fimbrin). RDX (radixin) and related ERM proteins link actin filaments to the membrane (Shin et al. 2013). At its base, a stereocilium tapers and passes into the cuticular plate, an actin- and spectrin-rich meshwork lying just under the cell's apical surface. The outer actin filaments end, and the inner filaments coalesce into a dense rootlet that is bundled by the protein TRIOBP (Kitajiri et al. 2010). The dense cross-linking of the actin core and the narrow rootlet at the base determine the mechanical properties of the stereocilia. When force is applied to their tips, stereocilia do not bend along their lengths but pivot at their bases (Hudspeth 1983; Karavitaki and Corey 2010). In addition, stereocilia in many species display a striking "sliding adhesion" whereby adjacent stereocilia adhere to each other at their tips but shear along their lengths when the bundle is deflected (Kozlov et al. 2007; Karavitaki and Corey 2010). The degree of adhesion also varies among hair cells. In the bullfrog (*Rana catesbeiana,* now *Lithobates catesbeiana*), for instance, pulling on the single kinocilium entrains the entire bundle, with stereocilia separating by less than $\sim$10 nm (Karavitaki and Corey 2010), whereas movement of a stereocilium in a mammalian cochlear hair cell moves only a few nearby stereocilia but not the whole bundle (Nam et al. 2015).

Different mechanical stimuli are conveyed to hair bundles in different ways in different organs. In the lateral line organs of aquatic vertebrates, fluid motion past the animal deflects an acellular gelatinous cupula that extends from the body wall and encloses the hair bundles of all the hair cells in a sensory patch called a neuromast. Hair cells are stimulated when the cupula moves. In "otolith organs" of the vestibular system, in which a gelatinous otolithic membrane overlies the hair cell epithelium and bears otoliths or otoconia of calcium carbonate, the kinocilium and sometimes the tallest stereocilia are embedded in the otolithic membrane and are moved when translational forces (including gravity) result in force on the otoconia. Hair cell bundles of the semicircular canals of the vestibular system are

similarly embedded in a cupula that spans the canal, and the cupula is deflected by fluid forces within the canals when the head rotates. In the cochleae of many vertebrates, the hair cell epithelium is suspended between two bony or soft tissue walls, and the vibrations due to sound move the entire epithelium with each cycle of sound. Hair bundles are, in almost all cases, attached to an overlying, acellular "tectorial membrane," and sound causes shearing between the tectorial membrane and the epithelium that deflects the bundles. A further elaboration of the mammalian cochlea is a separation of the hair cell population into 3–4 rows of outer hair cells (OHCs), the bundles of which attach to the tectorial membrane, and a single row of inner hair cells (IHCs), with bundles that do not contact the tectorial membrane but are moved by fluid forces caused by shear between the tectorial membrane and the sensory epithelium. In all cases, the mechanical stimulus leads to deflection of the hair bundle and the generation of a receptor current.

4.1.2 Measuring Mechanotransduction In Vivo and In Vitro

The first electrical correlate of hair cell transduction, the "cochlear microphonic" response, was discovered by Wever and Bray (1930) as a sound-evoked electrical potential that could be measured from sites near the cochlear nerve and brainstem. Although Wever and Bray interpreted it as a neural response, Adrian (1931) and later Hallpike and Rawdon-Smith (1934) recognized that the cochlear microphonic is an extracellular potential generated by the flow of receptor current through the cochlear partition. It is best measured near the hair cells, usually with an electrode placed near the round window of the cochlea. Because the electrical time constant of the scala media is small, the microphonic reflects the receptor current with high fidelity, although it is filtered by cellular capacitance at higher frequencies. It measures functioning hair cells, especially OHCs, directly (Dallos and Cheatham 1976).

More direct, but also more difficult, are methods for direct stimulation and direct recording from hair cells. Hair bundles can be moved by several methods. In the bullfrog saccule and zebrafish (*Danio rerio*) lateral line organs, the overlying otolithic membrane or the cupula of the neuromast can be moved by a blunt probe; the tens or hundreds of hair bundles embedded in these structures follow the movement (Corey and Hudspeth 1983a). For this and similar methods, the probe is moved by a piezoelectric driver, which can produce movements of several micrometers with submillisecond speed. To move a single bundle, many investigators use a glass probe with a 1- to 5-μm tip diameter placed against the tips of stereocilia (Hudspeth 1982). In the mammalian cochlea, the probe is placed within the curve of an OHC bundle, stimulating most of the stereocilia in a bundle. A problem is that such probes can push in the positive direction but often cannot pull in the negative direction, and so they allow exploration of just part of the bidirectional activation curve. In bundles that retain kinocilia, a thin fiber of clean glass can stick to the kinocilium, producing both positive and negative deflections.

For mechanical measurements of hair bundle stiffness or force production, flexible stimulus probes are used with a stiffness that is similar to or less than the bundle stiffness of ~1 mN/m (Crawford and Fettiplace 1985). Long glass fibers of ~1 μm diameter have an appropriate stiffness (Howard and Ashmore 1986). Another method is to adhere a 1- to 2-μm-diameter glass bead to the kinocilium and place it at the focus of an intense beam of infrared light. This "gradient force light trap" or "laser tweezers" can produce forces up to ~100 pN on the bead (Cheung and Corey 2006). Like a flexible glass fiber, the bead can move within the trap and so forces produced by the bundle can be measured. Many of these methods work well for frog or turtle hair bundles, which have kinocilia and are cohesive. They are less effective for mammalian cochlear hair cells, which have stereocilia in a distributed array that is not very cohesive (Nam et al. 2015). A blunt probe therefore moves some stereocilia more than others, and the measured activation curve is a sum of different curves. New probes, microfabricated from silicon to fit the specific geometry of a bundle, may provide more uniform stimulation to different stereocilia of a bundle (Karavataki, personal communication). Finally, in many studies, a hair bundle is more uniformly deflected by a fluid jet placed near the bundle (Kros et al. 1992). A disadvantage is that fluid jets are not as fast as stiff probes.

For stimulating with stiff probes, flexible probes, or fluid jets, the actual bundle motion must be measured. The best methods are optical, using either cameras or photodiodes. Fast video cameras have kilohertz frame rates, and frame-by-frame image analysis can reveal movement on a nanometer and millisecond scale. Alternatively, the image of a flexible probe or the bundle itself can be projected onto a photodiode so that the photocurrent changes with bundle position.

To measure the receptor current, whole cell patch-clamp recording is the method of choice. In high-frequency mammalian hair cells, the total current can be 10 nA or more, and so a pipette series-resistance compensation must be used to avoid voltage errors. It has not been possible to measure single MET channels in the stereocilia by conventional cell-attached patch clamping. However, when only a few functional channels remain because tip links are broken either by tissue dissection (Ohmori 1985; Géléoc et al. 1997) or by exposing bundles to a calcium chelator (Assad et al. 1991; Crawford et al. 1991), then the large single-channel currents (10–30 pA) and the low noise of patch recording make it possible to observe single channels opening with whole cell recording and to measure the channel conductance. This has been useful in correlating single-channel properties with the putative molecular composition of proposed transduction channels.

Fluorescent indicator dyes have also been used to assess transduction. The transduction channel pore is large enough to allow influx of fluorescent styryl dyes like FM1-43. These are trapped in the cytoplasm by their positive charge. If channels are present and functional, FM1-43 can make a hair cell brightly fluorescent in tens of seconds (Gale et al. 2001; Meyers et al. 2003). Although not very quantitative, such dyes are quick and efficient markers for cells with functional transduction. Ca^{2+} influx through the transduction channel can also be measured.

Indicators include organic dyes, loaded into the cytoplasm through the patch pipette, and genetically encoded dyes with the coding sequence stably inserted in a mouse genome (Denk et al. 1995; Delling et al. 2016).

4.1.3 Generation of the Receptor Current

Complementary biophysical and morphological descriptions of hair cell transduction have produced an integrated understanding of the mechanotransduction process. Deflection of a hair bundle toward its taller stereocilia (a positive deflection) evokes a depolarizing receptor potential by opening nonselective cation channels (Hudspeth and Corey 1977). Some fraction of channels are open at rest, positioning the cell in its most sensitive range and allowing both depolarizing and hyperpolarizing responses to positive and negative deflections. The observed activation range depends on the geometry of the hair bundle and on the method of stimulation, but the full range from all channels closed to all channels open is usually 0.1–1.0 μm as measured at the tip of the bundle (Howard and Hudspeth 1988; Crawford et al. 1989). Channel opening is remarkably fast. After a step deflection, the receptor current turns on with a time constant of 30–150 μs at room temperature, opening faster with larger deflections; it is likely to activate in less than 10 μs at mammalian temperatures (Corey and Hudspeth 1983b; Ricci et al. 2005). As a benchmark, the most optimistic estimated time constant of a single ion-channel opening, in this case for the acetylcholine receptor, is 0.9 μs (Chakrapani and Auerbach 2005), equivalent to a frequency of about 180 kHz.

The fast kinetics has been taken as evidence against a diffusible second-messenger intermediate in hair cell transduction and as evidence for a model in which the channels are directly opened by mechanical force applied to the channel protein. In this model, positive movement of the bundle stretches a hypothetical "gating spring" attached to the channel. The force on the channel thus increases with deflection. If the opening of the channel is associated with movement along the force axis, then the relative energy of the open state is reduced by force, favoring the open state. The energy of the transition state between open and closed conformations is also reduced by force, and this model explains both the shape of the activation curve and the faster opening with larger deflections. Detailed analysis of the opening kinetics suggests additionally that the channel has at least three conformational states, two closed and one open (Corey and Hudspeth 1983b). Sensitive mechanical measurements of frog hair bundles indicate that the gating spring stiffness is $\sim$1 mN/m and the channel movement with opening is $\sim$4 nm (Howard and Hudspeth 1988). When bundle force is plotted as deflection-dependent stiffness, the channel opening produces a drop in apparent stiffness (see Sect. 4.3.1). The kinetics and drop in stiffness are strong evidence for a force-gated ion channel in hair cell transduction.

Analysis of the ultrastructure of the hair bundle has revealed some morphological correlates of these elements. First, measurement of extracellular field potentials indicated that the force-gated transduction channels are located at the tips of stereocilia in frog hair cells (Hudspeth 1982), and this location was confirmed by fluorescence imaging of calcium influx through the channels (Denk et al. 1995; Lumpkin and Hudspeth 1995). Fast calcium imaging in a mammalian cochlea showed that calcium enters the tips of all but the tallest stereocilia (Beurg et al. 2009). This localization focused attention on the tips of stereocilia, where Pickles et al. (1984) found a distinct set of filamentous "tip links," each about 150 nm long and 10 nm diameter, extending from the tip of each cilium to the side of its taller neighbor but only along the excitatory axis and not from side to side. This correlates with the observation that deflection of a hair bundle perpendicular to the excitatory axis has no effect (Shotwell et al. 1981). Further electron microscopy revealed that each tip link is double stranded, with a slight twist (Kachar et al. 2000). Pickles et al. (1984) recognized that positive deflection of the bundle would tension tip links and suggested that they pull directly on transduction channels. The importance of tip links was confirmed by the immediate abolition of receptor current when tip links are chemically disrupted (Assad et al. 1991). Absence of stimulus-evoked calcium influx into the tallest stereocilia thus suggests that the transduction apparatus is located at the lower but not upper end of each tip link. Comparison of the single-channel current and total transduction current also suggests that each stereocilium has about two functional channels (Ricci et al. 2003), perhaps related structurally to the two strands of the tip link.

Although the tip link was initially thought to be the gating spring, molecular analysis of the tip link (see Sect. 4.2.1) suggested that its stiffness is too high, that the tip link is a cablelike structure that might bend but not appreciably stretch under physiological loads. What, then, is the gating spring? One possibility is that the lipid membrane at the tip of each stereocilium, in which the transduction channels are embedded, acts as a spring. Modeling of membrane properties indicates that membrane elasticity is almost but perhaps not quite adequate to be the gating spring in all hair cells (Powers et al. 2014). Instead, it seems more likely that the gating spring is a distinct, elastic tether protein connecting transduction channels to the actin cores of the stereocilia.

4.1.4 Fast and Slow Adaptation

When a hair bundle is deflected and held, there is a rapid influx of current that then declines over milliseconds, even when bundle deflection is maintained (Corey and Hudspeth 1983a; Eatock et al. 1987). During and after the decline, larger deflections can evoke the maximum current, showing that this adaptation is not due to an inactivation of channels (such as that found for voltage-dependent sodium

channels). Instead, adaptation is best characterized as a time-dependent shift of the hair cell activation curve along the stimulus axis. It acts to reduce the response to either positive or negative stimuli and thus to keep mechanotransduction within its activation range. A positive deflection that opens channels shifts the curve to the right, so channels close; a negative deflection shifts the curve to the left, so they reopen. This process allows hair cells to continue to respond with high sensitivity when large static stimuli would otherwise saturate the response. The extent of the shift is usually not quite as large as the deflection, so adaptation is not complete.

Two mechanisms might explain such a shift: adaptation could be mediated by a mechanical adjustment of the force on transduction channels or it could be mediated by a change in channel open probability for a certain force. Both mechanisms may operate in hair cells.

4.1.4.1 Slow Adaptation

In bullfrog hair cells, adaptation has a time course of 20–50 ms. To reconcile an apparent relaxation in the stimulus with the tip-link model for transduction, Howard and Hudspeth (1987) suggested that the upper attachment point of the tip link could slip down or climb up the stereocilium to maintain tip-link tension, perhaps using a myosin-based motor complex. The stall force of the motor would set the resting tension and thus the resting open probability. The rate of adaptation is Ca^{2+}-dependent in the frog (Assad et al. 1989) and turtle (*Pseudemys scripta elegans*; Crawford et al. 1989), with higher Ca^{2+} promoting faster slipping. Moreover, Ca^{2+} accelerates slipping more than climbing, so the net effect of high Ca^{2+} is to reduce resting open probability, apparently by reducing tension. Depolarization of a hair cell to positive potentials, which would reduce Ca^{2+} influx through transduction channels, greatly slows adaptation and also increases resting open probability; increasing intracellular Ca^{2+} buffering has the same effect. The site of Ca^{2+} action is apparently intracellular, consistent with an intracellular Ca^{2+}-modulated motor.

4.1.4.2 Fast Adaptation

Further studies in the frog and turtle revealed a faster form of adaptation, with a time course of $\sim$1 ms (Howard and Hudspeth 1988; Ricci and Fettiplace 1997). Fast adaptation is also Ca^{2+} dependent and seems also to be controlled at an intracellular Ca^{2+}-binding site. A careful analysis of the effects of intracellular fast and slow buffers suggested that slow adaptation is controlled by Ca^{2+} at an intracellular site $\sim$200 nm from the channel but that the fast adaptation site is very close to the channel (Wu et al. 1999). Unlike slow adaptation, viewed as a motor-mediated modulation of tension on the channel, fast adaptation is proposed to be mediated by Ca^{2+} binding to the channel to change its force dependence.

4.1.4.3 Mechanical Correlates of Adaptation

Both forms of adaptation have measurable mechanical correlates. These offer independent windows into the mechanisms. A constant force applied to a bundle will deflect it by an amount equal to the force divided by the stiffness, but when a slow adaptation motor slips, it allows the bundle to move further with the time course of adaptation. Similarly, depolarization that reduces intracellular Ca^{2+} and promotes motor climbing will increase tip-link tension, pulling stereocilia tips together and moving the bundle negatively (Assad et al. 1989; Crawford et al. 1991). For fast adaptation, a particularly important motion is predicted: a positive deflection that opens channels allows Ca^{2+} to enter, bind to the channel, and promote channel closure in $\sim$1 ms or less. When the channel closes, its gate moves back toward the channel by $\sim$4 nm (Howard and Hudspeth 1988), tightening tip links and causing a fast negative bundle movement of $\sim$20 nm. Such movement, when the timing and amplitude are optimal, produces force that may drive active amplification in the cochlea (Sect. 4.3.5).

4.1.4.4 Mammalian Hair Cells

The simple separation of adaptation into fast and slow components is not so clear in mammalian cochlear hair cells nor are the components as well understood. Cochlear hair cells do show fast adaptation, which can be very fast (<0.1 ms; Ricci et al. 2005). However, the Ca^{2+} dependence is less pronounced and intracellular buffers have less effect in slowing adaptation or shifting the resting activation curve (Beurg et al. 2010; Peng et al. 2013; Corns et al. 2014). Further confusion arises in distinguishing between fast ($\sim$1 ms) and very fast ($\sim$0.1 ms) components of adaptation and from the possibility that probe slippage might be interpreted as adaptation. Because the mechanical feedback produced by fast adaptation is potentially important in driving amplification and tuning in the mammalian cochlea, it is essential, despite the technical challenges of measuring at nanometer and microsecond scales, to understand this process better.

4.1.5 Generation of the Receptor Potential

As a first approximation, the receptor potential that drives synaptic release is the product of the receptor current and the membrane resistance (R_m) of the hair cell. When the bundle is deflected, the receptor current (carried mainly by K^+ ions from the endolymph flowing through the transducer conductance) alters the membrane potential in the cell body. The precise effect, especially at high frequencies (say above 1 kHz), depends on whether the cell is an isolated cell or in the hair cell epithelium (Fig. 4.2).

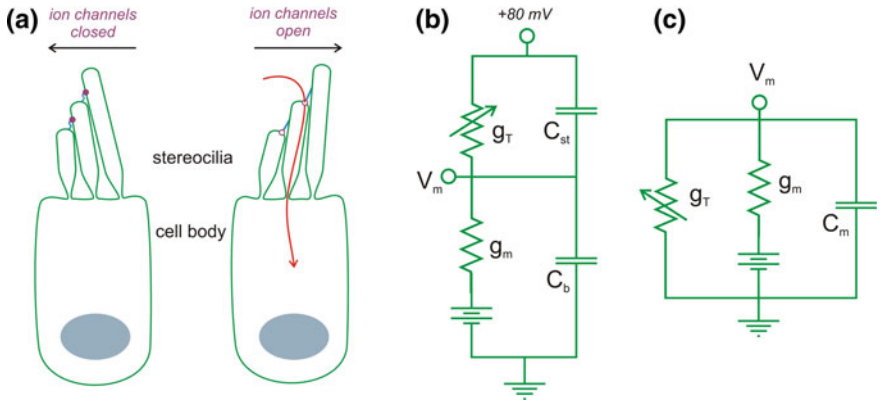

Fig. 4.2 The electrical current flow in hair cells. **a** The MET channels are located at the tips of all but the tallest stereocilia. Deflection of the bundle toward the taller stereocilia tensions the tip links, which pull the MET channels open and allow the flow of positive current into the cell body to depolarize it. **b** For hair cells in vivo, when part of a tight epithelium, the current flows from the endolymphatic compartment (at +80 mV in mammals; *top*) and the MET conductance (g_T) is in series with the basolateral membrane conductance ($g_m = 1/R_m$). The battery represents the resting potential (V_m) for the basolateral membrane. **c** In vitro, the cell is surrounded by the same solution and g_T is in parallel with g_m. C_{st} and C_b represent the separate capacitance of the stereocilia and basolateral membranes, respectively. C_m is the total membrane capacitance ($=C_{st} + C_b$) that would be measured in patch-clamp experiments

The receptor current can be 1 nA or more, and at hyperpolarized potentials, the R_m can be many hundreds of megohms, leading to calculated values for receptor potentials of hundreds of millivolts that is clearly impossible. Several factors shape the receptor potential so that it is not directly proportional to receptor current. These include nonlinear R_m and membrane capacitance (C_m).

Hair cells express a variety of voltage- and calcium-dependent potassium channels that activate at −80 to −40 mV and reduce the effective R_m. At potentials at which these potassium conductances are active, the cell resistance is much lower: as low as 6 MΩ in bullfrog hair cells and 4 MΩ in mammalian OHCs (Mammano and Ashmore 1996; Johnson et al. 2011). Because the transduction channels have a nonzero resting open probability, they generate a standing current that depolarizes the hair cell to a region of lower resistance. The receptor potential is consequently in the range of tens of millivolts but is sufficient to activate the voltage-dependent calcium channels that mediate transmitter release.

Auditory hair cells can operate at frequencies of hundreds to thousands of hertz. At these frequencies, an additional limitation on receptor potential is the time it takes the receptor current to charge the C_m. The charging time acts as a low-pass filter for sinusoidal receptor currents, with a corner frequency (f_0) = $1/2\pi\tau$, where the time constant (τ) = R_mC_m. A small hair cell with a capacitance of 10 pF and a (low) input resistance of 10 MΩ will have a membrane τ = 100 μs and a f_0 = 1.6 kHz. The filter limit seems to preclude high-frequency hearing. However,

most hair cells have fewer than 50% of their transduction channels open at rest, so there is more current that enters during the positive phase of a periodic stimulus than is inhibited during the negative phase, leading to a net inward current with stimulation. Although filtered in time, the receptor potential is thus depolarizing (Russell and Sellick 1983). The R_mC_m τ additionally limits models for mechanical amplification (Sect. 4.4.3).

4.2 Molecular Components of the Hair Bundle Transduction Apparatus

Nearly all of the known proteins of the hair cell mechanotransduction apparatus have been discovered by positional cloning of deafness genes in humans, mice, and zebrafish. Many of these function in the retina as well, so mutations in them also cause blindness, resulting in various forms of Usher syndrome. Components of the transduction apparatus are illustrated in Fig. 4.3.

4.2.1 Tip Links

Two cadherins, PCDH15 and CDH23, both of which are members of the large cadherin superfamily (Sotomayor et al. 2014), together form the tip link. PCDH15 is mutated in the deaf *Ames waltzer* mouse (Alagramam et al. 2001) and in the human Usher syndrome type 1F (Ahmed et al. 2001). CDH23 is mutated in the *waltzer* mouse (Di Palma et al. 2001), in Usher 1D, and in the human recessive deafness DFNB12 (Bork et al. 2001). These cadherins have 11 or 27 extracellular cadherin (EC) repeats, respectively, in an extracellular N-terminal domain. Both have a single transmembrane domain and a short intracellular domain that binds to other transduction components. A single tip link is a tetramer composed of a parallel dimer of PCDH15 joining a parallel dimer of CDH23 in a tip-to-tip configuration, with CDH23 at the upper end and PCDH15 at the lower end (Kazmierczak et al. 2007). The atomic structure of the first two EC domains, bound together, has been solved (Sotomayor et al. 2010, 2012) and reveals a large overlap of the two EC domains. Steered molecular dynamic simulations indicate that a force of many hundreds of piconewtons (pN), much more than normal physiological forces on the tip link, is required to *unfold* the EC domains, and so it is thought that they do not normally unfold. The overall stiffness of the tip link, calculated from these simulations with the assumption that all EC domains have the same properties, is much higher than the measured stiffness of the gating-spring element. The tip link is thus thought not to be the gating spring; it pulls on transduction channels but does itself not stretch much. More than 400 pN are also required for *unbinding* the two cadherins in high-speed simulations, but the unbinding force may be much

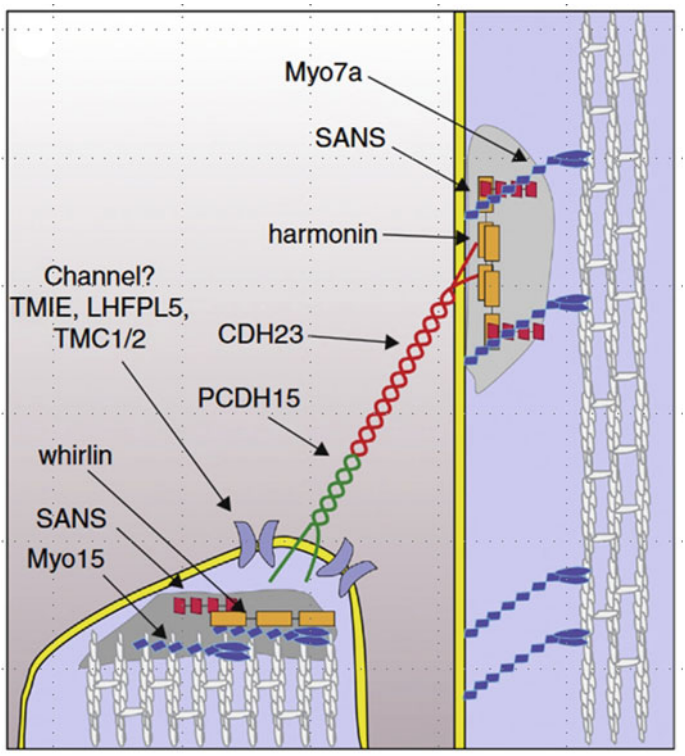

Fig. 4.3 The molecular organization of the tip-link and MET-complex proteins. The location of tip-link proteins (CDH23 and PCDH15) is well understood, but the precise organization of the MET-complex proteins (TMC1/2, LHFPL5, TMIE, and perhaps others) is currently unknown (*left*). The rigid core of the stereocilia is made up of actin filaments to which myosins bind to maintain tip-link tension (*right*). From Zhao and Müller (2015), with permission

less at lower at more physiological speeds. The two-stranded configuration of the tip link may provide a safety factor that greatly prolongs the tip-link lifetime at physiological forces and times.

4.2.2 Tip-Link Upper End

A molecular motor maintains resting tension on the tip link and so mediates at least one component of adaptation. Two different myosins have been proposed for this motor. MYO1C is located at the upper ends of tips links in the bullfrog (Garcia et al. 1998), and chemical genetic inactivation of MYO1C in mouse vestibular hair cells abolishes the slow component of adaptation in a few minutes (Holt et al. 2002).

MYO7A, mutated in Usher 1B (Weil et al. 1995) and the shaker-1 mouse (Gibson et al. 1995), is located at the upper ends of tip links in mammalian hair cells (Grati and Kachar 2011), and mice lacking MYO7A appear to have lower resting tip-link tension (Kros et al. 2002). It will be important to clarify the various roles of these myosins and perhaps others in conveying transduction components to the tips of stereocilia and in maintaining tip-link tension.

Closely associated with both CDH23 and MYO7A are two scaffolding proteins. Harmonin, an intracellular protein with three protein-binding PDZ domains, is mutated in the human Usher 1C syndrome and the recessive nonsyndromic deafness DFNB18 (Verpy et al. 2000) and also in the *deaf circler* mouse (Johnson et al. 2003). Sans, an intracellular protein with at least three ankyrin repeats, is mutated in the human Usher 1G and the *Jackson shaker* mouse (Weil et al. 2003). Both are located near the upper tip-link insertion in stereocilia. USH1C/harmonin, USH1G/sans, and MYO7A all interact with each other, and they bind to CDH23 (Adato et al. 2005).

4.2.3 Tip-Link Lower End

At least five integral membrane proteins form a complex at the lower end of the tip link. One, of course, is PCDH15. Two more were found as products of genes mutated in hereditary deafness. TMHS/LHFPL5 is a small protein with four transmembrane domains and is similar to claudins. It is mutated in the deaf *hurry-scurry* mouse (Longo-Guess et al. 2005) and the human DFNB67 (Shabbir et al. 2006). Tiny TMIE has a single transmembrane domain and an intracellular C-terminus. It was discovered as the protein mutated in the *spinner* mouse (Mitchem et al. 2002) and the human deafness DFNB6 (Naz et al. 2002). Two more, TMC1 and TMC2, are candidates for the transduction channel itself and are discussed in Sect. 4.2.5. All five are required for mechanotransduction, although TMC1 and TMC2 can substitute for each other. They apparently form a transduction complex. PCDH15 binds both TMC1 and TMC2 (Maeda et al. 2014; Beurg et al. 2015). TMIE binds both PCDH15 and LHFPL5 (Zhao et al. 2014). LHFPL5 binds TMC1 and seems to be required for its function because LHFPL5-knockout mice have improper targeting of TMC1 and show transduction currents much like those in TMC1-knockout mice.

4.2.4 Coupling of the Hair Bundle

In many nonmammalian species and in mammalian vestibular epithelia, the hair bundle is deflected through the coupling of the kinocilium to the overlying structures (for example, the otolithic membrane in the case of the frog sacculus). In the

mammalian cochlea, a slightly different situation is found because the tallest stereocilia of the OHCs are directly anchored to the underside of the tectorial membrane by stereocilins (Verpy et al. 2011). It may even be the case that the stereocilins are the partners for the tectorins (see Gummer, Dong, Ghaffari, and Freeman, Chap. 6). All of these coupling points offer a degree of compliance in the mechanical excitation of the hair bundle.

4.2.5 Transduction Channel

The hair cell transduction channel, sometimes called the MET channel, is the element that converts the physical stimulus of sound into the electrical currency of the nervous system. Although it is a core protein of the sense of hearing, its identity has eluded researchers for decades and only in recent years has a strong molecular candidate emerged.

The biophysical characteristics of the transduction channel have long been known. It is a nonselective cation channel that passes all alkali cations (Corey and Hudspeth 1979). It also passes a surprising range of small organic cations, including the fluorescent dye FM1-43, indicating a pore diameter of at least 12 Å. The channel is highly permeable to Ca^{2+}, passing Ca^{2+} about 20 times as well as Na^{+} at low concentrations, but Ca^{2+} is also a partial blocker, inhibiting monovalent cation influx by $\sim$50% (Lumpkin et al. 1997). The pore is blocked in the low micromolar range by a variety of small organic cations such as benzamil, curare, ruthenium red, and streptomycin and by trivalent cations such as La^{3+} and Gd^{3+}. With the exception of certain polycationic peptides, blockers with nanomolar affinity have not been found. The single-channel conductance varies among species and hair cell types but is generally 100–300 pS (Ricci et al. 2003; Pan et al. 2013). Surprisingly, single-channel conductances can vary from the low-frequency to the high-frequency end of the auditory organ in both turtles (Ricci et al. 2003) and mammals (Beurg et al. 2006). This may be a consequence of heteromultimerization of different subunits with different properties or may reflect posttranscriptional or posttranslational modification of a single gene product.

A molecular candidate for the transduction channel should have permeation properties similar to those above. It should meet other criteria as well. (1) The candidate should be required for mechanotransduction; (2) its gene should be expressed in hair cells at the developmental onset of mechanosensitivity; (3) the protein should be located at the site of mechanotransduction, which for hair cells is the tips of all but the tallest stereocilia; (4) it should be mechanosensitive when expressed in a heterologous system; and (5) its permeation properties such as selectivity and conductance should be altered by appropriate mutation of the candidate protein.

A variety of channel candidates has been proposed in the past decade or so but none have experimentally stood the test of time (Corey and Holt 2016). However, the two promising candidates were discovered by positional cloning of a deafness gene. *TMC1* was found to be the gene defective in the human recessive deafness DFNB7/DFNB11 and the dominant deafness DFNA36 (Kurima et al. 2002). The mouse *Tmc1* is mutated in the recessive *dn* mouse and the dominant *Bth* mouse. TMC1 is one of eight members of the TMC membrane protein family, and the close homolog TMC2 is also found in hair cells. TMCs have between 6 and 10 transmembrane domains, but the topology is unclear. Although hair cells in mice lacking TMC1 are still mechanically sensitive at early postnatal ages (Marcotti et al. 2006), this was shown to be a result of compensation by TMC2 (Kawashima et al. 2011). The *Tmc2* gene is downregulated by the second postnatal week in mouse cochlea, and in the absence of TMC2, TMC1 is absolutely required for hearing.

In both auditory and vestibular hair cells in mice, *Tmc1* and *Tmc2* are expressed during development when hair cells become mechanically sensitive (Géléoc and Holt 2003; Kawashima et al. 2011). They are not expressed in other cells of the inner ear, meeting another criterion. In mice expressing TMC1 or TMC2 proteins tagged with mCherry or GFP, fluorescence was observed where transduction channels should be, at the tips of all but the tallest stereocilia (Kurima et al. 2015). Mice expressing just *Tmc1* or just *Tmc2* have transduction channels with differing conductance and Ca^{2+} selectivity, and a point mutation in TMC1 further changes the conductance, selectivity, and pharmacological block, all consistent with the TMC proteins forming the transduction channel pore (Pan et al. 2013). Finally, TMC1 and TMC2 participate in a complex with other proteins mentioned above that are required for mechanotransduction.

Although alternative hypotheses can be proposed (Corey and Holt 2016), TMC1 and TMC2 meet almost all the criteria for the hair cell transduction channel. Further studies of structure and function will provide additional evidence that may confirm this identity.

4.3 Hair Bundle Mechanics and Motility

Hair bundles often exhibit active motility, that is, they may twitch at the onset of step stimuli, resonate in response to periodic stimuli, and even oscillate spontaneously. These behaviors require a source of activity (Sect. 4.3.6). Active hair bundle motility has been observed in fishes, amphibians, reptiles and birds but not (yet) in mammals. The absence of evidence for active motility in mammals does not mean it is not there but may indicate that experimental conditions have not yet replicated conditions in vivo. However, observations in nonmammalian species can show how active motion arises and indicate the circumstances in which active hair bundle motility might be expected in mammals.

4.3.1 Nonlinear Mechanics and Channel Gating

As a result of the transduction channel gating, hair bundle mechanics is inherently nonlinear (Howard and Hudspeth 1988). The theoretical consequences for bundle mechanics can be developed as follows.

For simplicity, assume that a channel has two states and that adaptation is not present. The probability (P_O) of the channel being open is then given by

$$P_O = 1/[1 + \exp(-Z(X - X_0)/(k_B T))] \tag{4.1}$$

in which X is the displacement of the tip of a hair bundle, X_0 is the bundle's position when $P_O = 0.5$, k_B is Boltzmann's constant, and T is absolute temperature. The single-channel "gating force" ($Z = \gamma k_{GS} d$) depends on the stiffness of the gating spring (k_{GS}), the gating swing (d), and the geometric factor ($\gamma = x/X$) relating gating-spring extension x to bundle displacement X. Z is a measure of a channel's sensitivity and is equal to the change in gating-spring tension when the channel opens.

If the hair bundle moves as a unit, then the N channels of the bundle gate in parallel. Denoting K_{SP} as the combined stiffness of the stereociliary pivots with reference position (X_{SP}), the external force (F_E) required to hold the bundle at a fixed displacement (X) is

$$F_E = K_\infty X - NZP_O + F_R \tag{4.2}$$

where $K_\infty = K_{SP} + N\gamma^2 k_{GS}$ and $F_R = -K_{SP}X_{SP} - N\gamma k_{GS}x_{GS}$ is a constant force that depends on the reference extension of the gating springs x_{GS}. The slope of the displacement-force relationship (Eq. 4.2) corresponds to a hair bundle stiffness and is negative if Z is sufficiently large (Fig. 4.4). When $P_O = 0.5$, the bundle possesses negative stiffness for the condition

$$Z > Z_{NS} = (4k_B T K_\infty / N)^{1/2} \tag{4.3}$$

The single-channel gating force Z can be estimated from the transduction current, which is proportional to P_O (Eq. 4.1) or from the displacement-force relationship (Eq. 4.2). The maximum gating forces in the mammalian cochlear apex (>0.3 pN; van Netten and Kros 2000) are on the same order of magnitude as those in the turtle (0.3–0.7 pN; Ricci et al. 2002) or in the frog (Martin et al. 2000). The mammalian measurements may underestimate the gating force, however, because they assume that adaptation does not affect channel opening significantly and that the stimulus is uniform across stereocilia, neither of which is likely to be true (Ó Maoiléidigh and Hudspeth 2013; Nam et al. 2015).

Adaptation can also create a region of negative slope in measured displacement-force relationships. Because adaptation can produce forces that are not dependent on bundle position alone, this slope is not a stiffness (Kennedy et al. 2005).

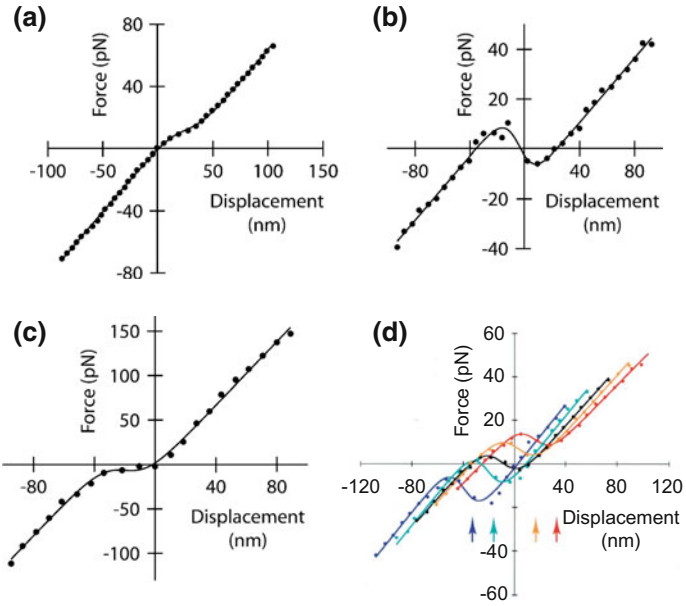

Fig. 4.4 Empirical displacement-force relationships. **a** A quiescent hair bundle has a nonlinear displacement-force relationship. A fit to Eq. 4.2 yields Z = 0.41 pN such that $Z < Z_{NS}$, where Z_{NS} is given by Eq. 4.3. **b** A spontaneously oscillating hair bundle possesses negative stiffness as Z = 0.68 pN > Z_{NS}. **c** Another quiescent bundle has a displacement-force region with a slope close to zero, corresponding to Z = 0.44 pN ≈ Z_{NS}. **d** Adaptive shift of the displacement-force relationship. Displacement-force relationships are measured after the bundle has adapted to offsets from its initial position by 0 nm (*black*), 16 nm (*orange*), 33 nm (*red*), −16 nm (*cyan*), and −33 nm (*blue*). Fits yield Z = 0.53–0.64 pN. The relationships shift along a line of slope 400 μN/m. **a**–**c** From Tinevez et al. (2007), with permission; **d** from Martin et al. (2000), with permission

Negative stiffness is a passive property of hair bundles but is necessary for the spontaneous oscillations of bundles seen in many experiments (Martin et al. 2003).

4.3.2 Adaptation and Active Motility

"Slow adaptation" (Sects. 4.1 and 4.2) in the vestibular systems of frogs and mice is likely the consequence of myosin motors that maintain tension in the tip links (Howard and Hudspeth 1987; Holt et al. 2002). An increase in tension is thought to cause the upper end of a tip link to slip down along the side of a stereocilium, reducing the gating-spring extension by an amount x_a. In nonmammalian vertebrates this process is accelerated by intracellular Ca^{2+}. In the presence of adaptation, the open probability of the channels P_O is given by

$$P_O = 1/\{1 + \exp[-Z(X - X_a - X_0)/(k_B T)]\} \quad (4.4)$$

where $X_a = x_a/\gamma$. Adaptation changes the force on the channel resulting in a displacement-force relationship with an additional term $K_{GS}X_a$ given by

$$F_E = K_\infty X - NZP_O + F_R - K_{GS}X_a, \quad (4.5)$$

where $K_{GS} = N\gamma^2 k_{GS}$ is a stiffness due to all the gating springs. Holding the adaptation variable X_a at different constant values shifts the displacement-force curve along a line of slope K_{SP} (Fig. 4.4d).

Active hair bundle motility can be described by combining Eq. 4.5 with a dynamical equation for myosin-based adaptation and a term that takes hair bundle damping into account (Martin et al. 2003). The resulting model produces transduction-current dynamics with two relaxation timescales, fast and slow, suggesting that adaptation can be explained by just one mechanism (Tinevez et al. 2007). However, myosin activity is likely to be too slow to account for fast adaptation in mammals (Sect. 4.1.4.2). In addition, the transduction channels are 200 nm or more distant from the motors so the speed of myosin-based adaptation is severely limited by calcium diffusion (and there are no channels that could modulate Ca^{2+} for motors in the tallest stereocilia).

4.3.3 Mechanical Loading

Hair bundles from different organs and organisms produce a variety of active behaviors (Fig. 4.5). The myosin-based model can account for these movements (Tinevez et al. 2007), but this does not necessarily imply that myosin motors are the basis for activity in all of these systems. The myosin model depends on a large number of adjustable parameters, which can reproduce many different observations but obscure understanding of why the model matches experiments so well.

The behavior of the myosin-based model can be depicted as a function of the stiffness of the pivot springs plus the stiffness (K_{AS}) of any accessory structures attached to the bundle (i.e., $K = K_{SP} + K_{AS}$) and the constant force produced by their reference extensions ($F_C = K_{SP}X_{SP} + K_{AS}X_{AS}$; Fig. 4.6). Different operating points correspond to bundles or accessory structures with distinct properties. A bundle can be bistable, possessing two stable resting positions and can oscillate spontaneously, or it can have a single stable position. Models for adaptation based on channel or calcium dynamics possess state diagrams with the same structure leading to difficulties in determining which model corresponds best to reality (Ó Maoiléidigh et al. 2012).

To understand why many quantitative models produce the same behaviors, it is useful to consider a qualitative model constructed using only a few key features of bundle dynamics. First, the adaptation process produces a force (F) on the bundle. Second, the hair bundle displacement-force relationship is nonlinear due to channel

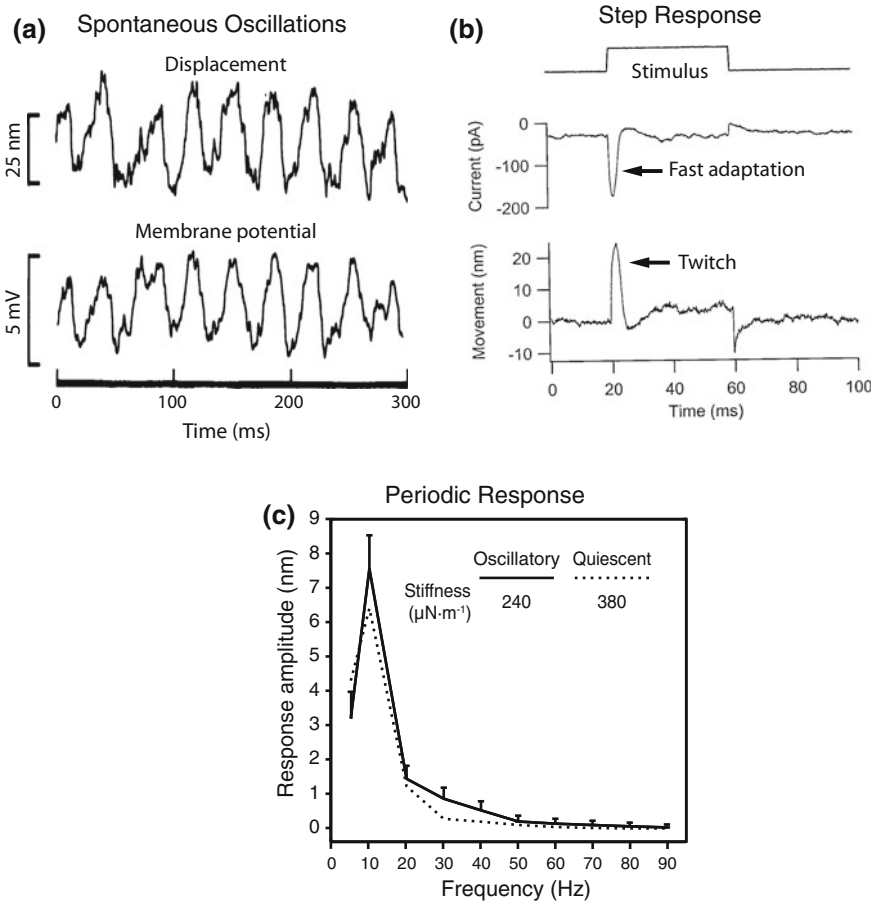

Fig. 4.5 Active hair bundle motility. **a** Spontaneous oscillations of a hair bundle from the auditory organ of the turtle create oscillations in the receptor potential. **b** A hair bundle from the auditory organ of the turtle twitches in response to a step stimulus. The dynamics of the twitch's recoil matches that of fast adaptation. **c** Spontaneous oscillations of a frog saccular hair bundle can be suppressed by increasing its load stiffness. This hair bundle resonates when it is oscillating spontaneously and can be induced to oscillate when it is quiescent. **a** From Crawford and Fettiplace (1985), with permission; **b** from Ricci et al. (2000), with permission; **c** from Salvi et al. (2015), with permission

gating (Fig. 4.4), possibly with a region of negative slope, and most simply described by the cubic equation $A(X - F) - (X - F)^3 + F_E = 0$. Third, adaptation shifts the displacement-force relationship, which consequently must depend on the force (Fig. 4.4d). Finally, the dynamics of the adaptation force must exhibit two properties. The adaptation force is a function of bundle displacement, most simply described by a linear term proportional to X, and adaptation takes time to act. To reduce the number of independent parameters, the model can be rescaled such that

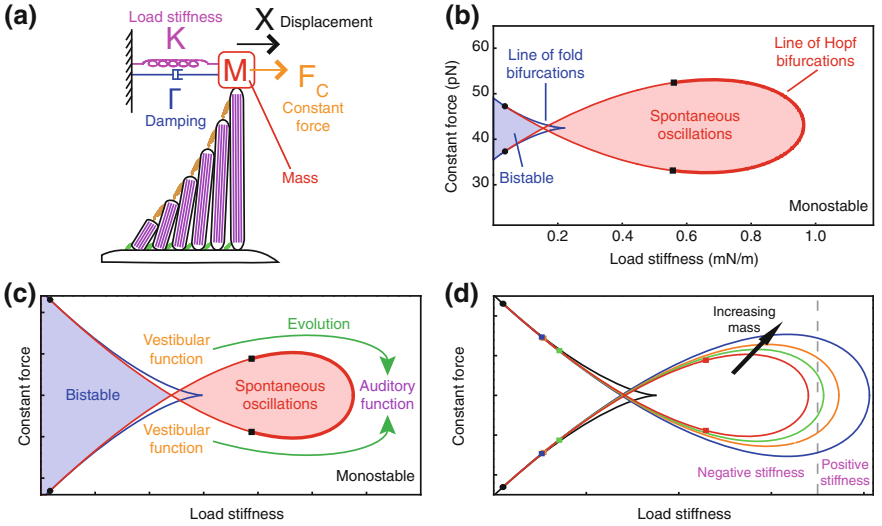

Fig. 4.6 Modeling hair bundle dynamics. **a** A hair bundle and an accessory structure load the hair bundle with a constant force (F_C), a stiffness (K), a damping constant (Γ), and a mass (*M*). **b** The state diagram for a physically detailed model. A line of supercritical (*thick red*) and subcritical (*thin red*) Hopf bifurcations encloses the region of spontaneous oscillations. The bistable region is bounded by a line of fold bifurcations. A hair bundle is monostable for other operating points. **c** A general model captures the qualitative structure of a hair-bundle state diagram described by Eqs. 4.6 and 4.7. A hair bundle operating near the line of subcritical Hopf bifurcations is suitable for vestibular organs. An auditory hair bundle is expected to display great sensitivity to periodic stimuli when it operates close to the line of supercritical Hopf bifurcations. Bundles with vestibular function may have evolved to have auditory function (*green arrows*). **d** State diagrams for hair bundles with different mass loads (Eqs. 4.6, 4.7). A hair bundle lacks negative stiffness for large values of the load stiffness but can still oscillate spontaneously due to its mass load. Modified from Ó Maoiléidigh et al. (2012), with permission

X and F have the same units. The hair bundle mechanical load possesses a stiffness (K), a damping constant (Γ), a mass (*M*), and a constant force (F_C; see Fig. 4.6a). The resulting equations describing a mechanically loaded hair bundle are

$$dX/dt = A(X - F) - (X - F)^3 - KX - \Gamma dX/dt - Md^2X/dt^2 + F_C + F_E \quad (4.6)$$

$$\tau dF/dt = BX - F \quad (4.7)$$

Here A is a stiffness resulting from channel gating, τ is the adaptation time constant, and B is the sensitivity of adaptation to bundle displacement. These equations describe the qualitative features of active hair bundle motility independently of whether it arises from channel reclosure, myosin motors, or any other type of active adaptation.

It is instructive to consider a mechanical load without damping ($\Gamma = 0$) or mass ($M = 0$). The qualitative model's state diagram has the same structure as diagrams resulting from many types of adaptation mechanisms (Fig. 4.6c). The diagram depicts the loci of several types of bifurcation, a qualitative change in the dynamics of a system. In response to shifting the operating point from the monostable region to the oscillatory regime, the amplitude of spontaneous oscillations increases continuously from zero at a supercritical Hopf bifurcation line or jumps discontinuously to a nonzero value at a subcritical Hopf bifurcation line. Raising the load stiffness increases the frequency of oscillations but decreases their amplitude. Experimentally, hair bundles possess state diagrams with all these features (Salvi et al. 2015).

The parameter A is analogous to the single-channel gating force Z, and a bundle possesses negative stiffness when $A > K$. Spontaneous oscillations have not been seen in mammalian bundles, perhaps because they are much stiffer than those of nonmammals and consequently do not possess negative stiffness. Spontaneous oscillations in this model also only occur for a limited range of constant forces (F_C), as found experimentally.

Increasing the damping constant Γ causes the spontaneously oscillatory region of a bundle's state diagram to shrink. In contrast, a rise in the mass M increases the size of the oscillatory region (Fig. 4.6d). Thus, a mass-loaded hair bundle is predicted to oscillate spontaneously even if it does not possess negative stiffness.

Spontaneous oscillations in the hair bundle could be the source of spontaneous otoacoustic emissions (SOAEs). In mammalian OHCs, spontaneous bundle oscillations would produce receptor potential oscillations and drive somatic electromotility. A hair bundle state diagram therefore implies that a decrease in the tectorial membrane's stiffness, decreasing the load on OHC bundles, would lead to an increase in the number and magnitude of SOAEs, accompanied by a decrease in their frequency (Ó Maoiléidigh and Hudspeth 2013). These predictions have recently been confirmed in a mutant mouse with a tectorial membrane that is detached from the bony wall of the cochlea (Cheatham et al. 2016).

Hair bundles can exhibit mixed-mode oscillations at low-load stiffnesses (Roongthumskul et al. 2011). Spontaneous oscillations appear and disappear as if the bundle were moving periodically across a subcritical Hopf bifurcation. To account for these observations, an additional variable would have to be added to Eqs. 4.6 and 4.7. It is unclear, though, whether such oscillations are associated with hair bundle function.

4.3.4 Response to Step Deflections

A hair bundle can respond to the onset of a positive force step by generating a twitch (Fig. 4.5b). This has been described above as resulting from a Ca^{2+}-dependent channel closure, which pulls the stereocilia back. It can alternatively be understood as adaptation moving the hair bundle moving across the nonlinear

portion of the displacement-force relationship and causing a recoil (Tinevez et al. 2007). Bundles do not twitch if their operating point is too far from the region of spontaneous oscillation, in agreement with observations (Salvi et al. 2015). Equations 4.6 and 4.7 predict that twitches are especially large when a bundle operates near a subcritical Hopf bifurcation. Vestibular organs that respond to step stimuli corresponding to head tilting, rotation, and acceleration are predicted to have hair bundles that operate near subcritical Hopf bifurcations.

The timescales of fast adaptation and twitches match (Fig. 4.5b), but mammalian bundles showing fast adaptation have not been observed to twitch (Kennedy et al. 2005). Due to the large stiffness of the bundle, the operating point of a mammalian bundle loaded by a stimulus fiber is too far from the region of spontaneous oscillation for twitches to arise. Mass-loaded hair bundles from mammals are still predicted to twitch, however, despite their large stiffness (Ó Maoiléidigh et al. 2012).

Hair bundles have been observed in experiments to move farther than the base of the stimulus fiber without recoil (Kennedy et al. 2005; Salvi et al. 2015). Such a movement is expected to take place when the stimulus moves the bundle so far across the nonlinear portion of the displacement-force relationship that adaptation cannot cause the bundle to recoil. In principle, neither negative stiffness nor adaptation is necessary for this movement; the only requirement is nonlinear stiffness.

4.3.5 Amplification of Periodic Stimuli

Spontaneously oscillating and quiescent hair bundles can resonate in response to periodic stimuli (Martin and Hudspeth 2001; Fig. 4.5). A quiescent bundle is most sensitive and frequency selective, however, when it operates near a boundary of spontaneous motion, a supercritical Hopf bifurcation (Fig. 4.6b). In addition, the response at the resonant frequency can depend sublinearly on the stimulus amplitude, compressing the input range onto a smaller output scale. When the range of forces over which compression occurs is larger, the closer the bundle operates to a Hopf bifurcation.

A stimulus fiber is most effective at extracting energy from a spontaneously oscillating or spiking hair bundle when the fiber entrains the bundle (Martin and Hudspeth 1999). Weak periodic stimuli are most easily entrained when a bundle is close to a Hopf bifurcation, and so the operating point of a bundle determines whether it can produce mechanical work (Salvi et al. 2015).

Sensitive, sharply tuned, and compressed responses to sound are characteristic features of auditory organs. All systems operating near a supercritical Hopf bifurcation exhibit these properties and possess the same dynamics regardless of their underlying mechanisms (Hudspeth 2014). Correspondingly, auditory systems might have evolved to operate close to supercritical Hopf bifurcations. Individual hair

bundles can be experimentally manipulated to operate near such a bifurcation and consequently exhibit the three signature response characteristics (Salvi et al. 2015).

The mass of the tectorial membrane is sufficiently large to poise an OHC bundle close to a supercritical Hopf bifurcation such that it resonantly amplifies periodic input (Ó Maoiléidigh and Hudspeth 2013). A similar argument may also explain why a lizard with hair bundles loaded by tectorial sallets exhibits lower thresholds and shaper tuning than a lizard with free-standing bundles (Manley 2000, 2001).

Theoretically, the sensitivity, frequency selectivity, and range of compression of a spontaneously oscillating hair bundle are limited by noise (Dierkes et al. 2008; Lindner et al. 2009). Observations and calculations show, however, that the effects of noise may be mitigated by coupling groups of bundles together so that they synchronize (Barral et al. 2010). The gain of an individual hair bundle, the ratio of the sensitivities at high and low input levels, is only about 10 (Martin and Hudspeth 2001). It remains to be seen whether coupling contributes significantly to the gain and bandwidth of the mammalian cochlea (see Gummer, Dong, Ghaffari, and Freeman, Chap. 6). In mammals, the gain can be as large as 1000 in the high-frequency cochlear region (Robles and Ruggero 2001). Coupling was similarly predicted to increase sensitivity in the tokay gecko (*Gekko gecko*; Authier and Manley 1995).

4.3.6 The Energy for Amplification

Amplification, that is, the increase in amplitude over any passive response, does not necessarily require energy. It is widely thought, however, that amplification in the cochlea arises from an active process that adds energy to sound-induced vibrations, and so it is essential to understand the cellular basis of the energy source. In the mammalian cochlea, the endocochlear potential and the resting potential of an OHC determine the magnitude of the transducer current (Patuzzi 1998). The endocochlear potential is determined by the metabolic activity of the stria vascularis. For hair bundle amplification, two possible sources are the electrochemical gradients of permeant ions, especially Ca^{2+}, and ATP-driven molecular motors.

An electrochemical Ca^{2+} gradient is created by ATP-driven calcium pumps on the hair cell apical surface (Crouch and Schulte 1995; Yamoah et al. 1998), by the resting potential of the hair cell, and in the mammalian cochlea, by the endocochlear potential. The gradient ensures that calcium will always flow into the stereocilia. As result, cyclic entry of Ca^{2+} and binding to the transduction channel could be capable of transducing this electrochemical gradient into mechanical work. In addition, myosin motors could also perform mechanical work by applying forces on tip links and consequently displacing the bundle (Howard and Hudspeth 1987).

Negative stiffness can shape an active process, but it is a passive consequence of channel gating and cannot power activity. During stimulation, some of the energy required to displace a hair bundle into its region of negative stiffness is provided by the adaption process. Subsequently, a hair bundle moves away from the unstable

negative-stiffness region and performs work on its environment. This cyclic process can amplify the response to periodic driving by reducing the input energy required for motion (Martin et al. 2000).

4.3.7 Stimulation with Two Frequencies

The passive nonlinearity resulting from channel gating produces distortion products in the response of a hair bundle to stimulation with two primary frequencies $f_1 < f_2$ (Jaramillo et al. 1993). The distortions from an active hair bundle are, however, different from those of a passive system. For example, with an active process, the odd distortion products $2f_1 - f_2$ and $2f_2 - f_1$ can be manipulated by setting the operating point so as to be larger than the even products $f_2 - f_1$ and $f_1 + f_2$, when the input is weak and the stimulus frequencies are close to the resonant frequency of the bundle. Additionally, for stimuli near the resonant frequency, the magnitude of the odd distortion products relative to the responses at the primary frequencies is almost independent of the stimulus level, in agreement with psychophysical studies and direct observations of basilar membrane motion. These and other properties of distortions from an active hair bundle can be explained by its operation near a Hopf bifurcation (Jülicher et al. 2001; Barral and Martin 2012).

4.3.8 Calcium Effects on Bundle Movement

Because adaptation is Ca^{2+} dependent, altering extracellular Ca^{2+} elicits bundle movements (Fig. 4.7). The same step change in extracellular Ca^{2+} can, however, induce motion in either the positive or negative direction, with or without a twitch. The response to a sudden change in Ca^{2+} depends qualitatively on the constant force load (Tinevez et al. 2007). Depending on the operating point, spontaneous oscillations can be suppressed by raising or lowering the extracellular Ca^{2+} but elevating Ca^{2+} always increases the oscillation frequency (Martin et al. 2003; Manley et al. 2004; Fig. 4.7b).

4.3.9 Electrically Driven Motion

Depolarizing a hair cell can lower the calcium level within stereocilia. As a consequence, spontaneous oscillations can be slowed or suppressed by depolarization (Fig. 4.7c). Membrane potential changes evoke bundle movements with timescales similar to both slow and fast adaptation (Fig. 4.7d).

Hair bundles also exhibit voltage-induced motions that are independent of calcium entry through the transduction channels (Fig. 4.7d). Blocking the transduction

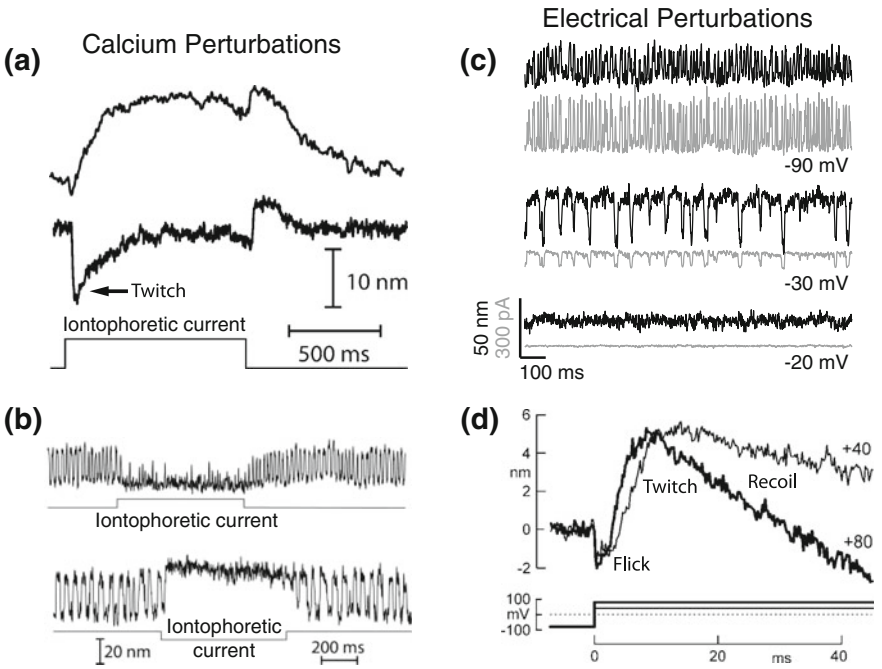

Fig. 4.7 Dependence of hair bundle dynamics on Ca^{2+} and membrane potential in the bullfrog sacculus. **a** Iontophoretic changes in extracellular Ca^{2+} evoke hair bundle movements. Hair bundles move in the positive direction (*top*) or twitch in the negative direction (*bottom*) in response to the same increase in extracellular Ca^{2+}. **b** An increase in extracellular Ca^{2+} can suppress spontaneous hair bundle oscillations (*top*). An iontophoretic pulse of ATP lowered the extracellular Ca^{2+}, quenching spontaneous oscillations (*bottom*). **c** Spontaneous oscillations become slower and more erratic as the membrane potential is increased until they are eventually suppressed. **d** A bundle can flick and twitch with a slow recoil in response to depolarizing steps in the membrane potential. **a** From Tinevez et al. (2007), with permission; **b** from Martin et al. (2003), with permission; **c** from Meenderink et al. (2015), with permission; **d** from Cheung and Corey (2006), with permission

channels does not abolish this motion, known as a "flick," but it does require intact tip links (Ricci et al. 2000; Cheung and Corey 2006). Flicks are likely the result of an unknown voltage-sensitive element associated with the transduction apparatus.

4.4 Electromotility of Mammalian Outer Hair Cells and Its Role in Amplification

Mammalian cochleae have two types of hair cells: IHCs that signal cochlear activity to the nerve and three or more rows of OHCs that have a motor function, amplifying the partition amplitude at low stimulus levels and thus the input to IHCs by

100-fold or more. Amplification, in principle, may be produced by a combination of two mechanisms: one produced by the hair bundle (discussed in Sect. 4.3) and one by the cell body.

OHCs rapidly shorten with depolarization, lengthen with hyperpolarization, and produce mechanical force. This process is known as electromotility and is driven by the protein SLC26A5/prestin, a member of the SLC26/SulP anion transporter family (see Santos-Sacchi, Navaratnam, Raphael, and Oliver, Chap. 5). Electromotility can be studied in vivo (Zha et al. 2012), in isolated temporal bones (Mammano and Ashmore 1993), in isolated strips, and in single isolated cells.

Electromotility can be measured in several ways. Although the length can be measured directly by fast video cameras, this method has a limited bandwidth. More common is to project an image of the OHC cuticular plate through the microscope onto a differential pair of photodiodes. With suitable circuitry, such a detector has a bandwidth of at least 20 kHz (Dallos and Evans 1995). An alternative is to measure velocity with a laser Doppler vibrometer, focused either on the cuticular plate to measure electromotility or on the cantilever of an atomic force microscope positioned against the cuticular plate to measure electromechanical force. With this method, the bandwidth of the measurement system exceeds 100 kHz (Frank et al. 1999). Voltage control must be similarly fast. With whole cell recording, the bandwidth is seldom over 20 kHz, but with an OHC sucked into a snugly fitting glass capillary, the measured frequency limit is nearly 80 kHz. Such measurements show that OHC electromotility faithfully follows the membrane potential to at least 50 kHz, above the hearing range of many mammals.

A variety of other voltage-induced length changes are known, but these are slower and often involve the movement of fluid in and out of the cells (reviewed in Ashmore 2008).

4.4.1 Active Hair Bundle Motility in the Cochlea

Active hair bundle motility has yet to be observed in OHCs. However, observations in isolated cochleae indicate that somatic electromotility and active hair bundle motility could coexist in mammals. In the gerbil (*Meriones unguiculatus*), replacing K^+ in the endolymph with a large monovalent cation that does not permeate the MET channel eliminates the receptor potential, abolishing the drive for somatic electromotility, but still allows Ca^{2+} entry that could drive hair bundle motility. The response of the cochlea remains nonlinear and dependent on the endocochlear potential, apparently due to active hair bundle motility (Chan and Hudspeth 2005). In rat cochlear hair cells in vitro, OHC bundles move by up to 60 nm in response to depolarization under conditions when most of the somatic electromotility is blocked (Kennedy et al. 2006). Bundle movement was blocked by dihydrostreptomycin, which blocks the transduction channel, or by reducing extracellular Ca^{2+}. Both are consistent with the idea that Ca^{2+} entry at negative potentials drives hair bundle motility.

4.4.2 Modeling Motile Forces in the Cochlea

The relative roles of hair bundle motility and somatic electromotility have been explored in mathematical models of cochlear micromechanics. This has not led to a consensus because the complexity of cochlear mechanics and uncertainties associated with the components of the cochlea. Different simplifications and assumptions have led to a variety of conclusions.

In one class of models, explicit mechanisms for active hair bundle motility are not included. Instead, it is only assumed that active hair bundle motility formally produces an active force. This force increases the sensitivity of the cochlea significantly (Reichenbach and Hudspeth 2010) and can deform the cochlear partition as much as somatic electromotility (Nam and Fettiplace 2010).

A second class of models includes an explicit description for active hair bundle motility. According to such models, active hair bundle motility either reduces the sensitivity of the cochlea (Meaud and Grosh 2011), increases the cochlear vibrations only slightly in comparison to somatic electromotility (Nam and Fettiplace 2012), or raises the sensitivity of the cochlea significantly if the parameters controlling bundle activity are chosen appropriately (Ó Maoiléidigh and Jülicher 2010).

A third class of models supposes that somatic electromotility alone can account for most experimental observations, including the sensitivity of the cochlea to weak stimuli (Nobili and Mammano 1996; Ramamoorthy et al. 2007). Experimentally, somatic electromotility is required for amplification (Dallos et al. 2008), but unlike active hair bundle motility, somatic electromotility *alone* does not amplify mechanical stimuli. A nonlinear active process that amplifies mechanical input can be constructed by a combination of somatic electromotility with the nonlinearity of mechanotransduction, with the endocochlear potential as an energy source, and with feedback due to mechanical coupling between OHCs and other components of the cochlea such as the tectorial membrane. This system can possess a Hopf bifurcation and consequently exhibit great sensitivity, sharp tuning, and a large dynamic range (Ó Maoiléidigh and Jülicher 2010).

4.4.3 The RC Time-Constant Problem and Interaction Between Active Hair Bundle Motility and Somatic Electromotility

As mentioned in Sect. 4.1.5, the low-pass filter created by the membrane time constant (the product of the membrane resistance and capacitance, equal to RC) limits the speed at which the membrane potential can change and thus the speed of somatic electromotility. How can electromotility drive amplification at many tens of kilohertz when the filter reduces the oscillatory receptor potential above about 1 kHz? This is the “RC time-constant problem.”

There have been numerous suggested solutions to this problem. These include (1) that the extracellular potential gradients are large enough to cancel the potential drop across the basolateral membrane (Dallos and Evans 1995); (2) that there is a tuned resonant current in OHCs sufficient to compensate for the low-pass filter (Ospeck et al. 2003); (3) that the piezoelectricity of the basolateral membrane enhances voltage changes (Weitzel et al. 2003); (4) that the hair bundle generates sufficient force to obviate the need for electromotility; (5) that there are stretch-activated anion channels that effectively convert a voltage-driven mechanism into a current-driven one (Rybalchenko and Santos-Sacchi 2003); (6) that a parallel resonance between tectorial membrane inertia and OHC bundle radial stiffness compensates the phase delay of the low-pass filter (Gummer et al. 1996); (7) that active hair bundle motility amplifies the receptor potential driving somatic motility (Ó Maoiléidigh and Hudspeth 2013); and (8) that the membrane time constant in vivo is much smaller than originally thought (Johnson et al. 2011).

The last solution has considerable merit. In vivo, high-frequency OHCs have a resting open probability close to 50%, which produces a large standing current that depolarizes the hair cell to a region that would activate the KCNQ4 K^+ channel. In addition, high-frequency hair cells are smaller and have less capacitance. Both reduce the time constant and increase the low-pass filter frequency. For hair cells responding best to a 10-kHz sound, the predicted filter frequency (6–7 kHz) is only slightly less, indicating that electromotility could function at such frequencies (Johnson et al. 2011).

Finally, somatic electromotility can influence active hair bundle motility. In one scenario, somatic electromotility creates a force on the hair bundle that is in phase with its velocity (Ó Maoiléidigh and Jülicher 2010). This force opposes the damping forces on the hair bundle, allowing active hair bundle motility to operate at higher frequencies. In contrast, forces produced by active hair bundle motility do not appear to have a significant effect on the OHC soma.

4.5 Unresolved Problems

Although there has been extraordinary progress since *The Cochlea* was published 21 years ago (Dallos et al. 1996), many problems remain.

4.5.1 The Upper Frequency Limit of Hearing

Some species can hear into the ultrasonic acoustic range, which may exceed 100 kHz, but it is not known which factors set this limit. Although thermodynamic considerations determine the mean open probability of the MET channel, it is

necessary to know more about the rates at which the MET channel can open and close. These frequencies are at the limit or beyond the bandwidth of current cellular recording methods and so techniques need to improve, for both stimulating the hair bundle and measuring transduction kinetics.

4.5.2 The Nature of the Transduction Complex

Five proteins are known to be located in or near the transduction complex at the lower end of each tip link, and something is known about the way they are connected. But their atomic structures and how they are linked (or not) in the complex remain unknown. How force is transmitted along the tip link to the proteins of the complex needs to be understood and how that causes a channel to open. The motor complex at the upper end of the tip link, which mediates the tip-link attachment and regulates its tension, must also still be understood. Finally, there are likely to be additional protein components that remain to be discovered.

4.5.3 Fast Adaptation and the Nature of Active Hair Bundle Motility

The fast Ca^{2+}-dependent closure of channels after they are opened by mechanical stimuli has been fairly well characterized in nonmammalian vertebrates but remains confusing in mammals. How (or even whether) Ca^{2+} controls fast adaptation needs to be better understood, and how Ca^{2+} interacts with the transduction complex proteins to do so. How (or even whether) fast adaptation drives active hair bundle motility in the mammalian cochlea remains unknown. Because active hair bundle motility may be an essential component of amplification and tuning in the cochlea, cochlear function can probably not be understood without understanding fast adaptation.

4.5.4 Somatic Electromotility

SLC26A5/prestin is also required for tuning of the basilar membrane, yet it is still unclear exactly how it operates as a molecular actuator. There is no atomic structure for the molecule as yet, although there are some excellent starting points (as described by Santos-Sacchi, Navaratnam, Raphael, and Oliver, Chap. 5). Structural techniques, computational or experimental, are needed to visualize the molecular processes in operation.

4.5.5 The Origin of Cochlear Amplification

Finally, to fully understand the basis of cochlear amplification, active hair bundle motility and somatic electromotility need to be integrated into a model that also incorporates the cellular and acellular mechanics of the cochlea. This is a very hard problem, but, with luck, this question will have been already answered when the next volume on the cochlea appears 21 years from now.

Compliance with Ethics Requirements David P. Corey declares that he has no conflict of interest. Dáibhid Ó Maoiléidigh declares that he has no conflict of interest. Jonathan F. Ashmore declares that he has no conflict of interest.

References

Adato, A., Michel, V., Kikkawa, Y., Reiners. J., Alagramam, K. N., Weil, D., Yonekawa, H., Wolfrum, U., El-Amraoui, A., & Petit, C. (2005). Interactions in the network of Usher syndrome type 1 proteins. *Human Molecular Genetics,* 14, 347–356.

Adrian, E. D. (1931). The microphonic action of the cochlea: An interpretation of Wever and Bray's experiments. *Proceedings of the Physiological Society, The Journal of Physiology*, 71, xxviii–xxix.

Ahmed, Z. M., Riazuddin, S., Bernstein, S. L., Ahmed, Z., Khan, S., Griffith, A. J., Morell, R. J., Friedman, T. B., Riazuddin, S., & Wilcox, E. R. (2001). Mutations of the protocadherin gene *PCDH15* cause Usher syndrome type 1F. *American Journal of Human Genetics,* 69, 25–34.

Alagramam, K. N., Murcia, C. L., Kwon, H. Y., Pawlowski, K. S., Wright, C. G., & Woychik, R. P. (2001). The mouse Ames waltzer hearing-loss mutant is caused by mutation of *Pcdh15*, a novel protocadherin gene. *Nature Genetics,* 27, 99–102.

Ashmore, J. (2008). Cochlear outer hair cell motility. *Physiological Reviews*, 88, 173–210.

Assad, J. A., Hacohen, N., & Corey, D. P. (1989). Voltage dependence of adaptation and active bundle movement in bullfrog saccular hair cells. *Proceedings of the National Academy of Sciences of the United States of America,* 86, 2918–2922.

Assad, J. A., Shepherd, G. M., & Corey, D. P. (1991). Tip-link integrity and mechanical transduction in vertebrate hair cells. *Neuron,* 7, 985–994.

Authier, S., & Manley, G. A. (1995). A model of frequency tuning in the basilar papilla of the Tokay gecko, *Gekko gecko*. *Hearing Research* 82, 1–13.

Barral, J., & Martin, P. (2012). Phantom tones and suppressive masking by active nonlinear oscillation of the hair cell bundle. *Proceedings of the National Academy of Sciences of the United States of America,* 109, E1344–E1351.

Barral, J., Dierkes, K., Lindner, B., Jülicher, F., & Martin, P. (2010). Coupling a sensory hair cell bundle to cyber clones enhances nonlinear amplification. *Proceedings of the National Academy of Sciences of the United States of America,* 107, 8079–8084.

Beurg, M., Evans, M. G., Hackney, C. M., & Fettiplace, R. (2006). A large-conductance calcium-selective mechanotransducer channel in mammalian cochlear hair cells. *The Journal of Neuroscience,* 26, 10992–11000.

Beurg, M., Fettiplace, R., Nam, J. H., & Ricci, A. J. (2009). Localization of inner hair cell mechanotransducer channels using high-speed calcium imaging. *Nature Neuroscience,* 12(5), 553–558.

Beurg, M., Nam, J. H., Chen, Q., & Fettiplace, R. (2010). Calcium balance and mechanotransduction in rat cochlear hair cells. *Journal of Neurophysiology,* 104, 18–34.

Beurg, M., Xiong, W., Zhao, B., Müller, U., & Fettiplace, R. (2015). Subunit determination of the conductance of hair cell mechanotransducer channels. *Proceedings of the National Academy of Sciences of the United States of America,* 112, 1589–1594.

Bork, J. M., Peters, L. M., Riazuddin, S., Bernstein, S. L., Ahmed, Z. M., Ness, S. L., Polomeno, R., Ramesh, A., Schloss, M., Srisailpathy, C.,R., Wayne, S., Bellman, S., Desmukh, D., Ahmed, Z., Khan, S. N., Kaloustian, V. M., Li, X. C., Lalwani, A., Riazuddin, S,, Bitner-Glindzicz, M., Nance, W. E., Liu, X. Z., Wistow, G., Smith, R. J., Griffith, A. J., Wilcox, E. R., Friedman, T. B., & Morell, R. J. (2001). Usher syndrome 1D and nonsyndromic autosomal recessive deafness DFNB12 are caused by allelic mutations of the novel cadherin-like gene *CDH23*. *American Journal of Human Genetics,* 68, 26–37.

Chakrapani, S., & Auerbach, A. (2005). A speed limit for conformational change of an allosteric membrane protein. *Proceedings of the National Academy of Sciences of the United States of America,* 102, 87–92.

Chan, D. K., & Hudspeth, A. J. (2005). Ca^{2+} current-driven nonlinear amplification by the mammalian cochlea in vitro. *Nature Neuroscience,* 8, 149–155.

Cheatham, M. A., Ahmad, A., Zhou, Y., Goodyear, R. J., Dallos, P., & Richardson, G. P. (2016). Increased spontaneous otoacoustic emissions in mice with a detached tectorial membrane. *Journal of the Association for Research in Otolaryngology*, 17, 81–88.

Cheung, E. L., & Corey, D. P. (2006). Ca^{2+} changes the force sensitivity of the hair cell transduction channel. *Biophysical Journal,* 90, 124–139.

Corey, D. P., & Hudspeth, A. J. (1979). Ionic basis of the receptor potential in a vertebrate hair cell. *Nature,* 281, 675–677.

Corey, D. P., & Hudspeth, A. J. (1983a). Analysis of the microphonic potential of the bullfrog's sacculus. *The Journal of Neuroscience*, 3, 942–961.

Corey, D. P., & Hudspeth, A. J. (1983b). Kinetics of the receptor current in bullfrog saccular hair cells. *Journal of Neuroscience,* 3, 962–976.

Corey, D. P., & Holt, J. R. (2016). Are TMCs the mechanotransduction channels of vertebrate hair cells? *The Journal of Neuroscience*, 36, 10921–10926.

Corns, L. F., Johnson, S. L., Kros, C. J., & Marcotti, W. (2014). Calcium entry into stereocilia drives adaptation of the mechanoelectrical transducer current of mammalian cochlear hair cells. *Proceedings of the National Academy of Sciences of the United States of America*, 111, 14918–14923.

Crawford, A. C., & Fettiplace, R. (1985). The mechanical properties of ciliary bundles of turtle cochlear hair cells. *The Journal of Physiology,* 364, 359–379.

Crawford, A. C., Evans, M. G., & Fettiplace, R. (1989). Activation and adaptation of transducer currents in turtle hair cells. *The Journal of Physiology*, 419, 405–434.

Crawford, A. C., Evans, M. G., & Fettiplace, R. (1991). The actions of calcium on the mechano-electrical transducer current of turtle hair cells. *The Journal of Physiology,* 434, 369–398.

Crouch, J. J., & Schulte, B. A. (1995). Expression of plasma membrane Ca-ATPase in the adult and developing gerbil cochlea. *Hearing Research*, 92, 112–119.

Dallos, P., & Cheatham, M. A. (1976). Production of cochlear potentials by inner and outer hair cells. *The Journal of the Acoustical Society of America,* 60, 510–512.

Dallos, P., & Evans, B. N. (1995). High-frequency motility of outer hair cells and the cochlear amplifier. *Science,* 267, 2006–2009.

Dallos, P., Popper, A. N., & Fay, R. R. (Eds.). (1996). *The Cochlea.* New York: Springer-Verlag.

Dallos, P., Wu, X., Cheatham, M. A., Gao, J., Zheng, J., Anderson, C. T., Jia, S., Wang, X., Cheng, W. H. Y., Sengupta, S., He, D. Z. Z., & Jian Zuo, J. (2008). Prestin-based outer hair cell motility is necessary for mammalian cochlear amplification. *Neuron,* 58, 333–339.

Delling, M., Indzhykulian, A. A., Liu, X., Doerner, J., Xie, T., Corey, D. P., & Clapham, D. E. (2016). Primary cilia are not calcium-responsive mechanosensors. *Nature,* 531, 656–660.

Denk, W., Holt, J. R., Shepherd, G. M. G., & Corey, D. P. (1995). Calcium imaging of single stereocilia in hair cells: Localization of transduction channels at both ends of tip links. *Neuron,* 15, 1311–1321.

Dierkes, K., Lindner, B., & Jülicher, F. (2008). Enhancement of sensitivity gain and frequency tuning by coupling of active hair bundles. *Proceedings of the National Academy of Sciences of the United States of America,* 105, 18669–18674.

Di Palma, F., Holme, R. H., Bryda, E. C., Belyantseva, I. A., Pellegrino, R., Kachar, B., Steel, K. P., & Noben-Trauth, K. (2001). Mutations in Cdh23, encoding a new type of cadherin, cause stereocilia disorganization in waltzer, the mouse model for Usher syndrome type 1D. *Nature Genetics*, 27, 103–107.

Eatock, R. A., Corey, D. P., & Hudspeth, A. J. (1987). Adaptation of mechanoelectrical transduction in hair cells of the bullfrog's sacculus. *The Journal of Neuroscience,* 7, 2821–2836.

Fettiplace, R., & Kim, K. X. (2014). The physiology of mechanoelectrical transduction channels in hearing. *Physiological Reviews*, 94, 951–986.

Flock, Å., & Wersäll, J. (1962). A study of the orientation of the sensory hairs of the receptor cells in the lateral line organ of fish, with special reference to the function of the receptors. *Journal of Cell Biology,* 15, 19–27.

Frank, G., Hemmert, W., & Gummer, A. W. (1999). Limiting dynamics of high-frequency electromechanical transduction of outer hair cells. *Proceedings of the National Academy of Sciences of the United States of America,* 96, 4420–4425.

Gale, J. E., Marcotti, W., Kennedy, H. J., Kros, C. J., & Richardson, G. P. (2001). FM1-43 dye behaves as a permeant blocker of the hair cell mechanotransducer channel. *The Journal of Neuroscience*, 21, 7013–7025.

Garcia, J. A., Yee, A. G., Gillespie, P. G., & Corey, D. P. (1998). Localization of myosin-Iβ near both ends of tip links in frog saccular hair cells. *The Journal of Neuroscience*, 18, 8637–8647.

Géléoc, G. S., & Holt, J. R. (2003). Developmental acquisition of sensory transduction in hair cells of the mouse inner ear. *Nature Neuroscience*, 6, 1019–1020.

Géléoc, G. S., Lennan, G. W., Richardson, G. P., & Kros, C. J. (1997). A quantitative comparison of mechanoelectrical transduction in vestibular and auditory hair cells of neonatal mice. *Proceedings of the Royal Society of London B: Biological Sciences,* 264, 611–621.

Gibson, F., Walsh, J., Mburu, P., Varela, A., Brown, K. A., Antonio, M., Beisel, K. W., Steel, K. P., & Brown, S. D. (1995). A type VII myosin encoded by the mouse deafness gene shaker-1. *Nature*, 374, 62–64.

Grati, M., & Kachar, B. (2011). Myosin VIIa and sans localization at stereocilia upper tip-link density implicates these Usher syndrome proteins in mechanotransduction. *Proceedings of the National Academy of Sciences of the United States of America,* 108, 11476–11481.

Gummer, A. W., Hemmert, W., & Zenner, H. P. (1996). Resonant tectorial membrane motion in the inner ear: Its crucial role in frequency tuning. *Proceedings of the National Academy of Sciences of the United States of America*, 93, 8727–8732.

Hallpike, C. S., & Rawdon-Smith, A. F. (1934). The "Wever and Bray phenomenon." A study of the electrical response in the cochlea with especial reference to its origin. *The Journal of Physiology,* 81, 395–408.

Holt, J. R., Gillespie, S. K., Provance, D. W., Shah, K., Shokat, K. M., Corey, D. P., Mercer, J. A., & Gillespie, P. G. (2002). A chemical-genetic strategy implicates myosin-1c in adaptation by hair cells. *Cell*, 108, 371–381.

Howard, J., & Ashmore, J. F. (1986). Stiffness of sensory hair bundles in the sacculus of the frog. *Hearing Research*, 23, 93–104.

Howard, J., & Hudspeth, A. J. (1987). Mechanical relaxation of the hair bundle mediates adaptation in mechanoelectrical transduction by the bullfrog's saccular hair cell. *Proceedings of the National Academy of Sciences of the United States of America*, 84, 3064–3068.

Howard, J., & Hudspeth, A. J. (1988). Compliance of the hair bundle associated with gating of mechanoelectrical transduction channels in the bullfrog's saccular hair cell. *Neuron*, 1, 189–199.

Hudspeth, A. J. (1982). Extracellular current flow and the site of transduction by vertebrate hair cells. *The Journal of Neuroscience*, 2, 1–10.

Hudspeth, A. J. (1983). The hair cells of the inner ear. *Scientific American*, 248, 54–64.

Hudspeth, A. J. (2014). Integrating the active process of hair cells with cochlear function. *Nature Reviews of Neuroscience*, 15, 600–614.

Hudspeth, A. J., & Corey, D. P. (1977). Sensitivity, polarity, and conductance change in the response of vertebrate hair cells to controlled mechanical stimuli. *Proceedings of the National Academy of Sciences of the United States of America*, 74, 2407–2411.

Jaramillo, F., Markin, V. S., & Hudspeth, A. J. (1993). Auditory illusions and the single hair cell. *Nature*, 364, 527–529.

Johnson, K. R., Gagnon, L. H., Webb, L. S., Peters, L. L., Hawes, N. L., Chang, B., & Zheng, Q. Y. (2003). Mouse models of USH1C and DFNB18: Phenotypic and molecular analyses of two new spontaneous mutations of the *Ush1c* gene. *Human Molecular Genetics,* 12, 3075–3086.

Johnson, S. L., Beurg, M., Marcotti, W., & Fettiplace, R. (2011). Prestin-driven cochlear amplification is not limited by the outer hair cell membrane time constant. *Neuron*, 70, 1143–1154.

Jülicher, F., Andor, D., & Duke, T. (2001). Physical basis of two-tone interference in hearing. *Proceedings of the National Academy of Sciences of the United States of America*, 98, 9080–9085.

Kachar, B., Parakkal, M., Kurc, M., Zhao, Y., & Gillespie, P. G. (2000). High-resolution structure of hair cell tip links. *Proceedings of the National Academy of Sciences of the United States of America,* 97, 13336–13341.

Karavitaki, K. D., & Corey, D. P. (2010). Sliding adhesion confers coherent motion to hair cell stereocilia and parallel gating to transduction channels. *The Journal of Neuroscience*, 30, 9051–9063.

Kawashima, Y., Géléoc, G. S., Kurima, K., Labay, V., Lelli, A., Asai, Y., Makishima, T., Wu, D. K., Della Santina, C. C., Holt, J. R., & Griffith, A. J. (2011). Mechanotransduction in mouse inner ear hair cells requires transmembrane channel-like genes. *Journal of Clinical Investigation,* 121, 4796–4809.

Kazmierczak, P., Sakaguchi, H., Tokita, J., Wilson-Kubalek, E. M., Milligan, R. A., Müller, U., & Kachar, B. (2007). Cadherin 23 and protocadherin 15 interact to form tip-link filaments in sensory hair cells. *Nature*, 449, 87–91.

Kennedy, H. J., Crawford, A. C., & Fettiplace, R. (2005). Force generation by the mammalian hair bundle supports a role in cochlear amplification. *Nature*, 433, 880–883.

Kennedy, H. J., Evans, M. G., Crawford, A. C., & Fettiplace, R. (2006). Depolarization of cochlear outer hair cells evokes active hair bundle motion by two mechanisms. *The Journal of Neuroscience*, 26, 2757–2766.

Kitajiri, S., Sakamoto, T., Belyantseva, I. A., Goodyear, R. J., Stepanyan, R., Fujiwara, I., Bird, J. E., Riazuddin, S., Riazuddin, S., Ahmed, Z. M., Hinshaw, J. E., Sellers, J., Bartles, J. R., Hammer, J. A., 3rd, Richardson, G. P., Griffith, A. J., Frolenkov, G. I., & Friedman, T. B. (2010). Actin-bundling protein TRIOBP forms resilient rootlets of hair cell stereocilia essential for hearing. *Cell*, 141, 786–798.

Kozlov, A. S., Risler, T., & Hudspeth, A. J. (2007). Coherent motion of stereocilia assures the concerted gating of hair cell transduction channels. *Nature Neuroscience*, 10, 87–92.

Kros, C. J., Rusch, A., & Richardson, G. P. (1992). Mechano-electrical transducer currents in hair cells of the cultured neonatal mouse cochlea. *Proceedings of the Royal Society of London B: Biological Sciences*, 249, 185–193.

Kros, C. J., Marcotti, W., van Netten, S. M., & Self, T. J. (2002). Reduced climbing and increased slipping adaptation in cochlear hair cells of mice with Myo7a mutations. *Nature Neuroscience*, 5, 41–47.

Kurima, K., Peters, L. M., Yang, Y., Riazuddin, S., Ahmed, Z. M., Naz, S., Arnaud, D., Drury, S., Mo, J., Makishima, T., Ghosh, M., Menon, P. S., Deshmukh, D., Oddoux, C., Ostrer, H., Khan, S., Riazuddin, S., Deininger, P. L., Hampton, L. L., Sullivan, S. L., Battey, J. F., Jr., Keats, B. J., Wilcox, E. R., Friedman, T. B., & Griffith, A. J. (2002). Dominant and recessive deafness caused by mutations of a novel gene, TMC1, required for cochlear hair cell function. *Nature Genetics,* 30, 277–284.

Kurima, K., Ebrahim, S., Pan, B., Sedlacek, M., Sengupta, P., Millis, B. A., Cui, R., Nakanishi, H., Fujikawa, T., Kawashima, Y., Choi, B. Y., Monahan, K., Holt, J. R., Griffith, A. J., & Kachar, B. (2015). TMC1 and TMC2 localize at the site of mechanotransduction in mammalian inner ear hair cell stereocilia. *Cell Reports*, 12, 1606–1617.

Lindner, B., Dierkes, K., & Jülicher, F. (2009). Local exponents of nonlinear compression in periodically driven noisy oscillators. *Physical Review Letters*, 103, 250601.

Longo-Guess, C. M., Gagnon, L. H., Cook, S. A., Wu, J., Zheng, Q. Y., & Johnson, K. R. (2005). A missense mutation in the previously undescribed gene *Tmhs* underlies deafness in hurry-scurry (*hscy*) mice. *Proceedings of the National Academy of Sciences of the United States of America*, 102, 7894–7899.

Lumpkin, E. A., & Hudspeth, A. J. (1995). Detection of Ca^{2+} entry through mechanosensitive channels localizes the site of mechanoelectrical transduction in hair cells. *Proceedings of the National Academy of Sciences of the United States of America*, 92, 10297–10301.

Lumpkin, E. A., Marquis, R. E., & Hudspeth, A. J. (1997). The selectivity of the hair cell's mechanoelectrical–transduction channel promotes Ca^{2+} flux at low Ca^{2+} concentrations. *Proceedings of the National Academy of Sciences of the United States of America*, 94, 10997–11002.

Maeda, R., Kindt, K. S., Mo, W., Morgan, C. P., Erickson, T., Zhao, H., Clemens-Grisham, R., Barr-Gillespie, P. G., & Nicolson, T. (2014). Tip-link protein protocadherin 15 interacts with transmembrane channel-like proteins TMC1 and TMC2. *Proceedings of the National Academy of Sciences of the United States of America*, 111, 12907–12912.

Mammano, F., & Ashmore, J. F. (1993). Reverse transduction measured in the isolated cochlea by laser Michelson interferometry. *Nature*, 365, 838–841.

Mammano, F., & Ashmore, J. F. (1996). Differential expression of outer hair cell potassium currents in the isolated cochlea of the guinea-pig. *The Journal of Physiology,* 496, 639–646.

Manley, G. A. (2000). Cochlear mechanisms from a phylogenetic viewpoint. *Proceedings of the National Academy of Sciences of the United States of America,* 97, 11736–11743.

Manley, G. A. (2001). Evidence for an active process and a cochlear amplifier in nonmammals. *Journal of Neurophysiology,* 86, 541–549.

Manley, G. A., Sienknecht, U., & Köppl, C. (2004). Calcium modulates the frequency and amplitude of spontaneous otoacoustic emissions in the bobtail skink. *Journal of Neurophysiology,* 92, 2685–2693.

Marcotti, W., Erven, A., Johnson, S. L., Steel, K. P., & Kros, C. J. (2006). Tmc1 is necessary for normal functional maturation and survival of inner and outer hair cells in the mouse cochlea. *The Journal of Physiology* 574, 677–698.

Martin, P., & Hudspeth, A. J. (1999). Active hair-bundle movements can amplify a hair cell's response to oscillatory mechanical stimuli. *Proceedings of the National Academy of Sciences of the United States of America*, 96, 14306–14311.

Martin, P., & Hudspeth, A. J. (2001). Compressive nonlinearity in the hair bundle's active response to mechanical stimulation. *Proceedings of the National Academy of Sciences of the United States of America*, 98, 14386–14391.

Martin, P., Mehta, A. D., & Hudspeth, A. J. (2000). Negative hair-bundle stiffness betrays a mechanism for mechanical amplification by the hair cell. *Proceedings of the National Academy of Sciences of the United States of America*, 97, 12026–12031.

Martin, P., Bozovic, D., Choe, Y., & Hudspeth, A. J. (2003). Spontaneous oscillation by hair bundles of the bullfrog's sacculus. *The Journal of Neuroscience,* 23, 4533–4548.

Meaud, J., & Grosh, K. (2011). Coupling active hair bundle mechanics, fast adaptation, and somatic motility in a cochlear model. *Biophysical Journal*, 100, 2576–2585.

Meenderink, S. W., Quiñones, P. M., & Bozovic, D. (2015). Voltage-mediated control of spontaneous bundle oscillations in saccular hair cells. *The Journal of Neuroscience,* 35, 14457–14466.

Meyers, J. R., MacDonald, R. B., Duggan, A., Lenzi, D., Standaert, D. G., Corwin, J. T., & Corey, D. P. (2003). Lighting up the senses: FM1-43 loading of sensory cells through nonselective ion channels. *The Journal of Neuroscience,* 23, 4054–4065.

Mitchem, K. L., Hibbard, E., Beyer, L. A., Bosom, K., Dootz, G. A., Dolan, D. F., Johnson, K. R., Raphael, Y., & Kohrman, D. C. (2002). Mutation of the novel gene *Tmie* results in sensory cell defects in the inner ear of spinner, a mouse model of human hearing loss DFNB6. *Human Molecular Genetics*, 11, 1887–1898.

Nam, J. H., & Fettiplace, R. (2010). Force transmission in the organ of Corti micromachine. *Biophysical Journal*, 98, 2813–2821.

Nam, J. H., & Fettiplace, R. (2012). Optimal electrical properties of outer hair cells ensure cochlear amplification. *PLoS ONE*, 7, e50572.

Nam, J. H., Peng, A. W., & Ricci, A. J. (2015). Underestimated sensitivity of mammalian cochlear hair cells due to splay between stereociliary columns. *Biophysical Journal,* 108, 2633–2647.

Naz, S., Giguere, C. M., Kohrman, D. C., Mitchem, K. L., Mitchem, K. L., Riazuddin, S., Morell, R. J., Ramesh, A., Srisailpathy, S., Deshmukh, D., Riazuddin, S., Griffith, A. J., Friedman, T. B., Smith, R. J., & Wilcox, E. R. (2002). Mutations in a novel gene, TMIE, are associated with hearing loss linked to the DFNB6 locus. *American Journal of Human Genetics,* 71, 632–636.

Nobili, R., & Mammano, F. (1996). Biophysics of the cochlea. II: Stationary nonlinear phenomenology. *The Journal of the Acoustical Society of America,* 99, 2244–2255.

Ohmori, H. (1985). Mechano-electrical transduction currents in isolated vestibular hair cells of the chick. *The Journal of Physiology,* 359, 189–217.

Ó Maoiléidigh, D., & Jülicher, F. (2010). The interplay between active hair bundle motility and electromotility in the cochlea. *The Journal of the Acoustical Society of America,* 128, 1175–1190.

Ó Maoiléidigh, D., & Hudspeth, A. J. (2013). Effects of cochlear loading on the motility of active outer hair cells. *Proceedings of the National Academy of Sciences of the United States of America,* 110, 5474–5479.

Ó Maoiléidigh, D., Nicola, E. M., & Hudspeth, A. J. (2012). The diverse effects of mechanical loading on active hair bundles. *Proceedings of the National Academy of Sciences of the United States of America,* 109, 1943–1948.

Ospeck, M., Dong, X. X., & Iwasa, K. H. (2003). Limiting frequency of the cochlear amplifier based on electromotility of outer hair cells. *Biophysical Journal,* 84, 739–749.

Pan, B., Géléoc, G. S., Asai, Y., Horwitz, G. C., Kurima, K., Ishikawa, K., Kawashima, Y., Griffith, A. J., & Holt, J. R. (2013). TMC1 and TMC2 are components of the mechanotransduction channel in hair cells of the mammalian inner ear. *Neuron,* 79, 504–515.

Patuzzi, R. (1998). The Goldman-Hodgkin-Katz equation and graphical 'load-line' analysis of ionic flow through outer hair cells. *Hearing Research*, 125, 71–97.

Peng, A. W., Effertz, T., & Ricci, A. J. (2013). Adaptation of mammalian auditory hair cell mechanotransduction is independent of calcium entry. *Neuron,* 80, 960–972.

Pickles, J. O., Comis, S. D., & Osborne, M. P. (1984). Cross-links between stereocilia in the guinea pig organ of Corti, and their possible relation to sensory transduction. *Hearing Research*, 15, 103–112.

Powers, R. J., Kulason, S., Atilgan, E., Brownell, W. E., Sun, S. X., Barr-Gillespie, P. G., & Spector, A. A. (2014). The local forces acting on the mechanotransduction channel in hair cell stereocilia. *Biophysical Journal*, 106, 2519–2528.

Ramamoorthy, S., Deo, N. V., & Grosh, K. (2007). A mechano-electro-acoustical model for the cochlea: Response to acoustic stimuli. *The Journal of the Acoustical Society of America,* 121, 2758–2773.

Reichenbach, T., & Hudspeth, A. J. (2010). A ratchet mechanism for amplification in low-frequency mammalian hearing. *Proceedings of the National Academy of Sciences of the United States of America*, 107, 4973–4978.

Ricci, A. J., & Fettiplace, R. (1997). The effects of calcium buffering and cyclic AMP on mechano-electrical transduction in turtle auditory hair cells. *The Journal of Physiology*, 501, 111–124.

Ricci, A. J., Crawford, A. C., & Fettiplace, R. (2000). Active hair bundle motion linked to fast transducer adaptation in auditory hair cells. *The Journal of Neuroscience,* 20, 7131–7142.

Ricci, A. J., Crawford, A. C., & Fettiplace, R. (2002). Mechanisms of active hair bundle motion in auditory hair cells. *The Journal of Neuroscience,* 22, 44–52.

Ricci, A. J., Crawford, A. C., & Fettiplace, R. (2003). Tonotopic variation in the conductance of the hair cell mechanotransducer channel. *Neuron,* 40, 983–990.

Ricci, A. J., Kennedy, H. J., Crawford, A. C., & Fettiplace, R. (2005). The transduction channel filter in auditory hair cells. *The Journal of Neuroscience,* 25, 7831–7839.

Robles, L., & Ruggero, M. A. (2001). Mechanics of the mammalian cochlea. *Physiological Reviews,* 81, 1305–1352.

Roongthumskul, Y., Fredrickson-Hemsing, L., Kao, A., & Bozovic, D. (2011). Multiple-timescale dynamics underlying spontaneous oscillations of saccular hair bundles. *Biophysical Journal,* 101, 603–610.

Russell, I. J., & Sellick, P. M. (1983). Low-frequency characteristics of intracellularly recorded receptor potentials in guinea-pig cochlear hair cells. *The Journal of Physiology*, 338, 179–206.

Rybalchenko, V., & Santos–Sacchi, J. (2003). Cl^- flux through a non-selective, stretch-sensitive conductance influences the outer hair cell motor of the guinea-pig. *The Journal of Physiology*, 547, 873–891.

Salvi, J. D., Ó Maoiléidigh. D., Fabella, B. A., Tobin, M., & Hudspeth, A. J. (2015). Control of a hair bundle's mechanosensory function by its mechanical load. *Proceedings of the National Academy of Sciences of the United States of America*, 112, E1000–E1009.

Shabbir, M. I., Ahmed, Z. M., Khan, S. Y., Riazuddin, S., Waryah, A. M., Khan, S. N., Camps, R. D., Ghosh, M., Kabra, M., Belyantseva, I. A., Friedman, T. B., & Riazuddin, S. (2006). Mutations of human *TMHS* cause recessively inherited non-syndromic hearing loss. *Journal of Medical Genetics*, 43, 634–640.

Shin, J. B., Krey, J. F., Hassan, A., Metlagel, Z., Tauscher, A. N., Pagana, J. M., Sherman, N. E., Jeffery, E. D., Spinelli, K. J., Zhao, H., Wilmarth, P. A., Choi, D., David, L. L., Auer, M., & Barr-Gillespie, P. G. (2013). Molecular architecture of the chick vestibular hair bundle. *Nature Neuroscience*, 16, 365–374.

Shotwell, S. L., Jacobs, R., & Hudspeth, A. J. (1981). Directional sensitivity of individual vertebrate hair cells to controlled deflection of their hair bundles. *Annals of the New York Academy of Sciences*, 374, 1–10.

Sotomayor, M., Weihofen, W. A., Gaudet, R., & Corey, D. P. (2010). Structural determinants of cadherin-23 function in hearing and deafness. *Neuron*, 66, 85–100.

Sotomayor, M., Weihofen, W. A., Gaudet, R., & Corey, D. P. (2012). Structure of a force-conveying cadherin bond essential for inner-ear mechanotransduction. *Nature*, 492, 128–132.

Sotomayor, M., Gaudet, R., & Corey, D. P. (2014). Sorting out a promiscuous superfamily: Towards cadherin connectomics. *Trends in Cell Biology*, 24, 524–536.

Tinevez, J.-Y., Jülicher, F., & Martin, P. (2007). Unifying the various incarnations of active hair-bundle motility by the vertebrate hair cell. *Biophysical Journal*, 93, 4053–4067.

van Netten, S. M., & Kros, C. J. (2000). Gating energies and forces of the mammalian hair cell transducer channel and related hair bundle mechanics. *Proceedings of the Royal Society of London B: Biological Sciences*, 267, 1915–1923.

Verpy, E., Leibovici, M., Zwaenepoel, I., Liu, X.-Z., Gal, A., Salem, N., Mansour, A., Blanchard, S., Kobayashi, I., Keats, B. J., Slim, R., & Petit, C. (2000). A defect in harmonin, a PDZ domain–containing protein expressed in the inner ear sensory hair cells, underlies Usher syndrome type 1C. *Nature Genetics*, 26, 51–55.

Verpy, E., Leibovici, M., Michalski, N., Goodyear, R. J., Houdon, C., Weil, D., Richardson, G. P., & Petit, C. (2011). Stereocilin connects outer hair cell stereocilia to one another and to the tectorial membrane. *The Journal of Comparative Neurology*, 519, 194–210.

Weil, D., Blanchard, S., Kaplan, J., Guilford, P., Gibson, F., Walsh, J., Mburu, P., Varela, A., Levilliers, J., Weston, M. D., Kelley, P. M., Kimberling, W. J., Wagenaar, M., Levi-Acobas, F., Larget-Piet, D., Munnich, A., Steel, K. P., Brown, S. D. M., & Petit, C. (1995). Defective myosin VIIA gene responsible for Usher syndrome type 1B. *Nature,* 374, 60–61.

Weil, D., El-Amraoui, A., Masmoudi, S., Mustapha, M., Kikkawa, Y., Lainé, S., Delmaghani, S., Adato, A., Nadifi, S., Zina, Z. B., Hamel, C., Gal, A., Ayadi, H., Yonekawa, H., & Petit, C. (2003). Usher syndrome type I G (USH1G) is caused by mutations in the gene encoding SANS, a protein that associates with the USH1C protein, harmonin. *Human Molecular Genetics,* 12, 463–471.

Weitzel, E. K., Tasker, R., & Brownell, W. E. (2003). Outer hair cell piezoelectricity: Frequency response enhancement and resonance behavior. *The Journal of the Acoustical Society of America*, 114, 1462–1466.

Wever, E. G., & Bray, C. W. (1930). Action currents in the auditory nerve in response to acoustical stimulation. *Proceedings of the National Academy of Sciences of the United States of America*, 16, 344–350.

Wu, Y. C., Ricci, A. J., & Fettiplace, R. (1999). Two components of transducer adaptation in auditory hair cells. *Journal of Neurophysiology*, 82, 2171–2181.

Yamoah, E. N., Lumpkin, E. A., Dumont, R. A., Smith, P. J., Hudspeth, A. J., & Gillespie, P. G. (1998). Plasma membrane Ca^{2+}-ATPase extrudes Ca^{2+} from hair cell stereocilia. *The Journal of Neuroscience*, 18, 610–624.

Zha, D., Chen, F., Ramamoorthy., S., Fridberger, A., Choudary, N., Jacques, S. L., Wang, R. K., & Nuttall, A. L. (2012). *In vivo* outer hair cell length changes expose the active process in the cochlea. *PLoS ONE,* 7, e32757.

Zhao, B., & Müller, U. (2015). The elusive mechanotransduction machinery of hair cells. *Current Opinion in Neurobiology*, 34, 172–179.

Zhao, B., Wu, Z., Grillet, N., Yan, L., Xiong, W., Harkins-Perry, S., & Müller, U. (2014). TMIE is an essential component of the mechanotransduction machinery of cochlear hair cells. *Neuron*, 84, 954–967.

Chapter 5
Prestin: Molecular Mechanisms Underlying Outer Hair Cell Electromotility

Joseph Santos-Sacchi, Dhasakumar Navaratnam, Rob Raphael, and Dominik Oliver

Abstract Prestin is a member of the SLC26 family of anion transporters that has evolved to serve as a molecular motor in outer hair cells (OHCs) of the mammalian inner ear. The protein is piezoelectric-like, exhibiting voltage and tension sensitivity, with significant modulation by anions, chiefly intracellular chloride. Receptor potentials of OHCs drive molecular conformational changes in prestin, as evidenced by voltage sensor charge movements, that evoke robust length changes in OHCs, thereby contributing to a mechanical feedback mechanism and, therefore, to cochlear amplification, which enhances our auditory sensitivity. Current research has been focused on tertiary structural determinations, prestin interactions with other proteins and membrane lipids, trafficking, and the mechanism of anion effects. One of the key remaining questions is the determination of structural changes induced by membrane voltage perturbations and how those changes result in forces exerted by the OHCs. Indeed, much remains to be understood about this extraordinary molecule.

J. Santos-Sacchi (✉)
Departments of Surgery (Otolaryngology), Neuroscience, and Cellular and Molecular Physiology, Yale University School of Medicine, 333 Cedar Street, New Haven, CT 06520-8018, USA
e-mail: joseph.santos-sacchi@yale.edu

D. Navaratnam
Departments of Neurology and Neuroscience, Yale University School of Medicine, 333 Cedar Street, New Haven, CT 06520-8018, USA
e-mail: dhasakumar.navaratnam@yale.edu

R. Raphael
Department of Biomedical Engineering, Rice University, 6100 Main Street, Houston, TX 77521, USA
e-mail: rraphael@rice.edu

D. Oliver
Department of Neurophysiology, Philipps-Universität Marburg, Deutschhausstrasse 2, 35037 Marburg, Germany
e-mail: oliverd@staff.uni-marburg.de

G.A. Manley et al. (eds.), *Understanding the Cochlea*, Springer Handbook of Auditory Research 62, DOI 10.1007/978-3-319-52073-5_5

Keywords Chloride · Cochlea · Cochlear amplifier · Hearing · Membrane · Membrane curvature · Motor protein · Nonlinear capacitance · Nonsteroidal anti-inflammatory drug · Protein interactions · Protein structure · SCL26A5 · Voltage sensor

5.1 Introduction

Prestin is a remarkable protein that underlies our keen sense of hearing. It is a member of an anion transporter family (SLC26) that has role changed into a fast molecular motor that drives outer hair cell (OHC) somatic electromechanical activity, the transduction of the receptor potential of the cell (see Corey, Ó Maoiléidigh, and Ashmore, Chap. 4) into pronounced cell length changes at acoustic rates, thereby boosting perceptual thresholds by 40–60 dB. In this chapter, three broad areas focus on how this protein works. They include an overview of the protein's biophysical traits, the structural features of the protein that will lead to detailed structure-function relationships, and the role of accessory protein/lipid partners in helping this protein to carry out its important work. Much is to be learned. Pertinent reviews on the subjects of this chapter are available in the literature (He et al. 2006; Ashmore 2008; Ashmore et al. 2010).

5.2 Known Biophysical Properties of Prestin

5.2.1 The OHC Sensor/Motor: Prestin

An intense investigation of this somatic motility began soon after its discovery by Bill Brownell and colleagues (Brownell et al. 1985; Kachar et al. 1986). Surprisingly, when OHCs are stimulated electrically by a current injection within or across the cell, their length changes as a function of stimulus intensity and waveform. It soon became clear that OHC somatic motility [also known as electromotility (eM)] was driven by voltage and not any particular ionic current (Ashmore 1987; Santos-Sacchi and Dilger 1988), evidencing movements of 15 nm/mV on average (Santos-Sacchi 1989). One of the most powerful pieces of evidence that eM was driven by voltage was the observation of displacement currents, capacitive-like currents, similar in some respects to the gating currents of ion channels (Bezanilla 2000), which are evoked by membrane voltage steps under whole cell voltage clamp (Ashmore 1989; Santos-Sacchi 1990). These displacement currents, or, equivalently, a voltage-dependent or nonlinear membrane capacitance (NLC), arise from the movements of a voltage sensor charge across the electric field of the membrane. The identification of such a charge movement immediately led to the notion of a sensorimotor unit residing in the OHC plasma membrane that obeyed

two-state Boltzmann statistics (Ashmore 1990; Santos-Sacchi 1991), where characterization of the charge-voltage (Q-V) or, equivalently, the capacitance-voltage (C-V) relationship provides estimates of the unitary sensor charge (z; assuming full passage of the sensor charge through the field of the membrane), the maximum charge transferred (Q_{max}), and, the voltage where charge is equally distributed across the membrane (V_h; Fig. 5.1). The Boltzmann characterization of motor charge movement also provided the impetus for the development of "molecular" models of motor action that incorporated Boltzmann statistics, including area and conformational state models (Kalinec et al. 1992; Dallos et al. 1993; Iwasa 1994). Given the Q_{max} and an elementary sensor charge estimate, the number of motors residing in the membrane can be estimated, giving a density in OHCs of about 10,000/μm^2 (Huang and Santos-Sacchi 1993; Gale and Ashmore 1997a; Mahendrasingam et al. 2010), although this number may need to be reevaluated (Santos-Sacchi and Song 2016). V_h and z have been used to define the voltage operating range of the motor, with V_h localizing the eM-V function relative to the resting membrane potential of the cell and z defining the extent over which the motor is voltage sensitive. With z being less than unity, the motor has a quite shallow voltage dependence compared with ion channels. The two-state formalism also imposes strict correspondence between charge movement and eM, where according to a now widely accepted area-state model (Iwasa 1994; Santos-Sacchi and Song 2014a), motors will fluctuate between a compact and expanded surface area state, with unitary motor area change estimates varying between 0.37 and 8 nm^2 (Iwasa 1993; Santos-Sacchi 1993; Gale and Ashmore 1994; Adachi and

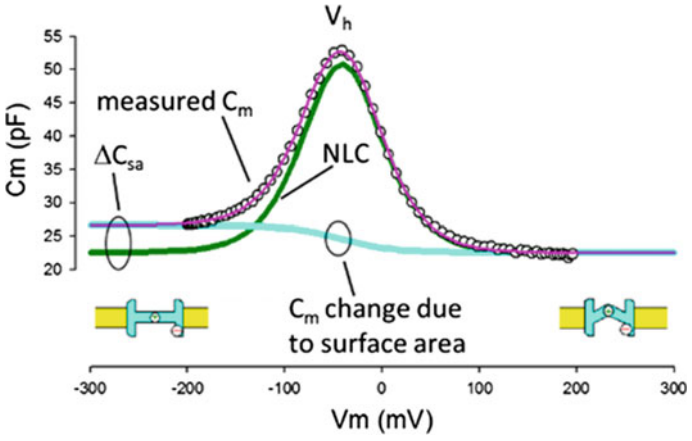

Fig. 5.1 Outer hair cell (OHC) nonlinear membrane capacitance (NLC). OHC voltage-dependent capacitance (*circles*) is composed of two components, both riding atop a linear capacitance corresponding to the cell's surface area. One is associated with the voltage sensor charge of prestin (NLC; *green*), and the other is associated with motor state occupancy (*blue*). Cartoon depicts prestin in either state, expanded or contracted. V_h, voltage where charge is equally distributed across the membrane; C_m, membrane capacitance; ΔC_{sa}, state-dependent capacitance; V_m, membrane voltage. See text for further details. Modified from Santos-Sacchi and Navarrete (2002)

Iwasa 1999). As indicated in Fig. 5.1, voltage-dependent C_m possesses an additional component, state-dependent capacitance (ΔC_{sa}), that has been attributed to area/membrane thickness changes associated with motor state occupancy, each motor contributing an additional 17 aF when residing in the expanded state (Santos-Sacchi and Navarrete 2002). The high variance of area estimates highlights the need for structural observations at the molecular level.

During the ensuing years, a host of biophysical attributes of the OHC plasma membrane motor were characterized, and these traits, together with its NLC, would be crucial in identifying the molecular nature of the motor. One of the most important discoveries was the piezoelectric nature of the motor (Iwasa 1993). On introducing tension into the OHC membrane, NLC shifts along the voltage axis. The shift in V_h effects the charge movement in the membrane, and this phenomenon is intrinsic to the membrane (Gale and Ashmore 1994; Kakehata and Santos-Sacchi 1995). These data are fully consistent with a direct voltage-to-mechanical (and vice versa) transduction process that does not directly require any intermediate steps (e.g., second messengers) or biochemical energy sources (except, of course, those sources required to maintain the membrane voltage). Other early observations that defined the nature of the motor and set the stage for its molecular identification included the simultaneous block of the NLC and motor activity by intracellularly acting salicylate and extracellularly acting gadolinium (Santos-Sacchi 1991; Tunstall et al. 1995; Kakehata and Santos-Sacchi 1996), the influence of altered membrane potential (prepulse effect) on V_h (Santos-Sacchi et al. 1998), the tension and turgor pressure effects (piezoelectric-like) on the NLC (Iwasa 1993; Gale and Ashmore 1994; Kakehata and Santos-Sacchi 1995), and the temperature susceptibility of the NLC (Santos-Sacchi and Huang 1998; Meltzer and Santos-Sacchi 2001).

5.2.2 Enter Prestin

Zheng et al. (2000) identified the OHC motor protein as prestin (SLC26A5), a member of an anion transporter family. Key to this identification was the localization of the protein to the OHC lateral membrane where electromechanical activity is restricted (Dallos et al. 1991; Huang and Santos-Sacchi 1994) and biophysical demonstrations of OHC motor-like activity in heterologously transfected cells, including the NLC, the voltage-driven membrane movement, and a block by salicylate. Subsequently, prestin was shown to exhibit membrane tension (Ludwig et al. 2001; Santos-Sacchi et al. 2001), prepulse (Santos-Sacchi et al. 2001), and temperature sensitivities similar to those in the native OHCs (Meltzer and Santos-Sacchi 2001). It was clear at that point that all known biophysical traits of prestin matched those that had been identified before its discovery. Another fundamental observation that indisputably linked prestin to OHC eM was the absence of eM in the prestin-knockout mouse (Liberman et al. 2002).

5.2.3 Importance of Prestin for Cochlear Amplification

Interestingly, while the knockout implicated the importance of prestin in cochlear amplification, issues were quickly identified that dampened such a conclusion, including the obvious mechanical impedance changes in the OHCs (and consequently the cochlear partition) that result from removal of the abundant protein content within the OHC lateral membrane, which substantially shortened OHCs. Subsequently, persuasive evidence that prestin predominantly underlies cochlear amplification was obtained from a knockin of mutated prestin (499 mutant) that has its voltage operating range (assessed by NLC V_h) shifted far out of the physiological range while maintaining other features of normal OHC function, structure, and mechanics (Dallos et al. 2008). That mutation also altered the kinetics of prestin (Homma et al. 2013). Another important observation linking prestin to cochlear amplification was that manipulations of chloride, previously shown to control the electromechanical activity of prestin (Oliver et al. 2001), reversibly altered the basilar membrane tuning in vivo (Santos-Sacchi et al. 2006). Salicylate, which competes with chloride for the anion binding site of prestin and reduces the NLC (Oliver et al. 2001), also adversely affects basilar membrane motion (Santos-Sacchi et al. 2006; Fisher et al. 2012). Finally, there is evidence for prestin mutations causing deafness (Mutai et al. 2013).

5.2.4 How Does Prestin Sense Voltage?

The voltage-dependent nature of eM naturally begs the question, What makes the protein sensitive to voltage? It is clear that prestin must possess a charged voltage sensor that is moved by voltage drops across the plasma membrane. In other well-studied voltage-dependent membrane proteins, charged amino acid residues serve this function. For example, the S4 segment in the voltage sensor domain of all classical voltage-gated ion channels comprises the voltage sensor domain (Bezanilla 2000). In a fundamental study investigating this issue, Oliver et al. (2001) found that neutralization of candidate electrically charged amino acid residues had little effect on voltage sensitivity of prestin, whereas removal of monovalent intracellular anions, namely intracellular chloride or bicarbonate, abolished charge movement and hence voltage sensitivity. Recently, careful examination of this phenomenon indicated that the OHC eM magnitude (Song and Santos-Sacchi 2013) and the total Q_{max} (Santos-Sacchi and Song 2016) do not decrease with intracellular chloride level, but rather chloride levels influence the rate of prestin transitions (Santos-Sacchi and Song 2016), resulting in an apparent reduction of NLC when the membrane potential is changed at rates exceeding the Cl^--dependent kinetics of prestin. Based on the observation of anion sensitivity, Oliver et al (2001) concluded that the voltage sensor of prestin is not made up from intrinsic residues in prestin, but instead, monovalent anions serve as extrinsic voltage sensors, i.e., that

charge movements (NLC) arise directly from the translocation of the anion across the electrical field along some hypothetical access channel in the protein. This anion translocation, in turn, would then drive simultaneous conformational changes between the expanded and contracted states, thus producing eM. In fact, the voltage dependence of prestin varied with the size of the monovalent anion present, as if bulkier anions can travel a smaller fraction of the electrical field (Oliver et al. 2001). However, other findings are difficult to reconcile with this simple external voltage sensor model. First, a shift of the voltage dependence (V_h) toward depolarized potentials observed when the anion concentration is lowered is contrary to the prediction of the model (Rybalchenko and Santos-Sacchi 2003a). Interestingly, a variety of anion substitutes can markedly shift V_h in either the depolarizing or hyperpolarizing direction to varying degrees (Oliver et al. 2001; Rybalchenko and Santos-Sacchi 2008). Second, if other than monovalent anions can maintain prestin function, the charge number z moved per prestin molecule should correspond to the valence of the anion serving as voltage sensor (assuming that the electrical distance traveled remains the same). However, an increase in z has not been observed when monovalent anions are substituted with di- or trivalent anions (Rybalchenko and Santos-Sacchi 2008). Third, hyperpolarization, which drives prestin into the expanded state, should move the anion toward a more extracellular position, but in the expanded state, the apparent affinity for the anions is reduced, suggesting the release toward the cytosol (Song and Santos-Sacchi 2010). Observations such as these have led to a counter theory that anions serve as allosteric-like modulators of prestin charge movement, anion binding conformationally transitioning the protein into a voltage-enabled state, with sensor charge contributed by a wide-ranging distribution of charged residues within the protein (Bai et al. 2009). A current structural view of anion interaction with prestin is provided in Sects. 5.3.4 and 5.3.5.

5.2.5 *How Many States/Transitions Does Prestin Have?*

Simply based on standard fits of the NLC, it was not possible to differentiate between two-state and multistate behavior in the motor protein prestin (Huang and Santos-Sacchi 1993; Scherer and Gummer 2005). For example, fits with two-state Boltzmann or infinite state Langevin equations each adequately fit the NLC because of measurement uncertainty at the extreme voltages needed to interrogate the very shallow voltage dependence of the protein. The NLC has been used routinely as a surrogate for eM under the assumption that sensor charge movement exhibits fast two-state behavior directly linked to eM. It was natural to assume such fast kinetics because eM had been measured in the acoustic frequency range (Ashmore 1987; Santos-Sacchi 1992; Dallos and Evans 1995), even out to about 80 kHz (Frank et al. 1999) at room temperature. Interestingly, the NLC cutoff frequency was near 10 kHz at room temperature (Gale and Ashmore 1997b). The recent observation that characteristics of the NLC and eM can diverge as a function of reduced anion

concentration revealed that prestin activity is not governed by a simple two-state process but is instead multistate (Song and Santos-Sacchi 2013). A basis for disparity between the two measures may be related to slow, chloride-controlled intermediate transitions between chloride-binding and voltage-enabled states (Song and Santos-Sacchi 2013; Santos-Sacchi and Song 2014a). Essentially, steady-state (or low-frequency) evaluations of eM do not correspond to sensor charge movement that is measured at higher frequencies because each will only be equal when measured at the same frequency. Although the simple model developed in that work (*meno presto* model) can recapitulate features of the behavior of prestin, thus revealing its multistate nature with attendant time/phase delays (Santos-Sacchi and Song 2014b), it is likely that models incorporating transporter characteristics expected from the SLC heritage of prestin will offer greater insight (Muallem and Ashmore 2006; Schaechinger et al. 2011), provided they can account for all known biophysical properties exhibited by prestin.

Clearly, a lack of consensus on the structure of prestin based on software prediction algorithms, as indicated by the wide range of secondary topologies attributed to the membrane protein such as the 12 transmembrane domain (TMD) model (Oliver et al. 2001; Deak et al. 2005; Rajagopalan et al. 2006), the 10 TMD model (Navaratnam et al. 2005), and the 8 TMD model (Lovas et al. 2015), has led to difficulties in understanding the biophysical basis of the NLC and eM. Additionally, the limited information on the interacting partners of prestin and the influence of its membrane environment has contributed to these difficulties. Fortunately, significant progress is currently being made on these fronts.

5.3 Structure and Function of Prestin

5.3.1 Molecular and Functional Features of Prestin

Prestin is the fifth member of the SLC26 family of anion exchangers (hence SLC26A5; Zheng et al. 2000), a group of 10 mammalian proteins (Mount and Romero 2004; Alper and Sharma 2013). SLC26 proteins belong to a large, ubiquitous, and evolutionarily ancient "sulfate permease" (SulP) family of anion transporters present in animals, plants, fungi, and bacteria. Although the SLC26 nomenclature was originally used for the mammalian SulP proteins (Mount and Romero 2004), the SulP and SLC26 nomenclature may be used interchangeably (Dorwart et al. 2008; Geertsma et al. 2015). These evolutionary and molecular relationships are of particular relevance because structural information on mammalian prestin has emerged only very recently and is entirely based on crystallographic data for close (i.e., within the SLC26/SulP family) or remotely homologous relatives of mammalian SLC26 proteins.

The mammalian SLC26 proteins are diverse in terms of both their transport substrates and the transport modes. Thus, SLC26 transport activities include

electrogenic or electroneutral exchange of monovalent (e.g., chloride, iodide) and divalent anions (e.g., sulfate, oxalate). Two members, SLC26A7 and SLC26A11, mediate uncoupled flux of chloride at high rates, which may indicate that these members function as anion channels. Detailed reviews on SLC26 transport function and roles in physiology and pathophysiology are available (Mount and Romero 2004; Dorwart et al. 2008; Alper and Sharma 2013).

The closest prestin relatives of mammalian prestin, nonmammalian orthologs of SLC26A5 (e.g., chicken and zebrafish prestin), are highly active anion transporters that mediate the stoichiometric exchange of monovalent anions such as chloride against divalent anions (either sulfate or oxalate; Schaechinger and Oliver 2007; Schaechinger et al. 2011). Because this transport mode is electrogenic, i.e., one electrical charge is transferred per transport cycle, nonmammalian prestins generate robust transport currents in the presence of divalent transport substrates (Schaechinger and Oliver 2007). In contrast, transport currents were not observed with mammalian prestin in the presence of divalents (Schaechinger and Oliver 2007; Schaechinger et al. 2011), indicating that prestin has no transport activity, that it acts in an electroneutral mode that does not generate electrical current, or that transport rates are much lower than in its nonmammalian orthologs. In fact, by using fluorescent pH sensors and electrophysiology, Mristik et al. (2012) showed that prestin may function as a $Cl^-/2HCO_3^-$ exchanger, however with a low transport rate. Recently, prestin has been shown to allow ion currents through a pathway distinct from its transporter pathway (Bai et al. 2017). Moreover, based on a tracer-flux assay, one study suggested transport capability for formate and chloride (Bai et al. 2009), although another group could not reproduce this finding while confirming transport in nonmammalian orthologs (Tan et al. 2011). Interestingly, prestin, as well as other SLC26 proteins, mediates uncoupled permeation of thiocyanate (SCN^-) at appreciable rates (Schanzler and Fahlke 2012). Although the permeation of this anion has no obvious physiological relevance, this finding underscores the high degree of mechanistic and structural similarity between prestin and other SLC26 transporters and may turn out as helpful in deciphering potential common molecular mechanisms of transport and eM.

Mammalian prestin is a 744-amino acid protein with a high degree of sequence conservation across mammalian species (Zheng et al. 2000). As with other SLC26 proteins, prestin consists of a large TMD containing numerous hydrophobic stretches indicative of multiple transmembrane segments. This TMD is flanked by hydrophilic intracellular N- and C-termini (Ludwig et al. 2001; Zheng et al. 2001). The detailed topology of the TMD had long remained enigmatic, but it is now clear that it contains 14 membrane-spanning domains (Gorbunov et al. 2014; Geertsma et al. 2015). Within this TMD, two regions have been recognized for their particularly high sequence conservation across the SLC26/SulP family. One is located more N-terminally and is designated as the "SulP consensus signature" (Prosite PS01130); the other one located in the C-terminal half of the TMD is known as the Saier motif (Saier et al. 1999; Mount and Romero 2004). The high degree of conservation suggested that these protein regions are of particular importance for SLC26 function and may be critically involved in anion transport and possibly in eM. This is supported by the finding that transplantation of protein regions, including these motifs from mammalian prestin into

the prestin ortholog from zebrafish, is sufficient to confer mammalian-like function (i.e., fast charge transfer and eM) onto the nonmammalian prestin, which otherwise functions as a transporter (Schaechinger et al. 2011).

Another well-conserved domain of all mammalian and most bacterial SLC26/SulP proteins is the sulfate transporter and anti-sigma factor antagonist (STAS) domain, which occupies most of the cytoplasmic C-terminus (Sharma et al. 2011). The name refers to sequence and structural similarity with bacterial anti-sigma factor antagonist (ASA) proteins. In prestin from rats, the STAS domain approximately comprises amino acids 505–714 (Pasqualetto et al. 2010). Although the TMD mediates and determines the eM and transport function of SLC26 members as shown by transplantation of domains between mammalian and transport-active nonmammalian prestin (Schaechinger et al. 2011), mutagenesis studies indicated that the STAS domain is indispensable both for proper membrane targeting (Navaratnam et al. 2005; Zheng et al. 2005) and for protein function (Bai et al. 2006) in prestin and in other SLC26 transporters (Sharma et al. 2011). How the cytosolic domain affects eM or transport function is yet unknown. Nevertheless, as also found with other SLC26 transporters (Ko et al. 2004), the STAS domain is implicated in the interaction of prestin with other proteins including MAP1S (Bai et al. 2010) and calmodulin (Keller et al. 2014; see Sect. 5.4.2).

Although the prestin sequence is generally highly conserved across mammalian species, parallel or convergent evolution of the prestin gene has been discovered in echolocating bats and whales (Li et al. 2010; Liu et al. 2010). Thus, the same amino acid substitutions are found specifically in these phylogenetically unrelated lineages of echolocating mammals. Most of these sites cluster in the cytoplasmic C-terminus including the STAS domain (Li et al. 2010; Liu et al. 2010). Some of these residue replacements were found to modulate the voltage dependence of prestin (Liu et al. 2014), but the physiological consequences of these specific molecular traits are unknown. Given the parallel occurrence in echolocating species that use particularly high frequencies, it has been speculated that these amino acid changes may support the function of prestin in ultrasonic hearing (Li et al. 2010; Liu et al. 2010).

5.3.2 *Molecular Structure of Prestin*

Two papers in 2014 and 2015 revealed the molecular structure of SLC26/SulP transporters and of prestin in particular. Gorbunov et al. (2014) used a homology modeling approach based on the X-ray crystal structure of the bacterial uracil transporter UraA (Lu et al. 2011), which belongs to the NCS2 family of nucleobase/cation symporters, as the template. Although direct sequence conservation between UraA and prestin (or other mammalian SLC26 members) is low, advanced remote homology detection methods indicate that SLC26/SulP and NCS transporters are directly related, arguing that they share a common molecular architecture (Hoglund et al. 2011; Wong et al. 2012; Vastermark and Saier 2014). Homology models of mammalian and chicken prestin were scrutinized and refined

by molecular dynamics (MD) simulations (Gorbunov et al. 2014), which supported the validity of this conclusion. Soon afterward, this homology model was confirmed by the first experimental atomic structure of a SLC26/SulP transporter, the bacterial fumarate transporter SLC26Dg from *Deinococcus geothermalis* (Geertsma et al. 2015).

Modeling and X-ray crystallography consistently revealed a 7 + 7 inverted-repeat architecture for the TMD of SLC26 transporters and thus prestin (Gorbunov et al. 2014; Geertsma et al. 2015). As illustrated in Fig. 5.2, the central domain (TMD) of prestin is made up of 14 mostly helical transmembrane (TM) segments of variable length. The two halves (or repeats) of the TMD, each containing seven TM segments, are related to each other by a twofold pseudosymmetry such that they are inversely oriented with respect to the intracellular side. TMs from both repeats are interdigitated with their counterparts from the other repeat (Fig. 5.3a), forming the inverted-repeat organization that is characteristic of many different transporters (Forrest and Rudnick 2009). The topology of prestin was further probed by examining the intra- and extracellular accessibility of

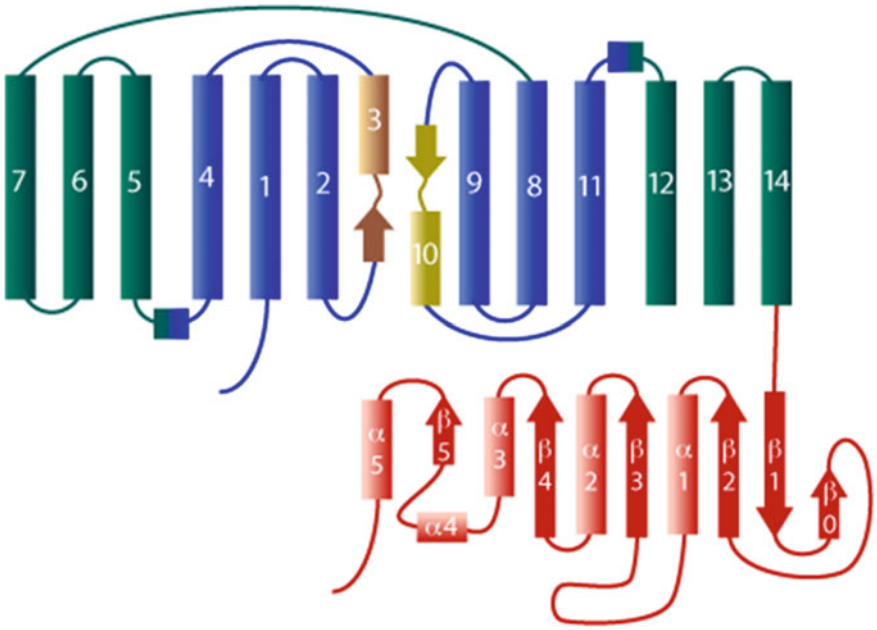

Fig. 5.2 Topology of prestin. The transmembrane domain (TMD) contains 14 largely helical membrane-spanning domains, forming two inverted repeats (TMs 1–7 and TMs 8–14). Colors indicate the three-dimensional structural organization into two main helix bundles, the "core" domain (*blue*) and the "gate" domain (*green*). Two central, partially helical and antiparallel TMs within the core domain are highlighted in *brown* (TM3) and *yellow* (TM10). *Arrows*: short β-strand segments. The cytoplasmic C-terminus (*red*) is mostly folded into a sulfate transporter and anti-sigma factor antagonist (STAS) domain consisting of several α-helical and β-strand segments

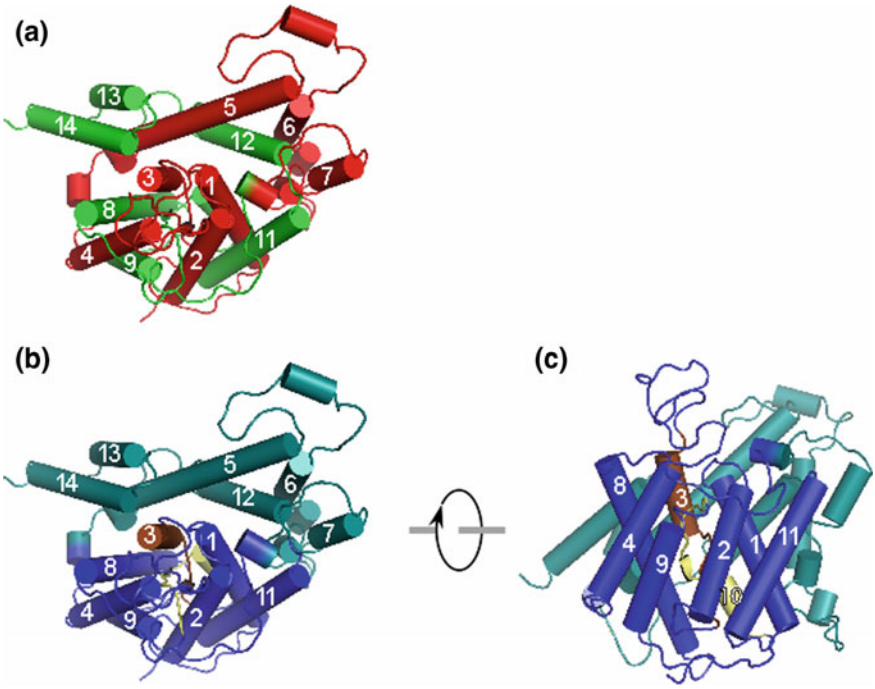

Fig. 5.3 Three-dimensional structure of prestin. **a** Extracellular surface view of overall TMD structure of prestin as derived from homology modeling with the experimental structure of SLC26Dg (Geertsma et al. 2015) as the template. *Red*: inverted repeat I; *green*: inverted repeat II. Transmembrane segments are labeled as in Fig. 5.2; helical part of TM 10 is largely hidden by TM1. **b** Same structure colored according to structural organization in core and gate domain. Color code as in Fig. 5.2. **c** Side view

mutationally inserted cysteine residues to cysteine-reactive, membrane-impermeant reagents (Gorbunov et al. 2014). These experiments unequivocally showed that the topology of mammalian prestin is fully consistent with the architecture of the bacterial homolog and the homology model based on UraA.

The TMD is organized into two structural units, each consisting of a bundle of TM helices containing segments from both inverted repeats (Figs. 5.2, 5.3b, c). TMs 1–4 and the pseudosymmetry-related counterpart TMs 8–11 form a compact bundle that has been designated the core domain. TMs 5–7 and 12–14 fold into a more planar (extended) bundle of helices termed the gate domain, which aligns with one side of the core domain, forming an extensive interface between both domains (Fig. 5.3b).

Attempts were also made to address the molecular structure of SLC26A6 and prestin by homology modeling based on the crystal structures of a bacterial chloride transporter, CLC-ec1 (Ohana et al. 2011), or the bacterial amino acid transporter Glt_{PH} (Lovas et al. 2015) as the templates, respectively. However, these approaches produced structures that can now be excluded given the lack of similarity with the

SLC26 crystal structure (Geertsma et al. 2015), disagreement with the experimentally determined topology (Gorbunov et al. 2014), and the lack of a sufficiently close evolutionary relationship between the respective transporter families and the SLC26/SulP family (Hoglund et al. 2011; Vastermark and Saier 2014).

The structure of the cytosolic STAS domain of prestin was solved at atomic resolution both for mammalian prestin (from the rat; Pasqualetto et al. 2010) and nonmammalian prestin (from the chicken; Lolli et al. 2015), revealing an ovoid domain assembled from a central β-sheet surrounded by five α-helices (Fig. 5.2). The core of the domain is structurally similar to STAS domains of bacterial SulP/LC26 proteins and to bacterial ASA proteins, but there are significant differences at the N- and C-termini, most notably an N-terminal extension including some rigid turns and an extra β-strand. Interestingly, the mammalian, but not the chicken, STAS domain harbors an anion binding site, the function of which is yet unknown (Lolli et al. 2015). Given its impact on prestin function, a close structural interaction with the TMD would seem likely. Although Pasqualetto et al. (2010) identified a molecular surface that may interact with either the lipid bilayer or the intracellular face of the TMD, the STAS orientation relative to the TMD remains unknown in the vertebrate SLC26 proteins. In the bacterial SLC26Dg full-length structure, the domain is facing away from the TMD and occupies a position corresponding to the inner lipid bilayer, which is apparently an artifact from cocrystallization with a nanobody (Geertsma et al. 2015). Low-resolution structural data from additional prokaryotic SLC26 homologs suggested that the STAS domain may project away from the TMD (Compton et al. 2014).

5.3.3 Oligomerization

Biochemical and low-resolution structural findings indicated that eukaryotic and bacterial SLC26 transporters share a conserved dimeric architecture (Detro-Dassen et al. 2008; Compton et al. 2011, 2014). However, some studies suggest that prestin forms tetramers (Zheng et al. 2006; Hallworth and Nichols 2012). Tetramers might be expected because particles in the lateral membrane of OHCs that are observed by freeze-fracture electron microscopy (EM) and believed to represent native prestin molecules, showed estimated diameters somewhat above 10 nm (Forge 1991; Kalinec et al. 1992). Given the dimensions of an SLC26 monomer of about 4.5 × 6 nm in the membrane plane (Gorbunov et al. 2014; Geertsma et al. 2015), these EM-resolved particles may correspond to tetrameric prestin assemblies. Also, a low-resolution structure of recombinant prestin, as obtained by a three-dimensional reconstruction based on single-particle EM images, exhibited four-fold symmetry consistent with tetrameric stoichiometry (Mio et al. 2008). It remains to be shown if these observations are due to the formation of higher order oligomers (i.e., dimers of dimers) and, if so, whether tetrameric assembly is important for functional or cell biological behavior.

The recent crystal structure of the bacterial SLC26Dg as well as the prestin homology structure provided no direct clues to the structural nature of dimerization. However, Geertsma et al. (2015) noted that the surface of the gate domain (opposite to the interface with the core domain) stood out due to high sequence conservation, which suggested that it may mediate dimerization. Interestingly, a recent crystal structure of the human anion exchanger AE1 (SLC4A1; also known as erythrocyte band 3 protein) showed that SLC4 transporters also share the 7 + 7 inverted-repeat architecture with SLC26 transporters, including an essentially superimposable arrangement of core and gate domains (Arakawa et al. 2015). This is consistent with the fact that together with the NCS2 family, the SLC4 family of bicarbonate transporters is one of the closest SulP/SLC26 relatives as indicated, e.g., by the Pfam database of protein families (Finn et al. 2014). This AE1 structure revealed a dimeric structure mediated by dimerization of the gate domains, lending support to a similar dimeric assembly of SLC26 proteins through the gate domains as proposed for SLC26 by Geertsma et al. (2015).

Although the mechanistic role of oligomerization in the transport or motor function of SLC26 proteins is unknown, for prestin it has been shown that subunits interact functionally, likely by an allosteric mechanism (Detro-Dassen et al. 2008). However, the atomic structure revealed the complete anion binding site and putative translocation pathway within the monomeric subunit (see Sect. 5.3.4), indicating that each subunit is basically functioning as an independent unit rather than forming an oligomeric common transport or motor domain with the other subunit.

5.3.4 Anion Binding Site

The SLC26/prestin structures provided a fresh mechanistic view into the anion dependence of the electromotile activity of prestin and the relationship to the transport function of related SLC26 proteins. Thus, the SLC26 structures feature a central cavity in the TMD, located halfway through the membrane and close to the interface between the core and gate domains. In both computational and X-ray structures, this cavity is accessible to solutes from the cytoplasm but is occluded from the extracellular space. Structural considerations and experimental evidence indicate that this central cavity is the principal binding site for the transport substrate in SLC26 transporters and specifically for the anion that enables eM in mammalian prestin. The pocket is formed largely by the two complementary pseudosymmetry-related, partially helical TMs 3 and 10 and by two complementary TM helices 1 and 8 (Fig. 5.4). Notably, these regions overlap with the Saier motif comprising TMs 9 and 10 (Saier et al. 1999; Mount and Romero 2004; Gorbunov et al. 2014), consistent with the high functional importance of this protein region as suggested by sequence conservation. Moreover, two protein regions previously recognized as molecular determinants of electromotile capability in prestin (Schaechinger et al. 2011) largely coincide with the domains forming the central pocket, further emphasizing the functional importance of these domains.

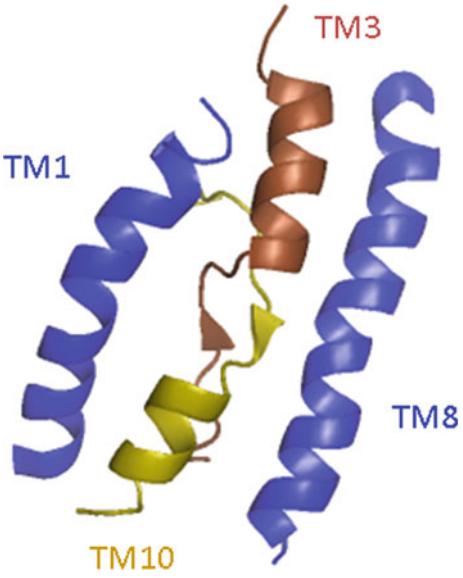

Fig. 5.4 Anion binding site. Main structural elements that contribute to the proposed central anion binding site. Anions are thought to bind at a central binding site with contributions from the nonhelical segments and the inward-pointing (N-terminal) ends of the partial helices of TMDs 3 and 10

In the crystal structure of the (non-SLC26) transporter UraA, a substrate molecule, uracil, occupies the structurally equivalent central site (Lu et al. 2011). Although the SLC26Dg crystal structure lacked bound substrate, the high similarity to UraA and structural details support the identity of the binding site. The dimensions of the cavity in computational and experimental SLC26 structures are compatible with the range of the substrate anions accepted by SLC26Dg and prestin, respectively (Gorbunov et al. 2014; Geertsma et al. 2015). Furthermore, the N-terminal ends of the partial helices from TM segments 3 and 10 point toward the binding site from opposite directions, providing likely hydrogen-bond partners for the substrate (Geertsma et al. 2015; Fig. 5.4). In UraA, a similar arrangement has been observed, with additional coordination of the substrate by side-chain interactions (Lu et al. 2011). For prestin, Gorbunov et al. (2014) directly tested the role of the structurally corresponding positions by introducing point mutations. Such mutations either altered the anion selectivity of prestin, affected the efficacy of the competitive inhibitory anion salicylate, or abolished function. Similarly, mutations at the homologous positions in transport-competent prestin orthologs from non-mammals (chicken; cPres) altered anion selectivity or abolished transport function (Gorbunov et al. 2014). Altogether, as expected for a transporter, a substrate binding site is located centrally in SLC26 proteins, including prestin. Importantly, the mutational analysis suggested that this same binding site not only mediates transport in SLC26 transporters (including nonmammalian prestin) but also is responsible for the anion-dependence of eM and NLC mediated by mammalian prestin.

How can these structural findings be reconciled with the functional knowledge on prestin? Kinetic analysis of the charge movement and motility of prestin indicated that rapid initial binding of a monovalent anion (chloride) is followed by a

slower transition and, subsequently, by the fast voltage-dependent rearrangement that generates both molecular motion and charge movement (Song and Santos-Sacchi 2013). Given that mutating the binding site disrupts prestin function, a plausible conclusion is that the first fast binding step corresponds to the binding of chloride into the SLC26 substrate binding site.

5.3.5 *Electromotile Molecular Transitions*

Here we consider the prestin structure in the context of the prevailing area-motor model that postulates (at least) two major states with different cross-sectional dimensions. Although this issue awaits its elucidation, some considerations can be made on the basis of the current knowledge.

Functionally, binding of an anion and a subsequent slower conformational transition appear to precede the mechanically productive fast structural rearrangement in mammalian prestin (Oliver et al. 2001; Song and Santos-Sacchi 2013). The concept of molecular rearrangements following binding of an anion into the central substrate binding site shared with other SLC26 homologs (Gorbunov et al. 2014) has been taken to indicate that the mechanical activity of prestin is mechanistically related to the anion transport cycle (Schaechinger et al. 2011; Gorbunov et al. 2014; Geertsma et al. 2015).

In many secondary transporters, substrate translocation occurs via an alternate access mechanism. Thus, a central binding site is alternately exposed to the extra- and intracellular environment, thereby allowing binding of a substrate on one site and dissociation/release at the opposite site of the membrane (Rudnick 2013). Such a mechanism involves at least one major conformational rearrangement and may additionally involve an intermediate occluded state (Fig. 5.5). For some

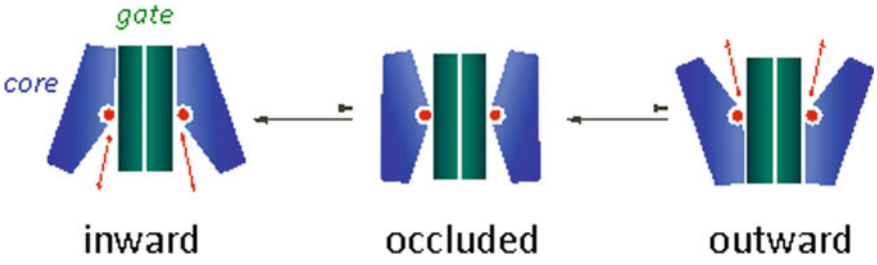

Fig. 5.5 Structural model for anion transport by SLC26. Alternating access of the central anion binding site may result from rotational movement of the core domains against the dimerized gate domains acting as a central scaffold. Experimental crystal structure of SLC26Dg and computational structures of prestin have an inward-facing conformation, but the experimental structure of the structurally homologous exchanger, AE1, revealed an outward-facing conformation (Arakawa et al. 2015). The conformational repertoire of mammalian prestin may be restricted to inward-open and hypothetical occluded states. Modified from Geertsma et al. (2015)

transporters, the conformational change mediating alternate access transport has been structurally resolved. Notably, these transporters also conform to the principle of inverted-repeat architecture, although they are not directly related to SLC26 transporters (Vastermark and Saier 2014). It was shown that there, the conformational switch between inward and outward orientation occurs by a tilting motion between rigid TM bundles (Forrest and Rudnick 2009; Rudnick 2013). For SLC26 transporters, the available structure of SLC26Dg and the UraA-based homology model (as well as the UraA structure itself) describe essentially the same inward-open conformation; therefore, the nature of the molecular rearrangements could not be inferred directly from the structural data (Lu et al. 2011; Gorbunov et al. 2014; Geertsma et al. 2015). However, it has been suggested that a relative motion between core and gate domains mediates transport in SLC26 transporters and UraA (Lu et al. 2011; Gorbunov et al. 2014; Geertsma et al. 2015). Indeed, this idea is strongly supported by the AE1 structure, which revealed an (inhibitor-bound) outside-out state. This structure superposes closely with the UraA and SLC26 structures, with the exception of altered relative positions of core and gate domains (Arakawa et al. 2015). The AE1 structure thus supports the idea of rotation between core and gate domain as the conformational mechanism mediating substrate transport as previously suggested by Gorbunov et al. (2014) and Geertsma et al. (2015; Fig. 5.5). Additional experimental support comes from the finding that a cysteine residue introduced into the central binding site of the transport-active prestin ortholog from chicken is accessible to nonpermeable cysteine-modifying reagents both from the intra- and extracellular sites, consistent with the alternate exposure of this site to both faces of the membrane (Gorbunov et al. 2014).

Given that anion binding into the central binding site in prestin enables eM, it is tempting to speculate that (voltage-dependent) motor activity arises from subsequent conformational transitions equivalent to those mediating anion translocation in other SLC26 transporters (Schaechinger et al. 2011; Gorbunov et al. 2014; Geertsma et al. 2015). In fact, a chimeric SLC26A5 construct based on the zebrafish prestin ortholog ("synthetic prestin") has both electromechanical and transport activity, consistent with the idea that the transport cycle may accommodate transitions that produce eM (Schaechinger et al. 2011). Also, observations on native chicken hair cells suggested that even nonmammalian, i.e., transport-competent, prestin orthologs may be able to generate forces sufficient for motions at the cellular scale (Beurg et al. 2013). However, in contrast to the transport-active prestin orthologs, the central binding of mammalian prestin is exclusively exposed to the intracellular side (Gorbunov et al. 2014), which is consistent with its interaction with anions selectively at the intracellular, cytoplasmic side (Oliver et al. 2001; Rybalchenko and Santos-Sacchi 2003b, 2008). In structural terms, this indicated that mammalian prestin is unable to reach a state where the binding site is fully exposed to the extracellular medium (Schaechinger et al. 2011; Gorbunov et al. 2014). Therefore, if eM arises from structural rearrangements similar to those that mediate anion transport, these states should be equivalent to a segment of the transport cycle from the fully inward-open conformation to a state preceding full exposure to the extracellular face (Schaechinger et al. 2011; Gorbunov et al. 2014).

Another open issue is the molecular nature of the voltage sensitivity of prestin. The steepness of the voltage-induced motility or charge movement suggests that roughly one elementary electrical charge is moved across the electrical field of the membrane to drive electromechanical activity (Santos-Sacchi 1991). Either exchanging the prevalent intracellular monovalent anion (Oliver et al. 2001) or neutralizing the charged amino acids by mutation (Bai et al. 2009) affects the steepness of the voltage dependence of prestin. Accordingly, anions or polar protein domains have been postulated as extrinsic or intrinsic voltage sensors, respectively. Structural identification of the mechanically effective conformational rearrangements should help to identify the molecular nature of the voltage sensor. Understanding the dynamic electromechanical behavior on this structural level will be one of the most fascinating challenges for future work on prestin.

5.4 Interaction of Prestin with Its Cellular Environment

5.4.1 Localization of Prestin Along the Basolateral Wall

After the identification of prestin (Zheng et al. 2000), immunolocalization studies showed the protein along the basolateral surface of OHCs (Belyantseva et al. 2000; Yu et al. 2006). These observations were presaged by electrophysiological localization of motor activity along the lateral membrane (Kalinec et al. 1992; Dallos et al. 1993; Huang and Santos-Sacchi 1993). This localization pattern has important physiological significance because the electromotile force generated by prestin is directed along the longitudinal axis of these elongated cells (Holley and Ashmore 1990; Holley et al. 1992; Matsumoto et al. 2010). It is believed that the unusual structure of the lateral wall of the OHCs, encompassing a prestin-containing plasma membrane, the underlying cortical cytoskeleton, and subsurface cisternae, plays a critical role in eM. The plasma membrane is connected to the underlying cytoskeleton by "pillars," ultrastructurally identified electron-dense entities (Holley and Ashmore 1990; Forge 1991). Nonetheless, the molecular links of prestin to the underlying cytoskeleton are unknown.

The delivery of prestin to the basolateral wall of OHCs has several potential confounding mechanisms. Protein sorting has been best studied in polarized epithelial cells, where work has established a dichotomy of targeting to the apical or basolateral surface. Although hair cells are polarized epithelial cells, they also show properties of neurons, with an apical-receptive area housing the mechanosensitive channels corresponding to a dendritic end and a basal pole housing the synaptic machinery that corresponds to a neuronal axonal end. A long-standing hypothesis first proposed by Dotti and Simons (1990) posited the dendritic end of a neuron to be equivalent to the basolateral surface and the axonal end to correspond to the apical end of polarized epithelial cells. Hair cells, however, confound this neat

division. Thus, hair cells have to be categorized in terms of protein sorting as either epithelial cell-like or neuronal-like.

It has long been established that classic basolateral markers such as β-catenin and Na^+/K^+-ATPase are localized along the basolateral surface of hair cells (Schneider et al. 1987; Leonova and Raphael 1997; Zhang et al. 2015). Zheng et al. (2010) demonstrated that stereociliary proteins, including harmonin and cadherin 23, are targeted to the apical surface of the CL4 cell, a model polarized epithelial cell. The authors also established that prestin was targeted to the basolateral surface of CL4 cells. These data confirm that, at least for these proteins, hair cell protein-sorting mechanisms are akin to those of polarized epithelial cells. Interestingly, using the apically targeted pendrin as a vehicle, Zheng et al. (2010) showed that basolateral targeting of prestin is determined by the C-terminus of prestin. Using site-directed mutagenesis, Zhang et al. (2015) established that two tyrosine residues, Y520 and Y667, are important for targeting prestin to the basolateral surface of polarized MDCK cells. Moreover, these authors demonstrated that this targeting is also dependent on APμ1-B, which is present in hair cells (and epithelial cells) but absent in neuronal cells (Zhang et al. 2015).

5.4.2 Prestin's Interactome

As alluded to in Sect. 5.2, the identity of prestin as the protein responsible for OHC eM has been well established. Recent efforts have also focused on identifying the role of ancillary proteins in the function of prestin. Because prestin has all the molecular features of the motor responsible for eM, this raises the question, Why look for other associated proteins? The response to this lies in three parts. First, in parallel with other systems, in particular ion channels, ancillary proteins modify the biophysical properties of the protein while establishing its localization and transport between different vesicular compartments as well as modifying its rates of turnover. Thus, protein partners may play a similar role with prestin. Second, although many of the biophysical attributes of prestin in OHCs are comparable to those of prestin expressed in heterologous cells, important discrepancies exist (for instance, the V_h of prestin in OHCs lies between −40 and −80 mV, whereas prestin in heterologous cells consistently shows more negative V_h values). Third, although prestin is clearly responsible for eM, there is evidence that links to the underlying cytoskeleton are important for harnessing forces generated by prestin along the longitudinal axis of the cell (Holley and Ashmore 1990; Holley et al. 1992; Matsumoto et al. 2010). How this is brought about is still unknown.

5.4.2.1 Vesicle-Associated Membrane Protein

To date, many proteins that interact with prestin have been identified, although definitive interactions and a clear physiological role have yet to be defined for the

vast majority of these proteins. An initial membrane yeast two-hybrid screen identified several proteins as potential prestin interactors (Zheng et al. 2009). Chief among these interacting proteins were those known for transport between different vesicular compartments. These include vesicle-associated membrane protein, vesicle-associated protein A (VAPA), and Yip1 domain family member 6 (Yipf6; Zheng et al. 2009). Association with VAPA, important for integrity of the endoplasmic reticulum (ER), was found to increase the surface expression of prestin. Interestingly, the effect seemed reciprocal, with decreased amounts of VAPA in prestin-knockout OHCs (Zheng et al. 2009). Although a role for Yipf6 in prestin transport has not been demonstrated, its closest yeast homolog, Yip1p, has been demonstrated to be important for Rab-mediated transport from the ER to the Golgi apparatus (Matern et al. 2000; Barrowman et al. 2003; Spang 2004). Yipf6 mutants have intestinal inflammatory disease, although a clear mechanism has yet to be identified and a hearing phenotype has not yet been defined (Brandl et al. 2012). A second group of proteins (38%) identified by the membrane yeast two-hybrid screen included several mitochondrial membrane proteins (cytochrome *b*, subunits of NADH-ubiquinone oxidoreductase, and ATP synthase 6; Zheng et al. 2009). Mitochondrial proteins are known to be nonspecific interactors in yeast two-hybrid screens. In their screens, mitochondrial proteins were a dominant fraction, and they saw no interactions between mitochondrial proteins and the tip-link protein cadherin 23, arguing against a nonspecific interaction. OHCs from prestin knockouts and knock-in mice with altered voltage sensitivity showed early cell death. Actual measures of mitochondrial dysfunction in prestin knockouts have, however, yet to be demonstrated.

5.4.2.2 Cystic Fibrosis Transmembrane Conductance Regulator

The cystic fibrosis transmembrane conductance regulator (CFTR) was identified by Homma et al. (2010) as interacting with prestin. Interest in the CFTR was piqued because a lateral wall conductance that carries Cl^- has been identified in OHCs (Rybalchenko and Santos-Sacchi 2003b) and because Cl^- is a critical modulator of prestin activity (see Sect. 5.2.5). Like the lateral wall Cl^- conductance, the CFTR also shows mechanosensitivity (Zhang et al. 2010). The CFTR has been shown to interact with a number of other SLC26 family members through their STAS domain (Ko et al. 2004). Although many of these interactions are dependent on PKA phosphorylation of the CFTR R domain, the interactions also result in a mutual activation of CFTR and SLC26 transporter activity (Ko et al. 2004). Homma et al. (2010) convincingly showed interactions between prestin and the CFTR (although the interaction is not dependent on PKA phosphorylation). They also showed that the presence of prestin results in the localization of CFTR from its exclusively apical location to a partial basolateral location in OHCs. Unexpectedly, however, there was little reciprocal functional effect on prestin or the CFTR in OHCs; no effects on NLC or CFTR conductance were observed. In contrast, the interaction in heterologous cells results in enhanced prestin charge movement in response to PKA

activation; a reciprocal enhanced effect on CFTR conductance was not demonstrable in the presence of prestin. Although the findings of the CFTR in the lateral membrane of OHCs in the presence of prestin is intriguing, a physiological role for the CFTR in OHCs has yet to be established. Blockers of CFTR had no effect on OHC lateral wall Cl^- conductance (Rybalchenko and Santos-Sacchi 2003b). Furthermore, mutations of CFTR that causes cystic fibrosis are not associated with hearing defects. Hearing phenotypes in these patients have been well studied, and sensorineural hearing loss was described only in the context of toxic levels of gentamicin that is used for treating repeated pulmonary infections in these patients (Homma et al. 2010).

5.4.2.3 Calmodulin

A recent paper by Keller et al. (2014) identified calmodulin as an interactor of prestin. The identity of calmodulin as an interactor was determined after initial assessments showed intrinsically disordered regions in the C-terminus of prestin in proximity to its STAS domain (Keller et al. 2014). Intrinsically disordered regions have been shown to interact with calmodulin, and Keller et al. (2014) go on to show that prestin binds to calmodulin using these regions in a Ca^{2+}-dependent manner. Importantly, they show a 35-mV shift in V_h with increasing Ca^{2+}, an effect that was reversed by the calmodulin inhibitor trifluoperazine (Keller et al. 2014). The authors then speculate that the Ca^{2+}-induced changes in V_h could have physiological importance, with efferent modulation from the olivocochlear bundle effecting changes in OHC stiffness through increases in Ca^{2+}. These interpretations may not be complete, with changes in V_h induced by Ca^{2+} perfusion being secondary to the effects on turgor pressure and not entirely due to the effects on V_h by a direct effect from calmodulin binding to prestin. Thus, the changes in V_h were not evident when the cells were collapsed before Ca^{2+} perfusion (Song and Santos-Sacchi 2015).

5.4.2.4 Microtubule-Associated Proteins

Microtubule-associated protein 1S (MAP1S) is a protein that was identified as interacting with prestin using a conventional Gal4-based yeast two-hybrid assay (Surguchev et al. 2012). In this assay, the C-terminus of prestin was used as bait. MAP1S is a member of the microtubule-associated protein family. MAP1S coexpression enhanced the surface expression of prestin as established by both biochemical and electrophysiological measures (Surguchev et al. 2012). These findings are paralleled by a gradient of MAP1S mRNA expression along the tonotopic axis, suggesting that MAP1S may bring about the higher amounts of prestin in the plasma membrane of high-frequency hair cells. Interestingly, MAP1S has also been shown to interact with actin, and its concentration in proximity to the lateral wall of OHCs raises the possibility that it serves as the link between prestin and the underlying cytoskeleton. As previously referred to, the lateral wall of OHCs

includes a cortical cytoskeleton sandwiched between subsurface cisternae and the lateral plasma membrane. The cortical cytoskeleton consists of circumferentially arranged actin filaments linked to longitudinally arranged spectrin (α2, β5) filaments (Forge 1991; Kalinec et al. 1992; Legendre et al. 2008). Previous work identified pillars that are electron-dense entities linking OHC lateral membranes to circumferentially arranged actin filaments (Holley and Ashmore 1990; Forge 1991; Kalinec et al. 1992). The molecular composition of pillars is unknown. Because MAP1S also forms a complex with a host of other actin-binding proteins (Liu et al. 2002; Liu and McKeehan 2002), these data raise the possibility that MAP1S is one component of a complex of proteins that form pillar structures.

5.4.2.5 Spectrin and Spectrin-Interacting Proteins

Although prior reports have shown a concentration of two spectrin-interacting proteins (ankyrin or protein 4.1) along the periphery of OHCs (Knipper et al. 1995; Zine and Schweitzer 1997), the wide gap (50 nm) between the cytoskeleton and the lateral membrane makes it unclear whether these proteins have a physiological role or not (Legendre et al. 2008). Moreover, there are no data showing a direct interaction between prestin and ankyrin or protein 4.1. Interestingly, a paper identifying β5 spectrin as a component of the OHC cytoskeleton showed no interaction between prestin and this spectrin isoform (Legendre et al. 2008). However, these authors found an unknown component in OHC lysates that enabled such an interaction. A key area of research in the future will be exploring the interactions between prestin and other components of the lateral wall.

5.4.2.6 Calcium/Calmodulin-Dependent Serine Protein Kinase

A subsequent study using yeast two-hybrid screens identified calcium/calmodulin-dependent serine protein kinase (CASK) as an interacting partner of prestin (Cimerman et al. 2013). CASK is a membrane-associated guanylate kinase (MAGUK). Members of this family have been shown in other systems to bind membrane proteins linking them to actin through protein 4.1 (Zhu et al. 2016). The subcellular distribution of CASK showed a developmental change that correlated with prestin and was affected by thyroid hormone levels. Normally, by postnatal day (P) 18, both NLC and eM reach mature levels. In hypothyroid animals, there is a delay in the expression of prestin, with NLC levels taking until P28 to reach normal levels. Prestin is normally expressed along the entire basolateral surface early in development and is then localized predominantly along the lateral wall while being largely excluded from the basal pole. In contrast, CASK is found predominantly at the basal pole where OHCs contact Deiters cells. In hypothyroid animals, CASK is expressed at low levels, with prestin expressed over the entire basolateral surface at P28. Coincidentally, although NLC levels were normal, eM responses were markedly reduced. Zhu et al. (2016) reasoned that the interactions

with CASK may be involved in the redistribution of prestin to the lateral wall and in generating force, possibly through the cytoskeleton or OHC interactions with Deiter's cells.

5.4.3 *Prestin in the Membrane Environment*

It is becoming increasingly appreciated that an interplay of membrane structure, organization, and mechanics regulates the function of membrane proteins. It is thus important to understand how the membrane environment affects the function of prestin. From a thermodynamic point of view, the lipid environment is the "solvent" in which prestin operates, just as water is the solvent for biochemical reactions. Thus, changes in the composition, fluidity, and mechanical properties of the membrane can all affect the molecular function of prestin. At the same time, prestin has a large C-terminus that contains a STAS domain possessing a number of potential protein-protein interaction motifs. It is reasonable to postulate that the STAS domain connects prestin to the cytoskeleton of the cell and places constraints on its mobility. Understanding these supramolecular interactions of prestin is necessary to ultimately understand how the molecular nanoscale events that occur in the prestin protein proper result in the mesoscale rearrangements that must ultimately be responsible for OHC eM.

5.4.3.1 Prestin as a Mechanosensitive Protein

After the original discovery that the membrane capacitance of the OHC was sensitive to membrane stress (Iwasa 1993), the tension sensitivity of prestin was further characterized in both OHCs and HEK cells expressing prestin (Kakehata and Santos-Sacchi 1995; Ludwig et al. 2001; Santos-Sacchi et al. 2001). These studies implied that the application of mechanical force results in a geometric rearrangement in prestin that, in turn, affects its ability to move charge in response to voltage changes, establishing prestin as similar to mechanosensitive channels such as MscL, Piezo1, and TREK1 (Sukharev et al. 1996; Coste et al. 2010; Brohawn et al. 2014). Given that the OHC is under turgor pressure, this mechanical sensitivity is likely to be physiologically important.

The question may be raised as to how prestin senses membrane mechanical forces. Membranes are thin structures that have a large resistance to changes in surface area but a very small resistance to changes in curvature. Curvature stress can be induced by differential partitioning of molecules into the two leaflets of the membrane, corresponding to the classic "bilayer couple" explanation of red blood cell shape changes (Singer and Oster 1992). It has become increasingly appreciated that many mechanosensitive membrane proteins sense mechanical force through the lipid bilayer in accordance with the "force from lipid" principle (Anishkin et al. 2014). Forces may be applied to the lipid bilayer by stretching the area or through

the direct or indirect application of membrane curvature stress. Indeed, many reagents that affect prestin function are also known to change membrane curvature (Oghalai et al. 2000; Brownell et al. 2001). It has been postulated that in the intact OHC, turgor pressure would supply a force leading to nanoscale bending of the membrane between the pillar proteins (Raphael et al. 2000; Spector et al. 2006). Although this is difficult to directly measure in living cells with current technology, measurements using fluorescence polarization microscopy (Greeson and Raphael 2009) are consistent with both the existence of nanoscale curvature and pharmacological-induced changes in this curvature. Specifically, reagents that changed the curvature in opposite directions were found to be consistent with the corresponding changes in the function of prestin as measured by the Boltzmann parameter (V_h) of the NLC (Fang et al. 2007; Greeson and Raphael 2009). Other studies have obtained evidence that prestin is also sensitive to the thickness of the membrane (Fang et al. 2010).

One of the challenges in prestin research has been the lack of pharmacological compounds that inhibit its function. This is an also issue for other mechanosensitive proteins such as MscL (Hamill 2006). The most utilized inhibitor of prestin function is salicylate, an active metabolite of aspirin related to nonsteroidal anti-inflammatory drugs (NSAIDs). NSAIDs and analgesics are associated with ototoxicity, hearing loss, and tinnitus (ringing in the ears). In other membrane proteins, NSAID effects have been attributed to both indirect effects on membrane properties and direct binding to functional regions of proteins (Lichtenberger et al. 2006; Manrique-Moreno et al. 2009). Additional research is needed to identify specific inhibitors of prestin function.

5.4.3.2 Prestin as a Confined Protein

The original fluid-mosaic membrane model proposed that proteins diffuse freely in a sea of lipids (Singer and Nicolson 1972). This picture has been refined by the discovery that different proteins have varying degrees of confinement in the membrane. In the membrane biophysics community, many concepts such as "membrane microdomains" and "lipid rafts" have been espoused to characterize the restricted mobility of membrane proteins. Here, the important questions are, Can prestin diffuse freely or is it constrained? If it is constrained, does this occur through interactions with the cytoskeleton?

The lateral diffusion of prestin was first directly measured using fluorescence recovery after photobleaching (FRAP) in HEK cells expressing prestin (Organ and Raphael 2007). These studies revealed that the diffusion of prestin is relatively slow when compared with proteins of similar molecular weight. In addition, using a dual-bleach protocol, these studies suggested that prestin was transiently confined. To confirm transient confinement and better understand the membrane dynamics of prestin, single-molecule imaging studies were performed (Kamar et al. 2012). Individual molecules of prestin labeled with a highly stable fluorophore were expressed in HEK cells and tracked using total internal fluorescence microscopy.

These studies confirmed that prestin is indeed confined in the membrane and undergoes anomalous diffusion (Kamar et al. 2012). The results could be fit to a "hop-diffusion" model in which prestin molecules diffuse within a limited area, then "hop" to a different area of the membrane. In this model, there is a timescale associated with confinement that corresponds to the strength of the intermolecular interactions restricting free diffusion of the protein. These studies raised the question of how prestin diffuses in the native OHCs. Later studies in knock-in mice expressing prestin fused to yellow fluorescent protein (YFP) obtained results consistent with the minimal diffusion of prestin in OHCs as measured with traditional FRAP (Yamashita et al. 2015). When compared with the HEK cell single-molecule results, it appears that OHCs contain additional mechanisms that further confine prestin (Yamashita et al. 2015). This raises the question whether robust electromechanical activity seen in OHCs as opposed to HEK cells could be related to the presence of additional interactions that limit the membrane lateral mobility of prestin, i.e., whether membrane confinement has implications for prestin function. One of the key ways to alter the confinement of membrane proteins is to manipulate membrane cholesterol, which changes the structure of membrane microdomains. Depletion of membrane cholesterol with MBCD was shown to have a dramatic impact on prestin confinement (Kamar et al. 2012). Taking into account an earlier study that indicated that cholesterol affects the Boltzmann parameter (V_h) of the NLC in OHCs (Rajagopalan et al. 2007), it suggests that alterations in prestin confinement affect at least the operating voltage range of prestin. Similar cholesterol depletion experiments were also carried out in the knock-in mouse model (Yamashita et al. 2015), but here the addition of salicylate was also required to enable prestin to undergo free membrane diffusion. Identifying the molecular mechanisms responsible for prestin confinement and understanding whether they affect prestin function is an important priority for future research.

5.5 Conclusions and Open Questions

Gaining a molecular and cellular understanding of eM function has been the major driving force for the research summarized above. Considering the major advances achieved over the last decade, a mechanistic framework for prestin function is finally emerging.

Only recently have experimental and computational data on the structure of prestin and its relatives been obtained. Yet, these findings already provide unprecedented insights and show remarkable agreement between structure and the wealth of biophysical data assembled since the discovery of eM. This initial structural picture of prestin should now provide a productive ground for well-directed structural and functional approaches toward understanding how molecular conformational dynamics generate eM. Given this goal, it should be kept in mind that the present structural data provide only a snapshot of one particular state, that many structural details are still missing, and, importantly, that the structure of prestin itself

has not been determined experimentally. Thus, much remains to be explored. Additionally, such work may also provide important insights into the inner workings of other SLC26 transporters, including pendrin, another SLC26 member with high relevance for cochlear homeostasis and pathophysiology.

Structure-function results are consistent with the idea that prestin works as a conformationally constrained alternate access transporter (see Fig. 5.5). In such a model, eM would arise from the transition between distinct states within an anion transport cycle that differ mechanically and electrostatically, in turn rendering prestin mechanosensitive. The conformational transition may result in a change of cross-sectional area as proposed by the prevailing area motor model (Iwasa 1994); alternatively, the tilting motion between helical bundles suggested by the available structural data may also indicate the generation of differential stresses between the two leaflets of the membrane bilayer, consistent with a previously proposed membrane bending model of eM based on flexoelectricity (Raphael et al. 2000).

Beyond these molecular mechanisms, many observations suggest that integration of prestin into a complex cellular structure, i.e., the highly specialized trilaminate lateral wall of OHCs, is important for effectively channeling the molecular movements into the generation of macroscopic cellular eM. Yet, components of this cortical structure as well as how it is assembled and whether prestin is part of it remain unknown. Despite identification of various potential interaction partners of prestin described in this chapter, their involvement in the OHC lateral wall and thus their relevance for eM remain unknown. Other important interaction partners likely await identification. Future work on the function of prestin-associated proteins will not only require elucidation of their ultrastructural localization and molecular interactions within the supramolecular OHC cortex but should also include selective manipulation of these proteins and disruption of their interactions in living OHCs.

It can be anticipated that the molecular and supramolecular characterization of prestin will lead to new approaches for selective alteration of eM that can, in turn, increase our overall understanding of the role of eM in cochlear mechanics (i.e., amplification). Ultimately, research along these avenues will increase our understanding of this unique protein that is so important for our sense of hearing.

Compliance with Ethics Requirements Joseph Santos-Sacchi declares that he has no conflict of interest. Dhasakumar Navaratnam declares that he has no conflict of interest. Robert Raphael declares that he has no conflict of interest. Dominik Oliver declares that he has no conflict of interest.

References

Adachi, M., & Iwasa, K. H. (1999). Electrically driven motor in the outer hair cell: Effect of a mechanical constraint. *Proceedings of the National Academy of Sciences of the United States of America,* 96(13), 7244–7249.

Alper, S. L., & Sharma, A. K. (2013). The SLC26 gene family of anion transporters and channels. *Molecular Aspects of Medicine,* 34(2–3), 494–515.

Anishkin, A., Loukin, S. H., Teng, J., & Kung, C. (2014). Feeling the hidden mechanical forces in lipid bilayer is an original sense. *Proceedings of the National Academy of Sciences of the United States of America,* 111(22), 7898–7905.

Arakawa, T., Kobayashi-Yurugi, T., Alguel, Y., Iwanari, H., Hatae, H., Iwata, M., Abe, Y., Hino, T., Ikeda-Suno, C., Kuma, H., Kang, D., Murata, T., Hamakubo, T., Cameron, A. D., Kobayashi, T., Hamasaki, N., & Iwata, S. (2015). Crystal structure of the anion exchanger domain of human erythrocyte band 3. *Science,* 350(6261), 680–684.

Ashmore, J. (2008). Cochlear outer hair cell motility. *Physiological Reviews,* 88(1), 173–210.

Ashmore, J., Avan, P., Brownell, W. E., Dallos, P., Dierkes, K., Fettiplace, R., Grosh, K., Hackney, C. M., Hudspeth, A. J., Juelicher, F., Lindner, B., Martin, P., Meaud, J., Petit, C., Santos-Sacchi, J. R., & Canlon, B. (2010). The remarkable cochlear amplifier. *Hearing Research,* 266(1–2), 1–17. Corrigendum. *Hearing Research*, 280(1–2), 245.

Ashmore, J. F. (1987). A fast motile response in guinea-pig outer hair cells: The cellular basis of the cochlear amplifier. *The Journal of Physiology,* 388, 323–347.

Ashmore, J. F. (1989). Transducer motor coupling in cochlear outer hair cells. In D. Kemp & J. P. Wilson (Eds.), *Mechanics of Hearing* (pp. 107–113). New York: Plenum Press.

Ashmore, J. F. (1990). Forward and reverse transduction in the mammalian cochlea. *Neuroscience Research Supplement,* 12, S39–S50.

Bai, J. P., Navaratnam, D., Samaranayake, H., & Santos-Sacchi, J. (2006). En block C-terminal charge cluster reversals in prestin (SLC26A5): Effects on voltage-dependent electromechanical activity. *Neuroscience Letters,* 404(3), 270–275.

Bai, J. P., Surguchev, A., Montoya, S., Aronson, P. S., Santos-Sacchi, J., & Navaratnam, D. (2009). Prestin's anion transport and voltage-sensing capabilities are independent. *Biophysical Journal,* 96(8), 3179–3186.

Bai, J. P., Surguchev, A., Ogando, Y., Song, L., Bian, S., Santos-Sacchi, J., & Navaratnam, D. (2010). Prestin surface expression and activity are augmented by interaction with MAP1S, a microtubule-associated protein. *Journal of Biological Chemistry,* 285(27), 20834–20843.

Bai, J.P., Moeini-Naghani, I., Zhong, S., Li, F.Y., Bian, S., Sigworth, F.J., Santos-Sacchi, J., & Navaratnam, D. (2017). Current carried by the Slc26 family member prestin does not flow through the transporter pathway. *Scientific Reports*, 7:46619.

Barrowman, J., Wang, W., Zhang, Y., & Ferro-Novick, S. (2003). The Yip1p•Yif1p complex is required for the fusion competence of endoplasmic reticulum-derived vesicles. *Journal of Biological Chemistry,* 278(22), 19878–19884.

Belyantseva, I. A., Adler, H. J., Curi, R., Frolenkov, G. I., & Kachar, B. (2000). Expression and localization of prestin and the sugar transporter GLUT-5 during development of electromotility in cochlear outer hair cells. *The Journal of Neuroscience,* 20(24), RC116.

Beurg, M., Tan, X., & Fettiplace, R. (2013). A prestin motor in chicken auditory hair cells: Active force generation in a nonmammalian species. *Neuron,* 79(1), 69–81.

Bezanilla, F. (2000). The voltage sensor in voltage-dependent ion channels. *Physiological Reviews,* 80(2), 555–592.

Brandl, K., Tomisato, W., Li, X., Neppl, C., Pirie, E., Falk, W., Xia, Y., Moresco, E. M., Baccala, R., Theofilopoulos, A. N., Schnabl, B., & Beutler, B. (2012). Yip1 domain family, member 6 (Yipf6) mutation induces spontaneous intestinal inflammation in mice. *Proceedings of the National Academy of Sciences of the United States of America,* 109(31), 12650–12655.

Brohawn, S. G., Su, Z., & MacKinnon, R. (2014). Mechanosensitivity is mediated directly by the lipid membrane in TRAAK and TREK1 K^+ channels. *Proceedings of the National Academy of Sciences of the United States of America*, 111(9), 3614–3619.

Brownell, W. E., Bader, C. R., Bertrand, D., & de Ribaupierre, Y. (1985). Evoked mechanical responses of isolated cochlear outer hair cells. *Science,* 227(4683), 194–196.

Brownell, W. E., Spector, A. A., Raphael, R. M., & Popel, A. S. (2001). Micro- and nanomechanics of the cochlear outer hair cell. *Annual Review of Biomedical Engineering,* 3, 169–194.

Cimerman, J., Waldhaus, J., Harasztosi, C., Duncker, S. V., Dettling, J., Heidrych, P., Bress, A., Gampe-Braig, C., Frank, G., Gummer, A. W., Oliver, D., Knipper, M., & Zimmermann, U.

(2013). Generation of somatic electromechanical force by outer hair cells may be influenced by prestin-CASK interaction at the basal junction with the Deiter's cell. *Histochemistry and Cell Biology,* 140(2), 119–135.

Compton, E. L., Karinou, E., Naismith, J. H., Gabel, F., & Javelle, A. (2011). Low resolution structure of a bacterial SLC26 transporter reveals dimeric stoichiometry and mobile intracellular domains. *Journal of Biological Chemistry,* 286(30), 27058–27067.

Compton, E. L., Page, K., Findlay, H. E., Haertlein, M., Moulin, M., Zachariae, U., Norman, D. G., Gabel, F., & Javelle, A. (2014). Conserved structure and domain organization among bacterial Slc26 transporters. *Biochemical Journal,* 463(2), 297–307.

Coste, B., Mathur, J., Schmidt, M., Earley, T. J., Ranade, S., Petrus, M. J., Dubin, A. E., & Patapoutian, A. (2010). Piezo1 and Piezo2 are essential components of distinct mechanically activated cation channels. *Science*, 330(6000), 55–60.

Dallos, P., & Evans, B. N. (1995). High-frequency motility of outer hair cells and the cochlear amplifier. *Science,* 267(5206), 2006–2009.

Dallos, P., Evans, B. N., & Hallworth, R. (1991). Nature of the motor element in electrokinetic shape changes of cochlear outer hair cells. *Nature, 350*(6314), 155–157.

Dallos, P., Hallworth, R., & Evans, B. N. (1993). Theory of electrically driven shape changes of cochlear outer hair cells. *Journal of Neurophysiology,* 70(1), 299–323.

Dallos, P., Wu, X., Cheatham, M. A., Gao, J., Zheng, J., Anderson, C. T., Jia, S., Wang, X., Cheng, W. H., Sengupta, S., He, D. Z., & Zuo, J. (2008). Prestin-based outer hair cell motility is necessary for mammalian cochlear amplification. *Neuron,* 58(3), 333–339.

Deak, L., Zheng, J., Orem, A., Du, G. G., Aguinaga, S., Matsuda, K., & Dallos, P. (2005). Effects of cyclic nucleotides on the function of prestin. *The Journal of Physiology,* 563(2), 483–496.

Detro-Dassen, S., Schanzler, M., Lauks, H., Martin, I., zu Berstenhorst, S. M., Nothmann, D., Torres-Salazar, D., Hidalgo, P., Schmalzing, G., & Fahlke, C. (2008). Conserved dimeric subunit stoichiometry of SLC26 multifunctional anion exchangers. *Journal of Biological Chemistry,* 283(7), 4177–4188.

Dorwart, M. R., Shcheynikov, N., Yang, D., & Muallem, S. (2008). The solute carrier 26 family of proteins in epithelial ion transport. *Physiology,* 23, 104–114.

Dotti, C. G., & Simons, K. (1990). Polarized sorting of viral glycoproteins to the axon and dendrites of hippocampal neurons in culture. *Cell,* 62(1), 63–72.

Fang, J., & K. H. Iwasa. (2007). Effects of chlorpromazine and trinitrophenol on the membrane motor of outer hair cells. *Biophysical journal*, 93:1809–1817.

Fang, J., Izumi, C., & Iwasa, K. H. (2010). Sensitivity of prestin-based membrane motor to membrane thickness. *Biophysical Journal,* 98(12), 2831–2838.

Finn, R. D., Bateman, A., Clements, J., Coggill, P., Eberhardt, R. Y., Eddy, S. R., Heger, A., Hetherington, K., Holm, L., Mistry, J., Sonnhammer, E. L., Tate, J., & Punta, M. (2014). Pfam: The protein families database. *Nucleic Acids Research,* 42, D222–D230.

Fisher, J. A., Nin, F., Reichenbach, T., Uthaiah, R. C., & Hudspeth, A. J. (2012). The spatial pattern of cochlear amplification. *Neuron,* 76(5), 989–997.

Forge, A. (1991). Structural features of the lateral walls in mammalian cochlear outer hair cells. *Cell and Tissue Research,* 265(3), 473–483.

Forrest, L. R., & Rudnick, G. (2009). The rocking bundle: A mechanism for ion-coupled solute flux by symmetrical transporters. *Physiology,* 24, 377–386.

Frank, G., Hemmert, W., & Gummer, A. W. (1999). Limiting dynamics of high-frequency electromechanical transduction of outer hair cells. *Proceedings of the National Academy of Sciences of the United States of America,* 96(8), 4420–4425.

Gale, J. E., & Ashmore, J. F. (1994). Charge displacement induced by rapid stretch in the basolateral membrane of the guinea-pig outer hair cell. *Proceedings of the Royal Society of London B: Biological Sciences,* 255(1344), 243–249.

Gale, J. E., & Ashmore, J. F. (1997a). The outer hair cell motor in membrane patches. *Pflügers Archiv - European Journal of Physiology,* 434(3), 267–271.

Gale, J. E., & Ashmore, J. F. (1997b). An intrinsic frequency limit to the cochlear amplifier. *Nature,* 389(6646), 63–66.

Geertsma, E. R., Chang, Y. N., Shaik, F. R., Neldner, Y., Pardon, E., Steyaert, J., & Dutzler, R. (2015). Structure of a prokaryotic fumarate transporter reveals the architecture of the SLC26 family. *Nature Structural & Molecular Biology,* 22, 803–808.

Gorbunov, D., Sturlese, M., Nies, F., Kluge, M., Bellanda, M., Battistutta, R., & Oliver, D. (2014). Molecular architecture and the structural basis for anion interaction in prestin and SLC26 transporters. *Nature Communications,* 5, 3622.

Greeson, J. N., & Raphael, R. M. (2009). Amphipath-induced nanoscale changes in outer hair cell plasma membrane curvature. *Biophysical Journal,* 96(2), 510–520.

Hallworth, R., & Nichols, M. G. (2012). Prestin in HEK cells is an obligate tetramer. *Journal of Neurophysiology,* 107(1), 5–11.

Hamill, O. P. (2006). Twenty odd years of stretch-sensitive channels. *Pflügers Archiv - European Journal of Physiology*, 453(3), 333–351.

He, D. Z., Zheng, J., Kalinec, F., Kakehata, S., & Santos-Sacchi, J. (2006). Tuning into the amazing outer hair cell: Membrane wizardry with a twist and shout. *Journal of Membrane Biology,* 209(2–3), 119–134.

Hoglund, P. J., Nordstrom, K. J., Schioth, H. B., & Fredriksson, R. (2011). The solute carrier families have a remarkably long evolutionary history with the majority of the human families present before divergence of bilaterian species. *Molecular Biology and Evolution,* 28(4), 1531–1541.

Holley, M. C., & Ashmore, J. F. (1990). Spectrin, actin and the structure of the cortical lattice in mammalian cochlear outer hair cells. *Journal of Cell Science,* 96(2), 283–291.

Holley, M. C., Kalinec, F., & Kachar, B. (1992). Structure of the cortical cytoskeleton in mammalian outer hair cells. *Journal of Cell Science,* 102(3), 569–580.

Homma, K., Miller, K. K., Anderson, C. T., Sengupta, S., Du, G. G., Aguinaga, S., Cheatham, M., Dallos, P., & Zheng, J. (2010). Interaction between CFTR and prestin (SLC26A5). *Biochimica et Biophysica Acta,* 1798(6), 1029–1040.

Homma, K., Duan, C., Zheng, J., Cheatham, M. A., & Dallos, P. (2013). The V499G/Y501H mutation impairs fast motor kinetics of prestin and has significance for defining functional independence of individual prestin subunits. *Journal of Biological Chemistry,* 288(4), 2452–2463.

Huang, G., & Santos-Sacchi, J. (1993). Mapping the distribution of the outer hair cell motility voltage sensor by electrical amputation. *Biophysical Journal,* 65(5), 2228–2236.

Huang, G. J., & Santos-Sacchi, J. (1994). Motility voltage sensor of the outer hair cell resides within the lateral plasma-membrane. *Proceedings of the National Academy of Sciences of the United States of America,* 91(25), 12268–12272.

Iwasa, K. H. (1993). Effect of stress on the membrane capacitance of the auditory outer hair cell. *Biophysical Journal,* 65(1), 492–498.

Iwasa, K. H. (1994). A membrane motor model for the fast motility of the outer hair cell. *The Journal of the Acoustical Society of America,* 96(4), 2216–2224.

Kachar, B., Brownell, W. E., Altschuler, R., & Fex, J. (1986). Electrokinetic shape changes of cochlear outer hair cells. *Nature,* 322(6077), 365–368.

Kakehata, S., & Santos-Sacchi, J. (1995). Membrane tension directly shifts voltage dependence of outer hair cell motility and associated gating charge. *Biophysical Journal,* 68(5), 2190–2197.

Kakehata, S., & Santos-Sacchi, J. (1996). Effects of salicylate and lanthanides on outer hair cell motility and associated gating charge. *The Journal of Neuroscience,* 16(16), 4881–4889.

Kalinec, F., Holley, M. C., Iwasa, K. H., Lim, D. J., & Kachar, B. (1992). A membrane-based force generation mechanism in auditory sensory cells. *Proceedings of the National Academy of Sciences of the United States of America,* 89(18), 8671–8675.

Kamar, R. I., Organ-Darling, L. E., & Raphael, R. M. (2012). Membrane cholesterol strongly influences confined diffusion of prestin. *Biophysical Journal,* 103(8), 1627–1636.

Keller, J. P., Homma, K., Duan, C., Zheng, J., Cheatham, M. A., & Dallos, P. (2014). Functional regulation of the SLC26-family protein prestin by calcium/calmodulin. *The Journal of Neuroscience,* 34(4), 1325–1332.

Knipper, M., Zimmermann, U., Kopschall, I., Rohbock, K., Jungling, S., & Zenner, H. P. (1995). Immunological identification of candidate proteins involved in regulating active shape changes of outer hair cells. *Hearing Research,* 86(1–2), 100–110.

Ko, S. B., Zeng, W., Dorwart, M. R., Luo, X., Kim, K. H., Millen, L., Goto, H., Naruse, S., Soyombo, A., Thomas, P. J., & Muallem, S. (2004). Gating of CFTR by the STAS domain of SLC26 transporters. *Nature Cell Biology,* 6(4), 343–350.

Legendre, K., Safieddine, S., Kussel-Andermann, P., Petit, C., & El-Amraoui, A. (2008). αII-βV spectrin bridges the plasma membrane and cortical lattice in the lateral wall of the auditory outer hair cells. *Journal of Cell Science,* 121(20), 3347–3356.

Leonova, E. V., & Raphael, Y. (1997). Organization of cell junctions and cytoskeleton in the reticular lamina in normal and ototoxically damaged organ of Corti. *Hearing Research,* 113(1–2), 14–28.

Li, Y., Liu, Z., Shi, P., & Zhang, J. (2010). The hearing gene prestin unites echolocating bats and whales. *Current Biology,* 20(2), R55–R56.

Liberman, M. C., Gao, J., He, D. Z., Wu, X., Jia, S., & Zuo, J. (2002). Prestin is required for electromotility of the outer hair cell and for the cochlear amplifier. *Nature,* 419(6904), 300–304.

Lichtenberger, L. M., Zhou, Y., Dial, E. J., & Raphael, R. M. (2006). NSAID injury to the gastrointestinal tract: Evidence that NSAIDs interact with phospholipids to weaken the hydrophobic surface barrier and induce the formation of unstable pores in membranes. *Journal of Pharmacy and Pharmacology*, 58(11), 1421–1428.

Liu, L., & McKeehan, W. L. (2002). Sequence analysis of LRPPRC and its SEC1 domain interaction partners suggests roles in cytoskeletal organization, vesicular trafficking, nucleo-cytosolic shuttling, and chromosome activity. *Genomics,* 79(1), 124–136.

Liu, L., Amy, V., Liu, G., & McKeehan, W. L. (2002). Novel complex integrating mitochondria and the microtubular cytoskeleton with chromosome remodeling and tumor suppressor RASSF1 deduced by in silico homology analysis, interaction cloning in yeast, and colocalization in cultured cells. *In Vitro Cellular & Developmental Biology - Animal,* 38(10), 582–594.

Liu, Y., Cotton, J. A., Shen, B., Han, X., Rossiter, S. J., & Zhang, S. (2010). Convergent sequence evolution between echolocating bats and dolphins. *Current Biology,* 20(2), R53–R54.

Liu, Z., Qi, F. Y., Zhou, X., Ren, H. Q., & Shi, P. (2014). Parallel sites implicate functional convergence of the hearing gene prestin among echolocating mammals. *Molecular Biology and Evolution,* 31(9), 2415–2424.

Lolli, G., Pasqualetto, E., Costanzi, E., Bonetto, G., & Battistutta, R. (2015). The STAS domain of mammalian SLC26A5 prestin harbors an anion-binding site. *Biochemical Journal*, 473(4), 365–370.

Lovas, S., He, D. Z., Liu, H., Tang, J., Pecka, J. L., Hatfield, M. P., & Beisel, K. W. (2015). Glutamate transporter homolog-based model predicts that anion-π interaction is the mechanism for the voltage-dependent response of prestin. *Journal of Biological Chemistry,* 290(40), 24326–24339.

Lu, F., Li, S., Jiang, Y., Jiang, J., Fan, H., Lu, G., Deng, D., Dang, S., Zhang, X., Wang, J., & Yan, N. (2011). Structure and mechanism of the uracil transporter UraA. *Nature,* 472(7342), 243–246.

Ludwig, J., Oliver, D., Frank, G., Klöcker, N., Gummer, A. W., & Fakler, B. (2001). Reciprocal electromechanical properties of rat prestin: The motor molecule from rat outer hair cells. *Proceedings of the National Academy of Sciences of the United States of America,* 98(7), 4178–4183.

Mahendrasingam, S., Beurg, M., Fettiplace, R., & Hackney, C. M. (2010). The ultrastructural distribution of prestin in outer hair cells: A post-embedding immunogold investigation of low-frequency and high-frequency regions of the rat cochlea. *European Journal of Neuroscience,* 31(9), 1595–1605.

Manrique-Moreno, M., Garidel, P., Suwalsky, M., Howe, J., & Brandenburg, K. (2009). The membrane-activity of ibuprofen, diclofenac, and naproxen: A physico-chemical study with lecithin phospholipids. *Biochimica et Biophysica Acta*, 1788(6), 1296–1303.

Matern, H., Yang, X., Andrulis, E., Sternglanz, R., Trepte, H. H., & Gallwitz, D. (2000). A novel Golgi membrane protein is part of a GTPase-binding protein complex involved in vesicle targeting. *The EMBO Journal,* 19(17), 4485–4492.

Matsumoto, N., Kitani, R., Maricle, A., Mueller, M., & Kalinec, F. (2010). Pivotal role of actin depolymerization in the regulation of cochlear outer hair cell motility. *Biophysical Journal,* 99(7), 2067–2076.

Meltzer, J., & Santos-Sacchi, J. (2001). Temperature dependence of non-linear capacitance in human embryonic kidney cells transfected with prestin, the outer hair cell motor protein. *Neuroscience Letters,* 313(3), 141–144.

Mio, K., Kubo, Y., Ogura, T., Yamamoto, T., Arisaka, F., & Sato, C. (2008). The motor protein prestin is a bullet-shaped molecule with inner cavities. *Journal of Biological Chemistry,* 283(2), 1137–1145.

Mistrik, P., Daudet, N., Morandell, K., & Ashmore, J. F. (2012). Mammalian prestin is a weak Cl^-/HCO_3^- electrogenic antiporter. *The Journal of Physiology,* 590(22), 5597–5610.

Mount, D. B., & Romero, M. F. (2004). The SLC26 gene family of multifunctional anion exchangers. *Pflügers Archiv - European Journal of Physiology,* 447(5), 710–721.

Muallem, D., & Ashmore, J. (2006). An anion antiporter model of prestin, the outer hair cell motor protein. *Biophysical Journal,* 90(11), 4035–4045.

Mutai, H., Suzuki, N., Shimizu, A., Torii, C., Namba, K., Morimoto, N., Kudoh, J., Kaga, K., Kosaki, K., & Matsunaga, T. (2013). Diverse spectrum of rare deafness genes underlies early-childhood hearing loss in japanese patients: A cross-sectional, multi-center next-generation sequencing study. *Orphanet Journal of Rare Diseases,* 8, 172.

Navaratnam, D., Bai, J. P., Samaranayake, H., & Santos-Sacchi, J. (2005). N-terminal-mediated homomultimerization of prestin, the outer hair cell motor protein. *Biophysical Journal,* 89(5), 3345–3352.

Oghalai, J. S., Zhao, H. B., Kutz, J. W., & Brownell, W. E. (2000). Voltage- and tension-dependent lipid mobility in the outer hair cell plasma membrane. *Science,* 287(5453), 658–661.

Ohana, E., Shcheynikov, N., Yang, D., So, I., & Muallem, S. (2011). Determinants of coupled transport and uncoupled current by the electrogenic SLC26 transporters. *The Journal of General Physiology,* 137(2), 239–251.

Oliver, D., He, D. Z., Klocker, N., Ludwig, J., Schulte, U., Waldegger, S., Ruppersberg, J. P., Dallos, P., & Fakler, B. (2001). Intracellular anions as the voltage sensor of prestin, the outer hair cell motor protein. *Science,* 292(5525), 2340–2343.

Organ, L. E., & Raphael, R. M. (2007). Application of fluorescence recovery after photobleaching to study prestin lateral mobility in the human embryonic kidney cell. *Journal of Biomedical Optics,* 12(2), 021003.

Pasqualetto, E., Aiello, R., Gesiot, L., Bonetto, G., Bellanda, M., & Battistutta, R. (2010). Structure of the cytosolic portion of the motor protein prestin and functional role of the STAS domain in SLC26/SulP anion transporters. *Journal of Molecular Biology,* 400(3), 448–462.

Rajagopalan, L., Patel, N., Madabushi, S., Goddard, J. A., Anjan, V., Lin, F., Shope, C., Farrell, B., Lichtarge, O., Davidson, A. L., Brownell, W. E., & Pereira, F. A. (2006). Essential helix interactions in the anion transporter domain of prestin revealed by evolutionary trace analysis. *The Journal of Neuroscience,* 26(49), 12727–12734.

Rajagopalan, L., Greeson, J. N., Xia, A., Liu, H., Sturm, A., Raphael, R. M., Davidson, A. L., Oghalai, J. S., Pereira, F. A., & Brownell, W. E. (2007). Tuning of the outer hair cell motor by membrane cholesterol. *Journal of Biological Chemistry,* 282(50), 36659–36670.

Raphael, R. M., Popel, A. S., & Brownell, W. E. (2000). A membrane bending model of outer hair cell electromotility. *Biophysical Journal,* 78(6), 2844–2862.

Rudnick, G. (2013). How do transporters couple solute movements? *Molecular Membrane Biology,* 30(7), 355–359.

Rybalchenko, V., & Santos-Sacchi, J. (2003a). Allosteric modulation of the outer hair cell motor protein prestin by chloride. In A. Gummer (Ed.), *Biophysics of the Cochlea: From Molecules to Models* (pp. 116–126). Singapore: World Scientific Publishing.

Rybalchenko, V., & Santos-Sacchi, J. (2003b). Cl^- flux through a non-selective, stretch-sensitive conductance influences the outer hair cell motor of the guinea-pig. *The Journal of Physiology,* 547(3), 873–891.

Rybalchenko, V., & Santos-Sacchi, J. (2008). Anion control of voltage sensing by the motor protein prestin in outer hair cells. *Biophysical Journal,* 95(9), 4439–4447.

Saier, M. H., Jr., Eng, B. H., Fard, S., Garg, J., Haggerty, D. A., Hutchinson, W. J., Jack, D. L., Lai, E. C., Liu, H. J., Nusinew, D. P., Omar, A. M., Pao, S. S., Paulsen, I. T., Quan, J. A., Sliwinski, M., Tseng, T. T., Wachi, S., & Young, G. B. (1999). Phylogenetic characterization of novel transport protein families revealed by genome analyses. *Biochimica et Biophysica Acta,* 1422(1), 1–56.

Santos-Sacchi, J. (1989). Asymmetry in voltage-dependent movements of isolated outer hair cells from the organ of Corti. *The Journal of Neuroscience,* 9(8), 2954–2962.

Santos-Sacchi, J. (1990). Fast outer hair cell motility: How fast is fast? In P. Dallos, C. D. Geisler, J. W. Matthews, M. A. Ruggero, & C. R. Steele (Eds.), *The Mechanics and Biophysics of Hearing* (pp. 69–75). Berlin: Springer-Verlag.

Santos-Sacchi, J. (1991). Reversible inhibition of voltage-dependent outer hair cell motility and capacitance. *The Journal of Neuroscience,* 11(10), 3096–3110.

Santos-Sacchi, J. (1992). On the frequency limit and phase of outer hair cell motility: Effects of the membrane filter. *The Journal of Neuroscience,* 12(5), 1906–1916.

Santos-Sacchi, J. (1993). Harmonics of outer hair cell motility. *Biophysical Journal,* 65(5), 2217–2227.

Santos-Sacchi, J., & Dilger, J. P. (1988). Whole cell currents and mechanical responses of isolated outer hair cells. *Hearing Research,* 35(2–3), 143–150.

Santos-Sacchi, J., & Huang, G. J. (1998). Temperature dependence of outer hair cell nonlinear capacitance. *Hearing Research,* 116(1–2), 99–106.

Santos-Sacchi, J., & Navarrete, E. (2002). Voltage-dependent changes in specific membrane capacitance caused by prestin, the outer hair cell lateral membrane motor. *Pflügers Archiv - European Journal of Physiology,* 444(1–2), 99–106.

Santos-Sacchi, J., & Song, L. (2014a). Chloride and salicylate influence prestin-dependent specific membrane capacitance. *Journal of Biological Chemistry,* 289(15), 10823–10830.

Santos-Sacchi, J., & Song, L. (2014b). Chloride-driven electromechanical phase lags at acoustic frequencies are generated by SLC26a5, the outer hair cell motor protein. *Biophysical Journal,* 107(1), 126–133.

Santos-Sacchi, J., & Song, L. (2016). Chloride anions regulate kinetics but not voltage-sensor Q_{max} of the solute carrier SLC26a5. *Biophysical Journal,* 110, 1–11.

Santos-Sacchi, J., Kakehata, S., & Takahashi, S. (1998). Effects of membrane potential on the voltage dependence of motility-related charge in outer hair cells of the guinea-pig. *The Journal of Physiology,* 510(1), 225–235.

Santos-Sacchi, J., Shen, W., Zheng, J., & Dallos, P. (2001). Effects of membrane potential and tension on prestin, the outer hair cell lateral membrane motor protein. *The Journal of Physiology,* 531(3), 661–666.

Santos-Sacchi, J., Song, L., Zheng, J. F., & Nuttall, A. L. (2006). Control of mammalian cochlear amplification by chloride anions. *The Journal of Neuroscience,* 26(15), 3992–3998.

Schaechinger, T. J., & Oliver, D. (2007). Nonmammalian orthologs of prestin (SLC26A5) are electrogenic divalent/chloride anion exchangers. *Proceedings of the National Academy of Sciences of the United States of America,* 104(18), 7693–7698.

Schaechinger, T. J., Gorbunov, D., Halaszovich, C. R., Moser, T., Kugler, S., Fakler, B., & Oliver, D. (2011). A synthetic prestin reveals protein domains and molecular operation of outer hair cell piezoelectricity. *The EMBO Journal,* 30(14), 2793–2804.

Schanzler, M., & Fahlke, C. (2012). Anion transport by the cochlear motor protein prestin. *The Journal of Physiology,* 590(2), 259–272.

Scherer, M. P., & Gummer, A. W. (2005). How many states can the motor molecule, prestin, assume in an electric field? *Biophysical Journal: Biophysical Letters*, 88(5), L27–L29.

Schneider, M. E., Cotanche, D. A., Fambrough, D. M., Saunders, J. C., & Matschinsky, F. M. (1987). Immunocytochemical and quantitative studies of Na^+,K^+-ATPase distribution in the developing chick cochlea. *Hearing Research,* 31(1), 39–53.

Sharma, A. K., Rigby, A. C., & Alper, S. L. (2011). STAS domain structure and function. *Cellular Physiology and Biochemistry,* 28(3), 407–422.

Singer, S. J., & Nicolson, G. L. (1972). The fluid mosaic model of the structure of cell membranes. *Science,* 175(4023), 720–731.

Singer, S. J., & Oster, G. F. (1992). The bilayer couple hypothesis. *Trends in Cell Biology*, 2(3), 69–70.

Song, L., & Santos-Sacchi, J. (2010). Conformational state-dependent anion binding in prestin: Evidence for allosteric modulation. *Biophysical Journal,* 98(3), 371–376.

Song, L., & Santos-Sacchi, J. (2013). Disparities in voltage-sensor charge and electromotility imply slow chloride-driven state transitions in the solute carrier SLC26a5. *Proceedings of the National Academy of Sciences of the United States of America,* 110(10), 3883–3888.

Song, L., & Santos-Sacchi, J. (2015). Intracellular calcium affects prestin's voltage operating point indirectly via turgor-induced membrane tension. In K. D. Karavitaki & D. P. Corey (Eds.), *Mechanics of Hearing: Protein to Perception: Proceedings of the 12th International Workshop on the Mechanics of Hearing,* Cape Sounio, Greece, June 23–29, 2014. Melville, NY: American Institute of Physics Conference Proceedings 1703, 030009.

Spang, A. (2004). Vesicle transport: A close collaboration of Rabs and effectors. *Current Biology,* 14(1), R33–R34.

Spector, A. A., Deo, N., Grosh, K., Ratnanather, J. T., & Raphael, R. M. (2006). Electromechanical models of the outer hair cell composite membrane. *Journal of Membrane Biology,* 209(2–3), 135–152.

Sukharev, S. I., Blount, P., Martinac, B., Guy, H. R., & Kung, C. (1996). MscL: A mechanosensitive channel in *Escherichia coli*. *Society of General Physiologists Series*, 51, 133–141.

Surguchev, A., Bai, J. P., Joshi, P., & Navaratnam, D. (2012). Hair cell BK channels interact with RACK1, and PKC increases its expression on the cell surface by indirect phosphorylation. *American Journal of Physiology - Cell Physiology,* 303(2), C143–C150.

Tan, X., Pecka, J. L., Tang, J., Okoruwa, O. E., Zhang, Q., Beisel, K. W., & He, D. Z. (2011). From zebrafish to mammal: Functional evolution of prestin, the motor protein of cochlear outer hair cells. *Journal of Neurophysiology,* 105(1), 36–44.

Tunstall, M. J., Gale, J. E., & Ashmore, J. F. (1995). Action of salicylate on membrane capacitance of outer hair cells from the guinea-pig cochlea. *The Journal of Physiology,* 485(3), 739–752.

Vastermark, A., & Saier, M. H. (2014). Evolutionary relationship between 5 + 5 and 7 + 7 inverted repeat folds within the amino acid-polyamine-organocation superfamily. *Proteins: Structure, Function, and Bioinformatics,* 82(2), 336–346.

Wong, F. H., Chen, J. S., Reddy, V., Day, J. L., Shlykov, M. A., Wakabayashi, S. T., & Saier, M. H., Jr. (2012). The amino acid-polyamine-organocation superfamily. *Journal of Molecular Microbiology and Biotechnology,* 22(2), 105–113.

Yamashita, T., Hakizimana, P., Wu, S., Hassan, A., Jacob, S., Temirov, J., Fang, J., Mellado-Lagarde, M., Gursky, R., Horner, L., Leibiger, B., Leijon, S., Centonze, V. E., Berggren, P. O., Frase, S., Auer, M., Brownell, W. E., Fridberger, A., & Zuo, J. (2015). Outer hair cell lateral wall structure constrains the mobility of plasma membrane proteins. *PLoS Genetics,* 11(9), e1005500.

Yu, N., Zhu, M. L., & Zhao, H. B. (2006). Prestin is expressed on the whole outer hair cell basolateral surface. *Brain Research,* 1095(1), 51–58.

Zhang, W. K., Wang, D., Duan, Y., Loy, M. M., Chan, H. C., & Huang, P. (2010). Mechanosensitive gating of CFTR. *Nature Cell Biology,* 12(5), 507–512.

Zhang, Y., Moeini-Naghani, I., Bai, J., Santos-Sacchi, J., & Navaratnam, D. S. (2015). Tyrosine motifs are required for prestin basolateral membrane targeting. *Biology Open,* 4(2), 197–205.

Zheng, J., Shen, W., He, D. Z., Long, K. B., Madison, L. D., & Dallos, P. (2000). Prestin is the motor protein of cochlear outer hair cells. *Nature,* 405(6783), 149–155.

Zheng, J., Long, K. B., Shen, W., Madison, L. D., & Dallos, P. (2001). Prestin topology: Localization of protein epitopes in relation to the plasma membrane. *NeuroReport,* 12(9), 1929–1935.

Zheng, J., Du, G. G., Matsuda, K., Orem, A., Aguinaga, S., Deak, L., Navarrete, E., Madison, L. D., & Dallos, P. (2005). The C-terminus of prestin influences nonlinear capacitance and plasma membrane targeting. *Journal of Cell Science,* 118(13), 2987–2996.

Zheng, J., Du, G. G., Anderson, C. T., Keller, J. P., Orem, A., Dallos, P., & Cheatham, M. (2006). Analysis of the oligomeric structure of the motor protein prestin. *Journal of Biological Chemistry,* 281(29), 19916–19924.

Zheng, J., Anderson, C. T., Miller, K. K., Cheatham, M., & Dallos, P. (2009). Identifying components of the hair cell interactome involved in cochlear amplification. *BMC Genomics,* 10, 127.

Zheng, L., Zheng, J., Whitlon, D. S., Garcia-Añoveros, J., & Bartles, J. R. (2010). Targeting of the hair cell proteins cadherin 23, harmonin, myosin XVa, espin, and prestin in an epithelial cell model. *The Journal of Neuroscience,* 30(21), 7187–7201.

Zhu, J., Shang, Y., & Zhang, M. (2016). Mechanistic basis of MAGUK-organized complexes in synaptic development and signalling. *Nature Reviews Neuroscience,* 17(4), 209–223.

Zine, A., & Schweitzer, L. (1997). Localization of proteins associated with the outer hair cell plasma membrane in the gerbil cochlea. *Neuroscience,* 80(4), 1247–1254.

Chapter 6
Electromechanical Feedback Mechanisms and Power Transfer in the Mammalian Cochlea

Anthony W. Gummer, Wei Dong, Roozbeh Ghaffari, and Dennis M. Freeman

Abstract The basis of the extraordinary sensitivity and frequency selectivity of the mammalian cochlea is an electromechanical feedback system that amplifies the deflection of the hair cell stereocilia. Electromechanical force is generated by the soma of the outer hair cell and acts against viscous forces. These forces are expected to be particularly large in the narrow subtectorial space between the reticular lamina and the overlying tectorial membrane. Fundamental aspects of this amplifying process are not fully understood. Three main questions are addressed in this chapter. First, given capacitive and inertial characteristics of cellular and acellular cochlear components, how is the electromechanical force coupled to the stereocilia locally, radially, and longitudinally, with correct phase to produce gain rather than attenuation? Second, how is temporal fidelity achieved in the presence of high gain? Third, what is the evidence for power amplification rather than just amplitude amplification? This chapter presents modern experimental approaches that are addressing these issues. Presented in a conceptual framework of experiment and theory, three approaches are highlighted: (1) combined pressure and voltage

A.W. Gummer (✉)
Section of Physiological Acoustics and Communication, Faculty of Medicine, University of Tübingen, Elfriede-Aulhorn-Strasse 5, 72076 Tübingen, Germany
e-mail: anthony.gummer@uni-tuebingen.de

W. Dong
Research Service, VA Loma Linda Healthcare System, Loma Linda, CA 92357, USA
e-mail: wei.dong@va.gov

W. Dong
Department of Otolaryngology and Head and Neck Surgery, Loma Linda University Health, Loma Linda, CA 92354, USA

R. Ghaffari · D.M. Freeman
Research Laboratory of Electronics, Massachusetts Institute of Technology, Cambridge, MA 02139, USA
e-mail: rooz@mit.edu

D.M. Freeman
e-mail: freeman@mit.edu

G.A. Manley et al. (eds.), *Understanding the Cochlea*, Springer Handbook of Auditory Research 62, DOI 10.1007/978-3-319-52073-5_6

measurements near the organ of Corti, (2) vibration measurements at the reticular lamina and tectorial membrane, and (3) mechanical and electrokinetic properties of the tectorial membrane. The experimental evidence supports the thesis that average power gain in the region of maximum amplitude response and coupling through the tectorial membrane are both crucial for shaping the frequency response of the cochlear amplifier and, therefore, of stereocilia deflection.

Keywords Active amplification · Basilar membrane vibration · Cochlear mechanics · Electrokinetics · Electromechanical transduction · Longitudinal coupling · Optical coherence tomography · Otoacoustic emissions · Outer hair cell · Pressure waves · Reticular lamina vibration · Stereocilia · Tectorial membrane vibration · Traveling wave

6.1 Introduction

The mammalian cochlea is a remarkable sensor capable of detecting subatomic motions and performing high-quality, intensity-dependent spectral analysis. These extraordinary properties underlie our ability to communicate and to navigate through acoustically rich environments. Nevertheless, some fundamental aspects of signal processing in the cochlea are not fully understood. Measurements of basilar membrane (BM) motions have shown that both sensitivity and frequency selectivity are already manifest in the mechanical stage of auditory processing (Robles and Ruggero 2001). The sharpness of BM tuning, Q_{10dB}, defined as the frequency of the amplitude maximum divided by the bandwidth 10 dB below the maximum, is as high as 11 (Robles and Ruggero 2001). Both the sensitivity and frequency selectivity of BM motion are surprising because cochlear structures are surrounded by fluid whose viscosity would naturally dissipate energy and thereby limit frequency tuning and responses to low-intensity sounds. On that basis, "electromechanical action" (Gold 1948) has been implicated in providing the energy that is necessary to act against viscous forces.

This chapter focuses on recent concepts and experiments for elucidating the mechanisms of cochlear sensitivity and frequency selectivity in mammals. Central to this issue are the electromechanical action of the outer hair cell (OHC) and the mechanisms for coupling this force into the motion of the cochlear partition (CP) and, in particular, to the hair cell stereocilia. To this end, Sect. 6.2 considers fluid-pressure and velocity conditions within the cochlea and Sect. 6.3 the mechanical, electrical, kinematical, and material properties of the tectorial membrane (TM). Measurement of the relative phase of pressure and velocity is essential for understanding the timing of OHC electromechanical force and deciding whether this action yields net power gain. TM properties are crucial for understanding the coupling of OHC force because mechanical energy is transferred to the hair cells at the interface between the TM, stereocilia, and reticular lamina (RL). In Sect. 6.4, a number of outstanding problems are presented.

6.2 Cochlear Fluid Pressure and Amplification

Objects are moved by forces, and in the case of the cochlea, it is fluid pressure that initiates force. Despite this rather trivial statement, it is displacement, or equivalently velocity, that has been the focus of experimental cochlear mechanics. For comprehensive reviews of this vast field, the reader is referred to, for example, Robles and Ruggero (2001) and Olson et al. (2012). The pioneering book by von Békésy (1960) is also recommended.

Today, due to technological advances in the miniaturization of pressure sensors, it is now possible to probe pressure fields near cochlear structures and thereby directly address central issues such as the mechanisms of cochlear amplification. This section provides an update on crucial pressure experiments and their importance for understanding cochlear amplification.

6.2.1 Cochlear Pressure Waves: Classical Hydrodynamics

Sound pressure waves stimulating the eardrum are transmitted via vibrations of the middle ear ossicles to the oval window at the base of the cochlea where vibration of the stapes footplate initiates fluid waves in the cochlea.

The cochlea is divided by the CP into three fluid-filled compartments called the scala tympani (ST), scala vestibuli (SV), and scala media (SM). The ST and SV connect through the helicotrema, a small hole close to the apical end of the cochlea (Fig. 6.1). At the basal end of the cochlea, the cochlear fluid connects to the stapes via the oval window. The round window membrane releases the fluid pressure to air pressure in the middle ear cavity.

Sound transmission in the forward direction has been well described (de Boer 1980; Olson et al. 2012). Vibration of the stapes longitudinally compresses the cochlear fluid, causing a compressive pressure wave that is approximately instantaneous and spatially invariant. This compressive wave can be thought of as a background pressure that varies in time with the piston-like motion of the stapes; it is known as the cochlear "compression wave" (CW) or "fast wave" (Fig. 6.1, *thin dashed lines*). In addition to the CW, the stapes vibration creates a pressure difference between the ST and SV, which displaces the CP transversally, causing a transversal displacement wave to propagate longitudinally along the cochlea. This wave is slower than the CW because it depends on interactions between the fluids and the mechanical elements of the CP. This wave is called the cochlear "traveling wave" (TW) or "slow wave" (Fig. 6.1, *solid line*).

The TW and CW are distinguishable with respect to (1) timing because the TW propagates along the CP much slower than the CW, which travels near the speed of sound in cochlear fluid; (2) amplitude because the TW is locally filtered by hydrodynamic interactions between the fluid and CP and also enhanced and tuned by an amplifying process internal to the CP; and (3) spatial variation because the

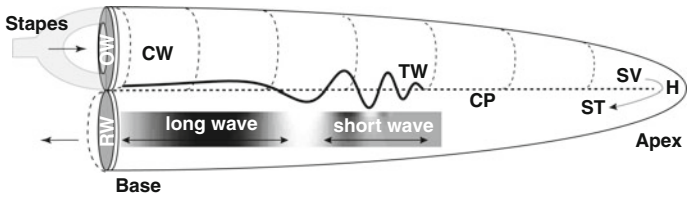

Fig. 6.1 Pressure waves in the cochlear fluids. "Compression wave" (CW; *thin dashed lines*) moves longitudinally from base to apex of the cochlea, through the scala vestibuli (SV) and the helicotrema (H) and from apex to base through the scala tympani (ST). "Traveling wave" (TW; *solid line*) is created by the pressure difference between the SV and ST, transversally displacing the cochlear partition (CP; *thick dashed line*) and propagating longitudinally along the cochlea. Although only depicted on the CP, TW fronts (surfaces of equal phase) also propagate along the cochlea through the fluids, with amplitudes that depend on wavelength and distance from the CP. TW motion can be partitioned into two wavelength-associated regions: the "long-wave" region and the "short-wave" region. OW, oval window; RW, round window. Cochlea is unrolled for illustration purposes

TW varies substantially spatially, slows (wavelength shortens), and grows in amplitude as it travels along the CP, reaching a maximum at the "characteristic" or "best" frequency (BF) place. Apical to the BF place, the TW gradually disappears, leaving a so-called evanescent wave as evidenced by an approximately frequency-independent response at a given measurement place. (An evanescent wave occurs where the imaginary part of the wave number, which defines the wave-decay constant, becomes much larger than the real part of the wave number, which defines the wavelength. Experimentally, evanescent waves are distinguishable from the CW because their amplitudes decay longitudinally as given by their wave-decay constants.)

Based on the wavelength of the TW and the dimensions of the scalae, TW propagation can be divided into two regions along the cochlea (de Boer 1980). In the first region, called the "long-wave" region, the wavelength (λ) of the TW is long compared with the height (h) of the cochlear duct ($\lambda \gg 2\pi h$). In this region, the motion of fluid particles can be considered as a plane wave of equal amplitude throughout the depth of the fluid, similar to a wall of fluid moving back and forth in a tube. In the second region, called the "short-wave" region, λ is short compared with h ($\lambda \ll 2\pi h$). Here, wave propagation is similar to ripples on the surface of a deep pond and fluid particles travel in elliptical trajectories with largest amplitudes near the surface. In contrast, the CW moves in phase with the stapes between the oval and round windows and is nearly unchanging in space. The CW appears to be relatively unimportant for cochlear micromechanics because it causes little BM vibration (Robles and Ruggero 2001) and neural excitation at only very high sound levels (Huang and Olson 2011).

6.2.2 *Measurement of Cochlear Fluid Pressure*

Intracochlear pressure measurements can be made by introducing a hydrophone into the cochlea. This device is effectively a microphone adapted to sensing changes in fluid pressure. Olson (1998, 1999) developed a hydrophone small enough (inner/outer diameter 100/150 μm) to make pressure measurements near the BM, potentially without damaging the cochlea. This device, commonly known as a micropressure sensor, functions as a fiber-optic lever and has a broadband sensitivity up to at least 50 kHz.

Even with more advanced miniaturized devices, being developed at this time with outside diameters of about 80 μm (Olson, personal communication), the use of pressure sensors at different places along the cochlea is still limited by the spiral anatomy of the cochlea. As a result, there are only a few locations within the cochlea that are surgically accessible for making direct measurements. To date, the greatest success has come from micropressure sensor placement in the SV and ST of the basal cochlear turn (Fig. 6.2).

Changes in the pressure in the SV (P_{SV}) near the stapes (Fig. 6.2a) can be produced by two mechanisms: (1) by sound-induced vibration of the middle ear (forward transmission) and (2) by otoacoustic emissions (OAEs) generated within

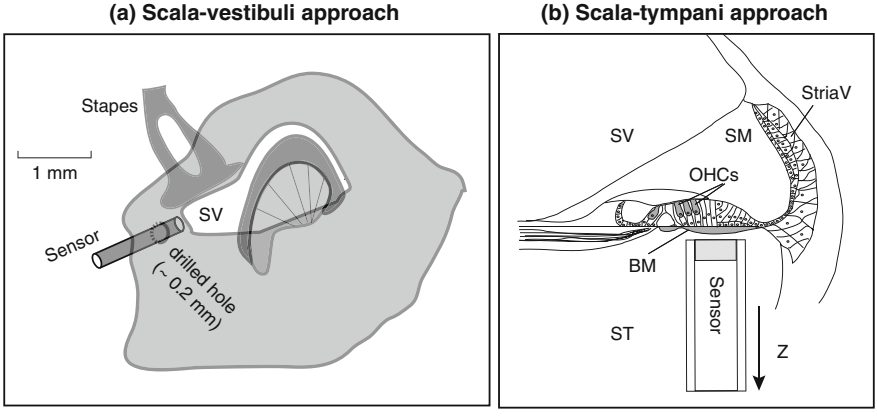

Fig. 6.2 Surgical approaches for intracochlear pressure measurements. Such measurements require introducing a micropressure sensor into the cochlear fluid with the least possible influence on cochlear condition and, therefore, cochlear mechanics. The most surgically accessible locations are the SV and ST of the first (basal) cochlear turn; these scalae are larger than at more apical cochlear locations. The sensor is introduced through a hole made in the cochlear bony wall, into the SV next to the stapes (**a**) or into the ST close to the basilar membrane (BM; **b**). Smaller next-generation probes are expected for insertion into scala media (SM); this is a challenging problem because it requires penetration of the spiral ligament and stria vascularis (StriaV) and, therefore, means increased likelihood of cochlear damage. **a** Reprinted from Dong and Olson (2006, Fig. 1), with permission from the American Physiological Society; **b** reprinted from Olson (1999, Fig. 1), with permission from Macmillan Publishers Ltd: Nature, Copyright 1999 and E. S. Olson

the cochlea by the electromechanical action of the OHCs (reverse transmission). Thus, measurements of the P_{SV} together with stapes vibration measurements enable assessment of both forward- and reverse-transmission parameters (Olson 1998; Dong and Olson 2006), such as the input and output impedances of the cochlea, the acoustic power entry to the cochlea (Slama et al. 2010), and the driving pressure difference across the CP (Nakajima et al. 2009).

Pressure in the ST (P_{ST}) can also be mapped at different locations relative to the BM (Fig. 6.2b, *Z* direction), the resulting measurement being the summed pressures of the TW and CW at each location. Depending on the measurement location, either the TW or CW can dominate. For example, when the micropressure sensor is positioned close to the BM, the P_{ST} is dominated by the pressure of the TW as fluid particles move in concert with the BM. At some frequencies and stimulus amplitudes, the TW and CW can have similar amplitudes and, dependent on their relative phases, can constructively or destructively interfere. Thus, quantifying the P_{ST} is crucial for understanding the TW motion of the BM and the fluids, the mechanical impedance of the CP, and the electromechanical force generated by the OHCs.

6.2.3 *Electromechanical Basis of Responses to Electrical Stimulation*

Previous studies have demonstrated that the BM responds not only to acoustic but also to electrical stimuli (Robles and Ruggero 2001). The response to electrical current appears to be due to the electromechanical action of the OHCs. Somatic electromotility was first observed in studies showing that OHCs are capable of mechanical deformation at acoustic frequencies when electrically stimulated (Brownell et al. 1985). Stimulus-evoked axial changes of cell length are driven by voltage changes across the plasma membrane rather than by the passage of ionic current (Ashmore 2008). For OHCs isolated from the cochlea, somatic electromechanical displacement and force have been measured up to at least 70 kHz (Frank et al. 1999). (To date, there are no corresponding data for stereocilia so that in this chapter, it is assumed that OHC electromechanical force is predominantly somatic.) This lower bound of maximum frequency (70 kHz) is a consequence of the limited bandwidth of the laser interferometric measurement system. The amplitudes and phases of these electromechanical responses are independent of stimulus frequency up to at least an octave above the frequencies that need to be amplified at a given place along the CP. Moreover, the electromechanical response of the isolated OHC is approximately linear for the range of receptor potentials recorded in vivo. Similar wideband electromechanical responses have been demonstrated in situ by applying a voltage across the CP in an in vitro preparation and measuring (1) the electromechanical force at the RL in the absence of the TM (Scherer and Gummer 2004a) or (2) RL vibration in the presence (Nowotny and Gummer 2006) or absence (Scherer and Gummer 2004a) of the TM. Bipolar

electrical stimulation in vivo across the CP between the ST and SV can elicit BM vibration responses (in the guinea pig) up to at least 100 kHz (Grosh et al. 2004; Grosh, Chap. 11). In the mouse, intracochlear electrical stimulation in vivo across the CP between the ST and SM has shown that, in addition to a tuned response similar to that of the BM, the RL also possesses a broadband frequency-response component *directly* attributable to the electromechanical action of the OHC soma (Ren et al. 2016). That is, whether isolated, in situ, or in vivo, the OHC acts as an ideal electromechanical transducer, its response relative to transmembrane potential being independent of frequency and distortionless over its functionally relevant frequency and intensity ranges.

These ideal transducer properties enable energy propagation within the in vivo cochlea to be studied by electrical stimulation, the OHC acting as an ideal source of electromechanical force. The first evidence for electromechanical activity in the cochlea was provided by injection of a sinusoidal current into the SM during acoustic stimulation (Hubbard and Mountain 1983). The currents generated OAEs at the frequency of the electrical stimulus. Intracochlear electrical stimulation is capable of yielding BM amplitude and phase responses that closely resemble those produced for acoustic stimuli (Nuttall and Ren 1995; Ren et al. 2016). Such data demonstrate that electrical stimulation is capable of producing conventional TWs and that the OHCs produce sufficient electromechanical force at all functionally relevant stimulus frequencies to guarantee the required sensitivity of the in vivo cochlea.

6.2.4 *Pressure Responses to Acoustic or Electrical Stimulation*

The physical concepts involved are illustrated in Fig. 6.3 for intracochlear pressure measured in response to acoustic or electrical stimulation. Entry into the ST allows the tip of the micropressure sensor, represented here by a telescope cartoon (Fig. 6.3a), to be placed close to the BM (down to about 10 μm). At this distance, the P_{ST} is dominated by BM motion.

Normalized to the stimulus, a similar pattern is seen in P_{ST} responses to either electrical (Fig. 6.3b, d) or acoustical (Fig. 6.3c, e) stimuli. The amplitude responses show the tuning characteristics of the recording location. The phase curves provide information on the timing of wave propagation to the recording location relative to the stimulus. Although amplitude responses appear highly dependent on stimulus amplitudes, phase changes little with stimulus amplitude. A similar situation exists for the vibration responses of the BM (Robles and Ruggero 2001). Superposition of

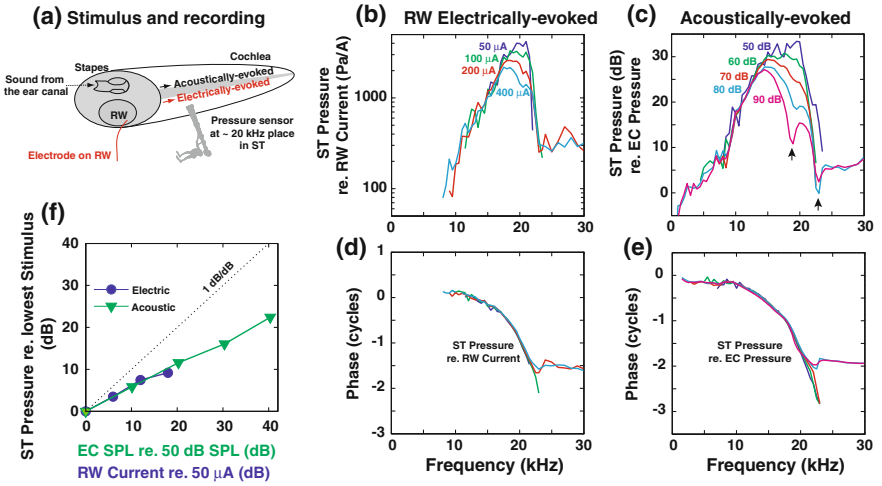

Fig. 6.3 Characteristics of intracochlear pressure responses to acoustic and electrical stimulation. **a** Pressure responses were measured in the ST of the basal turn of the gerbil cochlea with a micropressure sensor positioned close to the BM (about 10 μm) at the 20-kHz place. The stimulus was either sound in the ear canal (EC), swept tones of 0.2–30 kHz at 50–90 dB sound pressure level (SPL; re 20 μPa) in 10-dB steps, or current at the RW, swept sinusoids of 8–30 kHz at 50–400 μA in 6-dB steps, with the reference electrode on neck muscle. Amplitude (**b** and **c**) and phase (**d** and **e**) of fluid pressure relative to sound pressure (**c** and **e**) or current (**b** and **d**). *Arrows* in **c** indicate evidence of destructive interference between the TW and the CW. **f** Pressure amplitude relative to stimulus amplitude as function of either EC SPL or RW current amplitude, expressed on dB axes. *Dotted line* has a slope of 1 dB/dB and represents the input/output function for a linear system. Note that the responses to both stimuli are nonlinear compressive and of similar slope (0.5 dB/dB)

(relative) response curves independent of stimulus amplitude is a characteristic of linear systems.[1]

Based on pressure measurements, here from the 20-kHz place, three different frequency regions can be distinguished in P_{ST} responses.

(1) At frequencies below about 15 kHz, TWs pass by the sensor on their way towards their BF places. In this frequency region, the slope of the phase response is approximately independent of frequency, meaning that the sensor is located in the long-wave region of the TW (Fig. 6.1). As described in Sect. 6.2.1, in such a region, the cochlear fluid behaves as a plane TW that changes little in amplitude and phase throughout the depth of the fluid. Superposition of the responses means that the response amplitudes increase in

[1]By definition, a linear system is one that satisfies the following property. Denoting time by t, if $r_1(t)$ is the response to stimulus $s_1(t)$ and $r_2(t)$ is the response to stimulus $s_2(t)$, then $r_1(t) + r_2(t)$ is the response to $s_1(t) + s_2(t)$ irrespective of the choice of $s_1(t)$ and $s_2(t)$. A natural consequence of this definition is that both the amplitude and the phase responses of a linear system are independent of stimulus amplitude.

direct proportion to stimulus amplitudes and that the phases are independent of frequency. That is, the system is linear in this frequency range.

(2) At frequencies above about 23 kHz, TWs peak at locations basal to the sensor. For these frequencies, measured pressure amplitude increases in direct proportion to stimulus amplitude, but the amplitude and phase responses change little with frequency. Being independent of frequency, this response region is often called the "plateau region" (Robles and Ruggero 2001). Because the phase is independent of BM place along this region apical to the 23-kHz place, there is no TW in this region.

(3) At frequencies between 15 and 23 kHz, the slope of the phase response increases with frequency, meaning that the sensor is located in the short-wave region of the TW (Fig. 6.1). In such a region, the cochlear fluid behaves as a TW, with amplitude decreasing throughout the depth of the fluid from its maximum at the BM (Olson 1998; Dong and Olson 2005). Thus, when measured at a location close to the BM, P_{ST} is dominated by the TW pressure for frequencies in the region of the peak amplitude response.

As frequency is increased within the short-wave region, the wavelength decreases and the amplitude increases in accordance with energy conservation, similar to the situation for an ocean wave approaching the shore. In addition to this purely hydrodynamical property—wavelength decrease and concomitant amplitude increase—the OHCs located in this region are presumed to inject electromechanical energy into the TW, which further increases the amplitude and frequency selectivity of the TW. Based on BM vibration responses, it has been estimated that approximately 53 OHCs inject energy into the TW at neural threshold at the 15-kHz point of the guinea pig BM (Russell and Nilsen 1997).

In the short-wave region, the amplitude responses (but not the phase responses) are dependent on stimulus amplitude. That is, the system is nonlinear in this region. The peak of the relative amplitude response is largest at the lowest stimulus amplitudes and, as such, the nonlinearity is said to be compressive. The largest peak is located near 20 kHz, namely, at the BF for this recording location. At this frequency, the response amplitude for both stimulus conditions increases by only about 0.5 dB for a 1-dB increase in stimulus amplitude (Fig. 6.3f). For sound-evoked BM vibration responses, the slope in this compressive region can be as small as 0.1 dB/dB (Robles and Ruggero 2001). There is strong experimental evidence that saturation of the mechanoelectrical transducers in the OHC stereocilia are the basis for this compression (Preyer and Gummer 1996; Cooper 2003).

Because the micropressure sensor sums the pressures of different wave modes at a particular location, the amplitude and phase of the P_{ST} enables the frequency dependence of the relative contributions of the TW and the CW to be evaluated. For example, the notches in the acoustically evoked amplitude of the P_{ST} at stimulus frequencies of 18 and 23 kHz and sound pressure levels of 80 and 90 dB are evidence of destructive interference of the TW and CW (Fig. 6.3c, *arrows*), with a corresponding phase transition from the TW to the CW dominating at 23 kHz.

6.2.5 Estimation of Velocity Responses from Pressure Responses

Pressure differences within the fluid can be used to estimate fluid and BM velocities, which, in turn, can also be used to estimate the mechanical impedance of the CP (Olson 2001), a parameter necessary for calculating power transfer directly (Sects. 6.2.6, 6.2.7, and 6.2.8). This possibility relies on an equation, called the Navier-Stokes equation, that relates fluid pressure to velocity. For an incompressible, isotropic fluid this equation can be written as

$$\nabla p = -\rho \frac{\partial \boldsymbol{v}}{\partial t} - \rho(\boldsymbol{v} \cdot \nabla)\boldsymbol{v} + \mu \nabla^2 \boldsymbol{v}$$

where ∇ is the del vector operator, ∇p is the pressure gradient, $\boldsymbol{v}$ is the fluid-velocity vector, and ρ and μ are fluid density and dynamic viscosity, respectively. The values of ρ and μ for perilymph can be assumed to be identical to those for water, namely, 10^3 kg/m^3 and 10^{-3} kg/(m s), respectively.

Using a dimensional analysis, Dong and Olson (2013) have shown that the inertial term (first term) is larger than the nonlinear (second) and the viscous (third) terms. For example, at the 24-kHz place in the gerbil cochlea, the nonlinear term is at least three orders of magnitude smaller than the other two terms; the inertial term is larger than the viscous term by a factor of 34 at 24 kHz and a factor of 7 at 5 kHz. Thus, in its present application, the Navier-Stokes equation can be further simplified to $\nabla p = -\rho \frac{\partial \boldsymbol{v}}{\partial t}$.

With this simplification, velocity in a given direction can be estimated by measuring the pressure gradient in that direction. In particular, because the BM remains in contact with the fluid, BM velocity (v_{BM}) can be estimated using a pressure measurement made close to the BM (typically, 10–30 μm away; denoted by p_B) and one made at a deeper place in the fluid along the sensor axis perpendicular to the BM (Z direction in Fig. 6.2b; denoted by p_A). The separation (Δz) between measurement points is typically 10–20 μm. Then, for sinusoidal stimulation, v_{BM} can be approximated as $v_{BM} \approx \frac{j}{\rho\omega}\frac{(p_B - p_A)}{\Delta z}$, where ω is the radial stimulus frequency and $j = \sqrt{-1}$. Equivalently, BM displacement (x_{BM}) can be estimated as $x_{BM} \approx \frac{1}{\rho\omega^2}\frac{(p_B - p_A)}{\Delta z}$.

Concepts involved in interpreting combined vibration and electrical data are illustrated in Fig. 6.4. At stimulus frequencies between 17 and 33 kHz, the P_{ST} decreased by about 5 dB when the sensor was placed 10 μm further from the BM (Fig. 6.4a, *dotted lines*). The pronounced notch at 24 kHz in the amplitude response (Fig. 6.4a, *arrow*) evoked by the 70-dB stimulus and the correspondingly smaller phase accumulation (Fig. 6.4b, *dotted gray line*) is evidence of destructive interference between the two wave modes, TW and CW. The spatial variation of pressure at frequencies around the BF, in the short-wave region, has been previously discussed both theoretically (de Boer 1980) and experimentally (Olson 1998;

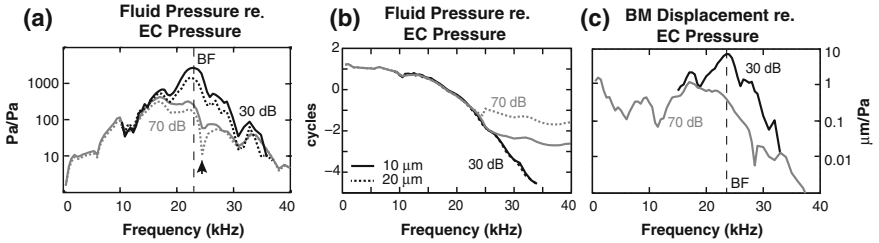

Fig. 6.4 Spatial variation of intracochlear fluid pressure and derived BM displacement. Amplitude (**a**) and phase (**b**) of fluid pressure in ST relative to sound pressure close to the tympanic membrane in the EC for sound intensities of 30 dB SPL (*black lines*) and 70 dB SPL (*gray lines*). Fluid pressure was measured at distances of about 10 µm (*solid lines*) and 20 µm (*dotted lines*) from the BM. **c** Amplitude response of BM displacement derived from the Navier-Stokes equation for linear motion in an inviscid fluid. Note that, similar to the pressure-amplitude response, the displacement response is compressively nonlinear from about 0.7 octave below the best frequency (BF) to about 0.5 octave above BF. Reprinted from Dong and Olson (2013, Fig. 2), Copyright 2013 with permission from Elsevier

Dong and Olson 2005). In this vein, at low and high frequencies relative to the BF (about 0.7 octave below and 0.5 octave above the BF in Fig. 6.4a), there appears to be little pressure gradient within the fluid. This is almost certainly due to the TW being in the long-wave region at the lower frequencies and the CW dominating the pressure response at the higher frequencies.

Figure 6.4c shows the amplitude of BM displacement estimated from the pressure difference measurements using the simplified form of the Navier-Stokes equation. Similar to the pressure responses, the derived BM displacement response is tuned to the pressure BF and varies compressively with the sound pressure level (SPL). Normalized to sound pressure, the fluid-pressure and derived BM displacement responses at 30 dB SPL are, respectively, 12 and 22 times greater than those at 70 dB SPL. These factors represent the amount of signal compression. The difference in the amount of compression for pressure and displacement is likely due in part to the source of the compression. The OHC electromechanical force acts "directly" on the BM through the relatively stiff supporting Deiters cells, giving a relatively large compressive nonlinearity for BM displacement, whereas within the fluid, the TW pressure for short waves is less than that at the BM surface so that the recorded pressure signal will have a relatively large CW component.

6.2.6 *Active Mechanisms and Cochlear Amplification*

To achieve tuned mechanical responses in the presence of high damping, Gold (1948) suggested that "an electromechanical action takes place whereby a supply of electrical energy is employed to counteract the damping." Because energy is supplied, Gold (1948) called the mechanism "active" as opposed to a passive

mechanism that simply dissipates energy. Within the realms of a discussion of the properties of "regenerative receivers" in radio engineering, Gold (1948) pointed out that the "external source of power is required, not necessarily to obtain an output of greater power than that obtained in the input, but in order to make the output [amplitude] a sufficiently critical function of frequency." Assuming that damping forces are directly proportional to velocity, Gold (1948) argued that to counteract damping losses, the active mechanism must provide negative damping and, therefore, that the electromechanical force must be in phase with BM velocity. Later, Davis (1983) introduced the term "cochlear amplifier": "I shall call the active process 'the cochlear amplifier.'" Based on a review of physiological experiments, Davis (1983) concluded that the OHCs are crucial for cochlear amplification.

In the meantime, the brilliant insights provided by Gold almost 70 years ago have been supported theoretically (Neely and Kim 1986; Diependaal et al. 1987) and experimentally using measurements of BM vibration (Nilsen and Russell 2000; Lukashkin et al. 2007), intracochlear pressure and derived BM velocity (Dong and Olson 2013), and RL vibration relative to BM vibration (Zha et al. 2012; Ren et al. 2016). The sound-evoked OAEs first reported by Kemp (1978) confirmed the existence of a source of acoustic energy originating from within the cochlea. There is general agreement that the BM (often used as synonym for the CP) is locally active basal to the resonant place for a given stimulus frequency (Neely and Kim 1986; de Boer and Nuttall 2000). Based on prestin (Liberman et al. 2002; Dallos et al. 2008) and tectorin (Mellado Lagarde et al. 2008) knock-out experiments, as well as vibration measurements at the basal and apical boundaries of the OHCs (Zha et al. 2012; Ren et al. 2016), it was shown that electromechanical forces generated by the OHC soma are responsible for this activity.

The term "cochlear amplification" has been used in different ways, either amplitude or power amplification.

Amplitude amplification means the amplitude of either velocity or displacement. Even here, at least two definitions of amplitude amplification can be found in the literature (Robles and Ruggero 2001; de Boer et al. 2005). In one case, it is defined as the ratio of the amplitude at the peak measured in the healthy functioning cochlea to the amplitude at the same frequency in the dead cochlea. In the other case, it is defined as the amplitude ratio at the respective peak frequencies in the healthy and dead cochleae. In the first case, the gain can be as much as 80 dB, and in the second, typically 50 dB in the basal to midfrequency regions of the cochlea.

Power amplification refers to the amplification of acoustical power flowing from the stapes to the place of peak amplitude response. Power flux calculations based on applying two- or three-dimensional cochlear models to BM vibration data have suggested that power amplification is no more than about 20 dB (Diependaal et al. 1987; de Boer and Nuttall 2001). Results of the Allen-Fahey experiment (Allen and Fahey 1992) and its derivatives (de Boer et al. 2005; Shera and Guinan 2007), all designed to estimate power amplification using distortion product OAEs (DPOAEs), suggested that there is practically no power amplification (<10 dB). To explain this unexpected result, Shera and Guinan (2007) presented evidence that the DPOAE amplitude might be reduced by destructive interference when the primary stimulus

frequencies (f_1 and f_2) are close to the DPOAE frequency, $f_{DP} = 2f_1 - f_2 \approx f_1$ when $f_1 \approx f_2$. These authors conjectured that the DPOAE source is not a point source but rather a distributed source, and that, as such, phase differences between the many sources can lead to destructive interference and the apparent near absence of power amplification. If power amplification really is on the order of 20 dB, as estimated theoretically (Diependaal et al. 1987; de Boer and Nuttall 2001), then it is perhaps not surprising that these experiments did not provide evidence for it.

If the OHCs are producing electromechanical force to counteract viscous forces, that is, producing negative damping as postulated by Gold (1948), then there must be power amplification in that region of the cochlea because negative resistance results in negative average-power dissipation or, in other words, power gain. Therefore, one can define cochlear power amplification as a region on the BM where the real part of the BM impedance is negative, as, for example, in the paradigm of Allen and Fahey (1992).

Before proceeding with concepts of power amplification, it is emphasized that OHC electromechanical forces are supposed to act against viscous forces not to reduce them. Indeed, as emphasized by Wang et al. (2016), one of the outcomes of a functional cochlear amplifier is increased viscous losses because viscous force is proportional to velocity.

6.2.7 *Evidence For and Against Cochlear Power Amplification from Single-Parameter Measurements*

To demonstrate power amplification directly requires the measurement of velocity and fluid pressure because instantaneous power is the product of these two parameters. With the exception of the Olson group, experimenters have measured only velocity or displacement and inferred pressure or force from physical principles. Such experiments cannot provide *direct* evidence of power amplification.

The experiments of Lukashkin et al. (2007) produced indirect evidence for power amplification at low intensities. Here, BM displacement was measured in response to a high-frequency sound stimulus that was sinusoidally biased in amplitude by a low-frequency, high-level tone. The phase of the electromechanical force applied to the BM by the OHCs at the measurement place relative to BM displacement at that place was inferred from Lissajous orbits of instantaneous amplitudes of displacement and sound pressure. The technique is based on two plausible assumptions supported by earlier experiments. (1) The low-frequency bias tone modulates the open probability of the mechanoelectrical channels in the OHC stereocilia (as a second-order Boltzmann function), which at the low bias frequency (28 Hz) modulates the amplitude of the receptor potential in phase with the amplitude of the sound pressure (Patuzzi et al. 1989). (2) The instantaneous BM displacement amplitude is directly proportional to the instantaneous electromechanical force

applied to the BM because the OHCs act as receptor-potential driven, mechanical force sources independent of frequency, both with (Frank et al. 1999) and without (Scherer and Gummer 2004a) mechanical load. The inferred electromechanical force was found to be in phase with BM velocity and, therefore, presumably counterphasic to viscous forces acting to impede BM motion. Although indirect, Lukashkin et al. (2007) thus presented evidence for negative resistance and, therefore, power amplification at the measurement site.

The experiments of Zha et al. (2012) produced direct evidence for the OHCs being the source of local BM activity. These authors measured vibration of both the BM and the RL of the overlying OHC associated with that BM measurement point. The BM and RL presented an intensity-dependent phase difference, on average, of 90° at low intensities (30 dB SPL) that decreased to 40° at high intensities (100 dB SPL) and vanished postmortem. That is, the relative phase (and also amplitude) was a compressive function of sound intensity and physiologically vulnerable, as required if OHCs are to be responsible for the active, compressive, and physiologically vulnerable motion of the BM. However, contrary to expectation for negative resistance, OHC electromotility was counterphasic to BM velocity and, therefore, presumably in phase with fluid friction at the BM surface. However, because it is OHC force that is acting on the BM, it is the phase of this parameter that must be measured before conclusions can be made about the sign of resistance and, therefore, the existence of power amplification. The importance of force delivered by the OHCs is emphasized in a companion, theoretical publication from the same research group, in which Ramamoorthy and Nuttall (2012) provide theoretical evidence for the OHC load impedance being conjugately matched to the OHC source impedance, thus enabling maximum power transfer from the OHCs.

In contrast, the experiments and modeling of van der Heijden and Versteegh (2015) produced indirect evidence for the absence of power amplification at low intensities *and* for active power attenuation above 40 dB SPL. In these experiments, BM vibration was measured at two adjacent locations, and the energy flux of the TW was calculated and compared with the power input to the middle ear. Although an improvement on flux estimates based on vibration responses at a single point, in the absence of a measured second independent parameter — fluid pressure or impedance — the evidence remains indirect. Moreover, the middle ear impedance required for their calculation of the power input to the middle ear was taken from the literature, and the choice may well have had an important influence on their conclusions, especially if the power gain is, in reality, small (<20 dB; Sect. 6.2.6). Nevertheless, the authors do make the important point that OHC activity does not necessarily imply negative resistance and present a model by which amplitude amplification is produced by rapid vibration-mode transitions from a nondispersive and stiff mode into a dispersive and compliant mode. That is, an intensity-dependent attenuator is proposed instead of a saturating power amplifier. As pointed out by the authors, rather than being a positive-feedback mechanism synchronized cycle-by-cycle to the stimulus, as is the case for negative resistance, it is a negative-feedback system without the need for phase locking to the stimulus and, therefore, is less vulnerable to instability.

6.2.8 *Evidence for Cochlear Power Amplification from Multiparameter Measurements*

To date, the most compelling evidence for cochlear power amplification derives from studies that have compared fluid pressure and velocity with spatially and temporarily coincident extracellular voltage (Dong and Olson 2013). At low-to-moderate stimulus levels, the extracellular voltage can be interpreted as originating predominantly from the local OHC receptor current (Kössl and Russell 1992) while the sound-evoked pressure at the BM is a result of local mechanical effects. Accordingly, to fully understand the electromechanical interactions that produce cochlear activity, the key is in comparing the phases between (1) voltage and BM displacement and (2) BM displacement and fluid pressure. BM displacement can be derived using the differential-pressure technique with the sensor tip placed at different distances from the BM (Sect. 6.2.5).

The concepts involved in interpreting such mechanical and electrical data are illustrated in Fig. 6.5 for the 24-kHz place of the gerbil cochlea. At frequencies from 9 to 17 kHz (i.e., 1.4–0.5 octave below the BF), the voltage and displacement responses are approximately in phase (Fig. 6.5a). This observation is consistent with (1) the simple mechanoelectrical transduction model of Davis (1957), but also see Dallos (2003) for a detailed kinematic analysis, and (2) the intra- and extracellular voltage recordings reported by Kössl and Russell (1992) from OHCs

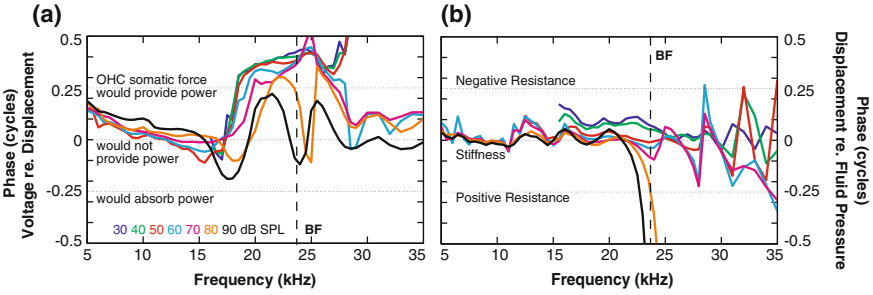

Fig. 6.5 Phase comparison of voltage, pressure, and displacement. **a** Phase of voltage in the ST relative to derived BM displacement. **b** Phase of derived BM displacement relative to fluid pressure. Voltage and pressure were measured at the same location using a dual voltage-pressure sensor. Phase conventions were positive displacement for BM motion toward the SV and positive voltage for positive ionic current into ST. *Curves* are *color coded* according to the stimulus SPLs (in dB) given above the frequency axis in (**a**). Differential measurements were made at 10 and 20 μm from the BM. **a** Positive phase near the BF implies that the outer hair cell (OHC) electromechanical force delivers average power to the BM. **b** Zero phase implies stiffness-dominated BM motion; positive phase at 30 and 40 dB SPL for 15–25 kHz implies net power gain, that is, power amplification at low sound intensity in that frequency range. The large phase swings at 80 and 90 dB SPL and the phase swings above approximately 27 kHz occur when pressure is dominated by the CW while the displacement is dominated by the TW (Dong and Olson 2013). Reprinted from Dong and Olson (2013, Fig. 4), Copyright 2013 with permission from Elsevier

in vivo (from the basal turn of the guinea pig cochlea). Namely, BM displacement toward the SV opens the mechanosensitive channels in the OHC stereocilia, causing an influx of positive ions and depolarization. The positive current passes through the cell and causes positive voltage in ST. Accordingly, BM displacement toward the SV and voltage in the ST are in phase.

At frequencies above 17 kHz, the ST voltage leads BM displacement, amounting to about 0.44 cycle at the BF and intensities below 70 dB SPL. To relate this phase difference to OHC somatic force, it is necessary to know the phase of the receptor potential. Depending on which experimental data is used for this purpose — in vivo intracellular recordings (Kössl and Russell 1992) or in vitro whole cell patch-clamp recordings from OHCs in situ (Johnson et al. 2011) or isolated (Preyer et al. 1996) — the receptor potential lags the receptor current and, therefore, the voltage in the ST by somewhere between 0.17 and 0.25 cycle. That is, the inferred receptor potential leads BM displacement by somewhere between 0.19 and 0.27 cycle. OHC electromechanical force has been shown to be in phase with the change in transmembrane potential in isolated OHCs (Frank et al. 1999), and model calculations suggest that the OHC source impedance is matched to provide maximum power when loaded by the organ of Corti (Ramamoorthy and Nuttall 2012). Therefore, approximating the range of 0.19–0.27 cycle by 0.25 cycle, the phase data in Fig. 6.5a suggest that OHC force leads BM displacement by approximately 0.25 cycle; that is, the force is in phase with BM velocity for frequencies near the BF and sound intensities below 70 dB SPL. As explained in Sect. 6.2.6, when velocity and force are in phase, the result is delivery of average power to the system.

Having provided evidence for power injection, the next question is whether OHC electromechanical force is of sufficient magnitude to produce power amplification? This question can be answered by examining the phase of BM displacement relative to fluid pressure, the rationale being that for a noninertial BM impedance, the phase of BM displacement relative to fluid pressure is zero for a compliant element, negative for a dissipative element, and positive for an absorbing element (of average power). That is, positive relative phase means power amplification. The phase data in Fig. 6.5b show that for sound intensities of 50 to 70 dB SPL, the phase is approximately zero up to about 28 kHz (0.2 octave above the BF). That is, in this intensity range, the impedance of the CP is stiffness dominated up to and above the BF, as proposed theoretically by Steele and Taber (1981) and found experimentally by Dong and Olson (2009). However, at the lowest SPLs (30 and 40 dB), the displacement consistently leads the pressure at frequencies ranging from 15 to 25 kHz (0.7 octave below to 0.1 octave above the BF). That is, in these frequency and intensity ranges, the impedance is dominated by negative resistance, thus providing evidence for power amplification. The phase lead is 0.1 cycle rather than the 0.25 cycle that would be the case for a point resistance. However, this should not be surprising because the CP is a viscoelastic, distributed system. For example, point impedance measurements along the RL (in vitro) have shown that this structure cannot be physically described by a classical point impedance with frequency-independent components; instead, it is a viscoelastic material for which

the real part of the impedance decreases with increasing frequency (Scherer and Gummer 2004b).

In summary, the phase lead of ST voltage relative to BM displacement provides direct evidence for OHC electromechanical activity and the phase lead of BM displacement relative to fluid pressure provides direct evidence that this activity results in power amplification at low sound intensities in the region of the BF.

6.3 Tectorial Membrane Mechanics and Cochlear Amplification

How electromechanical force from the OHCs is coupled to the BM and stereocilia to produce not only amplification but also the appropriate bandwidth remains unknown. First, there is theoretical (Mammano and Nobili 1993) and experimental (Gummer et al. 1996) evidence that delays caused by the electrical time constant of the OHC basolateral membrane and the inertia of the TM might act synergistically to couple OHC electromechanical force in the appropriate phase to ensure amplification. Consider a child on a swing: the phase of the applied force is "critical." Second, there is theoretical (Meaud and Grosh 2010) and experimental (Ghaffari et al. 2007) evidence that longitudinal mechanical coupling of the OHCs by the TM ensures that the amplifier bandwidth is sufficiently wide to yield temporal fidelity. Consider a second-order resonant system: with a gain of 60 dB relative to the low-frequency response, its Q_{10dB} is 316 rather than the experimental value of 5–11 observed for the BM (Robles and Ruggero 2001). Such a large Q_{10dB} would mean, for example, that the step response would require 1,245 cycles of the ringing frequency to settle down (to within 2% of its steady-state response), a prohibitively long time for any system.

Recent genetic studies have confirmed the importance of the TM for cochlear amplification. Changes in genes that encode TM proteins, such as Tecta (Xia et al. 2010), Tectb (Russell et al. 2007), and Otoa (Lukashkin et al. 2012), cause moderate-to-severe hearing deficits even when the TM is nearly unchanged in its physical orientation and structural attachments to the sensory receptors.

Despite the prominent role of the TM in cochlear mechanics, the basic dynamic physical properties and mechanistic role of the TM remain unclear. Classical cochlear models have represented the TM as a stiff lever (Davis 1957), a resonant mass-spring system (Allen 1980; Zwislocki 1980), and an inertial load (Mammano and Nobili 1993); refer to Fig. 6.6 for schematics of the mechanical elements and their motion. However, these models ignore longitudinal coupling through which excitations at one location could spread to other longitudinal locations throughout the cochlea (Abnet and Freeman 2000; Meaud and Grosh 2010). Recent experiments have demonstrated that the TM is poroelastic (Masaki et al. 2006), that its physical properties change with longitudinal position (Ghaffari et al. 2007; Gavara and Chadwick 2010), that its mechanical matrix supports TWs at audio frequencies

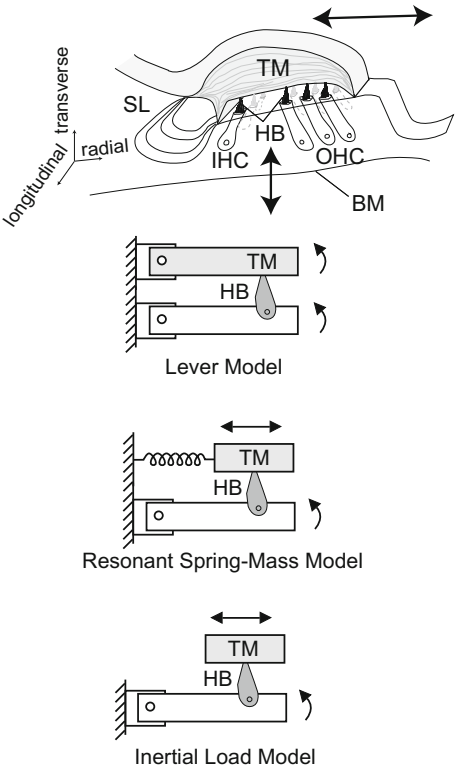

Fig. 6.6 Schematic showing the cochlear partition (spiral limbus [SL], hair bundles [HBs], TM, BM, inner hair cell [IHC], and OHCs) and three different mechanical models of the TM: (1) a rigid body that moves with the organ of Corti and the HBs that protrude from its apical surface as a system of levers (*top*), (2) a mass attached via a spring to the HBs (*middle*), and (3) an inertial load overlying the HBs (*bottom*) *Arrows,* directions of motion

(Ghaffari et al. 2007; Sellon et al. 2014), and that a fixed charge in the matrix produces electrostatic repulsion effects (Freeman et al. 2003a; Ghaffari et al. 2013). Taken together, these results along with anatomical studies (Kronester-Frei 1978; Thalmann 1993) collectively show that the TM is a highly charged, nanoporous matrix capable of supporting longitudinally propagating TWs at audio frequencies.

There has been significant progress in understanding the response properties of isolated hair cells, including the ability of OHCs to generate electromechanical forces (see Santos-Sacchi, Navaratnam, Raphael, and Oliver, Chap. 5) that underlie cochlear amplification (Sects. 6.2.6, 6.2.7, and 6.2.8). However, there has been slower progress (and considerable debate) in characterizing how accessory structures, like the TM, help to shape cochlear responses to acoustic stimulation. Here, concepts based on recent in vitro, in situ, and in vivo results are presented that shed light on the critical role of this enigmatic extracellular matrix in cochlear mechanics. The findings help to (1) clarify the local and distributed interactions of the TM with the hair bundles and the organ of Corti, (2) demonstrate how TM dynamic properties change in response to genetic manipulations, and (3) show how the TM interacts with other cochlear structures and fluids during normal and impaired cochlear function.

6.3.1 *Local Interactions of the Tectorial Membrane with Hair Bundles*

Hair cells are sensitive to shear forces that displace hair bundles along their axis of symmetry. Based on its strategic position overlying the hair bundles, the TM is poised to deliver the shear forces that stimulate hair cells at audio frequencies through viscous and elastic mechanisms.

6.3.1.1 Quasi-Static Point Impedance Measurements

In situ studies of the TM using static probe displacements were first developed by von Békésy (1953) and Zwislocki and Cefaratti (1989). Static and dynamic mechanical properties of the TM have been further examined using isolated TM preparations, which can tease apart the material properties of the TM from those of surrounding tissues, such as the underlying hair bundles or fluid in the subtectorial space (Freeman et al. 2003a, b).

Several groups have used atomic force microscope (AFM) cantilevers to deliver quasi-static point forces to isolated TM samples. Measurements in mouse (Gueta et al. 2006) and guinea pig (Shoelson et al. 2004) preparations have shown that TM point stiffness varies from the base to the apex of the cochlea. However, there is considerable variability across studies (as much as a 100-fold), in part because the TM is anisotropic and the methods range from quasi-static to audio frequencies. Furthermore, the transverse point indentations applied by an AFM cantilever are different from the shear interactions at the interface between the TM and the hair bundles. Moreover, the TM is highly hydrated, composed of 97% water and 3% macromolecules by weight. Its mechanical matrix is surrounded by water, suggesting that the TM is viscoelastic.

6.3.1.2 Dynamic Point Impedance Measurements

The first comprehensive study of TM dynamic shear properties used a magnetic bead to deliver point shear forces to isolated TM preparations (Abnet and Freeman 2000). These results demonstrated that the TM is viscoelastic at audio frequencies, and, therefore, its properties are not consistent with assumptions made in classical lever, inertial, and resonant models of cochlear micromechanics and macromechanics. Furthermore, the mechanical point shear impedance of the TM is not well represented by lumped mass, spring, and dashpot equivalent mechanical circuits but rather as a viscoelastic material.

Video images obtained in the magnetic bead measurements also indicated that there is significant coupling through the TM. Forces acting on the magnetic bead generated motions by as much as 30 μm away from the point of bead contact. The fact that the TM couples motion over large distances motivated the development of

new techniques that exploit microfabrication technologies to deliver shear forces to the TM at the level of a few rows of hair cells.

Gu et al. (2008) developed microfabricated shear probes (Fig. 6.7a) to deliver shear forces locally over a broad range of frequencies (0.1–10 kHz). Because the probes are made of silicon and are bulk fabricated, they can be made in large numbers with mechanical properties that are fairly consistent across probes. Moreover, the probe design enables testing material properties over a wide range of impedances by varying the geometry. The microscale design allows the shear probe to be operated at audio frequencies; the probe impedance is dominated by stiffness

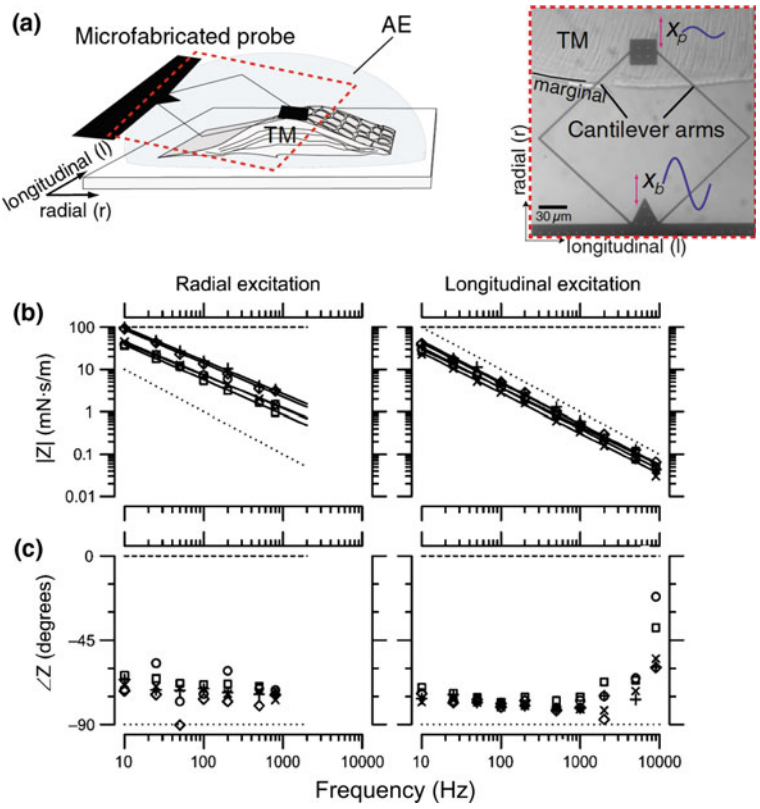

Fig. 6.7 TM shear impedance measured with a microfabricated probe. **a** Schematic of the probe, consisting of a base and shearing plate connected by two flexible arms (*left*). *Right* Optical image of shear probe with the shearing plate attached to the surface of the TM in artificial endolymph (AE). Amplitude (**b**) and phase (**c**) of TM shear impedance as function of frequency for radially (*left*) and longitudinally (*right*) probe-applied forces. *Symbols* represent individual TMs. *Solid lines* are regression lines for individual TMs; average amplitude slopes are −16 ± 0.4 dB/decade and −19 ± 0.4 dB/decade for radial and longitudinal forces, respectively. A purely elastic spring has an amplitude slope of −20 dB/decade and phase of −90° (*dotted lines*). Reprinted from Gu et al. (2008, Figs. 1 and 7), Copyright 2008 with permission from Elsevier

at frequencies up to at least 9 kHz. The TM shear-impedance measurements in wild-type and mutant mouse models indicate that the TM is mostly elastic, with the viscous component of impedance at least three times smaller at all frequencies in both the radial and longitudinal directions (Gu et al. 2008; Fig. 6.7b, c). The amplitudes of both the elastic and viscous components of TM shear impedance decreases with frequency. In the longitudinal direction, this decrease is nearly linear, but in the radial direction, the amplitude decreases significantly slower than linearly with frequency. Gavara and Chadwick (2010) developed an AFM-based technique to deliver point forces at higher frequencies (about 25 kHz) and confirmed that the TM exhibits viscoelastic behaviors at high frequencies.

6.3.1.3 Electrokinetic Properties of the Tectorial Membrane

The TM mechanically stimulates cochlear sensory receptors, but the presence of fixed charge in TM constituents suggests that TM electromechanical properties may also play an important role in cochlear mechanisms. TM macromolecules comprise both mechanical constituents such as collagen fibrils and charged constituents such as glycosaminoglycans (GAGs; Fig. 6.8a). GAGs in the TM carry sulfate (SO_3^-) and carboxyl (COO^-) charge groups, which are fully ionized at physiological pH and neutralized at acidic pH values. The presence of a fixed charge in the TM suggests the possibility that electrical stimuli might generate a mechanical response. The application of oscillating electric fields at audio frequencies (1–1000 Hz) directed along the transverse axis of the TM in a microaperture chamber (Fig. 6.8b, c) generated displacements of the TM. TM displacements had peak amplitudes at positions on the undersurface of the TM above the microaperture (Fig. 6.8d, e). Displacement amplitudes dropped significantly with distance away from the microaperture, increased with electric field strength, and decreased as a function of stimulus frequency, consistent with viscous-dominated interactions (Fig. 6.8f).

Electrically evoked displacements of the TM may have important implications for studies that apply electrical stimulation to the CP. Mechanical responses to electrical stimulation generally have been attributed to OHC somatic electromotility (Sects. 6.2.6–6.2.8) and hair bundle motility (Corey, Ó Maoiléidigh, and Ashmore, Chap. 4) mechanisms. However, electrically induced TM motions must also be taken into account if applied electrical currents flow through the TM.

Electrokinetic properties of the TM could interact directly with stereociliary ion channels. Although the exact position of these channels relative to the undersurface of the TM remains unclear, it is well-known that the TM is in close proximity (nanometer-scale separation) to the tallest rows of channels, driven predominantly by potassium and calcium currents, which in turn might exert large (local) electrical forces on TM macromolecules near the TM-hair bundle interface (Fig. 6.8g–i). Based on the amplitude of these motions, it is plausible that local electrically induced deformations of the TM could occur near stereociliary ion channels.

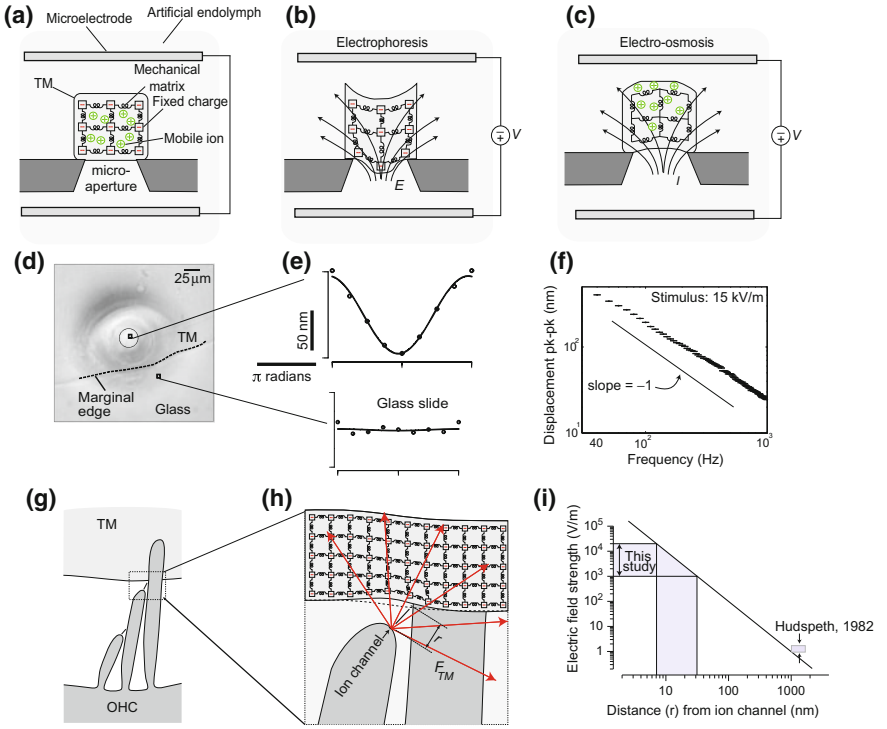

Fig. 6.8 Electrically evoked motions of the TM. **a** Schematic of an isolated TM segment composed of a network of mechanical springs, fixed negative-charge groups, and mobile positive ions. The segment is mounted on a microaperture, positioned between two microelectrodes, to create an electrochemical barrier between the two fluid compartments of a microchamber. **b** The applied electric field (*E*) exerts an electrophoretic force on the *fixed* negative charge, which results in the mechanical matrix deflecting toward the positive microelectrode. **c** An equal and opposite electroosmotic force from the electric current (*I*) sends *mobile* counterions in the opposite direction toward the negative microelectrode. **d** Optical image of TM overlying the microaperture. **e** Displacement-time waveforms show TM electrically evoked nanometer-scale motions of the TM in the region around the microaperture. **f** Displacement amplitudes decreased with increasing stimulus frequency, with the slope approaching −1 (for the double logarithmic plot). **g** Schematic illustrating the longest stereocilium of an OHC embedded in the TM. Note that the uppermost tip link is located close to the TM. **h** Magnified view showing the OHC mechanoelectrical transduction (MET) channel acting as a point electric source. The electric field (*arrows*) exerts force (F_{TM}) on fixed-charge macromolecules of the TM, locally over small distances (*r*) from the opening of the channel. **i** Model predictions of electric field strength as a function of *r*. Although MET currents are small, they flow through nanoscale ion channels and generate large electric fields near the TM (Hudspeth 1982). **a**–**c** Reprinted from Ghaffari et al. (2015, Fig. 1), with the permission from AIP Publishing; **d**–**i** reprinted from Ghaffari et al. (2013, Figs. 3b, d and 4, with permission from the National Academy of Sciences of the United States of America

6.3.1.4 Implications of Local Tectorial Membrane Interactions with Hair Bundles

The TM has been shown to undergo local deformations in response to intracochlear sound stimulation (Chan and Hudspeth 2005). This motion is presumably driven by local interactions with the hair bundles of OHCs, which are inserted into the TM and may couple active as well as passive mechanical forces to the TM. For this reason, it is important to compare the relative point stiffness and shear impedance of the TM and hair bundles (Chan and Hudspeth 2005; Corey, Ó Maoiléidigh, and Ashmore, Chap. 4). The TM would be relatively easy to move if its impedance matched that of the RL. In this context, it is relevant to note that OHC bundles have been shown to generate mechanical force in response to deflections (Jia and He 2005; Ashmore 2008). Such forces could contribute to the local motions of the TM or may be enhanced by the mechanoelectrical transduction currents, which may exert electrokinetic forces locally near the surface of the TM (Ghaffari et al. 2013). TM electrokinetics raises the intriguing notion that the TM may not behave as a purely mechanical structure locally but, instead, exhibits frequency-dependent electromechanical properties across multiple rows of hair cells.

6.3.2 Radial Modes of Tectorial Membrane Interactions with the Hair Bundles

Sound-induced and electrically evoked motions of the BM, TM, and RL have been shown to cause deflections of the hair bundles and are, therefore, of fundamental importance to cochlear mechanics (Chan and Hudspeth 2005; Ashmore 2008). For example, the phase of RL motion in the radial direction provides insight into the coupling of BM motion to OHC bundle deflection and thus to feedback processes associated with cochlear amplification. To understand the role of OHC motility on TM motion, several groups have stimulated isolated cochlear turns and studied radial modes of TM interactions with the hair bundles.

6.3.2.1 Effect of Electromechanical Force from Outer Hair Cells on Tectorial Membrane Motion

Jia and He (2005) reported that forces generated by OHC electromotility are sufficient to generate radial motions of the TM. This finding suggests that force generation by multiple rows of OHCs via somatic electromotility or hair bundle motility might excite radial motion of the TM, particularly in light of the physical attachment of the undersurface of the TM to the OHC hair bundles (Pickles et al. 1984; Verpy et al. 2011). In contrast to the OHC hair bundles, the inner hair cell (IHC) hair bundles are solely coupled to the TM through viscous coupling in the

subtectorial space (Patuzzi 1996; Nowotny and Gummer 2006). Recent measurements using electrical stimulation across isolated turns of the guinea pig cochlea indicate that OHC electromechanical force also drives a pulsatile, radial motion of fluid in the subtectorial space. This type of motion is thought to stimulate the IHC hair bundles at frequencies below 3 kHz (Nowotny and Gummer 2006; Fig. 6.9).

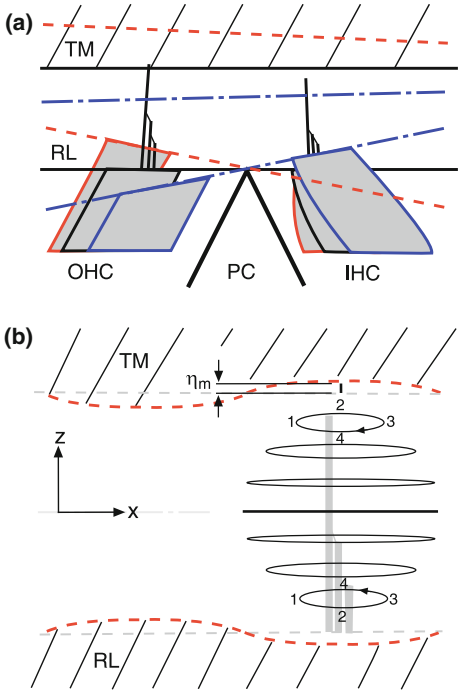

Fig. 6.9 Hydrodynamics of the subtectorial space in response to electromechanical force from the OHC soma. **a** Phase differences between the RL and TM. At the OHC, TM and RL move in phase because the longest OHC stereocilia are rigidly connected to the overlying TM. In contrast, at the IHC, the TM and RL move counterphasic because the RL rotates as a rigid plate about the apex of the pillar cells (PCs). Rotation is shown counterclockwise for OHC contraction (*blue lines*) and clockwise for OHC elongation (*red lines*). This mechanism, evidenced experimentally in all turns of the guinea pig cochlea at stimulus frequencies up to 3 kHz, modulates the depth of the subtectorial space at the IHC. *Gray areas*, cell somata. **b** Elliptical fluid-particle trajectories for counterphasic sinusoidal motion in the region of the IHC stereocilia (*three gray vertical rectangles*). *Numbers 1–4*, relative phases of the trajectories. Calculations suggest that the radial component of fluid motion (*x* direction) can be about an order of magnitude greater than the transverse component (*z* direction) near the center of the subtectorial space in the region of the tip links. Theoretically, this OHC-evoked pulsatile-like fluid motion is capable of directly modulating the open probability of the mechanoelectrical transduction channels. The transverse components at the TM and RL surfaces (*red dashed lines*) have equal amplitude denoted by η_m. Anatomical and mechanical features are not equally scaled. The measured value of η_m was 1–10 nm, whereas the depth of the subtectorial space is 4–8 μm for the first to third cochlear turns of the guinea pig cochlea, respectively. Reprinted from Nowotny and Gummer (2006, Fig. 3), Copyright 2006 with the permission from the National Academy of Sciences of the United States of America

6.3.2.2 Radial Modes of Tectorial Membrane Motion in Mutants

The *Tectb* and *Tecta* mutations have been shown to disrupt the striated sheet matrix of the TM (Russell et al. 2007) and cause significant changes in cochlear function (Xia et al. 2010). $Tecta^{C1509G}$ is a Tecta mouse model with TMs in heterozygotes that extend across only one row of OHCs (Xia et al. 2010). The $Tecta^{C1509G}$ mutation did not have visible alterations in the striated sheet matrix within the body of the TM. However, the $Tecta^{C1509G/+}$ TMs had significantly reduced stiffness and the heterozygote mouse exhibited partial hearing loss: 10–30 dB DPOAE threshold elevation (Xia et al. 2010). This change in cochlear response is likely caused by fewer OHCs being involved in electromechanical transduction, amplification, and coupling the mechanical output from the OHCs to the IHCs.

6.3.2.3 Implications of Radial Modes of Tectorial Membrane Interactions with the Hair Bundles

Currently, there is significant debate about the prevalent modes of motion that stimulate the hair bundles (Robles and Ruggero 2001; Guinan 2012). Specifically, the classical shearing motion between the TM and RL does not account for many of the important observations. For example, in all cochlear turns, OHC-evoked counterphasic motion between the TM and the RL at the IHCs has been observed for stimulus frequencies up to 3 kHz (Nowotny and Gummer 2006; Fig. 6.9). Such observations suggest the possibility of a second mechanism of cochlear amplification, producing mechanical force acting "directly" at the IHC stereocilia rather than "indirectly" via the BM. Thus, it is critical to understand the modes of motion that excite the stereocilia and mechanically couple the OHC electromechanical transducer to the IHC mechanoelectrical transducer. The recent studies detailing relative radial motions of the TM, hair bundles, and RL in wild types and mutants ultimately demonstrate that TM inertia, damping, and elasticity, which are comparable to those of the entire CP (Freeman et al. 2003b; Chan and Hudspeth 2005), allow significant motion of the TM even in the presence of loads imposed by fluid in the subtectorial space, the OHC hair bundles, and the limbal attachment. These new modes of radial motion raise important questions about how the TM couples motion longitudinally across different regions of the cochlea.

6.3.3 Longitudinal (Wave) Modes of Tectorial Membrane Motion

The point-stiffness and dynamic-shear impedance studies have implicated local mechanical properties (i.e., mass, stiffness) of the TM in stimulating the sensory hair bundles of hair cells. However, recent discovery of TM TWs and new cochlear

models suggest that the TM exhibits significant longitudinal coupling with large spatial extents (hundreds of rows of hair cells), capable of shaping the tuned frequency response of the cochlear amplifier.

6.3.3.1 Traveling-Wave Measurements of Isolated Tectorial Membrane

TM TWs were first observed in an experiment chamber in which a segment of an isolated TM was suspended between two parallel-aligned supports in artificial endolymph (Ghaffari et al. 2007, 2010; Fig. 6.10a, b). Sinusoidal forces applied in the radial direction at one support launched waves that propagated longitudinally

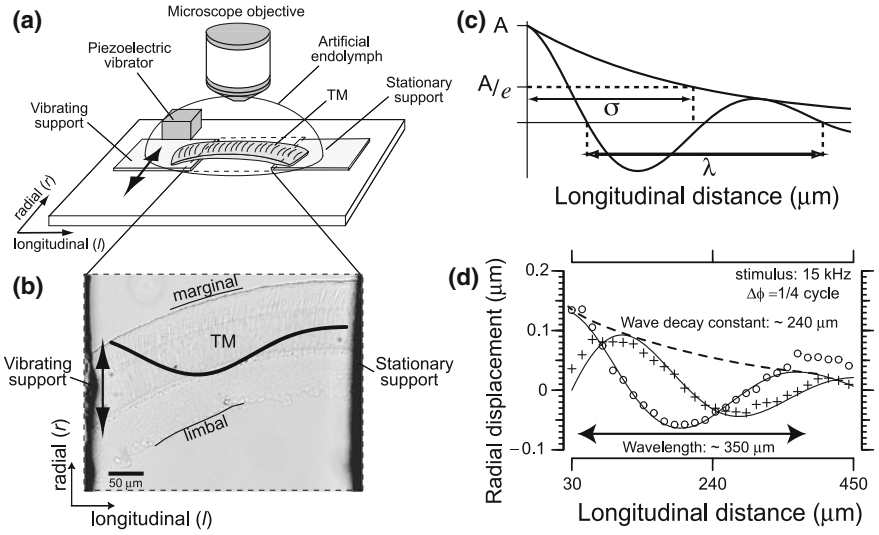

Fig. 6.10 Propagation of traveling waves along isolated TM. **a** Schematic of TM segment suspended between two supports, one of which is vibrated sinusoidally (*double arrow*) with a piezo actuator. Radial displacement was measured stroboscopically. **b** Image of a TM segment in artificial endolymph, with a superimposed cartoon of the measured radial displacement at one time instant (*not to scale*). The *lines* labeled marginal and limbal delineate the radial boundaries of the TM. **c** Schematic of a decaying wave of wavelength (λ) and peak amplitude (A), decaying with an exponential envelope of a wave-decay constant (σ). *Dashed lines*, envelope magnitude (A/*e*) at a longitudinal distance of σ from the stimulus, where *e* is Euler's constant. **d** TM radial displacement as function of longitudinal distance at two time instants separated by a quarter cycle (ΔΦ) of a 15-kHz stimulus. *Solid lines,* least mean square fits of a distributed impedance TM model to measured displacement responses (o and +). The spatial phase difference between the waves means that the TM is vibrating as a traveling wave. The wavelength is ∼350 µm (*double arrow*). *Dashed line*, exponential envelope of the traveling wave. The wave-decay constant is ∼240 µm. **a**, **b**, and **d** Reprinted from Ghaffari et al. (2007, Figs. 1A, B and 3B), Copyright 2007 with permission from the National Academy of Sciences of the United States of America; **c** reprinted from Ghaffari et al. (2010, Fig. 1B) with permission from Macmillan Publishers Ltd: Nature, Copyright 2010

along the TM toward the other support. Figure 6.10b–d shows the spatial pattern of radial displacement of a typical TM segment. The waveform snapshots pasted on the image show radial displacements as a function of longitudinal distance at two instants of time. The exponentially decaying sinusoid fitted to each waveform indicates wave motion of the TM. In response to 15-kHz stimuli, the wave has a wavelength of 350 μm and its envelope decays with a space constant of 240 μm (Fig. 6.10d). These wavelengths yield wave speeds that are comparable to TW speed estimates from the BM (Ghaffari et al. 2007). Although the mechanisms differ, the BM and TM waves have similar speeds as a function of longitudinal distance and stimulus frequency.

To determine whether TM TWs can propagate in vivo requires a distributed impedance model of the TM that accounts for the effects of cochlear loads: in particular, hair bundle stiffness and viscous forces in the subtectorial space. Adding hair bundle stiffness to the distributed impedance model does not have a significant effect on wave speed or decay. Damping in the subtectorial space was estimated by assuming that fluid flow can be modeled as the flow induced by the relative shear velocity of two parallel flat surfaces, known as plane Couette flow (Currie 1974), whereby the surface separation is supposed to be much smaller than the surface extent. The height of the subtectorial space was set based on the height of OHC stereocilia (1–6 μm). Viscous damping in the subtectorial space was found to attenuate TM TWs only at 1-μm gap heights. These reductions in the space constants were insignificant for gaps >2 μm. The presence of TM TWs suggests that significant longitudinal spread of excitation occurs via the TM. The distributed impedance model provides support for this claim by showing that TM waves are robust enough to overcome viscous dissipation in the subtectorial fluid and to excite radial motions of the hair bundles. Via radial coupling through the TM, TM waves are also important in stimulating fluid motion in the subtectorial space (Jia and He 2005; Nowotny and Gummer 2006). Thus TM waves enhance the mechanical input to both OHCs and IHCs.

In contrast to the fluid coupling that underlies the classical BM TW, TM waves represent an entirely new mechanism for longitudinal coupling through the cochlea. This finding counters a fundamental assumption made in classical cochlear models: that coupling only occurs through the fluid. Meaud and Grosh (2010) and others (Hubbard 1993; Lamb and Chadwick 2011) have implemented cochlear models that account for TM longitudinal coupling with implications for attaining high sensitivity but with broadened tuning to ensure high temporal resolution (fidelity).

6.3.3.2 Traveling-Wave Measurements of Isolated Tectorial Membrane in *Tectb*$^{-/-}$ Mutants

Genetic studies provide further support that TM TWs may play a significant role in cochlear tuning. The *Tectb* gene encodes β-tectorin, a glycoprotein that interacts with α-tectorin in the TM. Mice with this mutation have reduced sensitivity and sharper BM tuning (Russell et al. 2007). These differences in physiological

response cannot be explained by changes in damping or a simple attenuation in amplification. However, this combination of hearing abnormalities was found to be consistent with measured changes in TM wave velocity and decay constants.

There was a factor of two decrease in the extent of TM waves in *Tectb*$^{-/-}$ mice (Ghaffari et al. 2010). This reduction in the spatial extent of TM waves could lead to fewer hair cells working in concert, thereby causing a moderate decrease in sensitivity. Moreover, such a reduction in the coordinated activity of hair cells in *Tectb*$^{-/-}$ mice would simultaneously lead to a reduction in the longitudinal spread of excitation, causing fewer adjacent regions of the cochlea to vibrate at their own local best frequencies. The shorter wave-decay constants in *Tectb*$^{-/-}$ mice would thus lead to sharper frequency selectivity, in good agreement with the increase in the sharpness of tuning (Q_{10dB}) at mid-to-high frequencies (Ghaffari et al. 2010).

TM TWs can also explain the differences in hearing phenotypes between Tectb and other mutants. For example, both *Tectb*$^{-/-}$ and *Tecta*$^{Y1870C/+}$ mutants have normal hair bundles and TM attachments but exhibit distinctly different hearing phenotypes. *Tectb*$^{-/-}$ mice have sharper BM tuning (by a factor of 2–3), whereas *Tecta*$^{Y1870C/+}$ mice have normal BM tuning and broader neural tuning (Russell et al. 2007). These differences cannot be explained by changes in TM point stiffness alone. In addition to stiffness, shear viscosity of the TM (caused by the interaction of water with TM macromolecules) plays a key role in determining TM wave properties. Although TM stiffness can be measured locally and statically, TM shear viscosity requires dynamic measurement techniques. Recent measurements (Sellon et al. 2014) at audio frequencies show that TM shear viscosity is significantly lower in *Tecta*$^{Y1870C/+}$ TMs than in *Tectb*$^{-/-}$ and wild-type TMs (Fig. 6.11a). Experiments with polyethylene glycol (PEG) molecules of different radii of gyration demonstrate that the smaller shear viscosity in *Tecta*$^{Y1870C/+}$ TMs can be accounted for by their larger nanoscale pores (Sellon et al. 2014). Reducing TM shear viscosity reduces wave transmission loss, which, in turn, allows TM waves in *Tecta*$^{Y1870C/+}$ mutants to propagate further than those in *Tectb*$^{-/-}$ mice (i.e., wave-decay constants are larger in *Tecta*$^{Y1870C/+}$ mutants than in *Tectb*$^{-/-}$ mutants). These findings demonstrate that the TM is not a purely elastic structure, but, rather, it has important viscoelastic properties that can account for differences in cochlear tuning phenotypes of *Tecta*$^{Y1870C/+}$ and *Tectb*$^{-/-}$ mutant mice (Fig. 6.11b).

6.3.3.3 Traveling-Wave Measurements of Tectorial Membrane In Vivo

Our understanding of in vivo cochlear mechanics is largely based on measurements made at the BM (Robles and Ruggero 2001). There are few measurements of the relative motion between the TM and the RL (Gummer et al. 1996; Chan and Hudspeth 2005), and those have primarily been obtained in isolated cochlear turns in response to acoustic and electrical stimuli (Scherer and Gummer 2004a; Nowotny and Gummer 2006). More recent in vivo measurements by Lee et al. (2015) have demonstrated that the TM exhibits wave phenomena (Fig. 6.12).

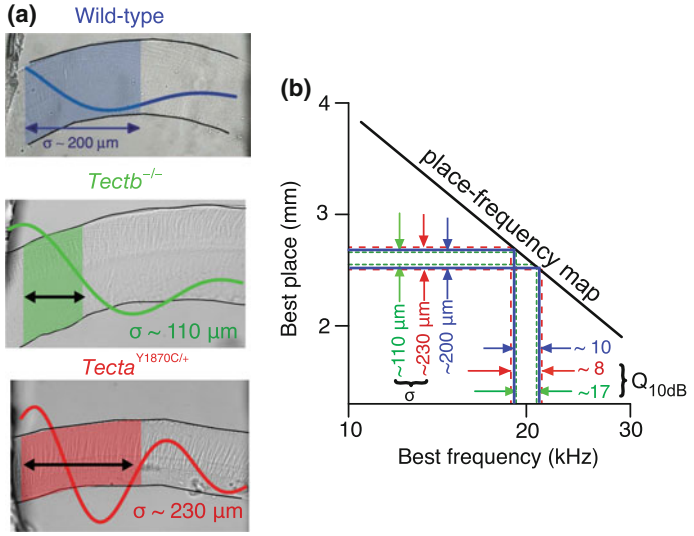

Fig. 6.11 TM wave-decay constant (σ) and quality of tuning (Q_{10dB}). **a** Images of wild-type (*top*), *Tectb*$^{-/-}$ (*middle*), and *Tecta*$^{Y1870C/+}$ (*bottom*) mouse TMs in artificial endolymph. The superimposed waveforms illustrate the radial displacement in response to a 20-kHz stimulus at one time instant (not to scale). **b** TM wave-decay constants predict frequency tuning, Q_{10dB}. *Horizontal lines*, wave-decay constant varies across *Tecta*$^{Y1870C/+}$ (230 µm; *red*), *Tectb*$^{-/-}$ (110 µm; *green*), and wild-type (200 µm; *blue*) TM samples. *Vertical lines*, equivalent differences in frequency yield Q_{10dB} estimates of ~10 for wild type and *Tecta*$^{Y1870C/+}$ and 17 for *Tectb*$^{-/-}$. Reprinted from Sellon et al. (2014, Fig. 6B). Used in accordance with the Creative Commons Attribution (CC BY) license

Compared to TWs on the BM, TWs on the TM have larger dynamic ranges and apically shifted positions of peak vibration (Lee et al. 2015). TM displacements were about twice BM displacements in response to 10 dB SPL sound stimuli. In contrast, at high sound intensity TM displacements were half the size of BM displacements. TM tuning was also found to be sharper than BM tuning, suggesting that the TM and BM waves are tightly coupled but have slight differences in phase. The phase of TM displacements leads that of the BM at low SPLs and lags BM phase at high SPLs. These differences in tuning and displacement amplitudes and phases could be governed by differences in the mechanical origin of TM and BM waves.

Recent advances in optical coherence tomography-based systems (Chen et al. 2011; Lee et al. 2015) have proven to have great value for studying cochlear mechanics because they provide both high-resolution motion measurements and imaging of fine cochlear structures (i.e., TM and RL). These techniques are poised to resolve the discrepancies that exist today between BM vibration data and auditory nerve responses (Lee et al. 2015) and will help elucidate the interactions of the TM and the organ of Corti.

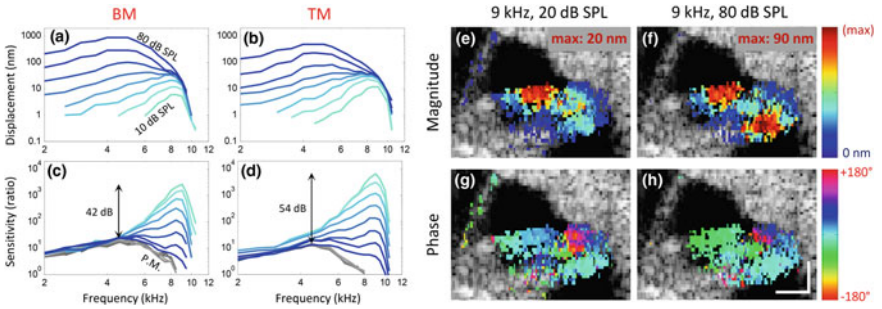

Fig. 6.12 Vibration measurements of the organ of Corti and TM in vivo. **a** and **b** BM and TM displacements in response to a range of sound stimuli (10–80 dB SPL). **c** and **d** Displacements of the BM and TM relative to displacement of the middle ear ossicular chain (sensitivity). In vivo, BM and TM motions exhibited nonlinear gain, with larger relative displacements at lower intensities. Postmortem (P.M.), the displacement responses (*gray lines*) overlapped for all stimulus intensities (30–80 dB SPL), demonstrating linearity. Displacement amplitude (**e** and **f**) and phase (**g** and **h**) responses of the BM and TM to low-intensity (**e** and **g**) and high-intensity (**f** and **h**) sound stimuli at the best frequency (9 kHz). Amplitudes are normalized to the maximum response in each image. These responses demonstrate that the organ of Corti and TM exhibit intensity-dependent wave motion. Reprinted from Lee et al. (2015, Fig. 3), with permission from the National Academy of Sciences of the United States of America and J. S. Oghalai

6.3.3.4 Implications of Longitudinal Modes of Tectorial Membrane Motion

Previous cochlear models have represented the TM as a single-point resonant structure with coupling occurring through the fluid. In models that incorporate TM longitudinal coupling, the TM would tend to increase the sensitivity of each resonator and thereby broaden the apparent tuning of the bank of resonators. TM wave-decay constants constitute the distance over which TM coupling is significant. Through the cochlear frequency-place map, these spatial bandwidth estimates can predict frequency bandwidth, thereby providing an estimate of the effective quality of tuning, Q (Fig. 6.11b). The Q_{10dB} values predicted from TM wave-decay constants closely match the tuning estimates from BM motion and neural recordings (Sellon et al. 2015).

Because wave-decay constants depend on stiffness and the Q_{10dB} depends on wave-decay constants, it follows that Q_{10dB} will also depend on stiffness. Estimates of Q_{10dB} as a function of a shear-storage modulus show that increasing TM stiffness broadens cochlear tuning. The opposite trend is predicted in resonant models, in which increasing TM stiffness would normally give rise to sharper cochlear tuning. This relationship between TM longitudinal coupling and Q_{10dB} fundamentally changes the way we think about the roles of viscosity and the spread of mechanical excitation in cochlear tuning.

6.4 Summary

This chapter has highlighted seminal concepts and experiments for elucidating mechanisms responsible for the extraordinary sensitivity and frequency selectivity of the cochlea. In vivo measurements of intracochlear voltage and pressure with a miniaturized, dual voltage-pressure sensor in the neighborhood of the BM provide *direct* evidence for a power injection in the region of the BF and for average-power gain relative to the average power from the middle ear. Experiments with isolated TMs have shown that the TM cannot be considered simply as a radial-point mechanical impedance with the function of locally deflecting OHC stereocilia. Instead, it is also an electrokinetic material with distributed viscoelastic properties. In response to direct mechanical stimulation, both in vitro and in vivo, the TM supports TWs, which can propagate in anterograde and retrograde directions over several wavelengths, conceivably coupling the OHC stereocilia dynamically over large longitudinal distances to shape cochlear amplification. Recent experiments with optical coherence tomography-based imaging techniques are unravelling in vivo phase relationships between the displacements of the TM, RL, and BM. Future technology will allow measurement of (1) mechanical forces acting on the stereocilia and (2) homeostatic events at the TM-stereociliary complex (e.g., Ca^{2+} regulation) in vivo. With such knowledge, it is hoped that paradigms for the clinical, differential diagnosis of the functional states of both the cochlear amplifier and the neural encoder will be attainable.

Compliance with Ethics Requirements Anthony W. Gummer declares that he has no conflict of interest. Wei Dong declares that she has no conflict of interest. Roozbeh Ghaffari declares that he has no conflict of interest. Dennis M. Freeman declares that he has no conflict of interest.

References

Abnet, C., & Freeman, D. (2000). Deformations of the isolated mouse tectorial membrane produced by oscillatory forces. *Hearing Research*, 144(1–2), 29–46.

Allen, J. B. (1980). Cochlear micromechanics–A physical model of transduction. *The Journal of the Acoustical Society of America*, 68(6), 1660–1670.

Allen, J. B., & Fahey, P. F. (1992). Using acoustic distortion products to measure the cochlear amplifier gain on the basilar membrane. *The Journal of the Acoustical Society of America,* 92(1), 178–188.

Ashmore, J. (2008). Cochlear outer hair cell motility. *Physiological Reviews*, 88(1), 173–210.

Brownell, W. E., Bader, C. R., Bertrand, D., and de Ribaupierre, Y. (1985). Evoked mechanical responses of isolated cochlear outer hair cells. *Science*, 227, 194–196.

Chan, D., and Hudspeth, A. J. (2005). Mechanical responses of the organ of Corti to acoustic and electrical stimulation in vitro. *Biophysical Journal*, 89, 4382–4395.

Chen, F., Zha, D., Fridberger, A., Zheng, J., Choudhury, N., Jacques, S. L., Wang, R. K., Shi, X., & Nuttall, A. L. (2011). A differentially amplified motion in the ear for near-threshold sound detection. *Nature Neuroscience*, 14(6), 770–774.

Cooper, N. P. (2003). Compression in the peripheral auditory system. In S. P. Bacon, R. R. Fay, & A. N. Popper (Eds.), *Compression from Cochlear to Cochlear Implants* (pp. 18–61). New York: Springer.

Currie, I. G. (1974). *Fundamental Mechanics of Fluids*. New York: McGraw-Hill Book Co.

Dallos, P. (2003). Organ of Corti kinematics. *Journal of the Association for Research in Otolaryngology*, 4(3), 416–421.

Dallos, P., Wu, X., Cheatham, M. A., Gao, J., Zheng, J., Anderson, C. T., Jia, S., Wang, X., Cheng, W. H. Y., Sengupta, S., He, D. Z. Z., & Zuo, J. (2008). Prestin-based outer hair cell motility is necessary for mammalian cochlear amplification. *Neuron*, 58(3), 333–339.

Davis, H. (1957). Biophysics and physiology of the inner ear. *Physiological Reviews*, 37(1), 1–49.

Davis, H. (1983). An active process in cochlear mechanics. *Hearing Research*, 9(1), 79–90.

de Boer, E. (1980). Auditory physics. Physical principles in hearing theory. I. *Physics Reports,* 62 (2), 87–174.

de Boer, E., & Nuttall, A. L. (2000). The mechanical waveform of the basilar membrane. III. Intensity effects. *The Journal of the Acoustical Society of America*, 107(3), 1497–1507.

de Boer, E., & Nuttall, A. L. (2001). Power gain of the cochlear amplifier. In D. J. Breebaart, A. J. M. Houtsma, A. Kohlrausch, V. F. Prijs, & R. Schoonhoven (Eds.), *Physiological and Psychological Bases of Auditory Function* (pp. 1–7). Maastricht, The Netherlands: Shaker.

de Boer, E., Nuttall, A. L., Hu, N., Zou, Y., & Zheng, J. (2005). The Allen-Fahey experiment extended. *The Journal of the Acoustical Society of America*, 117(3), 1260–1266.

Diependaal, R. J., de Boer, E., & Viergever, M. A. (1987). Cochlear power flux as an indicator of mechanical activity. *The Journal of the Acoustical Society of America*, 82(3), 917–926.

Dong, W., & Olson, E. S. (2005). Two-tone distortion in intracochlear pressure. *The Journal of the Acoustical Society of America,* 117(5), 2999–3015.

Dong, W., & Olson, E. S. (2006). Middle ear forward and reverse transmission in gerbil. *Journal of Neurophysiology,* 95(5), 2951–2961.

Dong, W., & Olson, E. S. (2009). In vivo impedance of the gerbil cochlear partition at auditory frequencies. *Biophysical Journal,* 97(5), 1233–1243.

Dong, W., & Olson, E. S. (2013). Detection of cochlear amplification and its activation. *Biophysical Journal,* 105(4), 1067–1078.

Frank, G., Hemmert, W., & Gummer, A. W. (1999). Limiting dynamics of high-frequency electromechanical transduction of outer hair cells. *Proceedings of the National Academy of Sciences of the United States of America*, 96(8), 4420–4425.

Freeman, D. M., Masaki, K., McAllister, A. R., Wei, J. L., & Weiss, T. F. (2003a). Static material properties of the tectorial membrane: A summary. *Hearing Research*, 180(1–2), 11–27.

Freeman, D. M., Abnet, C. C., Hemmert, W., Tsai, B. S., & Weiss T. F. (2003b). Dynamic material properties of the tectorial membrane: A summary. *Hearing Research*, 180(1–2), 1–10.

Gavara, N., & Chadwick, R. S. (2010). Noncontact microrheology at acoustic frequencies using frequency-modulated atomic force microscopy. *Nature Methods*, 7(8), 650–654.

Ghaffari, R., Aranyosi, A. J., & Freeman, D. M. (2007). Longitudinally propagating traveling waves of the mammalian tectorial membrane. *Proceedings of the National Academy of Sciences of the United States of America*, 104(42), 16510–16515.

Ghaffari, R., Aranyosi, A. J., Richardson, G. P., & Freeman, D. M. (2010). Tectorial membrane travelling waves underlie abnormal hearing in *Tectb* mutant mice. *Nature Communications*, 1, 96. doi:10.1038/ncomms1094.

Ghaffari, R., Page, S. L., Farrahi, S., Sellon, J. B., & Freeman D. M. (2013). Electrokinetic properties of the mammalian tectorial membrane. *Proceedings of the National Academy of Sciences of the United States of America*, 110(11), 4279–4284.

Ghaffari, R., Page S., Farrahi, S., Sellon, J. B., & Freeman, D. M. (2015). Electromechanical role of fixed charge in the mammalian tectorial membrane. In K. D. Karavitaki & D. P. Corey (Eds.), *Mechanics of Hearing: Protein to Perception* (pp. 080001-1–080001-5). Melville, New York: American Institute of Physics.

Gold, T. (1948). Hearing. II. The physical basis of the action of the cochlea. *Proceedings of the Royal Society B: Biological Sciences*, 135, 492–498.

Grosh, K., Zheng, J., Zou, Y., de Boer, E., & Nuttall, A. L. (2004). High-frequency electromotile responses in the cochlea. *The Journal of the Acoustical Society of America*, 115(5), 2178–2184.

Gu, J. W., Hemmert, W., Freeman, D. M., & Aranyosi, A. J. (2008). Frequency-dependent shear impedance of the tectorial membrane. *Biophysical Journal*, 95(5), 2529–2538.

Gueta, R., Barlam, D., Shneck, R. Z., & Rousso, I. (2006). Measurement of the mechanical properties of isolated tectorial membrane using atomic force microscopy. *Proceedings of the National Academy of Sciences of the United States of America*, 103(40), 14790–14795.

Guinan, J. J., Jr. (2012). How are inner hair cells stimulated? Evidence for multiple mechanical drives. *Hearing Research*, 292(1–2), 35–50.

Gummer, A. W., Hemmert, W., & Zenner, H. P. (1996). Resonant tectorial membrane motion in the inner ear: its crucial role in frequency tuning. *Proceedings of the National Academy of Sciences of the United States of America*, 93(16), 8727–8732.

Huang, S., & Olson, E. S. (2011). Auditory nerve excitation via a non-traveling wave mode of basilar membrane motion. *Journal of the Association for Research in Otolaryngology*, 12(5), 559–575.

Hubbard, A. (1993). A traveling-wave amplifier model of the cochlea. *Science*, 259(5091), 68–71.

Hubbard, A. E., & Mountain, D. C. (1983). Alternating current delivered into the scala media alters sound pressure at the eardrum. *Science,* 222, 510–512.

Hudspeth, A. (1982). Extracellular current flow and the site of transduction by vertebrate hair cells. *The Journal of Neuroscience*, 2(1), 1–10.

Jia, S., & He, D. Z. (2005). Motility-associated hair-bundle motion in mammalian outer hair cells. *Nature Neuroscience*, 8(8), 1028–1034.

Johnson, S. L., Beurg, M., Marcotti, W., & Fettiplace, R. (2011). Prestin-driven cochlear amplification is not limited by the outer hair cell membrane time constant. *Neuron*, 70(6), 1143–1154.

Kemp, D. T. (1978). Stimulated acoustic emissions from within the human auditory system. *The Journal of the Acoustical Society of America,* 64(5), 1386–1391.

Kössl, M., & Russell, I. J. (1992). The phase and magnitude of hair cell receptor potentials and frequency tuning in the guinea pig cochlea. *The Journal of Neuroscience*, 12(5), 1575–1586.

Kronester-Frei, A. (1978). Ultrastructure of the different zones of the tectorial membrane. *Cell and Tissue Research,* 193(1), 11–23.

Lamb, J. S., & Chadwick, R. S. (2011). Dual traveling waves in an inner ear model with two degrees of freedom. *Physical Review Letters*, 107(8), 088101.

Lee, H. Y., Raphael, P. D., Park, J., Ellerbee, A. K., Applegate, B. E., & Oghalai, J. S. (2015). Noninvasive in vivo imaging reveals differences between tectorial membrane and basilar membrane traveling waves in the mouse cochlea. *Proceedings of the National Academy of Sciences of the United States of America*, 112(10), 3128–3133.

Liberman, M. C., Gao, J., He, D. Z., Wu, X., Jia, S., & Zuo, J. (2002). Prestin is required for electromotility of the outer hair cell and for the cochlear amplifier. *Nature*, 419(6904), 300–304.

Lukashkin, A. N., Walling, M. N., & Russell, I. J. (2007). Power amplification in the mammalian cochlea. *Current Biology*, 17(15), 1340–1344.

Lukashkin, A. N., Legan, P.K., Weddell, T. D., Lukashkina, V. A., Goodyear, R. J., Welstead, L. J., Petit, C., Russell, I. J., & Richardson, G. P. (2012). A mouse model for human deafness DFNB22 reveals that hearing impairment is due to a loss of inner hair cell stimulation. *Proceedings of the National Academy of Sciences of the United States of America,* 109(47), 19351–19356.

Mammano, F., & Nobili, R. (1993). Biophysics of the cochlea: Linear approximation. *The Journal of the Acoustical Society of America*, 93(6), 3320–3332.

Masaki, K., Weiss, T. F., & Freeman, D. M. (2006). Poroelastic bulk properties of the tectorial membrane measured with osmotic stress. *Biophysical Journal*, 91(6), 2356–2370.

Meaud, J., & Grosh, K. (2010). The effect of tectorial membrane and basilar membrane longitudinal coupling in cochlear mechanics. *The Journal of the Acoustical Society of America*, 127(3), 1411–1421.

Mellado Lagarde, M. M., Drexl, M., Lukashkina, V. A., Lukashkin, A. N., & Russell, I. J. (2008). Outer hair cell somatic, not hair bundle, motility is the basis of the cochlear amplifier. *Nature Neuroscience*, 11(7), 746–748.

Nakajima, H. H., Dong, W., Olson, E. S., Merchant, S. N., Ravicz, M. E., & Rosowski, J. J. (2009). Differential intracochlear sound pressure measurements in normal human temporal bones. *Journal of the Association for Research in Otolaryngology*, 10(1), 23–36.

Neely, S. T., & Kim, D. O. (1986). A model for active elements in cochlear biomechanics. *The Journal of the Acoustical Society of America*, 79(5), 1472–1480.

Nilsen, K. E., & Russell, I. J. (2000). The spatial and temporal representation of a tone on the guinea pig basilar membrane. *Proceedings of the National Academy of Sciences of the United States of America*, 97(22), 11751–11758.

Nowotny, M., & Gummer, A. W. (2006). Nanomechanics of the subtectorial space caused by electromechanics of cochlear outer hair cells. *Proceedings of the National Academy of Sciences of the United States of America*, 103(7), 2120–2125.

Nuttall, A. L., & Ren, T. Y. (1995). Electromotile hearing: Evidence from basilar membrane motion and otoacoustic emissions. *Hearing Research*, 92(1–2), 170–177.

Olson, E. S. (1998). Observing middle and inner ear mechanics with novel intracochlear pressure sensors. *The Journal of the Acoustical Society of America*, 103(6), 3445–3463.

Olson, E. S. (1999). Direct measurement of intra-cochlear pressure waves. *Nature*, 402, 526–529.

Olson, E. S. (2001). Intracochlear pressure measurements related to cochlear tuning. *The Journal of the Acoustical Society of America,* 110(1), 349–367.

Olson, E. S., Duifhuis, H., & Steele, C. R. (2012). Von Békésy and cochlear mechanics. *Hearing Research,* 293(1–2), 31–43.

Patuzzi, R. B. (1996). Cochlear micromechanics and macromechanics. In P. Dallos, A. N. Popper, & R. R. Fay (Eds.), *The Cochlea* (pp. 186–257). New York: Springer-Verlag.

Patuzzi, R. B., Yates, G. K., & Johnstone, B. M. (1989). Changes in cochlear microphonic and neural sensitivity produced by acoustic trauma. *Hearing Research*, 39(1–2), 189–202.

Pickles, J. O., Comis, S. D. & Osborne, M. P. (1984). Cross-links between stereocilia in the guinea pig organ of Corti, and their possible relation to sensory transduction. *Hearing Research*, 15(2), 103–112.

Preyer, S., & Gummer, A. W. (1996). Nonlinearity of mechanoelectrical transduction of outer hair cells as the source of nonlinear basilar-membrane motion and loudness recruitment. *Audiology and Neurotology*, 1(1), 3–11.

Preyer, S., Renz, S., Hemmert, W., Zenner, H.-P., & Gummer, A. W. (1996). Receptor potential of outer hair cells isolated from base to apex of the adult guinea-pig cochlea: Implications for cochlear tuning mechanisms. *Auditory Neuroscience*, 2, 145–157.

Ramamoorthy, S., & Nuttall, A. L. (2012). Outer hair cell somatic electromotility in vivo and power transfer to the organ of Corti. *Biophysical Journal*, 102(3), 388–398.

Ren, T., He, W., & Barr-Gillespie, P. G. (2016). Reverse transduction measured in the living cochlea by low-coherence heterodyne interferometry. *Nature Communications*, 7, 10282. doi:10.1038/ncomms10282.

Robles, L., & Ruggero, M. A. (2001). Mechanics of the mammalian cochlea. *Physiological Reviews,* 81(3), 1305–1352.

Russell, I. J., & Nilsen, K. E. (1997). The location of the cochlear amplifier: Spatial representation of a single tone on the guinea pig basilar membrane. *Proceedings of the National Academy of Sciences of the United States of America,* 94(6), 2660–2664.

Russell, I. J., Legan, P. K., Lukashkina, V. A., Goodyear, R. J., & Richardson, G. P. (2007). Sharpened cochlear tuning in a mouse with a genetically modified tectorial membrane. *Nature Neuroscience*, 10(2), 215–223.

Scherer, M. P., & Gummer, A. W. (2004a). Vibration pattern of the organ of Corti up to 50 kHz: Evidence for resonant electromechanical force. *Proceedings of the National Academy of Sciences of the United States of America*, 101(51), 17652–17657.

Scherer, M. P., & Gummer, A. W. (2004b). Impedance analysis of the organ of Corti with magnetically actuated probes. *Biophysical Journal*, 87(2), 1378–1391.

Sellon, J. B., Ghaffari, R., Farrahi, S., Richardson G. P., & Freeman, D. M. (2014). Porosity controls spread of excitation in tectorial membrane traveling waves. *Biophysical Journal*, 106(6), 1406–1413.

Sellon, J. B., Farrahi, S., Ghaffari, R., & Freeman, D. M. (2015). Longitudinal spread of mechanical excitation through tectorial membrane traveling waves. *Proceedings of the National Academy of Sciences of the United States of America*, 112(42), 12968–12973.

Shera, C. A., & Guinan, J. J., Jr. (2007). Cochlear traveling-wave amplification, suppression, and beamforming probed using noninvasive calibration of intracochlear distortion sources. *The Journal of the Acoustical Society of America*, 121(2), 1003–1016.

Shoelson, B., Dimitriadis, E. K., Cai, H., Kachar, B., & Chadwick, R. S. (2004). Evidence and implications of inhomogeneity in tectorial membrane elasticity. *Biophysical Journal*, 87(4), 2768–2777.

Slama, M. C. C., Ravicz, M. E., & Rosowski, J. J. (2010). Middle ear function and cochlear input impedance in chinchilla. *The Journal of the Acoustical Society of America*, 127(3), 1397–1410.

Steele, C. R, & Taber, L. A. (1981). Three-dimensional model calculations for guinea pig cochlea. *The Journal of the Acoustical Society of America*, 69(4), 1107–1111.

Thalmann, I. (1993). Collagen of accessory structures of organ of Corti. *Connective Tissue Research*, 29(3), 191–201.

van der Heijden, M., & Versteegh, C. P. (2015). Energy flux in the cochlea: Evidence against power amplification of the traveling wave. *Journal of the Association for Research in Otolaryngology*, 16(5), 581–597.

Verpy, E., Leibovici, M., Michalski, N., Goodyear, R. J., Houdon, C., Weil, D., Richardson, G. P., & Petit, C. (2011). Stereocilin connects outer hair cell stereocilia to one another and to the tectorial membrane. *The Journal of Comparative Neurology,* 519(2), 194–210.

von Békésy, G. (1953). Shearing microphonics produced by vibration near the inner and outer hair cells. *The Journal of the Acoustical Society of America*, 25(4), 786–790.

von Békésy, G. (1960). *Experiments in Hearing*. New York: McGraw-Hill Book Company.

Wang, Y., Steele, C. R., & Puria, S. (2016). Cochlear outer-hair cell power generation and viscous fluid loss. *Scientific Reports*, 6, 19475. doi:10.1038/srep19475.

Xia, A., Gao, S. S., Yuan, T., Osborn, A., Bress, A., Pfister, M., Maricich, S. M., Pereira, F. A., & Oghalai, J. S. (2010). Deficient forward transduction and enhanced reverse transduction in the alpha tectorin C1509G human hearing loss mutation. *Disease Models and Mechanisms*, 3(3–4), 209–223.

Zha, D., Chen, F., Ramamoorthy, S., Fridberger, A., Choudhury, N., Jacques, S. L., Wang, R. K., & Nuttall, A. L. (2012). *In vivo* outer hair cell length changes expose the active process in the cochlea. *PLoS ONE,* 7(4), e32757.

Zwislocki, J. J. (1980). Five decades of research on cochlear mechanics. *The Journal of the Acoustical Society of America*, 67(5), 1679–1685.

Zwislocki, J. J, & Cefaratti, L. K. (1989). Tectorial membrane. II: Stiffness measurements in vivo. *Hearing Research*, 42(2–3), 211–227.

Chapter 7
Hair Cells and Their Synapses

Michael E. Schnee and Anthony Ricci

Abstract The peripheral auditory system acts like a spectrum analyzer to break down complex sounds into their frequency and intensity components. All of this information is transferred from sensory cell to afferent fiber via ribbon synapses where graded hair cell receptor potentials are transformed into synaptic events that generate postsynaptic action potentials. These synapses can operate at high frequencies with high temporal fidelity for long periods of time. This review discusses the most recent findings from the morphological to the molecular to the functional specializations of the hair cell ribbon synapse that allow for these unique synaptic properties. Afferent fiber properties vary greatly in terms of spontaneous activity, threshold sensitivity, and dynamic range; the potential mechanisms for these differences are presented. The role of the ribbon in regulating vesicle trafficking and in acting as a diffusion barrier to calcium is discussed. The role of otoferlin as it relates to vesicle fusion, vesicle trafficking, and endocytosis is presented. The potential roles for multiquantal vesicle fusion as well as the likely mechanisms underlying this phenomenon and its potential physiological relevance are addressed. Calcium homeostasis, the roles of nano- versus microdomains to synaptic properties, and the importance of calcium-induced calcium release are also elucidated.

Keywords Auditory · Calcium homeostasis · Calcium-induced calcium release · Capacitance · Cochlea · Excitatory postsynaptic current · Hair cells · Multivesicular release · Nanodomain · Otoferlin · Ribbon synapse · RIBEYE · Vesicle pools · Vesicle trafficking

M.E. Schnee
Department of Otolaryngology, Stanford University, 300 Pasteur Drive, Edwards Building R145, Stanford, CA 94305, USA
e-mail: mschnee@stanford.edu

A. Ricci (✉)
Department of Otolaryngology and Department of Molecular and Cellular Physiology, Stanford University, 300 Pasteur Drive, Edwards Building R145, Stanford, CA 94305, USA
e-mail: aricci@stanford.edu

G.A. Manley et al. (eds.), *Understanding the Cochlea*, Springer Handbook of Auditory Research 62, DOI 10.1007/978-3-319-52073-5_7

7.1 Introduction

The peripheral auditory system, including the external, middle, and inner ears, comprises an extraordinary engineering success. The middle ear overcomes a major impedance-matching problem that arises from translating sound from the air to the liquid interface while the inner ear (cochlea) acts as an exquisite spectrum analyzer, using a nonlinear mechanical gain as well as frequency tuning to discriminate more than five orders of magnitude for both sound intensity and frequency (Fig. 7.1). Yet all of this would be for naught if the information obtained from the mechanical separation of sound were not reliably transferred to the central nervous system. For this to happen, synapses convey graded information for intensity over extended time periods and in a manner that generates reliable postsynaptic firing. The primary focus of this chapter is to discuss specializations at the hair cell-afferent fiber synapse that aid in producing these remarkable characteristics. We discuss the molecular machinery, pre- and postsynaptic release properties, and calcium homeostatic mechanisms. Our goal is to provide a summary of recent data that contribute to existing hypotheses and controversies while helping to guide future directions for investigations of the hair cell-afferent fiber synapse.

7.1.1 Questions to Be Addressed

Cochlear hair cell-afferent fiber synapses differ from conventional neuronal synapses in several fundamental ways. In vivo recordings from single afferent fibers in response to sound stimulation are highly tuned, matching basilar membrane vibrations (Yates 1990), demonstrating high temporal fidelity and sensitivity. These synapses can operate at high vesicle release rates for long periods of time, intimating a rapid and robust vesicle release and resupply mechanism. Single-nerve recordings identify two populations of afferent fibers, one that has very low or no spontaneous activity, representing about 40% of fibers measured, and a second population where the range of spontaneous activity is quite broad, ranging from greater than 10 Hz to more than 150 Hz (Kawase and Liberman 1992; Fig. 7.2). Similar results were obtained across mammalian species: gerbil (Schmiedt 1989), mouse (Taberner and Liberman 2005), and cat (Liberman 1978). Because all afferent firing is driven synaptically, differences in spontaneous activity suggest differences in synaptic efficacy (Robertson and Johnstone 1979). A direct correlation between spontaneous firing rate and sound threshold levels led to a hypothesis where the broad sensitivity to sound intensity is conveyed across populations of fibers where each fiber has a narrow dynamic range and multiple fibers together create the broad range (Liberman 1978; Fig. 7.2). What mechanisms establish these individual dynamic ranges? We hypothesize that high firing rates result from hair cells releasing vesicles at high rates (Matthews and Fuchs 2010). Are there presynaptic specializations in vesicle fusion and trafficking or in calcium

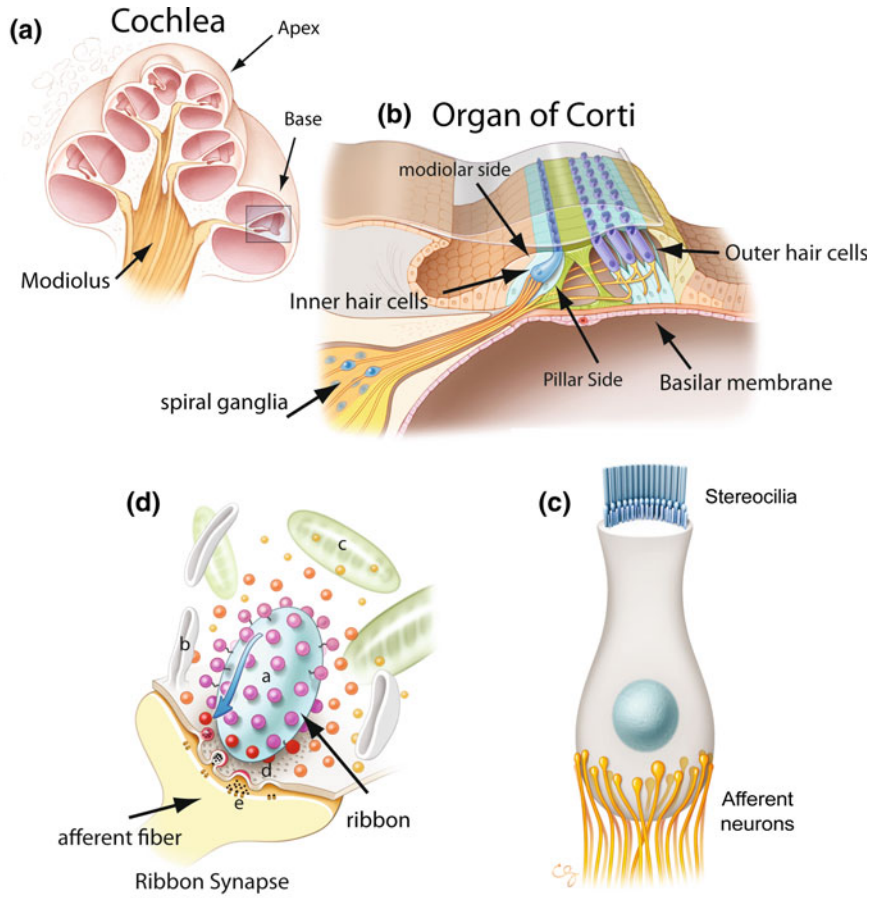

Fig. 7.1 Schematized description of the inner ear from cochlea to synapse. **a** Section showing multiple cochlea turns with the conical central modiolus where the spiral ganglia fibers project to the brainstem. **b** Wiring diagram of the organ of Corti showing the single row of inner hair cells (IHCs) innervated by type I spiral ganglion neurons and the 3 rows of outer hair cells (OHCs) with only the efferent fibers from the auditory brainstem shown. **c** Mature IHCs are innervated by 5–30 afferent fibers, each making a single synaptic contact. **d** Enlargement of a single synapse with the ribbon and tethered synaptic vesicles (SVs; *a*) that are color coded to illustrate different vesicle pools. *Blue arrow*: hypothesized flow of SVs down the ribbon to the base where docking may occur. Endocytic invaginations of the plasma membrane (*b*) are at the end of the presynaptic density where bulk endocytosis occurs. Mitochondria are concentrated at the synapse (*c*) and may have a role in sequestering Ca^{2+} and providing ATP that is required for Ca^{2+}-channel function and Ca^{2+} clearance. Dots indicate the stripes of $Ca_v1.3$ Ca^{2+} channels located adjacent to the ribbon (*d*), ranging in number from 80 to 700 depending on the species. When the Ca^{2+} channel(s) opens, nearby vesicles (*red*) fuse, releasing glutamate that activates postsynaptic AMPARs on the afferent fiber (*e*), triggering action potentials that travel to the cochlear nucleus

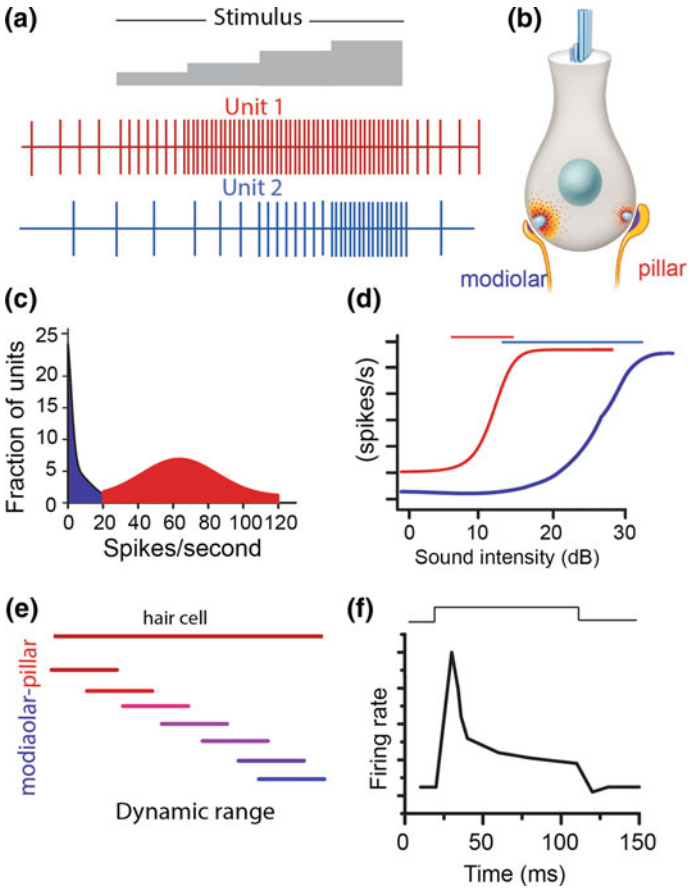

Fig. 7.2 Type I afferent fibers exhibit a heterogeneity in sound threshold, spontaneous release, and synaptic architecture. **a** High spontaneous-rate fiber (Unit 1; *red*) with a lower sound threshold than the low spontaneous-rate fiber (Unit 2; *blue*). Stimulus level (*gray*) is above the units. **b** IHC with two synapses illustrating the larger ribbon and smaller AMPAR patch (*purple*) characteristic of a modiolar synapse compared with the opposite in a pillar synapse. Ca^{2+} influxes (*red dots*) also differ. **c** Frequency histogram of afferent fiber spontaneous activity showing two distributions that are color coded to match the units and locations in **a** and **b**. **d** Plot of Units 1 and 2 from **a** showing the correlation between spontaneous activity and sound threshold to illustrate dynamic range differences between fibers. Lines above plot are dynamic ranges. **e** Theoretical representation of how small dynamic ranges of afferent fibers can align to provide the breadth of dynamic range found within a hair cell (range fractionation) or across a frequency range. **f** Illustration of spike-firing adaptation. Stimulus (*gray line*) and spike rate show two time components to the decrease in firing rate

homeostasis that support such robust synaptic activity (Figs. 7.3, 7.4)? Are the molecular mechanisms of vesicle fusion different at this ribbon synapse compared with more central synapses such as pyramidal cells? Does every vesicle fusion result in a postsynaptic spike and how is postsynaptic timing ensured? To this end,

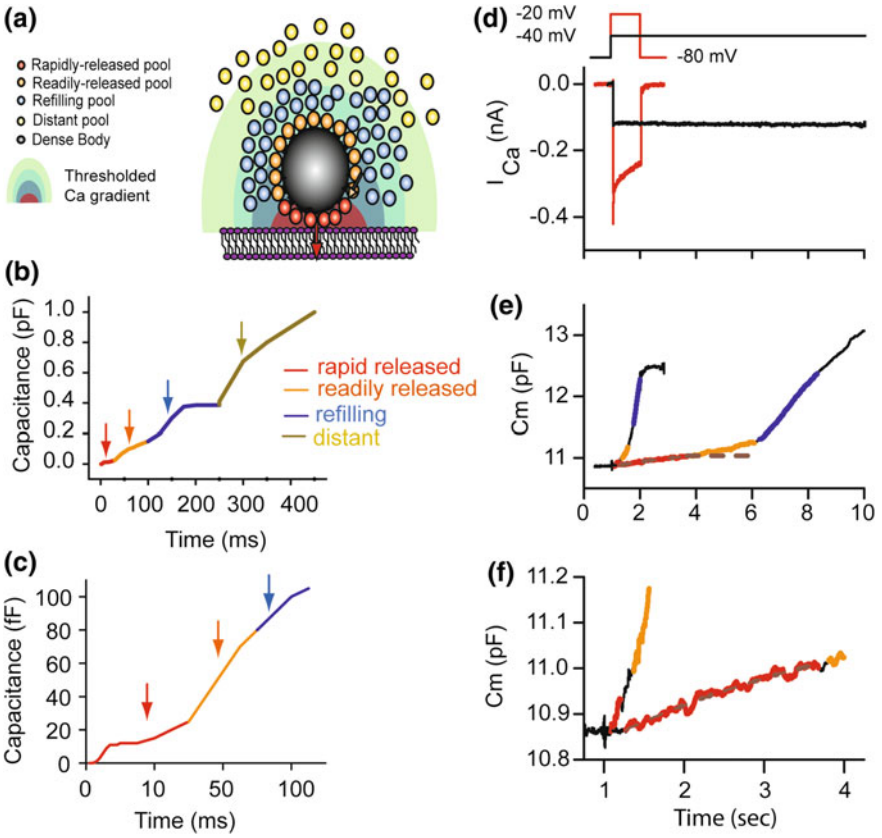

Fig. 7.3 Capacitance changes reflect vesicle fusion and identify vesicle pools. **a** Schematic based on transmission electron microscopy (TEM) reconstruction of hair cell ribbon synapse. **b** Plot of capacitance versus time as estimated from morphological counts of synaptic vesicles at turtle auditory hair cell ribbon synapses. Colors correspond to the vesicle populations in **a** and reflect the pool sizes listed. **c** Expansion of time in the plot in **b** to demonstrate the expected plateau associated with the initial release components. In both **b** and **c**, vesicle replenishment is assumed to be 10× slower than release and so does not mix between pools. **d** Examples of Ca^{2+} currents (I_{ca}) elicited from stimulations (*top lines*) for two turtle hair cells. **e** Capacitance response (Cm) elicited from responses in **d**. Colors are coded for predictions of pools. **f** Expansion of **e** to illustrate pool depletion with the reduced Ca^{2+} influx. **a** adapted from Schnee et al. (2005); **d–f** adapted from Schnee et al. (2011a)

excitatory postsynaptic currents (EPSCs) exhibit a broad range of amplitudes while maintaining consistently fast and uniform kinetic properties, prompting the hypothesis that these synapses use multivesicular release to ensure spike generation (Glowatzki and Fuchs 2002; Fig. 7.5). What mechanisms underlie the broad range of EPSC amplitudes at a given synapse? Synaptic output measured either pre- or postsynaptically appears linear in relation to stimulus intensity under physiological conditions. What does this mean in terms of release mechanisms and regulation?

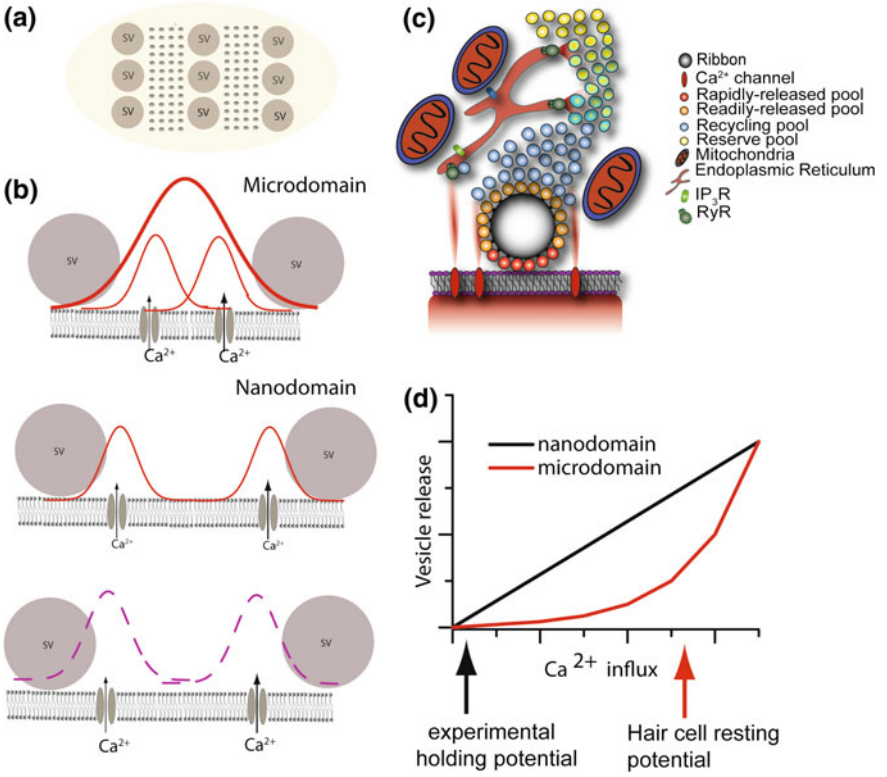

Fig. 7.4 Ca^{2+} homeostasis depends on molecular anatomy as well as hair cell excitability. **a** Likely distribution of Ca^{2+} channels (*small dots*) under the ribbon (*yellow spheroid*) with SVs intermixed. No data exist as to the number of release sites or their distribution near the ribbon, and Ca^{2+}-channel numbers are estimated to be between 70 and 800 per synapse. **b** *top*: Theoretical distribution of Ca^{2+} channels and SVs, showing the individual Ca^{2+} profile (*red*) for each channel (*thin lines*) and the summed response (*thick line*). For microdomain conditions, the channels are close enough that Ca^{2+} summations show that multiple channels can influence a given vesicle. *Middle*: Channels are further separated so that there is no overlap in Ca^{2+} distribution. Under these conditions, nanodomains prevail because individual channels regulate vesicle fusion. *Bottom*: Same distribution as a nanodomain condition but under conditions where Ca^{2+} channels are activated about the resting potential of the cell. Under these conditions, summation can occur, converting a nanodomain into a microdomain. **c** Broader view of the hair cell synapse depicting Ca^{2+}-induced Ca^{2+} release (CICR) components that provide a means of regulating vesicle trafficking independent of Ca^{2+}-channel activation. The ryanodine receptor (RyR) regulates uptake of Ca^{2+} into the endoplasmic reticulum and the inositol trisphosphate receptor (IP_3R) is a membrane glycoprotien complex that is responsible for Ca^{2+} release from the ER. **d** Plot of expected vesicle release under nanodomain or microdomain conditions. *Arrows*: Starting conditions with regard to the resting potential of the hair cell. **b** and **d** adapted from Wang and Augustine (2014); **c** adapted from Castellano-Muñoz and Ricci (2014)

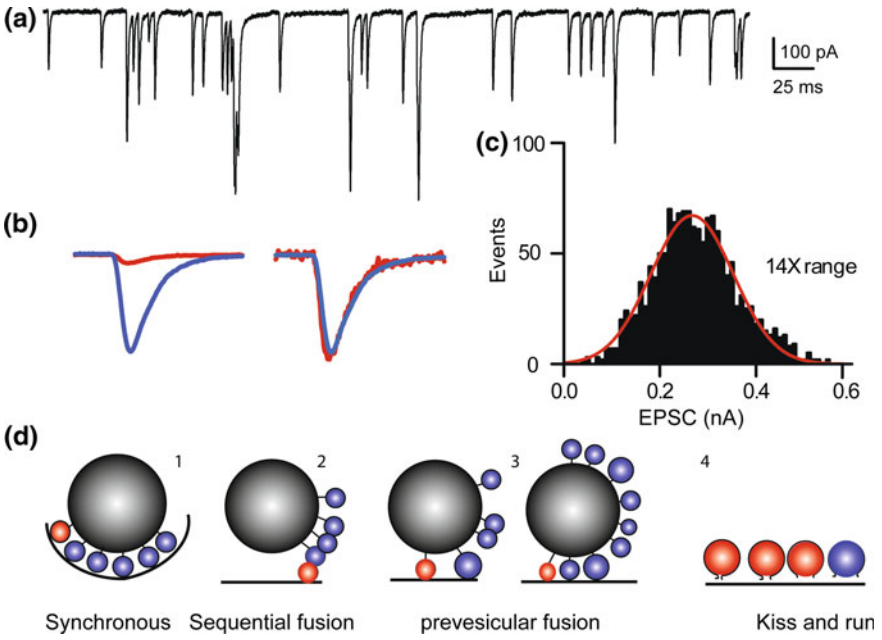

Fig. 7.5 A wide range of excitatory postsynaptic current (EPSC) amplitudes was recorded at multiple synapse fibers in nonmammalian vertebrates as well as at single synapse fibers in mammalian afferent boutons. **a** Recording of spontaneous activity from a low-frequency cell in the turtle auditory papilla that had a single fiber with an average of 20 ribbon synapses. **b** Single EPSCs have similar kinetics, as shown by scaling the smallest EPSCs (*red lines*) to match the largest (*blue lines*). **c** Frequency histogram of EPSC amplitudes shows a 14× range of single events from one fiber, which are well fit by a single Gaussian peak. **d** Various models have been put forward to explain the range in EPSC amplitudes including (1) synchronous fusion of multiple vesicles, which in this example is 6 vesicles fusing simultaneously, producing the mean response of the amplitude distribution in **c**. The red vesicle represents the response of a single vesicle or quanta for 1–3; (2) sequential fusion in which the first fusion triggers a chain of vesicles fusing together; (3) prevesicular fusion either on (*left*) or off (*right*) the ribbon; and (4) variable fusion pore release "kiss and run," in which the vesicle retains its identity

All of these questions remain highly controversial and the focus of multiple laboratories. The following systematically sheds light onto both the reason these questions are critical and also the data that make these questions controversial.

7.2 Anatomy

Unlike in low-frequency hearing end organs such as turtle and frog auditory papillae, where a single fiber innervates a single hair cell and can form up to 50 synapses, the mammalian cochlea has 5–30 fibers innervating a given hair cell where a single synapse drives fiber activity (Merchan-Perez and Liberman 1996; Fig. 7.1c).

Also unlike in frog or turtle hearing organs where the number of synapses varies tonotopically (Sneary 1988; Schnee et al. 2005), mammalian cochlea hair cells maintain a similar number of synapses tonotopically; however, there can be a frequency region where there is a greater number of synapses than in either the higher or lower frequency range (Frank et al. 2009). The tonotopic increase in synapses in low-frequency hearing organs was suggested to facilitate faithful high-frequency signal transfer, in particular using spatial and temporal summation between synapses (Schnee et al. 2013). The functional relevance of the mammalian innervation pattern remains to be determined but may be a means of reducing spatial or temporal overlap between synapses that could degrade timing information at higher frequencies.

Each hair cell-afferent fiber synapse has a presynaptic density called a ribbon or dense body because of its similarity to that observed in the visual system periphery (Fig. 7.1d). In the retina, ribbons are plate-like structures, 30–50 nm wide and up to 1 μm in length, the number and shape of which depend on the cell type, whereas hair cell ribbons vary from spherical, ellipsoid, or bar to a more teardrop shape in mature mammalian inner hair cells (IHCs; Regus-Leidig et al. 2010; Wichmann and Moser 2015). Ribbons come in different sizes and shapes that can be influenced by age, location within the hair cell and even in a circadian manner (Sobkowicz et al. 1982). Ribbons are found presynaptically in cells responding to graded stimuli that release transmitter tonically such as rods, cones, and bipolar cells within the retina; hair cells of the vestibular and auditory system; cells within the pineal gland; and cells in the electrical organs of eels and other fish (Matthews and Fuchs 2010). The function of these ribbons remains elusive, but several theories exist (see Sect. 7.7.2).

In addition to the ribbon, hair cell-afferent fiber synapses have a large synaptic density, typically on the order of 1 μm^2. Ca^{2+} channels cluster centrally under the ribbon (see Sect. 7.5.1 for more details) along with a variety of other traditional synaptic proteins. How many release sites (sites for vesicle fusion) exist per synapse and, specifically, where these release sites are located remains a critical, yet unresolved, question. Postsynaptically, glutamate receptors of the 2,3-benzodiazepine AMPA family type are distributed as a ring across from the dense body structure (Liberman et al. 2011). The ring structure is predicted to optimize uniform detection of glutamate released from vesicles within this ring structure. Other receptor types, such as *N*-methyl-D-aspartate (NMDA), have yet to be identified at this synapse, although metabotropic receptors have been implicated (Peng et al. 2004). Extrasynaptic glutamate receptors have not been reported.

7.3 Afferent Fiber Properties

7.3.1 Spontaneous Activity

Each mammalian afferent fiber makes a single synapse onto an IHC where it receives information about the frequency and amplitude of incoming sound (Fig. 7.1). During sound stimulation, the firing rate increases, adapts, and then

maintains steady-state rates up to 200 Hz for as long as the sound is present (Geisler et al. 1974). All afferent firing is driven synaptically (Robertson and Johnstone 1979; Siegel and Relkin 1987). Afferent spontaneous activity is driven by Ca^{2+} channels that are open at the hair cell resting potential, differentiating it from spontaneous activity in central neurons that may not always be Ca^{2+} driven (Glitsch 2008). Spontaneous activity of afferent fibers varies between 0 and 150 spikes/s despite the hair cell being isopotential. Given that each presynaptic element receives the same receptor potential, what then is responsible for variations in synaptic output (Fig. 7.2b)? Is spontaneous activity different for different hair cells or different between synapses on a given hair cell?

In the cat, synapses on the pillar face (Figs. 7.1b, 7.2) have lower acoustic thresholds and higher spontaneous rates compared with the modiolar synapses (Liberman 1978). Similarly, two populations of fibers are described based on spontaneous activity; one population had no or a very limited spontaneous activity and the other population had a very broad distribution of spontaneous activity (Fig. 7.2c). The limited dynamic range and the broad range of thresholds for firing led to the hypothesis that the broader cochlear dynamic range is encoded by a series of fibers operating at a particular characteristic frequency (CF), each with a unique but overlapping dynamic range (Fig. 7.2e). Thus fibers on a given hair cell would each be activated based on different sound intensities. This idea is somewhat confounded by the concept that the location of a particular CF varies with sound intensity, with louder sounds shifting the place map toward higher frequencies (Chatterjee and Zwislocki 1998). Together, these data may indicate that low spontaneous-rate fibers could correspond to a different CF than high-threshold fibers despite innervating the same hair cell.

The threshold difference between low and high spontaneous-rate fibers can be as large as 60 dB (Yates 1990). Differences in spontaneous activity and threshold are reflected in the synaptic architecture schematically illustrated in Fig. 7.2b, with the modiolar terminals having smaller synaptic ribbons and larger postsynaptic terminals. The latter would correspond to a larger glutamate-receptor area and more mitochondria than the pillar boutons (Liberman et al. 1990). The reduced number of mitochondria in the low spontaneous fibers may underlie their sensitivity to noise damage (Kujawa and Liberman 2009).

What then might account for the difference in sensitivity and spontaneous activity? The modiolar/pillar distribution was recently modified to a habenular (bottom)–to-cuticular (top) axis gradient based on glutamate-receptor (GluR) surface area. The postsynaptic GluR patch surface area varied inversely with ribbon size (Yin et al. 2014), and the difference in GluR numbers was postulated to account for the difference in spontaneous activity postsynaptically. A potential presynaptic mechanism accounting for variance in sensitivity and spontaneous rate between synapses is a difference in Ca^{2+}-channel density between synapses (Frank et al. 2009). Synapses with more Ca^{2+} channels would generate a greater Ca^{2+} signal for the same stimulation and so release vesicles at a higher rate. A third potential mechanism is a difference in the voltage dependence of Ca^{2+}-channel activation between synapses (Meyer et al. 2009). Here, channels that activate at

more negative membrane potentials would respond to smaller stimulations and have more channels open at the resting potential of the cell, leading to more vesicles being released for a given stimulus. Yet another potential difference between low and high spontaneously active fibers is that low spontaneously active synapses have more synaptic vesicles associated with a 350-nm "sphere of influence" around the ribbon (Kantardzhieva et al. 2013).

7.3.2 Stimulus-Driven Activity

Afferent firing is dynamic, responding to a constant-amplitude stimulus with an initial rapid increase in firing that reduces to a constant level, a process termed neural adaptation (Westerman and Smith 1984; Fig. 7.2f). Adaptation is a feature common to sensory systems in which graded stimulation rather than action potential drives vesicle release (Torre et al. 1995). Complete adaptation means that firing rates return to spontaneous levels in the face of a constant stimulus, whereas no adaptation implies a sustained firing rate during stimulation. Adaptation varies considerably depending on the species and how the sound stimulus is presented. For example, high spontaneous-rate fibers adapt more than low spontaneous-rate fibers for short interstimulus intervals, but the opposite applies for long intervals (Rhode and Smith 1985; for a review, see Heil and Peterson 2015). Rates of adaptation vary with species and experimental method, so it is difficult to make generalizations (Heil and Peterson 2015).

Adaptation may be due to the depletion of a small population of synaptic vesicles (Furukawa and Matsuura 1978). Early studies in the goldfish saccule first indicated that a reduction in vesicle release was responsible for spike-frequency adaptation (Furukawa and Matsuura 1978). Capacitance measurements coupled with a computational model confirmed this hypothesis (Schnee et al. 2005). Furthermore, simultaneous hair cell and afferent fiber recordings from rats found a reduction in release as an underlying adaptation (Goutman and Glowatzki 2007).

7.4 Presynaptic Vesicle Release

Communication at chemical synapses is accomplished by synaptic vesicle fusion with the presynaptic membrane in response to a rise in intracellular Ca^{2+} concentration ($[Ca^{2+}]$). Fusion dumps vesicle contents that diffuse across the synaptic cleft and bind with postsynaptic receptors to elicit an electrical response from the neuron. For hair cells, glutamate-filled vesicles must be moved to release sites where Ca^{2+} entry is sensed in order to direct vesicle fusion. Each step in the process requires a specific set of molecules to work cooperatively.

7.4.1 Vesicle Pools

Synaptic vesicles exist in pools (Rizzoli and Betz 2005) that can be defined spatially, functionally, and/or biochemically in terms of their readiness for release. Vesicles that are immediately released comprise the rapidly releasable pool (RaRP), those that can be released after slight preparation (priming) comprise the readily releasable pool (RRP), vesicles that need to be recruited and prepared for release make up the refilling pool, and, finally, typically the largest pool of vesicles that is not often activated is the reserve pool (Denker and Rizzoli 2010). At ribbon synapses, vesicle pools are often defined by location at the synapse or nearness to the ribbon. The RaRP represents vesicles between the ribbon and the plasma membrane, the RRP may be the remaining vesicles tethered to the ribbon, the refilling pool represents those vesicles not tethered to the ribbon but near the synapse, and the reserve pool are those vesicles that exist at a distance away from the ribbon (Schnee et al. 2005; Fig. 7.3a). An apparent difference between conventional synapses and ribbon synapses is the ease with which vesicles can move between pools in order to maintain release at high levels (Schnee et al. 2005). Although no direct evidence links vesicle pools monitored physiologically to ribbon location, there is compelling correlative data to this effect (Lenzi and von Gersdorff 2001). Figure 7.3 presents a cartoon that schematizes morphologically defined vesicle pools with their physiological correlate.

7.4.2 Membrane Capacitance Measurements

As vesicle fusion increases, the membrane surface area also increases (at least until the membrane is retrieved), and presynaptic monitoring of changes in the membrane capacitance has been used to monitor calcium-dependent synaptic vesicle fusion (Parsons 1994; Nouvian et al. 2006). Paired recordings that include postsynaptic nerve recordings and presynaptic capacitance measurements show a linear correspondence between EPSC charge and capacitance changes (Li et al. 2009). Vesicle pools have also been defined by identifying depletable pools of vesicles by monitoring capacitance in response to brief depolarizations that elicit Ca^{2+} influx (Parsons 1994; Beutner et al. 2001). The most carefully examined and accepted pool, the RaRP, shows good correlation with the number of synapses and vesicles counted in hair cells (Eisen et al. 2004; Khimich et al. 2005). Paired recordings of hair cells and afferent fibers in mammals and frogs confirm a rapidly depletable pool of EPSCs that may underlie fast adaptation of nerve firing (Keen and Hudspeth 2006; Goutman and Glowatzki 2007).

An example of the predicted capacitance measurement is presented in Fig. 7.3b, where plateaus are depicted based on morphological estimates of vesicle numbers in each pool. Isolating vesicle pools is particularly difficult at hair cell ribbon synapses because there is little vesicle depletion, presumably due to robust vesicle

trafficking (Schnee et al. 2005). The RaRP in mammalian IHCs can also be quite small, near the resolution of the measurement. Attempts at identifying pools using paired stimulation in which the first step duration is selected to deplete a given pool size and the second and subsequent pulses meant to track refilling gave the startling result that rather than depletion, facilitation was observed (Schnee et al. 2011b). Additionally, capacitance can continue to increase over a large range of values consistently greater than predicted for pool sizes Together these data support a robust vesicle trafficking mechanism whose variance might lead to masking (or prevention) of pool depletion.

The recently developed multi-sine wave method using Jclamp software (Santos-Sacchi 2004) continually monitors capacitance, providing a real-time monitor of capacitance changes during stimulation. The continuous monitoring of capacitance changes during Ca^{2+}-current activation revealed exocytic depression that was missed with the before and after measurements required of the single sine technique (Schnee et al. 2011a, b). Figure 7.3d–f shows an example of a capacitance recording from two turtle auditory hair cells stimulated with protocols that drove Ca^{2+} entry at different rates. Holding the cell at −80 mV and depolarizing to −20 mV (the maximal Ca^{2+} current) resulted in rapid capacitance changes with little evidence of pool depletion. The Ca^{2+} versus capacitance plot was best fit by a third-order Hill equation similar to that observed when Ca^{2+} was uncaged intracellularly (Beutner et al. 2001). However, with a depolarization that elicits only a portion of the Ca^{2+} current over a longer duration, depletable pools were more clearly delineated (Fig. 7.3d–f). Even when depletable pools were identified, there was considerable within-cell variance in pool size and in the stimulus size required to elicit the response. This variance is ascribed to the robust movement of vesicles between pools. Pool refilling may be very fast, making it difficult to deplete pools, but this also makes the pool size dependent on previous stimulation events.

7.4.3 Multiple Release Components

Afferent nerve firing rates increase linearly with sound level, and so it was expected and observed that capacitance changes would also increase linearly with Ca^{2+} load (representing stronger stimulation). Short-duration stimulations support the idea that release is linear with Ca^{2+} influx. In turtles, even long stimulations for seconds appear linear when monitored with the single sine technique (Schnee et al. 2005). However, continuous monitoring of capacitance demonstrated that vesicle release plotted as a function of Ca^{2+} influx is not linear (Fig. 7.3b). Typically, there is a first component whose rate and magnitude increases with Ca^{2+} load and where saturation can be observed. Longer or stronger stimulations result in a superlinear component where the release rate is greatly increased. Using steps eliciting the peak Ca^{2+} current, the two components of release tend to blur in time but are distinct for stimulations that slow Ca^{2+} entry by reducing channel open probabilities (Fig. 7.3e, f). Implications of these data in terms of Ca^{2+} homeostasis is discussed in Sect. 7.5,

but in terms of function, these data appear anomalous because single-unit measurements suggest a linear increase with stimulus intensity. The key to understanding this anomaly is that around the resting potential of the cell, the two release components overlap so that total release appears linear (Schnee et al. 2011b). A simple interpretation of the two release components is that release sites do not all have vesicles loaded when the hair cell is held at −80 mV and vesicle trafficking is not optimal. During depolarization, however, vesicle trafficking is more robust due to constant Ca^{2+} entry, filling all release sites faster than the vesicles can be exocytosed. Thus, superlinear release may represent a maximal release rate when all sites are filled. In agreement with this interpretation, holding the hair cell membrane depolarized increases the RaRP size and rate of release in vestibular and inner hair cells in Ca^{2+}-uncaging experiments (Vincent et al. 2014). Also, Ca^{2+}-dependent vesicle trafficking underlies potentiation of synaptic release at more physiological resting potentials (Cho et al. 2011; Levic et al. 2011). These results are consistent with the theoretical framework in which summation of multiple nonlinear processes with different sensitivities across active zones can produce a quasi-linear process (Heil and Neubauer 2010).

It is not surprising that vesicle trafficking is robust at hair cell ribbon synapses given that afferent firing is maintained for long periods of time (Fuchs and Parsons 2006). Few data exist as to the mechanism underlying vesicle trafficking at the auditory synapse, but trafficking is enhanced by Ca^{2+} (Goutman and Glowatzki 2011; Levic et al. 2011). Whether trafficking involves recycling of existing vesicles, recruitment of distant vesicles or creation of new vesicles remains to be determined. Also, the molecular mechanisms involved in trafficking need to be identified. The hair cell-specific protein otoferlin may be involved (Pangršič et al. 2010; Levic et al. 2011; see Sect. 7.7.4). Myosin VI is also implicated in trafficking of synaptic and basolateral machinery, although not explicitly for vesicle trafficking; its interactions with otoferlin make it a strong candidate (Heidrych et al. 2009; Roux et al. 2009).

7.5 Calcium Homeostasis

7.5.1 Calcium-Channel Molecular Components

Because each aspect of presynaptic synaptic activity, including vesicle priming, trafficking, fusion, and endocytosis, may be modulated by Ca^{2+} at some level, understanding the dynamics of Ca^{2+} homeostasis is critical to understanding synaptic activity. Cochlear hair cells use the $Ca_V1.3$ Ca^{2+} channel exclusively to drive synaptic release (Platzer et al. 2000). These channels are rapidly activating, show moderate Ca^{2+}-induced inactivation, and are sensitive to external pH changes (Zampini et al. 2014). The β2 subunit is responsible for inactivation and for anchoring the channel, and its absence results in a dramatic reduction in Ca^{2+}-channel density, a decrease in synaptic release, and defects in cochlear amplification

(Neef et al. 2009). The Rab3 interacting protein RIM2 may also play a role in regulating inactivation in mouse IHCs (Gebhart et al. 2010). The inactivation process can result in up to 50% of channels being inactivated at the resting potential of the hair cell (Schnee and Ricci 2003; Grant and Fuchs 2008). Ca^{2+} channels cluster in 2–3 strips of tightly packed channels at the synaptic zone right under the ribbons (Roberts 1994; Rutherford 2015; Fig. 7.4a) and the number of channels per synapse can range from 80 to 800 (Roberts et al. 1990; Brandt et al. 2005). The variance in channel number and their distribution per synapse may contribute to variations in synaptic efficacy (Wong et al. 2013). The physical location of these channels, particularly in reference to vesicle fusion sites, is a critical piece of missing information when trying to quantify how Ca^{2+} through these channels controls vesicle fusion (Schneggenburger et al. 2012).

7.5.2 Calcium Clearance

Equally important to Ca^{2+} entry is Ca^{2+} clearance. Because postsynaptic spike timing is controlled by the timing of presynaptic vesicle fusion, which in turn is tightly coupled to Ca^{2+} entry, it is critical that Ca^{2+} levels be rapidly and efficiently reduced after excitation (Ceriani and Mammano 2012). Free [Ca^{2+}] is typically reduced by diffusion, by binding to fixed or mobile Ca^{2+} buffers, and by Ca^{2+} being pumped either out of the cell using PMCA-type pumps or into intracellular storage compartments such as endoplasmic reticula via sarco(endo)plasmic reticulum Ca^{2+}-ATPase (SERCA) pumps. Mitochondria, which cluster around synapses, play a complex role in Ca^{2+} homeostasis, not only serving as a Ca^{2+} sink but also providing the ATP necessary for extrusion and uptake. Blocking Ca^{2+} uptake into mitochondria does not affect Ca^{2+}-current amplitude or affect heterogeneity in postnatal day 14–18 mouse IHCs (Frank et al. 2009), suggesting a limited role in hair cells as a Ca^{2+} sink (but see Zenisek and Matthews 2000). Estimates of mobile buffers range from 0.1 to 3 mM BAPTA equivalents, varying between hair cell types (Ricci et al. 2000; Beutner et al. 2001). Measurements of Ca^{2+} entry and clearance at presynaptic active zones in bullfrog saccular hair cells could be modeled with only a mobile buffer equivalent to 1 mM BAPTA (Issa and Hudspeth 1996). A triple knockout of parvalbumin, calbindin, and calretinin, three of the major Ca^{2+}-binding proteins in IHCs, was without effect except for a minor increase in exocytosis and enhanced Ca^{2+}-dependent inactivation of the Ca^{2+} current, suggesting buffering may not be that significant for synaptic Ca^{2+} clearance (Pangršič et al. 2015).

Another potential source of clearance is via plasma membrane Ca^{2+} pumps. PMCA1 localizes to the basolateral membrane but has not been reported to cluster near to synaptic zones (Polimeni et al. 2007). Indirect evidence from Ca^{2+} imaging (Frank et al. 2009; Schnee et al. 2011b) and also electrophysiological data investigating large-conductance Ca^{2+}-activated potassium (BK) channels may support the idea of a rapid clearance mechanism (Ricci et al. 2000).

7.5.3 Nanodomain Versus Microdomain

The molecular anatomy at the synapse is critical for determining how Ca^{2+} regulates vesicle fusion. Do single Ca^{2+} channels activate and drive vesicle fusion (nanodomains) or does release require summation between channels (microdomains)? At some conventional synapses, a single or few Ca^{2+} channels control synaptic vesicle fusion. In two classical synapses, the neuromuscular junction (NMJ) and the squid giant synapse, Ca^{2+} channels are located within 20 nm of the vesicles and opening of a single channel can drive release (Eggermann et al. 2012). Such nanodomain regulation is defined by insensitivity to the slow Ca^{2+} buffer EGTA and a block by millimolar concentrations of the fast buffer BAPTA, by the distance of the Ca^{2+} source from the vesicles, and by the linear relationship of $[Ca^{2+}]$ and release (Fig. 7.5). Microdomains are similarly defined but apply when the distance between the Ca^{2+} source and vesicle is 100 nm or greater or when release is more exponential and the response to EGTA can be as effective as that to BAPTA. Thus nanodomain and microdomain regulation can arise from the morphological distribution of channels relative to synaptic release sites as depicted in Fig. 7.4a. They are likely also regulated by factors modulating Ca^{2+} clearance as well as by the resting potential of the cell that dictates the Ca^{2+}-channel open probability. Additionally, the classical definitions of nanodomain and microdomain may not be directly adaptable to a synapse where hundreds of channels are packed tightly together in strips at an unknown distance from an unknown number of release sites. Nonetheless, data indicate that vesicle fusion in hair cells can operate from a nanodomain system (Brandt et al. 2005; Graydon et al. 2011). These experiments were performed from a negative holding potential to ensure that Ca^{2+} channels were closed and used brief duration depolarizations to voltages eliciting a maximal current, demonstrating that Ca^{2+} channels are close enough to release sites to create a nanodomain condition.

The closer Ca^{2+} channels are clustered, the more difficult it is to have a nanodomain (Fig. 7.4b) because the Ca^{2+} entering adjacent channels will overlap and sum in space. Biophysically, this can be controlled by limiting channel open times. However, under physiological conditions, hair cells have a resting potential at which approximately 20–30% of Ca^{2+} channels are continually activated (Farris et al. 2006; Johnson et al. 2011). For nanodomains to be maintained with this constant influx of Ca^{2+}, a very robust Ca^{2+} clearance mechanism must be in place to compensate for this constant Ca^{2+} load that can saturate local buffers, leading to summation of Ca^{2+} channels packed at high density. A second limitation to the nanodomain hypothesis is that if single Ca^{2+} channels are responsible for driving vesicle fusion, temporal fidelity would be limited by the stochastic nature of Ca^{2+}-channel activation so the ability to faithfully reproduce the analog receptor potential would be compromised (Coggins and Zenisek 2009) Thus more information is needed to determine if nanodomains are functionally relevant at hair cell synapses.

Another property of nanodomains is that release is linear with calcium influx because channels and release sites are recruited linearly and independently with depolarization (Wang and Augustine 2014). Microdomain release is better portrayed as an exponential relationship (Fig. 7.4b, d), where summation between channels augments vesicle release. Because in vivo single-unit activity shows a linear relationship with stimulus intensity, a nanodomain system might be implied. However, as described in Sect. 7.4.3, plots of capacitance as a function of Ca^{2+} entry are not linear, except over a very limited stimulus range. How can we reconcile these disparate pieces of data? In experiments in which capacitance measurements were made at the resting potential of the hair cell, the exponential relationship appeared linear because the set point on the Ca^{2+} entry versus release plot moves to the right where the curve is steep and apparently linear (Schnee 2011b; Fig. 7.4d). Thus, the hair cell may be a system that moves between nanodomain and microdomain behavior depending on the resting potential of the cell and also likely on Ca^{2+} clearance mechanisms.

7.5.4 Calcium-Induced Calcium Release

Two additional factors add to the complexity of understanding Ca^{2+} dynamics at ribbon synapses. First, does the ribbon provide a diffusion barrier to Ca^{2+} that might greatly impede nanodomain regulation by forcing comingling of Ca^{2+} from different channels or is it physically transparent to Ca^{2+} and so has no effect on diffusion (Graydon et al. 2011)? Theoretical approaches suggest that the ribbon can have a significant effect on Ca^{2+} distribution at the synapse. Direct data are, however, lacking due to the technical limitations of imaging such a confined space.

The second confounding issue is the presence of Ca^{2+}-induced Ca^{2+} release (CICR). Multiple reports demonstrate a clear role for CICR in hair cells, with several also demonstrating a role in modulating synaptic activity (Kennedy and Meech 2002; Lelli et al. 2003; for a review, see Castellano-Muñoz and Ricci 2014). It seems unlikely that CICR is directly altering vesicle fusion because the kinetics for onset and offset are too slow to maintain release timing. Thus it is more parsimonious (and is supported by data) that vesicle trafficking is Ca^{2+} dependent and regulated by CICR (Castellano-Muñoz et al. 2016). The requirements to control timing of vesicle fusion are that the Ca^{2+} signals turn on and off quickly. If vesicle replenishment is Ca^{2+} dependent, the tight control of the Ca^{2+} signal at the synapse would be quite inefficient at trafficking vesicles. With CICR, however, the signal could be maintained away from the synapse and promote trafficking in a more continuous fashion without compromising the tight regulation at the synapse. A significant amount of work remains to be done to fully elucidate Ca^{2+} homeostatic mechanisms.

7.6 Postsynaptic Measurements

Synaptic vesicle fusion at the hair cell synapse releases the excitatory neurotransmitter glutamate, activating the postsynaptic AMPA receptors Glur2 and Glur3 (Fujikawa et al. 2014), depolarizing the nerve fiber, and triggering action potentials. EPSCs have very rapid activation and deactivation kinetics and can range 20-fold in amplitude at a given synapse (Schnee et al. 2013; Fig. 7.5a). Cyclothiazide reduces AMPA-receptor desensitization, and slows the EPSC kinetics of afferent fibers, indicating desensitization occurs at this synapse (Glowatzki and Fuchs 2002). However, paired recordings of hair cell and afferent fiber show a linear relationship, indicating that receptor saturation and desensitization are minimal (Keen and Hudspeth 2006; Goutman and Glowatzki 2007).

Frequency histograms of EPSC amplitudes are skewed and typically biased toward larger amplitude responses (Glowatzki and Fuchs 2002; Grant et al. 2010). Variations in amplitude histograms have been ascribed to variance in vesicle transmitter content or to release of vesicles from multiple sites, thus summating in time and/or space. The content of synaptic vesicles can vary in transmitter concentration and vesicle volume can vary with synaptic vesicle size. At most synapses, larger EPSCs result from summation of multiple vesicles released in a short time frame so that temporal jitter in release leads to a slowing of the rise and decay times. At ribbon synapses, the rise and decay times of the smallest and largest EPSCs measured in a given fiber are generally very similar (Glowatzki and Fuchs 2002; Fig. 7.5b). The consistency in kinetics suggested a synaptic specialization termed multivesicular release (MVR). Multivesicular is classically defined as >1 synaptic vesicle released per release site at the active zone (Rudolph et al. 2015), so a prerequisite to defining a synapse as uni- or multivesicular is the identification of number and location of release sites at a given synapse. At auditory ribbon synapses, the number and location of release sites are unknown so to avoid confusion, multiquantal release (MQR) will be used to define potential mechanisms that might account for EPSCs larger than single-vesicle fusion. Of the potential mechanisms described in Fig. 7.5 to account for the broad distribution in EPSC amplitudes, only one actually represents multivesicular release, although all fit under the MQR umbrella.

7.6.1 Multiquantal Release

MQR may be due to synchronized fusion of multiple single vesicles (Fig. 7.5d1). Here, tightly controlled timing of vesicle release would underlie the lack of change in postsynaptic kinetics. Of course, the underlying assumption is that there are multiple release sites per ribbon synapse. MQR may also be due to release of large prefused vesicles (Matthews and Fuchs 2010; Fig. 7.5d3). Synaptic vesicle size variation can account for the 14× variability in EPSC amplitudes observed in

turtles (Schnee et al. 2013). Other proposed models include sequential fusion, true MVR (Fig. 7.5d2) in which the first vesicle docked to the plasma membrane fuses, promoting vesicles above it to attach and fuse together rather like a sausage, releasing their contents through the fusion pore formed by the first vesicle (Matthews and Fuchs 2010). The ribbon may facilitate prefusion of tethered vesicles (Fig. 7.5d3). Finally, kiss-and-run vesicle release (Fig. 7.5d4) has also been proposed as a potential mechanism for MQR. Here, the largest EPSC represents full fusion of a single vesicle, whereas smaller EPSCs represent varying fusion pore open times (Chapochnikov et al. 2014). One rationale for this hypothesis is that MQR can only support release at rates up to 120 Hz if, on average, 6 vesicles (mean EPSC; Fig. 7.5c) are required to trigger an action potential. Single-vesicle fusion per action potential on the other hand could theoretically support rates as high as 700 Hz (highest synaptic vesicle release rate for IHCs; Pangršič et al. 2010; Chapochnikov et al. 2014). At present, there is no direct evidence to support a particular mode of MQR, but there are hints that might support each of those listed. Although we are rapidly gaining knowledge, there remain major questions to be resolved, including whether MVR exists at all ribbon synapses.

7.6.2 *Alternate Interpretations from Multiquantal Release*

It remains plausible that classical quantal release can account for the broad and skewed EPSC amplitude histograms (Jarsky et al. 2010). The classical variance-mean analysis describing release at the NMJ (Del Castillo and Katz 1954) characterizes amplitude-frequency histograms with modal peaks that are multiples of the measured single quanta peak and release statistics follow a Poisson distribution. Amplitude histograms recorded from auditory synapses are quite skewed, particularly in rats and mice, which is not expected if EPSCs are generated by single vesicles (Glowatzki and Fuchs 2002). A confounding problem in non-mammal hearing animal models is the large number of synapses (up to 50) in a single afferent fiber, which may obscure peaks.

Altering the probability of release by modifying Ca^{2+} homeostasis is classically used as a means of identifying the miniature quantal size (Del Castillo and Katz 1954). Lowering external Ca^{2+} reduces EPSC amplitude and frequency in turtle, frog and mammalian auditory hair cells, suggesting a quantal component to release (Li et al. 2009; Schnee et al. 2013; Chapochnikov et al. 2014), although large EPSCs are still observed under these conditions. These data would therefore support models for MQR except for prevesicular fusion mechanisms where it is predicted that EPSC amplitude would remain high. However, regulating intracellular Ca^{2+} with buffers affects the probability of release but not the amplitude of the EPSC at mammalian synapses (Goutman and Glowatzki 2007). Ten millimoles of the fast intracellular Ca^{2+} buffer BAPTA shifted the range of uniquantal events to more depolarized potentials, showing MQR to be Ca^{2+} dependent in frog hair cells (Li et al. 2009). In addition, hyperpolarization, which reduces Ca^{2+} entry, also

reduced EPSC amplitude. A potential function for EPSC amplitude being Ca^{2+} independent at mammalian synapses may be to ensure that the response of individual afferent neurons is invariant with sound intensity (Fuchs 2004). These studies suggest a fundamental difference or at least multiple mechanism(s) between ribbon synapses of different end organs.

7.6.3 Functional Relevance of Multiquantal Release

One possible advantage of MQR at the auditory synapse is that the fast onset of a large EPSC can provide a rapid and precise signal for timing and ensure the generation of an action potential for each EPSC (Wittig and Parsons 2008). Recorded afferent fibers are suggested to spike with each excitatory postsynaptic potential so that the frequency of firing directly matches vesicle fusion (Siegel 1992; Rutherford et al. 2012). Misses in action potential generation are presently ascribed to postsynaptic refractoriness in the spike generation mechanism. If true, the significance of the breadth in EPSC amplitudes becomes more obscure. Perhaps EPSC amplitudes regulate the time to spike threshold where the time to spike shortens as EPSC amplitude increases (Fuchs 2004). Determining the underlying functional relevance of the EPSC distribution is critical for understanding signal processing and also will likely shed light into the existence and mechanism of the MQR.

7.7 Synaptic Proteins

The task of sensory ribbon synapses is to detect a wide range of graded analog sensory signals and convert this information into synaptic release events that, in turn, are transformed by the postsynaptic elements into a digital signal conveyed by action potentials for processing in the brain. Ribbon synapses are capable of temporally and spatially synchronized release of synaptic vesicles at rates up to hundreds of hertz (Meyer and Moser 2010). The protein structure of ribbon synapses is similar to conventional synapses, but there are notable exceptions for key proteins. In addition, the hair cell, unlike other ribbon-containing cells, has otoferlin, a protein implicated in most presynaptic aspects of synaptic transmission studied thus far (Fig. 7.6).

7.7.1 Ribbon Proteins

The synaptic ribbon is composed in part of individual subunits of RIBEYE that have an A and B domain. The A domain has a unique structure involved in establishing the ribbon scaffold, whereas the B domain is nearly identical to a

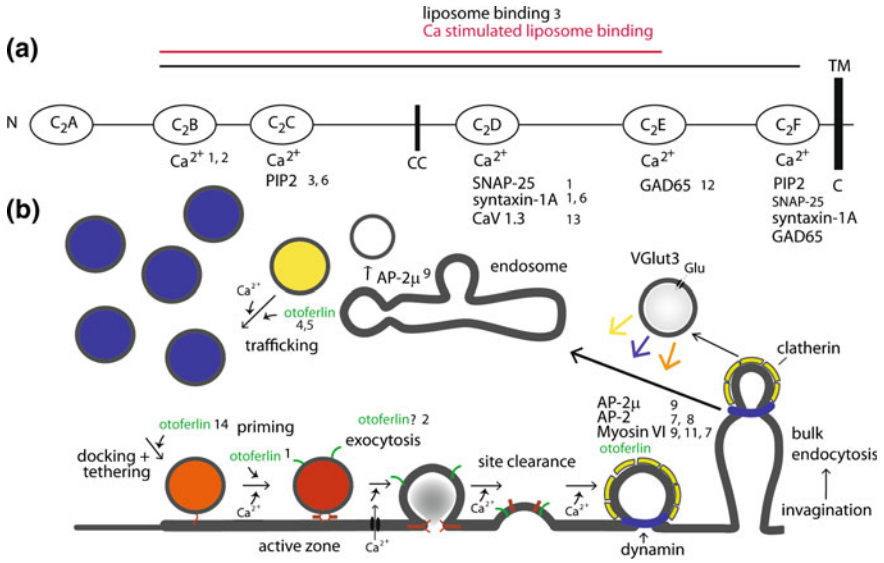

Fig. 7.6 Schematic diagram of otoferlin structure with binding interactions at the C2 domains and proposed roles in the synaptic vesicle cycle. **a** Otoferlin has six C2 domains and, with the exception of the C2A domain, all bind Ca^{2+} and phospholipids. CC, coiled-coiled domain; TM, proposed transmembrane domain. **b** Otoferlin is proposed to have multiple actions in the SV cycle, including trafficking, docking and tethering, priming, vesicle fusion, and clatherin-mediated endocytosis. *Red*: pool membership with readily releasable pool (RRP); *orange*: ribbon-attached vesicle; *blue*: refilling pool; *yellow*: distant pool. The synaptic ribbon has been removed for clarity. Numbers indicate the following references: 1, Roux et al. (2006); 2, Johnson and Chapman (2010); 3, Padmanarayana et al. (2014); 4, Pangršič et al. (2010); 5, Levic et al. (2011); 6, Ramakrishnan et al. (2014); 7, Duncker et al. (2013); 8, Neef et al. (2014); 9, Jung et al. (2015); 10, Roux et al. (2009); 11, Heidrych et al. (2009); 12, Wu et al. (2015); 13, Ramakrishnan et al. (2009); 14, Vogl et al. (2015). **b** adapted from Sudhof (2004)

transcription repressor, CtBP2, and may have enzyme activity (Zanazzi and Matthews 2009). The B domain opposes the plasma membrane and may be involved in tethering synaptic vesicles to the ribbon. RIBEYE is the only known ribbon-specific protein and is estimated to comprise about 65% of the total protein in goldfish retinal bipolar-cell ribbons (Schmitz et al. 2000). The A and B domains can polymerize when expressed together and form structures reminiscent of synaptic ribbons (Schmitz et al. 2000). The mature IHC ribbon has a distinct laminar substructure whose function is unknown. Knockdown of RIBEYE in zebrafish affected Ca^{2+}-channel clustering and afferent innervation, whereas over-expression produced ectopic aggregates of RIBEYE with associated Ca^{2+} channels (Sheets et al. 2011).

7.7.2 Ribbon Function

Multiple functions are ascribed to the ribbon. Ribbons may serve to increase the available pool size for synaptic vesicle release by acting as biological Velcro, catching freely diffusible vesicles and keeping them near to release sites (Matthews and Fuchs 2010; Safieddine et al. 2012; Sudhof 2012). They may similarly act as a conveyor belt to drive vesicles to release sites to maintain high levels of release (Vollrath and Spiwoks-Becker 1996). Ribbons may regulate timing of vesicle fusion or be important for prevesicular fusion, possibly needed to generate larger vesicles (Matthews and Sterling 2008). More recently, ribbons were suggested to be a location for vesicle production, where newly obtained endosomes might interact with CtBP2 to bud off a new supply of synaptic vesicles (Kantardzhieva et al. 2012). Alternatively, or in conjunction with these roles, ribbons could act as a physical diffusion barrier for Ca^{2+}, resulting in high local Ca^{2+} levels that drive vesicle fusion (Graydon et al. 2011). All are plausible, and data as yet do not distinguish between these possibilities.

7.7.3 Synaptic Density Proteins

Synapses have synaptic densities at the active zone that function in priming, docking, and maintaining vesicle populations. There are five main proteins that comprise the synaptic active zone, which are evolutionarily conserved across synapses: Rab3-interacting molecule (RIM); mammalian uncoordinated homology 13 (Munc13); RIM-binding protein (RIM-BP); α-liprin and glutamine; and leucine-, lycine-, and serine-rich protein (ELKS; Sudhof 2012). These proteins form a single large protein scaffold which docks and binds synaptic vesicles, recruits Ca^{2+} channels and regulates synaptic plasticity (Sudhof 2012). Three of these core proteins (α-liprin, RIM-BP, and ELKS) are missing from auditory ribbon synapses, whereas only α-liprin is absent from retinal ribbon synapses (Wichmann and Moser 2015). RIM-BP interacts with RIM in recruiting Ca^{2+} channels (mainly N and P/Q type), so it is not surprising that it is lacking only at the L-type auditory synapse. Harmonin, which is necessary for $Ca_v1.3$ function in IHCs, may replace RIM-BP (Gregory et al. 2013). Identifying the alternative proteins used and the functional consequences of the change are major goals of ribbon synapse investigations.

Bassoon, one of the largest proteins at the synapse, anchors the ribbon to the plasma membrane in hair cells and to the arciform density in the retina (tom Dieck et al. 2005). Genetic disruption of bassoon in mice results in a large number of floating ribbons in both photoreceptors and hair cells. At the auditory synapse, Ca^{2+}-channel density and geometry is disrupted and fast and sustained synaptic release is significantly reduced when bassoon is absent, resulting in degradation of spike timing and reduced spontaneous and sound-evoked nerve firing (Khimich et al. 2005; Buran et al. 2010). Piccolino, a shorter isoform of piccolo, was recently

discovered at ribbon synapses of photoreceptors and bipolar and inner hair cells and may also have an anchoring role (Regus-Leidig et al. 2013). Knockdown of piccolino results in abnormal ribbon structure in photoreceptors.

The synaptic vesicle cycle begins with filling the synaptic vesicle with glutamate transported by Vglut3 in the auditory IHC (Ruel et al. 2008). The filled synaptic vesicle is trafficked/diffused to the active zone, docks, is primed, and with a Ca^{2+} signal fuses to the active zone, releasing its content after which the synaptic vesicle (membrane and proteins) is cleared from the active zone and recovered by one of several endocytic pathways (see Sudhof 2004 for a review; Fig. 7.6b).

Synaptotagmins, transmembrane proteins associated with synaptic vesicles, are the Ca^{2+} sensor regulating the last steps of vesicle fusion (Tang et al. 2006). The role of synaptotagmins (15 isoforms, 8 with Ca^{2+}-binding domains in vertebrates; Sudhof 2002) in release dynamics in mammalian IHCs is controversial. Synaptotagmins-1, -2, and -4 are reported in mature gerbil IHCs (Johnson et al. 2010). Synaptotagmin-4 is proposed to be responsible for the Ca^{2+}-dependent linear release kinetics due to its lack of Ca^{2+}-binding sites (Sudhof 2002). In the early development of IHCs (up to postnatal day 4), synaptotagmins-1, -2, and -7 were detected but disappeared after the onset of hearing (Beurg et al. 2010). Hair cell vesicle fusion was unaffected in newborn mice lacking synaptotagmins-1, -2, and -7, and in posthearing animals lacking synaptotagmins-2 and -7, vesicle fusion was normal. mRNA for synaptotagmins-5, -6, -13, and -15 was detected in adult IHCs, but no functional role has been demonstrated (Nouvian et al. 2011). Possibly an unidentified protein may replace synaptotagmin as the Ca^{2+} sensor to regulate vesicle fusion in mature IHCs (like otoferlin) or an as yet unexplored isoform of synaptotagmin replaces the conventional isoforms in hair cells (see Sect. 7.7.4).

7.7.4 Otoferlin

7.7.4.1 Otoferlin Genetics

Mutations (60+) in the gene *OTOF*, which codes for the protein otoferlin, result in nonsyndromic hearing loss in humans (Yasunaga et al. 1999). The otoferlin mutation, together with other synaptic mutations affecting the $Ca_V1.3$ Ca^{2+} channel and synaptic vesicle protein Vglut3, are termed synaptopathies, and all underlie human deafness without altering cochlear mechanics (Brose et al. 2010). Loss of otoferlin results in a severe reduction in Ca^{2+}-dependent exocytosis without affecting the structural integrity of the synapse. Otoferlin is a member of the ferlin family of Ca^{2+}-binding proteins with 6 C2 regions that can bind Ca^{2+} and phospholipids (Pangršič et al. 2012; Fig. 7.6a). The C2 domains of otoferlin are universal Ca^{2+}-binding modules found in other synaptic proteins such as synaptotagmin-1 and Munc13. Otoferlin is a transmembrane protein that is expressed in mammalian inner, outer (immature), and vestibular hair cells and in four other vertebrate classes including sharks and rays, bony fish, amphibians, and

birds but not at ribbon synapses outside the inner ear (Goodyear et al. 2010). The amino acid sequence of the C2 domains shows remarkable homology across species, with the mouse sequence being the most homologous to human and to zebrafish the least (Chatterjee et al. 2015). The otoferlin knockout mouse is profoundly deaf due to a failure in synaptic transmission (Roux et al. 2006; Pangršič et al. 2010). Zebrafish lacking otoferlin have defects in hearing, balance, and locomotion, and truncated forms of otoferlin containing only C2 domains A to C restored function (Chatterjee et al. 2015). The pachanga mouse mutation has greatly reduced otoferlin levels, resulting in reduced vesicle fusion (Pangršič et al. 2010), and it was argued that otoferlin was critical for vesicle trafficking and fusion. Otoferlin colocalizes to the ribbon and the synaptic vesicles, as shown in immunogold electron microscopy from mouse IHCs (Roux et al. 2006) and is also found throughout the cell, often with a basolateral and apical surface concentration (Heidrych et al. 2008; Pangršič et al. 2012).

7.7.4.2 Otoferlin in Vesicle Fusion and Trafficking

Otoferlin is postulated to be the Ca^{2+} sensor in auditory and vestibular hair cells in an analogous manner to synaptotagmin-1 at conventional synapses. The knockout animal is deaf and exhibits a clear synaptopathy. Uncaging Ca^{2+} was not able to rescue vesicle fusion (Pangršič et al. 2010). In vitro assays show that otoferlin binds Ca^{2+} and has a Ca^{2+}-dependent interaction with SNARE proteins syntaxin-1 and SNAP25 (Roux et al. 2006; Ramakrishnan et al. 2014; Fig. 7.6a). The physiological role of this interaction is questionable because the SNARE proteins are not present at the auditory synapse (Nouvian et al. 2011). Five of the six C2 domains bind Ca^{2+} with affinities that are increased $7\times$ in the presence of membranes in vitro. These domains also stimulate membrane fusion in a Ca^{2+}-dependent manner that is the first proof that otoferlin can directly trigger membrane fusion (Johnson and Chapman 2010). Thus the biochemistry would support a role for otoferlin in modulating vesicle fusion.

Otoferlin is present in vestibular hair cells and may have a role in increasing the sensitivity of release. Knockout of otoferlin did not result in balance abnormalities in the mouse; however, vesicle fusion was greatly reduced and the kinetics of the remaining release changed from a linear to an exponential function (Dulon et al. 2009). Interestingly, spontaneous release was normal in the mutant, suggesting differences from IHC synapses. Conversely, knockout of otoferlin in zebrafish produces severe locomotive and balance abnormalities (Chatterjee et al. 2015).

If otoferlin is involved in vesicle release and trafficking, a high-affinity sensor would be advantageous if both processes have different Ca^{2+} sensitivities. Indeed, in the pachanga mouse model, where otoferlin is reduced but not absent, vesicle trafficking is impaired (Pangršič et al. 2010). Response to small stimuli is normal in the mutant, but sustained release is compromised; thus synaptic vesicles are rapidly

depleted. Otoferlin expression in chicken hair cells coincides with the development of rapid Ca^{2+}-dependent vesicle trafficking (Levic et al. 2011). Typical proteins responsible for priming, such as Munc13 and Ca^{2+}-dependent activator proteins (CAPS), are absent at IHC synapses, and mice lacking Munc13 and CAPS had no auditory defects (Vogl et al. 2015). Thus otoferlin is implicated in vesicle trafficking and priming.

7.7.4.3 Otoferlin and Endocytosis

The role of otoferlin in endocytosis is also controversial. Capacitance recordings of otoferlin knockout mice and pachanga mice show a lack of effect on fast and slow endocytosis (Roux et al. 2006; Pangršič et al. 2010; but see Duncker et al. 2013). Yeast 2 hybrid screens and immunological assays, however, show an intimate association of otoferlin and the endocytic proteins myosin-6, adaptor protein-2 (AP-2), and dynamin (Heidrych et al. 2009; Roux et al. 2009).

To date, otoferlin is implicated in vesicle fusion, vesicle priming, vesicle trafficking, and endocytosis (Fig. 7.6b). If true, this would be a remarkable feat. However, it also makes investigation of function more difficult. How do you study priming or trafficking in a cell that has no vesicle fusion? The coupling of these important steps in release makes them difficult to study in isolation, and this is particularly true if otoferlin plays a role in each step. Identifying the particular components of otoferlin involved in the various processes and selectively mutating them will provide some insight into the specific actions of this important molecule.

7.8 Summary

A great deal of progress was made over the past decades in understanding communication at the hair cell-afferent fiber synapse. Innervation patterns are well elucidated. Previously unknown molecules such as otoferlin shape synaptic functions. A robust vesicle trafficking mechanism underlies sustainable release. Variations in the number of Ca^{2+} channels per synapse as well as of postsynaptic glutamate receptors regulate afferent fiber threshold and spontaneous firing rates. As with any research topic, however, the more data uncovered, the more questions remain. Is multivesicular release a specialization of higher frequency hair cells and, if so, what is the functional relevance and what are the underlying mechanisms? Is the ribbon simply a means of increasing vesicle pools and promoting rapid vesicle trafficking? Does otoferlin have many functions and, if so, can we parcel out the specific functions with selective mutations of this large molecule? The list goes on. The advancement and implementation of new technology is opening new doors for experimentation that will yield answers to these important questions.

Acknowledgements Our thanks to Mamiko Niwa and Sara Talaei for careful reading of the manuscript and to Chris Gralapp for her excellent artwork. This work was supported by National Institute of Deafness and Other Communication Disorders (NIDCD) Grant R01 DC-00991306.

Compliance with Ethics Requirements Michael E. Schnee declares that he has no conflict of interest. Anthony Ricci declares that he has no conflict of interest.

References

Beurg, M., Michalski, N., Safieddine, S., Bouleau, Y., Schneggenburger, R., Chapman, E. R., Petit, C., & Dulon, D. (2010). Control of exocytosis by synaptotagmins and otoferlin in auditory hair cells. *The Journal of Neuroscience,* 30(40), 13281–13290.

Beutner, D., Voets, T., Neher, E., & Moser, T. (2001). Calcium dependence of exocytosis and endocytosis at the cochlear inner hair cell afferent synapse. *Neuron,* 29(3), 681–690.

Brandt, A., Khimich, D., & Moser, T. (2005). Few CaV1.3 channels regulate the exocytosis of a synaptic vesicle at the hair cell ribbon synapse. *The Journal of Neuroscience,* 25(50), 11577–11585.

Brose, N., O'Connor, V., & Skehel, P. (2010). Synaptopathy: Dysfunction of synaptic function? *Biochemical Society Transactions,* 38(2), 443–444.

Buran, B. N., Strenzke, N., Neef, A., Gundelfinger, E. D., Moser, T., & Liberman, M. C. (2010). Onset coding is degraded in auditory nerve fibers from mutant mice lacking synaptic ribbons. *The Journal of Neuroscience,* 30(22), 7587–7597.

Castellano-Muñoz, M., & Ricci, A. J. (2014). Role of intracellular calcium stores in hair cell ribbon synapse. *Frontiers in Cellular Neuroscience,* 8, 162.

Castellano-Muñoz, M., Schnee, M. E., & Ricci, A. J. (2016). Calcium-induced calcium release supports recruitment of synaptic vesicles in auditory hair cells. *Journal of Neurophysiology*, 115(1), 226–239. doi:10.1152/jn.00559.02015.

Ceriani, F., & Mammano, F. (2012). Calcium signaling in the cochlea - Molecular mechanisms and physiopathological implications. *Cell Communication and Signaling,* 10(1), 20.

Chapochnikov, N. M., Takago, H., Huang, C. H., Pangršič, T., Khimich, D., Neef, J., Auge, E., Gottfert, F., Hell, S. W., Wichmann, C., Wolf, F., & Moser, T. (2014). Uniquantal release through a dynamic fusion pore is a candidate mechanism of hair cell exocytosis. *Neuron,* 83(6), 1389–1403.

Chatterjee, M., & Zwislocki, J. J. (1998). Cochlear mechanisms of frequency and intensity coding. II. Dynamic range and the code for loudness. *Hearing Research,* 124(1–2), 170–181.

Chatterjee, P., Padmanarayana, M., Abdullah, N., Holman, C. L., LaDu, J., Tanguay, R. L., & Johnson, C. P. (2015). Otoferlin deficiency in zebrafish results in defects in balance and hearing: Rescue of the balance and hearing phenotype with full-length and truncated forms of mouse otoferlin. *Molecular and Cellular Biology,* 35(6), 1043–1054.

Cho, S., Li, G. L., & von Gersdorff, H. (2011). Recovery from short-term depression and facilitation is ultrafast and Ca^{2+} dependent at auditory hair cell synapses. *The Journal of Neuroscience,* 31(15), 5682–5692.

Coggins, M., & Zenisek, D. (2009). Evidence that exocytosis is driven by calcium entry through multiple calcium channels in goldfish retinal bipolar cells. *Journal of Neurophysiology,* 101(5), 2601–2619.

Del Castillo, J., & Katz, B. (1954). Quantal components of the end-plate potential. *The Journal of Physiology,* 124(3), 560–573.

Denker, A., & Rizzoli, S. O. (2010). Synaptic vesicle pools: an update. *Frontiers in Synaptic Neuroscience,* 2, 135.

Dulon, D., Safieddine, S., Jones, S. M., & Petit, C. (2009). Otoferlin is critical for a highly sensitive and linear calcium-dependent exocytosis at vestibular hair cell ribbon synapses. *The Journal of Neuroscience,* 29(34), 10474–10487.

Duncker, S. V., Franz, C., Kuhn, S., Schulte, U., Campanelli, D., Brandt, N., Hirt, B., Fakler, B., Blin, N., Ruth, P., Engel, J., Marcotti, W., Zimmermann, U., & Knipper, M. (2013). Otoferlin couples to clathrin-mediated endocytosis in mature cochlear inner hair cells. *The Journal of Neuroscience,* 33(22), 9508–9519.

Eggermann, E., Bucurenciu, I., Goswami, S. P., & Jonas, P. (2012). Nanodomain coupling between Ca^{2+} channels and sensors of exocytosis at fast mammalian synapses. *Nature Reviews Neuroscience,* 13(1), 7–21.

Eisen, M. D., Spassova, M., & Parsons, T. D. (2004). Large releasable pool of synaptic vesicles in chick cochlear hair cells. *Journal of Neurophysiology,* 91(6), 2422–2428.

Farris, H. E., Wells, G. B., & Ricci, A. J. (2006). Steady-state adaptation of mechanotransduction modulates the resting potential of auditory hair cells, providing an assay for endolymph $[Ca^{2+}]$. *The Journal of Neuroscience,* 26(48), 12526–12536.

Frank, T., Khimich, D., Neef, A., & Moser, T. (2009). Mechanisms contributing to synaptic Ca^{2+} signals and their heterogeneity in hair cells. *Proceedings of the National Academy of Sciences of the United States of America,* 106(11), 4483–4488.

Fuchs, P. (2004). Time and intensity coding at the hair cell's ribbon synapse. Presented at The Journal of Physiology Symposium on the Senses, San Diego, CA, October 22, 2004, *The Journal of Physiology,* 566(1), 5.

Fuchs, P. A., & Parsons, T. D. (2006). The synaptic physiology of hair cells. In R. A. Eatok, R. R. Fay, & A. N. Popper (Eds.), *Vertebrate Hair Cells* (pp. 249–312). New York: Springer.

Fujikawa, T., Petralia, R. S., Fitzgerald, T. S., Wang, Y. X., Millis, B., Morgado-Diaz, J. A., Kitamura, K., & Kachar, B. (2014). Localization of kainate receptors in inner and outer hair cell synapses. *Hearing Research,* 314, 20–32.

Furukawa, T., & Matsuura, S. (1978). Adaptive rundown of excitatory post-synaptic potentials at synapses between hair cells and eight nerve fibres in the goldfish. *The Journal of Physiology,* 276, 193–209.

Gebhart, M., Juhasz-Vedres, G., Zuccotti, A., Brandt, N., Engel, J., Trockenbacher, A., Kaur, G., Obermair, G. J., Knipper, M., Koschak, A., & Striessnig, J. (2010). Modulation of $Ca_v1.3$ Ca^{2+} channel gating by Rab3 interacting molecule. *Molecular and Cellular Neuroscience,* 44(3), 246–259.

Geisler, C. D., Rhode, W. S., & Kennedy, D. T. (1974). Responses to tonal stimuli of single auditory nerve fibers and their relationship to basilar membrane motion in the squirrel monkey. *Journal of Neurophysiology,* 37(6), 1156–1172.

Glitsch, M. D. (2008). Spontaneous neurotransmitter release and Ca^{2+}—How spontaneous is spontaneous neurotransmitter release? *Cell Calcium,* 43(1), 9–15.

Glowatzki, E., & Fuchs, P. A. (2002). Transmitter release at the hair cell ribbon synapse. *Nature Neuroscience,* 5(2), 147–154.

Goodyear, R. J., Legan, P. K., Christiansen, J. R., Xia, B., Korchagina, J., Gale, J. E., Warchol, M. E., Corwin, J. T., & Richardson, G. P. (2010). Identification of the hair cell soma-1 antigen, HCS-1, as otoferlin. *Journal of the Association for Research in Otolaryngology,* 11(4), 573–586.

Goutman, J. D., & Glowatzki, E. (2007). Time course and calcium dependence of transmitter release at a single ribbon synapse. *Proceedings of the National Academy of Sciences of the United States of America,* 104(41), 16341–16346.

Goutman, J. D., & Glowatzki, E. (2011). Short-term facilitation modulates size and timing of the synaptic response at the inner hair cell ribbon synapse. *The Journal of Neuroscience,* 31(22), 7974–7981.

Grant, L., & Fuchs, P. (2008). Calcium- and calmodulin-dependent inactivation of calcium channels in inner hair cells of the rat cochlea. *Journal of Neurophysiology,* 99(5), 2183–2193.

Grant, L., Yi, E., & Glowatzki, E. (2010). Two modes of release shape the postsynaptic response at the inner hair cell ribbon synapse. *The Journal of Neuroscience,* 30(12), 4210–4220.

Graydon, C. W., Cho, S., Li, G. L., Kachar, B., & von Gersdorff, H. (2011). Sharp Ca^{2+} nanodomains beneath the ribbon promote highly synchronous multivesicular release at hair cell synapses. *The Journal of Neuroscience,* 31(46), 16637–16650.

Gregory, F. D., Pangršič, T., Calin-Jageman, I. E., Moser, T., & Lee, A. (2013). Harmonin enhances voltage-dependent facilitation of $Ca_v1.3$ channels and synchronous exocytosis in mouse inner hair cells. *The Journal of Physiology,* 591(13), 3253–3269.

Heidrych, P., Zimmermann, U., Bress, A., Pusch, C. M., Ruth, P., Pfister, M., Knipper, M., & Blin, N. (2008). Rab8b GTPase, a protein transport regulator, is an interacting partner of otoferlin, defective in a human autosomal recessive deafness form. *Human Molecular Genetics,* 17(23), 3814–3821.

Heidrych, P., Zimmermann, U., Kuhn, S., Franz, C., Engel, J., Duncker, S. V., Hirt, B., Pusch, C. M., Ruth, P., Pfister, M., Marcotti, W., Blin, N., & Knipper, M. (2009). Otoferlin interacts with myosin VI: Implications for maintenance of the basolateral synaptic structure of the inner hair cell. *Human Molecular Genetics,* 18(15), 2779–2790.

Heil, P., & Neubauer, H. (2010). Summing across different active zones can explain the quasi-linear Ca^{2+}-dependencies of exocytosis by receptor cells. *Frontiers in Synaptic Neuroscience,* 2, 148.

Heil, P., & Peterson, A. J. (2015). Basic response properties of auditory nerve fibers: A review. *Cell and Tissue Research,* 361(1), 129–158.

Issa, N. P., & Hudspeth, A. J. (1996). The entry and clearance of Ca^{2+} at individual presynaptic active zones of hair cells from the bullfrog's sacculus. *Proceedings of the National Academy of Sciences of the United States of America,* 93(18), 9527–9532.

Jarsky, T., Tian, M., & Singer, J. H. (2010). Nanodomain control of exocytosis is responsible for the signaling capability of a retinal ribbon synapse. *The Journal of Neuroscience,* 30(36), 11885–11895.

Johnson, C. P., & Chapman, E. R. (2010). Otoferlin is a calcium sensor that directly regulates SNARE-mediated membrane fusion. *Journal of Cell Biology,* 191(1), 187–197.

Johnson, S. L., Franz, C., Kuhn, S., Furness, D. N., Ruttiger, L., Munkner, S., Rivolta, M. N., Seward, E. P., Herschman, H. R., Engel, J., Knipper, M., & Marcotti, W. (2010). Synaptotagmin IV determines the linear Ca^{2+} dependence of vesicle fusion at auditory ribbon synapses. *Nature Neuroscience,* 13(1), 45–52.

Johnson, S. L., Beurg, M., Marcotti, W., & Fettiplace, R. (2011). Prestin-driven cochlear amplification is not limited by the outer hair cell membrane time constant. *Neuron,* 70(6), 1143–1154.

Jung, S., Maritzen, T., Wichmann, C., Jing, Z., Neef, A., Revelo, N. H., Al-Moyed, H., Meese, S., Wojcik, S. M., Panou, I., Bulut, H., Schu, P., Ficner, R., Reisinger, E., Rizzoli, S. O., Neef, J., Strenzke, N., Haucke, V., & Moser, T. (2015). Disruption of adaptor protein 2mu (AP-2mu) in cochlear hair cells impairs vesicle reloading of synaptic release sites and hearing. *EMBO Journal,* 34(21), 2686–2702.

Kantardzhieva, A., Peppi, M., Lane, W. S., & Sewell, W. F. (2012). Protein composition of immunoprecipitated synaptic ribbons. *Journal of Proteome Research,* 11(2), 1163–1174.

Kantardzhieva, A., Liberman, M. C., & Sewell, W. F. (2013). Quantitative analysis of ribbons, vesicles, and cisterns at the cat inner hair cell synapse: Correlations with spontaneous rate. *Journal of Comparative Neurology,* 521(14), 3260–3271.

Kawase, T., & Liberman, M. C. (1992). Spatial organization of the auditory nerve according to spontaneous discharge rate. *Journal of Comparative Neurology,* 319(2), 312–318.

Keen, E. C., & Hudspeth, A. J. (2006). Transfer characteristics of the hair cell's afferent synapse. *Proceedings of the National Academy of Sciences of the United States of America,* 103(14), 5537–5542.

Kennedy, H. J., & Meech, R. W. (2002). Fast Ca^{2+} signals at mouse inner hair cell synapse: A role for Ca^{2+}-induced Ca^{2+} release. *The Journal of Physiology,* 539(1), 15–23.

Khimich, D., Nouvian, R., Pujol, R., tom Dieck, S., Egner, A., Gundelfinger, E. D., & Moser, T. (2005). Hair cell synaptic ribbons are essential for synchronous auditory signalling. *Nature,* 434(7035), 889–894.

Kujawa, S. G., & Liberman, M. C. (2009). Adding insult to injury: Cochlear nerve degeneration after "temporary" noise-induced hearing loss. *The Journal of Neuroscience,* 29(45), 14077–14085.

Lelli, A., Perin, P., Martini, M., Ciubotaru, C. D., Prigioni, I., Valli, P., Rossi, M. L., & Mammano, F. (2003). Presynaptic calcium stores modulate afferent release in vestibular hair cells. *The Journal of Neuroscience,* 23(17), 6894–6903.

Lenzi, D., & von Gersdorff, H. (2001). Structure suggests function: the case for synaptic ribbons as exocytotic nanomachines. *Bioessays,* 23(9), 831–840.

Levic, S., Bouleau, Y., & Dulon, D. (2011). Developmental acquisition of a rapid calcium-regulated vesicle supply allows sustained high rates of exocytosis in auditory hair cells. *PLoS ONE,* 6(10), e25714.

Li, G. L., Keen, E., Andor-Ardo, D., Hudspeth, A. J., & von Gersdorff, H. (2009). The unitary event underlying multiquantal EPSCs at a hair cell's ribbon synapse. *The Journal of Neuroscience,* 29(23), 7558–7568.

Liberman, L. D., Wang, H., & Liberman, M. C. (2011). Opposing gradients of ribbon size and AMPA receptor expression underlie sensitivity differences among cochlear-nerve/hair cell synapses. *The Journal of Neuroscience,* 31(3), 801–808.

Liberman, M. C. (1978). Auditory-nerve response from cats raised in a low-noise chamber. *The Journal of the Acoustical Society of America,* 63(2), 442–455.

Liberman, M. C., Dodds, L. W., & Pierce, S. (1990). Afferent and efferent innervation of the cat cochlea: Quantitative analysis with light and electron microscopy. *The Journal of Comparative Neurology,* 301(3), 443–460.

Matthews, G., & Sterling, P. (2008). Evidence that vesicles undergo compound fusion on the synaptic ribbon. *The Journal of Neuroscience,* 28(21), 5403–5411.

Matthews, G., & Fuchs, P. (2010). The diverse roles of ribbon synapses in sensory neurotransmission. *Nature Reviews Neuroscience,* 11(12), 812–822.

Merchan-Perez, A., & Liberman, M. C. (1996). Ultrastructural differences among afferent synapses on cochlear hair cells: Correlations with spontaneous discharge rate. *The Journal of Comparative Neurology,* 371(2), 208–221.

Meyer, A. C., & Moser, T. (2010). Structure and function of cochlear afferent innervation. *Current Opinion in Otolaryngology & Head and Neck Surgery,* 18(5), 441–446.

Meyer, A. C., Frank, T., Khimich, D., Hoch, G., Riedel, D., Chapochnikov, N. M., Yarin, Y. M., Harke, B., Hell, S. W., Egner, A., & Moser, T. (2009). Tuning of synapse number, structure and function in the cochlea. *Nature Neuroscience,* 12(4), 444–453.

Neef, J., Gehrt, A., Bulankina, A. V., Meyer, A. C., Riedel, D., Gregg, R. G., Strenzke, N., & Moser, T. (2009). The Ca^{2+} channel subunit β2 regulates Ca^{2+} channel abundance and function in inner hair cells and is required for hearing. *The Journal of Neuroscience,* 29(34), 10730–10740.

Neef, J., Jung, S., Wong, A. B., Reuter, K., Pangršič, T., Chakrabarti, R., Kugler, S., Lenz, C., Nouvian, R., Boumil, R. M., Frankel, W. N., Wichmann, C., & Moser, T. (2014). Modes and regulation of endocytic membrane retrieval in mouse auditory hair cells. *The Journal of Neuroscience,* 34(3), 705–716.

Nouvian, R., Beutner, D., Parsons, T. D., & Moser, T. (2006). Structure and function of the hair cell ribbon synapse. *Journal of Membrane Biology,* 209(2–3), 153–165.

Nouvian, R., Neef, J., Bulankina, A. V., Reisinger, E., Pangršič, T., Frank, T., Sikorra, S., Brose, N., Binz, T., & Moser, T. (2011). Exocytosis at the hair cell ribbon synapse apparently operates without neuronal SNARE proteins. *Nature Neuroscience,* 14(4), 411–413.

Padmanarayana, M., Hams, N., Speight, L. C., Petersson, E. J., Mehl, R. A., & Johnson, C. P. (2014). Characterization of the lipid binding properties of otoferlin reveals specific interactions between PI(4,5)P2 and the C2C and C2F domains. *Biochemistry,* 53(30), 5023–5033.

Pangršič, T., Lasarow, L., Reuter, K., Takago, H., Schwander, M., Riedel, D., Frank, T., Tarantino, L. M., Bailey, J. S., Strenzke, N., Brose, N., Muller, U., Reisinger, E., & Moser, T.

(2010). Hearing requires otoferlin-dependent efficient replenishment of synaptic vesicles in hair cells. *Nature Neuroscience,* 13(7), 869–876.

Pangršič, T., Reisinger, E., & Moser, T. (2012). Otoferlin: A multi-C2 domain protein essential for hearing. *Trends in Neurosciences,* 35(11), 671–680.

Pangršič, T., Gabrielaitis, M., Michanski, S., Schwaller, B., Wolf, F., Strenzke, N., & Moser, T. (2015). EF-hand protein Ca^{2+} buffers regulate Ca^{2+} influx and exocytosis in sensory hair cells. *Proceedings of the National Academy of Sciences of the United States of America,* 112(9), E1028–E1037.

Parsons, T. D. (1994). Calcium-triggered exocytosis and endocytosis in an isolated presynaptic cell: Capacitance measurements in saccular hair cells. *Neuron,* 13, 8.

Peng, B. G., Li, Q. X., Ren, T. Y., Ahmad, S., Chen, S. P., Chen, P., & Lin, X. (2004). Group I metabotropic glutamate receptors in spiral ganglion neurons contribute to excitatory neurotransmissions in the cochlea. *Neuroscience,* 123(1), 221–230.

Platzer, J., Engel, J., Schrott-Fischer, A., Stephan, K., Bova, S., Chen, H., Zheng, H., & Striessnig, J. (2000). Congenital deafness and sinoatrial node dysfunction in mice lacking class D L-type Ca^{2+} channels. *Cell,* 102(1), 89–97.

Polimeni, M., Prigioni, I., Russo, G., Calzi, D., & Gioglio, L. (2007). Plasma membrane Ca^{2+}-ATPase isoforms in frog crista ampullaris: Identification of PMCA1 and PMCA2 specific splice variants. *Hearing Research,* 228(1–2), 11–21.

Ramakrishnan, N. A., Drescher, M. J., & Drescher, D. G. (2009). Direct interaction of otoferlin with syntaxin 1A, SNAP-25, and the L-type voltage-gated calcium channel $Ca_v1.3$. *Journal of Biological Chemistry,* 284(3), 1364–1372.

Ramakrishnan, N. A., Drescher, M. J., Morley, B. J., Kelley, P. M., & Drescher, D. G. (2014). Calcium regulates molecular interactions of otoferlin with soluble NSF attachment protein receptor (SNARE) proteins required for hair cell exocytosis. *Journal of Biological Chemistry,* 289(13), 8750–8766.

Regus-Leidig, H., Specht, D., tom Dieck, S., & Brandstatter, J. H. (2010). Stability of active zone components at the photoreceptor ribbon complex. *Molecular Vision,* 16, 2690–2700.

Regus-Leidig, H., Ott, C., Lohner, M., Atorf, J., Fuchs, M., Sedmak, T., Kremers, J., Fejtova, A., Gundelfinger, E. D., & Brandstatter, J. H. (2013). Identification and immunocytochemical characterization of Piccolino, a novel Piccolo splice variant selectively expressed at sensory ribbon synapses of the eye and ear. *PLoS ONE,* 8(8), e70373.

Rhode, W. S., & Smith, P. H. (1985). Characteristics of tone-pip response patterns in relationship to spontaneous rate in cat auditory nerve fibers. *Hearing Research,* 18(2), 159–168.

Ricci, A. J., Gray-Keller, M., & Fettiplace, R. (2000). Tonotopic variations of calcium signalling in turtle auditory hair cells. *The Journal of Physiology,* 524(2), 423–436.

Rizzoli, S. O., & Betz, W. J. (2005). Synaptic vesicle pools. *Nature Reviews Neuroscience,* 6(1), 57–69.

Roberts, W. M. (1994). Localization of calcium signals by a mobile calcium buffer in frog saccular hair cells. *The Journal of Neuroscience,* 14(5), 3246–3262.

Roberts, W. M., Jacobs, R. A., & Hudspeth, A. J. (1990). Colocalization of ion channels involved in frequency selectivity and synaptic transmission at presynaptic active zones of hair cells. *The Journal of Neuroscience,* 10(11), 3664–3684.

Robertson, D., & Johnstone, B. M. (1979). Effect of divalent cations on spontaneous and evoked activity of single mammalian auditory neurones. *Pflügers Archiv: European Journal of Physiology,* 380(1), 7–12.

Roux, I., Safieddine, S., Nouvian, R., Grati, M., Simmler, M. C., Bahloul, A., Perfettini, I., Le Gall, M., Rostaing, P., Hamard, G., Triller, A., Avan, P., Moser, T., & Petit, C. (2006). Otoferlin, defective in a human deafness form, is essential for exocytosis at the auditory ribbon synapse. *Cell,* 127(2), 277–289.

Roux, I., Hosie, S., Johnson, S. L., Bahloul, A., Cayet, N., Nouaille, S., Kros, C. J., Petit, C., & Safieddine, S. (2009). Myosin VI is required for the proper maturation and function of inner hair cell ribbon synapses. *Human Molecular Genetics,* 18(23), 4615–4628.

Rudolph, S., Tsai, M. C., von Gersdorff, H., & Wadiche, J. I. (2015). The ubiquitous nature of multivesicular release. *Trends in Neurosciences,* 38(7), 428–438.

Ruel, J., Emery, S., Nouvian, R., Bersot, T., Amilhon, B., Van Rybroek, J. M., Rebillard, G., Lenoir, M., Eybalin, M., Delprat, B., Sivakumaran, T. A., Giros, B., El Mestikawy, S., Moser, T., Smith, R. J., Lesperance, M. M., & Puel, J. L. (2008). Impairment of SLC17A8 encoding vesicular glutamate transporter-3, VGLUT3, underlies nonsyndromic deafness DFNA25 and inner hair cell dysfunction in null mice. *American Journal of Human Genetics,* 83(2), 278–292.

Rutherford, M. A. (2015). Resolving the structure of inner ear ribbon synapses with STED microscopy. *Synapse,* 69(5), 242–255.

Rutherford, M. A., Chapochnikov, N. M., & Moser, T. (2012). Spike encoding of neurotransmitter release timing by spiral ganglion neurons of the cochlea. *The Journal of Neuroscience,* 32(14), 4773–4789.

Safieddine, S., El-Amraoui, A., & Petit, C. (2012). The auditory hair cell ribbon synapse: from assembly to function. *Annual Review of Neuroscience,* 35, 509–528.

Santos-Sacchi, J. (2004). Determination of cell capacitance using the exact empirical solution of partial differential Y/partial differential Cm and its phase angle. *Biophysical Journal,* 87(1), 714–727.

Schmiedt, R. A. (1989). Spontaneous rates, thresholds and tuning of auditory-nerve fibers in the gerbil: Comparisons to cat data. *Hearing Research,* 42(1), 23–35.

Schmitz, F., Konigstorfer, A., & Sudhof, T. C. (2000). RIBEYE, a component of synaptic ribbons: A protein's journey through evolution provides insight into synaptic ribbon function. *Neuron,* 28(3), 857–872.

Schnee, M. E., & Ricci, A. J. (2003). Biophysical and pharmacological characterization of voltage-gated calcium currents in turtle auditory hair cells. *The Journal of Physiology,* 549(3), 697–717.

Schnee, M. E., Lawton, D. M., Furness, D. N., Benke, T. A., & Ricci, A. J. (2005). Auditory hair cell-afferent fiber synapses are specialized to operate at their best frequencies. *Neuron,* 47(2), 243–254.

Schnee, M. E., Castellano-Muñoz, M., Kong, J. H., Santos-Sacchi, J., & Ricci, A. J. (2011a). Tracking vesicle fusion from hair cell ribbon synapses using a high frequency, dual sine wave stimulus paradigm. *Communicative and Integrative Biology,* 4(6), 785–787.

Schnee, M. E., Santos-Sacchi, J., Castellano-Muñoz, M., Kong, J. H., & Ricci, A. J. (2011b). Calcium-dependent synaptic vesicle trafficking underlies indefatigable release at the hair cell afferent fiber synapse. *Neuron,* 70(2), 326–338.

Schnee, M. E., Castellano-Muñoz, M., & Ricci, A. J. (2013). Response properties from turtle auditory hair cell afferent fibers suggest spike generation is driven by synchronized release both between and within synapses. *Journal of Neurophysiology,* 110(1), 204–220.

Schneggenburger, R., Han, Y., & Kochubey, O. (2012). Ca^{2+} channels and transmitter release at the active zone. *Cell Calcium,* 52(3–4), 199–207.

Sheets, L., Trapani, J. G., Mo, W., Obholzer, N., & Nicolson, T. (2011). Ribeye is required for presynaptic $Ca_V1.3a$ channel localization and afferent innervation of sensory hair cells. *Development,* 138(7), 1309–1319.

Siegel, J. H. (1992). Spontaneous synaptic potentials from afferent terminals in the guinea pig cochlea. *Hearing Research,* 59(1), 85–92.

Siegel, J. H., & Relkin, E. M. (1987). Antagonistic effects of perilymphatic calcium and magnesium on the activity of single cochlear afferent neurons. *Hearing Research,* 28(2–3), 131–147.

Sneary, M. G. (1988). Auditory receptor of the red-eared turtle: II. Afferent and efferent synapses and innervation patterns. *The Journal of Comparative Neurology,* 276(4), 588–606.

Sobkowicz, H. M., Rose, J. E., Scott, G. E., & Slapnick, S. M. (1982). Ribbon synapses in the developing intact and cultured organ of Corti in the mouse. *The Journal of Neuroscience,* 2(7), 942–957.

Sudhof, T. C. (2002). Synaptotagmins: Why so many? *Journal of Biological Chemistry,* 277(10), 7629–7632.

Sudhof, T. C. (2004). The synaptic vesicle cycle. *Annual Review of Neuroscience,* 27, 509–547.
Sudhof, T. C. (2012). The presynaptic active zone. *Neuron,* 75(1), 11–25.
Taberner, A. M., & Liberman, M. C. (2005). Response properties of single auditory nerve fibers in the mouse. *Journal of Neurophysiology, 93*(1), 557–569.
Tang, J., Maximov, A., Shin, O. H., Dai, H., Rizo, J., & Sudhof, T. C. (2006). A complexin/synaptotagmin 1 switch controls fast synaptic vesicle exocytosis. *Cell,* 126(6), 1175–1187.
tom Dieck, S., Altrock, W. D., Kessels, M. M., Qualmann, B., Regus, H., Brauner, D., Fejtova, A., Bracko, O., Gundelfinger, E. D., & Brandstatter, J. H. (2005). Molecular dissection of the photoreceptor ribbon synapse: Physical interaction of Bassoon and RIBEYE is essential for the assembly of the ribbon complex. *Journal of Cell Biology,* 168(5), 825–836.
Torre, V., Ashmore, J. F., Lamb, T. D., & Menini, A. (1995). Transduction and adaptation in sensory receptor cells. *The Journal of Neuroscience,* 15(12), 7757–7768.
Vincent, P. F., Bouleau, Y., Safieddine, S., Petit, C., & Dulon, D. (2014). Exocytotic machineries of vestibular type I and cochlear ribbon synapses display similar intrinsic otoferlin-dependent Ca^{2+} sensitivity but a different coupling to Ca^{2+} channels. *The Journal of Neuroscience,* 34 (33), 10853–10869.
Vogl, C., Cooper, B. H., Neef, J., Wojcik, S. M., Reim, K., Reisinger, E., Brose, N., Rhee, J. S., Moser, T., & Wichmann, C. (2015). Unconventional molecular regulation of synaptic vesicle replenishment in cochlear inner hair cells. *Journal of Cell Science,* 128(4), 638–644.
Vollrath, L., & Spiwoks-Becker, I. (1996). Plasticity of retinal ribbon synapses. *Microscopy Research and Technique,* 35(6), 472–487.
Wang, L. Y., & Augustine, G. J. (2014). Presynaptic nanodomains: A tale of two synapses. *Frontiers in Cellular Neuroscience,* 8, 455.
Westerman, L. A., & Smith, R. L. (1984). Rapid and short-term adaptation in auditory nerve responses. *Hearing Research,* 15(3), 249–260.
Wichmann, C., & Moser, T. (2015). Relating structure and function of inner hair cell ribbon synapses. *Cell and Tissue Research,* 361(1), 95–114.
Wittig, J. H., Jr., & Parsons, T. D. (2008). Synaptic ribbon enables temporal precision of hair cell afferent synapse by increasing the number of readily releasable vesicles: A modeling study. *Journal of Neurophysiology,* 100(4), 1724–1739.
Wong, A. B., Jing, Z., Rutherford, M. A., Frank, T., Strenzke, N., & Moser, T. (2013). Concurrent maturation of inner hair cell synaptic Ca^{2+} influx and auditory nerve spontaneous activity around hearing onset in mice. *The Journal of Neuroscience,* 33(26), 10661–10666.
Wu, W., Rahman, M. N., Guo, J., Roy, N., Xue, L., Cahill, C. M., Zhang, S., & Jia, Z. (2015). Function coupling of otoferlin with GAD65 acts to modulate GABAergic activity. *Journal of Molecular Cell Biology,* 7(2), 168–179.
Yasunaga, S., Grati, M., Cohen-Salmon, M., El-Amraoui, A., Mustapha, M., Salem, N., El-Zir, E., Loiselet, J., & Petit, C. (1999). A mutation in *OTOF*, encoding otoferlin, a FER-1-like protein, causes DFNB9, a nonsyndromic form of deafness. *Nature Genetics,* 21(4), 363–369.
Yates, G. K. (1990). Basilar membrane nonlinearity and its influence on auditory nerve rate-intensity functions. *Hearing Research,* 50(1–2), 145–162.
Yin, Y., Liberman, L. D., Maison, S. F., & Liberman, M. C. (2014). Olivocochlear innervation maintains the normal modiolar-pillar and habenular-cuticular gradients in cochlear synaptic morphology. *Journal of the Association for Research in Otolaryngology,* 15(4), 571–583.
Zampini, V., Johnson, S. L., Franz, C., Knipper, M., Holley, M. C., Magistretti, J., Russo, G., Marcotti, W., & Masetto, S. (2014). Fine Tuning of $Ca_V1.3$ Ca^{2+} channel properties in adult inner hair cells positioned in the most sensitive region of the Gerbil Cochlea. *PLoS ONE,* 9(11), e113750.
Zanazzi, G., & Matthews, G. (2009). The molecular architecture of ribbon presynaptic terminals. *Molecular Neurobiology,* 39(2), 130–148.
Zenisek, D., & Matthews, G. (2000). The role of mitochondria in presynaptic calcium handling at a ribbon synapse. *Neuron,* 25(1), 229–237.

Chapter 8
Afferent Coding and Efferent Control in the Normal and Impaired Cochlea

Mark Sayles and Michael G. Heinz

Abstract The auditory nerve is the neural transmission channel linking the cochlea and brainstem. After spectral decomposition of acoustic signals along the basilar membrane, afferent fibers convey information to the cochlear nucleus with astounding temporal precision, whereas efferent fibers form part of a negative-feedback control circuit thought to modulate the gain of cochlear signal transduction. Single-fiber spike-based neurophysiological recording in the auditory nerve continues to offer invaluable insights on cochlear mechanics and peripheral neural coding of sounds. Much has been learned over the past two decades regarding the effects of cochlear damage on coding and the relationship between neurophysiological and perceptual phenomena in audition. Here, a conceptual review of auditory nerve physiology in normal and impaired hearing is presented, including both afferent and efferent functions. Important historical foundations are covered as well as the most recent and exciting developments. The aim is to link neurophysiological findings with their perceptual counterparts wherever possible and to provide the reader a framework in which to understand the neural underpinnings of the everyday perceptual difficulties faced by hearing-impaired listeners.

Keywords Acoustic trauma · Auditory nerve · Cochlear gain control · Dynamic range · Frequency tuning · Hearing impairment · Loudness recruitment · Masking · Neural adaptation · Speech coding · Suppressive nonlinearity · Temporal coding

M. Sayles
Laboratory of Auditory Neurophysiology, Department of Neurosciences, Campus Gasthuisberg – O&N II, University of Leuven, Herestraat 49, bus 201, 3000 Leuven, Belgium
e-mail: saylesm@purdue.edu

M. Sayles · M.G. Heinz (✉)
Department of Speech, Language, and Hearing Sciences and Weldon School of Biomedical Engineering, Purdue University, 715 Clinic Drive, West Lafayette, IN 47907, USA
e-mail: mheinz@purdue.edu

G.A. Manley et al. (eds.), *Understanding the Cochlea*, Springer Handbook of Auditory Research 62, DOI 10.1007/978-3-319-52073-5_8

8.1 Introduction

The auditory nerve (AN) is the transmission channel linking the cochlea and brainstem. In response to sound, "analog" hair cell receptor potentials are transformed to a "digital" representation in trains of all-or-none action potentials, or "spikes," in a population of ~30,000 afferent AN fibers (ANFs) in each human ear. In addition, the cochlea receives efferent inputs from brainstem neurons. This chapter presents auditory afferent and efferent neurophysiology in normal and impaired hearing, emphasizing the relationship between physiology and perception.

8.1.1 Anatomy of Afferent and Efferent Cochlear Innervation

All acoustic information transduced by the cochlea is transmitted to the central nervous system by ANFs, which are the central projections of spiral ganglion neurons (SGNs). There are two varieties of SGN: type I and type II. The peripheral fibers of SGNs are known as type I and type II afferents (Fig. 8.1). Type I afferents make synaptic contact with inner hair cells (IHCs). Each type I afferent fiber receives input from a single IHC, although each IHC contacts 15 to 30 fibers (Liberman 1982). Type I ANFs form synapses onto neurons in the cochlear nucleus, the most peripheral structure in the auditory brainstem. Type I ANFs are the main source of auditory input to the brain, comprising 90–95% of the total SGNs in cats. Their physiological responses to sound are well characterized in both normal-hearing and hearing-impaired animals. The anatomy and function of type II SGNs are less well characterized (Robertson et al. 1999; Benson and Brown 2004). These neurons are unipolar, with thin slow-conducting axons. Each type II SGN peripherally innervates a group of outer hair cells (OHCs) over a relatively broad cochlear region (Brown 1987). Their central projection targets are a diverse set of neurons in the cochlear nucleus (Benson and Brown 2004). Recent work suggests that type II SGNs may form the afferent limb of a cochlear gain-control circuit involving the olivocochlear efferent system (Froud et al. 2015; Fig. 8.1).

The cochlea receives efferent innervation from neurons located in the superior olivary complex (SOC; Fig. 8.1). There are two types of olivocochlear efferent neuron: medial olivocochlear (MOC) and lateral olivocochlear (LOC) cells. Both MOC and LOC neurons receive excitatory input from the cochlear nucleus. MOC and LOC fibers travel in the vestibular nerve until close to the cochlea where they join auditory afferent fibers at the vestibulocochlear anastomosis. MOC fibers form cholinergic synapses bilaterally onto OHCs. These synapses are thought to function as a negative-feedback control system. MOC activation hyperpolarizes OHCs (Fuchs 2002), decreases their electromotility, and thereby reduces the gain of cochlear signal transduction. The "crossed" MOC pathway innervates the ipsilateral cochlea, and the "uncrossed" MOC pathway innervates the contralateral cochlea.

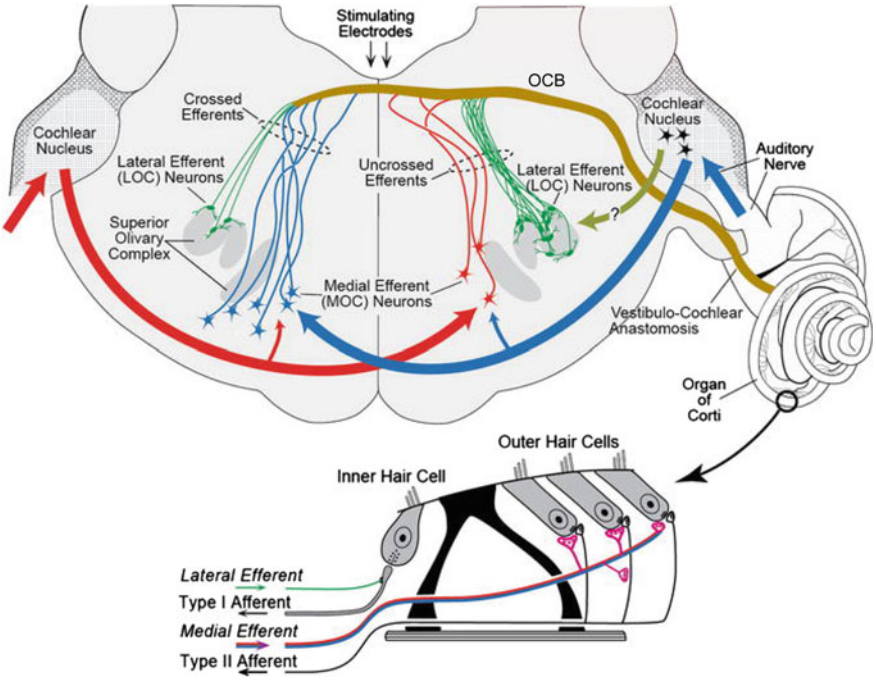

Fig. 8.1 The cochlea has afferent and efferent connections to the brainstem. *Top*: Schematized outline of a transverse brainstem section showing the lateral (LOC; *green lines*) and medial (MOC; *thin blue* and *thin red lines*) olivocochlear neurons and the olivocochlear bundle (OCB; *gold*). *Blue arrows*, inputs to the "crossed" pathways; *red arrows*, inputs to the "uncrossed" pathways. *Bottom*: Afferent and efferent innervation to the organ of Corti. Modified from Guinan (2013), with permission

The input to the MOC comes from the contralateral cochlear nucleus via the decussating fibers of the trapezoid body, so the "crossed" pathway is effectively "double crossed." In small mammals, the "crossed" pathway is two to three times stronger than the "uncrossed" pathway, both in terms of number of efferent fibers and the strength of the physiologically characterized reflex (Liberman et al. 1996). This may not be true in humans, where ipsilateral and contralateral MOC reflexes appear similar in strength.

LOC neurons have thin, unmyelinated axons that are difficult to record from or to stimulate separately from MOC axons. Therefore, relatively little is known about the physiology of LOC efferents. They project primarily to the ipsilateral cochlea and synapse onto type I afferent fibers immediately beneath IHCs rather than onto the hair cells. LOC neurons are cytochemically heterogeneous (Darrow et al. 2006b), receive excitatory and inhibitory synaptic inputs with slow kinetics (Sterenborg et al. 2010), and elicit either slow ($\tau \sim 10$ min) excitation or slow suppression of type I ANF output (Groff and Liberman 2003). For a detailed review of the olivocochlear efferent system, see Guinan (2006).

8.1.2 Noise-Induced Damage to Cochlear Anatomy

Noise overexposure is the main cause of preventable hearing impairment worldwide (Le Prell and Henderson 2012). Noise exposure causes mechanical and metabolic stress that can lead to temporary or permanent reductions in sensitivity through damage to or the death of OHCs and IHCs and supporting structures of the cochlea (Hu 2012). In cases of intense noise exposure, focal lesions (cochlea regions with >50% hair cell loss or "dead regions") can occur. The cochlear extent of hair cell lesions depends on the noise exposure spectral content, intensity, and duration (Harding and Bohne 2009). High-frequency exposures create lesions limited to the cochlear base, whereas low-frequency exposures produce lesions spanning a broad region due to traveling-wave properties. Significant variability in cochlear damage occurs across individuals exposed to the same noise but not generally across ears within an individual (Bohne et al. 1986). Some listeners' ears are "tender" and others "tough" (Cody and Robertson 1983). OHCs are generally more susceptible to noise exposure than IHCs in terms of cell survival (Hu 2012). This observation has led to the common audiological belief that mild-to-moderate hearing losses are primarily OHC based, with IHC damage only contributing to hearing losses greater than 60 dB (e.g., Moore 1995; Edwards 2004).

Single-neuron labeling studies have demonstrated that a combined measure of damage to IHC and OHC stereocilia is an accurate predictor of threshold shift in ANFs (Liberman and Dodds 1984). In contrast to hair cell death, IHCs and OHCs appear to be similarly susceptible to stereocilial damage but with IHCs generally demonstrating a greater fraction of stereocilial damage over broader cochlear regions than OHCs (Liberman and Dodds 1984; Hu 2012; Fig. 8.2). Thus, it is likely, as discussed in Sects. 8.4.2 and 8.7.1, that IHC dysfunction (in addition to OHC dysfunction) contributes to neural-coding deficits in many cases of mild-to-moderate sensorineural hearing loss (SNHL).

Cochlear synaptopathy can occur immediately after exposure to moderate noise levels that produce only a temporary threshold shift (Kujawa and Liberman 2015). Such temporary threshold shifts had long been assumed to imply no permanent cochlear damage. However, loss of 30–50% of the IHC synapses in cochlear regions basal to the noise exposure has been demonstrated in mice and guinea pigs (Kujawa and Liberman 2009; Furman et al. 2013). Cochlear synaptopathy is thought to result from glutamate excitotoxicity (Pujol and Puel 1999) and precedes delayed (months to years) loss of SGNs. Synaptopathy is hypothesized to underlie a form of hearing impairment for suprathreshold sounds despite normal thresholds. This phenomenon is termed "hidden hearing loss" because it is not detectable by standard audiometric threshold measures (Schaette and McAlpine 2011; Kujawa and Liberman 2015).

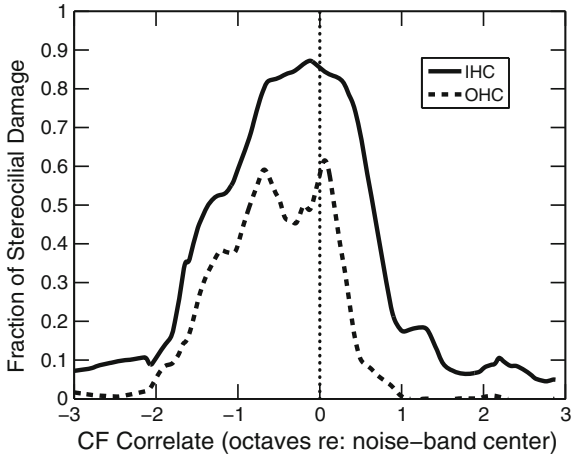

Fig. 8.2 The cochlear distribution and degree of inner hair cell (IHC) stereocilial damage from noise exposure are generally larger than they are for outer hair cells (OHCs). The fraction of IHC and OHC stereocilial damage is plotted versus the cochlear characteristic frequency (CF) associated with cochlear place (in octave difference relative to exposure-noise center frequency). Data were reanalyzed from Liberman and Dodds (1984) by averaging across animals exposed to narrowband noise with center frequencies from 1.5 to 5.5 kHz

8.1.3 Perceptual Effects of Noise Damage

8.1.3.1 Threshold Elevation

Perhaps the most obvious effect of noise damage is loss of audibility so that soft sounds are no longer perceived. Loss of audibility corresponds to threshold elevation for single ANFs in that soft sounds no longer alter the firing pattern of an ANF compared with silence (in neither terms of firing rate nor temporal synchrony). This is typically due to mechanically damaged and tangled hair cell stereocilia or hair cell death in more severe cases (see Sect. 8.1.2).

8.1.3.2 Loss of Frequency Selectivity

The ability to perceptually resolve frequency components of complex sounds is a fundamental component of audition (Fletcher 1940). This relies on ANF frequency selectivity, reflecting mechanical basilar membrane responses (Sellick et al. 1982). The cochlea is commonly thought of as a frequency analyzer that decomposes incoming broadband acoustic energy into narrow frequency bands. Damage to OHCs produces broadened frequency tuning in ANFs (see Sect. 8.3.3). Therefore, even when sounds are made audible for hearing-impaired listeners, loss of

frequency selectivity interferes with their ability to analyze complex sounds such as speech and music (Middlebrooks et al. 2016).

8.1.3.3 Impaired Speech-in-Noise Intelligibility

Speech intelligibility in environments with high levels of background noise and reverberation is dramatically reduced for hearing-impaired people (Duquesnoy 1983; Festen and Plomp 1990). Hypothesized deficits in temporal coding of sounds have been proposed as a mechanism underlying this degraded suprathreshold processing (Moore 2014).

8.1.3.4 Abnormal Growth of Loudness and Hyperacusis

Altered perception of loudness is a common effect of cochlear hearing loss. Despite elevated thresholds, loudness is often near normal at high sound levels ($\sim$90-dB sound pressure level [SPL]). This "catching up" of loudness results in a reduced dynamic range over which listeners with SNHL transition from just audible to painfully loud conditions. This "loudness recruitment" is typically described as an abnormally steep growth of loudness with increasing sound level. The severity of loudness recruitment generally scales with the degree of hearing loss; however, individual differences are common (Smeds and Leijon 2011). Hyperacusis, an intolerance (or hypersensitivity) to sound levels that would not be bothersome to normal-hearing listeners (Baguley 2003) is a related phenomenon in listeners with SNHL. Questions remain about the underlying neural basis of loudness recruitment and hyperacusis (see Sect. 8.4.2). At least part of the intersubject variability likely arises from individual differences in cochlear pathophysiology (e.g., OHC versus IHC dysfunction; Moore and Glasberg 2004).

8.2 Afferent Fiber Spontaneous Activity

8.2.1 Spontaneous Rate Categories

In the absence of acoustic stimulation, ANFs fire spontaneous spikes at rates between 0 and >100 spikes per second. The population spontaneous rate (SR) distribution is not unimodal (Liberman 1978). There are usually three SR groups described: low (SR < 1 spikes/s), medium (1 $\leq$ SR < 18 spikes/s), and high (SR $\geq$ 18 spikes/s). The SR correlates with many morphological and physiological characteristics of ANFs. High-SR fibers synapse on the pillar side of IHCs and are relatively thick ($\sim$1 μm diameter), whereas low-/medium-SR fibers synapse on the modiolar side of the IHC and are thinner ($\sim$0.5 μm diameter; Liberman 1980, 1982). The threshold at the *characteristic frequency* (CF) and the

dynamic range are inversely related to SR within the same CF region (Liberman 1978), with important implications for coding a wide range of sound levels (see Sect. 8.4.1). Temporal synchrony to fine structure and to envelope components of sounds is typically higher in low-SR fibers than in high-SR fibers (Johnson 1974; Joris and Yin 1992).

8.2.2 Selective Loss of Low-Spontaneous Rate Fibers

Cochlear synaptopathy (see Sect. 8.1.2) involves primarily excitotoxic damage to, and subsequent loss of, low-SR ANFs (Furman et al. 2013). This bias in susceptibility may be related to the relatively low number of mitochondria in low-SR SGCs compared with their high-SR counterparts (Liberman 1980). Mitochondria are important in buffering Ca^{2+} overload, which is a key trigger for excitotoxic neural damage.

8.3 Frequency Tuning

8.3.1 Physiological Measures of Auditory Nerve Fiber Frequency Tuning

Frequency selectivity is a fundamental response property of auditory neurons in that a narrow range of acoustic frequency components drive the response of a neuron. In ANFs, this frequency tuning largely reflects the mechanics of cochlear signal transduction (Narayan et al. 1998). The frequency to which an ANF is most sensitive (at which detection threshold is lowest) is called the CF. The CF derives from the particular *characteristic place* along the basilar membrane to which the ANF connects (Liberman 1982). The CF is typically determined from a frequency-threshold tuning curve, which is constructed by adaptively varying the sound level to find the level for each tone frequency that causes a criterion increase in spike rate (Liberman 1978). In addition, it is typical to quantify the "sharpness" of tuning using the tuning-curve quality factor at 10 dB above the CF threshold (Q_{10dB} = CF/10-dB bandwidth).

ANF tuning curves are often interpreted to represent the gain functions (albeit inverted) of cochlear band-pass filters. However, this is only partially true because there are nonlinear effects that complicate cochlear tuning as a function of sound level (Eustaquio-Martín and Lopez-Poveda 2011). Arguably, more accurate measures of tuning can be obtained by estimating the system impulse response for a fixed-level broadband stimulus (de Boer and de Jongh 1978; Recio-Spinoso et al. 2005). Filters obtained using this approach can be more explicitly thought of as true gain functions between the input to the cochlea and the output of SGCs.

8.3.2 Relating Physiological and Behavioral Estimates of Frequency Tuning

It is widely believed that behavioral frequency selectivity is a direct reflection of cochlear filtering. Animal experiments have shown a close correspondence between ANF tuning-curve bandwidths and behavioral frequency-resolution estimates in the same species (Evans 2001). Recent behavioral estimates of human cochlear tuning have emphasized that bandwidths are substantially smaller when derived using a forward-masking rather than a simultaneous-masking paradigm (Oxenham and Shera 2003). The discrepancy between tuning estimates from forward-masking and simultaneous-masking experiments can be understood by remembering that cochlear signal transduction involves an active nonlinear process. Due to saturation of the nonlinearity, one spectral component can reduce the response to another component ("two-tone suppression"; see Sect. 8.6.2). This reduction in cochlear-amplifier gain for broadband sounds increases the apparent bandwidth of filter estimates in simultaneous-masking paradigms. Putting this same argument in terms of single-unit physiology suggests tuning curves derived from responses to single tones may reflect sharp tuning that is rarely achievable under everyday listening conditions where broadband signals such as speech are typically encountered.

Noninvasive techniques for estimating frequency tuning based on stimulus-frequency otoacoustic emissions (SFOAEs) have been applied to many species, including humans (Shera et al. 2002; Bergevin, Verhulst, and van Dijk, Chap. 10). SFOAEs are sounds emitted from the cochlea in response to incoming sounds as a by-product of the mechanical amplification responsible for sharp basilar membrane tuning. The delay of SFOAEs is related to tuning bandwidth (i.e., sharper filters have longer impulse responses). Some evidence from this approach suggests that human cochlear filters are significantly sharper (by a factor of $\sim$2–3) than those of other mammals (Shera et al. 2010). The precise interpretation of SFOAE data related to the question of whether human cochlear filter bandwidths differ substantially from those in other animals has been, and continues to be, controversial. Different experimental approaches and interpretations of data can yield very different results (Ruggero and Temchin 2005; Manley and van Dijk 2016). However, a close correspondence between SFOAE-derived tuning estimates and invasive physiological measures of tuning has been established in several animal models (Shera et al. 2010; Joris et al. 2011). Interestingly, ANF threshold tuning curves in old-world monkeys are a factor of two narrower than threshold tuning curves from cat ANFs at the same CF (Joris et al. 2011).

8.3.3 *Selective Effects of Inner and Outer Hair Cell Damage on Tuning*

Anatomical evidence that both IHC and OHC damage occur with acoustic trauma (see Sect. 8.1.2) suggests that functional effects of hair cell damage must be considered at the output of the cochlea (the AN) or higher, because basilar-membrane responses do not reflect the contribution of IHC dysfunction. The most significant difference between IHC and OHC dysfunction is in terms of frequency selectivity, which can be understood by considering the differing roles of IHCs and OHCs. IHCs transduce basilar membrane motion into neural responses in individual ANFs (Corey, Ó Maoiléidigh, and Ashmore, Chap. 4), whereas OHCs are responsible for the high sensitivity and sharp tuning characteristic of normal hearing (Santos-Sacchi, Navaratnam, Raphael, and Oliver, Chap. 5; Gummer, Dong, Ghaffari, and Freemann, Chap. 6). High sensitivity allows very soft sounds to be heard, whereas sharp tuning allows sounds that differ in spectral features to be discriminated.

Liberman and Dodds' (1984) study established a strong correlation between abnormalities in ANF tuning-curve shapes after cochlear damage and hair cell status at the characteristic place of ANFs (Fig. 8.3). Hair cell stereocilial status is much more strongly correlated with threshold and tuning than is hair cell survival. An important implication of this observation is that hair cells are not simply either normally functioning or completely dysfunctional, but rather they can range in functionality after cochlear insult. Normal ANF tuning curves have well-defined "tip" and "tail" regions for CFs greater than ~2–3 kHz in cats, which requires normal stereocilia on both IHCs and OHCs (Fig. 8.3a). Selective OHC loss and/or significant OHC stereocilial damage is associated with elevated tips and hypersensitive tails ("W-shaped" tuning curves; Fig. 8.3b). Complete OHC loss (Fig. 8.3c) results in the complete absence of a tip, with the resulting broad "bowl-shaped" tuning curves thought to represent passive cochlear tuning after loss of the cochlear active process. Damage to IHC stereocilia (Fig. 8.3d), specifically disarray or loss of the tallest row of stereocilia, results in an elevated threshold at all frequencies, with very little effect on frequency selectivity. Passive ("component 2"; see Sect. 8.4.2) response properties, including severely elevated thresholds (90- to 100-dB SPL), greatly broadened tuning, and steepened rate-level functions (not shown) are observed when there is a complete absence of the tallest row of IHC stereocilia without damage to the shorter stereocilia (Fig. 8.3e). Note that all hair cell damage scenarios shown in Fig. 8.3b–d represent a 40-dB shift in ANF threshold, despite quite different frequency-selectivity effects, and thus represent a possible peripheral basis for individual differences in speech recognition despite similar audiometric thresholds.

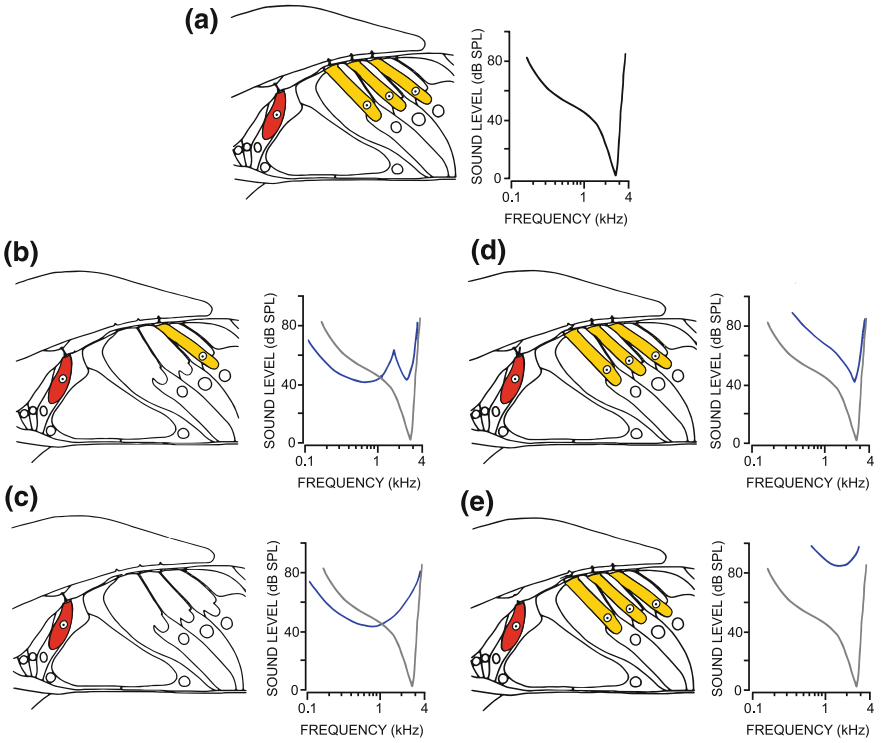

Fig. 8.3 Schematic representation of the structure-function correlation between IHC (*red*) and OHC (*gold*) damage (*left*) and frequency selectivity (*right*) characterized by pure-tone auditory nerve fiber (ANF) tuning curves (*black and gray*, *normal; blue*, *impaired*). **a** Normal IHC and OHC function. **b** Selective OHC loss and/or significant OHC stereocilial damage. **c** Complete loss of OHCs. **d** Disarray or loss of tallest row IHC stereocilia. **e** Complete absence of tallest row IHC stereocilia. SPL, sound pressure level. Modified from Liberman and Dodds (1984), with permission

8.3.4 Advances in Computational Modeling of Cochlear Impairment

Knowledge of the mechanistic and physiological aspects of cochlear function has increased dramatically in the decades since the first book on the cochlea in the *Springer Handbook of Auditory Research* (Dallos et al. 1996). Much of this knowledge is captured in computational auditory-nerve models, which simulate neural spike trains for single ANFs in response to arbitrary sounds. Several general translational applications (relating physiological properties to perception, modeling the effects of IHC vs. OHC dysfunction) have focused this work on phenomenological auditory-nerve models (reviewed by Heinz 2010, 2016). This style of model is not based on cochlear biophysics but rather represents the salient

signal-processing modules for transduction and focuses on simulating response properties at the output of the cochlea.

Significant advances have been made in modeling the effects of IHC and OHC dysfunction on the neural coding of complex sounds (Bruce et al. 2003; Zilany et al. 2014). Key insight toward modeling OHC dysfunction was the recognition that a number of nonlinear cochlear-response properties (compression, level-dependent tuning, and suppression) were all related to a single OHC-based cochlear gain-control mechanism (Patuzzi 1996). Thus, auditory-nerve models that represent each of these nonlinear response properties as depending on the functionality of a single OHC-based module are able to successfully model the systematic effects of OHC dysfunction with a single parameter, including broadened tuning and loss of compression (Carney 1993). Similarly, a single parameter has been used to model the range of IHC dysfunction, including effects on the shapes and slopes of ANF rate-level functions (see Sect. 8.4.2) and speech coding (see Sect. 8.7.1). Recent advances include adding synaptic power-law dynamics, which improved modulation coding and dynamic-range adaptation (Zilany and Carney 2010), and modeling the temporal dynamics and level dependence for efferent control of cochlear tuning (Smalt et al. 2014). It is certainly difficult to understand the combined (and often confounding) effects of IHC and OHC dysfunction experimentally. Phenomenologically based computational models provide great potential for disentangling the relative contributions of IHC and OHC dysfunction and may help in the development of diagnostic tests and rehabilitative strategies for addressing some of the individual differences that currently challenge audiology.

8.4 Coding of Sound Level

8.4.1 Afferent Rate-Level Functions and the "Dynamic-Range Problem"

Absolute and relative sound levels are fundamental acoustic attributes underlying many aspects of auditory processing. Listeners with normal hearing use level cues to perceive speech robustly across a wide range of signal and background-noise levels. In contrast, listeners with cochlear damage struggle with a limited dynamic range and experience difficulty understanding speech in background noise. Despite the fundamental importance of level coding, the discrepancy ("dynamic-range problem") between the wide perceptual dynamic range (up to $\sim$120 dB) and the limited dynamic range of individual neurons ($\sim$30–50 dB) remains unresolved (Viemeister 1988; reviewed by Heinz 2012).

Level coding in single neurons is typically characterized by rate-level function (Fig. 8.4c), where the discharge rate averaged over the duration of a CF tone is plotted against sound level. For ANFs, rate varies monotonically with sound level, increasing from spontaneous rate to maximum (saturated) rate but only over a limited

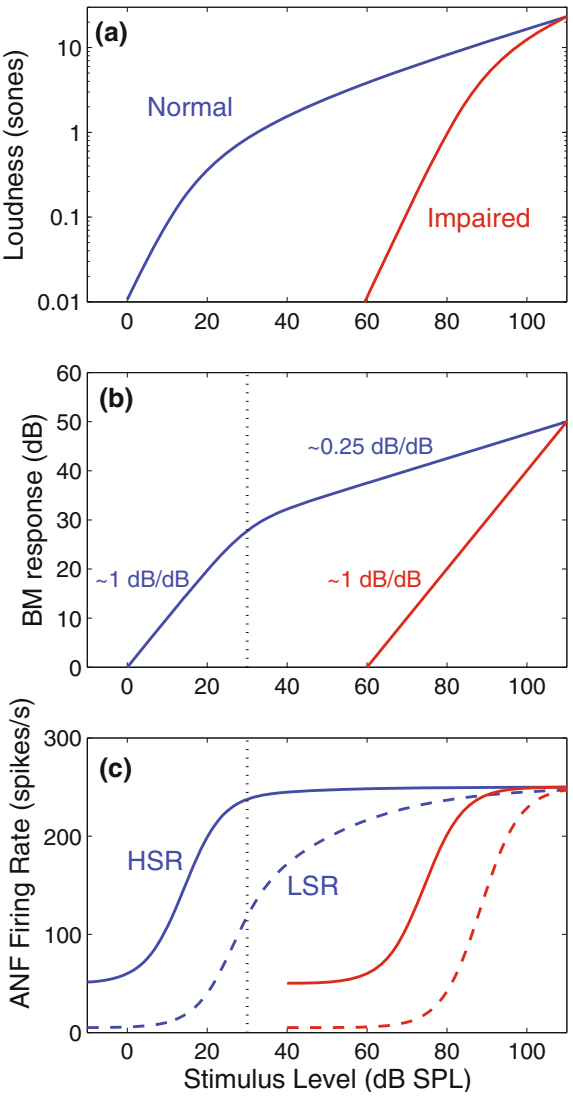

Fig. 8.4 Schematic of the relationship between perceptual and physiological representations of sound level for normal (*blue*) and impaired (*red*) hearing. **a** Typical loudness functions, with reduced dynamic range after cochlear damage. **b** and **c** Effects of OHC loss on input-output functions for basilar-membrane (BM) and ANF responses, respectively. **c**, *solid lines*: low-threshold, high-spontaneous rate (HSR) ANFs; *dashed lines*: higher threshold, low-SR (LSR) fibers

range of sound levels (less than ∼50 dB). Both threshold sound level and dynamic range depend systematically on SR (see Sect. 8.2), with high-SR fibers having lower thresholds and smaller dynamic ranges than low-SR fibers (Sachs and Abbas 1974). The wider dynamic ranges of low-SR fibers can be understood from the interaction of their higher thresholds and the sound level of basilar-membrane compression onset (Fig. 8.4b, c). Because low-SR ANFs saturate at SPLs above compression onset, the shallower basilar-membrane responses create shallower ANF rate-level functions, extending their dynamic range (Sachs and Abbas 1974; Yates 1990).

Several quantitative studies have attempted to solve the dynamic-range problem, each highlighting response properties that extend the neural dynamic range to account for more (but still not all) of the perceptual dynamic range (Siebert 1968; Colburn et al. 2003). Predictions of optimal just-noticeable differences (JNDs) in intensity, which factor in Poisson-like variability of ANF discharge counts, demonstrate that individual ANF rate saturation can be overcome by considering pooled ANF responses that include spread of excitation to CFs away from the tone frequency (Siebert 1968; Delgutte 1996). Although spread of excitation extends the predicted perceptual dynamic range for tones in quiet, robust intensity discrimination in notched-noise maskers suggests that a wide dynamic range must be accounted for by a restricted CF range (Viemeister 1983). A wider dynamic range within a limited set of CFs can be obtained by pooling across all SR groups because the low-SR ANFs have higher thresholds and wider dynamic ranges (Fig. 8.4c). However, predicted-intensity JNDs still increase significantly above 40- to 50-dB SPL due to Poisson variability (increased variance with increased rate) and thus do not account for human intensity JNDs remaining robust up to ~100-dB SPL (Delgutte 1987; Winslow and Sachs 1988). Alternate mechanisms have been proposed to help solve the dynamic-range problem, such as level-dependent temporal synchrony and phase responses (Heinz et al. 2001; Colburn et al. 2003), dynamic-range adaptation (see Sect. 8.4.3), and efferent feedback (see Sect. 8.8).

The benefit of low-SR ANFs for level coding is particularly interesting with respect to cochlear synaptopathy and hidden hearing loss (see Sects. 8.1.2 and 8.2). Low-SR fibers are more resilient to the saturating effects of background noise than high-SR fibers, suggesting that they may be important for listening in noise (Costalupes et al. 1984; Young and Barta 1986). Because low-SR fibers are more susceptible to moderate noise exposures, cochlear synaptopathy is an important factor to consider in explaining the difficulties listeners face in understanding speech in noisy environments, even with normal audiograms (Kujawa and Liberman 2015).

8.4.2 Loudness Correlates in Normal and Impaired Hearing

Loudness is a subjective measure of the perceived magnitude of a sound. The neural correlates of normal and impaired loudness perception remain unresolved (Heinz 2012). A long-standing hypothesis is that loudness relates to the total number of spikes in the ANF population (Fletcher and Munson 1933). Two important factors contribute to total ANF-response growth with sound level: response growth for ANFs with CFs at the tone frequency and recruitment of additional CFs above and below the tone frequency. Analytical AN models incorporating these factors demonstrate a power-law relationship between whole-nerve rate and sound level similar to perceptual loudness growth (Goldstein 1974). However, this spread-of-excitation model predicts a reduction in loudness growth in high-pass noise that is much more severe than observed perceptually. Experimental

approaches using a gross action potential measured from the AN trunk to evaluate the summed AN spike-count hypothesis show that total activity grows less steeply than loudness, with a frequency dependency that is inconsistent with the frequency-independent perceptual loudness growth above 1 kHz (Relkin and Doucet 1997). Furthermore, although experimental approaches show a general ability of the total spike count hypothesis to account for loudness summation (i.e., the effect of bandwidth on loudness), there are significant inconsistencies with perceptual data (Pickles 1983).

Loudness recruitment is a common effect of cochlear hearing loss (Fig. 8.4a; see Sect. 8.1.3.4). At first glance, recruitment appears to be well accounted for in terms of altered basilar membrane response growth after OHC dysfunction (Fig. 8.4b). In line with this observation, it has been hypothesized that steeper ANF response growth could be a correlate of loudness recruitment. However, experimental support for this idea is largely limited to specific near-CF and midlevel conditions (Harrison 1981). A theoretical evaluation of the predicted effects of OHC dysfunction on ANF rate-level function slopes suggests that only a subset of ANFs become steeper with impairment (Sachs and Abbas 1974; Heinz and Young 2004). Because the dynamic range of low-SR fibers depends on basilar-membrane compression (Fig. 8.4c; see Sect. 8.4.1), their response growth is predicted to become steeper. In contrast, the dynamic range of high-SR ANFs is entirely within the linear portion of basilar-membrane response growth for both normal and impaired systems. When studied empirically, tone rate-level functions after acoustic trauma were actually *shallower* than normal (Heinz and Young 2004; Fig. 8.5a). This unexpected outcome can be understood in terms of the confounding effects of IHC stereocilial damage, which has been hypothesized and modeled to make the IHC transduction

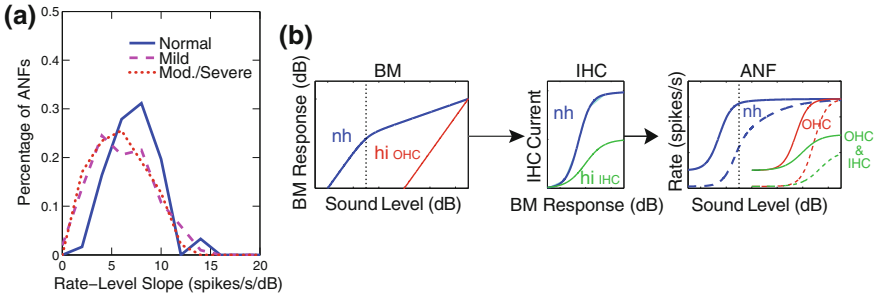

Fig. 8.5 In contrast to the predicted effects of OHC dysfunction, ANF rate-level slopes are on average shallower than normal after acoustic trauma. **a** Distributions of cat ANF rate-level slopes for normal hearing and mild and moderate-severe hearing losses. **b** Schematic of the opposing effects of OHC and IHC dysfunction on ANF level coding. *Left*: BM responses for normal hearing (nh; *blue*) and OHC dysfunction (hi_{OHC}; *red*); *middle*: IHC transduction for normal hearing and IHC dysfunction (hi_{IHC}; *green*); *right*: ANF rate-level functions for HSR (*solid*) and LSR fibers (*dashed*) for normal hearing and OHC dysfunction (*red*) and combined OHC and IHC dysfunction (*green*). **a** redrawn from Heinz and Young (2004); **b** modified from Heinz et al. (2005), with permission

function shallower than normal, thus counteracting the steepening effects of OHC dysfunction (Zilany and Bruce 2006; Fig. 8.5b; see Sect. 8.3.4). Very steep responses were observed in some fibers, but they were limited to cases in which fiber thresholds were severely elevated (>80 dB) and thus were inconsistent with perceptual findings that loudness recruitment occurs for all degrees of SNHL. These very steep, high-threshold rate-level functions likely represent "component 2" responses associated with an entirely passive cochlea (Liberman and Kiang 1984). These high-level irregularities have been largely ignored in the interpretation of studies of normal hearing but may be extremely relevant for hearing-impaired listeners because hearing aids operate at these high SPLs. Furthermore, alternative hypotheses that considered pooling spike counts across ANFs did not account for loudness recruitment (Heinz et al. 2005). However, steeper response growth has

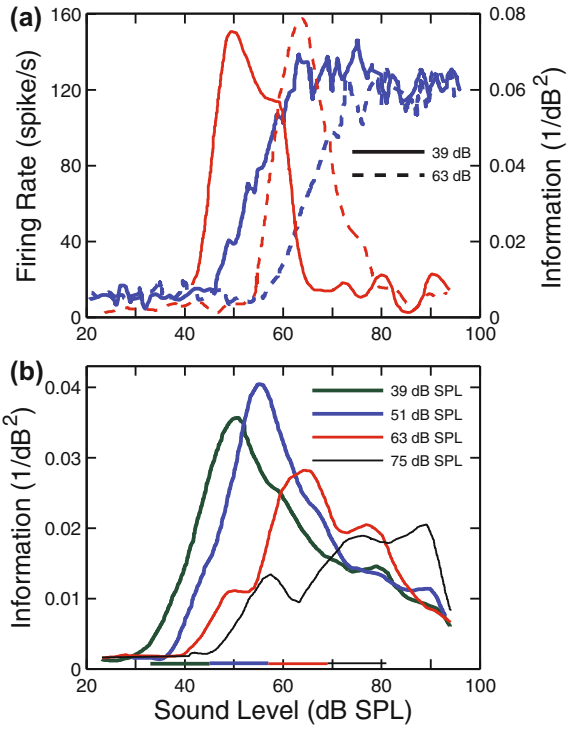

Fig. 8.6 The dynamic range over which individual-neuron firing rates provide information to discriminate small increments in sound level that can adapt toward the most frequently occurring sound levels. **a** Rate-level functions (*thick blue lines*) for an individual inferior colliculus neuron for mean sound levels of 39 (*solid blue*) and 63 (*dashed blue*) dB SPL. *Red lines*, level-discrimination information computed from the response of this neuron. **b** Pooled population information versus sound level for four different mean sound level conditions. *Horizontal bars*, high-probability ranges. Data redrawn from Dean et al. (2005) and reprinted from Heinz (2012), with permission

been observed in certain ventral cochlear nucleus cell types, perhaps consistent with a contribution from central compensatory mechanisms (Cai et al. 2009).

8.4.3 *Dynamic-Range Adaptation*

Although natural sounds (e.g., speech) occur across a wide range of levels, in the short term (i.e., a single listening situation), they tend to have a fairly narrow (~30-dB) dynamic range that is comparable to that of individual neurons (see Sect. 8.4.1). Recent evidence shows that neurons throughout the auditory system can rapidly shift their dynamic range toward the most frequently occurring sound level (Dean et al. 2005; Wen et al. 2012; Fig. 8.6a), suggesting that this mechanism helps to solve the dynamic-range problem. Originally described in inferior colliculus neurons, this adaptive level coding also occurs (to a smaller degree) in ANF responses (Wen et al. 2012), perhaps related to synaptic power-law dynamics (Zilany and Carney 2010). Quantitative pooled-response analyses of the more prominent inferior colliculus effects show that level-coding information still degrades at high SPLs, suggesting that this effect may not be sufficient to resolve the dynamic-range problem entirely (Fig. 8.6b). However, because this mechanism does

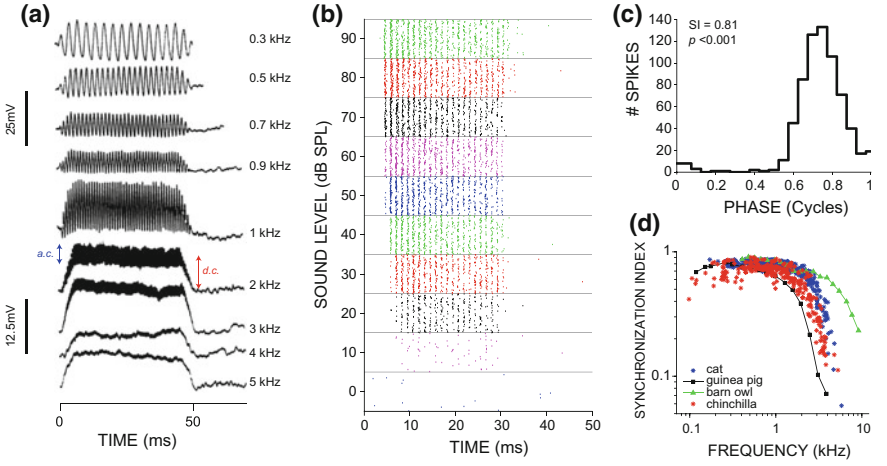

Fig. 8.7 ANF phase locking to single tones. **a** Intracellular single-IHC recordings in response to 50-ms tones at 0.3–5 kHz. Modified from Palmer and Russell (1986), with permission. *Blue arrows*, alternating current (a.c.) component for the 2-kHz response; *red arrows*, direct current (d.c.) component for the 2-kHz response. **b** Spike-raster plot representing spike times recorded from a single low-SR chinchilla ANF (CF = 812 Hz) in response to a CF tone as a function of SPL (Sayles and Joris, unpublished data). **c** Period histogram of spike times expressed modulo stimulus phase. Spikes are well synchronized to the stimulus, with a synchronization index (SI) of 0.81. **d** CF tone synchronization index versus frequency. Replotted data are for guinea pig (population trend schematized; *black*; Palmer and Russell 1986), chinchilla (*red*; Sayles and Joris, unpublished data), cat (*blue*; Johnson 1980), and barn owl (population trend schematized; *green*; Köppl 1997)

appear to contribute to normal auditory processing, it will be important to determine whether the selective loss of low-SR ANFs in cochlear synaptopathy reduces the robustness of level coding in cases of hidden hearing loss (see Sects. 8.1.2 and 8.2).

8.5 Temporal Coding

8.5.1 Phase Locking to Temporal Fine Structure and Envelope

Any acoustic signal can be mathematically decomposed into the product of a rapid "temporal fine structure" (TFS) oscillation and a slower "envelope" (ENV) oscillation. The earliest descriptions of ANF tone responses noted that the timing of spikes from low-CF fibers is a function of the stimulus phase (Galambos and Davis 1943; Rose et al. 1967). Spikes are "phase locked" to the pattern of oscillation induced on the basilar membrane (Fig. 8.7b–d). In this way, TFS is represented in the temporal pattern of spiking. However, ANF spike phase locking is *not* typically on a cycle-by-cycle "entrained" basis. Phase-locking strength is commonly quantified by the "synchronization index" (a.k.a. "vector strength"). This metric is the magnitude of the vector sum over all spike times, where each spike is considered a unit vector with phase corresponding to the instantaneous stimulus phase (Goldberg and Brown 1969). Equivalently, the synchronization index is the ratio of the second to first Fourier components of a histogram of spike phases (a "period histogram"; Johnson 1980). The temporal information present in phase-locked spike trains is thought to be critical for many aspects of normal audition, such as sound localization and musical pitch perception. Moreover, disorders of auditory perception may reflect abnormal phase locking after damage to the nervous system (Moore 2014).

ANF synchronization decreases with increasing stimulus frequency, reaching the measurement noise floor at some upper frequency limit (Johnson 1980; Palmer and Russell 1986). This upper frequency limit varies across species (Fig. 8.7d), whereas the degree of low-pass roll-off appears species invariant (Weiss and Rose 1988a). For cats, the upper frequency limit is ~5 kHz (Johnson 1980). Other common laboratory mammals have slightly lower limits: guinea pig, ~3.5 kHz (Palmer and Russell 1986) and chinchilla, ~4.5 kHz (Temchin and Ruggero 2009). The barn owl is exceptional, having the highest reported phase-locking limit at ~9 kHz (Köppl 1997). The origin of the low-pass behavior of phase locking is commonly thought to relate to the capacitive filtering properties of the IHC membrane and other synaptic properties (Weiss and Rose 1988b). There is a close correspondence between the roll-off in the modulation of IHC receptor potentials and the roll-off in ANF synchronization index (Palmer and Russell 1986; Fig. 8.7a).

ANFs also synchronize spiking to ENV components of multicomponent sounds. The most common method of characterizing temporal coding of ENV is with

sinusoidal amplitude-modulated (SAM) tones (Joris et al. 2004). Strength of ANF spike synchrony to ENV is typically a low-pass function of modulation frequency, with a 3-dB cutoff frequency that increases with CF. Because the filter bandwidth increases with the CF, the increase in temporal-modulation frequency cutoff has been interpreted to imply that filter bandwidth has a significant effect on ENV coding. However, the modulation cutoff frequency saturates for CFs greater than

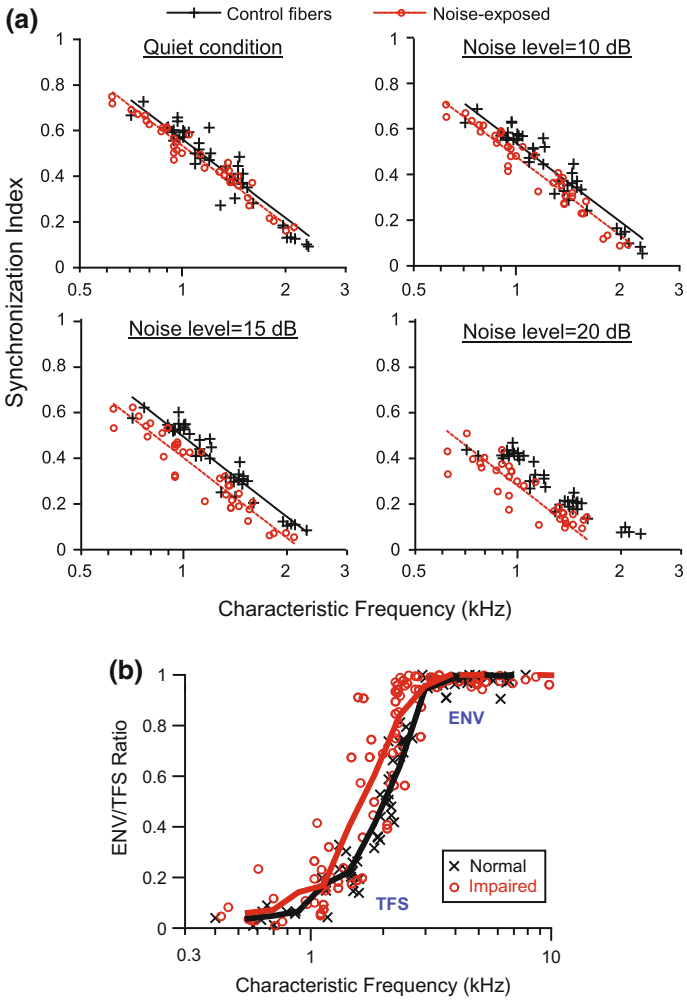

Fig. 8.8 Effects of acoustic trauma on temporal coding of temporal fine structure (TFS) and envelope (ENV). **a** Synchronization index for ANF CF tone responses from normal-hearing (*black*) and hearing-impaired (*red*) chinchillas. Each panel shows responses at a different broadband (20-kHz) noise-to-tone overall-level ratio (in dB). Modified from Henry and Heinz (2012), with permission. **b** Ratio of ENV to TFS coding in ANF responses to sinusoidal amplitude-modulated (SAM) tones. Modified from Kale and Heinz (2010), with permission

~10 kHz in cats (Joris and Yin 1992). This observation implies the existence of a separate mechanism that limits ENV coding at high frequencies, perhaps akin to the roll-off in TFS phase locking.

8.5.2 *Effects of Acoustic Trauma on Temporal Coding in Auditory Nerve Fibers*

Psychophysical studies have suggested that deficits in TFS processing underlie some suprathreshold perceptual abnormalities for hearing-impaired listeners (Moore 2014). Studies in hearing-impaired chinchillas demonstrate that under quiet listening conditions, the phase-locking synchronization index is similar to that found in normal-hearing animals. However, in the presence of background noise, the ability of ANFs of hearing-impaired animals to synchronize to a CF tone is severely diminished (Henry and Heinz 2012; Fig. 8.8a). This finding can be understood conceptually in terms of broadened frequency tuning in impaired animals (see Sect. 8.3.3). Broader filters pass more total masking-noise power, effectively decreasing the signal-to-noise ratio within the passband of the receptive field of the neuron. Thus, although there is no evidence for fundamentally impaired temporal precision in the ANF spike-generation mechanism, a deficit in temporal coding emerges in noisy listening situations due to impaired basilar-membrane filtering. This physiological finding is consistent with the perceptual observation that noisy environments are particularly troublesome for hearing-impaired listeners (see Sect. 8.1.3.3).

ANFs from hearing-impaired animals show a remarkable loss of tonotopicity in TFS coding for complex sounds (Henry et al. 2016). In ANFs from hearing-impaired animals, TFS responses can be shifted down in frequency far away from the CF. For example, responses from fibers with CFs around 4 kHz become dominated by aberrant TFS information between 0.5 and 1 kHz. This loss of tonotopicity for complex sounds can be related conceptually to the interaction between W-shaped tuning curves (Fig. 8.3b) and the roll-off in phase locking (Heinz and Henry 2013; Fig. 8.7d). The perceptual consequences of this tonotopically altered brainstem input pattern for complex-sound perception are likely to be substantial.

Although perceptual studies suggest that humans with cochlear damage experience difficulty exploiting TFS-based cues, it is thought that ENV processing is less affected. Some studies have actually suggested improved amplitude-modulation coding for hearing-impaired listeners compared with normal-hearing controls (e.g., Moore et al. 1996). This finding has been interpreted to reflect a loss of basilar-membrane compression resulting from decreased OHC gain. Neurophysiological studies have examined ENV coding in ANF responses from chinchillas with noise-induced hearing loss (Kale and Heinz 2010, 2012; Henry et al. 2014). ENV coding increases in strength following noise-induced cochlear damage, especially in ANFs with very steep rate-level functions associated with severe IHC damage (Fig. 8.3e; see Sect. 8.4.2). Despite substantially broadened

tuning curves, the upper frequency limit of modulation synchrony is unchanged (Kale and Heinz 2012). The major change in temporal-coding strength after noise-induced cochlear damage is a shift in the *balance* of TFS and ENV coding in mid-CF ANFs. Although hearing impairment does not change the fundamental ability of ANFs to code TFS, there is a substantial downward shift in the CF range over which temporal coding in response to complex sounds transitions mainly between TFS and ENV (Kale and Heinz 2010; Fig. 8.8b).

8.5.3 *Effects of Acoustic Trauma on Across-Fiber Spatiotemporal Coding*

Significant changes occur in the relative timing of phase-locked spikes across ANFs with slightly different CFs after acoustic trauma. These spatiotemporal patterns have been hypothesized to be perceptually relevant for speech (Shamma 1985), pitch (Loeb et al. 1983; Larsen et al. 2008), sound-level coding (Carney 1994; Heinz et al. 2001), tone-in-noise detection (Carney et al. 2002), and binaural processing of interaural time differences (Shamma et al. 1989; Joris et al. 2006). Furthermore, altered spatiotemporal patterns have been suggested to contribute to loudness recruitment (Carney 1994) and degraded processing of frequency modulation (Moore and Skrodzka 2002) after OHC dysfunction.

The primary origin of across-CF phase differences in ANFs responding to the same spectral feature is the cochlear traveling wave (Ruggero 1994), whereby basal locations respond to sound earlier than do apical locations. Phase differences across cochlear locations with CFs near a spectral feature also depend in part on the degree of resonance (cochlear gain and sharpness of tuning), with broader tuning creating more coincident responses across nearby CFs (Carney 1994). Thus, it is not surprising that cochlear damage appears to change delays in direct basilar-membrane measurements (Ruggero 1994) and in derived estimates based on human evoked responses (Strelcyk et al. 2009). Sparse sampling and imprecise CF estimates make accurate quantification of across-CF delays extremely difficult in ANF recordings. However, to overcome this limitation, the effect of acoustic trauma on across-CF delays has been estimated from single ANF responses to a set of frequency-shifted complex sounds (Heinz et al. 2010). Across-CF delays were up to one-quarter cycle smaller in noise-exposed ANFs, representing a more coincident spatiotemporal pattern after cochlear damage. Although this phase shift appears small, a quarter-cycle shift is very significant for spatiotemporal coding theories because it represents the difference between correlated and uncorrelated activity across CFs.

8.6 Adaptation, Suppression and Masking

8.6.1 Auditory Nerve Fiber Adaptation

Sensory systems adapt to stimulation. At the single-neuron level, this typically means that spike probability decreases from some initial peak at the stimulus onset to some lower value during sustained stimulation. After the stimulus offset, the "excitability," or spontaneous spiking probability, is initially depressed and then recovers with a certain characteristic time course. The precise pattern of neural adaptation is thought to have a variety of functional roles in processing time-varying physical stimuli, such as sound. Temporal-adaptation patterns of mammalian ANFs are well characterized, typically showing a peak of onset-related activity followed by a rapid decline to a quasi-steady discharge rate (Westerman and Smith 1984). The underlying mechanism is thought to involve primarily the depletion of a pool of readily releasable synaptic vesicles at the IHC-ANF synapse (Moser and Beutner 2000; Goutman and Glowatzki 2007). ANF adaptation kinetics are thought to be advantageous for the coding of complex sounds containing transients, such as consonants in speech (Delgutte and Kiang 1984b), and to contribute to the coding of amplitude-modulated sounds (Smith and Brachman 1980). After sound offset, spontaneous activity recovers with a quasi-exponential time course over ~200 ms (Harris and Dallos 1979). This form of recovery from adaptation is considered a neurophysiological correlate of the time course of perceptual forward masking, although central contributions appear necessary to account fully for the perceptual effect (Relkin and Turner 1988; Ingham et al. 2016).

After acoustic trauma, ANF-response patterns are more dominated by the initial onset peak of activity, with a more rapid onset-adaptation time constant and a

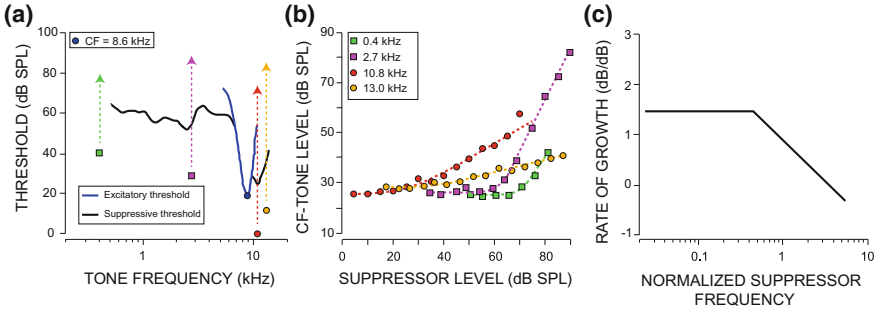

Fig. 8.9 Two-tone rate-suppression threshold and suppression growth in normal hearing. **a** Excitatory (*blue*) and suppressive (*black*) threshold tuning curves for a single cat ANF. Colored symbols and dashed lines indicate frequencies and sound-level range for the growth functions in **b**. **b** Suppression growth functions: two above and two below CF. **c** ANF population trend showing the growth rate of suppression versus normalized (re CF) suppressor frequency. Redrawn from Delgutte (1990b, Figs. 5 and 13), with permission

slower offset recovery (Scheidt et al. 2010). These altered kinetics are hypothesized to relate to changes in IHC intracellular calcium dynamics after noise damage. For example, noise overexposure is associated with elevated hair cell intracellular Ca^{2+} levels (Fridberger et al. 1998). This may alter the balance between the onset and sustained responses by differential action on rapidly inactivating Ca^{2+} channels and voltage-gated Ca^{2+} channels (Heil and Irvine 1997).

8.6.2 Two-Tone Suppression

The compressive nonlinearity of healthy cochlear signal transduction manifests as suppressive interactions between frequency components. In ANFs, these suppressive nonlinearities can be revealed using a two-tone stimulation paradigm (Sachs and Kiang 1968). The spike rate in response to one tone can be reduced by the *simultaneous* presence of a second tone. Hence, the term "two-tone rate suppression" (2TS) has been used (Delgutte 1990b). A similar phenomenon is observed in terms of spike synchrony. Synchrony to one tone can be reduced by the presence of a second, which "captures" the spike synchronization of the ANF (Javel 1981). The underlying basis is thought to be, at least partially, saturation of OHC receptor currents (Geisler et al. 1990). This mechanical phenomenon has almost-instantaneous action, hence the requirement for simultaneous tones (Arthur et al. 1971; van der Heijden and Joris 2005).

Suppressive frequency regions exist above the CF ("high-side suppression") and below the CF ("low-side suppression"; Fig. 8.9). Suppression threshold as a function of frequency for single ANFs has been studied using adaptive-tracking approaches similar to those used to map excitatory-threshold tuning curves (Schmiedt 1982; Delgutte 1990b). Low-side suppression typically has higher thresholds than high-side suppression (Fig. 8.9a). However, low-side suppression grows at a faster rate (up to 3 dB/dB) compared with high-side suppression (<1 dB/dB; Delgutte 1990b; Fig. 8.9b, c).

Instantaneous and frequency-dependent suppressive nonlinearities are important for the neural coding of complex sounds. When listening to broadband sounds, such as speech and music, there are suppressive interactions between multiple-frequency components (van der Heijden and Joris 2005; Sayles et al. 2016), which shape their neural representation (Sachs and Young 1980; Young 2008).

Acoustic trauma-induced OHC damage is associated with cochlear-response linearization. Aging in a noisy environment is associated with a reduction or loss of 2TS, with high-side suppression being the most vulnerable (Schmiedt et al. 1990). The low-side suppression threshold can remain relatively unchanged by hearing loss, even in cochlear regions with up to 60% OHC loss (Schmiedt and Schulte 1992).

8.6.3 Relationship of Adaptation and Suppression to Perceptual Masking

Adaptation and suppression in ANF responses are thought to be important for the neural coding of complex sounds and for the detection and discrimination of signals in background noise (Sachs and Young 1980; Miller et al. 1997). In the simple case of a two-tone stimulus, one at the CF (the signal) and one off the CF (the masker), both excitatory and suppressive masking can occur. If the masker itself excites the ANF, the threshold for signal detection will increase. Alternatively, if the masker acts to suppress the signal response but does not itself drive an increase in spike rate, the threshold for signal detection will also increase. The two mechanisms are not mutually exclusive, in that a masker may have both excitatory and suppressive influences simultaneously. Because suppressive masking effects only occur when the signal and masker overlap in time (simultaneous masking), but excitatory masking can also occur when the masker precedes the signal (forward masking), it is possible to tease apart physiologically the relative contributions of these two mechanisms to masking. Exploiting this approach, Delgutte (1990a) found suppressive masking to dominate for maskers much lower in frequency than the signal where suppressive growth rates are higher (Fig. 8.9b). This finding suggests that the perceptual "upward spread of masking" phenomenon may be derived largely from suppressive rather than excitatory masking, although this remains a topic of debate.

8.7 Coding of Complex Sounds

8.7.1 Speech Coding in the Auditory Nerve

Many fundamental phenomena in audition, such as frequency tuning, adaptation, suppression, and phase locking, can be understood by studying ANF responses to one- or two-tone stimuli. However, in everyday life, auditory systems typically encounter complex acoustic signals having a broadband spectrum, such as vocalizations and music. Knowledge of ANF physiological response properties to simple stimuli is an important foundation for building a detailed conceptual understanding of neural coding of the rich spectrotemporal content of such complex sounds.

The perceptually important frequency content of speech is largely determined by the resonant frequencies of the speaker's vocal tract. These result in "formants," which are peaks in the spectral energy distribution that underlie identification of different vowel sounds (Fant 1970). Neurophysiological studies of speech coding have therefore focused on representations of formant frequencies (Young and Sachs 1979; Delgutte and Kiang 1984a). Typically, spikes from several hundred ANFs with different CFs are recorded in response to the same speech sound. These data are then analyzed from a population perspective, asking what response properties convey information useful to identify salient acoustic features. Broadly speaking,

two common schemes are usually considered: temporal codes based on interspike interval statistics (Young and Sachs 1979; Palmer et al. 1986) and rate-place codes based on the firing-rate distribution across the CF axis (Sachs and Young 1979; Recio et al. 2002). ANF response nonlinearities have large effects on both rate-place and temporal representations (Sachs and Young 1980).

At low sound levels, rate-place profiles of cat ANF responses provide a clear representation of synthetic human vowel sounds. Peaks in firing rate occur at CFs corresponding to the formants. However, as the sound level is increased toward those typical of conversational speech (above ~60-dB SPL), the formant-related pattern of peaks and valleys in the firing rate versus CF profile disappears (Sachs and Young 1979). This is due to a combination of firing-rate saturation and suppressive nonlinearity (Sachs and Young 1980). With increasing SPL, high-SR fibers tuned near formant peaks saturate their firing rate while high-SR fibers tuned away from formant peaks "catch up." Additionally, for fibers tuned near formant peaks, there is increasing rate suppression of on-CF components by off-CF components. Sound-level dependence is the main criticism of rate-place vowel coding. However, low-SR ANFs with higher thresholds and wider dynamic ranges (see Sect. 8.4.1) are still able to represent formant structure at relatively high SPLs (Sachs and Young 1979). In addition, when vowel spectra are scaled appropriately for species-specific cochlear length, rate-place profiles are less dependent on sound

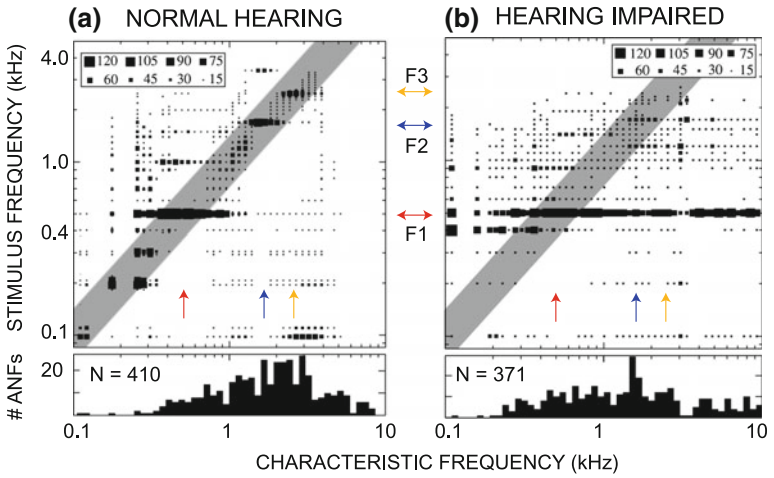

Fig. 8.10 ANF temporal coding of the vowel /ɛ/ in normal (**a**) and impaired (**b**) hearing at equal sensation levels. Spikes are phase locked to stimulus frequency components. Data are Fourier transform magnitudes (*insets*) from poststimulus time histograms, expressed as synchronized firing rate in spikes per second and averaged across fibers of similar CF. *Gray stripe*, response frequencies within 0.5-octave of the CF; *colored arrows*, formant frequencies along both axes. Histograms below the main plots represent the number of fibers in each bin. Modified from Young (2008), with permission

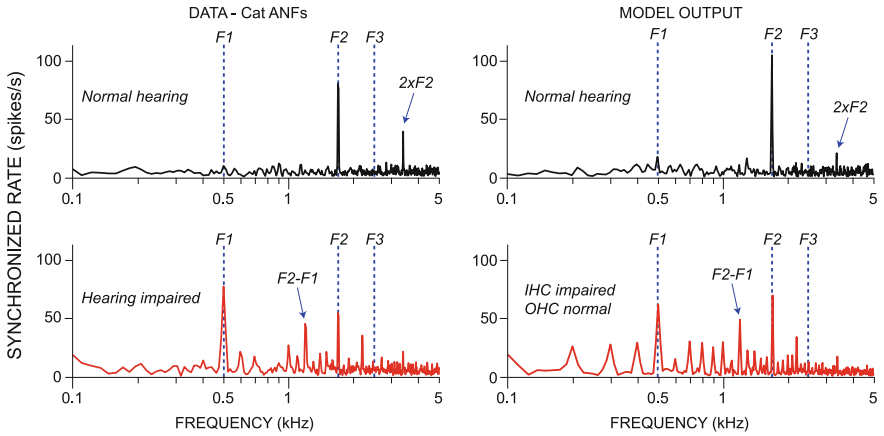

Fig. 8.11 IHC dysfunction contributes to the effects of acoustic trauma on synchrony-based vowel coding. *Left column*: Fourier transforms of PST histograms from a normal (*top*, *black line*) and an impaired cat ANF (*bottom*, *red line*) in response to the vowel /ɛ/; *blue dashed lines*, formant frequencies (F1, F2, F3). Both fibers had a CF near F2. Reprinted from Miller et al. (1997), with permission. *Right column*: AN model responses to the same vowel. *Top*, response of the normal-hearing model; *bottom*, response of a hearing-impaired model ANF with only IHC damage. Modified from Bruce et al. (2003), with permission

level than when "human-scaled" speech is presented to other species (Recio et al. 2002).

Fibers with CFs near formant peaks (particularly the first and second formants, F1 and F2, respectively) show strong phase locking to spectral components nearest to the formant. There is said to be "synchrony capture" of the response of the fiber by those components. Across the tonotopic array, there are narrow CF regions where fibers are dominated by synchrony to F1, to F2, or to higher formants (Young and Sachs 1979; Delgutte and Kiang 1984a; Fig. 8.10a). Between these regions, fibers generally synchronize to modulation at the fundamental frequency (F0) for voiced vowel sounds. As the sound level increases, synchrony suppression of F1 by components near F2 in a normal-hearing ear allows fibers tuned near F2 to maintain a temporal representation of the second formant frequency. Moreover, and in contrast to rate-place profiles, tonotopic temporal representations of vowel sounds are relatively stable with increasing sound level in normal-hearing animals. This is because synchrony to formants tends to capture the response of a fiber and suppress a temporal response to stimulus components away from the formants. In hearing-impaired animals, synchrony to F1 tends to spread across the CF array, degrading the tonotopic representation characteristic of the normal system (Fig. 8.10b).

In hearing-impaired animals, ANFs with CFs near F2 are unable to maintain a clear temporal representation of F2 (Miller et al. 1997; Fig. 8.11, *left column*).

Instead, their responses become dominated by phase locking to components near F1 and intermodulation distortion components such as F2–F1. These alterations (relative to normal hearing) are expected to reduce speech intelligibility for hearing-impaired listeners. Miller et al. (1997) interpreted these data in terms of broadened frequency tuning and weakened suppressive nonlinearities, reflecting OHC dysfunction. However, IHC dysfunction likely also contributes to this altered temporal representation after acoustic trauma, where mixed IHC and OHC pathology is typical (see Sect. 8.1.2). For example, Bruce et al. (2003) found that both IHC and OHC dysfunction contribute to the degraded tonotopic representation of formants in a computational model of ANF responses. Temporal responses similar to those recorded by Miller et al. (1997) were reproduced by *only* impairing the IHC component of the model (Fig. 8.11, *right column*).

Other aspects of ANF physiology, such as adaptation, likely also contribute to the coding of ongoing speech. The description here is limited to ANF representations of steady-state voiced vowel sounds. This view is simplistic because natural speech cannot simply be viewed as a temporal series of discrete isolated epochs. Moreover, the addition of background noise or a single concurrent talker adds significant complexity to the neural representation (Delgutte and Kiang 1984c; Palmer 1990). For a detailed review of speech coding, see Young (2008).

8.7.2 Auditory Scene Analysis

Ears are typically faced with a jumbled mixture of acoustic energy from more than one sound source. The auditory system must parse this mixture into several auditory "streams" to form distinct "auditory objects," thereby enabling a listener to follow a single voice during a conversation in a noisy situation (Bregman 1990). An F0 difference between sound sources is a particularly salient acoustic feature for this task (Brokx and Nooteboom 1982). For example, the high-pitched voice of a young child in the presence of the low-pitched voiced of an adult male can be followed with relative ease. Palmer (1990) studied the representation of "double vowels" in the spiking responses of single guinea pig ANFs. Fibers with CFs near a formant peak of one of the two vowels tended to phase lock to spectral components from that vowel sound, giving a temporal cue to that formant frequency. Fibers with CFs away from a formant of either vowel tended to phase lock to the envelope modulation corresponding to the F0 of either one or both vowels in the mixture. The relative strength of phase locking to the F0 of each vowel in the mixture depended on the balance of energy from each vowel at the basilar membrane location corresponding to the CF of the fiber. This temporal information in ANF spike patterns can be exploited for perceptual segregation of the competing voices (de Cheveigné 1993; Keilson et al. 1997).

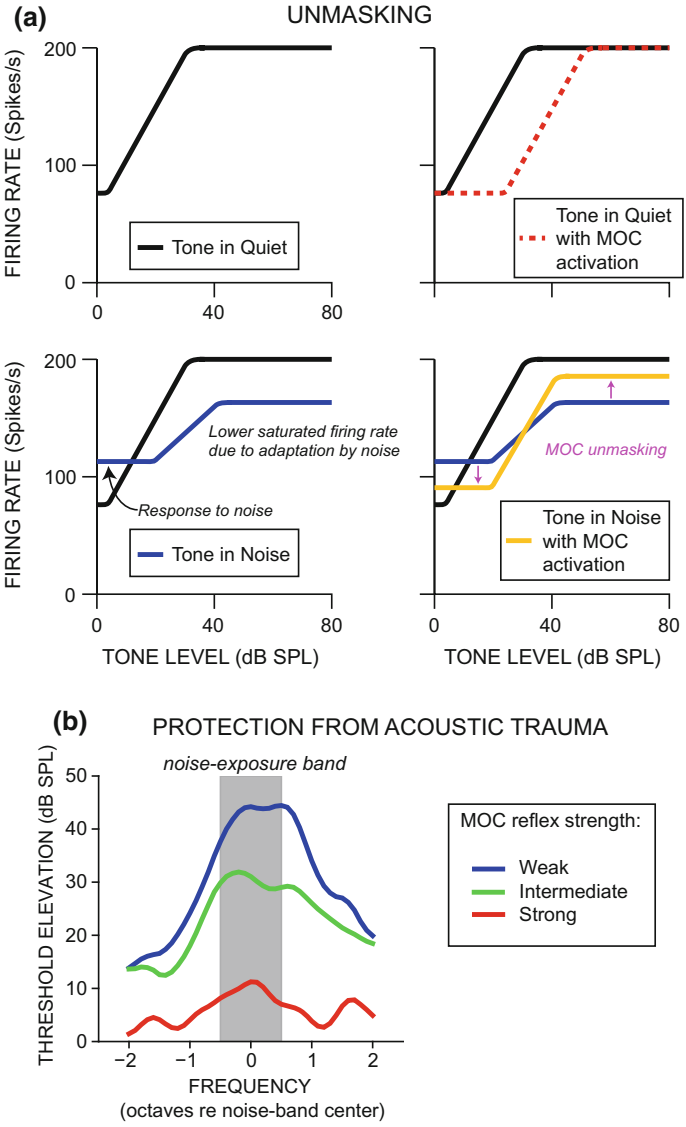

Fig. 8.12 Hypothesized functions of the MOC efferent system: signal unmasking and protection from acoustic trauma. **a** Schematic rate-level functions for a HSR ANF in response to CF tones in quiet, in background noise, and with and without MOC efferent activation. Based on a similar figure in Guinan (2006), with permission. **b** Permanent threshold shifts measured from compound action potential recordings in guinea pigs exposed to an octave-band noise. Data from Maison and Liberman (2000) grouped according to estimated MOC reflex strength and averaged across three noise-exposure bands

8.8 Role of Olivocochlear Efferents

8.8.1 Sensory-Context Modulation of Cochlear Function

MOC efferent activation is thought to improve signal detection in noisy backgrounds (Dewson 1968; Kawase et al. 1993). MOC activation decreases ANF responses to tones in a quiet background (Guinan and Gifford 1988); therefore, a role for MOC efferents in improving signal detection may appear counterintuitive. However, in the presence of background noise, MOC activation can actually increase ANF responses to transient sounds by decreasing neural adaptation to the background noise (Winslow and Sachs 1988; Kawase et al. 1993; Fig. 8.12a). Such improvements in the detectability of transient sounds may be particularly important for the coding of modulated signals, such as speech. A related "sensory-context" functional role for the MOC efferent system is the modulation of cochlear gain by other sensory modalities. Attention to visual stimuli reduces the gain of cochlear signal transduction, suggesting that selective attention can modulate the gain of auditory afferents via olivocochlear efferents (Delano et al. 2007).

8.8.2 Protection from Acoustic Trauma

Efferents are thought to protect the cochlea from the damaging effects of intense-sound exposure (Rajan 2000). Recent work shows MOC innervation of OHCs is tonotopically aligned with ANFs in a manner consistent with that predicted to be optimal for cochlear protection (Brown 2014, 2016). Functionally, MOC reflex strength is inversely correlated with the degree of permanent threshold elevation after intense noise overexposure (Maison and Liberman 2000; Fig. 8.12b). Work on cochlear synaptopathy (Kujawa and Liberman 2015) has led to a greater understanding of the protective role of MOC efferents under everyday listening conditions. After exposure to moderate-level noise, mice with lesioned efferent neurons had a greater loss of IHC-ANF synapses compared with control mice (Maison et al. 2013). It therefore seems likely that protection from noise damage could be a major driving force for the evolution of such a negative-feedback control system operating at sound levels typical of conversational speech. The LOC system may also play a role in protection from acoustic trauma. Mice with selectively lesioned LOC neurons are more susceptible to ipsilateral acoustic trauma compared with control mice (Darrow et al. 2007).

8.8.3 *Balancing Interaural Sensitivity*

LOC neurons are located in the lateral superior olive, a brainstem nucleus that receives binaural inputs and is involved in the processing of interaural-level difference (ILD) cues for sound-source localization. One potential function of the LOC efferent system is to maintain the two cochleae in a state of balanced excitability, thereby contributing to effective ILD coding (Irving et al. 2011). Without precisely balanced excitability, any interaural difference in cochlear output may or may not reflect a true ILD. Darrow et al. (2006a) found a shift in the balance of excitability between the two cochleae after selectively lesioning LOC neurons. LOC lesions removed the tight interaural correlation in auditory brainstem response (ABR) wave-I amplitudes (reflecting the summed activity of all ANFs) seen in normal animals. These data therefore suggest that a functional LOC efferent system is required to maintain proper interaural balance in excitability, perhaps to enable high sensitivity to small ILDs.

8.9 Summary and Future Directions

This chapter has focused on the neural coding of sounds in the discharge patterns of ANFs in normal and impaired hearing. Work addressing the physiological effects of hearing loss on ANF responses has highlighted a number of perceptually and translationally relevant effects (e.g., broadened tuning and loss of tonotopicity) as well as the absence of some hypothesized physiological correlates of psychophysical phenomena (e.g., the lack of consistently steeper rate-level functions and the lack of degraded TFS phase-locking strength). This absence of hearing-loss effects on ANF physiology has led to important insights, such as the opposing effects of OHC and IHC dysfunction that complicate the interpretation of physiological correlates of loudness recruitment. It is critically important to study the effects of cochlear damage on the neural coding of complex sounds because the full impact of changes in tonotopicity and frequency-dependent nonlinearities may only be apparent for broadband sounds. More detailed work is needed to understand the effects of cochlear damage on suppressive nonlinearities, which are critical for robust speech coding in normal hearing. More generally, future work exploring the effects of OHC versus IHC dysfunction on auditory neural coding will be important for improving understanding of the basis for individual variability in speech perception across patients with similar audiograms. Such work may ultimately lead to diagnostic tests sensitive to differences in the balance of OHC and IHC dysfunction, thereby refining the currently singular category of SNHL and allowing individually tailored approaches to audiological therapy that are physiologically based.

Important insight into the salient features of neural coding has been garnered from both experimental and modeling studies quantifying correlations between peripheral physiology and perception. However, an enormous amount of neural

computation is performed by the brain. The consequences of altered peripheral processing for neural coding in the brainstem and beyond, at a single-neuron level, have received much less attention than the peripheral effects presented in this chapter. Hypothesis-driven exploration of the effects of hearing impairment on the central auditory nervous system, based on knowledge of cochlear damage and ANF physiology, is a fruitful avenue for future work in this field. In particular, the effects of hearing loss on binaural processing will be important for understanding and ameliorating the difficulties listeners with cochlear hearing loss have in spatial source segregation in real-world listening situations (Middlebrooks et al. 2016), for which hearing aids currently provide limited benefit (Popelka et al. 2016).

Exciting recent work has begun to link cochlear synaptopathy after moderate sound exposure to suprathreshold processing deficits, so-called "hidden hearing loss" (Bharadwaj et al. 2015). One limitation in this work is that the evoked physiological measures (e.g., ABRs, envelope following responses, and, more recently, middle ear reflexes) that have been correlated with perceptual deficits do not provide direct confirmation of the degree of cochlear synaptopathy in humans. Future work to provide quantitative links between single-ANF responses (e.g., of differing SRs) and evoked responses is critical to the development of fast and reliable assays of cochlear synaptopathy that can be applied in the audiology clinic. From the opposite angle, animal behavioral studies are also needed to establish the perceptual consequences of cochlear synaptopathy. Finally, the loss of synaptic connections between IHCs and ANFs characteristic of this form of hearing impairment does have one major saving grace. The sensory cells themselves and their neural connections to the brain survive for months to years after the synaptic insult. This offers a window of opportunity for future therapeutic intervention, perhaps exploiting neurotrophins to restore functional IHC-ANF connections (e.g., Suzuki et al. 2016) or stem cells to replace damaged or missing auditory neurons (Nayagam and Edge 2016).

Acknowledgements Preparation of this chapter was partially supported by a grant from the National Institute on Deafness and Other Communication Disorders (R01-DC009838). Mark Sayles was supported by a UK-US Fulbright Scholarship from Action on Hearing Loss and a postdoctoral fellowship from the Research Foundation, Flanders, Belgium.

Compliance with Ethics Requirements Mark Sayles declares that he has no conflict of interest. Michael G. Heinz declares that he has no conflict of interest.

References

Arthur, R. M., Pfeiffer, R. R., & Suga, N. (1971). Properties of "two-tone inhibition" in primary auditory neurones. *The Journal of Physiology*, 212(3), 593–609.

Baguley, D. M. (2003). Hyperacusis. *Journal of the Royal Society of Medicine*, 96(12), 582–585.

Benson, T. E., & Brown, M. C. (2004). Postsynaptic targets of type II auditory nerve fibers in the cochlear nucleus. *Journal of the Association for Research in Otolaryngology*, 5(2), 111–125.

Bharadwaj, H. M., Masud, S., Mehraei, G., Verhulst, S., & Shinn-Cunningham, B. G. (2015). Individual differences reveal correlates of hidden hearing deficits. *The Journal of Neuroscience*, 35(5), 2161–2172.

Bohne, B. A., Bozzay, D. G., & Harding, G. W. (1986). Interaural correlations in normal and traumatized cochleas: Length and sensory cell loss. *The Journal of the Acoustical Society of America*, 80(6), 1729–1736.

Bregman, A. S. (1990). *Auditory Scene Analysis*. Cambridge, MA: MIT Press.

Brokx, J. P. L., & Nooteboom, S. G. (1982). Intonation and the perceptual separation of simultaneous voices. *Journal of Phonetics*, 10(1), 23–36.

Brown, M. C. (1987). Morphology of labeled afferent fibers in the guinea pig cochlea. *The Journal of Comparative Neurology*, 260(4), 591–604.

Brown, M. C. (2014). Single-unit labeling of medial olivocochlear neurons: The cochlear frequency map for efferent axons. *Journal of Neurophysiology*, 111(11), 2177–2186.

Brown, M. C. (2016). Recording and labeling at a site along the cochlea shows alignment of medial olivocochlear and auditory nerve tonotopic mappings. *Journal of Neurophysiology*, 115 (3), 1644–1653.

Bruce, I. C., Sachs, M. B., & Young, E. D. (2003). An auditory-periphery model of the effects of acoustic trauma on auditory nerve responses. *The Journal of the Acoustical Society of America*, 113(1), 369–388.

Cai, S., Ma, W.-L. D., & Young, E. D. (2009). Encoding intensity in ventral cochlear nucleus following acoustic trauma: Implications for loudness recruitment. *Journal of the Association for Research in Otolaryngology*, 10(1), 5–22.

Carney, L. H. (1993). A model for the responses of low-frequency auditory-nerve fibers in cat. *The Journal of the Acoustical Society of America*, 93, 401–417.

Carney, L. H. (1994). Spatiotemporal encoding of sound level: Models for normal encoding and recruitment of loudness. *Hearing Research*, 76(1–2), 31–44.

Carney, L. H., Heinz, M. G., Evilsizer, M. E., Gilkey, R. H., & Colburn, H. S. (2002). Auditory phase opponency: A temporal model for masked detection at low frequencies. *Acta Acustica united with Acustica*, 88, 334–347.

Cody, A. R., & Robertson, D. (1983). Variability of noise-induced damage in the guinea pig cochlea: Electrophysiological and morphological correlates after strictly controlled exposures. *Hearing Research*, 9(1), 55–70.

Colburn, H. S., Carney, L. H., & Heinz, M. G. (2003). Quantifying the information in auditory-nerve responses for level discrimination. *Journal of the Association for Research in Otolaryngology*, 4, 294–311.

Costalupes, J. A., Young, E. D., & Gibson, D. J. (1984). Effects of continuous noise backgrounds on rate response of auditory nerve fibers in cat. *Journal of Neurophysiology*, 51(6), 1326–1344.

Dallos, P., Popper, A. N., & Fay, R. R. (Eds.). (1996). *The Cochlea*. New York: Springer-Verlag.

Darrow, K. N., Maison, S. F., & Liberman, M. C. (2006a). Cochlear efferent feedback balances interaural sensitivity. *Nature Neuroscience*, 9(12), 1474–1476.

Darrow, K. N., Simons, E. J., Dodds, L., & Liberman, M. C. (2006b). Dopaminergic innervation of the mouse inner ear: Evidence for a separate cytochemical group of cochlear efferent fibers. *The Journal of Comparative Neurology*, 498(3), 403–414.

Darrow, K. N., Maison, S. F., & Liberman, M. C. (2007). Selective removal of lateral olivocochlear efferents increases vulnerability to acute acoustic injury. *Journal of Neurophysiology*, 97(2), 1775–1785.

Dean, I., Harper, N. S., & McAlpine, D. (2005). Neural population coding of sound level adapts to stimulus statistics. *Nature Neuroscience*, 8(12), 1684–1689.

de Boer, E., & de Jongh, H. R. (1978). On cochlear encoding: potentialities and limitations of the reverse-correlation technique. *The Journal of the Acoustical Society of America*, 63(1), 115–135.

de Cheveigné, A. (1993). Separation of concurrent harmonic sounds: Fundamental frequency estimation and a time-domain cancellation model of auditory processing. *The Journal of the Acoustical Society of America*, 93(6), 3271–3290.

Delano, P. H., Elgueda, D., Hamame, C. M., & Robles, L. (2007). Selective attention to visual stimuli reduces cochlear sensitivity in chinchillas. *The Journal of Neuroscience*, 27(15), 4146–4153.

Delgutte, B. (1987). Peripheral auditory processing of speech information: Implications from a physiological study of intensity discrimination. In M. E. H. Schouten (Ed.), *The Psychophysics of Speech Perception* (pp. 333–353). Dordrecht, The Netherlands: Nijhof.

Delgutte, B. (1990a). Physiological mechanisms of psychophysical masking: Observations from auditory-nerve fibers. *The Journal of the Acoustical Society of America*, 87(2), 791–809.

Delgutte, B. (1990b). Two-tone rate suppression in auditory-nerve fibers: Dependence on suppressor frequency and level. *Hearing Research*, 49(1–3), 225–246.

Delgutte, B. (1996). Physiological models for basic auditory percepts. In H. L. Hawkins, T. A. McMullen, A. N. Popper, & R. R. Fay (Eds.), *Auditory Computation* (pp. 157–220). New York: Springer-Verlag.

Delgutte, B., & Kiang, N. Y.-S. (1984a). Speech coding in the auditory nerve. I. Vowel-like sounds. *The Journal of the Acoustical Society of America*, 75(3), 866–878.

Delgutte, B., & Kiang, N. Y.-S. (1984b). Speech coding in the auditory nerve. IV. Sounds with consonant-like dynamic characteristics. *The Journal of the Acoustical Society of America*, 75(3), 897–907.

Delgutte, B., & Kiang, N. Y. S. (1984c). Speech coding in the auditory nerve. V. Vowels in background noise. *The Journal of the Acoustical Society of America*, 75(3), 908–918.

Dewson, J. H. (1968). Efferent olivocochlear bundle: Some relationships to stimulus discrimination in noise. *Journal of Neurophysiology*, 31(1), 122–130.

Duquesnoy, A. J. (1983). Effect of a single interfering noise or speech source upon the binaural sentence intelligibility of aged persons. *The Journal of the Acoustical Society of America*, 74(3), 739–743.

Edwards, B. (2004). Hearing aids and hearing impairment. In S. Greenberg, W. A. Ainsworth, A. N. Popper, & R. R. Fay (Eds.), *Speech Processing in the Auditory System* (pp. 339–421). New York: Springer-Verlag.

Eustaquio-Martín, A., & Lopez-Poveda, E. A. (2011). Isoresponse versus isoinput estimates of cochlear filter tuning. *Journal of the Association for Research in Otolaryngology*, 12(3), 281–299.

Evans, E. F. (2001). Latest comparisons between physiological and behavioural frequency selectivity. In D. J. Breebart, A. J. M. Houtsma, A. Kohlrausch, V. F. Prijs, & R. Schoonhoven (Eds.), *Physiological and Psychophysical Bases of Auditory Function* (pp. 382–387). Maastricht, The Netherlands: Shaker Publishing BV.

Fant, G. (1970). *Acoustic Theory of Speech Production.* The Hague, The Netherlands: Mouton de Gruyter.

Festen, J. M., & Plomp, R. (1990). Effects of fluctuating noise and interfering speech on the speech-reception threshold for impaired and normal hearing. *The Journal of the Acoustical Society of America*, 88(4), 1725–1736.

Fletcher, H. (1940). Auditory patterns. *Review of Modern Physics*, 12, 47–65.

Fletcher, H., & Munson, W. A. (1933). Loudness, its definition, measurement and calculation. *The Journal of the Acoustical Society of America*, 5, 82–108.

Fridberger, A., Flock, Å., Ulfendahl, M., & Flock, B. (1998). Acoustic overstimulation increases outer hair cell Ca^{2+} concentrations and causes dynamic contractions of the hearing organ. *Proceedings of the National Academy of Sciences of the United States of America*, 95(12), 7127–7132.

Froud, K. E., Wong, A. C. Y., Cederholm, J. M. E., Klugmann, M., Sandow, S. L., Julien, J. P., Ryan, A. F., & Housley, G. D. (2015). Type II spiral ganglion afferent neurons drive medial olivocochlear reflex suppression of the cochlear amplifier. *Nature Communications*, 6, 7115.

Fuchs, P. (2002). The synaptic physiology of cochlear hair cells. *Audiology and Neurotology*, 7(1), 40–44.

Furman, A. C., Kujawa, S. G., & Liberman, M. C. (2013). Noise-induced cochlear neuropathy is selective for fibers with low spontaneous rates. *Journal of Neurophysiology*, 110(3), 577–586.

Galambos, R., & Davis, H. (1943). The response of single auditory nerve fibers to acoustic stimulation. *Journal of Neurophysiology*, 6, 39–57.

Geisler, C. D., Yates, G. K., Patuzzi, R. B., & Johnstone, B. M. (1990). Saturation of outer hair cell receptor currents causes two-tone suppression. *Hearing Research*, 44(2–3), 241–256.

Goldberg, J. M., & Brown, P. B. (1969). Responses of binaural neurons in the dog superior olivary complex to dichotic stimuli: Some physiological mechanisms of sound localization. *Journal of Neurophysiology*, 32, 613–636.

Goldstein, J. L. (1974). Is the power law simply related to the driven spike response rate from the whole auditory nerve? In H. R. Moskowitz, B. Scharf, & S. S. Stevens (Eds.), *Sensation and Measurement* (pp. 223–229). Dordrecht, The Netherlands: Reidel.

Goutman, J. D., & Glowatzki, E. (2007). Time course and calcium dependence of transmitter release at a single ribbon synapse. *Proceedings of the National Academy of Sciences of the United States of America*, 104(41), 16341–16346.

Groff, J. A., & Liberman, M. C. (2003). Modulation of cochlear afferent response by the lateral olivocochlear system: Activation via electrical stimulation of the inferior colliculus. *Journal of Neurophysiology*, 90(5), 3178–3200.

Guinan, J. J. (2006). Olivocochlear efferents: Anatomy, physiology, function, and the measurement of efferent effects in humans. *Ear and Hearing*, 27(6), 589–607.

Guinan, J. J. (2013). Physiology and function of cochlear efferents. In D. Jaeger & R. Jung (Eds.), *Encyclopedia of Computational Neuroscience* (pp. 1–11). New York: Springer-Verlag.

Guinan, J. J., & Gifford, M. L. (1988). Effects of electrical stimulation of efferent olivocochlear neurons on cat auditory-nerve fibers. III. Tuning curves and thresholds at CF. *Hearing Research*, 37(1), 29–45.

Harding, G. W., & Bohne, B. A. (2009). Relation of focal hair cell lesions to noise-exposure parameters from a 4- or a 0.5-kHz octave band of noise. *Hearing Research*, 254(1–2), 54–63.

Harris, D. M., & Dallos, P. (1979). Forward masking of auditory nerve fiber responses. *Journal of Neurophysiology*, 42(4), 1083–1107.

Harrison, R. V. (1981). Rate-versus-intensity functions and related AP responses in normal and pathological guinea pig and human cochleas. *The Journal of the Acoustical Society of America*, 70(4), 1036–1044.

Heil, P., & Irvine, D. R. F. (1997). First-spike timing of auditory-nerve fibers and comparison with auditory cortex. *Journal of Neurophysiology*, 78(5), 2438–2454.

Heinz, M. G. (2010). Computational modeling of sensorineural hearing loss. In R. Meddis, E. A. Lopez-Poveda, A. N. Popper, & R. R. Fay (Eds.), *Computational Models of the Auditory System* (pp. 177–202). New York: Springer US.

Heinz, M. G. (2012). Intensity coding throughout the auditory system. In K. L. Tremblay & R. F. Burkard (Eds.), *Translational Perspectives in Auditory Neuroscience: Normal Aspects of Hearing* (pp. 349–386). San Diego, CA: Plural Publishing.

Heinz, M. G. (2016). Neural modelling to relate individual differences in physiological and perceptual responses with sensorineural hearing loss. In S. Santurette, T. Dau, J. C. Dalsgaard, L. Tranebjaerg, T. Andersen, & T. Poulsen (Eds.), *Individual Hearing Loss – Characterization, Modelling, Compensation Strategies, International Symposium on Audiological and Auditory Research (ISAAR),* Danavox Jubilee Foundation, Nyborg, Denmark, August 23–25, 2017, pp. 137–148.

Heinz, M. G., & Young, E. D. (2004). Response growth with sound level in auditory-nerve fibers after noise-induced hearing loss. *Journal of Neurophysiology*, 91(2), 784–795.

Heinz, M. G., & Henry, K. S. (2013). Modeling disrupted tonotopicity of temporal coding following sensorineural hearing loss. *Proceedings of Meetings on Acoustics*, 19(1), 050177.

Heinz, M. G., Colburn, H. S., & Carney, L. H. (2001). Rate and timing cues associated with the cochlear amplifier: Level discrimination based on monaural cross-frequency coincidence detection. *The Journal of the Acoustical Society of America*, 110(4), 2065–2084.

Heinz, M. G., Issa, J. B., & Young, E. D. (2005). Auditory-nerve rate responses are inconsistent with common hypotheses for the neural correlates of loudness recruitment. *Journal of the Association for Research in Otolaryngology*, 6(2), 91–105.

Heinz, M. G., Swaminathan, J., Boley, J. D., & Kale, S. (2010). Across-fiber coding of temporal fine-structure: Effects of noise-induced hearing loss on auditory-nerve responses. In E. A. Lopez-Poveda, A. R. Palmer, & R. Meddis (Eds.), *The Neurophysiological Bases of Auditory Perception* (pp. 621–630). New York: Springer-Verlag.

Henry, K. S., & Heinz, M. G. (2012). Diminished temporal coding with sensorineural hearing loss emerges in background noise. *Nature Neuroscience*, 15(10), 1362–1364.

Henry, K. S., Kale, S., & Heinz, M. G. (2014). Noise-induced hearing loss increases the temporal precision of complex envelope coding by auditory-nerve fibers. *Frontiers in Systems Neuroscience*, 8, 20.

Henry, K. S., Kale, S., & Heinz, M. G. (2016). Distorted tonotopic coding of temporal envelope and fine structure with noise-induced hearing loss. *The Journal of Neuroscience*, 36(7), 2227–2237.

Hu, B. (2012). Noise-induced structural damage to the cochlea. In C. G. Le Prell, D. Henderson, R. R. Fay, & A. N. Popper (Eds.), *Noise-Induced Hearing Loss* (pp. 57–86). New York: Springer-Verlag.

Ingham, N. J., Itatani, N., Bleeck, S., & Winter, I. M. (2016). Enhancement of forward suppression begins in the ventral cochlear nucleus. *Brain Research*, 1639, 13–27.

Irving, S., Moore, D. R., Liberman, M. C., & Sumner, C. J. (2011). Olivocochlear efferent control in sound localization and experience-dependent learning. *The Journal of Neuroscience*, 31(7), 2493–2501.

Javel, E. (1981). Suppression of auditory nerve responses I: Temporal analysis, intensity effects and suppression contours. *The Journal of the Acoustical Society of America*, 69(6), 1735–1745.

Johnson, D. H. (1974). *The Response of Single Auditory-Nerve Fibers in the Cat to Single Tones: Synchrony and Average Discharge Rate.* Cambridge, MA: MIT.

Johnson, D. H. (1980). The relationship between spike rate and synchrony in responses of auditory-nerve fibers to single tones. *The Journal of the Acoustical Society of America*, 68(4), 1115–1122.

Joris, P. X., & Yin, T. C. T. (1992). Responses to amplitude-modulated tones in the auditory nerve of the cat. *The Journal of the Acoustical Society of America*, 91(1), 215–232.

Joris, P. X., Schreiner, C. E., & Rees, A. (2004). Neural processing of amplitude-modulated sounds. *Physiological Reviews*, 84(2), 541–577.

Joris, P. X., Van de Sande, B., Louage, D. H., & van der Heijden, M. (2006). Binaural and cochlear disparities. *Proceedings of the National Academy of Sciences of the United States of America*, 103(34), 12917–12922.

Joris, P. X., Bergevin, C., Kalluri, R., McLaughlin, M., Michelet, P., van der Heijden, M., & Shera, C. A. (2011). Frequency selectivity in Old-World monkeys corroborates sharp cochlear tuning in humans. *Proceedings of the National Academy of Sciences of the United States of America*, 108(42), 17516–17520.

Kale, S., & Heinz, M. G. (2010). Envelope coding in auditory nerve fibers following noise-induced hearing loss. *Journal of the Association for Research in Otolaryngology*, 11(4), 657–673.

Kale, S., & Heinz, M. G. (2012). Temporal modulation transfer functions measured from auditory-nerve responses following sensorineural hearing loss. *Hearing Research*, 286(1–2), 64–75.

Kawase, T., Delgutte, B., & Liberman, M. C. (1993). Antimasking effects of the olivocochlear reflex. II. Enhancement of auditory-nerve response to masked tones. *Journal of Neurophysiology*, 70(6), 2533–2549.

Keilson, S. E., Richards, V. M., Wyman, B. E., & Young, E. D. (1997). The representation of concurrent vowels in the cat anaesthetized ventral cochlear nucleus: Evidence for a periodicity-tagged spectral representation. *The Journal of the Acoustical Society of America*, 102(2), 1056–1070.

Köppl, C. (1997). Phase locking to high frequencies in the auditory nerve and cochlear nucleus magnocellularis of the barn owl, *Tyto alba*. *The Journal of Neuroscience*, 17(9), 3312–3321.

Kujawa, S. G., & Liberman, M. C. (2009). Adding insult to injury: Cochlear nerve degeneration after "temporary" noise-induced hearing loss. *The Journal of Neuroscience*, 29(45), 14077–14085.

Kujawa, S. G., & Liberman, M. C. (2015). Synaptopathy in the noise-exposed and aging cochlea: Primary neural degeneration in acquired sensorineural hearing loss. *Hearing Research*, 330, 191–199.

Larsen, E., Cedolin, L., & Delgutte, B. (2008). Pitch representations in the auditory nerve: Two concurrent complex tones. *Journal of Neurophysiology*, 100(3), 1301–1319.

Le Prell, C., & Henderson, D. (2012). Perspectives on noise-induced hearing loss. In C. G. Le Prell, D. Henderson, R. R. Fay, & A. N. Popper (Eds.), *Noise-Induced Hearing Loss* (pp. 1–10). New York: Springer-Verlag.

Liberman, M. C. (1978). Auditory-nerve responses from cats raised in a low-noise chamber. *The Journal of the Acoustical Society of America*, 63(2), 442–455.

Liberman, M. C. (1980). Morphological differences among radial afferent fibers in the cat cochlea: An electron-microscopic study of serial sections. *Hearing Research*, 3(1), 45–63.

Liberman, M. C. (1982). The cochlear frequency map for the cat: Labeling auditory-nerve fibers of known characteristic frequency. *The Journal of the Acoustical Society of America*, 72(5), 1441–1449.

Liberman, M. C., & Dodds, L. W. (1984). Single-neuron labeling and chronic cochlear pathology. III. Stereocilia damage and alterations of threshold tuning curves. *Hearing Research*, 16(1), 55–74.

Liberman, M. C., & Kiang, N. Y.-S. (1984). Single-neuron labeling and chronic cochlear pathology. IV. Stereocilia damage and alterations in rate- and phase-level functions. *Hearing Research*, 16(1), 75–90.

Liberman, M. C., Puria, S., & Guinan, J. J. (1996). The ipsilaterally evoked olivocochlear reflex causes rapid adaptation of the $2f_1$-f_2 distortion product otoacoustic emission. *The Journal of the Acoustical Society of America*, 99(6), 3572–3584.

Loeb, G. E., White, M. W., & Merzenich, M. M. (1983). Spatial cross-correlation. A proposed mechanism for acoustic pitch perception. *Biological Cybernetics*, 47(3), 149–163.

Maison, S. F., & Liberman, M. C. (2000). Predicting vulnerability to acoustic injury with a noninvasive assay of olivocochlear reflex strength. *The Journal of Neuroscience*, 20(12), 4701–4707.

Maison, S. F., Usubuchi, H., & Liberman, M. C. (2013). Efferent feedback minimizes cochlear neuropathy from moderate noise exposure. *The Journal of Neuroscience*, 33(13), 5542–5552.

Manley, G. A., & van Dijk, P. (2016). Frequency selectivity of the human cochlea: Suppression tuning of spontaneous otoacoustic emissions. *Hearing Research*, 336, 53–62.

Middlebrooks, J. C., Simon, J. Z., Popper, A. N., & Fay, R. R. (Eds.). (2016). *The Auditory System at the Cocktail Party*. New York: Springer International Publishing.

Miller, R. L., Schilling, J. R., Franck, K. R., & Young, E. D. (1997). Effects of acoustic trauma on the representation of the vowel "eh" in cat auditory nerve fibers. *The Journal of the Acoustical Society of America*, 101(6), 3602–3216.

Moore, B. C. J. (1995). *Perceptual Consequences of Cochlear Damage*. New York: Oxford University Press.

Moore, B. C. J. (2014). *Auditory Processing of Temporal Fine Structure: Effects of Age and Hearing Loss*. Singapore: World Scientific.

Moore, B. C. J., & Skrodzka, E. (2002). Detection of frequency modulation by hearing-impaired listeners: Effects of carrier frequency, modulation rate, and added amplitude modulation. *The Journal of the Acoustical Society of America*, 111(1), 327–335.

Moore, B. C. J., & Glasberg, B. R. (2004). A revised model of loudness perception applied to cochlear hearing loss. *Hearing Research*, 188(1–2), 70–88.

Moore, B. C. J., Wojtczak, M., & Vickers, D. A. (1996). Effect of loudness recruitment on the perception of amplitude modulation. *The Journal of the Acoustical Society of America*, 100(1), 481–489.

Moser, T., & Beutner, D. (2000). Kinetics of exocytosis and endocytosis at the cochlear inner hair cell afferent synapse of the mouse. *Proceedings of the National Academy of Sciences of the United States of America*, 97(2), 883–888.

Narayan, S. S., Temchin, A. N., Recio, A., & Ruggero, M. A. (1998). Frequency tuning of basilar membrane and auditory nerve fibers in the same cochleae. *Science*, 282, 1882–1884.

Nayagam, B. A., & Edge, A. S. B. (2016). Stem cells for the replacement of auditory neurons. In A. Dabdoub, B. Fritzsch, A. N. Popper, & R. R. Fay (Eds.), *The Primary Auditory Neurons of the Mammalian Cochlea* (pp. 263–286). New York: Springer-Verlag.

Oxenham, A. J., & Shera, C. A. (2003). Estimates of human cochlear tuning at low levels using forward and simultaneous masking. *Journal of the Association for Research in Otolaryngology*, 4(4), 541–554.

Palmer, A. R. (1990). The representation of the spectra and fundamental frequencies of steady-state single- and double-vowel sounds in the temporal discharge patterns of guinea pig cochlear-nerve fibers. *The Journal of the Acoustical Society of America*, 88(3), 1412–1426.

Palmer, A. R., & Russell, I. J. (1986). Phase-locking in the cochlear nerve of the guinea-pig and its relation to the receptor potential of inner hair-cells. *Hearing Research*, 24(1), 1–15.

Palmer, A. R., Winter, I. M., & Darwin, C. J. (1986). The representation of steady-state vowel sounds in the temporal discharge patterns of the guinea pig cochlear nerve and primarylike cochlear nucleus neurons. *The Journal of the Acoustical Society of America*, 79(1), 100–113.

Patuzzi, R. (1996). Cochlear micromechanics and macromechanics. In P. Dallos, A. N. Popper, & R. R. Fay (Eds.), *The Cochlea* (pp. 186–257). New York: Springer-Verlag.

Pickles, J. O. (1983). Auditory-nerve correlates of loudness summation with stimulus bandwidth in normal and pathological cochleae. *Hearing Research*, 12(2), 239–250.

Popelka, G. R., Moore, B. C. J., Fay, R. R., & Popper, A. N. (2016). *Hearing Aids*. New York: Springer International Publishing.

Pujol, R., & Puel, J.-L. (1999). Excitotoxicity, synaptic repair, and functional recovery in the mammalian cochlea: A review of recent findings. *Annals of the New York Academy of Sciences*, 884(1), 249–254.

Rajan, R. (2000). Centrifugal pathways protect hearing sensitivity at the cochlea in noisy environments that exacerbate the damage induced by loud sound. *The Journal of Neuroscience*, 20(17), 6684–6693.

Recio, A., Rhode, W. S., Kiefte, M., & Kluender, K. R. (2002). Responses to cochlear normalized speech stimuli in the auditory nerve of cat. *The Journal of the Acoustical Society of America*, 111(5), 2213–2218.

Recio-Spinoso, A., Temchin, A. N., van Dijk, P., Fan, Y. H., & Ruggero, M. A. (2005). Wiener-kernel analysis of responses to noise of chinchilla auditory-nerve fibers. *Journal of Neurophysiology*, 93(6), 3615–3634.

Relkin, E. M., & Turner, C. W. (1988). A reexamination of forward masking in the auditory nerve. *The Journal of the Acoustical Society of America*, 84(2), 584–591.

Relkin, E. M., & Doucet, J. R. (1997). Is loudness simply proportional to the auditory nerve spike count? *The Journal of the Acoustical Society of America*, 101(5), 2735–2740.

Robertson, D., Sellick, P. M., & Patuzzi, R. (1999). The continuing search for outer hair cell afferents in the guinea pig spiral ganglion. *Hearing Research*, 136(1–2), 151–158.

Rose, J. E., Brugge, J. F., Anderson, D. J., & Hind, J. E. (1967). Phase-locked response to low frequency tones in single auditory nerve fibers of the squirrel monkey. *Journal of Neurophysiology*, 30, 769–793.

Ruggero, M. A. (1994). Cochlear delays and traveling waves: Comments on "Experimental look at cochlear mechanics." *Audiology*, 33(3), 131–142.

Ruggero, M. A., & Temchin, A. N. (2005). Unexceptional sharpness of frequency tuning in the human cochlea. *Proceedings of the National Academy of Sciences of the United States of America*, 102(51), 18614–18619.

Sachs, M. B., & Kiang, N. Y.-S. (1968). Two-tone inhibition in auditory-nerve fibers. *The Journal of the Acoustical Society of America*, 43(5), 1120–1128.

Sachs, M. B., & Abbas, P. J. (1974). Rate versus level functions for auditory-nerve fibers in cats: Tone-burst stimuli. *The Journal of the Acoustical Society of America*, 56(6), 1835–1847.

Sachs, M. B., & Young, E. D. (1979). Encoding of steady-state vowels in the auditory nerve: Representation in terms of discharge rate. *The Journal of the Acoustical Society of America*, 66, 470–479.

Sachs, M. B., & Young, E. D. (1980). Effects of nonlinearities on speech encoding in the auditory nerve. *The Journal of the Acoustical Society of America*, 68, 858–875.

Sayles, M., Walls, M. K., & Heinz, M. G. (2016). Suppression measured from chinchilla auditory-nerve-fiber responses following noise-induced hearing loss: Adaptive-tracking and systems-identification approaches. In P. van Dijk, D. Başkent, E. Gaudrain, E. de Kleine, A. Wagner, & C. Lanting (Eds.), *Physiology, Psychoacoustics and Cognition in Normal and Impaired Hearing* (pp. 285–295). New York: Springer International Publishing.

Schaette, R., & McAlpine, D. (2011). Tinnitus with a normal audiogram: physiological evidence for hidden hearing loss and computational model. *The Journal of Neuroscience*, 31(38), 13452–13457.

Scheidt, R. E., Kale, S., & Heinz, M. G. (2010). Noise-induced hearing loss alters the temporal dynamics of auditory-nerve responses. *Hearing Research*, 269(1–2), 23–33.

Schmiedt, R. A. (1982). Boundaries of two-tone rate suppression of cochlear-nerve activity. *Hearing Research*, 7(3), 335–351.

Schmiedt, R. A., & Schulte, B. A. (1992). Physiologic and histopathologic changes in quiet- and noise-aged gerbil cochleas. In A. L. Dancer, D. Henderson, R. J. Salvi, & R. P. Hamernik (Eds.), *Noise-Induced Hearing Loss* (pp. 246–256). St. Louis, MO: Mosby.

Schmiedt, R. A., Mills, J. H., & Adams, J. C. (1990). Tuning and suppression in auditory nerve fibers of aged gerbils raised in quiet or noise. *Hearing Research*, 45(3), 221–236.

Sellick, P. M., Patuzzi, R., & Johnstone, B. M. (1982). Measurement of basilar membrane motion in the guinea pig using the Mossbauer technique. *The Journal of the Acoustical Society of America*, 72, 131–141.

Shamma, S. A. (1985). Speech processing in the auditory system. I: The representation of speech sounds in the responses of the auditory nerve. *The Journal of the Acoustical Society of America*, 78(5), 1612–1621.

Shamma, S. A., Shen, N. M., & Gopalaswamy, P. (1989). Stereausis: Binaural processing without neural delays. *The Journal of the Acoustical Society of America*, 86(3), 989–1006.

Shera, C. A., Guinan, J. J., & Oxenham, A. J. (2002). Revised estimates of human cochlear tuning from otoacoustic and behavioral measurements. *Proceedings of the National Academy of Sciences of the United States of America*, 99(5), 3318–3323.

Shera, C. A., Guinan, J. J., & Oxenham, A. J. (2010). Otoacoustic estimation of cochlear tuning: Validation in the chinchilla. *Journal of the Association for Research in Otolaryngology*, 11(3), 343–365.

Siebert, W. M. (1968). Stimulus transformations in the peripheral auditory system. In P. A. Kolers & M. Eden (Eds.), *Recognizing Patterns* (pp. 104–133). Cambridge, MA: MIT Press.

Smalt, C. J., Heinz, M. G., & Strickland, E. A. (2014). Modeling the time-varying and level-dependent effects of the medial olivocochlear reflex in auditory nerve responses. *Journal of the Association for Research in Otolaryngology*, 15(2), 159–173.

Smeds, K., & Leijon, A. (2011). Loudness and hearing loss. In M. Florentine, A. N. Popper, and R. R. Fay (Eds.), *Loudness* (pp. 223–259). New York: Springer-Verlag.

Smith, R. L., & Brachman, M. L. (1980). Response modulation of auditory-nerve fibers by AM stimuli: Effects of average intensity. *Hearing Research*, 2(2), 123–133.

Sterenborg, J. C., Pilati, N., Sheridan, C. J., Uchitel, O. D., Forsythe, I. D., & Barnes-Davies, M. (2010). Lateral olivocochlear (LOC) neurons of the mouse LSO receive excitatory and inhibitory synaptic inputs with slower kinetics than LSO principal neurons. *Hearing Research*, 270(1-2), 119–126.

Strelcyk, O., Christoforidis, D., & Dau, T. (2009). Relation between derived-band auditory brainstem response latencies and behavioral frequency selectivity. *The Journal of the Acoustical Society of America*, 126(4), 1878–1888.

Suzuki, J., Corfas, G., & Liberman, M. C. (2016). Round-window delivery of neurotrophin 3 regenerates cochlear synapses after acoustic overexposure. *Scientific Reports*, 6, 24907.

Temchin, A. N., & Ruggero, M. A. (2009). Phase-locked responses to tones of chinchilla auditory nerve fibers: Implications for apical cochlear mechanics. *Journal of the Association for Research in Otolaryngology*, 11(2), 297–318.

van der Heijden, M., & Joris, P. X. (2005). The speed of auditory low-side suppression. *Journal of Neurophysiology*, 93(1), 201–209.

Viemeister, N. F. (1983). Auditory intensity discrimination at high frequencies in the presence of noise. *Science*, 221, 1206–1207.

Viemeister, N. F. (1988). Intensity coding and the dynamic range problem. *Hearing Research*, 34, 267–274.

Weiss, T. F., & Rose, C. (1988a). A comparison of synchronization filters in different auditory receptor organs. *Hearing Research*, 33(2), 175–179.

Weiss, T. F., & Rose, C. (1988b). Stages of degradation of timing information in the cochlea: A comparison of hair cell and nerve-fiber responses in the alligator lizard. *Hearing Research*, 33 (2), 167–174.

Wen, B., Wang, G. I., Dean, I., & Delgutte, B. (2012). Time course of dynamic range adaptation in the auditory nerve. *Journal of Neurophysiology*, 108(1), 69–82.

Westerman, L. A., & Smith, R. L. (1984). Rapid and short-term adaptation in auditory nerve responses. *Hearing Research*, 15(3), 249–260.

Winslow, R. L., & Sachs, M. B. (1988). Single-tone intensity discrimination based on auditory-nerve rate responses in backgrounds of quiet, noise, and with stimulation of the crossed olivocochlear bundle. *Hearing Research*, 35(2–3), 165–189.

Yates, G. K. (1990). Basilar membrane nonlinearity and its influence on auditory nerve rate-intensity functions. *Hearing Research*, 50(1–2), 145–162.

Young, E. D. (2008). Neural representation of spectral and temporal information in speech. *Philosophical Transactions of the Royal Society of London B: Biological Sciences*, 363(1493), 923–945.

Young, E. D., & Sachs, M. B. (1979). Representation of steady-state vowels in the temporal aspects of the discharge patterns of populations of auditory-nerve fibers. *The Journal of the Acoustical Society of America*, 66, 1381–1403.

Young, E. D., & Barta, P. E. (1986). Rate responses of auditory nerve fibers to tones in noise near masked threshold. *The Journal of the Acoustical Society of America*, 79(2), 426–442.

Zilany, M. S. A., & Bruce, I. C. (2006). Modeling auditory-nerve responses for high sound pressure levels in the normal and impaired auditory periphery. *The Journal of the Acoustical Society of America*, 120(3), 1446–1466.

Zilany, M. S. A., & Carney, L. H. (2010). Power-law dynamics in an auditory-nerve model can account for neural adaptation to sound-level statistics. *The Journal of Neuroscience*, 30(31), 10380–10390.

Zilany, M. S. A., Bruce, I. C., & Carney, L. H. (2014). Updated parameters and expanded simulation options for a model of the auditory periphery. *The Journal of the Acoustical Society of America*, 135(1), 283–286.

Chapter 9
Ion and Fluid Homeostasis in the Cochlea

Philine Wangemann and Daniel C. Marcus

Abstract The transduction of sound into nerve impulses requires an ionic environment that depends on a variety of ion transport processes in epithelial and endothelial cells of the cochlea. Specific ion transport functions occur in specific cell types that coordinate the production and maintenance of endolymph, which is the fluid in the lumen of the cochlear duct that supports the sensory transduction process. The critical nature of these ion transport processes is underscored by observations of hearing loss when ion transport mechanisms malfunction as a result of mutations, drug exposure, or hormonal imbalance. This chapter describes our basic understanding of salient ion transport processes and their regulation by hormones and other regulatory pathways.

Keywords Acid-base balance · Aquaporin · Calcium homeostasis · Endolymph · Hereditary deafness · Hormone receptors · Hormonal regulation · Intrastrial fluid · Outer sulcus cells · Perilymph · Potassium secretion · Reissner's membrane · Sodium absorption · Spiral prominence · Stria vascularis

9.1 Introduction

The mechanosensory transduction of sound in the cochlea depends on large electrochemical gradients and an unusual composition of the luminal fluid in the inner ear. This chapter focuses on ion transport mechanisms that establish and maintain those gradients. Although the focus is on the cochlea, much of what we know is informed by closely analogous mechanisms in the vestibular labyrinth. As such, reference to knowledge of pertinent homeostatic mechanisms in the vestibular

P. Wangemann (✉)
Cell Physiology Laboratory, Kansas State University, Manhattan, KS 66506, USA
e-mail: wange@vet.k-state.edu

D.C. Marcus
Cellular Biophysics Laboratory, Kansas State University, Manhattan, KS 66506, USA
e-mail: marcus@k-state.edu

G.A. Manley et al. (eds.), *Understanding the Cochlea*, Springer Handbook of Auditory Research 62, DOI 10.1007/978-3-319-52073-5_9

labyrinth is included in this narrative. A short review of epithelial transport principles and nomenclature is provided next.

9.1.1 Transepithelial Vectorial Transport Between Compartments

Epithelial cells form sheets or tubules within the body that thereby separate two fluid compartments. Examples include glands, kidney tubules, digestive intestinal tract, airways, and the inner ear. In addition to the passive structural role of the epithelial cells, they engage in highly specialized transepithelial solute and water transport that can occur via a transcellular and/or paracellular pathway. Epithelial cells produce vectorial transcellular movements of solutes by virtue of an asymmetric distribution of transport proteins in the apical (luminal or mucosal) plasma membrane and in the basolateral (abluminal or nutrient) plasma membrane. The apical membrane is often the site of "gatekeeper" transport proteins that control the overall rate of transepithelial transport. The rate of transport is regulated by a variety of hormonal receptor and second-messenger signal pathways (e.g., β-adrenergic receptors via cyclic AMP [cAMP], purinergic receptors via extracellular ATP, intracellular Ca^{2+} levels; see Sect. 9.5).

The paracellular pathway is also important for mediating transepithelial transport and consists primarily of the tight junction barrier between cells. This barrier consists of combinations of intracellular and membrane proteins with widely varying functional properties provided by myriad expression patterns of junctional gene products and by cellular control of the junction proteins (Turner et al. 2014). Solutes cross the tight junction barrier driven by electrical and/or chemical concentration gradients, and the transport rates are regulated by the selective properties of the junction, which in turn are under cellular control.

Net transepithelial fluid transport results in fluid secretion (basolateral to apical) or absorption (apical to basolateral). The driving force for fluid movement results from net solute transport and the resulting local osmotic pressure differences generated, and the primary pathways for water are through plasma membrane proteins, especially the class known as aquaporins (AQPs).

Proteins that mediate transport across the apical and basolateral membranes of epithelia are of three broad types: primary active transporters (also referred to as "pumps"), transporters, and channels. The pumps consume metabolic energy, usually in the form of ATP, and transform that energy into creation of transmembrane solute gradients. The most pervasive of these is the Na^+, K^+-ATPase (a.k.a. the Na^+ pump) that pushes 2 K^+ ions into the cytosol and pulls 3 Na^+ ions out of the cytosol for each ATP cleaved. The energy from the ATP is then stored as an inward-directed Na^+ concentration gradient that can be utilized by secondary active transporters to move other solutes across the apical and/or basolateral plasma membranes. An example of such transporters includes Na^+/H^+ exchangers in which

the inward movement of Na^+ drives the obligatory movement of acid (H^+) out of the cell. The accumulation of cytosolic K^+ by the action of the Na^+, K^+-ATPase often establishes a negative electrical potential difference mediated by membrane K^+-selective channels, and this negative voltage can then drive electrogenic solute transport. Examples include efflux of negative ions such as Cl^- through Cl^--selective ion channels and Ca^{2+} movements via coupled electrogenic Na^+/Ca^{2+} exchange. The overall constellation of apical and basolateral transport activity must, of course, be coordinated and balanced to avoid catastrophic accumulation or depletion of any solutes in the cytosol during transepithelial secretion or absorption.

9.2 Fluid Composition

There are several fluid compartments in the inner ear that have distinct compositions and communication pathways among them. Blood vessels are adjacent to the perilymphatic space (see Sect. 9.2.1) and to the intrastrial space (see Sect. 9.2.3). The restricted communication between blood and perilymph is referred to as the blood-perilymph (or blood-labyrinth) barrier (see Sect. 9.2.1). The luminal compartment contains endolymph that provides the environment of the sensory stereocilia and enables the auditory transduction process. Perilymph is the extracellular fluid that surrounds the cochlear duct epithelium (Fig. 9.1, *blue areas*) and endolymph is the luminal fluid within the cochlear duct (Fig. 9.1, *pink areas*). The epithelial cell domains that form the cochlear duct and their locations are also shown (Fig. 9.1).

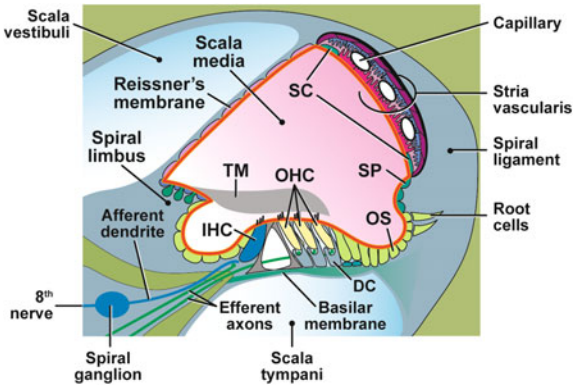

Fig. 9.1 Diagram of a cross section of the cochlear duct. The luminal compartment, scala media, contains endolymph and is bounded by epithelial cells whose apical membranes are designated by the *bold orange line around the scala media*. The abluminal fluid, perilymph, is within the scala tympani, scala vestibuli, extracellular spaces of the spiral ligament, and spiral limbus and is in contact with the basolateral membranes of all the epithelial cells except the marginal cells of the stria vascularis. *TM* tectorial membrane, *IHC* inner hair cell, *OHC* outer hair cells, *DC* deiters cells, *OS* outer sulcus cells, *SC* spindle-shaped cells. Adapted from Marcus (2012), with permission

9.2.1 Perilymph and the Blood-Perilymph Barrier

The perilymphatic space is contiguous throughout the inner ear. The cochlear cross section displays two perilymphatic compartments, which locally may have small differences in ion composition (e.g., K^+ is slightly higher in the scala vestibuli than in the scala tympani), but these "two compartments" are openly joined at the cochlear apex (helicotrema) and the perilymph diffuses rapidly between the two scalae through the spiral ligament of the lateral wall (Salt et al. 1991a, b). At the cochlear base, the scala tympani is bounded by the round window, with a connection to the cerebral spinal fluid via the cochlear aqueduct (Salt et al. 2003), but the scala vestibuli is openly continuous with the perilymph bathing the vestibular organs. The complexity of the perilymph-filled spaces and the fact that the perilymph and cerebrospinal fluid are under pressure compared with the atmosphere complicate the investigation of perilymph homeostasis (Salt et al. 2003).

The composition of the perilymph is closely similar to that of blood plasma and to cerebrospinal fluid, but the perilymph is not merely an ultrafiltrate of plasma or an extension of CSF. The differences can be seen in Table 9.1, and several studies have demonstrated a tightly regulated separation of perilymph from blood. This separation is termed the blood-perilymph barrier (Juhn et al. 1982), in analogy to the better characterized blood-brain barrier. The exchange of solutes between blood and perilymph has been proposed to be primarily localized at the vessels of the spiral limbus (Firbas et al. 1981). Glucose is known to be the primary fuel for inner ear metabolism, but it does not pass freely from the blood but rather is transferred via a regulated transendothelial facilitated transport pathway (Ferrary et al. 1987). Putative facilitated diffusion of glucose via the GLUT-1 transporter into the intrastrial space (see Sect. 9.2.3) may also occur from capillaries in the stria vascularis (Ando et al. 2008). Exchange of Ca^{2+} across the blood-perilymph barrier occurs at a remarkably slow rate, although the molecular basis of restricted transport across the barrier has not been identified (Juhn et al. 1982).

Table 9.1 Fluid composition of the inner ear and adjoining fluids

	Cochlear perilymph	Cochlear endolymph	Utricular endolymph	Endolymphatic sac endolymph	Cerebrospinal fluid	Plasma
Na^+ (mM)	148	1.3	9	129	149	145
K^+ (mM)	4.2	157	149	10	3.1	5.0
Cl^- (mM)	119	132	–	124	129	106
HCO_3^- (mM)	21	31	–	–	19	18
Ca^{2+} (mM)	1.3	0.023	0.28	–	–	2.6
Protein (mg/dl)	178	38	–	–	24	4238
pH	7.3	7.5	7.5	6.9	7.3	7.3
Potential (mV)	0	+80 to +100	0 to +4	+6 to +15	–	0

Reproduced from Marcus and Wangemann (2010), with permission

The blood-perilymph barrier can be compromised by systemic inflammation induced by lipopolysaccharides, similar to the blood-brain barrier (Hirose et al. 2014). By contrast, other insults to auditory function such as impulse noise, hypertension, and the ototoxic drugs cisplatin and gentamycin have not been found to cause compromise of the blood-perilymph barrier (Laurell et al. 2000, 2008; Mosnier et al. 2001).

9.2.2 Endolymph

Endolymph is a highly unusual extracellular fluid with its high K^+, low Na^+, and low Ca^{2+} concentrations. This composition is essential for the transduction of sound and acceleration into hearing and balance, respectively. The sensory cells employ apical mechanotransduction channels with very large single-channel conductance and that are permeable to all three of the above-named cations (Effertz et al. 2015; Corey, Ashmore, and Ó Maoiléidigh, Chap. 4). Endolymphatic Ca^{2+} concentration needs to be highly regulated due to the relatively high permeability of the mechanotransduction channel to Ca^{2+} over Na^+ but also due to the Ca^{2+} dependence of channel ion selectivity, rectification, and conductance (reviewed in Effertz et al. 2015). In addition, the low level of endolymphatic Ca^{2+} prevents sensory cell Ca^{2+} loading.

The special energetic advantage of the radically different cation compositions of endolymph and perilymph was recognized by Ruediger Thalmann over 45 years ago (Thalmann 1971) and elaborated by others (Patuzzi 2011a). The basic principle has 2 components. (1) The transduction process in hair cells requires very little energy when the transduction current is carried by K^+ ions (see below in this section) and therefore needs no dedicated vascular supply (although the lower turn has a single spiral vessel in the basilar membrane). (2) The high concentration of endolymphatic K^+ and the extra electrical driving force produced by the stria vascularis requires a massive energy supply provided by the high density of blood capillaries, as embodied in the name of the tissue. This separation of energy production and consumption sites allows the pulsations of the blood in the stria to be physically dampened by the spongy spiral ligament attached to the rigid outer bony shell of the cochlea so that we are not overwhelmed by the sound of our circulation instead of hearing the important external sounds.

The mechanotransduction current is carried passively by K^+ from endolymph through the apical cation channels in the hair cells, driven by the electrical potential difference between the endolymph and the hair cell cytosol. The low endolymphatic Na^+ maintains osmotic balance against K^+ and prevents Na^+ loading of the sensory cells through entry via the nonselective cation transduction channels. K^+ exits the basolateral side of the sensory cells passively through a high density of K^+-selective channels, driven by the membrane voltage that is slightly above electrochemical equilibrium at this membrane.

9.2.3 Intrastrial Fluid

The basolateral membrane of the strial marginal cells is in contact with the intrastrial fluid, which is a microenvironment that couples marginal cell function and intermediate cell function. This interdependence of cell functions is described in Sect. 9.4.2 on the endocochlear potential (EP).

The composition of the intrastrial fluid is maintained by the adjacent cells, but the extensive and intimate capillary network in the stria appears to serve for metabolic gas exchange but not for solutes such as K^+ (although some drugs such as furosemide pass through easily). This view derives from the observations that vascular perfusion with artificial blood devoid of K^+ or glucose has a long-delayed effect on the metabolically labile EP generated by the stria vascularis (see Sect. 9.4.2), whereas perilymphatic perfusion of K^+-free or glucose-free solution causes an immediate decline in EP (Wada et al. 1979; Kambayashi et al. 1982).

This exchange barrier at the strial capillaries provides a means to control drug delivery to the ear by synthesizing drug analogs with high or low permeability through this barrier. Loop diuretics of the furosemide family penetrate this barrier with tremendous ease but exchange with perilymph comparatively slowly. Vascular perfusion of furosemide causes a nearly instantaneous loss of EP, whereas perilymphatic perfusion of furosemide has a delay of more than 6 min due to the extremely low permeability of the basal cell tight junctions, which restrict access of the drug to the site of action at the basolateral membrane of strial marginal cells (see Sect. 9.4.1).

9.3 Transport Epithelia in the Cochlea

There are a large number of cell types that border the cochlear duct. Each type makes specific contributions to the maintenance of endolymph composition and electrical potential, with each cell type able to secrete and/or absorb solutes through one or more transport pathways under different control mechanisms.

9.3.1 Stria Vascularis

The stria vascularis is a complex epithelial structure on the cochlear lateral wall that (1) secretes K^+ into endolymph and (2) generates the EP (Table 9.1). The high level of endolymphatic K^+ provides the substrate for the transduction current through the sensory cells, and the EP provides a part of the driving force (in conjunction with the basolateral membrane voltage) for the flow of K^+ that is modulated by sound. The cellular transport model by which the stria vascularis secretes potassium and generates the EP is shown in Fig. 9.2 and described in Sects. 9.4.1 and 9.4.2. Recall

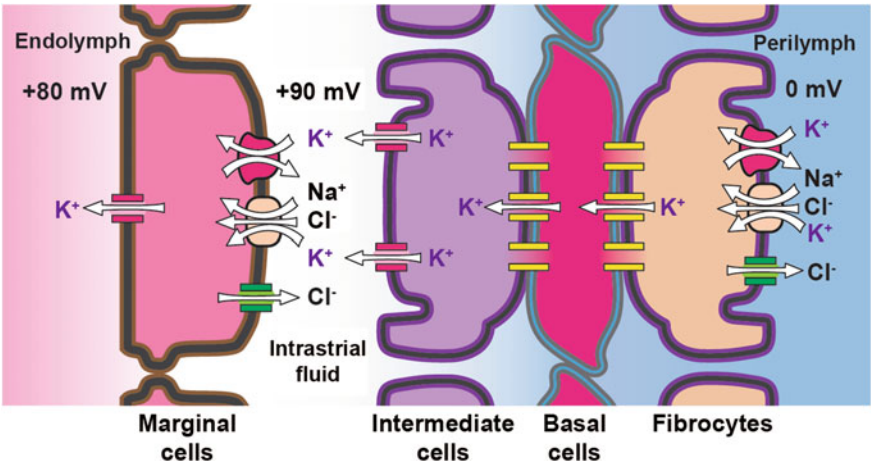

Fig. 9.2 Diagram of a cell model of K^+ transport from the perilymph by fibrocytes of the spiral ligament through the stria vascularis into the cochlear endolymph. The fibrocytes, basal cells, and intermediate cells form a syncytium through a dense network of gap junctions (*yellow channel symbols*), with K^+ flow indicated (*white arrows*), although other small solutes also pass. Fibrocytes take up perilymphatic K^+ via the Na^+, K^+-ATPase and Na^+, K^+, $2Cl^-$ cotransporter; Cl^- and Na^+ recycle across that membrane back into perilymph, while K^+ diffuses through gap junctions into the basal cells of stria vascularis and further into the intermediate cells. The high concentration of K^+ in the intermediate cells creates a large voltage across its high density of KCNJ10 K^+ channels (*red channel symbols*) in the membrane facing the intrastrial fluid space. Such a constellation of high cytosolic K^+ concentration bounded by a highly K^+-selective plasma membrane creates a negative resting membrane potential in "classical" examples of symmetrical cells such as nerve cell bodies. However, in this highly asymmetrical arrangement of cell membranes, the unusually low K^+ concentration of the intrastrial space, coupled with the cytosol that is effectively clamped to "ground" (held near zero, the potential of perilymph) by the syncytium, the intermediate cells then push the intrastrial space voltage to +80 to +100 mV. The transepithelial voltage of the marginal cell layer is small, so that most of the intrastrial space voltage is observed in the scala media. The marginal cells remove K^+ from the intrastrial space by the same transporter constellation as seen in the fibrocytes and secretes it into the endolymph through KCNQ1/KCNE1 K^+ channels (*red channel symbols*) in the apical membrane. Adapted from Marcus, D. C. (2012). Acoustic transduction. In N. Sperelakis (Ed.), *Cell Physiology Source Book: Essentials of Membrane Biophysics* (pp. 649-668). San Diego, CA: Academic Press, with permission

that all epithelial cells that produce a vectorial transport of substances do so by virtue of different membrane properties of their apical and basolateral membranes.

The basal cell layer of the stria vascularis adjoins a bed of fibrocytes (spiral ligament) that is sponge-like and pervaded by perilymph. The basal cell layer forms a very tight barrier between the perilymph in the spiral ligament and the intrastrial fluid space. The basal cells form a syncytium via a high density of gap junctions with fibrocytes and the intermediate cells, which are responsible for generating the EP (see Sect. 9.4.2). Finally, a monolayer of strial marginal cells forms a barrier between the intrastrial fluid space and the endolymph. The marginal cells are joined to each other by tight junctions but have no gap junction connections among

themselves. This barrier supports a large gradient in K^+ concentration and electrical potential difference (Table 9.1; Fig. 9.2). The physiological significance of the functional independence of marginal cells is not known.

9.3.2 Reissner's Membrane

Reissner's membrane epithelium (Fig. 9.1) accounts for more boundary surface of the cochlear duct than any of the other epithelial cell domains. It contributes to the maintenance of endolymph composition by the absorption of Na^+ mediated by epithelial Na^+ channels in its apical membrane (see Sect. 9.4.5) and may provide acid/base control of endolymph via $Ca^{2+}/2H^+$ exchange mediated by a putative apical Ca^{2+}-ATPase (see Sect. 9.4.7). The basolateral membrane expresses a Cl^- channel (SLC26A7) that is associated with pH control in other epithelial cells (Kim et al. 2014). The apical membrane also expresses P2X2-nonselective cation channels that are activated by luminal nucleotides, which implies that Reissner's membrane can contribute to absorption of Na^+ and K^+ under purinergic control (Lee and Marcus 2008; Morton-Jones et al. 2015; see Sect. 9.5.4.2).

9.3.3 Outer Sulcus, Spiral Prominence, and Strial Spindle Cells

These three epithelial cell types occur on the lateral wall and are contiguously adjacent to each other (Fig. 9.1). All of these cells express the Cl^-/HCO_3^- exchanger SLC26A4 and thereby contribute to the alkalinization of the endolymph (Wangemann et al. 2007). The outer sulcus epithelial cells have also been shown to absorb both K^+ and Na^+ via apical cation nonselective channels of two types, one of which is under purinergic control (Kim and Marcus 2011). It was also recently found that outer sulcus cells in the upper cochlear turns are involved with hormonal control of endolymph volume mediated by AQP translocation to the plasma membrane in response to hyperosmotic challenge or muscarinic agonist (see Sect. 9.5.2).

9.3.4 Spiral Limbus Epithelial Cells

The spiral limbus (Fig. 9.1) supports epithelial cells on its upper and lateral (inner sulcus) surfaces. Little is known about their respective transport functions.

9.4 Homeostasis

The cellular basis of ion and water transport in the cochlea and the ways in which these processes are regulated and coordinated among the many types of cells involved are presented here. The integration of these functions and their role in hearing have also been analyzed and discussed from molecular, pharmacological, and engineering perspectives (Patuzzi 2011a, b; Marcus 2012).

9.4.1 K^+ Secretion by Strial Marginal Cell Epithelium

Active K^+ secretion into the cochlear duct was first unambiguously demonstrated by radioactive K^+ fluxes from either the perilymph or blood vessels (Konishi et al. 1978; Sterkers et al. 1982), even though earlier indirect evidence supported the proposition. These K^+ fluxes were inhibited by drugs well characterized to block specific transport processes and by anoxia. The stria was taken to be the tissue source of secretion because the flux was nearly the same when the radiotracer was placed in either of the cochlear perilymphatic scalae; possible contributions by the spiral limbus were disregarded.

Another study demonstrated more directly that the stria vascularis secretes K^+ (Wangemann et al. 1995a). A K^+-selective self-referencing probe was positioned adjacent to the apical surface of the marginal cells, where an outward-directed K^+ flux was detected and was inhibited by basolateral bumetanide (specific inhibitor of the Na^+-K^+-$2Cl^-$ cotransporter [NKCC]). In concert with additional pharmacological and electrophysiological experiments, a cell model that explains the underlying transport pathways at the molecular level was developed (Fig. 9.2). Briefly, K^+ is taken up from the intrastrial fluid by the Na^+, K^+-ATPase (Na^+ pump) and NKCC1, the former being a primary-active process that consumes cellular energy supplies and the latter a secondary-active process that utilizes the energy contained in the Na^+ gradient established by the Na^+-pump. This combined uptake mechanism, in concert with the small volume of the intrastrial space and the barrier to K^+ between this space and the strial capillaries, yields the surprising result that the intrastrial space K^+ concentration is reduced markedly below that in blood plasma, to about 1.2 mM (Takeuchi et al. 2000), which has important ramifications for normal and pathological function of the stria (see Sect. 9.4.2). The Na^+ and Cl^- that enter the cell at the basolateral membrane via NKCC1 are removed across the same membrane via the Na^+ pump and Cl^- channels, while the K^+ accumulated in the cytosol is secreted across the apical membrane via K^+-selective channels (Fig. 9.2).

The apical K^+ channels are composed of α- and β-channel subunits (KCNQ1 and KCNE1, respectively), which are voltage-activated channels. They also occur in human cardiac myocytes, and a genetic disease due to mutations of this channel, Jervell and Lange-Nielsen syndrome, displays dysfunction of the heart and hearing

(Shen et al. 1997; Marcus and Wangemann 2010). The critical contributions of the apical K^+ channel and basolateral transport proteins of the model are supported by observations of collapsed scala media in gene knockout mice that lack either of the subunits of the channels or lack the cotransporter (Marcus 2012).

9.4.2 *Production of Endocochlear Potential by Strial Intermediate and Basal Cells*

The EP is functionally a transepithelial voltage that occurs across the monolayer of epithelial cells of the cochlear duct, including the sensory cells. However, it also occurs across the multilayered stria vascularis and originates predominantly from the basal cell-intermediate cell syncytial layer (see Sect. 9.3.1), in contrast to K^+ secretion carried out by the marginal cell layer (see Sect. 9.4.1). Despite this separation of function, the two cell layers are operationally coupled via the K^+ concentration of the intrastrial space.

The basal cell-intermediate cell layer maintains intracellular K^+ at a high level by the uptake from perilymph by fibrocytes in the spiral ligament and diffusion via gap junctions into basal cells and intermediate cells (Kikuchi et al. 2000; Fig. 9.2). These cells generate a large potential difference between the intrastrial space and the spiral ligament (perilymph) fluid by virtue of its high expression of KCNJ10 K^+ channels (also known as Kir4.1) in the intermediate cell membrane. The barrier between the intrastrial space and perilymph of the spiral ligament is formed by extremely tight junctions composed of claudin-11 proteins between the basal cells. The essential nature of these claudins was demonstrated by the collapse of the EP in claudin-11-null mice (Gow et al. 2004). The importance of the KCNJ10 channel to EP generation is supported by the observation that KCNJ10-knockout mice have no EP, but they maintain an elevated endolymphatic K^+ concentration (Marcus et al. 2002). The basal and intermediate cells are thought to have a strongly depolarized membrane voltage with respect to the perilymph and a high K^+ concentration (Fig. 9.2). This combination would create a canonical highly polarized intermediate cell membrane, made larger than in other K^+-conductive cells due to the unusually low K^+ concentration of the intrastrial space (see Sect. 9.4.1). This layer of cells thereby generates an intrastrial space voltage of 90 mV or more. Due to clamping of the basal/intermediate cell membrane voltage near zero, this potential difference of the intrastrial space is *positive* with respect to perilymph. The marginal cells contribute very little potential to the transepithelial difference, just as the physiologically analogous vestibular dark cells contribute little to the endolymphatic potential in the utricle, common crus, and ampullae. The vestibular dark cell epithelium is a K^+-secretory monolayer without the intermediate cell/basal cell layer.

Although penetration of the stria with sharp double-barrel microelectrodes unavoidably results in some cellular damage, the profile of the potential difference with respect to the perilymph and the K^+ concentration is consistent with the above

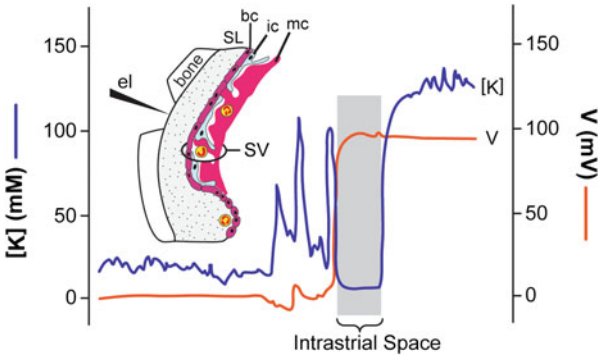

Fig. 9.3 Recording of profiles for voltage (*orange line*) and K^+ concentration ([K]; *blue line*) during penetration of the stria vascularis (SV). A region was found where the voltage with respect to the perilymph was highly positive but the K^+ concentration was low; this region was interpreted to be the intrastrial space. *SL* spiral ligament, *bc* basal cell, *ic* intermediate cell, *mc* marginal cell, *el* penetrating electrode advanced from *left* to *right*. *x*-Axis, time/distance of electrode advancement. Adapted from Marcus (2012), with permission

view (Salt et al. 1987; Fig. 9.3). In the spiral ligament perilymph, the voltage is defined as zero and the K^+ concentration is low. The electrode then enters a region where the K^+ concentration rises but the voltage remains low, which is taken to indicate entry into the basal and intermediate cells. Further advance of the electrode into the stria leads to the observation of suddenly low K^+ concentration that is accompanied by a high voltage, which is taken to indicate entry into the intrastrial space. Finally, the electrode traverses a barrier into a stable region of high K^+ concentration and high voltage, which is taken to be traversal across the marginal cell layer into cochlear endolymph.

The coupling of function of the two strial layers referred to above is illustrated by observations of the rapid decline in the EP during inhibition of marginal cell K^+ secretion by pharmacological or metabolic block of basolateral K^+ uptake (ouabain, bumetanide, anoxia) from the intrastrial space. The cessation of K^+ uptake from the intrastrial space would lead to a rapid rise in K^+ concentration due to the continued exit from intermediate cells through the KCNJ10 channels, leading to a rapid depolarization across these channels and the resulting collapse of the EP (Marcus and Wangemann 2010).

9.4.3 K^+ Cycling

K^+ is the main charge carrier that mediates the quiescent and stimulus-activated currents from the endolymph through the apical mechanosensitive ion channels into the cochlear and vestibular sensory cells. This current flow depolarizes the sensory cells, which leads to contraction of the motor protein prestin (SLC26A5) in cochlear

outer hair cells (the substrate of stimulus amplification) and to Ca^{2+} influx into cochlear inner hair cells and vestibular hair cells (the signal for vesicular neurotransmitter release and activation of the sensory neurons). This K^+ current into the sensory cells is balanced by an efflux of K^+ via basolateral K^+ channels into interstitial spaces that are continuous with the perilymph (Marcus and Wangemann 2010).

The molecular identities of the major K^+ channels in hair cells that mediate K^+ efflux have been established. Most prominently, these include the voltage-gated K^+ channel KCNQ4 and the Ca^{2+}-activated K^+ channel KCNMA1 (Robbins 2001; Sakai et al. 2011). Several splice variants of KCNQ4 are expressed in the inner ear and mutations of this channel are associated with hearing loss (Gao et al. 2013). The K^+ channel KCNQ4 associates with the β-subunit KCNE1 and possibly with other KCNE subunits that are expressed in hair cells (Strutz-Seebohm et al. 2006). K^+ released from the sensory hair cells is likely at least partially recycled by uptake into spiral ligament fibrocytes, transferred into the stria vascularis, and secreted back into the endolymph.

Two pathways have been proposed to shuttle K^+ from the base of the cochlear sensory cells toward the fibrocytes of the lateral wall, and both are likely to participate. The first is simple diffusion through the perilymph, and its involvement is supported by the observation of voltage gradients due to electric currents in the scala tympani (Zidanic and Brownell 1990). The second is diffusion through the gap junction-coupled epithelial cells located between the sensory cells and the fibrocytes of the lateral wall (Spicer and Schulte 1996). This intraepithelial pathway is posited to involve uptake of K^+ into Deiters cells, dispersion among the cells along the basilar membrane and outer sulcus via gap junctions, and release of K^+ from outer sulcus root cells into the interstitial space of the spiral ligament (Kikuchi et al. 2000). A comparable theory has also been advanced to account for diffusion from inner hair cells to the spiral limbus and release into the scala vestibuli, followed by diffusion through the perilymph to the suprastrial spiral ligament and back to the stria vascularis (Kikuchi et al. 2000). Deletion of expression of KCNK5 K^+ channels in developmentally mature mice leads to profound deafness, consistent with an essential role in K^+ cycling. These channels are normally expressed in Böttcher, Claudius, and outer sulcus root cells (Cazals et al. 2015).

The final step consists of K^+ uptake by specialized fibrocytes in the spiral ligament and diffusional movement via the gap junctions GJB2 (Cx26) and GJB6 (Cx30) into the strial basal and intermediate cells, followed by supply to marginal cells and the endolymphatic space, as described (Sect. 9.4.1). Fibrocyte types II, IV, and V express Na^+, K^+-ATPase, the NKCC1 SLC12A2 and the Cl^- channels CLCNKA and CLCNKB. The resemblance of this constellation of transporters to the basolateral membrane of strial marginal cells (Sect. 9.4.1) suggests that fibrocytes take up K^+ from the perilymph, although functional data from fibrocytes are lacking (Marcus and Wangemann 2010). Despite the attractiveness of this hypothesis, a number of observations are not consistent with it, such as a known human deafness genotype that is associated with a mutation in a cochlear gap junction connexin that nonetheless is as permeable to K^+ as the normal connexin, and are reviewed elsewhere (Mammano 2013).

9.4.4 K^+ Buffering

K^+ efflux from the basolateral membrane of sensory cells during acoustic stimulation was demonstrated to increase the adjacent perilymphatic K^+ concentration (Johnstone et al. 1989). Elevated K^+ in this region would be expected to depolarize the sensory cells, supporting cells, and nerve terminals, leading to hearing loss. It is thought that these increases in K^+ are limited in magnitude by local K^+-buffering mechanisms in neighboring supporting cells such as Deiters cells.

Deiters cells express basolateral K^+ channels (Nenov et al. 1998), the K^+, Cl^- cotransporter isoform KCC4 (Boettger et al. 2002) and gap junctions that connect to neighboring supporting cells of the epithelial gap junction network (see Sect. 9.4.3). The importance of K^+, Cl^- cotransporters in the inner ear is underscored by the observation that KCC4-knockout mice are deaf (Boettger et al. 2002). These observations support the speculation that Deiters cells buffer extracellular K^+ through the uptake of K^+ at the base of the hair cells and expel it across a part of the membrane facing away from the sensory cell and/or move the K^+ by diffusion from the Deiters cell to neighboring supporting cells via gap junctions. The former mechanism for buffering of extracellular K^+ by Müller glial cells has been proposed to explain a similar phenomenon in the retina (Kofuji et al. 2002). Whether K^+, Cl^- cotransporters participate in K^+ buffering as mediators of cellular K^+ uptake or efflux awaits experimental determination (Marcus and Wangemann 2009).

9.4.5 Na^+ Absorption

The cochlea regulates endolymphatic Na^+ concentrations to low levels to maintain sensory cell function. The cation nonselective permeability of the mechanotransduction channel would otherwise allow elevated Na^+ to flood the cytosol of the sensory cells, leading to cellular dysfunction and hearing loss (Shi et al. 2005). Pathologically elevated endolymphatic Na^+ occurs during transient ischemic anoxia, which is a putative etiology of sudden hearing loss (Sellick and Johnstone 1972). Mutations underlying nonsyndromic autosomal recessive deafness (DFNA8/10) due to dysfunction of the Na^+ transport regulatory gene *TMPRSS3* is also expected to disrupt Na^+ homeostasis (Guipponi et al. 2002). Furthermore, altered endolymphatic Na^+ concentration has been proposed as a mechanism of premenstrual exacerbation of Ménière's disease (Andrews and Honrubia 2010).

9.4.5.1 Na^+ Absorption Pathways

Normal Na^+ absorptive flux in the cochlea is only about 1% of the normal K^+ secretory flux (Konishi et al. 1978), suggesting a lower requirement for metabolic support of Na^+ absorption than for K^+ secretion. This supposition is supported by

the dense blood capillary network in the K^+-secreting stria vascularis as compared with the avascular Reissner's membrane and single-vessel metabolic supply of the outer sulcus and Claudius cells, which are all involved in Na^+ absorption (Kim and Marcus 2011).

The cochlea absorbs Na^+ from the endolymph via three types of apical ion channels expressed in several cell types. These cells all create an inward driving force for cations across the apical membrane by virtue of Na^+, K^+-ATPase in parallel with K^+ channels in the basolateral membrane (Fig. 9.4b, c), which create an inward electrochemical driving force for Na^+ (and K^+) across the apical membrane. Reissner's membrane and Claudius cells utilize the epithelial Na^+ channel (ENaC) to mediate transport across the apical membrane from the endolymph into the cytosol (Yoo et al. 2012; Kim and Marcus 2011; Fig. 9.4c). ENaC transport is regulated by several signal pathways, but one prominent mechanism is the genomic control of channel numbers in the membrane via glucocorticoid signaling (see Sect. 9.5.5). Both outer sulcus cells and sensory hair cells mediate apical cation entry via nonselective cation channels (Kim and Marcus 2011; Fig. 9.4b). The outer sulcus absorption of K^+ is referred to as parasensory K^+ absorption (see Sect. 9.4.6). All of these cell types mediate the cellular entry of both Na^+ and K^+ via ionotropic purinergic receptors (see Sect. 9.5.4), which are activated under conditions such as noise (Kim and Marcus 2011).

9.4.5.2 Na^+ Secretion Pathways

The entry of Na^+ into the endolymph has long been tacitly assumed to simply be via an undefined "leak" pathway. Although this view largely remains, it was found recently that an active H^+ flux can emanate from the apical surface of stria vascularis under energetically favorable conditions and that a part of this flux is mediated by a Na^+/H^+-exchanger (Miyazaki et al. 2016). Na^+/H^+-exchangers are secondary active transporters that can operate in either direction depending on the net chemical driving force. The apical Na^+/H^+-exchanger in the stria vascularis likely operates close to equilibrium under normal steady-state conditions but can either secrete or absorb Na^+ when away from equilibrium. In secretion mode, it may provide at least a part of the Na^+ "leak" into endolymph.

9.4.6 Parasensory K^+ Absorption

Auditory and vestibular transduction depend on the balance of secretion and absorption of cations by the epithelial cells bounding the endolymphatic spaces. Potassium is secreted by strial marginal cells in the cochlea (see Sect. 9.4.1), and there is both a quiescent and a stimulus-induced efflux of K^+ from the endolymphatic space through the hair cells. Variations in the intensity and duration of acoustic stimuli would cause fluctuations in endolymph cation composition if there

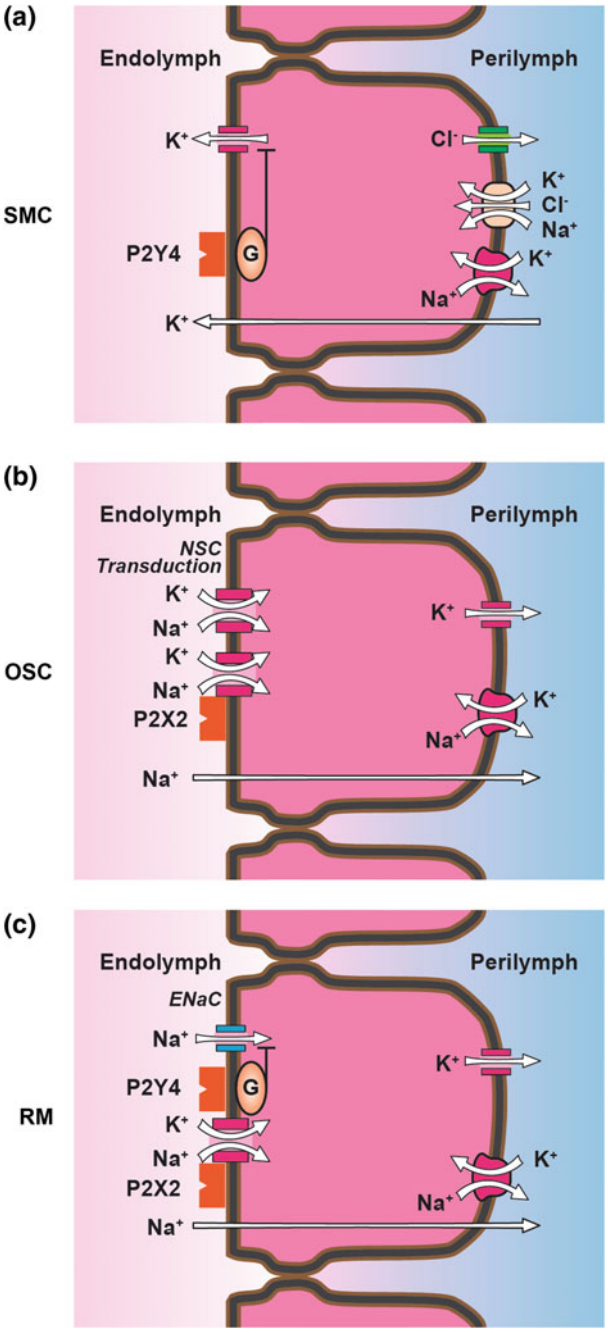
(a)
Endolymph
Perilymph
K+
Cl-
K+
Cl-
Na+
SMC
P2Y4
G
K+
Na+
K+
(b)
Endolymph
Perilymph
NSC
Transduction
K+
Na+
K+
Na+
K+
OSC
P2X2
K+
Na+
Na+
(c)
Endolymph
Perilymph
ENaC
Na+
K+
P2Y4
G
K+
Na+
K+
RM
P2X2
Na+
Na+

◂**Fig. 9.4** Purinergic signaling in the cochlear epithelium. **a** Stria vascularis marginal cells (SMC). Activation of P2Y4 receptors in the apical membrane reduce secretory K^+ flux via a G-protein (G) signal cascade. There are additional purinergic receptors on the basolateral side (not shown; Liu et al. 1995). **b** Outer sulcus cells (OSC). Activation of apical P2X2 receptors open the associated nonselective cation channels. Also shown are the apical purinergic-independent NSC channels; this model also applies to hair cells and the apical transduction channels. **c** Reissner's membrane epithelial cells (RM). Activation of P2Y4 receptors (membrane location unknown) reduces epithelial Na^+ channel (ENaC)-mediated Na^+ absorption via a G signal cascade, and activation of apical P2X2 receptors open the associated nonselective cation channels. *White arrows*, direction of flow. Adapted from Marcus (2012), with permission

were no coordinated regulation of the rates of secretion and absorption. Secretion is under the control of several extracellular hormones and factors, including purinergic agonists (see Sect. 9.5.4). It has been shown that the outer sulcus epithelial cells provide a parasensory pathway in the cochlea that sustains an apical-to-basal transepithelial cation current and that this current is regulated by purinergic agonists via P2X2 purinergic receptors (Lee et al. 2001; Kim and Marcus 2011). P2X2 receptors are ligand-gated nonselective cation channels; therefore, the Na^+- and K^+-absorptive currents through the outer sulcus epithelial cells have both constitutively active and regulated components. The K^+-mediated transduction current in hair cells is also accompanied by a Na^+ flux because the transduction channels are nonselective cation channels (Fig. 9.4).

9.4.7 Ca^{2+} Balance

Endolymphatic Ca^{2+} concentration is unusually low for an extracellular fluid (see Table 9.1) and its level is apparently maintained at its set point by a balanced secretion-absorption system. Ca^{2+} is secreted into the endolymph by the plasma membrane Ca^{2+}-ATPase PMCA2, which is located in the stereocilia of hair cells and also in Reissner's membrane (Furuta et al. 1998; Chen et al. 2011). Function of this protein was supported by the demonstration of PMCA activity on the apical membranes of Reissner's membrane (Yoshihara and Igarashi 1987) and stereocilia of hair cells (Yamoah et al. 1998). Mutation or deletion of the gene for PMCA2 leads to a reduced level of endolymphatic Ca^{2+} (Wood et al. 2004) and to deafness (Kozel et al. 1998).

A Ca^{2+}-absorptive system is expressed in the cochlea, and its gatekeeper apical channels, TRPV5 and TRPV6, are located in the inner and outer sulcus cells and have also been observed in the marginal cells (Yamauchi et al. 2010). The basic cell model components for Ca^{2+} absorption consist of the TRPV5 and TRPV6 epithelial Ca^{2+} channels in the apical membrane, cytosolic Ca^{2+} buffer, and basolateral Na^+/Ca^{2+} exchanger and Ca^{2+}-ATPase (Hoenderop et al. 2005). Ca^{2+} enters the cell from endolymph via the apical Ca^{2+} channels and is bound by the Ca^{2+} buffers. The bound Ca^{2+} diffuses across the cell to the basolateral membrane where the Ca^{2+} is released from the buffer and removed from the cell across the basolateral membrane by the combined action of the Ca^{2+}-ATPase and Na^+/Ca^{2+} exchanger. Surprisingly,

Ca^{2+}-ATPase activity was observed at the apical membrane of the outer sulcus cells as well as at the lateral membrane (Yoshihara and Igarashi 1987), although it is conceivable that the apical staining was in the subapical vesicles. The TRPV5 and TRPV6 transport system in the semicircular canal epithelium was found to be strongly inhibited by acidic shifts in the luminal pH (Nakaya et al. 2007) and stimulated by binding of vitamin D to its nuclear receptor (Yamauchi et al. 2005). Expression of all of these genes was also observed in the cochlea (Yamauchi et al. 2005, 2010).

9.4.8 Acid-Base Balance

Endolymphatic acid-base balance is also a secretion-absorption system. H^+ secretion from the stria vascularis has been observed with self-referencing pH electrodes (Miyazaki et al. 2016). In addition, HCO_3^- secretion occurs via the Cl^-/HCO_3^- exchanger pendrin (SLC26A4), which is expressed in the apical membrane of strial spindle cells, the spiral prominence, and outer sulcus epithelial cells (Wangemann 2013). Pendrin, and likely other HCO_3^- transporters, maintain endolymph alkaline with respect to perilymph (Table 9.1). As expected, adult *Slc26a4*-mutant mice have acidic endolymphatic pH (Wangemann et al. 2007). Further studies with conditional expression of *Slc26a4* point to a more complex acid-base regulatory system (Choi et al. 2011) that is under continuing investigation.

9.4.9 Water Movement: Aquaporins

The volume flow of water across biological membranes is always driven by osmotic differences across membranes and thereby follows active and passive movements of solutes, including ions. In other words, there are no known active "water pump" transporters. Diffusive water flow across biological membranes is mediated by a number of different proteins, but most attention has been paid to the 13 mammalian isoforms of AQP (reviewed in Hosoi 2016). Some AQPs are located in epithelial cells but others are in mesenchymal, vascular, or neural cells. Much interest has focused on epithelial cells in the cochlea (including stria vascularis and outer sulcus) and on the epithelium of the endolymphatic sac, an organ devoid of sensory cells that is involved in fluid absorption from endolymph. The expression and purported functions of AQPs in the inner ear was recently reviewed (Eckhard et al. 2012).

Movements of water across epithelia require a pathway in both the apical and basolateral membranes. These pathways may be mediated by different constellations of AQPs, some of which are constitutively expressed and others which are under hormonal control of translocation between cytosol and plasma membrane. AQP isoforms detected in inner ear tissues include AQP1, AQP4, and AQP5 in the cochlea (Li and Verkman 2001) and AQP2 in the endolymphatic sac (Maekawa

et al. 2010). Two prominent systems of regulated AQP-mediated water movement in the inner ear are mediated by AQP5 under muscarinic control (see Sects. 9.3.3 and 9.5.2) and by AQP2 under vasopressin control (see Sect. 9.5.3).

In addition to hormonal control of some AQPs, the isoforms are also characterized by their permeabilities to water and glycerol. Glycerol-permeable AQPs (aquaglyceroporins) include AQP3 and AQP8; others carry water but are impermeable to glycerol (AQP1, AQP2, AQP4, AQP5; Verkman and Mitra 2000). Another distinguishing characteristic is their sensitivity to inhibition by mercury compounds (mercurial-sensitive AQPs include AQP1, AQP2, and AQP3 but not AQP4; Verkman and Mitra 2000). Dependence of hearing on the expression of AQPs was tested in mice with individually knocked out AQP1, AQP3, AQP4, and AQP5. Auditory brainstem response to click stimulus was unaffected by the knockout of AQP1, AQP3, or AQP5. A significant hearing loss was observed in AQP4-null mice (Li and Verkman 2001).

9.5 Hormonal Regulation

In a changing environment, all cells respond to varying levels of systemic and local hormones, osmotic strength, and extracellular K^+ concentration. These extracellular influences modulate cell function via interaction with effector molecules in the plasma membrane (e.g., ionotropic receptors) or via intracellular signals (e.g., via metabotropic receptors and second-messenger signal molecules such as intracellular Ca^{2+} concentration, pH, and organic molecule signal pathways). These signal pathways modulate the rates of K^+ secretion, Na^+ and Ca^{2+} absorption, and water transport in the cochlea.

Homeostatic mechanisms in the inner ear occur in the absence of innervation of the stria vascularis and of the other extrasensory cells in the cochlea. Nonetheless, marginal cells contain receptors coupled to ion transport for several local or systemic hormones, including catecholamines, ATP, muscarinic agonists, and adrenocorticosteroid hormones. The sources of agonists for these receptors are systemic and/or paracrine rather than neural.

9.5.1 β-Adrenergic Receptors

Stimulation of β-adrenergic receptors in the stria vascularis leads to an increase in K^+ secretion, as represented by the transepithelial short-circuit current. The involvement of these receptors was established by determination of the potency order of specific antagonists and by demonstration of the presence of transcripts in cochlear tissue (Wangemann 2002). β-Adrenergic receptors are commonly coupled via G proteins to adenylate cyclase. Indeed, in addition to receptor stimulation, an increase in strial cytosolic cAMP via direct stimulation of adenylate cyclase,

by perfusion of a membrane-permeable cAMP analog, or by inhibition of phosphodiesterases that catalyze the breakdown of cAMP all lead to an increase of short-circuit current.

9.5.2 Muscarinic Receptors

Cholinergic signaling often occurs in functional units that are stimulated by activation of β-adrenergic receptors and inhibited by cholinergic receptors. Consistent with that constellation, activation of β-adrenergic receptors stimulates K^+ secretion, while activation of the (cholinergic) muscarinic receptors M3 and/or M4 on the basolateral membrane of strial marginal cells inhibit K^+ secretion. The source of the muscarinic agonists is not clear; however, they are likely arriving by the circulation from remote organs or from local paracrine release (Wangemann 2002). It is conceivable that acetylcholine levels would increase in the perilymph under conditions that overwhelm acetylcholinesterase activity in the synaptic clefts beneath the cochlear sensory cells and be carried by local blood vessels to the strial marginal cells (Hoya et al. 2001; Wangemann 2002).

Muscarinic receptors were recently found to also regulate water movements through AQP water channels expressed in outer sulcus cells of the upper cochlear turns (see Sect. 9.3.3). The isoform AQP4 is constitutively expressed in the basolateral membrane, and the isoform AQP5 is translocated into the apical plasma membrane in response to muscarinic agonists (Eckhard et al. 2015). The muscarinic control of AQP in outer sulcus cells is therefore poised to control transepithelial water flux in the cochlea, suggesting that one etiology of Ménière's disease could be dysfunction of this system. It has also been posited that the M3 receptors in the outer sulcus cells are constitutively activated in the absence of agonist, as found in an expression system study (Eckhard et al. 2012). This scenario would fit with findings of parasensory cation absorption by these cells (Kim and Marcus 2011; see Sect. 9.4.6); AQP5 and AQP4 in the apical and basolateral membranes could provide a pathway for reabsorptive water flux that accompanies the cation flux.

9.5.3 Vasopressin Control of Aquaporin 2

Transepithelial water fluxes across kidney tubules and across some other epithelia occur through AQP water channels (see Sect. 9.4.9) and the primary mode of regulation is via translocation of AQP2 between the cytosol and plasma membrane in response to vasopressin V2-receptor activation and the resultant downstream cAMP-protein kinase A (PKA) signaling (Brown et al. 2012). A long-standing interest in the possible role of V2/AQP2 in cochlear volume homeostasis has been pursued by many investigators who have searched for evidence of involvement of

this system in endolymph homeostasis and in the formation of cochlear hydrops in Ménière's disease.

The literature has been difficult to evaluate and integrate due to (1) uneven quality and resolution of expression studies, with widely conflicting results; (2) "expression" often defined only at the transcript level; (3) comparison of systemic versus local administration of receptor agonists and antagonists; and (4) the apparently blinding drive to support and adopt the kidney model. There have been varying degrees of stringency applied to the evaluation of antibody staining (the severity of the problem has been described; Delpire 2015), the selection of target tissues to stain, and often the exclusion of functional measures of hormonal signaling. Some of these conflicts in the literature have been reviewed by others (Eckhard et al. 2012; Takumida et al. 2012). Investigations that utilize systemically administered agents may result in effects either directly at the intended inner ear cellular targets or indirectly on the ear via alterations in the levels of hormones and other substances in the blood that then subsequently act in the inner ear, thereby confounding interpretations of drug actions. Nonetheless, we present here some of the most salient studies.

9.5.3.1 Kidney

In the kidney, key aspects of the V2/AQP2 system include binding of the agonist vasopressin (or antidiuretic hormone [ADH]) to the V2 receptor, followed by activation of the G_s protein, stimulation of adenylyl cyclase, increase in cytosolic cAMP, activation of PKA, and translocation and insertion of AQP2 into the apical cell membrane. Vasopressin thereby increases apical membrane water permeability through elevated numbers of AQP2 water channels in that membrane, which transports water in concert with constitutively expressed AQP3 and/or AQP4 in the basolateral membrane (Brown et al. 2012). This vasopressin-regulated system is a highly tempting story to adopt for the inner ear and could provide a basis for understanding the endolymphatic hydrops that often (but not always) accompanies the defining symptoms of Ménière's disease and would thereby be a possible drug target for treatment of Ménière's disease.

9.5.3.2 Cochlea

Several reports support the notion of this system contributing to the homeostasis of the cochlea at a local site. V2 receptors and AQP2 protein expression were both observed by fluorescence and immuno-gold immunolocalization in the basal cells of the stria vascularis; AQP2 was at the perilymph/spiral ligament side of the cells, while the V2 receptor and AQP3 were expressed at the intrastrial membrane (Nishioka et al. 2010). The two faces of the basal cells are separated by a barrier of tight junctions composed of claudin-11 (see Sect. 9.4.2). Expression of AQP2 in

the basal cells was also shown by another group (Takumida et al. 2012) but was not detected in another study (Li and Verkman 2001).

9.5.3.3 Endolymphatic Sac

Despite the incomplete and conflicting studies referred to in Sect. 9.5.3, some investigations of the V2/AQP2 system in the endolymphatic sac are more compelling than those in the cochlea. One conclusion from this body of work is that (1) the V2 receptor is located primarily in the basolateral membrane of the ribosome-rich cells in the endolymphatic sac; (2) in the absence of V2-receptor activation, the AQP2 water channels are localized primarily in intracellular vesicles and possibly in the apical membrane; and (3) the density of AQP2 channels in the basolateral membrane is increased by activation of the V2 receptors and subsequent translocation of the AQP2-containing vesicles. The most attractive hypothesis is that increased levels of vasopressin reduce transepithelial water permeability by removing gatekeeper AQP2 from the apical membrane of ribosomal-rich cells in the endolymphatic sac, which reduces absorption of fluid from the endolymph, leading to endolymphatic hydrops in the face of continued secretion in the cochlea.

This hypothesis is supported at several levels by the following observations.

- Importantly, two lines of evidence are consistent with the presence of AQP2 channels in the apical membrane that undergo endocytosis and translocation on activation of the V2 receptors (Kumagami et al. 1998; Maekawa et al. 2010). An acute primary culture of the rat endolymphatic sac maintained two types of cells with the appearance of ribosomal-rich and mitochondria-rich cells of the native sac. Functional V2 receptors were shown to inhibit endocytosis at the apical membrane in the cultured cells and to cause cochlear hydrops in guinea pigs chronically exposed to a V2 agonist (Kumagami et al. 1998).
- The correlation between Ménière's disease and elevated plasma vasopressin levels has been established by some teams (Eckhard et al. 2012), but see exception below in this section.
- Clinically relevant levels of vasopressin during chronic (1-week) infusion in guinea pigs were found to create significant cochlear hydrops compared with the control animals that received only saline infusions (Takeda et al. 2000).

If this hypothesis is correct, it implies a striking difference in the signal pathways in the kidney and endolymphatic sac. Activation of V2 receptors in the kidney lead to insertion of AQP2 in the apical membrane and consequent stimulation of transepithelial water flux, while in the endolymphatic sac, it leads to endocytosis of apical AQP2 and the consequent inhibition of transepithelial water flux. Problematic for this hypothesis is that (1) the obligatory correspondence of endolymphatic hydrops to Ménière's disease has been disputed (Merchant et al. 2005; Foster and Breeze 2013) and (2) some research teams found no elevation in plasma vasopressin in Ménière's patients (Eckhard et al. 2012).

9.5.4 Purinergic Signaling

Purinergic signaling in the cochlea is well-known, and evidence has been found to support a complete autocrine and/or paracrine signaling cycle (Lee and Marcus 2008). This includes observation of a local source of agonist, expression of purinergic receptors in the plasma membrane of inner ear epithelial cells, and termination of signaling. The signal pathway is apparently stimulated by stressful conditions such as noise. The level of endolymphatic ATP was observed to increase significantly after a short exposure to noise (Muñoz et al. 2001). Increases in endolymphatic ATP were correlated with decreases in the EP and in the input resistance of the cochlear duct, consistent with a protective effect on the sensory cells of purinergic signaling during noise exposure (Thorne et al. 2004).

9.5.4.1 Purinergic Agonist

The sources of purinergic agonist have been investigated, and it has been proposed that ATP is released from strial marginal cells into the endolymph via subapical membrane vesicles (Muñoz et al. 2001) and from nonsensory supporting cells in the organ of Corti mediated by connexin hemichannels (Anselmi et al. 2008). The involvement of pannexin-1 hemichannels in ATP release has also been proposed (Chen et al. 2015). Purinergic signaling in the cochlea is terminated through the breakdown of agonist catalyzed by ectonucleotidases (Vlajkovic et al. 2004). Effective concentrations of extracellular ATP on purinergic receptors are orders of magnitude less than those of intracellular ATP in metabolic reactions.

9.5.4.2 Purinergic Receptors

Electrophysiological and pharmacological investigations have demonstrated purinergic signaling in several cell types of the inner ear. Both ionotropic (P2X receptor) and metabotropic (P2Y receptor) types are expressed and control specific physiological processes.

Reissner's membrane, outer sulcus cells, and vestibular transitional epithelial cells express ionotropic P2X2 receptors in the apical membrane (Lee et al. 2001; Housley et al. 2013; Fig. 9.4b, c) that likely mediate a protective response to noise. P2X receptors are agonist-gated nonselective cation channels in the plasma membrane. As such, activation opens conductive pathways in the epithelial barrier and leads to a gated parasensory shunting of K^+ currents away from the sensory cells in overstimulated conditions. Inner and outer hair cells in the cochlea also express ionotropic P2X2 receptors in the apical membrane (Housley et al. 2013) (Fig. 9.4b) that likely mediate a protective response to noise by shunting the transduction channel in the same cell membrane.

Marginal cells in the stria vascularis secrete K^+ under the control of apical P2Y4 receptors (Fig. 9.4a). Activation of these receptors reduces K^+ secretion and the EP primarily via the diacylglycerol (DAG)-protein kinase C (PKC) branch of a G protein signal pathway (Lee and Marcus 2008), thereby contributing to the protective response to noise through reduction of the driving force for auditory transduction. Claudius cells utilize P2Y receptors to control transepithelial current, although the membrane location and electrogenic transport pathway coupled to the receptors are not known (Yoo et al. 2012). Activation of basolateral P2Y2 receptors in semicircular canal duct cells produced complex changes in transepithelial current and resistance (Pondugula et al. 2010). No electrical response to the apical purinergic agonists ATP or UTP was observed in this epithelium.

It was also reported that activation of P2Y2 and/or P2Y4 receptors, expressed on the apical membrane of Hensen, Böttcher, and Claudius cells of developing rats, by nanomolar levels of ATP initiates a complex pattern of Ca^{2+} waves through the coupled epithelial layer in the developing cochlea (Mammano 2013). Purinergic signaling thus plays a significant role in hearing through the regulation of endolymphatic ion composition and transduction currents (Housley et al. 2013).

9.5.5 Steroid Hormones

Steroid regulation of ion transport is exemplified by Reissner's membrane in the cochlea and by both saccular and semicircular canal duct epithelia in the vestibular system. These epithelia absorb Na^+ via highly Na^+-selective apical channels (ENaC) that are upregulated in expression and function specifically by glucocorticoids and not by mineralocorticoids (Kim and Marcus 2011). The signal pathway is illustrated in Fig. 9.5.

The corticosteroids diffuse into the target cells where the active form of glucocorticoid is increased by enzymatic action transforming inactive forms of glucocorticoid to the active form via 11β-hydroxysteroid dehydrogenase (HSD1). The active glucocorticoid binds to the receptor in the cytoplasm that then translocates into the nucleus where the agonist-receptor complex promotes expression of several proteins involved in the stimulation of Na^+ absorption. The stimulated signal pathway involves the increase in ENaC expression at the cell surface via SGK1 and Nedd4-2 through reduction of channel retrieval from the plasma membrane (Kim and Marcus 2011).

Binding sites for both glucocorticosteroid (ten Cate et al. 1993) and mineralocorticosteroid (Yao and Rarey 1996) have been demonstrated in the stria vascularis. Both corticoids control the activity of Na^+, K^+-ATPase in the stria vascularis (adrenalectomy reduced activity 60% and systemic administration of either the glucocorticosteroid dexamethasone or the mineralocorticosteroid aldosterone restored activity; Curtis et al. 1993), and the increase in Na^+, K^+-ATPase expression with aldosterone was not dependent on major changes in blood plasma cation concentration (ten Cate et al. 1994). However, despite the strong dependence of the

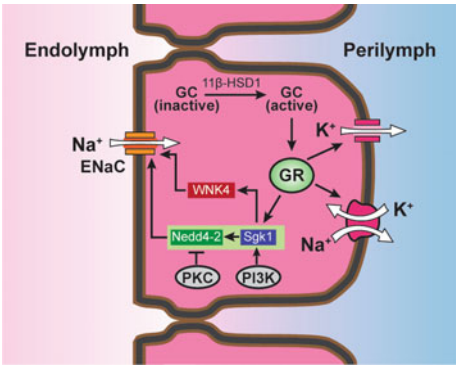

Fig. 9.5 Schematic diagram of glucocorticoid-regulated Na^+ absorption in mouse Reissner's membrane and rat semicircular canal duct epithelial cells. Inactive forms of glucocorticoid (GC) are activated by 11β-hydroxysteroid dehydrogenase 1 (11β-HSD1), which then increases ENaC expression via the glucocorticoid receptor (GR)-serum glucocorticoid-regulated kinase 1 (SGK1)-neural precursor cell-expressed developmentally downregulated 4-2 (Nedd4-2) pathway. WNK4 was also suggested to be involved in the glucocorticoid-regulated Na^+ transport pathway in Reissner's membrane. Glucocorticoid-stimulated Na^+ absorption is positively regulated by phosphatidylinositol 3-kinase (PI3K) and negatively regulated by protein kinase C (PKC) in semicircular canal epithelial cells. The rate of Na^+ absorption is stimulated by glucocorticoid activation of GR in mouse saccule; however, the mechanism of glucocorticoid-enhanced Na^+ absorption via ENaC was not molecularly defined. *White arrows*, direction of flow. Adapted from Kim and Marcus (2011), with permission

EP on strial Na^+, K^+-ATPase, a reduction in adrenocorticosteroids by adrenalectomy did not significantly reduce the EP in the presence or absence of strong acoustic stimulation (Ma et al. 1995). In addition, glucocorticoid hormones alone apparently do not stimulate the formation of Na^+, K^+-ATPase in the inner ear because no difference in the level of antibody binding to Na^+, K^+-ATPase was observed in glucocorticoid receptor-knockout mice (Erichsen et al. 1998).

9.5.6 Basolateral K^+ Concentration and Apical pH

Changes in extracellular ion composition, such as K^+ and H^+, can exert powerful control over ion transport by cells that are neighbors to the cells that produce those changes. In that regard, we may think of the controlling ions as paracrine-signaling hormones. The concentration of K^+ in the perilymph that surrounds the sensory cells and their nerve synapses is known to increase on sensory stimulation (see Sects. 9.4.3 and 9.4.4), and the K^+ thus exuded from the sensory cells is known to "recycle" to the stria vascularis in the cochlea and to the vestibular dark cells where it is pumped back into endolymph (see Sects. 9.4.3 and 9.4.4). The rate of basolateral uptake of K^+ in strial marginal cells and vestibular dark cells is exquisitely sensitive to the level of extracellular K^+ at that membrane so that small increases

supplied from the sensory cells would be expected to be avidly taken up and secreted across the apical (endolymphatic) membrane (Wangemann et al. 1996). This K^+ sensitivity is believed to play a significant role in regulating the recirculation of K^+ back into the endolymph (Wangemann et al. 1996).

The endolymphatic pH is regulated by several transport processes (see Sect. 9.4.8), and this in turn exerts control over the activity of at least two key transporters. The gatekeeper K^+ channel KCNQ1/KCNE1 in the apical membrane of strial marginal cells and vestibular dark cells is stimulated by acidification of endolymph (Wangemann et al. 1995b; Heitzmann et al. 2007), which thereby influences the rate of secretion of K^+ (see Sect. 9.4.1). The endolymphatic Ca^{2+} concentration in both the cochlea and the vestibular labyrinth is thought to be partially controlled by absorption through epithelial Ca^{2+} channels (see Sect. 9.4.7), and those channels have been shown to be strongly inhibited by acidic endolymphatic pH (Nakaya et al. 2007).

9.6 Genetic Diseases

Genetic factors underlie more than 50% of the cases of prelingual hearing impairment (Oonk et al. 2015). Genetic causes of hearing loss are classified and identified in several ways. Clinical presentations that are exclusively hearing related are "nonsyndromic" (70% of cases) and those with pathologies also in other organs are "syndromic" (30% of cases). The chromosomal loci of nonsyndromic hereditary DeaFNess are designated with DFN numbers, such as DFNA1 or DFNB1. The A and B refer to autosomal-dominant (roughly 20% of the nonsyndromic cases) and autosomal-recessive (roughly 80%) hereditary transmission of hearing loss (Bayazit and Yilmaz 2006). Cases that are not classified A or B (about 1–2%) are mitochondrial, X- or Y-linked inheritance (Oonk et al. 2015). Gene expression profiles for causative genes and the locations of the corresponding proteins involved in hereditary hearing loss are collected in a recent review (Nishio et al. 2015) and databases are maintained online (e.g., http://hereditaryhearingloss.org).

Many of the most prevalent types of sensorineural hearing loss with hereditary etiology arise from the dysfunction of cells that are responsible for ionic homeostasis of the endolymph. These include (1) DFNB1 caused by mutations of GJB2 (connexin-26) and/or GJB6 (connexin-30) gap junction genes, (2) DFNB4 (Pendred syndrome) caused by mutations in SLC26A4, a Cl^-/HCO_3^- transporter that is essential for normal development of the inner ear, and (3) Jervell and Lange-Nielsen syndrome, which results from mutations of the KCNQ1/KCNE1 K^+ channel in either of these subunits.

DFNB1 is the most common DFNB and can occur as either syndromic or nonsyndromic deafness (Jagger and Forge 2015). Gap junctions composed of CX26 homomers, CX30 homomers, and C26/CX30 heteromers connect epithelial and connective tissue cells in the cochlea and vestibular labyrinth in patterns that support multiple critical transport processes among cells (Jagger and Forge 2015).

The neuroepithelial sensory cells, however, have no gap junction connections to neighboring cells.

Multiple functions of connexins in the ear have been proposed. These include shuttling K^+ from the basolateral side of sensory cells during acoustic stimulation back to the stria vascularis for secretion into the endolymph (see Sect. 9.4.3); the transfer of essential second messengers such as inositol (1,4,5)-trisphosphate [Ins (1,4,5)P_3] and Ca^{2+} among the coupled cells; guidance of nutrients and hormones (e.g., glucose and locally produced thyroid hormone) to target cells (Wangemann et al. 2009; Jagger and Forge 2015); and paracrine signaling via connexins expressed in a single-cell membrane (hemichannels). Hemichannels of connexins are thought to participate in purinergic signaling in the ear by providing a route for ATP release from cells (Jagger and Forge 2015). Hemichannels can open when the extracellular fluid has a low divalent cation concentration. The apical membranes of cochlear epithelial cells face the endolymph, which contains only about 20 μM Ca^{2+} and Mg^{2+} each, thus providing a permissive environment. The mechanisms by which gap junctions participate in cochlear function are far from fully understood and continue to draw considerable attention.

Pendred syndrome results from mutations of the Cl^-/HCO_3^- exchanger coded by SLC26A4 and accounts for about 7.5% (varies by population) of cases of hereditary deafness. Deletion of this gene in mice results in an acidic shift of endolymphatic pH, as expected from the loss of a HCO_3^--secretory transporter (see Sect. 9.4.8). The effects of pendrin mutation, however, go far beyond this relatively obvious consequence and are described by Wangemann (2013) and Ito et al. (2014). A clinical diagnostic parameter for Pendred syndrome is an enlarged vestibular aqueduct and an endolymphatic hydrops throughout the inner ear. An enlarged vestibular aqueduct is readily observed in MRI scans, and the syndromic condition is hypothyroidism in humans (but not mice); although pendrin-knockout mice are euthyroid, there appears to be a local hypothyroidism in the cochlea (Wangemann et al. 2009).

Jervell and Lange-Nielsen syndrome (JLNS) is "syndromic" because the affected K^+ channel plays a prominent role in human cardiac function as well as providing the sole route of K^+ efflux from strial marginal cells and vestibular dark cells. Dysfunction of this channel results in a reduced volume of endolymph and concentration of K^+, and the EP is virtually abolished (Marcus et al. 2002). Patients with dysfunctional mutations of these K^+-channel subunits are profoundly deaf in both ears and their QTc EKG interval is associated with tachyarrhythmias (Tranebjaerg et al. 2014). Parents of a child with JLNS are usually heterozygotes and the inheritance is autosomal recessive.

The identification of genes underlying many of the clinically defined hereditary deafness types (Nishio et al. 2015) suggests that gene therapy may be a successful treatment option. This approach requires vectors that can hold the required amount of genetic information, can enter the desired target cells, and can stimulate gene expression over the necessary time period. There has been intense work on each of these aspects, with varied results (Chien et al. 2015). Hearing loss that originates from gene mutations whose expression is critical for function during only relatively

short time periods have the highest potential to be effective. The most severe effects of Pendred syndrome originate from a lack of normal expression in the ear during a 2-week period during development (Choi et al. 2011), which thereby offers a clear window of opportunity for gene therapy.

9.7 Free Radical Stress and Mitochondrial Dysfunction

Free radical stress that exceeds the capacity of defense mechanisms has been implicated in the inner ear pathogenesis of genetic (Pendred syndrome; see Sect. 9.6) and acquired (acoustic trauma, drug-induced ototoxicity, and age-related hearing loss) origins. Free radical stress originates largely from mitochondrial activity, but other mitochondrial actions have also been implicated in the cellular causes of these cochlear pathologies (Bottger and Schacht 2013). The stria vascularis is prone to free radical stress due to its high O_2-dependent metabolic activity and dense vascular system, and, indeed, EP generation over the KCNJ10 K^+ channel in intermediate cells is highly sensitive to local levels of free radical stress (Singh and Wangemann 2008). Hair cells are also susceptible to free radical stress even though they function at a lower level of metabolic activity because they produce a lower content of antioxidants (Bottger and Schacht 2013). In addition to free radical stress, mitochondrial modes of dysfunction include aberrant calcium regulation, mitochondrial DNA deletions, and the targeting of mitochondrial ribosomes (Bottger and Schacht 2013). A combined therapeutic strategy of administration of free radical scavengers and cochlear vasodilators has been proposed for the treatment of age-related hearing loss (Alvarado et al. 2015), but the widely variable results in the field has led to a measure of uncertainty in the general applicability of the proposal (Bottger and Schacht 2013).

9.8 Summary

Regulated solute and water transport in the cochlea is essential for hearing. This chapter describes the cellular mechanisms of transport in the different epithelial cells of the cochlear duct that produce and maintain the cochlear fluid composition in the face of local and systemic perturbations. Epithelial cells produce net secretory and/or absorptive fluxes by virtue of gene expression of specific transport proteins and asymmetrical placement in the apical and basolateral cell membranes. Transport is coordinated across the two membrane surfaces, and the net rate is further up- and downregulated by extracellular, intracellular, and transmembrane signals. Many genetic disorders that result in hearing loss relate to solute and water transport and their regulatory pathways.

Specific directions for future investigation include experimentally testing the hypotheses concerning (1) cellular mechanisms of putative K^+ buffering and

cycling in the cochlea, (2) the putative involvement of AQPs and hormonal signaling in the volume control of cochlear fluids, and (3) the ways in which the cochlea, vestibular organs, and endolymphatic sac communicate during development, as alluded to in this chapter. Furthermore, a rapidly expanding arsenal of techniques to manipulate inner ear genes and their modulation promises an exciting future of discovery and increased understanding of the importance of ion homeostasis in hearing and balance.

Acknowledgements This work was supported by Grant R01-DC012151 from the National Institute on Deafness and Other Communication Diseases, National Institutes of Health, and by the Kansas State University College of Veterinary Medicine.

Compliance with Ethics Requirements Philine Wangemann declares that she has no conflict of interest. Daniel C. Marcus declares that he has no conflict of interest.

References

Alvarado, J. C., Fuentes-Santamaria, V., Melgar-Rojas, P., Valero, M. L., Gabaldón-Ull, M. C., Miller, J. M., & Juiz, J. M. (2015). Synergistic effects of free radical scavengers and cochlear vasodilators: A new otoprotective strategy for age-related hearing loss. *Frontiers in Aging Neuroscience*, 7, 1–7.

Ando, M., Edamatsu, M., Fukuizumi, S., & Takeuchi, S. (2008). Cellular localization of facilitated glucose transporter 1 (GLUT-1) in the cochlear stria vascularis: Its possible contribution to the transcellular glucose pathway. *Cell and Tissue Research*, 331, 763–769.

Andrews, J. C., & Honrubia, V. (2010). Premenstrual exacerbation of Meniere's disease revisited. *Otolaryngologic Clinics of North America*, 43, 1029–1040.

Anselmi, F., Hernandez, V. H., Crispino, G., Seydel, A., Ortolano, S., Roper, S. D., Kessaris, N., Richardson, W., Rickheit, G., Filippov, M. A., Monyer, H., & Mammano, F. (2008). ATP release through connexin hemichannels and gap junction transfer of second messengers propagate Ca^{2+} signals across the inner ear. *Proceedings of the National Academy of Sciences of the United States of America*, 105, 18770–18775.

Bayazit, Y. A., & Yilmaz, M. (2006). An overview of hereditary hearing loss. *ORL Journal for Oto-Rhino Laryngology and Related Specialties*, 68, 57–63.

Boettger, T., Hubner, C. A., Maier, H., Rust, M. B., Beck, F. X., & Jentsch, T. J. (2002). Deafness and renal tubular acidosis in mice lacking the K-Cl co-transporter Kcc4. *Nature*, 416, 874–878.

Bottger, E. C., & Schacht, J. (2013). The mitochondrion: A perpetrator of acquired hearing loss. *Hearing Research*, 303, 12–19.

Brown, D., Bouley, R., Paunescu, T. G., Breton, S., & Lu, H. A. J. (2012). New insights into the dynamic regulation of water and acid-base balance by renal epithelial cells. *American Journal of Physiology - Cell Physiology*, 302, C1421–C1433.

Cazals, Y., Bevengut, M., Zanella, S., Brocard, F., Barhanin, J., & Gestreau, C. (2015). KCNK5 channels mostly expressed in cochlear outer sulcus cells are indispensable for hearing. *Nature Communications*, 6, 8780.

Chen, J., Zhu, Y., Liang, C., Chen, J., & Zhao, H.-B. (2015). Pannexin1 channels dominate ATP release in the cochlea ensuring endocochlear potential and auditory receptor potential generation and hearing. *Scientific Reports*, 5, 10762.

Chen, Q., Chu, H., Wu, X., Cui, Y., Chen, J., Li, J., Zhou, L., Xiong, H., Wang, Y., & Li, Z. (2011). The expression of plasma membrane Ca^{2+}-ATPase isoform 2 and its splice variants at

sites A and C in the neonatal rat cochlea. *International Journal of Pediatric Otorhinolaryngology*, 75, 196–201.

Chien, W. W., Monzack, E. L., McDougald, D. S., & Cunningham, L. L. (2015). Gene therapy for sensorineural hearing loss. *Ear and Hearing*, 36, 1–7.

Choi, B. Y., Kim, H. M., Ito, T., Lee, K. Y., Li, X., Monahan, K., Wen, Y., Wilson, E., Kurima, K., Saunders, T. L., Petralia, R. S., Wangemann, P., Friedman, T. B., & Griffith, A. J. (2011). Mouse model of enlarged vestibular aqueducts defines temporal requirement of *Slc26a4* expression for hearing acquisition. *Journal of Clinical Investigation*, 121, 4516–4525.

Curtis, L. M., ten Cate, W. J., & Rarey, K. E. (1993). Dynamics of Na, K-ATPase sites in lateral cochlear wall tissues of the rat. *European Archives of Oto-Rhino-Laryngology*, 250, 265–270.

Delpire, E. (2015). Research antibodies: Do not use them to stain your reputation. *American Journal of Physiology-Cell Physiology*, 309, C707–C708.

Eckhard, A., Gleiser, C., Arnold, H., Rask-Andersen, H., Kumagami, H., Müller, M., Hirt, B., & Löwenheim, H. (2012). Water channel proteins in the inner ear and their link to hearing impairment and deafness. *Molecular Aspects of Medicine*, 33, 612–637.

Eckhard, A., Dos, S. A., Liu, W., Bassiouni, M., Arnold, H., Gleiser, C., Hirt, B., Harteneck, C., Müller, M., Rask-Andersen, H., & Löwenheim, H. (2015). Regulation of the perilymphatic-endolymphatic water shunt in the cochlea by membrane translocation of aquaporin-5. *Pflügers Archiv - European Journal of Physiology*, 467, 2571–2588.

Effertz, T., Scharr, A. L., & Ricci, A. J. (2015). The how and why of identifying the hair cell mechano-electrical transduction channel. *Pflügers Archiv - European Journal of Physiology*, 467, 73–84.

Erichsen, S., Stierna, P., Bagger-Sjoback, D., Curtis, L. M., Rarey, K. E., Schmid, W., & Hultcrantz, M. (1998). Distribution of Na, K-ATPase is normal in the inner ear of a mouse with a null mutation of the glucocorticoid receptor. *Hearing Research*, 124, 146–154.

Ferrary, E., Sterkers, O., Saumon, G., Tran Ba Huy, P., & Amiel C. (1987). Facilitated transfer of glucose from blood into perilymph in the rat cochlea. *American Journal of Physiology - Renal Physiology*, 253, F59–F65.

Firbas, W., Gruber, H., & Wicke, W. (1981). The blood vessels of the limbus spiralis. *Archives of Oto-Rhino-Laryngology*, 232, 131–137.

Foster, C. A., & Breeze, R. E. (2013). The Meniere attack: An ischemia/reperfusion disorder of inner ear sensory tissues. *Medical Hypotheses*, 81, 1108–1115.

Furuta, H., Luo, L., Hepler, K., & Ryan, A. F. (1998). Evidence for differential regulation of calcium by outer versus inner hair cells: Plasma membrane Ca-ATPase gene expression. *Hearing Research*, 123, 10–26.

Gao, Y., Yechikov, S., Vazquez, A. E., Chen, D., & Nie, L. (2013). Impaired surface expression and conductance of the KCNQ4 channel lead to sensorineural hearing loss. *Journal of Cellular and Molecular Medicine*, 17, 889–900.

Gow, A., Davies, C., Southwood, C. M., Frolenkov, G., Chrustowski, M., Ng, L., Yamauchi, D., Marcus, D. C., & Kachar, B. (2004). Deafness in *Claudin 11*-null mice reveals the critical contribution of basal cell tight junctions to stria vascularis function. *The Journal of Neuroscience*, 24, 7051–7062.

Guipponi, M., Vuagniaux, G., Wattenhofer, M., Shibuya, K., Vazquez, M., Dougherty, L., Scamuffa, N., Guida, E., Okui, M., Rossier, C., Hancock, M., Buchet, K., Reymond, A., Hummler, E., Marzella, P. L., Kudoh, J., Shimizu, N., Scott, H. S., Antonarakis, S., & Rossier, B. C. (2002). The transmembrane serine protease ($TMPRSS_3$) mutated in deafness DFNB8/10 activates the epithelial sodium channel (ENaC) in vitro. *Human Molecular Genetics*, 11, 2829–2836.

Heitzmann, D., Koren, V., Wagner, M., Sterner, C., Reichold, M., Tegtmeier, I., Volk, T., & Warth, R. (2007). KCNE beta subunits determine pH sensitivity of KCNQ1 potassium channels. *Cellular Physiology and Biochemistry*, 19, 21–32.

Hirose, K., Hartsock, J. J., Johnson, S., Santi, P., & Salt, A. N. (2014). Systemic lipopolysaccharide compromises the blood-labyrinth barrier and increases entry of serum fluorescein into the perilymph. *Journal of the Association for Research in Otolaryngology*, 15, 707–719.

Hoenderop, J. G., Nilius, B., & Bindels, R. J. (2005). Calcium absorption across epithelia. *Physiological Reviews*, 85, 373–422.

Hosoi, K. (2016). Physiological role of aquaporin 5 in salivary glands. *Pflügers Archiv - European Journal of Physiology*, 468, 519–539.

Housley, G. D., Morton-Jones, R., Vlajkovic, S. M., Telang, R. S., Paramananthasivam, V., Tadros, S. F., Wong, A. C. Y., Froud, K. E., Cederholm, J. M. E. Sivakumaran, Y., Snguanwongchai, P., Khakh, B. S., Cockayne, D. A., Thorne, P. R., & Ryan, A. F. (2013). ATP-gated ion channels mediate adaptation to elevated sound levels. *Proceedings of the National Academy of Sciences of the United States of America*, 110, 7494–7499.

Hoya, N., Ogawa, K., Inoue, Y., Takiguchi, Y., & Kanzaki, J. (2001). The glutamate receptor agonist, AMPA, induces acetylcholine release in guinea pig cochlea; A microdialysis study. *Neuroscience Letters*, 311, 206–208.

Ito, T., Li, X., Kurima, K., Choi, B. Y., Wangemann, P., & Griffith, A. J. (2014). *Slc26a4*-insufficiency causes fluctuating hearing loss and stria vascularis dysfunction. *Neurobiology of Disease*, 66, 53–65.

Jagger, D. J., & Forge, A. (2015). Connexins and gap junctions in the inner ear—it's not just about K^+ recycling. *Cell and Tissue Researc*h, 360, 633–644.

Johnstone, B. M., Patuzzi, R., Syka, J., & Sykova, E. (1989). Stimulus-related potassium changes in the organ of Corti of guinea-pig. *The Journal of Physiology*, 408, 77–92.

Juhn, S. K., Rybak, L. P., & Fowlks, W. L. (1982). Transport characteristics of the blood-perilymph barrier. *American Journal of Otolaryngology*, 3, 392–396.

Kambayashi, J., Kobayashi, T., DeMott, J. E., Marcus, N. Y., Thalmann, I., & Thalmann, R. (1982). Effect of substrate-free vascular perfusion upon cochlear potentials and glycogen of the stria vascularis. *Hearing Research*, 6, 223–240.

Kikuchi, T., Kimura, R. S., Paul, D. L., Takasaka, T., & Adams, J. C. (2000). Gap junction systems in the mammalian cochlea. *Brain Research Reviews*, 32, 163–166.

Kim, K. X., Sanneman, J. D., Kim, H. M., Harbidge, D. G., Xu, J., Soleimani, M., Wangemann, P., & Marcus, D. C. (2014). Slc26a7 chloride channel activity and localization in mouse Reissner's membrane epithelium. *PLoS ONE*, 9, e97191.

Kim, S. H., & Marcus, D. C. (2011). Regulation of sodium transport in the inner ear. *Hearing Research*, 280, 21–29.

Kofuji, P., Biedermann, B., Siddharthan, V., Raap, M., Iandiev, I., Milenkovic, I., Thomzig, A., Veh, R. W., Bringmann, A., & Reichenbach, A. (2002). Kir potassium channel subunit expression in retinal glial cells: Implications for spatial potassium buffering. *Glia*, 39, 292–303.

Konishi, T., Hamrick, P. E., & Walsh, P. J. (1978). Ion transport in guinea pig cochlea. I. Potassium and sodium transport. *Acta Oto-Laryngologica*, 86, 22–34.

Kozel, P. J., Friedman, R. A., Erway, L. C., Yamoah, E. N., Liu, L. H., Riddle, T., Duffy, J. J., Doetschman, T., Miller, M. L., Cardell, E. L., & Shull, G. E. (1998). Balance and hearing deficits in mice with a null mutation in the gene encoding plasma membrane Ca^{2+}-ATPase isoform 2. *Journal of Biological Chemistry*, 273, 18693–18696.

Kumagami, H., Loewenheim, H., Beitz, E., Wild, K., Schwartz, H., Yamashita, K., Schultz, J., Paysan, J., Zenner, H.-P., & Ruppersberg, J. P. (1998). The effect of anti-diuretic hormone on the endolymphatic sac of the inner ear. *Pflügers Archiv - European Journal of Physiology*, 436, 970–975.

Laurell, G., Viberg, A., Teixeira, M., Sterkers, O., & Ferrary, E. (2000). Blood-perilymph barrier and ototoxicity: An in vivo study in the rat. *Acta Oto-Laryngologica*, 120, 796–803.

Laurell, G. F., Teixeira, M., Duan, M., Sterkers, O., & Ferrary, E. (2008). Intact blood-perilymph barrier in the rat after impulse noise trauma. *Acta Oto-Laryngologica*, 128, 608–612.

Lee, J. H., & Marcus, D. C. (2008). Purinergic signaling in the inner ear. *Hearing Research*, 235, 1–7.

Lee, J. H., Chiba, T., & Marcus, D. C. (2001). P2X2 receptor mediates stimulation of parasensory cation absorption by cochlear outer sulcus cells and vestibular transitional cells. *The Journal of Neuroscience*, 21, 9168–9174.

Li, J., & Verkman, A. S. (2001). Impaired hearing in mice lacking aquaporin-4 water channels. *Journal of Biological Chemistry*, 276, 31233–31237.

Liu, J., Kozakura, K., & Marcus, D. C. (1995). Evidence for purinergic receptors in vestibular dark cell and strial marginal cell epithelia of the gerbil. *Auditory Neuroscience*, 1, 331–340.

Ma, Y. L., Gerhardt, K. J., Curtis, L. M., Rybak, L. P., Whitworth, C., & Rarey, K. E. (1995). Combined effects of adrenalectomy and noise exposure on compound action potentials, endocochlear potentials and endolymphatic potassium concentrations. *Hearing Research*, 91, 79–86.

Maekawa, C., Kitahara, T., Kizawa, K., Okazaki, S., Kamakura, T., Horii, A., Imai, T., Doi, K., Inohara, H., & Kiyama, H. (2010). Expression and translocation of aquaporin-2 in the endolymphatic sac in patients with Meniere's disease. *Journal of Neuroendocrinology*, 22, 1157–1164.

Mammano, F. (2013). ATP-dependent intercellular Ca^{2+} signaling in the developing cochlea: Facts, fantasies and perspectives. *Seminars in Cell and Developmental Biology*, 24, 31–39.

Marcus, D. C. (2012). Acoustic transduction. In N. Sperelakis (Ed.), *Cell physiology source book: Essentials of membrane biophysics* (pp. 649–668). San Diego, CA: Academic Press.

Marcus, D. C., & Wangemann, P. (2009). Cochlear and vestibular function and dysfunction. In F. J. Alvarez-Leefmans, & E. Delpire (Eds.), *Physiology and Pathology of Chloride Transporters and Channels in the Nervous System: From Molecules to Diseases* (pp. 425–437). New York: Elsevier.

Marcus, D. C., & Wangemann, P. (2010). Inner ear fluid homeostasis. In P. A. Fuchs (Ed.), *The Oxford Handbook of Auditory Science: The Ear* (pp. 213–230). Oxford, UK: Oxford University Press.

Marcus, D. C., Wu, T., Wangemann, P., & Kofuji, P. (2002). KCNJ10 (Kir4.1) potassium channel knockout abolishes endocochlear potential. *American Journal of Physiology - Cell Physiology*, 282, C403–C407.

Merchant, S. M., Adams, J. C., & Nadol, J. B. (2005). Meniere's syndrome: Are symptoms caused by endolymphatic hydrops? *The Registry*, 12, 1–7.

Miyazaki, H., Wangemann, P., & Marcus, D. C. (2016). The gastric H, K-ATPase in stria vascularis contributes to pH regulation of cochlear endolymph but not to K secretion. *BMC Physiology,* 17(1), 1.

Morton-Jones, R. T., Vlajkovic, S. M., Thorne, P. R., Cockayne, D. A., Ryan, A. F., & Housley, G. D. (2015). Properties of ATP-gated ion channels assembled from $P2X_2$ subunits in mouse cochlear Reissner's membrane epithelial cells. *Purinergic Signalling*, 11, 551–560.

Mosnier, I., Teixeira, M., Loiseau, A., Fernandes, I., Sterkers, O., Amiel, C., & Ferrary, E. (2001). Effects of acute and chronic hypertension on the labyrinthine barriers in rat. *Hearing Research*, 151, 227–236.

Muñoz, D. J., Kendrick, I. S., Rassam, M., & Thorne, P. R. (2001). Vesicular storage of adenosine triphosphate in the guinea-pig cochlear lateral wall and concentrations of ATP in the endolymph during sound exposure and hypoxia. *Acta Oto-Laryngologica*, 121, 10–15.

Nakaya, K., Harbidge, D. G., Wangemann, P., Schultz, B. D., Green, E. D., Wall, S. M., & Marcus, D. C. (2007). Lack of pendrin HCO_3^- transport elevates vestibular endolymphatic $[Ca^{2+}]$ by inhibition of acid-sensitive TRPV5 and TRPV6 channels. *American Journal of Physiology - Renal Physiology*, 292, F1314–F1321.

Nenov, A. P., Chen, C., & Bobbin, R. P. (1998). Outward rectifying potassium currents are the dominant voltage activated currents present in Deiters' cells. *Hearing Research*, 123, 168–182.

Nishio, S. Y., Hattori, M., Moteki, H., Tsukada, K., Tsukada, K., Miyagawa, M., Naito, T., Yoshimura, H., Iwasa, Y., Mori, K., Shima, Y, Sakuma, N., & Usami, S. (2015). Gene expression profiles of the cochlea and vestibular endorgans: Localization and function of genes causing deafness. *The Annals of Otology, Rhinology and Laryngology*, 124 Suppl. 1, 6S–48S.

Nishioka, R., Takeda, T., Kakigi, A., Okada, T., Takebayashi, S., Taguchi, D., Nishimura, M., & Hyodo, M. (2010). Expression of aquaporins and vasopressin type 2 receptor in the stria vascularis of the cochlea. *Hearing Research*, 260, 11–19.

Oonk, A. M., Huygen, P. L., Kunst, H. P., Kremer, H., & Pennings, R. J. E. (2015). Features of autosomal recessive nonsyndromic hearing impairment: A review to serve as a reference. *Clinical Otolaryngology*, 41, 487–497. doi:10.1111/coa.12567.

Patuzzi, R. (2011a). Ion flow in cochlear hair cells and the regulation of hearing sensitivity. *Hearing Research*, 280, 3–20.

Patuzzi, R. (2011b). Ion flow in stria vascularis and the production and regulation of cochlear endolymph and the endolymphatic potential. *Hearing Research*, 277, 4–19.

Pondugula, S. R., Raveendran, N. N., & Marcus, D. C. (2010). Ion transport regulation by P2Y receptors, protein kinase C and phosphatidylinositol 3-kinase within the semicircular canal duct epithelium. *BMC Research Notes*, 3, 100.

Robbins, J. (2001). KCNQ potassium channels: Physiology, pathophysiology, and pharmacology. *Pharmacology and Therapeutics*, 90, 1–19.

Sakai, Y., Harvey, M., & Sokolowski, B. (2011). Identification and quantification of full-length BK channel variants in the developing mouse cochlea. *Journal of Neuroscience Research*, 89, 1747–1760.

Salt, A. N., Melichar, I., & Thalmann, R. (1987). Mechanisms of endocochlear potential generation by stria vascularis. *The Laryngoscope*, 97, 984–991.

Salt, A. N., Ohyama, K., & Thalmann, R. (1991a). Radial communication between the perilymphatic scalae of the cochlea. I: Estimation by tracer perfusion. *Hearing Research*, 56, 29–36.

Salt, A. N., Ohyama, K., & Thalmann, R. (1991b). Radial communication between the perilymphatic scalae of the cochlea. II: Estimation by bolus injection of tracer into the sealed cochlea. *Hearing Research*, 56, 37–43.

Salt, A. N., Kellner, C., & Hale, S. (2003). Contamination of perilymph sampled from the basal cochlear turn with cerebrospinal fluid. *Hearing Research*, 182, 24–33.

Sellick, P. M., & Johnstone, B. M. (1972). Changes in cochlear endolymph Na^+ concentration measured with Na^+ specific microelectrodes. *Pflügers Archiv - European Journal of Physiology*, 336, 11–20.

Shen, Z., Marcus, D. C., Sunose, H., Chiba, T., & Wangemann, P. (1997). I_{sK} channel in strial marginal cells: Voltage-dependence, ion-selectivity, inhibition by 293B and sensitivity to clofilium. *Auditory Neuroscience*, 3, 215–230.

Shi, X., Gillespie, P. G., & Nuttall, A. L. (2005). Na^+ influx triggers bleb formation on inner hair cells. *American Journal of Physiology - Cell Physiology*, 288, C1332–C1341.

Singh, R., & Wangemann, P. (2008). Free radical stress-mediated loss of *Kcnj10* protein expression in stria vascularis contributes to deafness in Pendred syndrome mouse model. *American Journal of Physiology - Renal Physiology*, 294, F139–F148.

Spicer, S. S., & Schulte, B. A. (1996). The fine structure of spiral ligament cells relates to ion return to the stria and varies with place-frequency. *Hearing Research*, 100, 80–100.

Sterkers, O., Saumon, G., Tran Ba, H. P., & Amiel, C. (1982). K, Cl, and H_2O entry in endolymph, perilymph, and cerebrospinal fluid of the rat. *American Journal of Physiology - Renal Physiology*, 243, F173–F180.

Strutz-Seebohm, N., Seebohm, G., Fedorenko, O., Baltaev, R., Engel, J., Knirsch, M., & Lang, F. (2006). Functional coassembly of KCNQ4 with KCNE-β-subunits in *Xenopus* oocytes. *Cellular Physiology and Biochemistry*, 18, 57–66.

Takeda, T., Takeda, S., Kitano, H., Okada, T., & Kakigi, A. (2000). Endolymphatic hydrops induced by chronic administration of vasopressin. *Hearing Research*, 140, 1–6.

Takeuchi, S., Ando, M., & Kakigi, A. (2000). Mechanism generating endocochlear potential: Role played by intermediate cells in stria vascularis. *Biophysical Journal*, 79, 2572–2582.

Takumida, M., Kakigi, A., Egami, N., Nishioka, R., & Anniko, M. (2012). Localization of aquaporins 1, 2, and 3 and vasopressin type 2 receptor in the mouse inner ear. *Acta Oto-Laryngologica*, 132, 807–813.

ten Cate, W. J., Curtis, L. M., Small, G. M., & Rarey, K. E. (1993). Localization of glucocorticoid receptors and glucocorticoid receptor mRNAs in the rat cochlea. *The Laryngoscope*, 103, 865–871.

ten Cate, W. J., Curtis, L. M., & Rarey, K. E. (1994). Effects of low-sodium, high-potassium dietary intake on cochlear lateral wall Na^+, K^+-ATPase. *European Archives of Oto-Rhino-Laryngology*, 251, 6–11.

Thalmann, R. (1971). Metabolic features of auditory and vestibular systems. *The Laryngoscope*, 81, 1245–1260.

Thorne, P. R., Muñoz, D. J., & Housley, G. D. (2004). Purinergic modulation of cochlear partition resistance and its effect on the endocochlear potential in the guinea pig. *Journal of the Association for Research in Otolaryngology*, 5, 58–65.

Tranebjaerg, L., Samson, R. A., & Green, G. E. (2014). Jervell and Lange-Nielsen syndrome. In R. A. Pagon, M. P. Adam, H. H. Ardinger, S. E. Wallace, H. C. Mefford, & K. Stephens (Eds.), *GeneReviews*. Available at https://www.ncbi.nlm.nih.gov/books/NBK1405/.

Turner, J. R., Buschmann, M. M., Romero-Calvo, I., Sailer, A., & Shen, L. (2014). The role of molecular remodeling in differential regulation of tight junction permeability. *Seminars in Cell and Developmental Biology*, 36, 204–212.

Verkman, A. S., & Mitra, A. K. (2000). Structure and function of aquaporin water channels. *American Journal of Physiology - Renal Physiology*, 278, F13–F28.

Vlajkovic, S. M., Housley, G. D., Muñoz, D. J., Robson, S. C., Sévigny, J., Wang, C. J. H., & Thorne, P. R. (2004). Noise exposure induces up-regulation of ecto-nucleoside triphosphate diphosphohydrolases 1 and 2 in rat cochlea. *Neuroscience*, 126, 763–773.

Wada, J., Kambayashi, J., Marcus, D. C., & Thalmann, R. (1979). Vascular perfusion of the cochlea: Effect of potassium-free and rubidium-substituted media. *Archives of Oto-Rhino-Laryngology*, 225, 79–81.

Wangemann, P. (2002). Adrenergic and muscarinic control of cochlear endolymph production. *Advances in Oto-Rhino-Laryngology*, 59, 42–50.

Wangemann, P. (2013). Mouse models for pendrin-associated loss of cochlear and vestibular function. *Cellular Physiology and Biochemistry*, 32, 157–165.

Wangemann, P., Liu, J., & Marcus, D. C. (1995a). Ion transport mechanisms responsible for K^+ secretion and the transepithelial voltage across marginal cells of stria vascularis in vitro. *Hearing Research*, 84, 19–29.

Wangemann, P., Liu, J., & Shiga, N. (1995b). The pH-sensitivity of transepithelial K^+ transport in vestibular dark cells. *Journal of Membrane Biology*, 147, 255–262.

Wangemann, P., Shen, Z., & Liu, J. (1996). K^+-induced stimulation of K^+ secretion involves activation of the I_{sK} channel in vestibular dark cells. *Hearing Research*, 100, 201–210.

Wangemann, P., Nakaya, K., Wu, T., Maganti, R. J., Itza, E. M., Sanneman, J. D., Harbidge, D. G., Billings, S., & Marcus, D. C. (2007). Loss of cochlear HCO_3^- secretion causes deafness via endolymphatic acidification and inhibition of Ca^{2+} reabsorption in a Pendred syndrome mouse model. *American Journal of Physiology - Renal Physiology*, 292, F1345–F1353.

Wangemann, P., Kim, H. M., Billings, S., Nakaya, K., Li, X., Singh, R., Sharlin, D. S., Forrest, D., Marcus, D. C., & Fong, P. (2009). Developmental delays consistent with cochlear hypothyroidism contribute to failure to develop hearing in mice lacking *Slc26a4*/pendrin expression. *American Journal of Physiology - Renal Physiology*, 297, F1435–F1447.

Wood, J. D., Muchinsky, S. J., Filoteo, A. G., Penniston, J. T., & Tempel, B. L. (2004). Low endolymph calcium concentrations in *deafwaddler*^{2J} mice suggest that PMCA2 contributes to endolymph calcium maintenance. *Journal of the Association for Research in Otolaryngology*, 5, 99–110.

Yamauchi, D., Raveendran, N. N., Pondugula, S. R., Kampalli, S. B., Singh, R., Wangemann, P., & Marcus, D. C. (2005). Vitamin D upregulates expression of ECaC1 mRNA in semicircular canal. *Biochemical and Biophysical Research Communications*, 331, 1353–1357.

Yamauchi, D., Nakaya, K., Raveendran, N. N., Harbidge, D. G., Singh, R., Wangemann, P., & Marcus, D. C. (2010). Expression of epithelial calcium transport system in rat cochlea and vestibular labyrinth. *BMC Physiology*, 10, 1.

Yamoah, E. N., Lumpkin, E. A., Dumont, R. A., Smith, P. J., Hudspeth, A. J., & Gillespie, P. G. (1998). Plasma membrane Ca^{2+}-ATPase extrudes Ca^{2+} from hair cell stereocilia. *The Journal of Neuroscience*, 18, 610–624.

Yao, X. F., & Rarey, K. E. (1996). Localization of the mineralocorticoid receptor in rat cochlear tissue. *Acta Oto-Laryngologica*, 116, 493–496.

Yoo, J. C., Kim, H. Y., Han, K. H., Oh, S. H., Chang, S. O., Marcus, D. C., & Lee, J. H. (2012). Na^{+} absorption by Claudius' cells is regulated by purinergic signaling in the cochlea. *Acta Oto-Laryngologica*, 132 Suppl. 1, S103–S108.

Yoshihara, T., & Igarashi, M. (1987). Cytochemical localization of Ca^{++}-ATPase activity in the lateral cochlear wall of the guinea pig. *Archives of Oto-Rhino-Laryngology*, 243, 395–400.

Zidanic, M., & Brownell, W. E. (1990). Fine structure of the intracochlear potential field. I. The silent current. *Biophysical Journal*, 57, 1253–1268.

Chapter 10
Remote Sensing the Cochlea: Otoacoustics

Christopher Bergevin, Sarah Verhulst, and Pim van Dijk

Abstract The ear is a remarkable detector. It is both highly sensitive and selective and operates over a large dynamic range spanning more than 12 orders of magnitude of energy. Perhaps surprisingly, not only does it respond to sound but emits it as well. These sounds, known as otoacoustic emissions (OAEs), provide a means to probe the fundamental biophysics underlying transduction and amplification in the ear. This chapter outlines the theoretical considerations describing the underlying biomechanics of OAE generation, highlights the various uses of OAEs (both scientific and clinical), including comparative approaches, and motivates open questions.

Keywords Cochlear biophysics · Comparative · Nonmonotonic growth · Hair cell · Otoacoustic emission

10.1 Introduction

10.1.1 Motivation: Remote Sensing the Cochlea

Despite significant technological advances in intracochlear measurements, many key facets (e.g., micromechanics, relative tuning throughout the organ of Corti)

C. Bergevin (✉)
Department of Physics and Astronomy and Centre for Vision Research,
York University, Toronto, ON M3J 1P3, Canada
e-mail: dolemitecb@gmail.com

S. Verhulst
Hearing Technology at WAVES, Department of Information Technology,
Ghent University, iGent, Technologiepark 15, 9052 Zwijnaarde, Belgium
e-mail: s.verhulst@ugent.be

P. van Dijk
Department of Otorhinolaryngology, Head and Neck Surgery,
University Medical Center Groningen, University of Groningen,
Hanzeplein 1, 9713 GZ Groningen, The Netherlands
e-mail: p.van.dijk@umcg.nl

G.A. Manley et al. (eds.), *Understanding the Cochlea*, Springer Handbook of Auditory Research 62, DOI 10.1007/978-3-319-52073-5_10

remain poorly characterized. This is in part due to surgical methods that can affect the fragile cochlea. A method to circumvent this limitation is via "remote sensing," observing the behavior of the cochlea in its normal physiological state without adversely affecting it. One approach is to use the fact that the ear emits sound, known as otoacoustic emissions (OAEs). For the most part, only healthy ears emit sound, which has led to the development of OAEs as a tool for hearing screening that has revolutionized pediatric audiology (Probst et al. 1991; Janssen and Müller 2008).

OAEs can be classified into two basic categories: spontaneous (SOAE) and evoked (eOAE). SOAEs typically appear as an idiosyncratic array of spectral peaks, unique to a given ear and relatively stable (e.g., Zurek 1981). eOAEs arise in response to an external stimulus. Whereas eOAEs are common in most ears (e.g., mammals, reptiles, birds, amphibians, insects), SOAEs are less prevalent. For example, prevalence among humans of different sexes and ethnicities can vary substantially (e.g., Talmadge et al. 1993; Whitehead et al. 1993; Kuroda 2007). Even within an individual, there can be differences with age and laterality. Implied throughout the chapter is the tacit assumption that OAEs are collectively generated via active amplification by the sensory hair cells in the inner ear, as evidenced by close relationships between hair cell physiology and OAEs.

10.1.2 A Starting Heuristic

The two primary functions of the inner ear are detection and spectral decomposition of sound (i.e., frequency selectivity or tuning). Evidence indicates that the ear employs energy-generating processes to facilitate these functions (i.e., the ear is *active*). Presumably OAE generation is tied to that process. To model these processes, myriad theoretical cochlear frameworks have at their heart the notion of driven oscillators. To frame this chapter, a single uncoupled second-order nonautonomous system oscillator (e.g., mass on a spring) is introduced here as a heuristic (French 1971). In its simplest form, a linear differential equation describes this system by

$$m\ddot{x} + b\dot{x} + kx = F(t) \tag{10.1}$$

Here x is the relevant physical dimension (e.g., displacement; diacritical dots indicate time derivatives), m is the effective mass, b is the damping, k is the stiffness, and F is an external driving force. Assuming damping is not relatively dominant, this system exhibits oscillatory behavior, with a peak response at the resonance frequency (i.e., it is tuned).

Many features in the cochlea can play the role of the various components described by Eq. 10.1. For example, "mass" can stem from the basilar (BMs) and/or tectorial (TMs) membranes, the stereovillar bundle, and/or entrained fluid. The damping term can arise in a number of different ways, such as viscous forces due to

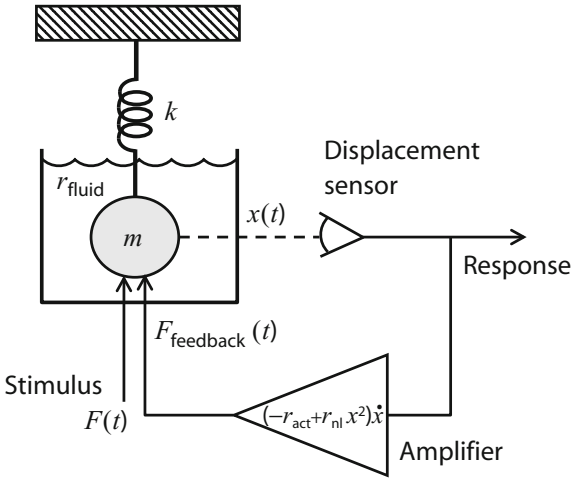

Fig. 10.1 Basic schematic of a vibration detector with active feedback. The mass (m) is set into motion by an external force [$F(t)$; referred to as the stimulus]. The mass is suspended from a spring with a spring constant (k). The motion of the mass is impeded by viscous forces of the surrounding fluid with a damping constant (r_{fluid}). A detector senses the position, leading to the displacement response [$x(t)$]. The motion in turn is fed back to the mass via a feedback force, which contains two terms: a negative component ($-r_{act}\dot{x}$, which compensates for viscous losses due to the fluid) and a nonlinear term ($r_{nl}x^2\dot{x}$; saturation of the amplifier). It can be shown that this form of feedback can enhance the frequency selectivity of the detector. If the feedback is too strong ($r = r_{act} - r_{fluid} > 0$), the mass will oscillate spontaneously but is stabilized due to the nonlinearity. Connecting back to the more general Eq. 10.2, the equation of motion would be $m\ddot{x} - [r_{act} - r_{fluid} - r_{nl}x^2]\dot{x} + kx = F(t)$. Adapted from Bialek and Wit (1984)

fluid coupling and/or friction internal to hair bundle linkage/channel dynamics. The drive could represent a combination of incident sound, (Brownian) noise inherent to the system, and/or some form of internal drive such as feedback.

One way to reduce the detrimental effect of damping on frequency selectivity is by adding a feedback loop (Fig. 10.1) that can act as an amplifier to inject energy into the response. With the appropriate phase of the feedback force, the amplitude of the oscillation can be boosted by the feedback and the frequency selectivity of the oscillator can be sharpened. Aside from feedback requiring a power source (e.g., metabolic energy), a drawback is that too much amplification can render the oscillator unstable and cause spontaneous oscillations. In fact, SOAEs are commonly believed to be related to such considerations and thus are pointed to as primary evidence of active feedback in the cochlea (e.g., connection to audiogram fine structure; Zwicker and Schloth 1984; Long and Tubis 1988). To ensure stability without resorting to collective "systems" level descriptions (see Sect. 10. 2.3), Eq. 10.1 is commonly modified to be nonlinear (see Fig. 10.1, Sects. 10.2.2.1 and 10.3.2.2).

Evidence suggests that a primary mechanism for feedback are the hair cells, which are known to provide a mechanical force either via the cell body ("somatic electromotility" in mammalian outer hair cells; Dallos 2008) and/or by the

stereovillar bundle ("bundle motility"; Hudspeth 2008; see also Corey, Ó Maoiléidigh, and Ashmore, Chap. 4). Although the details of the molecular components producing such feedback are still a matter of debate, many lines of evidence (including the presence of OAEs) argue for an active frequency-selective detector at the heart of cochlear mechanics. This chapter uses Eq. 10.1 (suitably modified) as a heuristic for OAE generation and the associated amplification process.

10.2 Modeling Otoacoustic Emission Generation

10.2.1 Overview

Models are indispensable in connecting our understanding of hair cell morphology and functionality to the generation of OAEs. Since the discovery of OAEs by David Kemp (1978), there has been a stimulating history of theoretical OAE modeling. Models come in a wide variety of forms, such as electric circuits (e.g., Zwicker 1986a, b), transmission lines (e.g., Zweig and Shera 1995; Talmadge et al. 1998), standing-wave cavities analogous to a laser (e.g., Shera 2003), single active/nonlinear "limit-cycle" oscillators (e.g., Wit 1986; Talmadge et al. 1991), and systems of coupled oscillators (e.g., Murphy et al. 1995b; Vilfan and Duke 2008). Note that the classifications made above are not necessarily mutually exclusive, and certain types such as "state-space" models (e.g., Elliott et al. 2007; Ku et al. 2009) could fit into multiple categories (e.g., transmission-line cochlear models are essentially coupled oscillators).

An interesting facet when looking across cochlear models is the range of biomechanical assumptions made, such as the form of coupling of outer hair cell (OHC)-related forces and the role of morphological irregularity (or "roughness;" see Sect. 10.2.3.3). Several open questions remain to be resolved.

- How do hair cells work together (and with accessory structures) to generate OAEs? How are such processes tied to forward auditory transduction?
- How does nonlinear emission growth link to cochlear compression and subsequent perceptual consequences?
- How critical is the distinction between SOAEs and eOAEs? Do they reveal fundamentally different insights into OAE generation mechanisms (e.g., Shera and Guinan 1999)?
- Both similarities and differences exist when comparing OAEs across species, but how do such meaningfully relate back to morphological differences?

These open questions will help focus the content of this chapter. Here, the discussion is limited to basic biophysical models of OAE generation and the experimental evidence that either supports or refutes these models. Exhaustive

comprehensive reviews regarding OAEs can be found elsewhere (e.g., Probst et al. 1991; Manley et al. 2008; Avan et al. 2013).

Understanding SOAE generation may be more tractable because there are fewer complicating factors (e.g., how an external stimulus may differentially drive/affect different mechanisms and/or sites). So although the bulk of otoacoustic research focuses on eOAEs, SOAE models will be the initial focal point here. The narrative highlights two (broadly categorized) classifications: single-source (see Sect. 10.2.2) and region (see Sect. 10.2.3) models.

10.2.2 Single-Source Models

Early theoretical studies of SOAE generation considered the underlying mechanism to be a single "source" (e.g., Johannesma 1980; Bialek and Wit 1984; see Fig. 10.1). That is, the complexities of the system were eschewed in favor of identifying to what extent the simplest model could describe the data. Conceptually, single-source models typically take the form of an isolated spatial element (e.g., a particular position along the BM). The foundations of such models are briefly described, and the features of the data that they are (and are not) capable of capturing are examined. Subsequently, similar efforts were also employed for eOAEs and are examined in Sect. 10.3.2.3.

10.2.2.1 Limit-Cycle Oscillators

As mentioned in Sect. 10.1.2, oscillators serve as the fundamental element. To make Eq. 10.1 produce a stable self-sustained oscillation (i.e., a limit cycle, somewhat akin to an SOAE peak), it must be modified to be both "active" (i.e., energy producing) and nonlinear (to ensure stability). Such a limit-cycle model for an SOAE peak was first proposed by Johannesma (1980). As shown in Fig. 10.1, the oscillator may correspond to an active feedback filter that becomes quasi-stable due to excessive feedback. One commonly employed formulation is the van der Pol system (Johannesma 1980)[1]

$$m\ddot{x} - \mu\left(a - x^2\right)\dot{x} + kx = F(t) \tag{10.2}$$

where the damping parameter μ is sometimes referred to as the "control parameter." For small displacements ($x^2 < a$), the damping is negative and energy is added to the system. For larger displacements, the damping becomes positive, which

[1]When using complex notation, this equation is sometimes expressed in a simplified complex form ("normal form") that captures qualitatively similar dynamics: $\dot{z} = -\mu z + i\omega_0 z + z\left|z^2\right| + F(t)$. See Hudspeth (2008).

stabilizes the motion. Note that some studies have suggested that a second-order oscillator (i.e., Eq. 10.2) is of too low an order to be able to sufficiently capture the essential aspects (e.g., Ó Maoiléidigh et al. 2012; see also Eqs. 10.3 and 10.4).

10.2.2.2 What Single-Source Models Do and Do Not Do

To first order, a large range of SOAE-related features are well captured by a single van der Pol oscillator. If the control parameter μ is relatively small, the oscillator exhibits a nearly sinusoidal response. The sinusoidal foundation of SOAEs can be confirmed by producing an amplitude distribution of a filtered SOAE peak. This exhibits two characteristic maxima (Bialek and Wit 1984; Talmadge et al. 1991) or a ring when considering the analytic signal (Shera 2003), closely corresponding to the van der Pol model. SOAEs can be suppressed by external tones, and the onset and release from suppression shows relaxation times on the order of 10–20 ms (Zwicker and Schloth 1984), again consistent with a van der Pol oscillator with a relatively small control parameter (μ). If the oscillator is assumed to interact with internal noise (e.g., thermal noise in the cochlea), it produces a sinusoidal signal with slow amplitude fluctuation and diffusing phase. Consistent with this model, the amplitude fluctuation spectrum of SOAEs displays slow fluctuations (Bialek and Wit 1984; van Dijk and Wit 1990a), and the peaks in the power spectrum of an SOAE have a Lorenzian shape (van Dijk and Wit 1990a; Talmadge et al. 1993; van Dijk et al. 2011). Finally, SOAEs phase lock to an external tone, as predicted by the van der Pol model. For weak tones, the phase locking is intermittent, which again is consistent with the assumption of weak internal noise interacting with the oscillator (van Dijk and Wit 1990b).

Despite these successes, OAE data indicate that the underlying generation mechanisms are more complex. First, a single van der Pol is only capable of generating energy predominantly at a single frequency, not at an idiosyncratic array of them that is commonly observed in SOAE spectra (see Fig. 10.2). Second, the relationship between amplitude fluctuation and frequency fluctuations is not consistent with the single oscillator model (van Dijk and Wit 1990a), with the probable exception of strong SOAEs (Bialek and Wit 1984). This suggests that interaction between SOAE peaks complicates the behavior of individual SOAE peaks. Third, detailed analysis of SOAE peak dynamics indicates there are interactions between different SOAE peaks (van Dijk and Wit 1998). The "relaxation dynamics" of multiple SOAEs requires interactions of several coupled van der Pol oscillators (Murphy et al. 1995a).

The limitations of single-source models are returned to in Sect. 10.3.2.3 within the context of eOAEs.

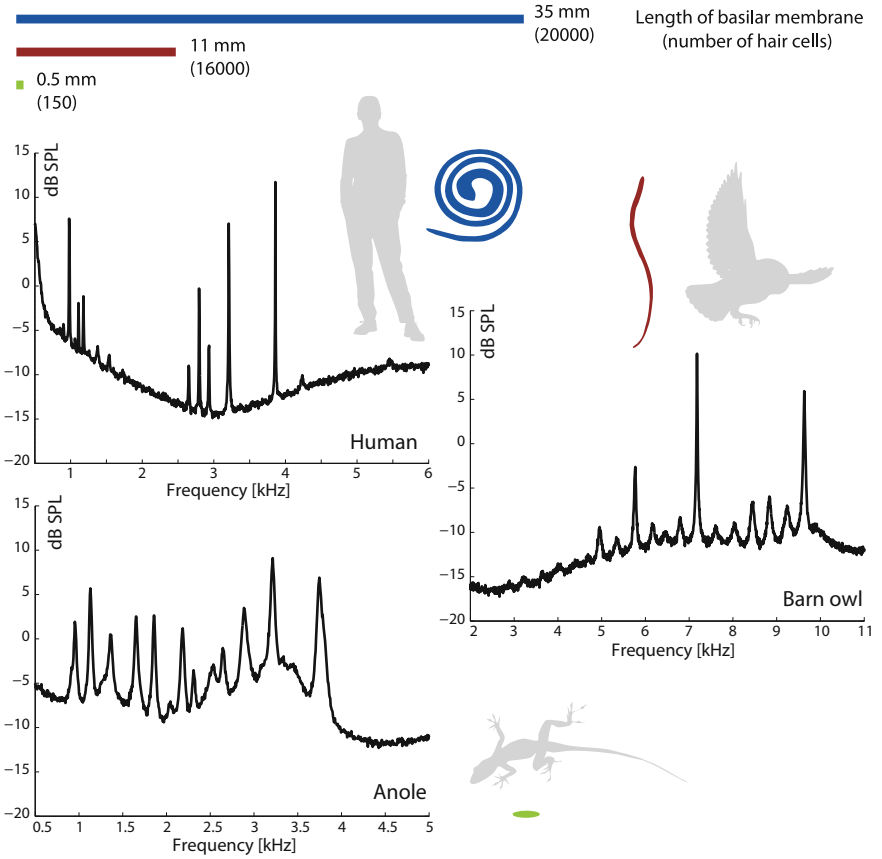

Fig. 10.2 Comparison of spontaneous optoacoustic emission (SOAE) activity from three different species. Each spectrum derives from an individual ear with relatively strong SOAE activity. Also shown is a visual comparison of the shape and length of the basilar membrane (BM) as well as the approximate total number of hair cells within a given ear for that species. SPL, sound pressure level. Modified from Bergevin et al. (2015a); graphic from Per Ruppel, University Information, University of Oldenburg, Germany, with permission

10.2.3 Region Models: Otoacoustic Emissions as an Emergent Property

Although single-source models provided a valuable starting point, the next generation of models takes a more global approach that considers the ear as a system of parts. To motivate them, evidence is highlighted here that compellingly points toward the importance of coupling between hair cells. For example, mice rarely exhibit SOAEs. However, when hair cell coupling is changed via a mutation in the TM structure (effectively changing its stiffness), SOAEs are more readily observed

(Cheatham et al. 2014). Also, in lizards, spectral characteristics of SOAEs correlate with TM structure (Manley 2001). These examples highlight the role of longitudinal coupling between sensory hair cells in the inner ear and its impact on emission characteristics.

It appears plausible that elements of the single-source model(s) are at work, but it is ultimately more fruitful to model OAEs as a summed response that represents the interaction of multiple generation sources. That is, the complexity of an OAE (e.g., input-output function [I/O] characteristics) is an *emergent* property due to the distributed nature of the cochlea. The most widely accepted theory posits two distinct generation mechanisms (Kemp 1986; Shera and Guinan 1999), each of which can be manifest as an array of different sources spread throughout the cochlea. That specific framework will be returned to in Sect. 10.3.1.

10.2.3.1 Basic Considerations for Coupled Oscillators

The heuristic of Eq. 10.1 can readily be modified to describe several connected oscillators, which can trade energy back and forth. For a simple 1-dimensional (1-D) collection of linear-coupled oscillators, a "normal mode" formulation is commonly employed (French 1971). The basic idea is that there are vibration patterns where all elements oscillate at the same frequency. All possible "modes" then form a basic space, from which any possible motion is a superposition. So, although the motion can appear complex, the decomposition into simpler components makes the problem analytically tractable. A common example is the nodal patterns that can be observed on a circular membrane (e.g., drum head).

When dealing with active/nonlinear oscillators, however, things become more complicated (see also Sect. 10.3.2.2). As an example, consider the "twin-engine" model (Aranyosi 2006), which comprises just two oscillators (x_1 and x_2) and was proposed in the context of explaining "glides" (i.e., frequency variations in the BM impulse response). The equations of motion are given by

$$m_c\ddot{x}_2 + k_c x_2 = m_1\ddot{x}_1 + [b_1 - g_1(x_1)]\dot{x}_1 + k_1 x_1 + F(t) \tag{10.3}$$

$$b_c\dot{x}_1 = m_2\ddot{x}_2 + [b_2 - g_2(x_2)]\dot{x}_2 + k_2 x_2 \tag{10.4}$$

where the subscript c denotes the coupling terms and g is "a nonlinear velocity-dependent term in each resonator, defined as the derivative of a Boltzmann function" (Aranyosi 2006). In this case, not only can the oscillators trade energy back and forth, but because they can also inject it, stability can arise through a form of feedback (e.g., Dallos and Corey 1991; Zweig 1991).

In the context of SOAE modeling, different approaches have been taken, such as standing waves via coherent reflection (Shera 2003), transmission lines (Choi et al. 2008; Epp et al. 2010), and a discretized array of oscillators (Murphy et al. 1995b; Vilfan and Duke 2008; Wit et al. 2012). Ultimately, these formulations are all in fact "coupled oscillator" models, just with different assumptions about the

"coupling." Coupling typically falls into two different categories: "global" arising hydrodynamically (e.g., Zweig 1976; Nobili et al. 1998; Epp et al. 2015) and "nearest neighbor only" (e.g., Vilfan and Duke 2008) via resistive and/or reactive elements (e.g., overlying TM). Going back to Sect. 10.2.2.1, although a single active oscillator may require nonlinearity for stability, an active system does not (e.g., Zweig 1991; see also Sect. 10.3.2). Or, conversely, SOAE models do not necessarily require limit-cycle oscillators per se because a self-sustained oscillation can arise as a consequence of the mechanics of the cochlea as a whole (Shera 2003). Regardless, two common threads arise between all classes of model: waves and randomness.

10.2.3.2 The Role of Waves

In his seminal paper first reporting the existence of OAE, Kemp (1978) began by stating "Cochlea wave propagation characteristics…," subsequently following up with a paper entitled *Otoacoustic Emissions, Travelling Waves and Cochlear Mechanisms* (Kemp 1986). It thus may not be surprising that much of the current understanding of OAE generation revolves around a wave-based framework (implicitly a region-model type). For example, the moniker "cochlear reflectance" has been proposed for a "normalized" measure of eOAE (Rasetshwane and Neely 2012).

In the context of OAE generation, clarification is needed regarding what precisely is meant by "wave." A 1-D wave is described by the function $f(x, t)$ (over spatial dimension x) that satisfies the partial differential equation (PDE), called the wave equation

$$\frac{\partial^2 f}{\partial x^2} = \frac{\partial^2 f}{\partial t^2}\frac{1}{c^2} \tag{10.5}$$

where c is independent of time. From a mechanical point of view, this PDE essentially amounts to the combination of two fundamental laws. For example, in the context of deriving a 1-D transmission-line model of the cochlea (Zweig et al. 1976; Zweig 1991), the wave equation is derived from Newton's second law (regarding BM displacement) and from the conservation of mass (regarding longitudinal fluid motion). A general solution to this equation has the form $f(x \pm ct)$ (d'Alembert's solution), such that time and space are scaled relative to one another. In many instances (but not all), the solutions have a periodic nature [e.g., $f(x,t) = F\cos(x \pm ct)$ or, more generally, $f(x,t) = Ae^{i(x\pm ct)} + Be^{i(-x\pm ct)}$ to allow for forward and reverse traveling waves].

Why is a wave defined here? If one considers the various dynamically relevant structures of the cochlea (e.g., hair cells, BM, TM) as oscillators, then the presence of a wave indicates some relative phase difference between them. Two consequences immediately arise, the first of which is the role of timing in the interactions and collective dynamics of the various constituents. Relative to Eq. 10.5, Shera and

Guinan (2008) provided a useful working definition for "wave" as the relative timing difference between different constituent parts of the cochlea. This is useful to bridge the gap they identified when they proposed that OAE properties "… are determined not by subcellular biophysics but by macromechanical (and emergent) properties of the cochlea … many features of OAEs … are perhaps best understood in this way" (Shera and Guinan 2008, p. 336). The field is arguably now well poised to bridge the microscopic (e.g., molecular motors or individual hair cells) and macroscopic (e.g., the cochlea as a whole or a system of coupled hair cells) descriptions; waves will likely play a key role. Second, the presence (in a 1-D sense) of both a forward and a backward traveling wave allows for the notion of SOAEs to arise via some sort of standing-wave mechanism (e.g., Shera 2003).

10.2.3.3 Stochastics: Role of Noise and Roughness

In a broad class of biophysical problems, the notion of some form of a stochastic element crucially at play has become increasingly accepted (Bialek 2012) and the cochlea is no exception. Randomness can be considered as arising in two different contexts: dynamic and static. With regard to dynamic randomness, the reference is chiefly to thermal noise. The study of hair cell bundle responses to noise has been revealing, such as the violation of the fluctuation-dissipation theorem (Duke and Jülicher 2008; Dinis et al. 2012). Internal cochlear noise also affects responses close to the threshold (van Dijk and Long 2015) and is responsible for the finite width of SOAE spectral peaks. For OAE modeling, three basic considerations are important.

First are the stochastic forces an individual bundle experiences. Recent work with bullfrog vestibular cells (Kozlov et al. 2012) has suggested that thermal forces cause fractional Brownian motion (i.e., temporal fractal-like correlations exist, indicative of "stochastic processes with memory"). Second, depending on the underlying potential energy configurations available, effects such as stochastic resonance may be at play (Jaramillo and Wiesenfeld 1998). Last, how are the thermal forces distributed across the oscillators? How independent are the stochastic driving forces between two adjacent oscillators?

In addition to dynamic irregularities (cochlear noise), the notion of static randomness, commonly referred to as irregularity or "roughness," is widely believed to play a crucial biomechanical role in OAE generation (Manley 1983; Zweig and Shera 1995; Mauermann et al. 1999). For example, within the context of a standing-wave model for SOAE generation (Shera 2003), the roughness provides a basis for reflection of waves in the cochlea. Because reflection also occurs at the round window, the conditions for a standing wave in the cochlea may arise. As stated by Ku et al. (2008), "only frequencies with a traveling wave that undergoes an integer round-trip phase change between the middle-ear boundary and the inhomogeneity will become unstable." Hence, SOAEs occur when the appropriate reflecting boundary condition is setup, depending on the underlying roughness. Because the roughness presumably differs between ears, each ear displays a unique pattern of SOAE peaks or possibly none at all.

Many classes of current OAE models implicitly include some static aspect of irregularity (e.g., Shera 2003; Vilfan and Duke 2008). How to best measure and subsequently quantify roughness is presently unclear. For example, hair cell arrangement may not be the only or even the chief consideration in anatomical roughness. Noisiness in BM stiffness, hair cell power output, or longitudinal TM coupling could also be factors. Previous studies have been stimulating (e.g., Lonsbury-Martin et al. 1988; Martin et al. 1988), but further physiological work is desirable along these lines, such as attempting to directly correlate SOAE patterns to morphology in individual ears (Manley 1983).

10.2.3.4 Comparing Macroscopic Models to Spontaneous Emission Data

In many cases, linear formulations of region models can be handled analytically (e.g., Zweig and Shera 1995), but nonlinear formulations are typically only tractable numerically. By shifting away from relatively simple single-source frameworks, region models have enough degrees of freedom to produce just about any type of behavior. So the issue arises as to how to most meaningfully compare back to empirical data. Consider, for example, the basic question, What precisely constitutes an SOAE peak? Clearly, not all "peaks" are created equal (Fig. 10.2). Using peaks as a benchmark (e.g., is a peak present or not?), some preexisting region models (e.g., Vilfan and Duke 2008; Wit and van Dijk 2012; Fruth et al. 2014) capture qualitative and quantitative aspects of the data, but they fail to capture other (key) properties, such as peak width. Thus, focusing primarily on peaks may be misleading, especially if the dynamics (e.g., Bialek and Wit 1984; Murphy et al. 1995b) are ignored. One could thus argue the necessity of characterizing SOAE activity beyond focusing on "peaks." For example, aspects such as "baseline" SOAE energy, readily apparent in nonmammals (e.g., Manley et al. 1996); temperature dependence (e.g., van Dijk et al. 1989); and differing SOAE interactions with external stimuli (e.g., Long and Tubis 1988; Hansen et al. 2014; Bergevin et al. 2015a) are yet unexplained.

One area where progress can be made is determining more effective ways to analyze OAE data. For example, a wide range of methodologies exist in an area broadly known as "nonlinear time-series analysis" (e.g., Kantz and Schreiber 2004) and may find valuable application to problems in hearing. This may allow for salient properties of SOAEs or SFOAEs to be more meaningfully extracted from recorded data, given inherent trade-offs between temporal and frequency resolution.

10.2.4 Summary

In summary, a basic biomechanical picture of the ear emerges as a collection of coupled nonlinear oscillators. The precise form of the oscillators and their coupling

is still open to debate, but this basic theoretical framework has provided a strong foundation for current theories of OAE generation. A recent study argued that wave-based and coupled-oscillator models are not orthogonal notions (Bergevin et al. 2015a), but the common ground between model classes remains unresolved. Despite the many basic open questions, a solid foundation for understanding OAE generation mechanisms is in place (e.g., Shera and Guinan 1999).

10.3 Evoked Emissions

10.3.1 Overview

To better understand the complexities of emission generation and the nonlinear and dynamic properties of cochlear mechanics, it is necessary to study how external sound can generate OAEs. Given that eOAEs deal with an external stimulus that "drives" the system and thereby injects energy, eOAEs are commonly defined by the sounds that evoke them (e.g., SFOAEs; distortion-product OAEs [DPOAEs]; transient eOAEs [TEOAEs]).

An alternative characterization has arisen from modeling efforts, primarily focused on considerations such as a coherence among scattering sites distributed along the BM as well as how energy propagates into and out of the cochlea (Shera and Guinan 2008; see also Sect. 10.4). eOAE models have furthermore incorporated "place-fixed" and "wave-fixed" generation mechanisms, where the place-fixed mechanism relies on spatially distributed reflection sources (e.g., OHC morphology differences along the cochlea; see Sect. 10.2.3.3) and where the wave-fixed mechanism relies on local cochlear nonlinearities that depend on the stimuli that elicited the emission (Zweig and Shera 1995; Shera and Guinan 2008). These two distinct OAE generation mechanisms are based on a widely accepted OAE "taxonomy" (Shera and Guinan 1999), where emissions are classified not by the location of their generation nor the type of stimulus used to evoke them but instead by their generation mechanism. As such, seemingly disparate emission types such as SOAEs and SFOAEs are predicted to arise from the same fundamental mechanism (Shera and Guinan 1999; Shera 2003), which is supported by experiment (e.g., Probst et al. 1986; Bergevin et al. 2011a, 2012a). Furthermore, the taxonomy has been particularly valuable for understanding DPOAE generation (e.g., Knight and Kemp 2000; Shera and Abdala 2012), one of the most commonly studied forms of emissions.

Despite the many OAE modeling studies, the precise nature by which OAE generation is in fact "distributed" over a wider cochlear region is still debated for transient and pure-tone eOAEs (e.g., Moleti et al. 2013; Sisto et al. 2015). Furthermore, most studies characterizing DPOAE generation assume that there are not only multiple mechanisms but also multiple spatial sources contributing from along the cochlea (e.g., Epp et al. 2010; Shera and Abdala 2012, Figs. 5–9).

10.3.2 Linearity: To Be or Not to Be?

As Zweig (2015) wrote, "The nonlinear response of the cochlea is of great interest. But what linear equation should be made nonlinear?" At face value, the commonly measured DPOAE $2f_1–f_2$ obviously stems from some form of nonlinearity. But in many regard, SFOAEs and click-evoked OAEs (CEOAEs; these are a type of TEOAE) are, with strong empirical support (e.g., Kalluri and Shera 2007), commonly assumed to arise from a linear reflection-based mechanism (Zweig and Shera 1995). Indeed, for low-level stimuli, SFOAE and CEOAE characteristics can be successfully described by linear models. Conceptually, the question arises as to which aspects of OAE models should be kept linear or not. Put another way, how essential is it to model cochlear nonlinearity to fully capture the key dynamics?

10.3.2.1 Basis of Cochlear "Nonlinearity"?

As a starting point, one might ask: What is the fundamental nonlinearity of the cochlea? A common assumption is that the sigmoidal nature of the mechanoelectrical transduction (MET) characteristic is the primary source of nonlinearity. An added virtue is that such a nonlinearity is commonly shared by all vertebrates (i.e., MET occurs via stereovillar hair cells). Two considerations argue that such a MET-centric view may be overly simplistic. First, numerous nonlinearities are readily observed in cochlear physiology. For example, consider just OHCs (Patuzzi 1996, Fig. 4.20). In addition to the nonlinear MET relationship, other nonlinear behavior includes potassium current through the basolateral wall, capacitive properties of the cell membrane, and prestin (Santos-Sacchi, Navaratnam, Raphael, and Oliver, Chap. 5), and length changes due to somatic electromotility. What their relative contribution is and how independent these are from one another is a subject of study but serve to indicate that there is more than just the MET source. Second, unlike linear systems, where heterogeneous nonlinear elements are coupled together, the dynamics of the resulting system can take a form that is difficult to predict (e.g., the interactions themselves can be nonlinear). That is, for coupled nonlinear systems, relatively complex behavior arises as an emergent property (Strogatz 2014), a facet true even for "simple" systems (e.g., May 1976). Thus, even if the MET is indeed the dominant nonlinearity of a given hair cell and no other sources contribute significantly, the net response of the cochlea as a whole can be difficult to characterize through the lens of just the superposition of many MET functions.

Another important modeling consideration is to what extent the nonlinearity is purely heuristic. For example, note that in Eq. 10.2, there is no obvious biophysical basis for either the nonlinearity or the active term. As mentioned in Sect. 10.1.2, at the cost of increasing an order of the model, a more salient physical basis can be introduced (e.g., the inclusion of an "adaptation system" as in Ó Maoiléidigh et al. 2012).

10.3.2.2 Nonlinearity in Cochlear Modeling

To account for the nonlinear properties of emissions, models typically either have included "local" nonlinearities (e.g., Talmadge et al. 1998; Verhulst et al. 2012) or have been made quasi linear (e.g., Zweig and Shera 1995; Choi et al. 2008). Quasi linear means the fundamental equations are linear, but some form of implicit/ad hoc assumption is made that mimics a nonlinearity (e.g., roughness does or does not matter between two different stimulus-level conditions). Thus, many experimentally observed nonlinear properties of CEOAEs and SFOAEs can be explained based on a linear reflection of local nonlinear cochlear mechanics. However, to date, it is unclear whether the nonlinear properties of eOAEs are best modeled using a combination of nonlinear cochlear mechanics and linear reflection from cochlear irregularities that either (1) show intensity-independent reflection strength properties, (2) demonstrate reflection strength dependent on cochlear gain changes, or (3) result from a reflection mechanism that shows nonlinear behavior different from that of the underlying local cochlear mechanics. Last, it should be noted that eOAE models can be stable while being both linear and active (e.g., energy input in one location can be dissipated at another location via other time-dependent forces; Zweig 1991), although most SOAE models have implicitly assumed some form of nonlinearity to avoid instability (e.g., Talmadge and Tubis 1993; Ku et al. 2009; Duifhuis 2012).

10.3.2.3 What Single-Source Models Do and Do Not Do (Revisited)

Returning to the theme of Sect. 10.2.2.2, the limitations of single limit-cycle OAE models become more evident when eOAEs are considered. A salient example is the nonlinear eOAE growth with respect to the evoking stimulus. These characterizations can be referred to as "level-growth functions" or "I/Os." In addition to the compressive (i.e., nonlinear) nature of the BM velocity as first shown in the early 1970s (Rhode 1971), it is well-known that I/Os for auditory nerve fibers (Kiang et al. 1986), BM responses (Robles and Ruggero 2001), and OAEs (Brown 1987; Bergevin 2007; Schairer et al. 2003) can also be sometimes nonmonotonic. That is, there are regions where higher level stimuli produce smaller magnitude responses than lower levels (Fig. 10.3a). If there is a limited region of nonmonotonic behavior, it is commonly referred to as a "notch." Typically, the notch in the magnitude is accompanied by a shift in the response phase. The nonmonotonic behavior is typically highly idiosyncratic, both to an individual ear and for a given frequency or level. Shift the stimulus frequency(ies) 100 Hz and an eOAE I/O shape could qualitatively change drastically, introducing a confounding reality, especially from a clinical perspective. Furthermore, in reports in which I/Os are shown averaged across individuals (e.g., Schairer et al. 2003; Johnson et al. 2006), nonmonotonic features tend to be averaged out.

Nonmonotonicity can simply arise from a single nonlinearity (Engebretson and Eldredge 1968; Weiss and Leong 1985; Lukashkin and Russell 1998). That basic idea was extended to explain DPOAE growth (Lukashkin et al. 2002), where the

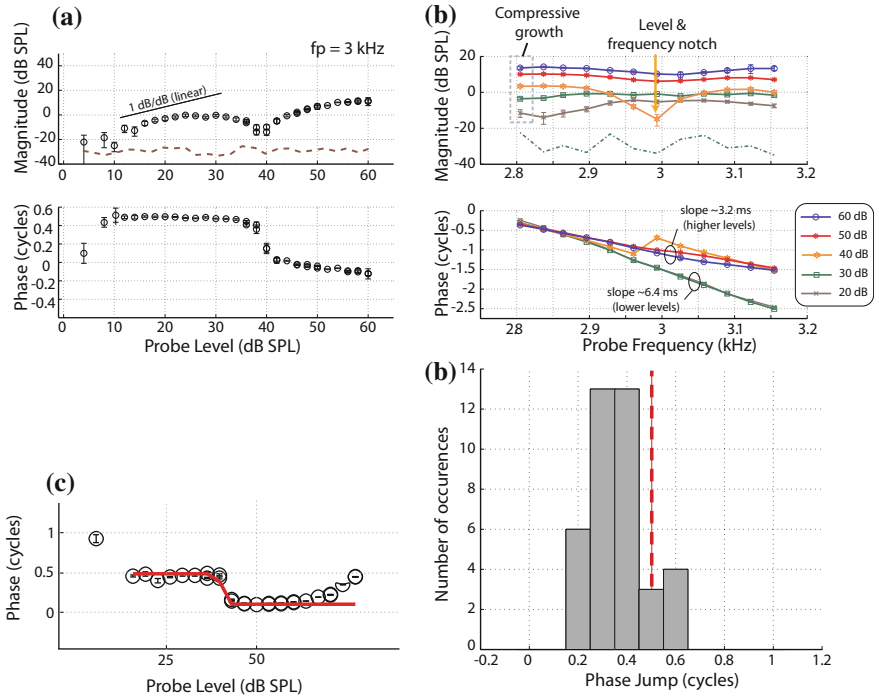

Fig. 10.3 Example of evoked otoacoustic emission (eOAE) dependence on stimulus level (Lp = Ls + 15 dB, fp = fs + 40 Hz; L length; p probe: s suppressor; f frequency; Bergevin 2007). **a** Representative stimulus-frequency otoacoustic emission (SFOAE) input/output function (I/O) for a human subject. *Dashed line* indicates the noise floor. Some phase values were shifted vertically by one cycle. The particular curve shown here is representative, but there can be significant qualitative variation in the shape across subjects (for a fixed set of parameters) and stimulus frequencies (in a given individual). **b** SFOAE frequency-dependence measured at different stimulus intensities in a human subject. A notch, with respect to both frequency and level, is apparent around 3 kHz and 40 dB SPL. Furthermore, there is a transition in the phase gradients depending on whether the stimulus level is below (larger gradient) or above (smaller gradient) 40 dB SPL. **c** Example of nonlinear regression (hyperbolic tangent) estimation of the phase jump for SFOAE probe-level dependence (*solid curve*). This was used as the basis for (**d**). **d** Size of SFOAE phase jump around a notch, compiled from multiple stimulus frequencies and species. The peak of the distribution indicates that the phase jumps tend to be smaller than 0.5 cycle (*dashed line*), typically 0.3–0.4 cycles

hypothesis is that distortions observable in the ear canal arise predominantly from "a single source, namely, a nonlinear amplifier with saturating I/O characteristic." It is important to critically examine this notion because there are wide implications for interpreting a broad range of eOAE behavior in terms of the underlying cochlear physiology, such as the inferred "operating point" of the transducer (e.g., Bian et al. 2002; Liberman et al. 2004).

At least two main lines of evidence argue against the applicability of the single-source model for eOAEs. First, many empirical aspects of nonmonotonic

features are not consistent with key predictions of the model (Bergevin 2007), such as linear growth at lower level (even for cubic distortion products), the size of the phase jump (not necessarily 0.5 cycle, as predicted by the model simply stemming from a sign change; Fig. 10.3d), phase varying smoothly with level (i.e., not just a "jump"), extended portions with highly compressed growth, and the frequency-dependent nature of the I/O (Fig. 10.3a, b).

Second, it is well-known that DPOAE source "unmixing" (e.g., Mauermann et al. 1999; Kalluri and Shera 2001) demonstrates that two generation components with differing latencies exist (see Sect. 10.3.1), that these can constructively/destructively interfere to yield a measured DPOAE at the ear canal (typically referred to as "fine structure"), and that these components can be differentially affected (e.g., Mauermann and Kollmeier 2004; Botti et al. 2016). In fact, there are numerous reviews of data indicating that both SOAEs and eOAEs are generated over multiple, spatially distributed areas (e.g., Shaffer et al. 2003; Siegel et al. 2005; Moleti et al. 2013).

10.3.3 Evoked Emission Delays

For eOAEs, there is a round-trip travel time, i.e., the time it takes an emission to come back out of the ear relative to the presentation of the stimulus. How exactly this delay informs us about cochlear mechanics is a topic of great debate. For example, do SFOAE delays relate to the group delay of the cochlear mechanical filter at the site of generation and can they then be used to infer tuning (see Sect. 10.3.4)? Examples of SFOAE delays for a variety of species are shown in Fig. 10.4.

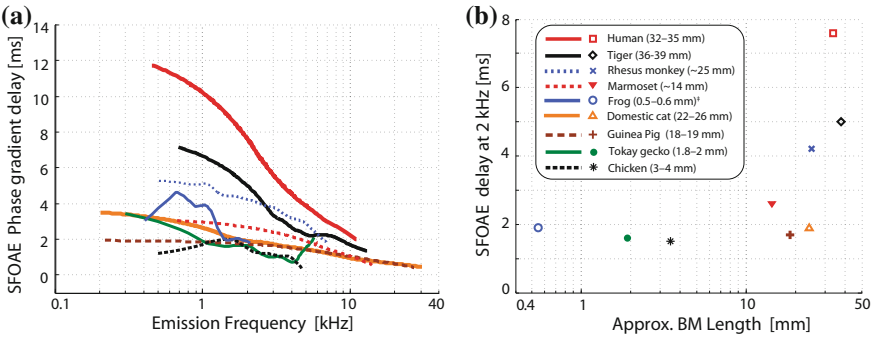

Fig. 10.4 **a** Comparison of SFOAE phase-gradient delays and BM lengths for several different species (40-dB SPL probe level; same stimulus paradigm/parameters used for all). Data from Shera and Guinan (2003), Bergevin et al. (2008, 2011b, 2012b), and Joris et al. (2011). **b** Mean delay at 2 kHz as a function of approximate BM length. ‡For the frog, the provided length corresponds only to the amphibian papilla

eOAE delays can be extracted from the ear canal recording in several ways. The first is by using ripples in the (steady-state) response of the probe (i.e., take the magnitude of the Fourier transform of the microphone response in the canal) that result from constructive and destructive interference between the stimulus and the (relatively delayed) eOAE (e.g., Zwicker and Schloth 1984; Shera and Guinan 1999). An alternative spectral method involves taking the slope of the unwrapped SFOAE phase versus frequency, called the "phase-gradient delay" (French 1971; Shera et al. 2010). For linear systems, the phase-gradient delay is equivalent to the group delay. Additionally, delays can be estimated directly in the time domain (Whitehead et al. 1996; Meenderink and Narins 2006); they show a good correspondence to those extracted from the steady-state frequency domain.

One example of how phase-gradient delays can be used to study the site of DPOAE generation is by comparing the delays of the $2f_2–f_1$ and the $2f_1–f_2$ evoked by the same stimulus. $2f_1–f_2$ DPOAE phase gradients are small compared with those of $2f_2–f_1$ (Knight and Kemp 2000; Bergevin et al. 2008). Does this mean that $2f_1–f_2$ is emitted from the cochlea much faster (almost instantaneously) relative to $2f_2–f_1$? It does not, as time-domain studies of delay have shown (e.g., Whitehead et al. 1996). Instead, this discrepancy is thought to arise from a difference in generation mechanisms stemming from wave- and place-fixed distinctions (e.g., Shera and Guinan 1999, 2008). This example shows that caution is required when correlating phase-gradient delays to actual time delays because the generation mechanism(s) could confound this relationship.

10.3.4 Stimulus-Frequency Emission Delays and Cochlear Tuning

Several studies have examined how SFOAE phase-gradient delays can be used as a proxy measure for cochlear tuning (e.g., Shera et al. 2002, 2010). A basic intuition is provided by Eq. 10.1. When the oscillator has low damping, it is more sharply resonant (i.e., it has a stronger "preference" for frequencies close to its characteristic frequency) and sluggish (i.e., it takes a longer time to build up a steady-state response because the oscillator can store more energy that can only be provided on a cycle-by-cycle basis by the external drive). Even though this method has been verified in animals (Bergevin and Shera 2010; Shera et al. 2010; Joris et al. 2011), suggestions that humans exhibit sharper cochlear mechanical tuning than other mammalian species have been more controversial (e.g., Ruggero and Temchin 2005; Siegel et al. 2005).

A psychophysical study in humans demonstrated that tuning derived from SFOAE delays compares well with perceptual auditory-filter tuning in an isoresponse forward-masking paradigm (Oxenham and Shera 2003). Subsequent investigations have provided further support for this relationship by comparing tuning estimates from neural, otoacoustic, and psychophysical estimates from a

single species (e.g., marmoset, Bergevin et al. 2011b; ferret, Sumner et al. 2014) and have shown that the SFOAE delays can also be in part explained by morphological aspects of the cochlea such as BM length (e.g., Bergevin et al. 2011b, 2012b; Fig. 10.4) and properties of the tectorial membrane (e.g., Bergevin et al. 2010). Despite this evidence, there are studies that do not support the view of sharp human frequency selectivity (e.g., Charaziak et al. 2013; Manley and van Dijk 2016). The OAE suppression properties investigated in those studies demonstrated human tuning values that are more consistent with the moderate frequency selectivity derived from simultaneous-masking psychoacoustic tuning curves.

Additionally, OAEs provide means to characterize the cochlear mechanical filter at the base of the perceptual auditory filter. It is clear that changes in cochlear mechanical filters (e.g., due to stimulus level or OHC damage) affect the perceptual auditory filters, but the exact relationship between OAE-derived tuning measures, auditory nerve tuning curves, and perceptual auditory filters is not entirely established. Whereas in humans, the relationship between perceptual and OAE tuning can be established, one must rely on animal physiology to establish the relationship between OAE and auditory nerve tuning (e.g., Shera et al. 2010). One way to study how different tuning estimates reflect the underlying cochlear filter tuning is by adopting models of the human cochlea that can simulate emissions as well as BM and auditory nerve responses (e.g., Verhulst et al. 2012, 2015).

Model approaches can further help address practical considerations such as how SFOAEs are generated and subsequently exit the inner ear (e.g., Choi et al. 2008), which is important in the study of the relationship between cochlear mechanical filter tuning and SFOAE delays. For example, if SFOAE generation is purely based on place-fixed mechanisms stemming from a narrow region around the peak of the traveling wave to the evoking stimulus (e.g., Zweig and Shera 1995; Shera and Guinan 2008), the relationship between the SFOAE delay and the filter group delay would only hold for low stimulus levels where the linear relationship between filter group delays and tuning (Goldstein et al. 1971) is valid. As the role of a place-fixed mechanism for SFOAE generation has been heavily debated over the years (e.g., Siegel et al. 2005), it is presently unclear to what degree existing SFOAE methods can reliably assess cochlear mechanical filter tuning at higher stimulus levels. Another potentially important modeling consideration that requires further study is the difference between isoresponse and isoinput measures of tuning (Eustaquio-Martín and Lopez-Poveda 2011).

10.4 How Do Emissions Exit the (Inner) Ear?

The question regarding OAEs and waves (see Sect. 10.2.3.2) is further highlighted by the debate as to how emissions are emitted from the cochlea. That is, whether OAEs propagate via “slow” (i.e., BM-based) or “fast” (i.e., fluid compression-based) waves (e.g., He et al. 2008; Dong and Olson 2008; Meenderink and van der Heijden 2010).

Another key consideration is that on exiting the cochlea, OAE energy must essentially drive the middle and outer ears in "reverse." Despite the passive gain (in the range of 40 dB) going inward, the middle ear behaves in a reciprocal fashion by attenuating sound pressure going outward (Shera and Zweig 1993). Several studies have examined this aspect, using either DPOAEs as an "intracochlear" source (Magnan et al. 1997; Dong and Olson 2006; Dalhoff et al. 2011), extracted temporal bones (Puria 2003), or other methods. Detailed knowledge in this regard is crucial toward understanding the power produced by the ear in SOAE generation and attempts to relate this overall power to the function of individual hair cells (e.g., Manley and Gallo 1997). The frequency-specific attenuation of sound caused by the middle ear transfer is particularly important when interpreting OAE amplitudes. For example, when using eOAEs to estimate the stimulus level required for detecting cochlear compression at a given frequency place, it needs to be considered that not all stimuli are as effective in driving the cochlear location where the eOAE is generated. Second, when interpreting the magnitudes of spectral CEOAE components in a clinical screening setting, the middle ear attenuates higher frequency CEOAE components as opposed to those where middle ear transmission is more efficient (1–2 kHz region), even in ears where there is no cochlear damage.

10.5 Benefits of a "Comparative" Viewpoint

Since OAEs were first discovered in humans, researchers quickly realized that emissions arise in a wide variety of animal classes such as amphibians (Palmer and Wilson 1982), reptiles (Rosowski et al. 1984), and even insects (Kössl and Boyan 1998). Since then, numerous observations have systematically compared OAEs between humans and nonmammals, many of which lack a direct analog to BM traveling waves. Regardless of whether one's interest is human cochlear mechanics or neuroethology, the general biophysical considerations discussed combined with the observation that most types of ears produce OAEs provides an important opportunity to understand their mechanisms.

A common feature shared among all vertebrate ears is hair cells (see Sect. 10.1.2). The number within a given ear, how they are coupled together (i.e., presence and structure of TM), their molecular composition (e.g., density of prestin), their bundle properties (e.g., number and height of stereovilli, internal coupling), their ionic environment (e.g., calcium level, effective endocochlear potential), and even the underlying substrate they are embedded in or sit atop (i.e., flexible BM, or cartilage) can vary dramatically across taxonomic boundaries (Fig. 10.2). Despite this variety, OAE properties exhibit striking similarities.

One study (Bergevin et al. 2008) indicated that the empirical basis for the wave-fixed versus place-fixed distinction (Shera and Guinan 1999; see also Sect. 10.2.3) can be found in a wide class of ears, even those that presumably lack a BM traveling wave. A subsequent study (Bergevin et al. 2015a) examined predictions of the "standing-wave" model (Shera 2003) in nonmammalian ears and

found good agreement between data and model, indicating shared properties at work in the underlying generation mechanisms.

In terms of differences, one distinction has drawn significant attention. SFOAE phase-gradient delays are much longer in humans than in any other species examined thus far (Fig. 10.4). As discussed in Sect. 10.3.4, this difference in delay has been proposed to be indicative of relatively sharper cochlear tuning in humans (Shera et al. 2002). Another telling difference is that within lizards, species with a continuous TM, have relatively few/large SOAE peaks while species without a TM tend to have more numerous smaller peaks (Manley 1997).

In short, OAEs are a common property across land vertebrates, and there are many similarities (and differences) across (e.g., Bergevin et al. 2015a) and within (e.g., Bergevin 2011; Berezina-Greene and Guinan 2015) groups. Presumably, these interrelationships, in the face of vast morphological differences, point to a key underlying biophysical principle(s) at work in all types of ears. At a minimum, it is clear that neither two distinct hair cell types nor a flexible BM nor the presence of a TM are a priori required for OAE generation. Such knowledge can in turn stimulate advancements in the evolutionary theory about hearing (Manley 2000).

10.6 Putting Emissions to Work

Having examined the mechanisms underlying the generation and current models of OAE, this section describes the practical aspects and their current and potential use. Readers are also referred to extensive reviews (e.g., Robinette and Glattke 2007; Janssen and Müller 2008; Lonsbury-Martin and Martin 2008).

OAEs have been extensively developed to probe peripheral auditory function in both basic scientific (e.g., Is my genetically modified mouse deaf?) and clinical (e.g., Is this newborn deaf?) settings. For the most part, eOAEs are used as a proxy measure for hearing ability, based on their relative amplitude. If the signal is above the noise floor (or some sort of predetermined threshold), the ear is considered normal (or healthy). Generally, these screenings are efficient and cost effective, given their noninvasive and objective nature. Some salient examples include

- Clinical hearing screening, especially in pediatric audiology (Kemp et al. 1990; Abdala et al. 1996; Norton et al. 2000)
- Hearing screening in humans (Dorn et al. 2001; Boege and Janssen 2002; Goodman et al. 2009)
- Hearing screening in animals (Liberman et al. 2002; Cheatham et al. 2014)
- Veterinary diagnostics/care (McBrearty and Penderis 2011); McBrearty et al. 2012)

Note that caution is needed because auditory neuropathies (i.e., pathologies in the neural pathway connecting the cochlea to the brain) can sometimes allow for "normal" OAEs despite hearing impairment being present (e.g., Berlin et al. 2003;

Bharadwaj et al. 2015). Additionally, middle ear dysfunction (e.g., otitis media) can affect OAEs and the absence of OAEs can be due to both middle or inner ear pathology (e.g., Owens et al. 1992; see also Sect. 10.4). Thus, a failure to record OAEs requires additional measurement (e.g., compound action potentials and/or auditory brainstem responses) to reach a diagnosis.

Another intriguing avenue of exploration is how eOAEs can be used to assess auditory function in hearing-impaired individuals. Recent improvements in signal processing (e.g., Vetešník et al. 2009; Keefe 2012) help toward this end. Basic comparisons between normal hearing and hearing impairment are well established (e.g., Gorga et al. 2003; Prieve et al. 1993) and have served to provide a useful benchmark for clinical applications. But recent studies have begun to examine further aspects, such as changes associated with frequency selectivity (e.g., Gruhlke et al. 2012; Charaziak et al. 2013), and these may help with understanding the difficulties with speech recognition in noisy environments. Another interesting avenue is retrocochlear pathologies such as acoustic neuromas (Telischi et al. 1995). Further studies for "translational" applications of OAEs include

- Monitoring intracranial pressure (de Kleine et al. 2000; Voss et al. 2006)
- Measuring cochlear blood flow (Telischi et al. 1998; Mom et al. 1999)
- Effects of ototoxic drug exposure (Stavroulaki et al. 1999; Lonsbury-Martin and Martin 2001; Reavis et al. 2011)
- Efferent-related feedback effects (Francis and Guinan 2010; Garinis et al. 2011; Boothalingam et al. 2015)
- Attention-related effects (Walsh 2012)
- SFOAEs as a measure of tuning (see Sect. 10.3.4)
- Basis of absolute pitch (Bergevin et al. 2015b)
- Biometric applications (Liu and Hatzinakos 2014; see also Nura headphones)
- Assessing (forward and reverse) middle ear function (Dalhoff et al. 2011; see also Sect. 10.4)
- Understanding OAE differences across human groups, such as ethnic and sex disparities (Whitehead et al. 1993; McFadden and Pasanen 1998)

One difficult obstacle in several of these potential applications is establishing an appropriate baseline (e.g., Reavis et al. 2015). For example, what are reasonable fluctuations in OAE properties that an audiologist could expect and thereby meaningfully detect a significant change (e.g., due to ototoxic exposure)?

10.7 Looking Ahead: Next Steps

Having described basic biophysical considerations that can be investigated using OAEs and highlighted a fraction of the literature that has attempted to address these questions, the chapter now ends on a note looking further ahead, drawing attention to several open areas of otoacoustic-related research.

- Can OAEs be used to clarify the role played by viscous forces of the inner ear fluids? Although a single hair bundle is presumably subject to a low Reynolds number environment, perhaps their collective behavior can cause a net decrease in the relevant frictional forces (in a fashion similar to motile bacteria; e.g., López et al. 2015).
- A recent study has argued for a "staircase"-like structure to the individual ears tonotopic map such that extended spatial regions effectively share a similar characteristic frequency (Shera 2015; Bell and Wit 2015). In what ways might these be related/connected to arguments for "frequency plateaus" in coupled oscillator models of SOAE generation (Vilfan and Duke 2008; Wit and van Dijk 2012)?
- Although many aspects of cochlear function are linear (or quasi-linear), the overall behavior is very nonlinear (e.g., compression is a fundamental means of operation). Thus, repeating Ku et al. (2008), "How does the cochlea behave in such a relatively linear fashion when it is so inherently nonlinear in terms of its basic building blocks?" Is the ear chaotic (e.g., Keefe et al. 1990)?
- The existence of SOAEs suggests that the cochlea is close to an instability (see Zweig 2003 as well as Corey, Ó Maoiléidigh, and Ashmore, Chap. 4) but obviously shows that the system is ultimately stable. Many classes of (active) cochlear models, however, have difficulty producing SOAE patterns with stability comparable to those seen physiologically. Why? Put another way, what aspects of cochlear function allow it to be quasi-stable?
- What is the biophysical basis for the general frequency stability of SOAEs, even after exposure to moderate sounds, or for temperature-dependent changes in SOAEs (e.g., van Dijk et al. 1989)?
- Idiosyncrasy of SOAEs. Why don't all ears emit SOAEs despite common sensitivity thresholds? Why do some species exhibit more robust SOAE activity than others? What is this telling us about the notion of "irregularity"? How might cochlear roughness be quantified and be correlated to OAEs? How level dependent is the role of irregularity and what does that tell us?
- Reconciling how a vast array of morphologies (including insect ears) give rise to OAEs. How are various morphological (e.g., BM length, number of hair cells) and functional (e.g., number of octaves spanned in audiogram, tuning) aspects interrelated?
- Elucidating the level dependence of eOAE phase-gradient delays (e.g., at low stimulus levels, do they become level independent?) and the implications for linearity and tuning.
- Can OAEs be used to offer an objective estimate of an individual's frequency selectivity aside from being able to assess sensitivity? How might OAEs be more effectively used in quantifying cochlear health in hearing-impaired individuals?
- "Suppression tuning curves" for SOAEs have been demonstrated to match auditory nerve fiber responses in lizards and the barn owl remarkably well (e.g., Köppl and Manley 1994). A recent study measured SOAE suppression in humans (Manley and van Dijk 2016), which suggested relatively moderate

frequency tuning in the cochlea. Given that these observations contradict the sharp tuning estimates found comparing SFOAE phase-gradient delays and auditory nerve tuning curves in Old World monkeys (Joris et al. 2011), the exact relationship between various tuning measures requires further research.

This chapter ends with a quote of the final sentence in Kemp's landmark paper (1978, p. 1391) announcing the discovery of OAEs: "If proven, it [the hypothesis that OAEs are generated by normal cochlear function] would provide a new insight into the microscopic behavior of the cochlear transduction mechanism which is not adequately understood." Kemp was certainly correct, although his discovery yielded much more than just "a new insight," and there is still a long way to go….

Acknowledgements Input from Glenis Long, Larissa McKetton, Jung-Hoon Nam, Elizabeth Olson, and Christopher Shera is gratefully acknowledged. Support from the Fields Institute, The Natural Sciences and Engineering Research Council of Canada (NSERC), and Deutsche Forschungsgemeinschaft (DFG) Cluster of Excellence EXC 1077/1 "Hearing4all" is acknowledged.

Compliance with Ethics Requirements Christopher Bergevin declares that he has no conflict of interest. Sarah Verhulst declares that she has no conflict of interest. Pim van Dijk declares that he has no conflict of interest.

References

Abdala, C., Sinninger, Y. S., Ekelid, M., & Zeng, F. G. (1996). Distortion product otoacoustic emission suppression tuning curves in human adults and neonates. *Hearing Research,* 98, 38–53.

Aranyosi, A. J. (2006). A "twin-engine" model of level-dependent cochlear motion. In A. L. Nuttall, T. Ren, P. Gillespie, K. Grosh, & E. de Boer (Eds.), *Auditory Mechanisms: Processes and Models* (pp. 500–501). Singapore: World Scientific Publishing Co.

Avan, P., Büki, B., & Petit, C. (2013). Auditory distortions: Origins and functions. *Physiological Reviews,* 93, 1563–1619.

Bell, A., & Wit, H. P. (2015). The vibrating reed frequency meter: Digital investigation of an early cochlear model. *PeerJ,* 3, e1333. doi:10.7717/peerj.1333.

Berezina-Greene, M. A., & Guinan, J. J. (2015). Stimulus frequency otoacoustic emission delays and generating mechanisms in guinea pigs, chinchillas, and simulations. *Journal of the Association for Research in Otolaryngology,* 16(6), 679–694.

Bergevin, C. (2007). *Comparative Approaches to Otoacoustic Emissions: Towards an Understanding of Why the Ear Emits Sound*. PhD Thesis, Massachusetts Institute of Technology, Cambridge, MA.

Bergevin, C. (2011). Comparison of otoacoustic emissions within gecko subfamilies: Morphological implications for auditory function in lizards. *Journal of the Association for Research in Otolaryngology*, 12(2), 203–217.

Bergevin, C., & Shera, C. A. (2010). Coherent reflection without traveling waves: On the origin of long-latency otoacoustic emissions in lizards. *The Journal of the Acoustical Society of America,* 127(4), 2398–2409.

Bergevin, C., Freeman, D. M., Saunders, J. C., & Shera, C. A. (2008). Otoacoustic emissions in humans, birds, lizards, and frogs: Evidence for multiple generation mechanisms. *Journal of Comparative Physiology A*, 194, 665–683.

Bergevin, C., Velenovsky, D. S., & Bonine, K. E. (2010). Tectorial membrane morphological variation: Effects upon stimulus frequency otoacoustic emissions. *Biophysical Journal*, 99, 1064–1072.

Bergevin, C., Velenovsky, D. S., & Bonine, K. E. (2011a). Coupled, active oscillators and lizard otoacoustic emissions. In C. A. Shera & E. S. Olson (Eds.), *What Fire Is in Mine Ears: Progress in Auditory Biomechanics: Proceedings of the 11th International Mechanics of Hearing Workshop,* Williamstown, MA, July 16–22, 2011 (pp. 453–460). Melville, NY: American Institute of Physics Conference Proceedings 1403.

Bergevin, C., McDermott, J., Roy, S., Li, F., Shera, C., & Wang, X. (2011b). Stimulus-frequency otoacoustic emissions as a probe of cochlear tuning in the common marmoset. *Association for Research in Otolaryngology Abstracts,* 34, 371.

Bergevin, C., Fulcher, A., Richmond, S., Velenovsky, D., & Lee, J. (2012a). Interrelationships between spontaneous and low-level stimulus-frequency otoacoustic emissions in humans. *Hearing Research*, 285(1–2), 20–28.

Bergevin, C., Walsh, E. J., McGee, J., & Shera, C. A. (2012b). Probing cochlear tuning and tonotopy in the tiger using otoacoustic emissions. *Journal of Comparative Physiology A*, 198(8), 617–624.

Bergevin, C., Manley, G. A., & Köppl, C. (2015a). Salient features of otoacoustic emissions are common across tetrapod groups and suggest shared properties of generation mechanisms. *Proceedings of the National Academy of Sciences of the United States of America,* 112(11), 3362–3367.

Bergevin, C., McKetton, L., Stone, V., Grahn, J., & Purcell, D. (2015b). No otoacoustic evidence for a peripheral basis underlying absolute pitch. *The Journal of the Acoustical Society of America,* 137, 2409.

Berlin, C. I., Hood, L., Morlet, T., Rose, K., & Brashears, S. (2003). Auditory neuropathy/dys-synchrony: Diagnosis and management. *Mental Retardation and Developmental Disabilities Research Reviews*, 9, 225–231.

Bharadwaj, H. M., Masud, S., Mehraei, G., Verhulst, S., & Shinn-Cunningham, B. G. (2015). Individual differences reveal correlates of hidden hearing deficits. *The Journal of Neuroscience*, 35(5), 2161–2172.

Bialek, W. (2012). *Biophysics: Searching for Principles*. Princeton, NJ: Princeton University Press.

Bialek, W., & Wit, H. P. (1984). Quantum limits to oscillator stability: Theory and experiments on acoustic emissions from the human ear. *Physics Letters A*, 104(3), 173–178.

Bian, L., Chertoff, M. E., & Miller, E. (2002). Deriving a cochlear transducer function from low-frequency modulation of distortion product otoacoustic emissions. *The Journal of the Acoustical Society of America*, 112(1), 198–210.

Boege, P., & Janssen, T. (2002). Pure-tone threshold estimation from extrapolated distortion product otoacoustic emission I/O-functions in normal and cochlear hearing loss ears. *The Journal of the Acoustical Society of America*, 111(4), 1810–1818.

Boothalingam, S., Allan, C., Allen, P., & Purcell, D. (2015). Cochlear delay and medial olivocochlear functioning in children with suspected auditory processing disorder. *PLoS ONE*, 10(8), e0136906.

Botti, T., Sisto, R., Sanjust, F., Moleti, A., & D'Amato, L. (2016). Distortion product otoacoustic emission generation mechanisms and their dependence on stimulus level and primary frequency ratio. *The Journal of the Acoustical Society of America*, 139(2), 658–673.

Brown, A. M. (1987). Acoustic distortion from rodent ears: A comparison of responses from rats, guinea pigs and gerbils. *Hearing Research*, 31(1), 25–37.

Charaziak, K. K., Souza, P., & Siegel, J. H. (2013). Stimulus-frequency otoacoustic emission suppression tuning in humans: Comparison to behavioral tuning. *Journal of the Association for Research in Otolaryngology*, 14, 843–862.

Cheatham, M. A., Goodyear, R. J., Homma, K., Legan, P. K., Korchagina, J., Naskar, S., Siegel, J. H., Dallos, P., Zheng, J., & Richardson, G. P. (2014). Loss of the tectorial membrane protein CEACAM16 enhances spontaneous, stimulus-frequency, and transiently evoked otoacoustic emissions. *The Journal of Neuroscience*, 34(31), 10325–10338.

Choi, Y. S., Lee, S. Y., Parham, K., Neely, S. T., & Kim, D. O. (2008). Stimulus-frequency otoacoustic emission: Measurements in humans and simulations with an active cochlear model. *The Journal of the Acoustical Society of America*, 123(5), 2651–2669.

Dalhoff, E., Turcanu, D., & Gummer, A. W. (2011). Forward and reverse transfer functions of the middle ear based on pressure and velocity DPOAEs with implications for differential hearing diagnosis. *Hearing Research*, 280, 86–99.

Dallos, P. (2008). Cochlear amplification, outer hair cells and prestin. *Current Opinion in Neurobiology*, 18, 370–376.

Dallos, P., & Corey, M. E. (1991). The role of outer hair cell motility in cochlear tuning. *Current Opinion in Neurobiology*, 1(2), 215–220.

de Kleine, E., Wit, H. P., & van Dijk, P. (2000). The behavior of spontaneous otoacoustic emissions during and after postural changes. *The Journal of the Acoustical Society of America*, 107(6), 3308–3316.

Dinis, L., Martin, P., Barral, J., Prost, J., & Joanny, J. (2012). Fluctuation-response theorem for the active noisy oscillator of the hair cell bundle. *Physical Review Letters*, 109, 160602.

Dong, W., & Olson, E. S. (2006). Middle ear forward and reverse transmission in gerbil. *Journal of Neurophysiology*, 95(5), 2951–2961.

Dong, W., & Olson, E. S. (2008). Supporting evidence for reverse cochlear traveling waves. *The Journal of the Acoustical Society of America,* 123(1), 222–240.

Dorn, P. A., Konrad-Martin, D., Neely, S. T., Keefe, D. H., Cyr, E., & Gorga, M. P. (2001). Distortion product otoacoustic emission input/output functions in normal-hearing and hearing-impaired human ears. *The Journal of the Acoustical Society of America,* 110(6), 3119–3131.

Duifhuis, H. (2012). *Cochlear Mechanics: Introduction to a Time Domain Analysis of the Nonlinear Cochlea.* New York: Springer-Verlag.

Duke, T. A. J., & Jülicher, F. (2008). Critical oscillators as active elements in hearing. In G. A. Manley, R. R. Fay, & A. N. Popper (Eds.), *Active Processes and Otoacoustic Emissions in Hearing* (pp. 63–92). New York: Springer-Verlag.

Elliott, S. J., Ku, E. M., & Lineton, B. (2007). A state space model for cochlear mechanics. *The Journal of the Acoustical Society of America,* 122(5), 2759–2771.

Engebretson, A. M., & Eldredge, D. H. (1968). Model for the nonlinear characteristics of cochlear potentials. *The Journal of the Acoustical Society of America,* 44(2), 548–554.

Epp, B., Verhey, J. L., & Mauermann, M. (2010). Modeling cochlear dynamics: Interrelation between cochlea mechanics and psychoacoustics. *The Journal of the Acoustical Society of America,* 128(4), 1870–1883.

Epp, B., Wit, H. P., & van Dijk, P. (2015). Clustering of cochlear oscillations in frequency plateaus as a tool to investigate SOAE generation. In K. D. Karavitaki & D. P. Corey (Eds.), *Mechanics of Hearing: Protein to Perception: Proceedings of the 12th International Workshop on the Mechanics of Hearing,* Cape Sounio, Greece, June 23–29, 2014 (pp. 090025-1–090025-6). Melville, NY: American Institute of Physics Conference Proceedings 1703.

Eustaquio-Martín, A., & Lopez-Poveda, E. A. (2011). Isoresponse versus isoinput estimates of cochlear filter tuning. *Journal of the Association for Research in Otolaryngology,* 12, 281– 299.

Francis, N. A., & Guinan, J. J. (2010). Acoustic stimulation of human medial olivocochlear efferents reduces stimulus-frequency and click-evoked otoacoustic emission delays: Implications for cochlear filter bandwidths. *Hearing Research,* 267(1–2), 36–45.

French, A. P. (1971). *Vibrations and Waves*. New York: W. W. Norton & Company.

Fruth, F., Jülicher, F., & Lindner, B. (2014). An active oscillator model describes the statistics of spontaneous otoacoustic emissions. *Biophysical Journal,* 107(4), 815–824.

Garinis, A., Werner, L., & Abdala, C. (2011). The relationship between MOC reflex and masked threshold. *Hearing Research,* 282, 128–137.

Goldstein, J. L., Baer, T., & Kiang, N. Y.-S. (1971). A theoretical treatment of latency, group delay, and tuning characteristics for auditory nerve responses to clicks and tones. In M. B. Sachs (Ed.), *Physiology of the Auditory System*, (p. 133–141). Baltimore, MD: National Education Consultants.

Goodman, S. S., Fitzpatrick, D. F., Ellison, J. C., Jesteadt, W., & Keefe, D. H. (2009). High-frequency click-evoked otoacoustic emissions and behavioral thresholds in humans. *The Journal of the Acoustical Society of America,* 125(2), 1014–1032.

Gorga, M. P., Neely, S. T., Bergman, B., Beauchaine, K. L., Kaminski, J. R., Peters, J., & Jesteadt, W. (2003). Otoacoustic emissions from normal-hearing and hearing-impaired subjects: Distortion product responses. *The Journal of the Acoustical Society of America,* 93(4), 2050–2060.

Gruhlke, A., Birkholz, C., Neely, S. T., Kopun, J., Tan, H., Jesteadt**, W.,** Schmid, K., & Gorga, M. P. (2012). Distortion-product otoacoustic emission suppression tuning curves in hearing-impaired humans. *The Journal of the Acoustical Society of America,* 132(5), 3292–3304.

Hansen, R., Santurette, S., & Verhulst, S. (2014). Effects of spontaneous otoacoustic emissions on pure-tone frequency difference limens. *The Journal of the Acoustical Society of America,* 136(6), 3147–3158.

He, W., Fridberger, A., Porsov, E., Grosh, K., & Ren, T. (2008). Reverse wave propagation in the cochlea. *Proceedings of the National Academy of Sciences of the United States of America,* 105(7), 2729–2733.

Hudspeth, A. J. (2008). Making an effort to listen: Mechanical amplification in the ear. *Neuron,* 59(4), 530–545.

Janssen, T., & Müller, J. (2008). Otoacoustic emissions as a diagnostic tool in a clinical context. In G. A. Manley, R. R. Fay, & A. N. Popper (Eds.), *Active Processes and Otoacoustic Emissions in Hearing* (pp. 421–460). New York: Springer-Verlag.

Jaramillo, F., & Wiesenfeld, K. (1998). Mechanoelectrical transduction assisted by Brownian motion: A role for noise in the auditory system. *Nature Neuroscience,* 1(5), 384–388.

Johannesma, P. (1980). Narrow band filters and active resonators. In G. van den Brink & F. Bilsen (Eds.), *Psychophysical, Physiological and Behavioural Studies in Hearing: Proceedings of the 5th International Symposium on Hearing*, Noordwikjkerhout, The Netherlands, April 8–12, 1980 (pp. 62–63). Delft, The Netherlands: Delft University Press.

Johnson, T. A., Neely, S. T., Garner, C. A., & Gorga, M. P. (2006). Influence of primary-level and primary-frequency ratios on human distortion product otoacoustic emissions. *The Journal of the Acoustical Society of America,* 119(1), 418– 428.

Joris, P. X., Bergevin, C., Kalluri, R., McLaughlin, M., Michelet, P., van der Heijden, M., & Shera, C. A. (2011). Frequency selectivity in Old-World monkeys corroborates sharp cochlear tuning in humans. *Proceedings of the National Academy of Sciences of the United States of America,* 108(42), 17516–17520.

Kalluri, R., & Shera, C. A. (2001). Distortion-product source unmixing: A test of the two-mechanism model for DPOAE generation. *The Journal of the Acoustical Society of America,* 109(2), 622–637.

Kalluri, R., & Shera, C. A. (2007). Near equivalence of human click-evoked and stimulus-frequency otoacoustic emissions. *The Journal of the Acoustical Society of America,* 121(4), 2097–2110.

Kantz, H., & Schreiber, T. (2004). *Nonlinear Time Series Analysis.* Cambridge, UK: Cambridge University Press.

Keefe, D. H. (2012). Moments of click-evoked otoacoustic emissions in human ears: Group delay and spread, instantaneous frequency and bandwidth. *The Journal of the Acoustical Society of America,* 132(5), 3319–3350.

Keefe, D., Burns, E., Ling, R., & Laden, B. (1990). Chaotic dynamics of otoacoustic emissions. In P. Dallos, C. D. Geisler, J. W. Matthews, M. A. Ruggero, & C. R. Steele (Eds.), *The Mechanics and Biophysics of Hearing* (pp. 194–201). New York: Springer-Verlag.

Kemp, D. T. (1978). Stimulated acoustic emissions from within the human auditory system. *The Journal of the Acoustical Society of America,* 64(5), 1386–1391.

Kemp, D. T. (1986). Otoacoustic emissions, travelling waves and cochlear mechanisms. *Hearing Research,* 22, 95–104.

Kemp, D. T., Ryan, S., & Bray, P. (1990). A guide to the effective use of otoacoustic emissions. *Ear and Hearing,* 11(2), 93–105.

Kiang, N., Liberman, M., Sewell, W., & Guinan, J. J. (1986). Single unit clues to cochlear mechanisms. *Hearing Research,* 22, 171–182.

Knight, R. D., & Kemp, D. T. (2000). Indications of different distortion product otoacoustic emission mechanisms from a detailed f_1,f_2 area study. *The Journal of the Acoustical Society of America,* 107(1), 457.

Köppl, C., & Manley, G. A. (1994). Spontaneous otoacoustic emissions in the bobtail lizard. II: Interactions with external tones. *Hearing Research,* 72, 159–170.

Kössl, M., & Boyan, G. S. (1998). Otoacoustic emissions from a nonvertebrate ear. *Naturwissenschaften,* 85, 124–127.

Kozlov, A. S., Andor-Ardó, D., & Hudspeth, A. J. (2012). Anomalous Brownian motion discloses viscoelasticity in the ear's mechanoelectrical-transduction apparatus. *Proceedings of the National Academy of Sciences of the United States of America,* 109(7), 2896–2901.

Ku, E. M., Elliott, S. J., & Lineton, B. (2008). Statistics of instabilities in a state space model of the human cochlea. *The Journal of the Acoustical Society of America,* 124(2), 1068–1079.

Ku, E. M., Elliott, S. J., & Lineton, B. (2009). Limit cycle oscillations in a nonlinear state space model of the human cochlea. *The Journal of the Acoustical Society of America,* 126, 739–750.

Kuroda, T. (2007). Clinical investigation on spontaneous otoacoustic emission (SOAE) in 447 ears. *Auris Nasus Larynx,* 34, 29–38.

Liberman, M. C., Gao, J., He, D. Z., Wu, X., Jia, S., & Zuo, J. (2002). Prestin is required for electromotility of the outer hair cell and for the cochlear amplifier. *Nature,* 419, 300–304.

Liberman, M. C., Zuo, J., & Guinan, J. J. (2004). Otoacoustic emissions without somatic motility: Can stereocilia mechanics drive the mammalian cochlea? *The Journal of the Acoustical Society of America,* 116(3), 1649–1655.

Liu, Y., & Hatzinakos, D. (2014). Earprint: Transient evoked otoacoustic emission for biometrics. *IEEE Transactions on Information Forensics and Security*, 9(12), 2291–2301.

Long, G. R., & Tubis, A. (1988). Investigations into the nature of the association between threshold microstructure and otoacoustic emissions. *Hearing Research,* 36(2–3), 125–138.

Lonsbury-Martin, B. L., & Martin, G. K. (2001). Evoked otoacoustic emissions as objective screeners for ototoxicity. *Seminars in Hearing,* 22(4), 377–392.

Lonsbury-Martin, B. L., & Martin, G. K. (2008). Otoacoustic emissions: Basic studies in mammalian models. In G. A. Manley, R. R. Fay, & A. N. Popper (Eds.), *Active Processes and Otoacoustic Emissions in Hearing* (pp. 261–304). New York: Springer-Verlag.

Lonsbury-Martin, B. L., Martin, G. K., Probst, R., & Coats, A. C. (1988). Spontaneous otoacoustic emissions in a nonhuman primate. II. Cochlear anatomy. *Hearing Research,* 33(1), 69–93.

López, H. M., Gachelin, J., Douarche, C., Auradou, H., & Clément, E. (2015). Turning bacteria suspensions into superfluids. *Physical Review Letters,* 115, 028301.

Lukashkin, A. N., & Russell, I. J. (1998). A descriptive model of the receptor potential nonlinearities generated by the hair cell mechanoelectrical transducer. *The Journal of the Acoustical Society of America,* 103(2), 973–980.

Lukashkin, A. N., Lukashkina, V. A., & Russell, I. J. (2002). One source for distortion product otoacoustic emissions generated by low- and high-level primaries. *The Journal of the Acoustical Society of America,* 111(6), 2740–2748.

Magnan, P., Avan, P., Dancer, A., Smurzynski, J., & Probst, R. (1997). Reverse middle-ear transfer function in the guinea pig measured with cubic difference tones. *Hearing Research,* 107(1–2):41–45.

Manley, G. A. (1983). Frequency spacing of acoustic emissions: A possible explanation. In W. R. Webster (Ed.), *Mechanisms of Hearing* (pp. 36–39). Clayton, VIC, Australia: Monash University Press.

Manley, G. A. (1997) Diversity in hearing-organ structure and the characteristics of spontaneous otoacoustic emissions in lizards. In E. R. Lewis, G. R. Long, R. F. Lyon, P. M. Narins & C. R. Steele (Eds.), *Diversity in Auditory Mechanics* (pp. 32–38), Singapore: World Scientific Publishing Co.

Manley, G. A. (2000). Cochlear mechanisms from a phylogenetic viewpoint. *Proceedings of the National Academy of Sciences of the United States of America,* 97(22), 11736–11743.

Manley, G. A. (2001). Evidence for an active process and a cochlear amplifier in nonmammals. *Journal of Neurophysiology,* 86(2), 541–549.

Manley, G. A., & Gallo, L. (1997). Otoacoustic emissions, hair cells, and myosin motors. *The Journal of the Acoustical Society of America*, 102(2), 1049–1055.

Manley, G. A., & van Dijk, P. (2016) Frequency selectivity of the human cochlea: Suppression tuning of spontaneous otoacoustic emissions. *Hearing Research,* 336, 53–62.

Manley, G. A., Gallo, L., & Köppl, C. (1996). Spontaneous otoacoustic emissions in two gecko species, *Gekko gecko* and *Eublepharis macularius*. *The Journal of the Acoustical Society of America, 99*:1588–1603.

Manley, G. A., Popper, A. N., & Fay, R. R. (2008). *Active Processes and Otoacoustic Emissions in Hearing*. New York: Springer-Verlag.

Martin, G. K., Lonsbury-Marin, B. L., Probst, R., & Coats, A. C. (1988). Spontaneous otoacoustic emissions in a nonhuman primate. I. Basic features and relations to other emissions. *Hearing Research,* 33(1), 49–68.

Mauermann, M., & Kollmeier, B. (2004). Distortion product otoacoustic emission (DPOAE) input/output functions and the influence of the second DPOAE source. *The Journal of the Acoustical Society of America,* 116(4), 2199–2212.

Mauermann, M., Uppenkamp, S., van Hengel, P. W., & Kollmeier, B. (1999). Evidence for the distortion product frequency place as a source of distortion product otoacoustic emission (DPOAE) fine structure in humans. I. Fine structure and higher-order DPOAE as a function of the frequency ratio f_2/f_1. *The Journal of the Acoustical Society of America,* 106(6), 3473–3483.

May, R. M. (1976). Simple mathematical models with very complicated dynamics. *Nature*, 261, 459–467.

McBrearty, A. R., & Penderis, J. (2011). Evaluation of auditory function in a population of clinically healthy cats using evoked otoacoustic emissions. *Journal of Feline Medicine and Surgery,* 13(12), 919–926.

McBrearty, A., Auckburally, A., Pollock, P. J., & Penderis, J. (2012). Evoked otoacoustic emissions: An alternative test of auditory function in horses. *Equine Veterinary Journal,* 45, 60–65.

McFadden, D., & Pasanen, E. G. (1998). Comparison of the auditory systems of heterosexuals and homosexuals: Click-evoked otoacoustic emissions. *Proceedings of the National Academy of Sciences of the United States of America,* 95, 2709–2713.

Meenderink, S. W., & Narins, P. M. (2006). Stimulus frequency otoacoustic emissions in the northern leopard frog, *Rana pipiens pipiens*: Implications for inner ear mechanics. *Hearing Research,* 220, 67–75.

Meenderink, S. W., & van der Heijden, M. (2010). Reverse cochlear propagation in the intact cochlea of the gerbil: Evidence for slow traveling waves. *Journal of Neurophysiology,* 103, 1448–1455.

Moleti, A., Al-Maamury, A. M., Bertaccini, D., Botti, T., & Sisto, R. (2013). Generation place of the long- and short-latency components of transient-evoked otoacoustic emissions in a nonlinear cochlear model. *The Journal of the Acoustical Society of America,* 133(6), 4098–4108.

Mom, T., Telischi, F. F., Martin, G. K., & Lonsbury-Martin, B. L. (1999). Measuring the cochlear blood flow and distortion-product otoacoustic emissions during reversible cochlear ischemia: A rabbit model. *Hearing Research,* 133(1–2), 40–52.

Murphy, W. J., Talmadge, C. L., Tubis, A., & Long, G. R. (1995a). Relaxation dynamics of spontaneous otoacoustic emissions perturbed by external tones. I. Response to pulsed single-tone suppressors. *The Journal of the Acoustical. Society of America,* 97(6), 3702–3710.

Murphy, W. J., Tubis, A., Talmadge, C. L., & Long, G. R. (1995b). Relaxation dynamics of spontaneous otoacoustic emissions perturbed by external tones. II. Suppression of interacting emissions. *The Journal of the Acoustical. Society of America,* 97(6), 3711–3720.

Nobili, R., Mammano, F., & Ashmore, J. (1998). How well do we understand the cochlea? *Trends in Neuroscience,* 21(4), 159–167.

Norton, S. J., Gorga, M. P., Widen, J. E., Folsom, R. C., Sininger, Y., Cone-Wesson, B., Vohr, B. R., & Fletcher, K. A. (2000). Identification of neonatal hearing impairment: Summary and recommendations. *Ear and Hearing,* 21(5), 529–535.

Ó Maoiléidigh, D., Nicola, E. M., & Hudspeth, A. J. (2012). The diverse effects of mechanical loading on active hair bundles. *Proceedings of the National Academy of Sciences of the United States of America,* 109(6), 1943–1948.

Owens, J. J., McCoy, M. J., Lonsbury-Martin, B. L., & Martin, G. K. (1992). Influence of otitis media on evoked otoacoustic emissions in children. *Seminars in Hearing,* 13(1), 53–65.

Oxenham, A. J., & Shera, C. A. (2003). Estimates of human cochlear tuning at low levels using forward and simultaneous masking. *Journal of the Association for Research in Otolaryngology*, 4, 541–554.

Palmer, A. R., & Wilson, J. P. (1982). Spontaneous and evoked acoustic emissions in the frog *Rana esculenta*. *The Journal of Physiology*, 324, P66.

Patuzzi, R. (1996). Cochlear micromechanics and macromechanics. In P. Dallos, A. N. Popper, & R. R. Fay (Eds.), *The Cochlea* (pp. 186–257). New York: Springer-Verlag.

Prieve, B. A., Gorga, M. P., Schmidt, A., Neely, S., Peters, J., Schultes, L., & Jesteadt, W. (1993). Analysis of transient-evoked otoacoustic emissions in normal-hearing and hearing-impaired ears. *The Journal of the Acoustical Society of America,* 93(6), 3308–3319.

Probst, R., Coat, A. C., Martin, G. K., & Lonsbury-Martin, B. L. (1986). Spontaneous, click-, and toneburst-evoked otoacoustic emissions from normal ears. *Hearing Research,* 21, 261–275.

Probst, R., Lonsbury-Martin, B. L., & Martin, G. K. (1991). A review of otoacoustic emissions. *The Journal of the Acoustical Society of America,* 89(5), 2027–2067.

Puria, S. (2003). Measurements of human middle ear forward and reverse acoustics: Implications for otoacoustic emissions. *The Journal of the Acoustical Society of America,* 113(5), 2773–2789.

Rasetshwane, D. M., & Neely, S. T. (2012). Measurements of wide-band cochlear reflectance in humans. *Journal of the Association for Research in Otolaryngology,* 13, 591–607.

Reavis, K. M., McMillan, G., Austin, D., Gallun, F., Fausti, S. A., Gordon, J. S., Helt, W. J., & Konrad-Martin, D. (2011). Distortion-product otoacoustic emission test performance for ototoxicity monitoring. *Ear and Hearing,* 32(1), 61–74.

Reavis, K. M., McMillan, G. P., Dille, M. F., & Konrad-Martin, D. (2015). Meta-analysis of distortion product otoacoustic emission retest variability for serial monitoring of cochlear function in adults. *Ear and Hearing,* 36(5), 251–260.

Rhode, W. S. (1971). Observations of the vibration of the basilar membrane in squirrel monkeys using the Mössbauer technique. *The Journal of the Acoustical Society of America,* 49, 1218–1231.

Robinette, M. S., & Glattke, T. J. (2007). *Otoacoustic Emissions: Clinical Applications*, 3rd ed. New York: Thieme.

Robles, L., & Ruggero, M. A. (2001). Mechanics of the mammalian cochlea. *Physiological Reviews,* 81(3), 1305–1352.

Rosowski, J. J., Peake, W. T., & White, J. R. (1984). Cochlear nonlinearities inferred from two-tone distortion products in the ear canal of the alligator lizard. *Hearing Research,* 13, 141–158.

Ruggero, M. A., & Temchin, A. N. (2005). Unexceptional sharpness of frequency tuning in the human cochlea. *Proceedings of the National Academy of Sciences of the United States of America,* 102(51), 18614–18619.

Schairer, K. S., Fitzpatrick, D., & Keefe, D. H. (2003). Input-output functions for stimulus-frequency otoacoustic emissions in normal-hearing adult ears. *The Journal of the Acoustical Society of America,* 114(2), 944–966.

Shaffer, L. A., Withnell, R. H., Dhar, S., Lilly, D. J., Goodman, S. S., & Harmon, K. M. (2003). Sources and mechanisms of DPOAE generation: Implications for the prediction of auditory sensitivity. *Ear and Hearing,* 24(5), 367–379.

Shera, C. A. (2003). Mammalian spontaneous otoacoustic emissions are amplitude-stabilized cochlear standing waves. *The Journal of the Acoustical Society of America,* 114(1), 244–262.

Shera, C. A. (2015). The spiral staircase: Tonotopic microstructure and cochlear tuning. *The Journal of Neuroscience,* 35(11), 4683–4690.

Shera, C. A., & Zweig, G. (1993). Middle-ear phenomenology: The view from the three windows. *The Journal of the Acoustical Society of America,* 92(3), 1356–1370.

Shera, C. A., & Guinan, J. J. (1999). Evoked otoacoustic emissions arise by two fundamentally different mechanisms: A taxonomy for mammalian OAEs. *The Journal of the Acoustical Society of America,* 105(2), 782–798.

Shera, C. A., & Guinan, J. J. (2003). Stimulus-frequency-emission group delay: A test of coherent reflection filtering and a window on cochlear tuning. *The Journal of the Acoustical Society of America*, 113(5), 2762–2772.

Shera, C. A., & Guinan, J. J. (2008). Mechanisms of mammalian otoacoustic emission. In G. A. Manley, R. R. Fay, & A. N. Popper (Eds.), *Active Processes and Otoacoustic Emissions in Hearing* (pp. 305–342). New York: Springer-Verlag.

Shera, C. A., & Abdala, C. (2012). Otoacoustic emissions: Mechanisms and applications. In K. L. Tremblay & R. F. Burkard (Eds.), *Translational Perspectives in Auditory Neurocience: Hearing Across the Life Span-Assessment and Disorders* (pp. 123–159). San Diego, CA: Plural Publishing.

Shera, C. A., Guinan, J. J., & Oxenham, A. J. (2002). Revised estimates of human cochlear tuning from otoacoustic and behavioral measurements. *Proceedings of the National Academy of Sciences of the United States of America*, 99(5), 3318–3323.

Shera, C. A., Guinan, J. J., & Oxenham, A. J. (2010). Otoacoustic estimation of cochlear tuning: Validation in the chinchilla. *Journal of the Association for Research in Otolaryngology,* 11, 343–365.

Siegel, J. H., Cerka, A. J., Recio-Spinoso, A., Temchin, A. N., van Dijk, P., & Ruggero, M. A. (2005). Delays of stimulus-frequency otoacoustic emissions and cochlear vibrations contradict the theory of coherent reflection filtering. *The Journal of the Acoustical Society of America,* 118(4), 2434–2443.

Sisto, R., Moleti, A., & Shera, C. A. (2015). On the spatial distribution of the reflection sources of different latency components of otoacoustic emissions. *The Journal of the Acoustical Society of America,* 137(2), 768–776.

Stavroulaki, P., Apostolopoulos, N., Dinopoulou, D., Vossinakis, I., Tsakanikos, M., & Douniadakis, D. (1999). Otoacoustic emissions – An approach for monitoring aminoglycoside induced ototoxicity in children. *International Journal of Pediatric Otorhinolaryngology,* 50, 177–184.

Strogatz, S. H. (2014). *Nonlinear Dynamics and Chaos: With Applications to Physics, Biology, Chemistry, and Engineering*. Boulder, CO: Westview Press.

Sumner, C. J., Wells, T. T., Bergevin, C., Palmer, A. R., Oxenham, A. J., & Shera, C. A. (2014). Comparing otoacoustic, auditory-nerve, and behavioral estimates of cochlear tuning in the ferret. *Association for Research in Otolaryngology Abstracts*, 37, PD-017.

Talmadge, C., & Tubis, A. (1993). On modeling the connection between spontaneous and evoked otoacoustic emissions. In H. Duifhuis, J. Horst, P. van Dijk, & S. van Netten (Eds.), *Biophysics of Hair-Cell Sensory Systems* (pp. 25–32). Singapore: World Scientific Press.

Talmadge, C. L., Tubis, A., Wit, H. P., & Long, G. R. (1991). Are spontaneous otoacoustic emissions generated by self-sustained cochlear oscillators? *The Journal of the Acoustical Society of America,* 89(5), 2391–2399.

Talmadge, C. L., Long, G. R., Murphy, W. J., & Tubis, A. (1993). New off-line method for detecting spontaneous otoacoustic emissions in human-subjects. *Hearing Research,* 71, 170–182.

Talmadge, C. L., Tubis, A., Long, G. R., & Piskorski, P. (1998). Modeling otoacoustic emission and hearing threshold fine structures. *The Journal of the Acoustical Society of America,* 104(3), 1517–1543.

Telischi, F. F., Roth, J., Stagner, B. B., Lonsbury-Martin, B. L., & Balkany, T. J. (1995). Patterns of evoked otoacoustic emissions associated with acoustic neuromas. *Laryngoscope,* 105(7), 675–682.

Telischi, F. F., Stagner, B., Widick, M. P., Balkany, T. J., & Lonsbury-Martin, B. L. (1998). Distortion-product otoacoustic emission monitoring of cochlear blood flow. *Laryngoscope,* 108(6), 837–842.

van Dijk, P., & Wit, H. P. (1990a). Amplitude and frequency fluctuations of spontaneous otoacoustic emissions. *The Journal of the Acoustical Society of America,* 88(4), 1779–1793.

van Dijk, P., & Wit, H. P. (1990b). Synchronization of spontaneous otoacoustic emissions to a $2f_1$-f_2 distortion product. *The Journal of the Acoustical Society of America,* 88(2), 850–855.

van Dijk, P., & Wit, H. P. (1998). Correlated amplitude fluctuations of spontaneous otoacoustic emissions. *The Journal of the Acoustical Society of America*, 104(1), 336–343.

van Dijk, P., & Long, G. (2015). A comparison of psychometric functions for tone detection at and away from spontaneous otoacoustic emissions. *Association for Research in Otolaryngology Abstracts,* 38, 480.

van Dijk, P., Wit, H. P., & Segenhout, J. M. (1989). Spontaneous otoacoustic emissions in the European edible frog (*Rana esculenta*): Spectral details and temperature dependence. *Hearing Research,* 42, 273–282.

van Dijk, P., Maat, B., & de Kleine, E. (2011). The effect of static ear canal pressure on human spontaneous otoacoustic emissions: Spectral width as a measure of inter-cochlear oscillation amplitude. *Journal of the Association for Research in Otolaryngology,* 12, 13–28.

Verhulst, S., Dau, T., & Shera, C. A. (2012). Nonlinear time-domain cochlear model for transient stimulation and human otoacoustic emission. *The Journal of the Acoustical Society of America,* 132(6), 3842–3848.

Verhulst, S., Bharadwaj, H. M., Mehraei, G., Shera, C. A., & Shinn-Cunningham, B. G. (2015). Functional modeling of the human auditory brainstem response to broadband stimulation. *The Journal of the Acoustical Society of America,* 138(3), 1637–1659.

Vetešník, A., Turcanu, D., Dalhoff, E., & Gummer, A. W. (2009). Extraction of sources of distortion product otoacoustic emissions by onset-decomposition. *Hearing Research,* 256, 21–38.

Vilfan, A., & Duke, T. (2008). Frequency clustering in spontaneous otoacoustic emissions from a lizard's ear. *Biophysical Journal,* 95(10), 4622–4630.

Voss, S. E., Horton, N. J., Tabucchi, T. H., Folowosele, F. O., & Shera, C. A. (2006). Posture-induced changes in distortion-product otoacoustic emissions and the potential for noninvasive monitoring of changes in intracranial pressure. *Neurocritical Care*, 4, 251–257.

Walsh, K. (2012). *Nonlinear Cochlear Responses Differ During Selective and Inattentive Listening*. PhD Thesis, University of Texas at Austin.

Weiss, T. F., & Leong, R. (1985). A model for signal transmission in an ear having hair cells with free-standing stereocilia. IV. Mechanoelectric transduction stage. *Hearing Research*, 20, 157–174.

Whitehead, M. L., Kamal, N., Lonsbury-Martin, B. L., & Martin, G. K. (1993). Spontaneous otoacoustic emissions in different racial groups. *Scandinavian Audiology,* 22(1), 3–10.

Whitehead, M. L., Stagner, B., Martin, G. K., & Lonsbury-Martin, B. L. (1996). Visualization of the onset of distortion-product otoacoustic emissions, and measurement of their latency. *The Journal of the Acoustical Society of America,* 100(3), 1663–1679.

Wit, H. P. (1986). Statistical properties of a strong otoacoustic emission. In J. Allen, J. L. Hall, A. E. Hubbard, S. T. Neely, & A. Tubis (Eds.), *Peripheral Auditory Mechanisms* (pp. 221–228). Berlin Heidelberg: Springer-Verlag.

Wit, H. P., & van Dijk, P. (2012). Are human spontaneous otoacoustic emissions generated by a chain of coupled nonlinear oscillators? *The Journal of the Acoustical Society of America,* 132(2), 918–926.

Wit, H. P., van Dijk, P., & Manley, G. A. (2012). A model for the relation between stimulus frequency and spontaneous otoacoustic emissions in lizard papillae. *The Journal of the Acoustical Society of America,* 132(5), 3273–3279.

Zurek, P. M. (1981). Spontaneous narrowband acoustic signals emitted by human ears. *The Journal of the Acoustical Society of America,* 69(2), 514–523.

Zweig, G. (1976). Basilar membrane motion. *Cold Spring Harbor Symposium on Quantum Biology,* 40, 619–633.

Zweig, G. (1991). Finding the impedance of the organ of Corti. *The Journal of the Acoustical Society of America,* 89(3), 1229–1254.

Zweig, G. (2003). Cellular cooperation in cochlear mechanics. In A. W. Gummer (Ed.), *Biophysics of the Cochlea: From Molecules to Models* (pp. 315–329). Hackensack, NJ: World Scientific Publishing Co.

Zweig, G. (2015). Linear cochlear mechanics. *The Journal of the Acoustical Society of America,* 138(2), 1102–1121.

Zweig, G., & Shera, C. A. (1995). The origin of periodicity in the spectrum of evoked otoacoustic emissions. *The Journal of the Acoustical Society of America,* 98(4), 2018–2047.

Zweig, G., Lipes, R., & Pierce, J. R. (1976). The cochlear compromise. *The Journal of the Acoustical Society of America,* 59, 975–982.

Zwicker, E. (1986a). A hardware cochlear nonlinear preprocessing model with active feedback. *The Journal of the Acoustical Society of America,* 80(1), 146–153.

Zwicker, E. (1986b). "Otoacoustic" emissions in a nonlinear cochlear hardware model with feedback. *The Journal of the Acoustical Society of America,* 80(1), 154–162.

Zwicker, E., & Schloth, E. (1984). Interrelation of different otoacoustic emissions. *The Journal of the Acoustical Society of America,* 75(4), 1148–1154.

Chapter 11
Localized Internal Stimulation of the Living Cochlea Using Electrical and Optical Methods

Karl Grosh

Abstract In this chapter, methods to locally stimulate the complex and fragile microstructures of the living cochlea in a repeatable, nondestructive, and quantifiable manner are described. Electrical stimulation of the intracochlear fluids causes the sensory epithelium of the cochlea to vibrate and sound to be emitted from the ear canal. Different strategies for localized electrical stimulation are presented along with advantages and disadvantages of each approach. The basilar membrane and reticular lamina motion in response to electrical excitation along with the dependence of the response on stimulation location and exposure to pharmacological agents known to affect hearing are shown. The active electromechanical function of the cochlea is necessary for proper function. These results provide insights into the interaction of outer hair cell-generated forces and the dynamics of the surrounding structures of the cochlea and fluid. Optical means for locally exciting the cochlea using an ultrafast laser pulse are also presented. The basilar membrane response to this spatially confined stimulation shows that the active enhancement of the response cannot be initiated instantly by a localized force applied to the basilar membrane but rather requires the presence of a forward traveling wave to effectively engage this process. Electrical and optical stimulation uncover features of the cochlear response not addressable by normal acoustic stimulation. These experiments have not only uncovered fundamental global and local characteristics of the cochlea but also have pointed out gaps in the existing knowledge and the need for further investigation.

Keywords Basilar membrane vibration · Cochlear mechanics · Electrical stimulation · Electrically evoked otoacoustic emissions · Laser stimulation · Reticular lamina vibration

K. Grosh (✉)
Department of Mechanical Engineering, The University of Michigan,
3646 G. G. Brown Building, Ann Arbor, MI 48109-2125, USA
e-mail: grosh@umich.edu

K. Grosh
Department of Biomedical Engineering, The University of Michigan,
3646 G. G. Brown Building, Ann Arbor, MI 48109-2125, USA

G.A. Manley et al. (eds.), *Understanding the Cochlea*, Springer Handbook of Auditory Research 62, DOI 10.1007/978-3-319-52073-5_11

11.1 Introduction

The development of methods to locally and internally stimulate the complex and fragile microstructures of the living cochlea in a repeatable, nondestructive, and quantifiable manner has been a longstanding challenge in cochlear mechanics (probably since researchers first peered into the organ). Quite early, it was found that any local mechanical forcing gave rise to an almost immediate increase in the threshold of hearing at characteristic frequencies (CFs) at the location of the stimulation in an in vivo preparation. This is not surprising, of course, because the cochlea did not evolve to withstand mechanically opening the organ and subsequent mechanical loading of the structures. This vulnerability combined with the inaccessibility of most parts of the cochlea have made methods for achieving spatially confined in vivo mechanical forcing nearly impossible. Hence, methods for locally and focally exciting the cochlea have required a more indirect approach. In this chapter, methods for stimulating the cochlea optically or electrically will be presented along with the existing limitations and future approaches as a method for exciting the cochlea in a controlled manner. Such localized stimulations probe the operating principles of the cochlea in two main ways.

First, disturbances propagate along the sensory epithelium away from the local force, displaying the emergent behavior of the organ in response to a stimulus very different from that via the normal auditory path. Using the response from internal stimulation for answering questions about the system-level response of the cochlea has come to the fore as localized intracochlear active processes mediated by outer hair cells (OHCs) were discovered (Brownell et al. 1985; discussed by Santos-Sacchi, Navaratnam, Raphael, and Oliver, Chap. 5) and their importance for normal cochlear function confirmed (Liberman et al. 2002; Dallos et al. 2008). Furthermore, otoacoustic emissions, whose use as a diagnostic clinical tool is widespread (see Bergevin, Verhulst, and van Dijk, Chap. 10), are generated from nonlinear interactions within the cochlea that then propagate to the outer ear. Intracochlear forcing quantifies the manner in which sound leaves the cochlea, with the ultimate objective of specifically understanding the physiological correlation of the emitted sound to either pathology or normal function. At the same time, local stimulation of the cochlea is a source of excitation independent from normal acoustic excitation. The responses to these stimuli can challenge different hypotheses of cochlear function, which may have been developed using only responses to external acoustic stimulation as a basis for hypothesis formation. If electromechanical force is applied to the sensory epithelium by the OHCs, what is the precise local deformation and global wave propagation arising from this localized internal force from within the organ of Corti? The answer to this question has been sought using light and electrical stimulation. Intracochlear stimulation holds the promise of not only accelerating the science of hearing but also of enriching the information obtained from clinical tools.

Second, these focal stimuli enable a more reductionist lens for viewing the response of the organ of Corti and the sensory epithelium. In the time domain, the

immediate, short-time response (<100 μs after the stimulus is applied) represents the local transfer function rather than the emergent response of the cochlea as a whole. Alternatively, by driving the system at frequencies higher than the local CF, a local analysis of the structures is likewise possible because the wave propagation at these higher frequencies is evanescent (in the longitudinal direction along the length of the cochlea). Determining the in situ electromechanical localized behavior of cells enables a link to measurements from a living animal to those measured in isolated, in vitro configurations. The key question to answer here is, Are the experimental measurements on isolated cells or excised cochlear preparations, such as temporal bone or hemicochlear preparations, recapitulated in the intact cochlea? As highlighted in this volume, measurements of the structure and function of individual cells, extracellular fluids, and extracellular materials have and continue to provide insights to normal hearing and pathology. These studies have revealed important contributors to the mechanical, electrical, and chemical functions even though the organ itself is severely compromised or destroyed before testing. These studies involve stripping apart portions of the cochlea to study the properties of individual components, be they extracellular, such as the structurally important basilar membrane (BM; e.g., Naidu and Mountain 2001), the tectorial membrane (TM; Ghaffari et al. 2010), and reticular lamina (RL; Scherer and Gummer 2004a, b) and the electrical resistance of the cochlear fluids (Strelioff 1973), or cellular, such as inner hair cells (IHCs) and OHCs (He and Dallos 1999). Intricate isolated preparations that strike the balance between maintaining cell health and a realistic electrochemical milieu, such as replacing potassium with sodium in artificial endolymph (Kennedy et al. 2003), have allowed for cells to be isolated and survive outside the living cochlea long enough to be characterized. Using these preparations, chemoelectromechanical experimentation combined with ingenious genetic manipulation led to the discovery of prestin, the motor protein of the OHCs (Zheng et al. 2000; discussed by Santos-Sacchi, Navaratnam, Raphael, and Oliver, Chap. 5). Now, using nanoelectromechanical techniques, identification of the transduction channel is even closer as reported, for example, by Kumira et al. (2015) and Corey, Ó Maoiléidigh, and Ashmore (Chap. 4). These remarkable results on the response of individual cells and their channels represent a detailed nanomechanical analysis that still must be viewed within the setting of the entire cochlea as described by Manley and Gummer (Chap. 1) and in the framework of theories of cochlear mechanics (Corey, Ó Maoiléidigh, and Ashmore, Chap. 4; Gummer, Dong, Ghaffari, and Freeman, Chap. 6). The action of isolating the cells still modifies their chemical, mechanical, and electrical equilibrium states. Hence, measurements like those described in this chapter put these cells back into the cochlea and determine if the role implicated by single-cell or isolated measurement are verified within in the living animal's configuration. The cellular- and the organ-level measurements complement one another because they act as checks and balances, avoiding entrenchment that may come from looking at the cochlear behavior through only one point of view.

11.2 Localized Electrical Excitation of the Cochlea

11.2.1 Overview

Hubbard and Mountain (1983) discovered that applying a sinusoidal current to a stimulating electrode in the scala media (SM) (referenced to a return electrode in the neck) would elicit robust acoustic emission called an electrically evoked otoacoustic emission (EEOAE). This finding coupled with the discovery of OHC electromotility spurred the use of EEOAEs by a number of other groups (e.g., Ren and Nuttall 1995; Xue et al. 1995; Kirk and Yates 1996) to explore electromotility in the cochlea. Two example configurations for electrically stimulating the cochlea are shown in Fig. 11.1.

As shown in Fig. 11.2a, a central finding was that the upper frequency of emissions arising from intracochlear electrical current injection was dictated by the location of the electrode (the more apical the electrode, the more bandlimited the emission; Kirk and Yates 1996; Nuttall et al. 2001). This indicated that the current spread away from the intracochlear source is minimal and showed promise that such stimulation can be used as a local interrogator of cochlear function near the stimulating electrode. In Fig. 11.2b, the phase was found to depend on the location of the electrode as well, although that dependence was not monotonic, as discussed in the caption. When the measurement and stimulus were collocated, the intracochlear electrical stimulation evoked a BM velocity that showed a multipeaked response at the CF (Figs. 11.3, 11.4, 11.5) along with a robust high-frequency response (well above the CF, as shown in Figs. 11.4 and 11.5). In Fig. 11.3a, the amplitude response of the BM to electrical stimulation was very different from that of the RL, especially at low frequencies where the RL amplitude was at least 10 times greater. Near the CF (45–55 kHz), the RL motion was only three times greater than that of the BM and the RL and BM phases nearly overlapped. The diversity of information that can come from local electrical stimulus is demonstrated by He and Ren (2013), where the BM velocity response to distant electrical stimulus was shown to possess only a single peak at the CF of the measurement location (Fig. 11.6c, e). Next, the underlying approach to performing these experiments and a more detailed description of the results are discussed along with limitations.

11.2.2 Experimental Approach

The rationale behind various stimulus strategies is presented here along with an outline of the experimental methods used. More details can be found in Ren and Nuttall (1995), Zheng et al. (2007), and He and Ren (2013).

For intracochlear bipolar stimulation, fenestrae are created in the walls of the scalae of the cochlea, the scala tympani (ST) and scala vestibuli (SV) or the bony

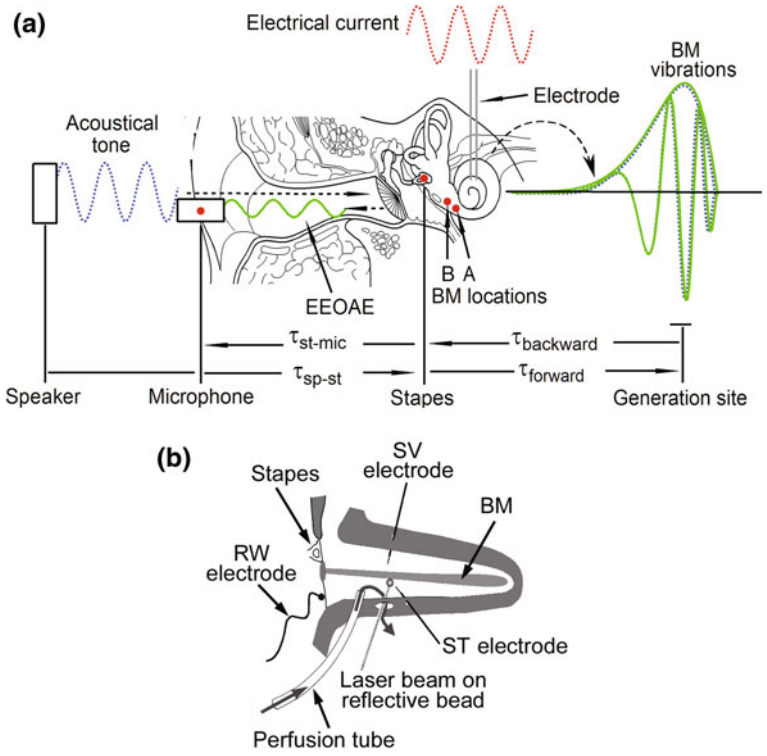

Fig. 11.1 **a** Schematic of a test setup to measure basilar membrane (BM) velocity and acoustic emissions evoked by an electrode pair placed in the second turn. The BM velocity was measured at two locations (**A**, **B**) through an opened round window (RW) at this location. To calculate intracochlear delay using electrically evoked optoacoustic emissions (EEOAEs), the time delay (τ) from stapes to microphone ($\tau_{st\text{-}mic}$) was subtracted from the microphone to electrical stimulus transfer delays to provide the correct timing. The BM velocity response to acoustic stimulation was also measured along with the time delay from speaker to stapes ($\tau_{sp\text{-}st}$) to provide the correct phase reference for intracochlear delay. Reproduced from He and Ren (2013), under Creative Commons License 3.0. **b** Simplified (uncoiled) rendition of the cochlea showing one configuration for local intracochlear or RW electrical stimulation. The local BM velocity was measured using a laser Doppler vibrometer. The scala tympani (ST) opening for the laser was also used to as the exit for the perfusate introduced via a small perfusion tube inserted in a separate fenestra. *SV* Scala vestibuli. From Zheng et al. (2007)

wall near the scala media (SM), to introduce the electrodes, allow for optical access for vibration measurement, and (sometimes) enable drug perfusion. Bipolar intracochlear stimulation was used and consisted of one of three strategies: (1) ST-SV, (2) ST-SM, and (3) ST-ST. The ST-SV electrode configuration is exemplified in Fig. 11.1b. In this case, two openings of $\sim$75 μm in diameter are made to insert the SV and ST electrode wires [50 μm platinum-iridium (Pt-Ir)] into the perilymph to form a bipolar pair across the cochlear duct in the first turn (Fig. 11.1b). For the ST-SM electrode configuration, as described by He and Ren (2013) and Ren et al.

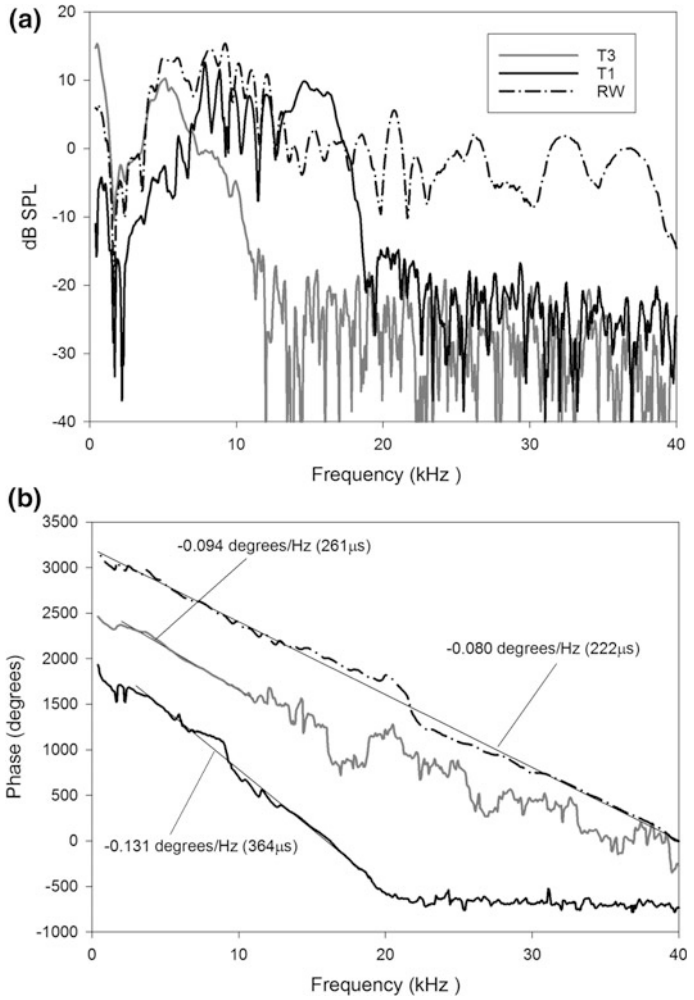

Fig. 11.2 **a** The EEOAE measured with an ear canal microphone and stimulated from three different electrode positions: the RW, the first turn (T1), and the third turn (T3). T1 and T3 data were evoked using a dipole-like ST–ST electrode configuration placed close to the BM. The ground electrode for the RW spectrum is located in the neck muscles. Each location was stimulated with 35 μA_{rms}. The amplitude of the transfer function was a function of the location of the electrode, with the more apical locations having a lower maximum EEOAE frequency. SPL, sound pressure level. **b** The phase slopes of the phase spectra are a function of tonotopic position. RW and T1 phase relationships were very consistent from animal to animal (the standard deviation was <18 μs in the delay). The slope of the T3 evoked emission was less consistent, sometimes (as in this example) having a smaller delay than the T1 evoked emission. The CF at the T1 location is around 17 kHz, whereas that for the T3 location is near 1 kHz. From Nuttall et al. (2001)

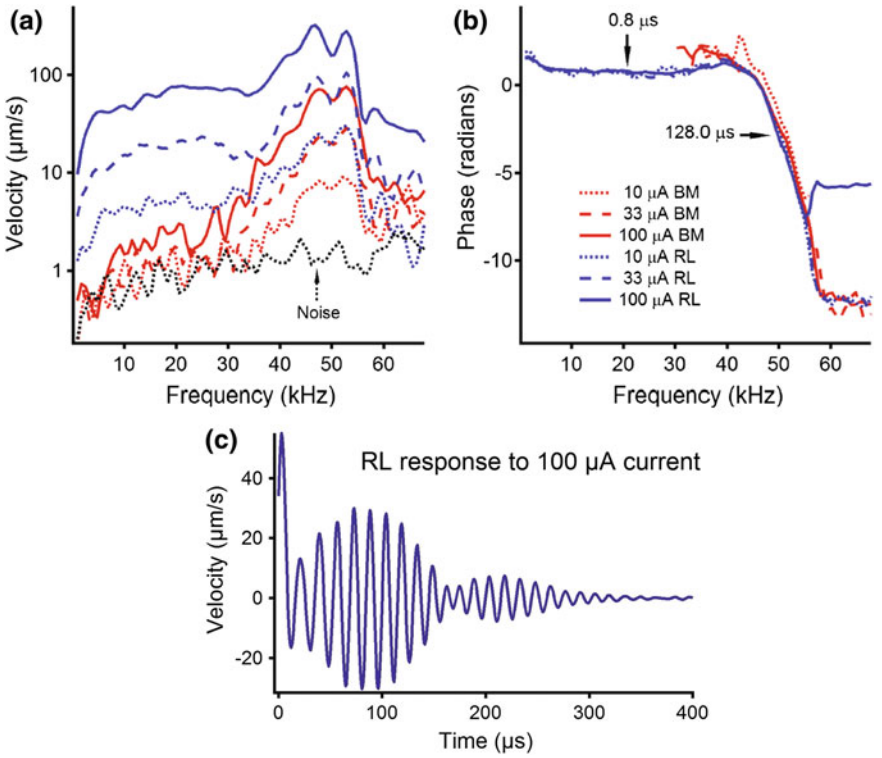

Fig. 11.3 Amplitude (**a**) and phase (**b**) of the velocity of the RL (*blue*) and BM (*red*) relative to current injection in a wild-type mouse measured using low-coherence heterodyne interferometry. The striking broadband response of the RL indicates the relative stiffness of the RL compared with that of the BM as actuated by the outer hair cells (OHCs; the BM is stiffer). **c** Inverse Fourier transform of the reticular lamina (RL) velocity due to 100-μA current shows an immediate impulse (~15 μs in duration) and subsequent delayed response in the sensitive animal. The echo (or second-wave packet) in the time response is a hallmark of a sensitive preparation. The BF at this location is 48 kHz and positive motion is toward the ST for both the RL and BM recordings. Reproduced from Ren et al. (2016), under Creative Commons License 4.0. Thanks to Dr. Ren for modifying the figures from displacement responses to the velocity as shown here

(2016), two holes <50 μm in diameter are drilled, one in the ST (e.g., a Pt-Ir wire inserted with the tip close to the BM) and one in the SM at the same longitudinal location. Placement of the SM electrode requires great care in this instance, as described by Ren et al. (2016), where the opening in the bony wall at the SM never penetrated into the soft tissue to avoid damage to the stria vascularis during electrode insertion. In the third configuration, the ST–ST stimulation, both the return and supply electrodes are placed in the ST. Such a bipolar stimulation paradigm is similar to that used for cochlear implants. One means to realize the ST–ST electrode configuration is to create a single 50-μm hole and insert two 25-μm wires subsequently positioned near the BM (Nuttall et al. 2001). These three approaches to

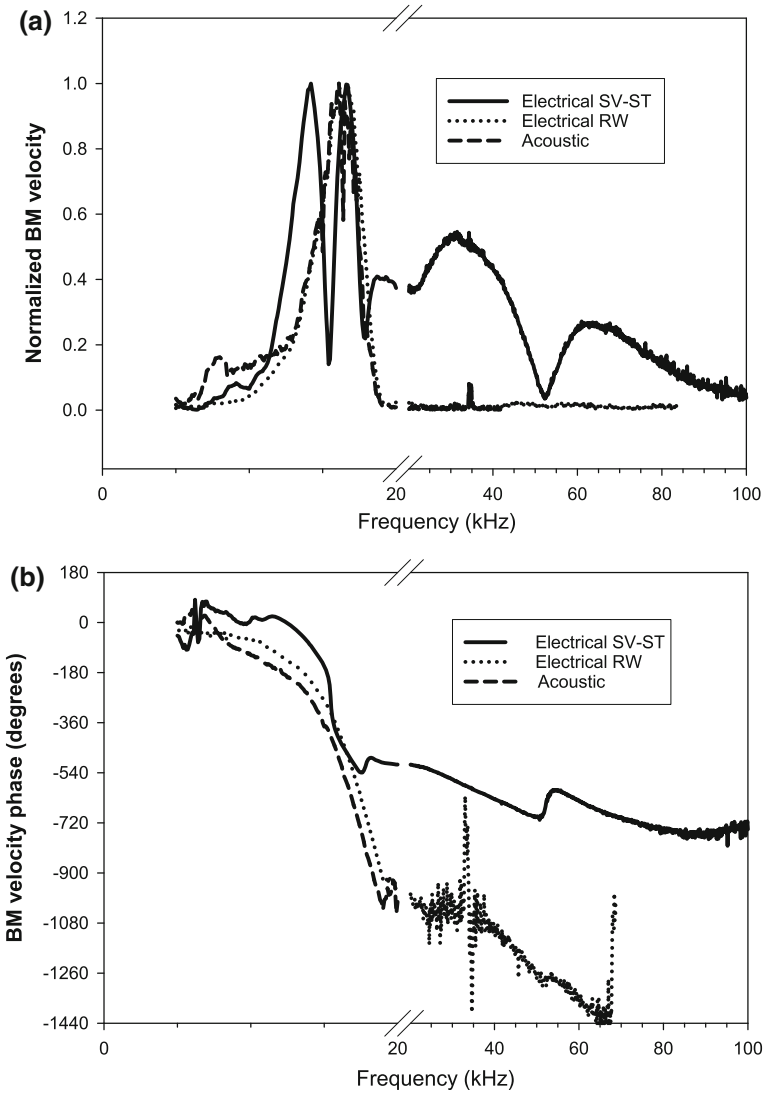

Fig. 11.4 Normalized velocity amplitude (**a**) and phase (**b**). In each case, the amplitude is normalized to the maximum response to acoustic, RW electrical, and local electrical (SV-ST) stimulation. In the case of electrical stimulation, the voltage sent to the constant-current generator serves as the reference for the phase and the velocity was normalized to the applied current. In response to bipolar electrical stimulation, the BM response is seen to extend up to 100 kHz. An expanded scale of 5 kHz per tic mark is used for frequencies below 20 kHz. The CF for this location is 17 kHz. Reproduced from Grosh et al. (2004), with permission from the Acoustical Society of America

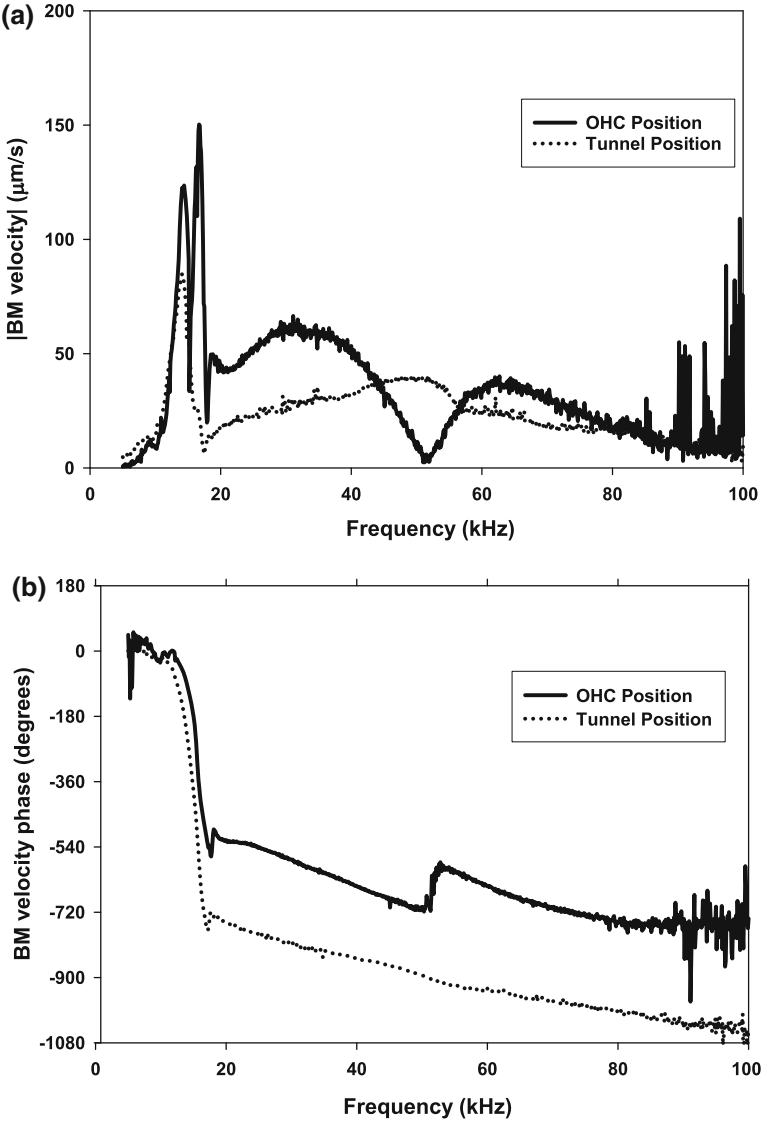

Fig. 11.5 BM velocity amplitude (**a**) and phase (**b**) in response to local electrical stimulation (bipolar electrode placed across the SV/ST). These data are from the tunnel and OHC radial locations on the BM of GP483 at the 17-kHz location. The BM velocity is seen to depend on the radial location. Reproduced from Grosh et al. (2004), with permission from the Acoustical Society of America

electrical stimulation represent a compromise between achieving a localized electrical stimulation while maintaining the sensitivity of the preparation. An ideal approach would be to place one electrode in the SM close to the apical pole of the

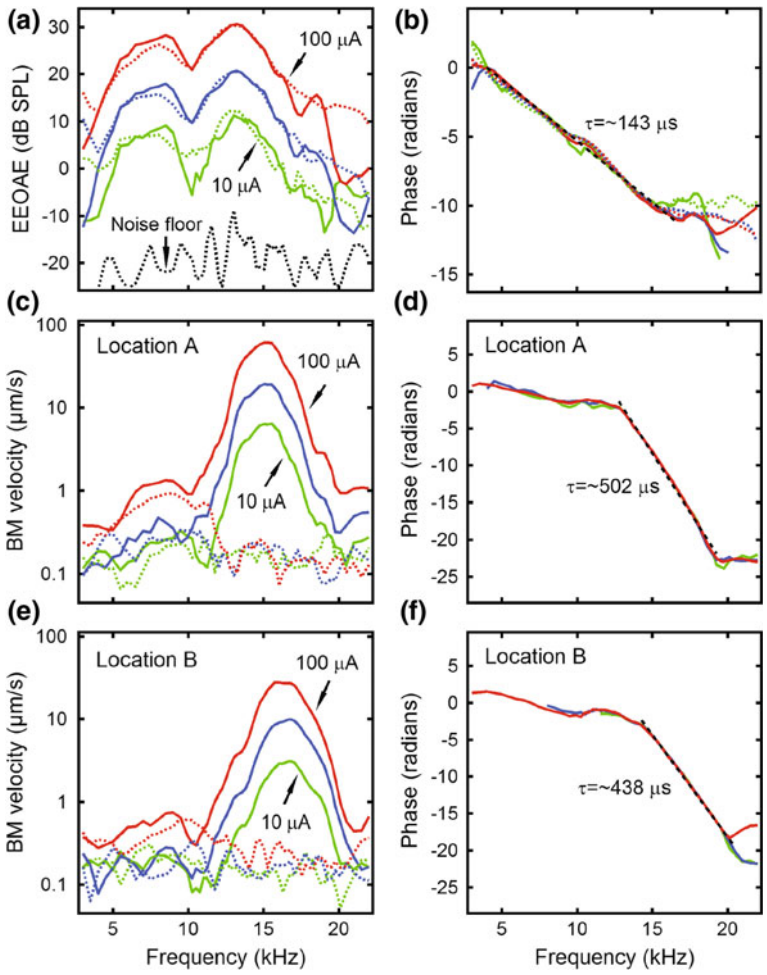

Fig. 11.6 EEOAE pressure amplitude (**a**) and phase (**b**) using the configuration shown in Fig. 11.1a. Amplitude and phase of the BM velocity at locations A (**c**, **d**) and B (**e**, **f**) for the case where the electrical stimulation is distant from the measurement location (note that location B is the closest to the stapes). *Solid lines* normal response, *dashed lines* for postmortem. *Red*, *blue*, and *green colors*, represent 100-, 33-, and 10-μA current levels, respectively. Phase is relative to current (subtraction of the delays associated with in-air propagation is described in Sect. 11.2.3.2) and positive motion is toward the ST. These curves demonstrate the relatively small changes in the EEOAE after death (other than removal of some fine structure) while the BM velocity changes dramatically after death. Furthermore, the delays seen in (**d**) and (**f**) indicate that the majority of the energy contained in the 15- to 20-kHz band arrives as a forward rather than reverse traveling wave. Separation of location A from location B is 106 μm (Tianying Ren, personal communication). Results are for the Mongolian gerbil. Reproduced from He and Ren (2013), under Creative Commons License 3.0

OHCs and the other in the ST near the BM and the basal pole of the OHCs. However, because disrupting the stria vascularis typically renders the preparation insensitive (possibly by reducing the endocochlear potential), repeatable insertion of an electrode into the SM while maintaining the sensitivity of preparation has thus far been elusive; hence this approach is not feasible for a reasonable experimental yield.

Extracochlear electrode placement can also be used as it minimizes or eliminates the need for opening the cochlea. The most popular is the round window (RW)-neck configuration because no openings in the cochlea are needed to affect this stimulation (Halsey et al. 2005; Drexl et al. 2008). Another alternative configuration is to pair a single SV electrode with the RW electrode as the return (Hu et al. 2005). In either case, the longitudinal current spread is greater than that for a completely intracochlear electrode pair because the return electrode is distant (either on the order of centimeters for the RW-neck configuration or millimeters for the SV-RW configuration). The spacing for the intracochlear electrode pairs is typically on the order of a few hundred micrometers (Nuttall et al. 2001; He and Ren 2013), thereby limiting the spread of current.

To allow for measurement of the BM velocity using traditional laser Doppler vibrometry (LDV), one opening $\sim$300 μm wide was made on the ST side of the cochlear basal turn (Parthasarthi et al. 2003). The RW has also been used as an optical window for mechanical measurements (Lukashkin et al. 2005), especially for experiments in mice (Russell et al. 2007; Ren et al. 2016). Sometimes, when drug perfusion is intended, a fourth opening is created (usually $\sim$70 μm in diameter) into which a small plastic tube can be used for passing the drugs. The larger hole for BM velocity measurements is used as the fluidic exit port for the drug (Zheng et al. 2007).

Naturally, the descriptions in this section are meant to provide a basis for understanding the experimental configurations in this chapter. Deviations from these approaches are possible. For example, techniques now allow for imaging through the cochlear wall itself (Lee et al. 2015), eliminating the need for a large cochleostomy for optical access. Also, a glass electrode can be used instead of a metal one (Kirk and Yates 1996).

Creating three or four openings in the cochlea presents a serious challenge because the trauma of the surgery holds the potential to significantly reduce the sensitivity at the measurement location. In a very good preparation of this kind, it is possible to have less than a 10-dB reduction in the compound action potential (CAP) threshold at the CF of the location of the surgery. However, a postsurgical 20-dB threshold shift is not unusual. The CAP measured from the RW electrode, with reference to a ground electrode in the soft tissues of the neck, is typically used to obtain information on the CAP threshold at a given acoustic frequency.

BM velocity measurement can be accomplished with commercially available LDVs, although custom-made interferometers (Lukashkin et al. 2005) can also be used. The laser beam of the LDV is directed through a compound microscope at a glass beads ($\sim$20 μm in diameter) placed onto the BM (Fig. 11.1). Finally, methods of optical coherence tomography (OCT) can be used to measure the

velocity of not only the BM but also the RL and the TM. OCT can be used with (Zha et al. 2011) or without (Lee et al. 2015) creating an opening in the cochlear wall. Recently, Ren et al. (2016) solved the technical difficulties of simultaneously using a scanning low-coherence heterodyne interferometer with electrical stimulation of the cochlea. This breakthrough allows for measuring the response of the BM and the RL to electrical *and* acoustic stimulation, holding significant promise to uncover the role of electromechanics in hearing.

11.2.3 Effects of Electrical Stimulation of the Cochlea

11.2.3.1 Cochlear Velocity Response at the Location of the Electrical Stimulus

Figure 11.4 shows the BM velocity response for three cases: (1) acoustic stimulation in the ear canal, (2) 35-μA root-mean-square (RMS) electrical stimulation at the RW, and (3) 100-μA RMS local bipolar electrical stimulation (Grosh et al. 2004). For acoustic stimulation (case 1), the velocity amplitude response of the BM is tuned and has a peak at ∼17 kHz, the CF for this cochlear location. For frequencies above the CF, the response falls to the noise floor (Fig. 11.4a, *dashed curve*). The corresponding phase response (Fig. 11.4b) shows a pattern of increasing phase lag that is characteristic of a traveling wave. For electrical stimulation from the RW-neck electrode pair (case 2), the pattern of response is similar to that for acoustic stimulation. This result confirmed earlier findings that electrical stimulation near the base of the cochlea results in forward propagating traveling waves on the BM (Nuttall and Ren 1995). In contrast, the response measured at the same location as the intracochlear bipolar electrical stimulation (case 3) produces a markedly different response (Fig. 11.4, *solid curves*). This amplitude-response curve has both a more complex multipeaked pattern near the CF and is detectable up to at least 100 kHz, the maximum stimulus frequency in these experiments. This response naturally decomposes into a high-frequency region (well above the CF; frequencies >20 kHz for this preparation) and a lower frequency region (near CF and below CF), each discussed in the sequel.

Response for Frequencies Near the CF and Below

In this frequency region, the amplitude response of the BM showed so-called "fine structure." Sometimes, as in Fig. 11.4a, a pronounced single notch was found. Although in others, such as the mouse data shown in Fig. 11.3a and some of the guinea pig response curves in Zheng et al. (2007), the fine structure more resembled undulations without a sharp null between the peaks. In all data, the BM response fell nearly to the noise floor ∼1 octave below the CF (30 kHz in mice and 9 kHz in guinea pigs). In both guinea pigs (Fig. 11.4b) and mice (Fig. 11.3b), the phase

accumulation induced by local electrical stimulation is lower than that induced by acoustic stimulation for frequencies below the CF. This lower phase accumulation is indicative of interference of multiple wave types (as would arise from a combination of standing waves, traveling waves, and local forced responses), resulting in a lower phase shift than for acoustically induced forward traveling wave alone. Near the CF, the rate of BM phase accumulation is similar to that induced by a normal acoustic input.

Because of its greater amplitude response compared with that of the BM, the RL velocity data provide a new window into low-frequency organ of Corti behavior. As seen in Fig. 11.3a, at low frequencies (between 10 and 40 kHz in the mouse), the RL velocity in response to a constant-amplitude current is nearly constant and $\sim 40°$ phase shifted from the current. The RL velocity response shows a very broadband low-frequency behavior. This is similar to what one expects for the lightly loaded OHC electromechanical transducer as measured by Frank et al. (1999) who found a flat displacement response from 100 Hz to 18 kHz due to a constant-voltage applied using the micropipette technique. They also showed a near-constant isometric force generation out to at least 50 kHz. The proportionality of the RL velocity to current (and *near* phase matching) may simply result from the excitation frequency exceeding the RC cutoff frequency of the OHC soma. However, such a simple model does not directly explain the 40° phase shift. Hence it is likely that the in vivo situation is more complicated.

Over the 10- to 40-kHz frequency range, the group delay is less than 1 μs; hence, under an impulsive electrical excitation, there is a significant arrival of low-frequency energy almost instantaneously. This can be seen quite clearly in Fig. 11.3c, where the time course of the RL velocity was obtained by performing the inverse Fourier transform of the velocity frequency response. For a linear system, this inverse Fourier transform represents the impulse response function. As noted in Ren et al. (2016), the response to 100-μA stimulation is very nearly three times that due to 33 μA over the entire frequency range, indicting near linearity over this level of current stimulation. The short-time behavior is composed of an initial large impulsive peak (which decays after ~ 15 μs), after which an oscillatory response of increasing frequency and longer delay is immediately evident (Fig. 11.3c). The initial peak is driven by the large current passing through the cochlear partition (much larger than usual transduction currents). After this 15-μs peak passes, the transduction current will be induced by mechanoelectrical transduction (MET) channel sensitivity and not by direct external stimulus. Hence, the electromechanical forces generated by the OHCs are smaller than those during the initial phase when the electrical current is applied. For very sensitive preparations, a secondary velocity response or ringing, as seen around 200 μs in Fig. 11.3c, is often present in the response to a short transient excitation. We speculate that this ringing is due either to coherent scattering, as suggested by Shera et al. (2005), from small perturbations in the properties of the cochlea (such as the MET sensitivity or somatic electromechanical coupling) or to active processes, as suggested by Lim and Steele (2003).

For frequencies near and above the CF, the BM phase information also becomes reliable (see Fig. 11.3b), uncovering possibly the most striking result of the Ren et al. (2016) paper. The RL and BM are in phase at these frequencies, indicating that they move together. This is contrary to a quasi-static viewpoint of the motion where one would expect the electrically induced motion of the OHC to push its apical and basal poles in opposite directions. Again, it is instructive to think of the response in the time domain. The group delay for energy above the CF is 120 μs (see Fig. 11.3b), well after the initial input current. This means that long after the extinction of the stimulating electrical impulse, a wave packet whose frequency content is near the CF will arrive at the measurement location (which is also the excitation location). Given this large delay, the response of the RL and BM are quite similar to an acoustically excited wave. In addition, around the CF, the structures of the organ of Corti are likely above their resonance, in which case driving forces can be out of phase with the motion of the structures (as in the case of a simple single degree of freedom system and as described in the context of cochlear mechanics in Gummer et al. 1996, Fig. 4). It is noteworthy that the peak response amplitude of the BM and the RL to electrical and acoustical stimulation in the base of the mouse occurs at the same frequency (Ren et al. 2016). This is different from the result of Chen et al. (2011) who showed that for guinea pigs, the peak response of the RL to acoustic stimulus occurred at a higher frequency than for the BM at the same location.

The interference of the multiple components due to wave propagation complicates interpretation of the local mechanics at the measurement location. In a temporal bone preparation, Gummer et al. (1996) used electrical excitation to find local amplitude minima and phase shifts around the CF as resonances in the TM and BM. This is one possible interpretation. There is no doubt that the local structural modal nature of the organ of Corti and TM is involved. Over the third row of OHCs, a notch, which could represent an antiresonance, is often seen to sit between the two peaks, one at the acoustical CF and another at a frequency nearly 0.5 octave below the CF (Figs. 11.4, 11.6). A less dramatic feature was seen in mice (Fig. 11.3a). A model that treats the BM, organ of Corti, and TM structures as a locally reacting (i.e., no longitudinal stiffness) two or more degree of freedom mechanical oscillator (Allen 1980; Ramamoorthy et al. 2007) predicts that OHC forcing of the TM and BM will possess a zero in the transfer function at the uncoupled resonance frequency of the TM (effective mass of TM combined with the effective stiffness of the TM and organ of Corti). If the cochlea were that simple, then the zero in the BM response would precisely locate the resonance of the TM. However, there is longitudinal stiffness in the cochlear structures, as modeled in Meaud and Grosh (2010), along with fluid-structure wave interference. Therefore, the complex behavior near the CF remains unresolved. Further modeling and analysis of measurements combining electrical stimulation with micromechanical measurements, such as in Ren et al. (2016), should enable identification of the in vivo electromechanical operational characteristics of the organ of Corti to determine if the complex behavior near the CF is due to local electromechanical forcing, reverse propagating waves (fast and slow), and actively generated forward propagating waves (as proposed by Li and Grosh 2012).

High-Frequency Response

A remarkable high-frequency (up to 4 times the CF) response of the BM velocity was consistently measured in several studies (Grosh et al. 2004; Hu et al. 2005; Zheng et al. 2007), with little animal-to-animal variation; this has not yet been measured in other species. The amplitude response at this radial location (over the third row of OHCs) and longitudinal location in the first turn of the guinea pig, ~4 mm from the stapes, shows a dip near 50 kHz and an approximate 180° phase reversal. The electrically evoked high-frequency response was present on all flexible portions in the radial direction of the BM. For instance, in the magnitude (Fig. 11.5a) and the phase (Fig. 11.5b) of the BM velocity over the third row of OHCs are compared with those measured over the tunnel region at the 17-kHz place (using two beads on the BM of the same animal). The velocity measured at the tunnel region presents an amplitude maximum at 50 kHz and only a small phase shift in this frequency region. This type of spatially varying amplitude and phase response is indicative of the interaction of two vibration modes. The fact that the presence or absence of the amplitude minimum/180° phase shift depended on radial position is consistent with the two superposition modes, the first whose motion is in-phase as a function of the radial coordinate and a second whose spatial pattern consists of a nodal line on the structure separating two out of phase lobes (think of the second mode of a simply supported string or of a beam). For the radial portion of the BM where the lobe of the second mode is in phase with the fundamental mode, no dip will occur (Fig. 11.5a), whereas the radial portion that is out of phase will present a spatially dependent dip. The minimum is determined by the forcing function, the modal participation, the spatial pattern of the modes, and the resonance frequencies. These factors are influenced by the mechanical properties of the organ of Corti. Perfusion of chlorpromazine, an agent known to alter the stiffness of the OHC, was found to reversibly shift the dip frequency (Zheng et al. 2007).

11.2.3.2 Cochlear Velocity Response Distant from the Electrical Stimulus

An important question is whether forward or backward propagating waves dominate the BM velocity response to a distant stimulus. In an effort to answer this question, He and Ren (2013) used ST-SM stimulus electrodes located in the second turn (CF ~ 3–8 kHz; Müller 1996) of the Mongolian gerbil and measured the BM velocity response at two locations in the first turn (in Fig. 11.1a, locations A and B are separated by a few hundred micrometers in the longitudinal direction and the most apical location, A, is at least 3 mm from the electrode location; Plassmann et al. 1987). Two measurement locations are needed to infer the direction of propagation. Intracochlear electrical stimulation gives rise to both evoked acoustic emissions in the ear canal (Fig. 11.6a, b) and to velocity emissions on the BM at locations distant to the stimulating electrodes (Fig. 11.6c–f); the velocity response is discussed first. When the electrical stimulation is distant, as in Fig. 11.6c–f, the BM response

pattern is quite different from the case in which the excitation and the response are collocated (Figs. 11.3, 11.4, 11.5). In He and Ren (2013), the only paper for which the BM velocity response to remote intracochlear stimulation is reported in a living cochlea, the phase between the two measurement locations is similar to that of a forward propagating wave generated by an external acoustic source. The BM velocity displays a peak response at the CF for both locations (Fig. 11.6c, e) along with a lower peak around 7.5 kHz but no high-frequency (above the CF) response. The peak near the CF is physiologically vulnerable, decreasing by two orders of magnitude under postmortem conditions. The lower frequency response did not change appreciably postmortem at either location. Consistent with this experimental result, a mathematical model by Li and Grosh (2012) predicted that a distant, apical force would generate a narrow band of frequencies where a forward propagating wave was generated (even though the force was apical to the measurement locations, as in the experiment). The theory predicted that the forward wave was locally generated by the active process, was only present near the CFs of the measurement and would disappear postmortem, consistent with the data of He and Ren (2013). That model, however, predicts a flat or negative-going phase profile for frequencies strictly less than the CF where such a reverse propagating phase profile is only indicated in the experiment at low frequencies (below 5 kHz). A phase lead at the basal measurement location, indicative of a forward traveling wave, is measured for frequencies just below the CF ($\sim$6–13 kHz; He and Ren 2013). Hence experiment and theory are not in complete agreement.

Another response measure that is distant from the stimulating electrode is the EEOAE. As mentioned previously (see Sect. 11.2.1), the EEOAE measured in the ear canal resulting from local, intracochlear electrical stimulation is bandlimited (Kirk and Yates 1996; Nuttall et al. 2001). These experiments show that the high-frequency cutoff of the EEOAE is correlated with the tonotopic place of the local electrical stimulation. For the guinea pig, as shown in Fig. 11.2, the frequency content of the EEOAE for RW electrical stimulation extends to 40 kHz; for first-turn excitation, the limit is roughly 20 kHz, and for the third-turn location, the limit is 10 kHz (Nuttall et al. 2001). The ST–ST bipolar electrodes used in Nuttall et al. (2001) are unusual in that both the supply and return are located in the same scala (ST). This dipole-like configuration appears to have been successful in enhancing the localization of the electric field. If the electrical stimulation were to spread basally from the electrode location, the evoked emissions would extend to higher frequencies by exciting the high-frequency, more basal OHCs. Unlike the EEOAE, the velocity data for local electrical stimulation in Figs. 11.4 and 11.5 show a local BM velocity response that is not bandlimited. Hence, the local mechanical response due to the OHC active process is engaged above the CF, but high-frequency disturbances (much greater than the CF) apparently are evanescent and, therefore, do not reach the ear canal at measurable levels. This is consistent with model predictions of EEOAEs (Grosh et al. 2003).

The amplitude spectra of the EEOAEs are consistent with the notion of a localized excitation. One might then assume that the magnitude of the slope of the phase data (and delays) should increase with the distance of the electrodes from the stapes; however, the data are equivocal on this point. The slope of the phase data at

a frequency gives the group delay (referred to as the delay in this text), which is the time the center of gravity of a wave packet with energy near that frequency arrives at a location (not the first arrival time). In Nuttall et al. (2001), repeatable delay data were obtained from RW and first-turn stimulation. The mean RW EEOAE delay to the microphone for multiple animals is 186 ± 17 μs, whereas for first-turn stimulation, the delay is 308 ± 18 μs, indicating an increase in delay with distance from the stapes. However, the data for the third-turn delay have a much greater variability, where delays near 1 ms were seen in a few experiments; more frequently, delays near ∼250 μs were measured, and intermediate delays (such as 472 μs given in Nuttall et al. 2001, Fig. 3) were also measured (no mean or standard error was reported for these third-turn delays). The authors noticed that distance of the electrodes to the BM affected the delay and attributed this spread to imprecision in placing the third-turn electrode in the ST (since there was no optical access to determine the proximity of the electrode to the BM). To compute the intracochlear delay, the transit time from the sound source to the stapes must be subtracted. In the guinea pig preparation of Nuttall et al. (2001), they estimate the acoustic delay to be 133 μs (the error associated with this measurement was not given nor whether this value varied from experiment to experiment; for convenience, an error of ±17 μs is assumed), resulting in a 53 ± 24 μs intracochlear delay for the RW electrode to stimulate to stapes motion and a 175 ± 25 μs delay for the first-turn electrode to the stapes.

He and Ren (2013) measured ST-SM EEOAEs with electrodes positioned in the second turn in the gerbil (Fig. 11.6b, d, f). At frequencies from 13 kHz (just below the CF of the BM velocity measurement location) to the upper frequency measured (25 kHz), the group delay of the electrically evoked BM velocity (438 μs) was much longer than the delay of the electrically evoked acoustic emission (133 μs). This is consistent with the hypothesis that (1) a nontraveling wave is emitted from the electrical excitation, (2) this wave is reflected by the RW/stapes asymmetric boundary condition, and (3) it propagated forward as a normal traveling wave (with long delay) back to the measurement location. Note that no EEOAE for frequencies higher than the CF of the electrode location are shown in this study or in the study by Grosh et al. (2004). From the intracochlear EEOAE results of Nuttall et al. (2001), it is expected that the emission would be bandlimited. Testing that hypothesis would help in the interpretation of the results by confirming a localized electric field.

The above-cited delays include the delay associated with propagation from the stapes to the microphone ($\tau_{st\text{-}mic}$). He and Ren (2013) found $\tau_{st\text{-}mic}$ to be ∼93 μs, resulting in an intracochlear delay of ∼50 μs from the electrode pair in the second turn to the stapes. When using an ST-SV electrode pair, Nuttall et al. (2001) found a similar result, that EEOAEs have an intracochlear delay of ∼100 μs, less than the forward delay of an externally acoustically evoked wave to the electrode location (∼300 μs). However, as fast as a 50 μs delay is, it is still much slower than the ∼8 μs it would take a compressional wave to travel from the electrode location to the stapes. Although these results are clear, their full interpretation awaits a more complete multicomponent analysis of the data (or some insightful modeling); an interesting but unresolved phenomenon is occurring.

11.2.3.3 Effect of Pharmacological Intervention and Postmortem Response

To determine if the active responses are due to electromechanical action of the OHCs, sodium salicylate was introduced to the cochlear fluids, either by diffusion through the RW (Ren et al. 2016) or by intracochlear perfusion (Grosh et al. 2004). Salicylate is known to reduce OHC electromotility (Tunstall et al. 1995; Kakehata and Santos-Sacchi 1996). In Fig. 11.7, the effect of perfusion of 20 μL of artificial perilymph containing 10 mM salicylate is shown to cause almost complete elimination of the electrically evoked BM amplitude response above 20 kHz and a 10-dB reduction of the response at the CF. This effect was reversible. Ren et al. (2016) showed an even more dramatic 40-dB reduction in both RL electrically evoked responses near the CF after salicylate application (shown in Ren et al. 2016, Fig. 4). This implies that electromechanical force produced by the OHCs is the main contributor to the electrically evoked responses seen when the stimulus and measurement locations are collocated.

Electromotility of the cells is expected to be present postmortem because OHCs exhibit robust electromotility in vitro. Indeed, this was found to be the case, but there was a significant difference between the postmortem responses for the collocated and distant electrode and measurement locations. Typical results for the collocated case are shown in Fig. 11.8. The in vivo and postmortem BM velocity-response patterns above 40 kHz differ by only a small amount, whereas the response around the CF is reduced by 10 dB postmortem (similar to the salicylate intoxicated state). The dip at 50 kHz is retained in the postmortem velocity response and there is a small reduction in the high-frequency response (very different from the salicylate result where near-complete extinction is seen). Hence, this ultrasonic electromotility seems to be most influenced by the local properties of the cochlea rather than by global wave propagation or distant properties of the cochlea. The reason for this is the evanescence of the wave propagation as shown by the robust responses at frequencies above the CF near the electrodes (Fig. 11.8) as opposed to postmortem responses below the noise floor for a BM location distant from the electrodes, as shown in Fig. 11.6c–f. These local properties include the organ of Corti stiffness and mass, OHC electromechanics, and the local effects of fluid loading. As such, localized high-frequency excitation holds the potential to provide information about the local material properties of the cochlea.

When the electrodes are distant from the measurement location, the BM response is reduced by $\sim$40 dB at the CF postmortem, as shown in Fig. 11.6c, e. Hence, this remotely generated forward propagating wave depends critically on the proper function of the cochlear machinery. On the other hand, the EEOAE is not reduced by death (Fig. 11.6a), although some of the fine structure is reduced, especially at the lowest current level. The presence of the above CF EEOAEs indicates that this energy does not require the contribution of a carefully tuned active process in order to be generated (only the fine structure of the EEOAE, which is a perturbation of the backbone of the pressure spectrum in Figs. 11.2a or 11.6a). In addition to the high-frequency response of the EEOAE, it would be very

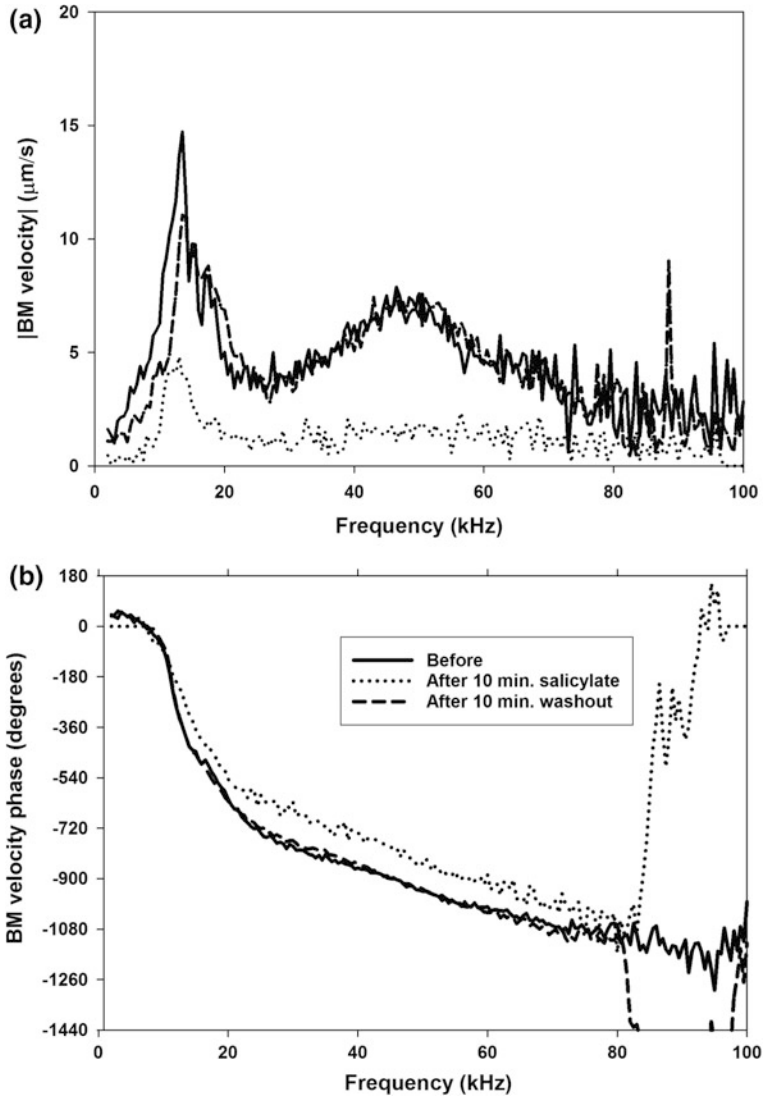

Fig. 11.7 BM velocity amplitude (**a**) and phase (**b**) in response to intracochlear electrical stimulation before, during, and after washout of sodium salicylate from the cochlea (GP 1-06-03). Salicylate reversibly reduces the motility in response to electrical stimulation. The CF for this location is 17 kHz. Reproduced from Grosh et al. (2004), with permission from the Acoustical Society of America

interesting to ascertain if the perfusion of salicylate would reduce this emitted pressure, thereby implicating mediation by the somatic OHC electromechanical transducer rather than by hair bundle-derived forcing. Similarly, the presence of

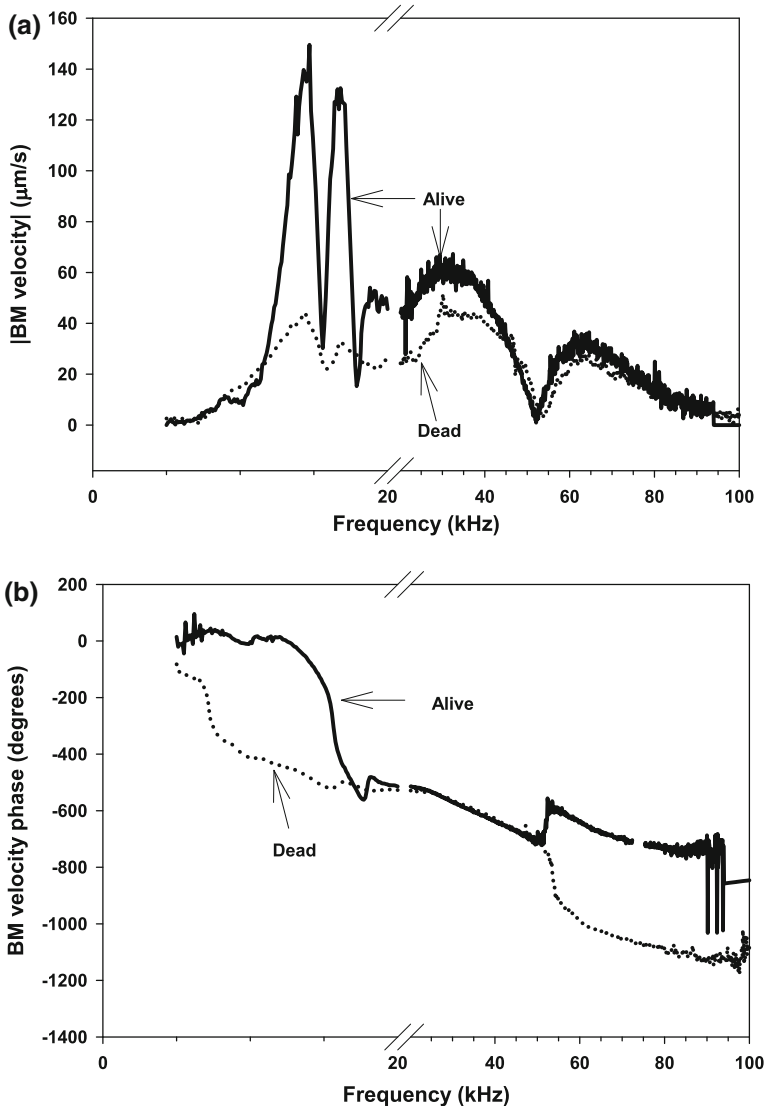

Fig. 11.8 Comparison of electrically evoked BM velocity amplitude (**a**) and phase (**b**) under postmortem and living conditions for the same animal (GP483). Results are for local electrical bipolar stimulation. An expanded scale of 5 kHz per tic mark is used for frequencies below 20 kHz. Again, the CF for this location is 17 kHz. Reproduced from Grosh et al. (2004), with permission from the Acoustical Society of America

EEOAEs in a genetically mutated mouse with a TM detached from the OHC hair bundles (the $Tecta^{C1509G/C1509G}$ mouse as studied in Ren et al. 2016) would likewise strongly point toward a prestin-based somatic active mechanism for EEOAEs.

11.2.3.4 Cochlear Velocity Response for Round Window Electrical Stimulation

Stimulation of emissions and BM velocity responses using a RW electrode paired with a distant return is often used. Some caution is needed when interpreting RW-evoked emissions. RW-evoked emissions extend up to and beyond the upper frequency of hearing for the animal. This technique has the advantage that the response to electrical stimuli can be obtained without the need for an opening. However, information about the health of the cochlea can only be determined indirectly through the emissions followed by a multicomponent signal-processing analysis. The signal has a long-delay component that is physiologically vulnerable and a short-delay component that is not vulnerable. It was a surprising finding that the elimination of OHCs through aminoglycoside treatment (Halsey et al. 2005) or prestin knockout (Drexl et al. 2008) did not completely eliminate the short-delay component of the RW EEOAE. In the Drexl et al. (2008) study, application of sodium salicylate was found to be an effective means to decrease the level of the EEOAE nearly to the noise floor in wild-type mice. In the Halsey et al. (2005) study, the electrode was chronically implanted on the perilymphatic side of the RW to enable long-term study of the effects of noise trauma (hence, this stimulation was slightly different than the usual extracochlear RW stimulation). There, the RW-evoked EEOAE fine structure was eliminated after trauma, but often the level of this smoothed, short-delay EEOAE actually increased compared with the baseline emission for reasons still unknown (Halsey et al. 2005). Drexl et al. (2008) attribute any residual EEOAE to an electrokinetic driving force and to the increased susceptibility of a more compliant organ of Corti in a prestin-knockout mouse to such stimulation, an argument that could also be applied to the effects of damage or aminoglycoside treatment.

11.2.4 Information from Intracochlear Electrical Stimulation

In a healthy cochlea, the BM vibration response due to acoustic input from the ear canal will be the sum of fluid pressure plus OHC electromechanical and other forces from the organ of Corti acting on the BM. High-frequency (above the CF) electrical excitation of the organ of Corti reveals a vibrational structure different from that for acoustical excitation. Due to the asymmetrical radial location of the OHCs, actuation of the OHCs will excite an asymmetrical structural mode. Because the asymmetrical BM mode has a higher resonance frequency than the more symmetric first mode, the excitation of this second structural mode will be more clearly detectable at higher frequencies. For acoustic input, the asymmetric mode is not as prominent for two reasons. First, the force of the fluid pressure on the BM due to acoustic input has a spatial pattern that is more uniform in the radial direction than

for excitation from the OHCs and, therefore, will preferentially excite a symmetric BM mode. Second, because the differential acoustic pressure excites this region of the BM at frequencies at and below the CF, the asymmetric modal response is low because there is very little acoustical energy input to this mode near its resonance frequency (above the CF).

Irrespective of the source of electromechanical action, intracochlear electrical stimulation serves as a mechanically noninvasive way to excite the cochlea that is complementary to acoustical excitation. The frequencies of excitation are not limited by the CF at the measurement location and the point of excitation is known. Experiments at the asymptotic tails of the cochlear response (either at high frequencies or at low frequencies relative to the CF) provide distinct opportunities. At ultrasonic frequencies, the response is dictated by local mechanical, electrical, and fluidic effects rather than global wave propagation. As such, this high-frequency excitation provides a means of interrogating the local response of a region of the cochlea as well as identifying parameters of a cochlear model that would be difficult to identify without high-frequency information. For instance, the frequency and spatial responses (mode shape) of a second structural mode would provide a measure of the local elastic and inertial properties of the organ of Corti and their contribution to the electromechanical response. Low-frequency electrical stimulation may be used to understand the electrical circuitry of the cochlea. The ability to measure the RL and BM motion concomitantly could enable in vivo measurement of the amplitude and phase between the electrical excitation and mechanical motion that would provide sufficient information to determine the RC cutoff frequency of the OHCs (or provide bounds on that frequency) or determine the presence of resonance of the TM, key elements of different hypotheses of cochlear function (Allen 1980; Ramamoorthy et al. 2007). Because these stimulation paradigms provide new information, they serve as independent tests of cochlear models. For instance, one could fit a mathematical model to match acoustical excitation and then make a prediction of the response to electrically induced motion. Although low- and high-frequency limits are interesting, the response at and near the CF is most important and most complicated. Multiple sources, including forcing from acoustic pressure and electromechanical effects along with long-delayed contributions due to reflection, comprise the overall response. Predicting this behavior from first principle models stands as a challenge.

11.3 Localized Optical Stimulation of the Cochlea with Laser Light

11.3.1 Overview

In the photoacoustic effect, laser light is absorbed, heating the material and causing an acoustic emission through its rapid expansion, subsequent rapid cooling, and

compression. Photoacoustic emission is widely used in imaging biological tissue (Wang and Hu 2012). In the cochlea, Fridberger and Ren (2006) pioneered the use of focused ultrafast laser pulses to stimulate the cochlea. This publication was followed by one (Ren et al. 2014) where focused light was used to repeatedly excite the internal structures of the living cochlea without disrupting normal function. To date, one other group has successfully used laser light to mechanically stimulate the cochlea (Zhang et al. 2009). However, this was in an in vitro preparation. Both groups were able to elicit motion of cochlear tissues by ultrafast laser stimulation of the tissues of the organ of Corti.

11.3.2 Methods

A schematic of the experimental setup used in Ren et al. (2014) is shown in Fig. 11.9. Salient methodological features, important for understanding the technique, are as follows. Laser light pulses of 30-μs duration and 930-nm wavelength were generated with an infrared laser diode. The maximum power of the laser was 0.5 W. A dichroic mirror was used to introduce the infrared laser beam into the optical path of the laser interferometer and to focus laser pulses on the BM (Fig. 11.9, *gray dashed line*). That is, a single optical path is used for both the laser

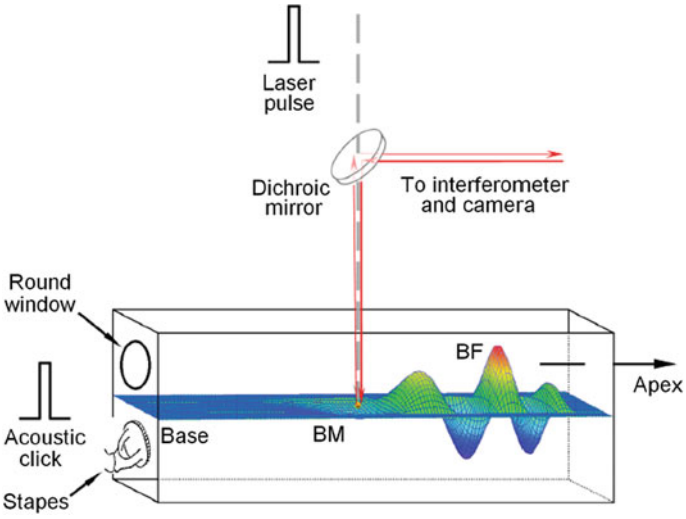

Fig. 11.9 Diagram of the experimental setup for laser-induced BM excitation of the cochlea. Infrared laser pulses were focused on the BM or on a bead on the basal turn of the cochlea. Acoustic clicks were delivered to the external ear canal, which vibrated the stapes and resulted in the BM vibration. The BM vibration was measured by focusing the object beam from a laser interferometer on the reflective bead. In this figure, BF represents the location of highest response for this excitation frequency (sometimes called the best place or characteristic location). Reproduced from Ren et al. (2014), under Creative Commons License 4.0

excitation and the measurement of BM vibration. The position of the laser focal spot was changed by moving the collimating lens with an *x*-*y* translation stage, whereas the focal spot of the object beam of the laser interferometer (Fig. 11.9, *solid red lines*) was unchanged. In other words, the excitation location changed while the measurement location remained fixed and focused (on a gold-coated reflective bead). The success of optical stimulation experiments is not only dependent on the physiological condition of the cochlea, as usual, but also on the optical transparency of the inner ear fluids that, in turn, depends on the amount of bleeding during surgery (which introduces light-scattering cells into the perilymph). Because of the presence of scatterers, it was not possible to conclusively determine the lateral spot size of the laser beam; however, a spot size of 25 μm was estimated from the experiments and theoretical predictions of Ren et al. (2014).

Note that Zhang et al. (2009) used a neodymium-doped yttrium aluminium garnet (Nd:YAG) laser frequency operating in the green spectrum (532 and 355 nm) and BM motion was elicited by focusing the beam on the osseous spiral lamina (these wavelengths of light are claimed to be better absorbed by bone than by tissue). Choice of the wavelength of light is impacted by factors such as tissue damage, lateral resolution, and laser source availability. The Zhang et al. (2009) study shows the possibility of a much shorter (10 ns vs. 30 μs) laser pulse that would allow for unambiguous discrimination between laser forcing and wave propagation effects in a living cochlea. However, the Zhang et al. (2009) study was performed on an excised cochlear segment where the laser light could be directly applied to the spiral lamina. When they retracted the fiber to a distance of 1 mm, the stimulation showed a 75% decrease in the forced response to this wavelength of light. Hence it is unclear whether or not this wavelength of light would penetrate the perilymph with sufficient intensity to vibrate the sensory epithelium in vivo.

Ren et al. (2014) found that the laser light had to be focused on cochlear tissue to elicit a response. This observation is consistent with the well-established results from photoacoustic tomography (Wang and Hu 2012). Infrared laser light can give rise to effects other than a photoacoustic emission in the cochlea. It has been demonstrated that optical stimulation with an infrared (1.8-μm) laser elicits action potentials in cells and was posited to change the cell membrane capacitance (Shapiro et al. 2012). Okunade and Santos-Sacchi (2013) showed that temperature increases in OHCs caused by infrared laser illumination induced changes in the membrane capacitance dependent on the holding potential. Both of these effects could also induce motion in the cochlea. However, the laser energy used in the study by Ren et al. (2014; 1.5–15 μJ/pulse) is roughly three orders of magnitude smaller than in either of those experiments, the wavelength of light was smaller, and the duration of the pulse was shorter (30 μs compared with minimum durations of 100 μs in Shapiro et al. 2012 and 1 ms in Okunade and Santos-Sacchi 2013). Therefore, optically induced electrical stimulation, neural activation, and thermally induced capacitance changes in OHCs were probably not involved in the experiments of Ren et al. (2014). If either of these techniques (Shapiro et al. 2012 or Okunade and Santos-Sacchi 2013) could be spatially confined, executed on a microsecond timescale, and shown to vibrate the sensory epithelium, they would

represent an acceptable means to excite the cochlea (provided they could do so without damaging the tissues).

11.3.3 Basilar Membrane Velocity Response

The results of Ren et al. (2014) are presented here. On laser excitation, the bead surface moved toward the laser beam and then returned to its equilibrium position as the light turned off (Fig. 11.10a). This polarity of motion is consistent with thermal expansion of the tissues or a net motion of the BM toward the ST. Because greater than 97% of the light is reflected from gold at a wavelength of 930 nm (Bass et al. 2009), the only significant absorption will be from the tissues themselves. After this initial spike of movement, there were physiologically vulnerable,

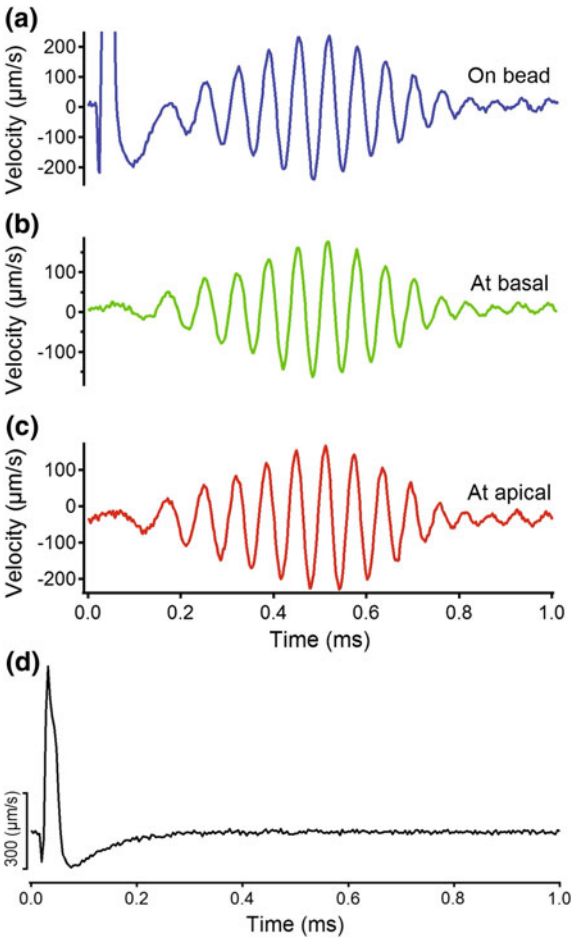

Fig. 11.10 Laser-induced motion of a gold-coated bead on the BM when the laser pulse (excitation point) is focused on the bead (**a**), 50 μm basal to the bead (**b**), and 50 μm apical to the bead (**c**). **d** Time response of the laser-induced BM velocity on the bead in a postmortem condition. Reproduced from Ren et al. (2014), under Creative Commons License 4.0

gradually increasing wavelets that peaked after ~0.5 ms and then decayed. Next, the laser pulse was focused 50 μm closer to the apex of the cochlea while maintaining the response measurement spot at the original location (Fig. 11.10b). Under this condition, the initial spike of motion was nearly extinguished. Third, the excitation location was moved 50 μm closer to the base of the cochlea (Fig. 11.10c; the slight DC shift in the velocity is likely a technical issue with the velocity coder because this was not a consistent finding). Cross-correlation analysis revealed no measurable time lag among the three delayed wavelet responses in the same animal.

Hence, with the exception of the initial spike, a 100-μm change of the excitation location did not alter the delayed response. The response was very different in the insensitive cochlea. In this case, the initial spike of motion remained, but the delayed response was absent (Fig. 11.10d). For times less than 200 μs from the start of the pulse, there was a close correspondence between responses recorded in the sensitive ear (Fig. 11.10a) and those recorded postmortem. These data confirm that the physiologically vulnerable force-generating mechanism of the OHCs was not involved in the immediate response of the BM to laser pulses. This also shows that the laser-induced heating causes a local and immediate excitation of the BM (because this local excitation is present in passive and active cochleae). When the measurement and excitation locations were not collocated, this large initial response was not seen, demonstrating the focal, localized nature of the light stimulation (around 25 μm as mentioned in Sect. 11.3.2). A distributed stimulus would have caused an early motion spike even after separation of the measurement and excitation locations. The amplitude spectrum of the laser pulse-induced responses of the BM revealed a peak centered at 16 kHz (Fig. 11.11, *red solid line*, left axis) and a rapid phase decrease with frequency (Fig. 11.11, *blue solid line*, right axis). The frequency response at the same location to an external acoustic impulse was also measured (Fig. 11.11). The shapes of the amplitude and phase responses of laser-evoked motions were similar to those evoked by a pressure stimulus of 30-dB sound pressure level (SPL; Fig. 11.11, *dashed lines*).

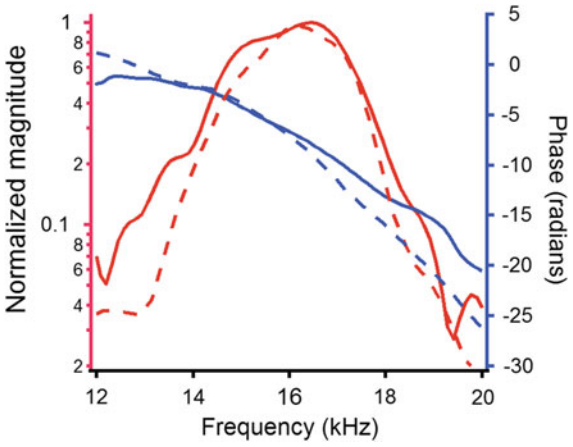

Fig. 11.11 Magnitude (*red*) and phase (*blue*) spectra of laser pulse-induced BM velocity response (*solid lines*) are very similar to those evoked by a 30-dB SPL swept-tone, external acoustic stimulus (*dashed lines*). Reproduced from Ren et al. (2014), under Creative Commons License 4.0

11.3.4 Interpretation of Optically Induced Vibration Response

The mathematical model of Li and Grosh (2012) was extended in Ren et al. (2014) to include heating sources to understand the laser pulse-induced BM response. This active model includes a two-duct acoustic domain so that both symmetric and nonsymmetric waves as well as fast and slow waves are admitted. The best fits to the experiment were obtained with 52% of the heat source in the SM and 48% below the BM in the ST; this asymmetric forcing launches both a fast wave in the fluid and locally forces the BM. The asymmetry in the forcing drove the BM, giving rise to the immediate localized displacement (similar to that seen in experiment) followed by the delayed wavelet.

Both experimental and modeling results indicate that energy is propagated rapidly from the location of the heating source to the base of the cochlea, subsequently generating a forward traveling wave by reflection from the stapes. When the electromechanical force produced by the OHCs was removed from the model, only the initial, highly damped, transient response remained, whereas the delayed wavelet response was eliminated, just as in the postmortem data shown in Fig. 11.10d. The model predicts that the delayed response is due to the electromechanical action of the OHCs. It is perhaps not surprising that an internal heat source generates a compressional wave that reflects from the asymmetric impedance presented by the stapes and RW, generating a forward propagating traveling wave. However, as reported by Ren et al. (2014), both the experiment and the model present a surprising result: the large initial response generated from the laser pulses does not result in an immediately amplified response. Hence, the effective engagement of the active mechanism that enhances the vibrational response of the cochlea to low-level sounds cannot be initiated instantly by a local point force applied to the BM. For either light or acoustical stimulation, the generation of an enhanced response requires the presence of a forward traveling wave. This wave coordinates the electromechanical response of the OHCs along the length of the BM to enhance hearing sensitivity. In retrospect, this is an appropriate design for processing external sounds that travel from the base of the cochlea toward the apex.

It is also instructive to compare the transient response to localized light stimulation shown in Fig. 11.10a with that due to electrical stimulation in Fig. 11.3c. For both laser light and electrical stimulation, there is a vigorous initial impulsive response at early times (less than 50 μs considering both stimuli), demonstrating a force at the measurement location. This initial response is not vulnerable, occurring postmortem in the light-stimulated experiment and in a TM-mutant mouse under electrical stimulation. Overall, the velocity responses are very similar where the initial impulse is followed by a delayed wave packet. The delayed energy at the physiologically vulnerable, higher frequencies (those close to the CF) for the light-stimulated case appear to arrive later than those for the electrically stimulated case (relative to the group delay due to acoustic input) as seen in the time-frequency analysis in He and Ren (2013) and Ren et al. (2016). This may be due to the spread

of current from the ST-SM bipolar electrode pair (possibly on the order of 1 mm) being greater than that of the focal light stimulation (estimated to be ∼25 μm), giving rise to a locally forced response. However, it is also possible that this is simply an animal- and frequency-dependent difference. Naturally, the generality of these results should be viewed with the caveat that they represent the response from one species at one location in the cochlea.

11.4 Summary and Future Directions

Intracochlear electrical stimulation and focused ultrafast laser light provide a localized reproducible means of exciting cochlear structures. Interpreting the results from local forcing using a mathematical model is a most effective way to establish connections between cellular measurements and organ-level measurements in the living cochlea. Advances in these measurement techniques hold the promise of answering important questions about cochlear function, such as the role of OHC electromechanics in hearing.

What are the forces required to move the BM? From Olson (2001), pressure differences across the BM are on the order of ∼2–16 Pa (at 45- and 85-dB SPL, respectively); a 10-Pa pressure translates to a force of 0.8 nN over a single OHC (10 μm diameter). Kössl and Russell (1992) measured transmembrane voltage differences on the order of 0.1–10 mV that would give rise to blocked OHC electromechanical forces on the order of 0.01–1 nN for each OHC (Iwasa and Adachi 1997). Therefore, force generation on the order of 0.01–10 nN in a cochlear cross section represents a reasonable, physiologically relevant range that new experimental techniques could target. Direct mechanical stimulation by conventional techniques, such as with glass fibers, are unacceptable for two reasons: (1) the geometrical constraints in accessing the living organ and (2) the mechanical contact with the BM gives rise to immediate reduction in sensitivity at the CF of the location (Alfred Nuttall, personal communication).

What stimulus current magnitudes are required to evoke detectable vibration responses in the cochlea? A stimulus current of 10 μA appears to be the minimum that is effective, with a maximum of ∼100 μA before undesirable effects occur (Nuttall et al. 2001; Ren et al. 2016). Assuming, for the ease of calculation, a uniform applied current spread of 2 mm from the electrodes and a 10-μA stimulus yields 50 nA per OHC, more than expected from normal MET. However, the cochlear microphonic voltage in the SM relative to the ST ground measured by Ren et al. (2016) in response to a 35-μA stimulus is 66 mV, from which they estimate the transmembrane potential of the OHC to be ∼4.1 mV. This estimate is reasonable considering that the cells are directly forced by an applied current. The current paths, however, are not yet completely characterized, although it is thought that most of the current enters through the MET channels of the OHC. Measurements of the current spread (i.e., the spatial dependence of the current, potentially enabled by multielectrode probes) would be a welcome addition to this

measurement suite because such data should enable estimation of model parameters as well as testing predictions of current and voltage levels and the spatial extent of the current excitation.

Alternatives to the approaches discussed in this chapter must be minimally invasive and flexible. Pt-Ir wires are preferable to glass microelectrodes because they enable easier positioning of the animal and other test apparatus. Laser light paths are fixed and cumbersome, but if alternate fiber-based stimulation were possible, as used, for example, by Zhang et al. (2009), then experiments using optical stimulation would be made significantly easier. Here, one experimental requirement is that microsecond stimuli are essential for testing cochlear function. Mechanical forcing of the BM using magnetic beads is possible, although electronic cross talk between stimulus and measurement systems (especially for the measurement of any electronic response variables) would be challenging in an in vivo preparation. Presently, yields for sensitive animals hover around 30% (for example, Ren et al. 2016). Any new approaches must seek to either improve or maintain such success rates so that the experiments may be concluded in a productive fashion.

The future prospects for electrical stimulation combined with micromechanical and microelectronic measurements of the response to uncover the workings of the cochlea is probably best exemplified in the recent paper by Ren et al. (2016). Concurrent OCT or low-coherence optical measurements of the RL and BM in response to both electrical and acoustic stimulation should enable a better understanding of active processes by combining these experiments with model predictions. Using OCT concurrently with laser-pulse stimulation of the cochlear structures is probably technically too difficult at this point.

However, the development of a laser stimulation technique where the light absorption is solely in the ST or the bony structures in the ST holds significant promise. This stimulation would still be localized but now only in one scala and hence would promote the generation of a slow pressure-difference wave as opposed to the fast wave. This would be much more like directly applying a force to the BM without the confounding effect of the fast wave (which reflects from the stapes-RW boundary and interacts with the local forcing). This could be achieved by focusing on a bead that is coated with a material or contains a gas that preferentially absorbs the laser wavelength or, as in the approach of Zhang et al. (2009), focuses the light on a tissue in one scala that absorbs the light and heats the surrounding fluid.

Genetic manipulation, as presented by Ren et al. (2016), and pharmacological disruption of MET, for example, by disconnecting/destroying tip links or blocking MET channels, will give insights into the role of coupling TM motion to BM (and organ of Corti) motion. The properties of OHCs can be altered in a defined region by focused laser activation of either optogenetically manipulated cells (Wu et al. 2016) or a pharmacological agent that permanently disables prestin after exposure to ultraviolet light (Fisher et al. 2012). Determining the effect of such local property changes on the cochlear response to local electrical or optical stimulation will give insights into structure-function relationships. Furthermore, measuring the motion of the OHCs and associated voltages is essential for understanding the power consumed or produced by the electromechanical processes. OCT techniques where the

longitudinal dependence of the motion of the cochlear structures can be measured, as by Lee et al. (2015), could be combined with localized electrical stimulation to uncover the manner in which waves propagate along the cochlea, not only demonstrating cochlear function but also the means by which otoacoustic emissions are generated. Careful combinations of OCT measurements along with electrical excitation *and* electrical response (e.g., the cochlear microphonic) are just now possible and hold the potential for major discoveries. With the work of Dong and Olson (2013), the potential for simultaneous measurement of intracochlear pressure, voltage and velocity measurements may even be possible. Performing these studies on other animals, especially those with lower frequency hearing, closer to human speech frequencies, stands as an important goal to understanding human hearing through animal studies.

Acknowledgements I thank Anthony Gummer for his guidance, careful editing, and outstanding suggestions for this chapter. I also thank Tianying Ren and Alfred Nuttall, who answered my numerous questions along the course of writing this chapter, made many useful suggestions on its content, and provided many of the figures that I have reproduced here. Moreover, our collaboration over the years has been essential in formulating my ideas on this topic; their patience, collegiality, and expertise are greatly appreciated. Finally, I thank Amir Nankali and Aritra Sasmal for helping proofread this chapter.

Compliance with Ethics Requirements Karl Grosh declares that he has no conflict of interest.

References

Allen, J. B. (1980). Cochlear micromechanics—A physical model of transduction. *The Journal of the Acoustical Society of America*, 68(6), 1660–1670.

Bass, M., DeCusatis, C., Enoch J. M., Lakshminarayanan, V., Li, G., MacDonald, C., Mahajan, V. N., & Van Stryland, E. (2009). *Handbook of Optics,* vol. 2, 3rd ed. (p. 35.14). New York: McGraw-Hill.

Brownell, W. E., Bader, C. R., Bertrand, D., & de Ribaupierre, Y. (1985). Evoked mechanical responses of isolated cochlear outer hair cells. *Science,* 227, 194–196.

Chen, F., Zha D., Zheng J., Choudhury N., Jacques, S. L., Wang R. K., Shi, X., & Nuttall, A. L. (2011). A differentially amplified motion in the ear for near-threshold sound detection. *Nature Neuroscience*, 14, 770–774.

Dallos, P., Wu, X., Cheatham, M., Gao, J., Zheng, J., Anderson, C., Jia, S., Wang, X., Cheng, W., Sengupta, S., He, D., & Zuo, J. (2008). Prestin-based outer hair cell motility is necessary for mammalian cochlear amplification. *Neuron*, 58(3), 333–339.

Dong, W., & Olson, E. S. (2013). Detection of cochlear amplification and its activation. *Biophysical Journal*, 105(4), 1067–1078.

Drexl, M., Lagarde, M. M. M., Zuo, J., Lukashkin, A. N., & Russell, I. J. (2008). The role of prestin in the generation of electrically evoked otoacoustic emissions in mice. *Journal of Neurophysiology*, 99, 1607–1615.

Fisher, J. A. N., Nin, F., Reichenbach, T., Uthaiah, R. C., & Hudspeth, A. J. (2012). The pattern of cochlear amplification. *Neuron*, 76, 989–997.

Frank, G., Hemmert, W., & Gummer, A. W. (1999). Limiting dynamics of high-frequency electromechanical transduction of outer hair cells. *Proceedings of the National Academy of Sciences of the United States of America*, 96(8), 4410–4425.

Fridberger, A., & Ren, T. (2006). Local mechanical stimulation of the hearing organ by laser irradiation. *Neuroreport,* 17, 33–37.

Ghaffari, R., Aranyosi, A. J., Richardson, G. P., & Freeman, D. P. (2010). Tectorial membrane travelling waves underlie abnormal hearing in *Tectb* mutant mice. *Nature Communications*, 1, 96. doi:10.1038/ncomms1094.

Grosh, K., Deo, N. V., Parthasarathi, A. A., Nuttall, A. L., Zheng, J. F., & Ren T. (2003). Modeling electrically evoked otoacoustic emissions. In A. W. Gummer (Ed.), *Biophysics of the Cochlea: From Molecules to Models* (pp. 539–546). Singapore: World Scientific.

Grosh, K., Zheng, J., Zou, Y., de Boer, E., & Nuttall, A. L. (2004). High-frequency electromotile responses in the cochlea. *The Journal of the Acoustical Society of America,* 115(4), 2178–2184.

Gummer, A. W., Hemmert, W., & Zenner, H.-P. (1996). Resonant tectorial membrane motion in the inner ear: Its crucial role in frequency tuning. *Proceedings of the National Academy of Sciences of the United States of America*, 93, 8727–8732.

Halsey, K., Fegelman, K., Raphael, Y., Grosh, K., & Dolan, D. F. (2005). Long-term effects of acoustic trauma on electrically evoked otoacoustic emission. *Journal of the Association for Research in Otolaryngology*, 6, 324–340.

He, D. Z., & Dallos, P. (1999). Somatic stiffness of cochlear outer hair cells is voltage-dependent. *Proceedings of the National Academy of Sciences of the United States of America*, 96, 8223–8228.

He, W., & Ren, T. (2013). Basilar membrane vibration is not involved in the reverse propagation of otoacoustic emissions. *Scientific Reports*, 3, 1874.

Hu, N., Nuttall, A. L., & Ren, R. (2005). Spatial distribution of electrically induced high frequency vibration on basilar membrane. *Hearing Research*, 202, 35–46.

Hubbard, A. E., & Mountain, D. C. (1983). Alternating current delivered into the scala media alters sound pressure at the eardrum. *Science*, 222(4623), 510–512.

Iwasa, K. H., & Adachi, M. (1997). Force generation in the outer hair cell of the cochlea. *Biophysical Journal*, 73, 546–555.

Kakehata, S., & Santos-Sacchi, J. (1996). Effects of salicylate and lanthanides on outer hair cell motility and associated gating charge. *The Journal of Neuroscience*, 16(16), 4881–4889.

Kennedy, H. J., Evans, M. G., & Fettiplace, R. (2003). Fast adaptation of mechanoelectrical transducer channels in mammalian cochlear hair cells. *Nature Neuroscience,* 6, 832–836.

Kirk, D. L., & Yates, G. K. (1996). Frequency tuning and acoustic enhancement of electrically evoked otoacoustic emissions in the guinea pig cochlea. *The Journal of the Acoustical Society of America,* 100(6), 3714–3725.

Kössl, M., & Russell, I. J. (1992). The phase and magnitude of hair cell receptor potentials and frequency tuning in the guinea pig cochlea. *The Journal of Neuroscience,* 12, 1575–1586.

Kurima, K., Ebrahim, S., Pan, B., Sedlacek, M., Sengupta, P., Millis, B. A., Cui, R., Nakanishi, H., Fujikawa, T., Kawashima, Y., Choi, B. Y., Monahan, K., Holt, J. R., Griffith, A. J., & Kachar, B. (2015). TMC1 and TMC2 localize at the site of mechanotransduction in mammalian inner ear hair cell stereocilia. *Cell Reports,* 12, 1606–1617.

Lee, H. Y., Raphael, P. D., Park, J., Ellerbee, A. K., Applegate, B. E., & Oghalai, J. S. (2015). Noninvasive in vivo imaging reveals differences between tectorial membrane and basilar membrane traveling waves in the mouse cochlea. *Proceedings of the National Academy of Sciences of the United States of America,* 112(10), 3128–3133.

Li, Y., & Grosh, K. (2012). Direction of wave propagation in the cochlea for internally excited basilar membrane. *The Journal of the Acoustical Society of America,* 131, 4710–4721.

Liberman, M. C., Gao, J. G., He, D. Z. Z., Wu, X. D., Jia, S. P., & Zuo, J. (2002). Prestin is required for electromotility of the outer hair cell and for the cochlear amplifier. *Nature*, 419(6904), 300–304.

Lim, K.-M., & Steele, C. R. (2003). Response suppression and transient behavior in a nonlinear cochlear model with feed-forward. *International Journal of Solids and Structures,* 40, 5097–5107.

Lukashkin, A. N., Bashtanov, M. E., & Russell, I. J. (2005). A self-mixing laser-diode interferometer for measuring basilar membrane vibrations without opening the cochlea. *Journal of Neuroscience Methods,* 148(2), 122–129.

Meaud, J., & Grosh, K. (2010). The effect of tectorial membrane and basilar membrane longitudinal coupling in cochlear mechanics. *The Journal of the Acoustical Society of America*, 127, 1411–1421.

Müller, M. (1996). The cochlear place-frequency map of the adult and developing Mongolian gerbil. *Hearing Research,* 94, 148–156.

Naidu, R. C., & Mountain, D. C. (2001). Longitudinal coupling in the basilar membrane. *Journal of the Association for Research in Otolaryngology*, 2, 257–267.

Nuttall, A., & Ren, T. (1995). Electromotile hearing: Evidence from basilar membrane motion and otoacoustic emissions. *Hearing Research*, 92, 170–177.

Nuttall, A. L., Zheng, J., Ren, T., & de Boer, E. (2001). Electrically evoked otoacoustic emissions from apical and basal perilymphatic electrode positions in the guinea pig cochlea. *Hearing Research,* 152(1–2), 77–89.

Okunade, O., & Santos-Sacchi, J. (2013). IR laser-induced perturbations of the voltage-dependent solute carrier protein SLC26a5. *Biophysical Journal,* 105(8), 1822–1828.

Olson, E. S. (2001). Intracochlear pressure measurements related to cochlear tuning. *The Journal of the Acoustical Society of America*, 110(1), 349–367.

Parthasarathi, A. A., Grosh, K., Nuttall, A. L., & Zheng, J. (2003). Effect of current stimulus on in vivo cochlear mechanics. *The Journal of the Acoustical Society of America*, 114, 442–452.

Plassmann, W., Peetz, W., & Schmidt, M. (1987). The cochlea in gerbilline rodents. *Brain, Behavior and Evolution*, 30, 82–101.

Ramamoorthy, S., Deo, N. V., & Grosh, K. (2007). A mechano-electro-acoustical model for the cochlea: Response to acoustic stimuli. *The Journal of the Acoustical Society of America*, 121(5), 2758–2773.

Ren, T., & Nuttall, A. L. (1995). Extracochlear electrically evoked otoacoustic emissions: A model for in vivo assessment of outer hair cell electromotility. *Hearing Research,* 92, 178–183.

Ren, T., He, W., Li, Y., Grosh, K., & Fridberger, A. (2014). Light-induced vibration in the hearing organ. *Scientific Reports,* 4, 5941.

Ren, T., He, W., & Gillespie-Barr, P. G. (2016). Reverse transduction measured in the living cochlea by low-coherence heterodyne interferometry. *Nature Communications*, 7, 10282. doi:10.1038/ncomms10282.

Russell, I. J., Legan, P. K., Lukashkina, V. A., Lukashkin, A. N., Goodyear, R. J., & Richardson, G. P. (2007). Sharpened cochlear tuning in a mouse with a genetically modified tectorial membrane. *Nature Neuroscience,* 10(2), 215–223.

Scherer, M. P., & Gummer, A. W. (2004a). Vibration pattern of the organ of Corti up to 50 kHz: Evidence for resonant electromechanical force. *Proceedings of the National Academy of Sciences of the United States of America*, 101(51), 17652–17657.

Scherer, M. P., & Gummer, A. W. (2004b). Impedance analysis of the organ of Corti with magnetically actuated probes. *Biophysical Journal*, 87(2), 1378–1391.

Shapiro, M. G., Homma, K., Villarreal, S., Richter, C. P., & Bezanilla, F. (2012). Infrared light excites cells by changing their electrical capacitance. *Nature Communications,* 3, 736.

Shera, C. A., Tubis, A., & Talmadge, C. L. (2005). Coherent reflection in a two-dimensional cochlea: Short-wave versus long-wave scattering in the generation of reflection-source otoacoustic emissions. *The Journal of the Acoustical Society of America*, 118(1), 287–313.

Strelioff, D. (1973). A computer simulation of generation and distribution of cochlear potentials. *The Journal of the Acoustical Society of America*, 54, 620–629.

Tunstall, M. J., Gale, J. E., & Ashmore, J. (1995). Action of salicylate on membrane capacitance of outer hair cells from the guinea-pig cochlea. *The Journal of Physiology,* 485(3), 739–752.

Wang, L. V., & Hu, S. (2012). Photoacoustic tomography: In vivo imaging from organelles to organs. *Science,* 335, 1458–1462.

Wu, T., Ramamoorthy, S., Wilson, T., Chen, F., Porsov, E., Subhash, H., Foster, S., Zhang, Y., Omelchenko, I., Bateschell, M., Wang, L., Brigande, J. V., Jiang, Z.-G., Mao, T., & Nuttall, A. L. (2016). Optogenetic control of mouse outer hair cells. *Biophysical Journal,* 110(2), 493–502.

Xue, S., Mountain, D. C., & Hubbard, A. (1995). Electrically evoked basilar membrane motion. *The Journal of the Acoustical Society of America*, 97(5), 3030–3041.

Zha, D., Chen, F., Ramamoorthy, S., Fridberger, A. Choudhury, N., Jacques, S. L., Wang, R. K., & Nuttall, A. L. (2011). In vivo outer hair cell length changes expose the active process in the cochlea. *PLoS ONE,* 7(4), e32757.

Zhang, K. Y., Wenzel, G. I., Balster, S., Lim, H. H., Lubatschowski, T., Lenarz, W., Ertmer, W., & Reuter, G. (2009). Optoacoustic induced vibrations within the inner ear. *Optics Express,* 17, 23037–23043.

Zheng, J., Deo, N., Zou, Y., Grosh, K., & Nuttall, A. L. (2007). Chlorpromazine alters cochlear mechanics and amplification: In vivo evidence for a role of stiffness modulation in the organ. *Journal of Neurophysiol*ogy, 97, 994–1004.

Zheng, J., Shen, W., He, D. Z., Long, K. B., Madison, L. D., & Dallos, P. (2000). Prestin is the motor protein of cochlear outer hair cells. *Nature*, 405(6783), 149–155.